VOLUME 115 NUMBER 3

THE ASTROPHYSICAL JOURNAL

AN INTERNATIONAL REVIEW OF SPECTROSCOPY AND ASTRONOMICAL PHYSICS

MAY 1952

SPECTROSCOPIC EVIDENCE OF MOLECULAR HYDROGEN IN THE ATMOSPHERES OF URANUS AND NEPTUNE — *G. Herzberg* — 337
THE INTENSITY OF CERTAIN LINES OF *He* I IN THE B STARS — *I. I. Ahmad* — 341
STUDIES OF THE SPECTRA OF K GIANTS. I. A TABLE OF WAVE LENGTHS AND IDENTIFICATIONS OF SPECTRAL LINES IN THE REGION λλ 4000–5000 — *Livio Gratton* — 346
VARIATIONS IN THE SPECTRUM OF SIGMA SCORPII — *Richard D. Lewis* — 402
THE SPECTRUM OF CHI OPHIUCHI — *E. Margaret Burbidge* — 418
MEAN DISTANCES IN SINGLE-LINE BINARIES — *Victor M. Blanco* — 423
THE SPACE DISTRIBUTION OF INTERSTELLAR MATERIAL IN THE MILKY WAY — *L. Binnendijk* — 428
OB STARS IN THE P CYGNI REGION — *J. J. Nassau and Daniel Harris III* — 459
A FINDING LIST OF F STARS OF HIGH LUMINOSITY — *J. J. Nassau and W. W. Morgan* — 475
VARIATIONS IN THE STELLAR LUMINOSITY FUNCTION. V. A REGION IN CAMELOPARDALIS — *S. W. McCuskey* — 479
SUNSPOT PROMINENCES AND THE YELLOW CORONAL LINE — *Walter Orr Roberts* — 488
REFLECTION FROM METEORITIC SURFACES — *F. A. Kleerekoper and W. A. Rense* — 495
THE ORIGIN OF ZODIACAL LIGHT — *W. A. Rense* — 501
MULTIPLET INTENSITIES FOR THE LINES $^4S - {}^4D$ OF *S* II, *O* II, AND *N* I — *R. H. Garstang* — 506
FORMATION OF ABSORPTION LINES BY NONCOHERENT SCATTERING — *Malcolm P. Savedoff* — 509
ON THE CURVE-OF-GROWTH METHOD — *Su-shu Huang* — 529
SUPERTHERMIC PHENOMENA IN STELLAR ATMOSPHERES. VII. COLLISIONAL EXCITATION FROM LEVELS OTHER THAN THE LOWEST — *Satoshi Matsushima* — 544
SUPERTHERMIC PHENOMENA IN STELLAR ATMOSPHERES. VIII. COMMENT ON THE CHROMOSPHERIC MODEL — *Richard N. Thomas* — 550
ON THE RADIUS OF GYRATION OF STARS — *Lloyd Motz* — 562

NOTES

NOTE ON THE IDENTIFICATION OF THE GROUND STATE OF THE *TiO* MOLECULE — *John G. Phillips* — 567
ON THE CORONAL LINES λλ 5445, 5694, AND 4086 — *R. H. Garstang* — 569
ABSOLUTE ABSORPTION OF THE H_2 CONTINUUM — *Po Lee and G. L. Weissler* — 570
ABSOLUTE OSCILLATOR STRENGTHS OF CHROMIUM — *Frank B. Estabrook* — 571
HERBIG'S NEBULOUS OBJECTS NEAR NGC 1999 — *Guillermo Haro* — 572
THE SHELL SPECTRUM OF OMICRON ANDROMEDAE — *Arne Slettebak* — 573
THE SPECTRUM OF 29 CYGNI — *Arne Slettebak* — 575
THE SPECTRUM OF THE HIGH-VELOCITY A-TYPE STAR HD 161817 — *Arne Slettebak* — 576
ON THE BOLOMETRIC CORRECTION FOR EARLY-TYPE STARS — *Jesse K. McDonald and Anne B. Underhill* — 577
THE SPECTRUM OF CPD—60°3278 — *Jorge Sahade* — 578
THE SPECTRUM OF NOVA SCORPII 1950 II ON AUGUST 16, 1950 — *Jorge Sahade and Jorge Landi Dessy* — 579
A NOTE ON THE CONCEPT OF EFFECTIVE WAVE LENGTH — *Ivan King* — 580
SEARCH FOR FLARES OF dM STARS ON THE SPROUL ASTROMETRIC PROGRAM — *Sarah Lee Lippincott* — 582
ERRATA — 585
INDEX — 587

THE UNIVERSITY OF CHICAGO PRESS
CHICAGO, ILLINOIS, U.S.A.

May 1952 Vol. 115, No. 3

THE ASTROPHYSICAL JOURNAL

AN INTERNATIONAL REVIEW OF SPECTROSCOPY AND ASTRONOMICAL PHYSICS

Published in Collaboration with the American Astronomical Society

W. W. MORGAN
Managing Editor

S. CHANDRASEKHAR
Associate Editor

Yerkes Observatory of the University of Chicago

EDITORIAL BOARD

G. HERZBERG (1952-56)
National Research Council, Ottawa

C. D. SHANE (1952-55)
Lick Observatory, University of California

FRED L. WHIPPLE (1952-54)
Harvard College Observatory

LYMAN SPITZER, JR. (1952-53)
Princeton University Observatory

PAUL W. MERRILL (1952)
Mount Wilson Observatory of the Carnegie Institution of Washington

---

The Astrophysical Journal is published bimonthly by the University of Chicago at the University of Chicago Press, 5750 Ellis Avenue, Chicago 37, Illinois, during July, September, November, January, March, and May. ¶Two volumes are published per year, one beginning with the January issue and the other beginning with the July issue. The subscription price is $6.00 per volume or $12.00 per year; the price of single copies is $3.00. (Orders for service of less than a volume will be charged at the single copy rate.) ¶Postage is prepaid by the publishers on all orders from the United States and its possessions. No extra charge is made for postage to countries in the Pan American Postal Union. ¶Postage is charged extra as follows: for Canada, 20 cents per volume, 40 cents per year (total $6.20 per volume, $12.40 per year); on single copies 5 cents (total $3.05); for all other countries in the Postal Union, 50 cents per volume, $1.00 per year (total $6.50 per volume, $13.00 per year), on single copies 10 cents (total $3.10). ¶Subscriptions are payable in advance. Please make all remittances payable to The University of Chicago Press, in United States currency or its equivalent by postal or express money orders or bank drafts.

The following is an authorized agent:

For the British Empire, except North America and Australasia: The Cambridge University Press, Bentley House, 200 Euston Road, London, N.W. 1, England. Prices of yearly subscriptions and of single copies may be had on application.

Claims for missing numbers should be made within the month following the regular month of publication. The publishers expect to supply missing numbers free only when losses have been sustained in transit, and when the reserve stock will permit.

Business correspondence should be addressed to The University of Chicago Press, Chicago 37, Illinois.

Communications for the editors and manuscripts should be addressed to: W. W. Morgan, Editor of THE ASTROPHYSICAL JOURNAL, Yerkes Observatory, Williams Bay, Wisconsin.

Line drawings and photographs should be made by the author, and all marginal notes such as co-ordinates, wave lengths, etc., should be included in the cuts. It will not be possible to set up such material in type.

One copy of the corrected galley proof should be returned as soon as possible to the editor, Yerkes Observatory, Williams Bay, Wisconsin. Authors should take notice that the manuscript will not be sent to them with the proof.

The cable address is "Observatory, Williamsbay, Wisconsin."

The articles in this journal are indexed in the *International Index to Periodicals*, New York, N.Y.

Applications for permission to quote from this journal should be addressed to The University of Chicago Press, and will be freely granted.

Microfilms of complete journal volumes are available to regular subscribers only and may be obtained at the end of the year. Orders and inquiries should be addressed to University Microfilms, 313 North First Street, Ann Arbor, Michigan.

Notice to subscribers: If you change your address, please notify us and your local postmaster immediately.

Entered as second-class matter, July 31, 1940, at the Post-Office at Chicago, Ill., under the Act of March 3, 1879.
Acceptance for mailing at special rate of postage provided for in United States Postal Act of October 3, 1917, Section 1103, amended February 28, 1925.

[PRINTED IN U.S.A.]

THE ASTROPHYSICAL JOURNAL

AN INTERNATIONAL REVIEW OF SPECTROSCOPY AND ASTRONOMICAL PHYSICS

VOLUME 115 MAY 1952 NUMBER 3

SPECTROSCOPIC EVIDENCE OF MOLECULAR HYDROGEN IN THE ATMOSPHERES OF URANUS AND NEPTUNE*

G. HERZBERG

Division of Physics, National Research Council, Ottawa, Canada

Received December 21, 1951

ABSTRACT

The unidentified diffuse feature at 8270 A observed by Kuiper in the spectra of Uranus and Neptune is reproduced in the laboratory in an 80-meter path of hydrogen at 100-atm pressure and a temperature of 78° K. It is the $S(0)$ line of the 3–0 pressure-induced rotation-vibration band of the H_2 molecule. Two other lines of this band, as well as three lines of a double transition (2–0, 1–0), are observed in the laboratory spectrum. Most of these features are hidden in the planetary spectra by strong CH_4 bands, but a line, 8166 A, of the double transition is only partially overlapped by an adjacent CH_4 band. Its low intensity in the planetary spectra can be accounted for by assuming that there are even larger amounts of helium than of hydrogen in the atmospheres of Uranus and Neptune. Helium does not induce the double transition. The observed spectra are very roughly compatible with a 3:1 (or higher) helium-hydrogen ratio, a temperature of 78° K (or lower), and a partial pressure of hydrogen at the bottom of the visible atmosphere of about 2 atm. The thickness of an equivalent atmosphere of uniform density would be about 18 km for Uranus.

Two years ago Kuiper[1] reported the presence of a diffuse band at 8270 A in the spectra of Uranus and Neptune and showed that this band is not due to CH_4. As I pointed out in a recent paper,[2] the 8270 A feature agrees closely with the $S(0)$ line of the 3–0 band of the quadrupole rotation-vibration spectrum[3] of H_2 but because of its large width cannot be identified with this line. On the other hand, Welsh, Crawford, and Locke[4] have observed, at high pressure, lines of the 1–0 band and, more recently,[5] of the 2–0 band of the pressure-induced spectrum of H_2 which occur at the same wave lengths as the quadrupole lines but are very broad features (at room temperature about 320 cm^{-1} wide). The width was found by them to be independent of pressure but to decrease with temperature. Therefore, it appeared possible to me[2] that the 8270 A feature might

* Contribution No. 2713 from the National Research Council of Canada.

[1] G. P. Kuiper, *The Atmospheres of the Earth and Planets* (Chicago: University of Chicago Press, 1949), p. 325; *Ap. J.*, **109**, 540, 1949.

[2] G. Herzberg, *J.R.A.S. Canada*, **45**, 100, 1951.

[3] G. Herzberg, *Canadian J. Res.*, **A28**, 144, 1950.

[4] H. L. Welsh, M. F. Crawford, and J. L. Locke, *Phys. Rev.*, **76**, 580, 1949; M. F. Crawford, H. L. Welsh, J. C. F. MacDonald, and J. L. Locke, *Phys. Rev.*, **80**, 469, 1950.

[5] H. L. Welsh, M. F. Crawford, J. C. F. MacDonald, and D. A. Chisholm, *Phys. Rev.*, **83**, 1264, 1951.

be the $S(0)$ line of the 3–0 band of the pressure-induced H_2 spectrum, reduced in width on account of the low temperature in the atmospheres of Uranus and Neptune.

More recently, experiments have been carried out in this laboratory with a view to checking the above suggestion in a direct way. For this purpose a 2-meter absorption tube with a mirror system for multiple traversals was set up in such a way that pressures up to 100 atm could be reached and the whole tube could be cooled with liquid nitrogen.

At room temperature and a path length of 80 meters at 100-atm pressure, three very diffuse features were observed at 8450, 8150, and 7830 A, as shown in Figure 1, *a*. By cooling to the temperature of liquid nitrogen (78° K) but maintaining the pressure at 100 atm (i.e., increasing the density by a factor of 4), the spectrum was radically changed, and five lines, each of a width of about 60 cm^{-1} (40 A), appeared as shown in Figure 1, *b*. In Figure 1, *c*, the spectrum of Uranus as obtained by Kuiper[6] is shown for comparison. One of the five laboratory lines, at 8258 A, agrees closely with Kuiper's planetary feature both in position and in width. The slight difference between the wave length of the planetary and that of the laboratory feature is probably not real, since it refers to a broad band 40 A wide.[7] Even if it were real, it might be accounted for by a slight shift of the intensity distribution due to different physical conditions (e.g., temperature, helium content).

The question arises, of course, as to why the remaining four laboratory lines have not been observed in the planetary spectrum. It is seen in Figure 1, *b* and *c*, that all but one of these (the line at 8166 A) are hidden by strong CH_4 absorptions in the planetary spectra. There is a faint feature at 8158 A on Kuiper's spectrum, but this may be at least partly due to the R branch of the H_2O band at 8228 A and partly to the adjacent strong CH_4 band. At any rate it would appear that the 8166 A feature, if present at all, is fainter in the Uranus spectrum than the 8270 A feature, contrary to the laboratory spectrum, in which it is much stronger. This fact can be understood on the basis of a more detailed discussion of the laboratory spectrum.

At the temperature of liquid nitrogen (78° K) only four lines of the pressure-induced 3–0 band are to be expected—$Q(0)$, $Q(1)$, $S(0)$, and $S(1)$—of which $Q(0)$, if it occurs at all, would nearly coincide with $Q(1)$. These lines account for the three longward members of the laboratory spectrum. The large intensity of the 8166 A feature compared to that at 8258 A is anomalous, since, on the basis of the Boltzmann factor and the statistical weights, $S(1)$ should be slightly less intense than $S(0)$. This anomaly and the two additional lines at shorter wave lengths can, however, be readily accounted for on the assumption of a double transition similar to the one observed by Welsh, Crawford, MacDonald, and Chisholm[5] near the 2–0 band. The double transition accompanying the 2–0 band is one in which the 1–0 transition takes place simultaneously in both collision partners. In the case of the 3–0 band the corresponding double transition would be one in which the 1–0 transition takes place in one collision partner and the 2–0 transition in the other.

In Table 1 the observed and predicted wave lengths are listed for both the single 3–0 transition and the double (2–0, 1–0) transition. The predicted values of the 3–0 band are the quadrupole wave lengths observed at low pressure;[3] those of the (2–0, 1–0) band were obtained from the quadrupole wave numbers of the 2–0 band by adding the wave number of the origin of the 1–0 band. The agreement between observed and calculated lines seems to leave no doubt of the presence of the double transition in the laboratory spectrum. As shown by Figure 1, *b*, the double transition is stronger than the single transition, just as was observed by Welsh, Crawford, *et al.* for the 2–0 band. It should be

[6] I am greatly indebted to Dr. Kuiper for supplying this spectrogram and for permission to include it here.

[7] Actually, I measured on Kuiper's print 8260 A, suggesting that the difference may be due to personal differences of measuring diffuse bands. A more recent measurement of several plates by Kuiper (private communication) has yielded 8267 ± 2 A.

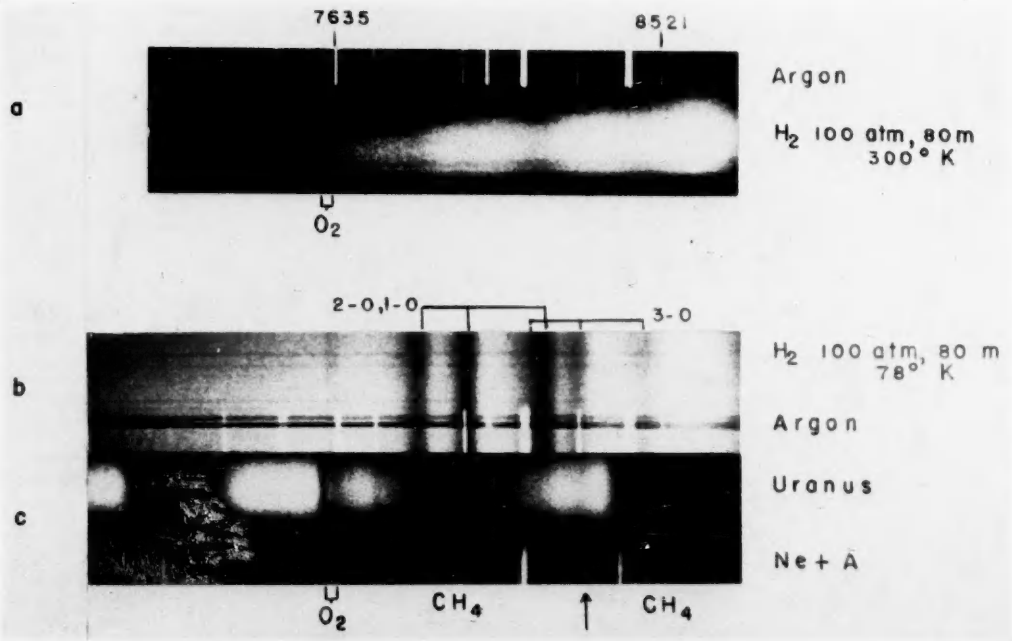

FIG. 1.—Pressure-induced spectra of hydrogen. *a*, spectrum at room temperature; *b*, spectrum at temperature of liquid nitrogen; *c*, spectrum of Uranus (Kuiper).

noted that the $Q(1)$ line of the double transition is not resolved from the $S(1)$ line of the single transition; but the 8166 A feature is distinctly asymmetric toward shorter wave lengths (see Fig. 1, *b*), as would be required by this overlapping.

The faintness of the feature at 8166 A in the spectrum of Uranus indicates that the double transition is weak compared to the single transition. One would expect the double transition to be absent in a gas mixture in which most collisions suffered by the H_2 molecules are with a partner different from H_2. The only collision partners that could be present in sufficient abundance in the atmospheres of Uranus and Neptune would appear to be helium atoms. It was shown by Crawford, Welsh, MacDonald, and Locke[4] in the case of the 1–0 band that helium can indeed induce the rotation-vibration spectrum of hydrogen. In the case of the 3–0 band, experiments were carried out with the same tube as described above, using a 3:1 and a 9:1 helium-hydrogen mixture. Unfortunately, with these dilutions the absorption is very weak and the spectra obtained are not suitable

TABLE 1

OBSERVED AND PREDICTED PRESSURE-INDUCED SPECTRUM OF H_2

Designation		Observed λ (A)	Predicted λ (A)
Single transition (3–0)	$Q(0)$	8469	8488
	$Q(1)$		8497
	$S(0)$	8258	8273
	$S(1)$		8151
Double transition (2–0, 1–0)	$Q(0)$	8166	8165
	$Q(1)$		8171
	$S(0)$	7958	7956
	$S(1)$	7830	7832

for reproduction. However, they do show the expected effect of a strengthening of the single band compared to the double band. The effect is not so great as might have been expected, since, apparently, helium atoms are not such efficient collision partners as H_2 molecules in inducing the single band.

It must be realized that, even if the double transition were completely absent in the planetary spectra, there would still be the line $S(1)$ of the single transition at 8151 A, which at 78° K would be only slightly weaker than $S(0)$ at 8258 A. It is not certain, because of the overlapping with the CH_4 band, whether the 8151 A feature is fainter than the 8270 A feature, although on casual inspection it appears to be weaker. If this were so, a temperature of Uranus lower than 78° K would be indicated. At 50° K the theoretical intensity ratio of $S(1)$ and $S(0)$ would be 0.18, instead of 0.60 as at 78° K. Of course, for these lower temperatures it becomes increasingly difficult to account for the large amounts of CH_4 observed to be present in the atmospheres of Uranus and Neptune. Also, the close agreement in width of the laboratory and planetary 8270 A features indicates that the temperature cannot be much lower than 78° K.

In addition to the temperature, information may be derived about the pressure in these planetary atmospheres by a comparison of the planetary and laboratory spectra, if an assumption is made about the helium-hydrogen ratio. At a temperature of 78° K the thickness of an equivalent atmosphere, having the same density throughout as the actual Uranus atmosphere has at the bottom of the visible atmosphere, is 31 km if it consists mainly of hydrogen and 16 km if it consists mainly of helium. The intensity of absorption of the pressure-induced spectrum is proportional to the product $p_{H_2}^2 \times l$,

where p_{H_2} is the pressure of H_2 and l the path length. This holds even when helium is present, since the absorption induced by helium is proportional to the product $p_{H_2} \times p_{He} \times l$, and p_{He} for a given helium-hydrogen ratio is proportional to p_{H_2}. Assuming a 3:1 helium-hydrogen mixture and considering the planetary spectrum to be matched by a laboratory spectrum of 120-meter path and 100-atm total pressure (this is a very rough estimate), one finds, since the product $p_{H_2}^2 \times l$ must be the same in the two cases, that the partial pressure p_{H_2} at the bottom of the visible atmosphere of Uranus (and similarly Neptune) is $p_{H_2} = 2.0$ atm (at 78° K), assuming $l_{\text{Uranus}} = 18$ km. This pressure does not depend much on the assumed helium-hydrogen ratio. The total pressure with the adopted helium-hydrogen ratio would be 8 atm. It might at first appear that the equivalent path length in the atmosphere should be twice the thickness of the equivalent atmosphere. However, a more detailed consideration shows that this factor 2 is just canceled out by the fact that the absorption is proportional to the square of the pressure, a fact that makes the lower part of the atmosphere much more effective in producing the absorption. It can be readily seen that in an isothermal atmosphere this effect just halves the effective length of the atmosphere.

Obviously it is desirable that a more detailed comparison be made of the envelope of the 8270 A feature in both the planetary and the laboratory spectra, using higher resolution in order to remove any remaining doubt that might exist of the correctness of the present identification. At the same time, by such a comparison it may be possible to separate the 8166 A feature from the overlapping CH_4 and H_2O bands and thus to get a better estimate of the helium-hydrogen ratio as well as of the temperature in the Uranus atmosphere.

I am greatly indebted to Mr. J. Shoosmith for his untiring and expert assistance in these experiments. I am also indebted to Drs. A. E. Douglas and B. P. Stoicheff for several helpful discussions.

THE INTENSITY OF CERTAIN LINES OF *He* I IN THE B STARS

I. I. AHMAD
Yerkes Observatory
Received January 7, 1952

ABSTRACT

The behavior of the *He* I lines λλ 4471, 4387, and 4144 is investigated in connection with spectral types determined on the system of the Yerkes spectral atlas for main-sequence stars and for supergiants. In the main-sequence stars the results are similar to those found earlier by Struve, Williams, and Rudnick; in the supergiants, however, the behavior is strikingly different for λ 4471, which appears to reach its maximum intensity near O9–B0.

Attention is called to the peculiar spectrum of the O9 star HD 93521; its spectral peculiarities and large distance from the galactic plane suggest a connection with Baade's Population II.

The behavior of the lines of *He* I with respect to spectral type and luminosity in the O and B stars has been described by—among others—Struve,[1] Williams,[2] and Rudnick.[3] Their results can be summarized as follows:

Struve found that with increasing temperature the singlets (λ 4387 and λ 4009) fade out more rapidly in the giants than in the dwarfs. For the cooler stars he found little, if any, difference in the ratio of triplets to singlets between giants and dwarfs; he placed the maximum intensity at about type B2 for both triplets and singlets. In connection with Harvard spectral types he found a null effect in the intensity of *He* I for the hottest stars; near maximum (B2) he found the *He* I lines to be systematically stronger in the giants than in the main-sequence stars.

Williams found the maximum intensity near type B3 and an absolute-magnitude effect opposite in sign to that found by Miss Payne[4] and Struve; he states: "An absolute magnitude effect similar in sign to that found for the H lines extends from the earliest types (within which the helium criterion is capable of distinguishing giants from dwarfs, although hydrogen intensity is not) to type B5 at least. . . ."[5]

Rudnick found the maximum to occur at B2 for both singlet and triplet systems, with the maximum sharper and better defined for the singlets than for the triplets. The asymmetry found by Struve[6] was confirmed. He found that λ 4471 fades out more slowly on either side of maximum in giants than in the main-sequence stars. For the singlet line λ 4387 the same is true for the later types; but in the range B2–O the situation is reversed, in that the intensities in giants drop faster than those in dwarfs. At class B2 Rudnick found that both λ 4471 and λ 4387 are about 50 per cent stronger in dwarfs than in giants; that is, he found a pronounced negative luminosity effect; he found this effect to be present as early as type B0. The results of Rudnick and Williams therefore agree that the strongest *He* I lines in the ordinary photographic region are enhanced in main-sequence stars over supergiants in the spectral range B0–B5.

It would seem to be of interest to investigate the behavior of these same lines on the

[1] *Ap. J.*, **78**, 73, 1933.

[2] *Ap. J.*, **83**, 109, 1936.

[3] *Ap. J.*, **83**, 439, 1936.

[4] *The Stars of High Luminosity* (Cambridge, Mass.: Harvard College Observatory, 1930), p. 268.

[5] The differences in the results from visual estimates and from the microphotometric measures can be accounted for by consideration of the inclusion of more of the wings of the lines in the latter than in the former. When very low dispersion is used, the visual intensity of strong lines is probably closer to the measures.

[6] *Ap. J.*, **78**, 82, 1933.

system of spectral classification described in the Yerkes spectral atlas.[7, 8] For this purpose the results of Rudnick were used, since a better selection of stars of different luminosity is possible than in the case of the measures of Williams. The spectral types were determined from plates taken with the parallax spectrograph attached to the 40-inch refractor of the Yerkes Observatory; they are on what will be described as the "revised Yerkes system." This system is very close to that of the Yerkes *Atlas of Stellar Spectra;* the changes are slight revisions in spectral type which have been possible because of the improved quality of spectrograms obtained during the past few years. For the main sequence the stars included are those in Rudnick's list of luminosity classes IV and V; the supergiants are those of luminosity classes I*a* and I*b*. Table 1 gives the

TABLE 1

EQUIVALENT WIDTHS (A) FOR MAIN SEQUENCE (RUDNICK)

Star	Sp. (RYS)*	λ 4471	λ 4387	λ 4144
ξ Per	O7	0.59	0.20	0.12
S Mon	O7	0.51	.21	.14
λ Ori	O8	0.61	.21	.11
10 Lac	O9 V	0.81	.32	.19
τ Sco	B0 V	1.07	.60	.37
ε Per	B0.5 V	1.41	.80	.53
γ Peg	B2 IV	1.42	.92	.69
δ Cet	B2 IV	1.36	.91	.76
θ Oph	B2 IV	1.13	.71	.59
ζ Cas	B2 V	1.42	.97	.78
102 Her	B2 V	1.14	.81	.58
η Aur	B3 V	1.06	.59	.55
η UMa	B3 V	1.08	.64	.47
ι Her	B3 V	1.18	.82	.66
π And	B5 V	0.84	.54	.45
λ Cyg	B5 V	0.74	.50	.35
2 Lac	B6 IV	0.69	.27	.26
ζ Peg	B8 V	0.29	.18	.05
ι And	B8 V	0.26	.25	.13
α Del	B9 V	0.34	0.30	0.14

* Revised Yerkes system.

data for the main-sequence stars and Table 2 those for the supergiants. The columns list the name of the star, the spectral type on the revised Yerkes system, and the equivalent width in angstroms of the diffuse triplet λ 4471 and of the diffuse singlets λ 4387 and λ 4144. The results are plotted in Figure 1, *a*, where the open circles refer to the supergiants and the closed circles to main-sequence stars.

The following conclusions can be drawn from an inspection of Figure 1, *a:*

a) There is a well-defined maximum for λ 4387 and λ 4144 at class B2 for the main-sequence stars and a less well-defined maximum near the same point for the supergiants.

b) The maximum for λ 4471 is also near B2 or slightly earlier.

c) The behavior of λ 4471 in the supergiants is quite different from that of λ 4387 and λ 4144, in that the intensity appears to increase with increasing temperature as far as the earliest supergiants plotted—of spectral type O9.5. At this spectral type there is probably a slight enhancement of λ 4471 with increasing luminosity.

[7] W. W. Morgan, P. C. Keenan, and E. Kellman, *An Atlas of Stellar Spectra* (Chicago: University of Chicago Press, 1943).

[8] See also W. W. Morgan and N. G. Roman, *Ap. J.*, **112**, 362, 1950.

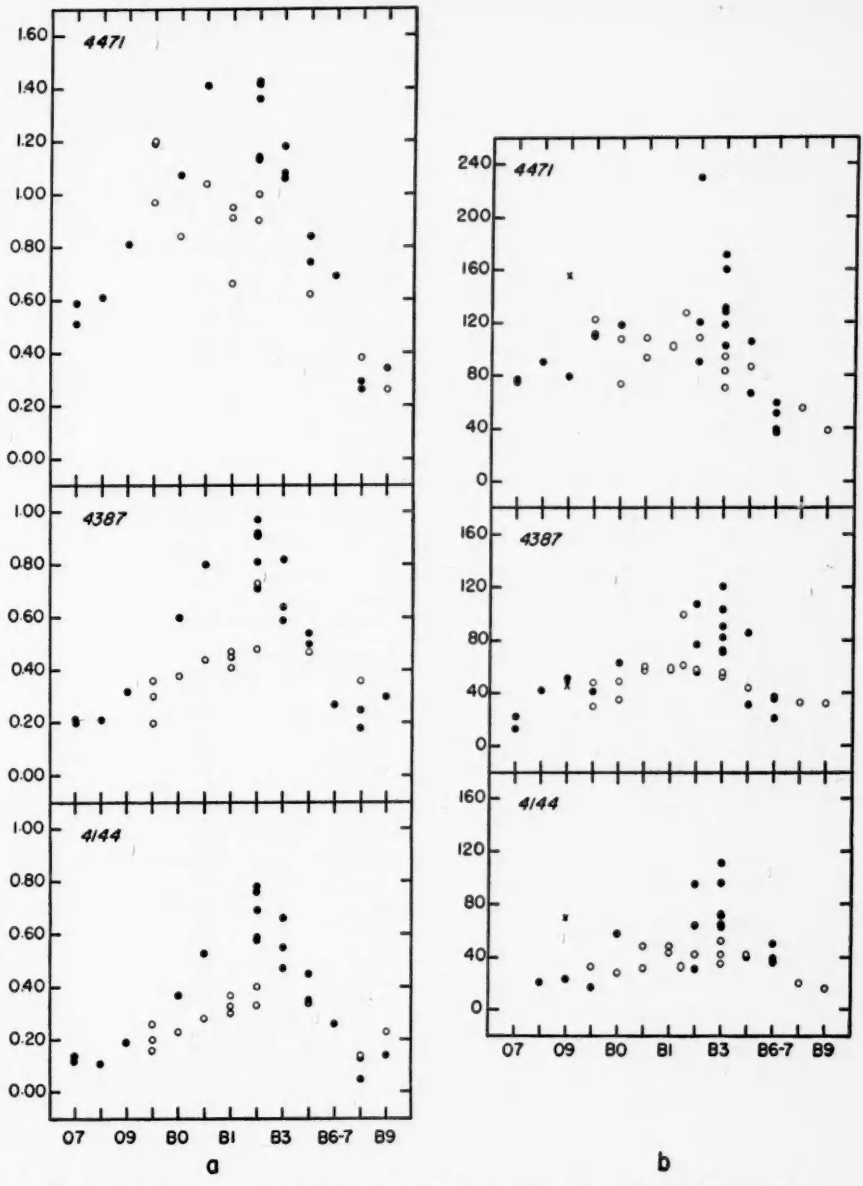

FIG. 1.—*a*, intensities of the *He* I lines λλ 4471, 4387, and 4144 (Rudnick) as a function of spectral type on the revised Yerkes system. Ordinates are equivalent widths in angstroms. Open circles refer to supergiants, filled circles to main-sequence stars. *b*, intensities of the same lines as determined by Williams. The cross refers to the peculiar O star HD 93521.

TABLE 2

EQUIVALENT WIDTHS (A) FOR SUPERGIANTS (RUDNICK)

Star	Sp. (RYS)	λ 4471	λ 4387	λ 4144
α Cam	O9.5 I*a*	1.19	0.30	0.20
19 Cep	O9.5 I*b*	0.97	.20	.16
ζ Ori	O9.5 I*b*	1.20	.36	.26
ε Ori	B0 I*a*	0.84	.38	.23
κ Ori	B0.5 I*a*	1.04	.44	.28
κ Cas	B1 I*a*	0.66	.45	.30
ρ Leo	B1 I*b*	0.91	.41	.33
ζ Per	B1 I*b*	0.95	.47	.37
χ^2 Ori	B2 I*a*	0.90	.73	.40
9 Cep	B2 I*b*	1.00	.48	.33
67 Oph	B5 I*b*	0.62	.47	.34
β Ori	B8 I*a*	0.38	.36	.14
4 Lac	B9 I*ab*	0.26	(0.24)*	0.23

* Values in parentheses are of lower accuracy.

TABLE 3

EQUIVALENT WIDTHS (A) FOR MAIN SEQUENCE (WILLIAMS)

HD No.	Sp. (RYS)	λ 4471	λ 4387	λ 4144
24912	O7	75	13	(14)*
47839	O7	77	22	(22)
36861	O8	90	42	21
93521	O9 Vp	156	47	70
214680	O9 V	79	51	23
149757	O9.5 V	110	41	17
149438	B0 V	118	63	58
4180	B2 V	90	56	31
39698	B2 V	120	77	64
208185	B2 V	230	107	95
32630	B3 V	171	120	71
74280	B3 V	102	71	64
100600	B3 V	131	72	111
120315	B3 V	128	82	64
187811	B3 V	118	90	72
208947	B3 V	160	103	96
22928	B5 III	66	31	40
147394	B5 III	105	85	.....
87901	B7 V	36	37	39
109387	B7 p	59	36	36
23480	B7 III	39	21	50
35497	B7 III	51	(21)	(49)

* Values in parentheses are of lower accuracy.

The effects noted above appear to be confirmed by the measures of Williams, although the scatter is rather large. Williams' observations are listed in Tables 3 and 4 and are plotted in Figure 1, *b*.

Especial attention should be called to the star HD 93521, which has an abnormally high intensity of λ 4471 for its spectral type. The intensity of λ 4471 is similar to that in

TABLE 4

EQUIVALENT WIDTHS (A) FOR SUPERGIANTS (WILLIAMS)

HD No.	Sp. (RYS)	λ 4471	λ 4387	λ 4144
30614	O9.5 I*a*	111	30	33
195592	O9.5 I*a*	122	48	(52)*
37128	B0 I*a*	73	35	28
204172	B0 I*b*	107	49	.....
38771	B0.5 I*a*	108	57	48
194839	B0.5 I*a*	93	60	31
24398	B1 I*b*	101	59	48
91316	B1 I*b*	102	58	43
190603	B1.5 I*a*	(86)	61	32
194279	B1.5 I*a*	127	99	33
206165	B2 I*b*	108	57	42
14134	B3 I*a*	70	.....	52
198478	B3 I*a*	83	52	35
36371	B3 I*b*	94	55	42
164353	B5 I*b*	86	44	42
34085	B8 I*a*	55	33	20
21291	B9 I*a*	38	32	16

* Values in parentheses are of lower accuracy.

main-sequence stars of classes B2 and B3, where the line reaches its greatest strength. It is of interest that HD 93521 is the only O-type star observable in northern latitudes which is located far above the galactic plane; the distance is approximately 800 psc. It thus may have some connection with Baade's Population II, and the spectral peculiarities may be associated with stars of the earliest type belonging to that category.

In conclusion, I wish to express my sincere thanks to Dr. W. W. Morgan for suggesting this problem and for his helpful advice and to Miss Irene Hansen for her kind assistance with the illustration.

STUDIES OF THE SPECTRA OF K GIANTS. I. A TABLE OF WAVE LENGTHS AND IDENTIFICATIONS OF SPECTRAL LINES IN THE REGION λλ 4000–5000*

LIVIO GRATTON
McDonald and La Plata Observatories
Received October 29, 1951

ABSTRACT

Accurate wave lengths and estimated intensities for about twenty-eight hundred lines in the spectral region λλ 4000–5000 of the two K giants α Serpentis and α Ursae Majoris have been obtained from coudé spectra having a dispersion ranging from 1.75 A/mm at λ 4000 to 6.25 A/mm at λ 5000. The identifications with atomic and molecular lines are discussed. Thirty-seven atoms and ions (some of them belonging to two ionization stages of the same element) have been definitely identified; twelve more are doubtful. Among the molecules, the strongest are *CN* and *CH*, followed by *SiH*, *TiO*, *AlH*, C_2, *SiN*, and *ZrO*. In addition, *SiF*, *AlO*, and *MgH* were also discussed, but the evidence is inconclusive. Attention is called to a faint line at λ 4339.27, one of whose contributors might be λ 4339.29 $D\gamma$.

I. INTRODUCTION

In recent years it has become evident that among stars of low and high velocity belonging to the same spectrum and luminosity class there exist noticeable differences in the intensities of spectral lines. It is generally believed that these correspond to differences in the basic chemical composition of stellar populations I and II.

It is well known that Morgan, Keenan, and Kellman discovered that the *CN* bands are abnormally weak[1] in high-velocity giants of spectral types G5–K2; the same was found by Popper[2] to be true for the K giants belonging to the globular clusters M3 and M13. On the other hand, Keenan[3] found that the *CH* band was enormously strengthened in the R stars of high velocity as compared with normal (low-velocity) stars of the same class, while the *CN* bands were again fainter in the high-velocity stars. Miczaika[4] investigated some selected K stars with somewhat higher dispersion, measuring photometrically line intensities for some eighty lines (mostly blends of *Fe* I, *Ti* I, *V* I, etc.); it was found again that the *CN* bands are fainter and *CH* stronger in the high-velocity stars; but apparently the Balmer lines and the strongest *Fe* lines did not show any marked differences between the two groups of stars, although Keenan, Morgan, and Münch[5] had suspected that the Balmer lines were somewhat stronger in the high-velocity stars. M. and B. Schwarzschild determined equivalent widths and central depths for a number of lines in nine F dwarfs from Mount Wilson coudé spectrograms of rather high dispersion.[6] The final data showed that the *CH* lines are stronger relative to the *Fe* lines in stars of high velocity, indicating a relative abundance of *C* to *Fe* two and a half times higher than in low-velocity stars; it was also suspected that the abundance ratio *H* to *Fe* might be larger in the high-velocity dwarfs by a factor of 2, as compared with those of low velocity. Finally, it may be mentioned that Roman[7] found that among giants and dwarfs of spectral types F5–G5 some stars have lines systematically weaker than others; if the stars were divided into two groups, those with weak lines were found to possess, in the mean, larger velocities and larger deviations from the mean velocity than those with strong

* *Contributions from the McDonald Observatory, University of Texas*, No. 207.

[1] *An Atlas of Stellar Spectra* (Chicago: University of Chicago Press, 1943).
[2] *Ap. J.*, **105**, 204, 1947.
[3] *Ap. J.*, **96**, 101, 1942.
[4] *Zs. f. Ap.*, **27**, 1, 1950.
[5] *A.J.*, **53**, 194, 1948.
[6] *Ap. J.*, **112**, 248, 1950.
[7] *Ap. J.*, **112**, 554, 1950.

lines; stars with high velocity (higher than 70 km/sec) were found only among those with weak lines.

During my stay at the McDonald Observatory in May and June, 1948, I took several spectra of K giants of high and low velocity with the prism coudé spectrograph, with the aim of studying the spectral differences (if any) in higher dispersion (of the order of 3 A/mm). But, although some differences could be detected by a simple inspection of the plates, it at once became evident that, in order to get a clear view of them, it was necessary to obtain very good identifications of the thousands of faint lines of those very rich spectra. Accordingly, it was decided to postpone all discussion and to measure first in great detail two spectra in order to identify as many lines as possible. As it was felt that the identifications might be useful to other investigators, it seemed worth while to publish them *in extenso*.

II. THE OBSERVATIONS

All the plates for this investigation (about thirty) were taken with the prism coudé spectrograph of the McDonald Observatory. With this instrument the region from λ 4000 to λ 5000 is brought into good focus at the same time by bending the plates rather strongly; however, on account of the high dispersion, it was not possible to photograph

TABLE 1

DATA ON SPECTROGRAMS MEASURED

Plate Cd	U.T. (1948)	Star	Spectrum	Reg.	Rad. Vel.	No. of Lines
759.....	May 20, 4^{h}10^m	α Ser	K2 III–IV	B	−2.0±0.24 (56)	1467
760.....	20, 5 15	α Ser		V	0.0± .19 (58)	1252
785.....	24, 5 14	α UMa	G8 II–III	B	−9.5± .28 (56)	1575
786.....	24, 5 41	α UMa		V	−8.2±0.15 (56)	1254

the whole spectrum on one single plate. This would have been impossible anyway because of the larger exposure times necessary for the violet end of the spectrum. For this reason two exposures were taken for each star, one for the violet (V) and the other for the blue (B) region. Occasionally a plate was found broken in the plateholder, and a few were repeated. The plates overlap between λ 4200 and λ 4400, but the V plates were measured only up to λ 4325 and the B plates from λ 4325 on.

Even with bright stars, the exposure times were rather long, so that it was necessary to use a fairly wide slit (0.05 mm) and very fast plates (103*a*-O), thus losing somewhat in resolving power. For the brightest star (α Bootis), the exposure times were 10 and 5 minutes for the V and B plates, respectively. The star was kept fixed on the slit during the exposure; the width of the spectra is, however, about 0.5 mm, owing to the size of the stellar image.

The focus was checked before the observations were started, and the spectrograph was first very carefully collimated. In the final position of the focus the lines are very sharp and show a little astigmatism only at the extremities of the spectrum, which is certainly harmless. During all the observations it was considered unnecessary to change the focal setting, because the temperature in the spectrograph case remained constant to one-tenth of a degree.

All plates were calibrated photometrically by means of a tube sensitometer using a common 6V-5A automobile lamp and a blue filter. They were developed 5 minutes in D19 developer at 65° F.

For measurement, one V and one B plate were selected of each of the two stars α Ursae Majoris and α Serpentis. These lay approximately at the two ends of the interval in spectral type covered by the investigation and have fine lines well suited for accurate measurement. The data for the plates are shown in Table 1. All are of excellent quality.

The dispersion at different wave lengths and the corresponding width of the slit projected on the plate are shown in Table 2. In practice it was found possible to measure separately two lines when their difference in wave length was a little less than the projected slit width, provided that the intensities were not too high or too different.

III. MEASUREMENT AND REDUCTION OF THE SPECTROGRAMS

The plates were measured at the Observatory of La Plata by means of a long-screw machine of the projection type. This instrument was constructed by a local firm according to the writer's specifications especially for the present investigation. Although the screw is unusually long (25 cm), the periodic errors were found to amount to less than

TABLE 2

DISPERSIONS AND SLIT WIDTHS

λ	Disp. (A/mm)	Slit (A)	λ	Disp. (A/mm)	Slit (A)
4000	1.75	0.08	4600	4.18	0.21
4200	2.48	.12	4800	5.17	.26
4400	3.29	0.16	5000	6.25	0.31

0.5μ throughout. The progressive error was not investigated, owing to the method used for the reduction, which permitted us to get free from its influence. However, from the measurements it may be estimated to be very small. I wish to stress the great gain in ease and probably in precision that is due to the use of a projecting machine. One plate with more than fifteen hundred lines could be measured in the customary two positions in less than 40 hours of effective work, with a total of about four thousand settings, including the time of writing down the readings. Not the least advantage of the projecting machine was the great ease with which the "wire" could be inclined to the dispersion; this was necessary, because the spectral lines from an autocollimating spectrograph are always inclined toward the dispersion.

The readings at the machine were reduced to wave lengths as follows. First, using the iron comparison lines, a table was constructed giving the λ's for intervals of 0.5 mm of the settings; by means of linear interpolation, the readings for the stellar lines were thus converted into wave lengths. Then, with the aid of a number of *Fe* I and *Mn* I lines directly identified, the Doppler shift was computed for each plate. Of course, this contains not only the true Doppler shift due to the star's motion relative to the observer but also the unknown errors of measurement due, for instance, to the curvature of the slit image. The observed values corrected for the motion of the observer, but *not* for systematic errors, are contained in Table 1, sixth column, together with their mean errors; the latter are internal errors from the agreement of the individual lines, whose number is indicated in parentheses.

The wave lengths of all the lines were corrected for the Doppler shift, and a first tentative identification was written down for each line, listing all reasonable contributors. With the help of the laboratory wave lengths of all lines whose intensity was greater than 2 and whose preliminary identification was considered reasonably certain, systematic corrections to the stellar preliminary wave lengths were derived graphically, as is shown in Figures 1 and 2. It is difficult to trace the cause of these systematic errors, but there is no doubt that part of them at least were due to variations of temperature in the room where the measurements were made. For instance, the discontinuities coincide with the points where the measurements were left at the end of one day's work and were resumed

on the following day.[8] In the preliminary wave lengths these irregularities were smoothed out by the process of reduction, the smoothing depending on the chance distribution of the comparison lines.

The final wave lengths were corrected accordingly. Their mean errors were found from a comparison with the laboratory wave lengths of all lines well identified, of intensity equal to or greater than 2. They are shown in Table 3 as a function of λ. These errors ob-

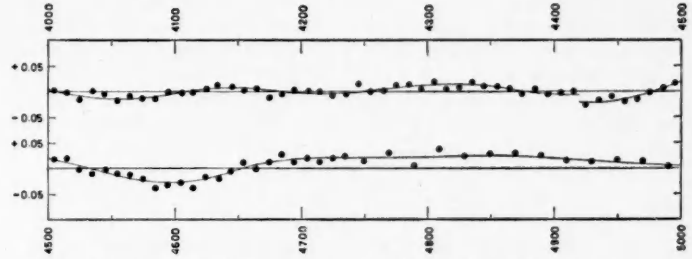

FIG. 1.—Systematic errors of the preliminary wave lengths for α Serpentis. Abscissae are wave lengths, ordinates systematic errors; each point is the mean value for some twenty or thirty lines.

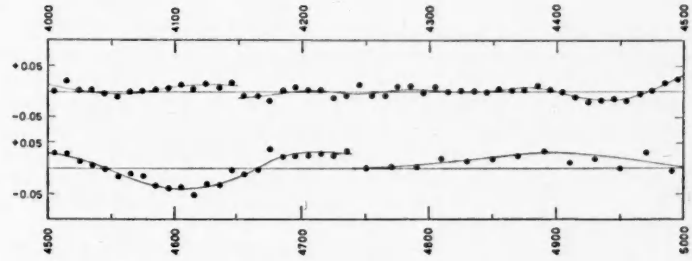

FIG. 2.—Systematic errors of the preliminary wave lengths for α Ursae Majoris. Abscissae and ordinates as in Fig. 1.

TABLE 3

MEAN ERRORS

λ	m.e.	λ	m.e.	λ	m.e.
4000	±0.018	4400	±0.024	4800	±0.034
4200	0.021	4600	0.028	5000	0.044

viously are partly due to errors of the laboratory wave lengths themselves or to a faulty identification. In the final table of wave lengths (Table 6) only the first two decimal figures were given. Of course, very wide or very faint lines may be in error by a much larger amount.

Owing to the systematic corrections and to the curvature of the slit image, there is

[8] It is obvious that the variation in temperature does not act simply as a dilatation or contraction of the scale; on account of possible flexure of the supports, it may also cause a deviation of the light-beam from the projecting lens. It was found, nevertheless, that the temperature variation in the room was very small during the measurements.

no point in comparing the radial velocities of Table 1 with those known for α Serpentis and α Ursae Majoris.

IV. THE ESTIMATED INTENSITIES

An extensive program of photometric measurement is planned for the near future. However, for the sake of identification, at least a rough estimate of the intensities is necessary. For this purpose, after various trials, very consistent estimates were obtained by comparing an enlarged reproduction of the spectra with an artificial scale. This consisted of a number of "spectral lines" drawn by hand with a very black pencil on a piece of white drawing paper; in this way the graininess of the enlarged image was imitated almost perfectly. The scale was compared by putting it very near to the spectrum to be examined and looking for the artificial line which best matched the stellar one. The "intensity" is simply the ordinal number of the line in the scale. After a little practice it was found that

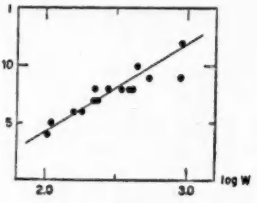

FIG. 3.—Comparison between estimated intensities and Pannekoek's equivalent widths for η Draconis. Abscissae are logarithms of equivalent width, ordinates estimated intensities for a small group of selected lines.

the effect of the density of the image could be accounted for well enough, but there is no doubt that the estimates are subjected to considerable systematic errors, depending on the mean photographic density of the continuous background. Actually, the estimates were made on a reproduction of a spectrum of β Ophiuchi; no difference could be detected between the spectrum of this star and that of α Serpentis after a careful examination by means of a Hartmann comparator.

In order to check the intensities, the following comparisons were made:

a) In his paper on line intensities in spectra of advanced type, Pannekoek[9] gives, among others, equivalent widths of a large number of lines of the G8 star η Draconis, which was also among the stars of my program. In order to compare my intensities with Pannekoek's equivalent widths, I estimated the intensities of a few lines of η Draconis. Owing to the different dispersion used, I thought it better to limit the comparison to a small group of lines free from blends in Victoria spectra and lying in a rather narrow spectral region from λ 4160 to λ 4210. The result is shown in Figure 3. The agreement is excellent; however, this is partly due to the use of a narrow spectral region. In comparing lines from a larger region, greater errors would be expected. The linearity of the relation is due to chance.

b) The equivalent widths of several *V* I and *Ti* I lines in α Bootis were determined at the Observatory of La Plata from the tracings in Hiltner and Williams' *Photometric Atlas of Stellar Spectra*. These may be compared with the estimated intensities in β Ophiuchi. The comparison is especially interesting because Hiltner and Williams employed the same spectral equipment as that used for the present investigation, so that the discrepancies cannot be attributed to the resolving power of the equipment. Figure 4 shows an agreement somewhat less satisfactory than Figure 3. This is due to the use of a wider spectral region but also to the fact that two different stars were compared. For instance, the greater intensity of the *Ti* lines relative to *V* in α Bootis may be due to chance but might also be real. The majority of the lines compared lie on the flat part of the curve of growth.

[9] *Pub. Dom. Ap. Obs. Victoria*, Vol. **8**, No. 5, 1950.

Although the comparison with the equivalent widths in α Bootis does not show very good agreement, the intensities of the present investigation may certainly be used for the purpose of the identification of the lines.

V. IDENTIFICATIONS OF ATOMIC LINES

The main source for the identification of atomic lines in an astrophysical source is Mrs. Moore-Sitterly's *Multiplet Table* (*MT*). For lines contained in this list no serious difficulty was usually encountered; a comparison of lines belonging to transitions between the same multiplets permitted us in almost all cases to decide whether or not a given ele-

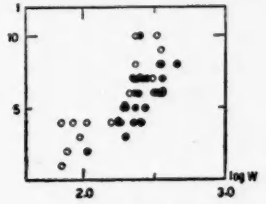

FIG. 4.—Comparison between estimated intensities and equivalent widths in α Bootis. Abscissae are logarithms of equivalent widths, ordinates estimated intensities; filled circles represent *Ti* I lines, empty circles *V* I lines.

ment contributed to a stellar line and in the majority of the cases to establish which was the main contributor. For this purpose in most cases the theoretical relative intensities were used as given in the tables of White and Eliason;[10] as, however, in many multiplets deviations from the LS-coupling are evident, for these and for all intersystem lines the observed laboratory intensities were used as given in the *MT*. For various blends a comparison with the *Revised Rowland Table of Solar Wave Lengths* was also very useful, in order to establish the order of importance of some of the contributors. Of course, the difference in excitation between the sun and a K giant was duly considered.

Table 4 contains a list of the elements observed in the spectra of the K giants. The numbers of lines there indicated do not correspond to that of the lines listed in the table of wave lengths, because some have been excluded, their contribution to the stellar lines being entirely negligible or the coincidences being due certainly to chance. In Table 6 some identifications have also been added from sources different from the *MT;* as these are considered very doubtful, they were not considered in the present discussion. The first column of Table 4 gives the atom or ion; the second, the ionization potential; the third, the numbers of coincidences observed with stellar lines which have no other atomic contributor; the fourth, the number of coincidences with stellar lines possessing other contributors; the fifth, the maximum intensity of a line in which the atom is the main contributor (numbers in parentheses refer to blended lines); and the notes in the sixth column usually refer to chance coincidences. The following comments to Table 4 can be made.

Na I.—Only faint lines in this spectral region. The maximum observed intensity is certainly due to other unknown contributors.

Si I.—Although one single line was observed, its attribution to *Si* I is quite certain.

Mn II.—The only observed coincidence (λ 4755.73) was eventually excluded from the table of wave lengths; the stellar line is probably due to *TiO*.

Cu I.—The only observed coincidence (λ 4530.78) was eventually excluded; the stellar line is well accounted for.

Zn I.—Rather doubtful, although, besides the coincidences indicated in the table, some coincidences with other unclassified lines have been listed.

[10] *Phys. Rev.*, **44**, 753, 1933.

TABLE 4

ELEMENTS OBSERVED

Element	I.P.	Fr. Line	Bl. Line	Max. Int.	Notes
1 *H*	13 54	3	.....	14	
4 *Be* I	9 28	1	.....	0	Probably a chance coincidence
11 *Na* I	5 12	3	5	6	
12 *Mg* I	7 61	4	4	10	
14 *Si* I	8 11	1	.....	10	
19 *K* I	4 32	1	1	8	
20 *Ca* I	6 09	15	18	100	
21 *Sc* I	6 7	5	12	8	
Sc II	12 8	5	13	(9)	
22 *Ti* I	6 81	129	222	10	
Ti II	13 6	32	55	9	
23 *V* I	6 71	67	127	10	
V II	14 1	18	31	7	Several chance coincidences
24 *Cr* I	6 74	189	260	20	Some coincidences may be due to chance
Cr II	16 6	16	12	3	The majority are chance coincidences
25 *Mn* I	7 40	34	36	25	
Mn II	15 6	1	.....	2	Only a chance coincidence
26 *Fe* I	7 86	442	494	60	Some coincidences may be due to chance
Fe II	16 16	17	24	7	Some coincidences may be due to chance
27 *Co* I	7 84	49	72	10	Some coincidences may be due to chance
28 *Ni* I	7 61	64	81	8	Some coincidences may be due to chance
29 *Cu* I	7 69	.....	1	.....	Only a chance coincidence
30 *Zn* I	9 35	2	2	3	Chance coincidences?
31 *Ga* I	5 97	.....	2	(1)	Chance coincidences?
32 *Ge* I	8 09	1	1	?	Chance coincidences?
38 *Sr* I	5 67	2	5	3	Some coincidences may be due to chance
Sr II	10 98	2	2	12	
39 *Y* I	6 5	11	14	5	
Y II	12 3	5	10	(7)	
40 *Zr* I	6 92	20	39	6	Some coincidences may be due to chance
Zr II	13 97	21	21	7	Several chance coincidences
41 *Cb* I	6 8	3	7	(3)	Some coincidences are due to chance
42 *Mo* I	7 06	1	.....	1	Probably a chance coincidence
Mo II	?	1	.....	3	Only a chance coincidence
44 *Ru* I	7 5	5	6	1	Several chance coincidences
45 *Rh* I	7 7	.....	2	(0)	Chance coincidences
46 *Pd* I	8 30	.....	1	(0)	Chance coincidence
55 *Cs* I	3 88	1	1	?	Chance coincidences?
56 *Ba* II	9 96	3	3	8	
57 *La* I	5 59	1	3	(1)	Chance coincidences?
La II	11 38	19	26	5	Several coincidences may be due to chance
58 *Ce* II	?	55	76	4	Several coincidences may be due to chance
59 *Pr* II	?	17	29	4	Some coincidences may be due to chance
60 *Nd* II	?	40	54	7	Some coincidences may be due to chance
62 *Sm* II	11 4	45	68	5	
63 *Eu* I	5 64	.....	2	.....	Chance coincidences
Eu II	11 21	1	6	9	Some coincidences may be due to chance
64 *Gd* I	6 16	1	1	0	Chance coincidences
Gd II	?	30	44	(4)	Several coincidences are due to chance
65 *Tb* II	?	3	5	.....	
66 *Dy* II	?	4	6	.....	
67 *Ho* II	?	.....	2	.....	Chance coincidences?
72 *Hf* II	14 8	11	5	2	Several coincidences are due to chance
74 *W* I	7 94	2	2	(2)	Chance coincidences?
76 *Os* I	8 7	1	3	(1)	Chance coincidences?
82 *Pb* I	7 38	.....	1	(8)	

Ga I.—The two ultimate lines λ 4172.05 and λ 4032.98 may be partly blended with strong lines of *Fe* I and *Mn* I.

Ge I.—Of the two observed coincidences, one is with a faint line in the wing of λ 4226.73 *Ca* I, and the other with a stellar line not otherwise accounted for.

Cb I.—Some of the coincidences listed are probably real, although the evidence is not conclusive.

Mo I.—The only observed coincidence may be due to chance; however, some strong unclassified lines have been listed.

Mo II.—Only one coincidence was noted (λ 4279.02); although the stellar line is not otherwise accounted for, this atom may be safely considered as absent.

Ru I.—Some of the coincidences listed are probably real, but the evidence is not conclusive.

Rh I.—Excluded from the table of wave lengths (Table 6).

Pd I.—Excluded from the table of wave lengths (Table 6).

Cs I.—Two coincidences were noted, one with a faint stellar line not otherwise explained; it is considered very doubtful.

La I.—Very doubtful, although the four noted coincidences are the only ones which might be expected in this spectral region.

Eu I.—Excluded from the table of wave lengths; the stellar lines are well accounted for.

Eu II.—Although the observed coincidences are rather few in number, the identification is quite certain.

Gd I.—Excluded from the table of wave lengths (Table 6).

Ce I, Pr I, Nd I, Tb I, Tb II, Dy I, Dy II, Ho I, Ho II.—The spectra of these rare earths have not yet been analyzed. Temperature classes by King[11] have been used. For neutral atoms, although several coincidences of stellar lines of low-temperature classes have been noted, the absence of the strongest lines permits us to conclude that they are not present in the spectra of the K giants, with the possible exception of *Dy* I; they have been excluded from the tables of wave lengths (Table 6). The ionized atoms are almost certainly present, as indicated in Table 4; the only doubtful one is *Ho* II.

Tm I, Tm II, Lu I, Lu II, Hf I.—The few observed coincidences may be accounted for; very doubtful.

Hf II.—Although several coincidences have been observed, the identification is rather doubtful.

W I, Os I.—Too few coincidences. Doubtful.

Pb I.—Although one single blended line has been observed, the identification is considered very probable.

Among the atoms not listed in Table 4 or in the comments, the great majority, like *He, C, N, O*, etc., do not possess strong lines of low excitation in the observed spectral region; the remaining ones have not been discussed for lack of sufficient laboratory data or because they are not expected on account of their scarcity.

VI. A LINE POSSIBLY DUE PARTLY TO DEUTERIUM

When the plates were examined, a faint line at λ 4339.27 was observed, which showed a rather peculiar behavior, being stronger in some stars and fainter in others. Owing to the possibility that *Dγ* (λ 4339.287) might be one of the contributors to the stellar line, special attention was dedicated to it. The stellar wave length measured on all the plates available where the line was present with sufficient intensity is shown in Table 5. The wave lengths of the third column are relative to other neighboring lines whose identification was practically certain; the mean errors are from the internal agreement of the plates of the same star.

As a rule, the line appears somewhat stronger in the three high-velocity stars γ Leo A,

[11] *Ap. J.*, **68**, 194, 1928; **72**, 221, 1930; **78**, 9, 1933.

η Cep, and α Boo, and in β Aql. It is interesting to note that the last-named star has a velocity below the limit but shows a spectral behavior in each respect more like that of high-velocity stars than that of normal stars.

To illustrate the variation in wave length of the line, the observed values are shown diagrammatically in Figure 5, with their respective mean errors. It may be easily seen that there is no clear run with the spectral class, and it is evident that the high-velocity group (including β Aql) shows a decidedly shorter wave length: an average λ of, say,

TABLE 5

STELLAR LINE AT λ 4339

Star	Spectrum	$\lambda \pm$ m.e.	No. of Pl.	Star	Spectrum	$\lambda \pm$ m.e.	No. of Pl.
α UMa	G8 II–III	4339.262 ± 0.003	2	ϵ Ser	K0 III–IV	4339.277 ± 0.003	3
η Dra	G8 III	4339.269 ± .006	2	ϵ Cyg	K0 III	4339.262 ± .003	2
β Aql	G8 IV	4339.253 ± .004	3	α Ser	K2 III–IV	4339.273	1
γ Leo A	K0p	4339.249	1	α Boo	K2p	4339.251	1
η Cep	K0 IV	4339.251 ± .009	3				

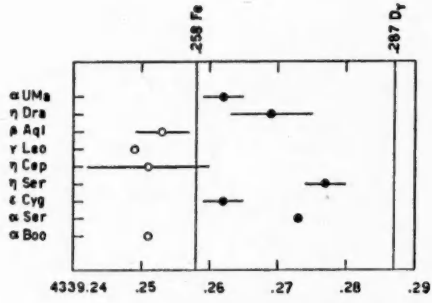

FIG. 5.—Wave lengths of a line near λ 4339.26. Abscissae are measured wave lengths in the stars shown at the left; the two vertical lines correspond to a line of *Fe* (sun) and to *D*γ. Open circles mean stars of the high-velocity group; full circles stars of low velocity; the lengths of the horizontal lines are twice the mean errors of the wave lengths.

4339.251 ± 0.003 against 4339.269 ± 0.006 (mean deviations) for the other stars. As the difference of the mean values is many times larger than their mean errors, the effect may be considered real.

In the neighborhood of this line the *MT* lists only 4339.287 *D*γ and λ 4339.317 *Ce* II. But the *Ce* II line seems to be ruled out not only on account of its wave length but also because the other component of the doublet, λ 4062.223, shows very different behavior. For instance, it is strong in β Oph, where λ 4339.27 could not be measured, being too faint, while it is faint in α Boo. The *Revised Rowland Table* gives a line at λ 4339.258, which is attributed to *Fe* (unclassified). This wave length coincides almost exactly with the general mean of all the K giants, but the *Fe* line is certainly very faint (it is not listed, for instance, in the wave length tables of the Massachusetts Institute of Technology, although it is contained in the table of *Fe* lines in Kayser's *Handbuch*); in any case, it is impossible to understand the observed behavior on the hypothesis of a single contributor of wave length equal to the mean.

Another possible contributor is λ 4339.25 *CH* (0, 0) $P_{1ed}5$. As other *CH* lines with the same rotational quantum number are fairly strong, this would account for the component of shorter wave length. It has already been mentioned that various authors have found the *CH* band strengthened in high-velocity stars. If we assume that the stellar line is a blend of λ 4339.25 *CH* and another component of longer wave length, the observed behavior both in intensity and in wave length would be easily understood.

As far as the unknown contributor of longer wave length is concerned, it would be tempting to identify it with $D\gamma$. But, of course, one cannot entirely rule out the possibility that the real contributor may be another atomic or molecular line. It may be remarked that a comparison with $H\gamma$ shows that an abundance ratio of the two hydrogen isotopes of the same order as that observed on earth would be quite sufficient to explain the intensity of the line, if it should be attributed to deuterium.

The matter cannot be settled by means of observations of $D\delta$ or $D\beta$, because these lines are in the wings of strong *Fe* lines and it would be very difficult to observe them on my spectra.

VII. IDENTIFICATION OF MOLECULAR LINES

The identification of the numerous molecular lines present in the spectra of K giants constitutes a very difficult problem. This is due essentially to the lack of suitable laboratory data. The rotational analyses are seldom available and, as a rule, are limited to a few bands of a given system. In her work on the spectrum of β Pegasi, D. Davis[12] found that when a rotational analysis was not available the best procedure was to take a laboratory spectrum of the molecule to be examined and to prepare from it a glass positive, with approximately the same dispersion as the stellar spectrogram; with a Hartmann comparator the glass positive may be compared directly with the stellar plate. It is obvious that this comparison would be much easier if the same spectrograph were used for both the laboratory and the stellar spectra.

For this purpose, during my stay at Mount Locke, I tried to obtain several molecular spectra with the coudé spectrograph used for the present investigation. Unfortunately, the facilities available at Mount Locke were not sufficient to take all the laboratory spectra in the condition of purity necessary for this comparison, so that little use could be made of them. For this reason in many cases the identifications of molecular lines are to be considered only provisional. The worst case is that of *TiO*.

It is highly desirable that more data (rotational analysis of more bands, assignment of quantum numbers to more lines, wave lengths, etc.) about molecular spectra should be made available in the near future, possibly in a form comparable with that existing for atomic spectra.

For the present investigation the following molecules were investigated; they probably comprise all important molecules which possess strong bands in the spectral region λλ 4000–5000.

CN.—The violet system of *CN* is, together with the G band of *CH*, the strongest molecular feature in the spectra of K giants. Indeed, with the exception of spectral types R and N, *CN* is stronger in K giants than in any other stars. Rotational analyses are available only for the (0, 1), (1, 2), and, partly, (2, 3) bands[13] ($^2\Sigma \rightarrow {}^2\Sigma$).

Owing to the importance of these bands for the general problem under investigation, an effort was made to identify as many individual lines as possible. For this purpose, the writer took some plates of the *CN* violet bands with the large grating spectrograph of the Physical Institute of the University of La Plata. Two sources were used, namely, ordinary carbon arc in air and a vacuum tube. It was found that in the arc the excitation was somewhat higher than in the stars, so that the members of low rotational quantum numbers could not be measured, while the lowest members could be easily seen in the vacuum

[12] *Ap. J.*, **106**, 28, 1947.

[13] Jevons, *Proc. R. Soc. London*, *A*, **112**, 407, 1927.

tube, in which the lines were much sharper. From the spectra of the two sources combined, 225 lines belonging to the (0, 1), (1, 2), (2, 3), (3, 4), (4, 5), and (5, 6) bands were measured. The wave lengths of the *CN* lines given in the table of wave lengths are from this investigation.

Of the 225 *CN* lines measured in the laboratory spectra, all but 9 coincide with stellar lines; the missing lines are faint in laboratory, and some might be due to impurities. Of the 216 coincidences, 59 are with stellar lines not otherwise explained, some of them being rather strong (7 on my scale), and 51 have a secondary or doubtful contributor. For the remaining 106, *CN* is a secondary contributor; some of these latter coincidences may be due to chance.

Of course, it is fairly probable that more lines than those measured may be attributed to *CN*, but it was not considered worth while to extend the laboratory work. No attempt has been made to identify bands with $\Delta v = 2$; if present, they must be rather faint.

CH.—The rotational analyses by Gerö[14] and Fagerholm[15] of the well-known G band $^2\Delta \rightarrow {}^2\Pi$ (0, 0) is quite sufficient. Of 240 lines classified by these authors, all but 17 were found to coincide with stellar lines; the lines missing have all very low or very high rotational quantum numbers. Because of the multiplet structure of the band and the crowding of lines near the band head, some of the lines were not separated. Fifty-six of them coincide with stellar lines not otherwise explained, and 49 with lines having other contributors faint or doubtful; usually these lines occur in pairs or even more numerous groups. There remain 118 coincidences, many of which are most probably due to chance. Several coincidences with solar lines attributed to *CH* (unclassified) were also noted.[16]

C_2.—Of the bands of the Swan system, the following heads were found to coincide with stellar absorption features: (1, 0), (2, 1), (3, 2), (4, 3), (5, 4), and (6, 5). The identification of the individual lines would be rather difficult, because each line is in reality a close triplet[17] just below the resolving power of our spectral equipment, thus producing a stellar line rather faint and fuzzy which would probably not be seen. Therefore, no attempt was made to identify them, although it is fairly possible that some contribute to stellar lines in the region λλ 4500–4737.

SiH.—Next to carbon compounds and possibly *TiO*, the $^2\Delta \rightarrow {}^2\Pi$ system of *SiH* gives the strongest bands in the observed region of the spectra of K giants. The rotational analysis by Jackson[18] was used to identify the individual lines. An arc with *H* streaming between *Si* electrodes was found to give all the *SiH* lines of the (0, 0) band, but it was not possible to use the spectrum thus obtained because of the impurities of the silicon used.

There were 185 lines investigated, including many unclassified lines, and all but 16 (mostly unclassified) were found to coincide with stellar lines. About half the coincidences are with unexplained or not well-explained stellar lines. For the remaining, *SiH* is a secondary contributor or the coincidence is due to chance.

SiN.—The band heads (0, 0), (1, 2), and (2, 2) of the $^2\Sigma \rightarrow {}^2\Sigma$ system were identified by comparison with laboratory spectra (arc with *Si* electrodes); they coincide with well-defined absorption features of the spectrum. No attempt was made to identify individual lines because of the compact structure of the bands; it is possible that some contribute to stellar lines in the region λλ 4117–4200.

SiF.—The bands of the well-analyzed α system ($^2\Pi \rightarrow {}^2\Pi$) have a rather compact structure[19] which cannot be well resolved on the stellar spectra. The strongest band heads

[14] *Zs. f. Phys.*, **118**, 27, 1941.

[15] *Ark. f. mat., astr. och fys.*, Vol. **27A**, No. 19, 1942.

[16] Richardson, *Ap. J.*, **77**, 195, 1933.

[17] Johnson, *Phil. Trans. R. Soc. London*, **226**, 157, 1926.

[18] *Proc. R. Soc. London, A*, **126**, 373, 1930.

[19] Johnson and Jenkins, *Proc. R. Soc. London, A*, **116**, 327, 1927.

were looked for, but the results were very uncertain. If present, this molecule must be very faint.

AlH.—Many lines belonging to the bands of the system $^1\Pi \rightarrow {}^1\Sigma$ were easily found by comparison with laboratory spectra. For the identification, the rotational analysis by Bengtsson[20] was used. The coincidences with lines of the band (1, 0) are rather unconvincing, but all the expected lines of the (0, 0) and also of the (1, 1) bands were found to coincide with stellar lines, several of which are otherwise unexplained.

MgH.—Only the (1, 0) band and a few lines of the (0, 0) band of the strong green system ($^2\Pi \rightarrow {}^2\Sigma$) fall in the observed region; no convincing coincidences were noted, and therefore this molecule was excluded from the table of wave lengths (Table 6). It may be remarked that Öhman[21] found that the *MgH* bands are stronger in dwarfs than in giants of spectral type M; as they begin to show in early K dwarfs, one may expect to find them very faint or absent in early K giants. Probably only the strongest lines of the (0, 0) band should be expected; they fall out of the region observed.

AlO.—The blue-green system ($^2\Sigma \rightarrow {}^2\Sigma$) is well developed in M stars, but no convincing coincidences with the strongest band heads were found when comparing the laboratory with the stellar spectra. We conclude that the bands must be absent or very faint.

TiO.—No rotational analysis of the bands of this very important molecule is available for bands falling to the violet of λ 5000; unfortunately, the attempt to obtain laboratory spectra at Mount Locke gave very unsatisfactory results. A comparison with the published wave lengths of the band heads showed that *TiO* is certainly present, although not very strong. In the final table of wave lengths (Table 6) all coincidences of stellar lines with *TiO* lines in the spectrum of β Pegasi were noted whenever other contributors were missing or doubtful, without an attempt to discuss them for lack of suitable data. Pending the publication of more laboratory data, these "identifications" must be considered very uncertain; a great number of them may be only chance coincidences.

ZrO.—We should expect this molecule to be fainter than *TiO*. The majority of the band heads seem to be faintly present, but the coincidences of individual lines with stellar ones were considered to be due to chance and were omitted from the final table.

VIII. A TABLE OF WAVE LENGTHS FOR K GIANTS IN THE SPECTRAL REGION λλ 4000–5000

The final table of wave lengths (Table 6) gives the wave lengths of all the absorption features measured in α Serpentis and α Ursae Majoris from λ 4000 to λ 5000, together with their intensity (in β Ophiuchi) and identifications.

The question about the data to be included in the column of identifications was carefully considered before they were entered in the table. Eventually it was decided to exclude only those contributors which seemed definitely improbable or whose contribution to the stellar line was certainly negligible. This was done for various reasons. In most investigations it is essential that the lines considered be due to only one well-determined contributor; it is better in these cases to eliminate a line because a secondary contributor was overestimated than to leave it in. Although the discussion of the identifications was very careful, it is, of course, fairly possible that a contributor which was considered secondary might turn out to be the main one. This is especially to be feared when molecular lines are involved.

It will be seen that, on account of this, for many lines the column of identifications contains three, four, or even more contributors. This should not cause confusion, because in almost all cases the principal contributor is in boldface; generally this contributes more than half the observed intensity and more than two-thirds of it if the contributors are only two. When more than one contributor is in boldface, it was impossible to decide which of them is predominating.

[20] *Nova acta r. soc. sci. Upsala*, Ser. IV, Vol. **8**, No. 4, 1932.

[21] *Stockholm Obs. Ann.*, Vol. **12**, No. 8, 1936.

TABLE 6

TABLE OF WAVE LENGTHS

α Ser	α UMa	Int.	Identifications	α Ser	α UMa	Int.	Identifications
3997.42			***.40 Fe*** **I** (***278***); .49 *Fe* Ip (556)	4006.15	4006.12	6	***.14 Ni*** **I** (***u***); .16 *Fe* Ip (564)
97.88			.90 *Co* I (32)	06.31	06.32	7	.31 *Fe* I (603)
3998.04			.05 *Fe* I (276)	06.63	06.60	18	.63 *Fe* I (488)—
98.53			.55 *Co* I (33)	06.78	06.77		.77 *Fe* I (320)—
98.69			.64 *Ti* I (12)	4007.00	06.99	6	.00 Sun; .99 β
98.98			.97 *Zr* II (16)	07.25	4007.26	8	***.23 Fe*** **I** (***119***); ***.28 Fe*** **I** (***277***) .20 *Ti* I (187)
3999.24			.24 *Ce* II (57)				
99.36			.36 *Ti* I (188)	07.46	07.43:	2	.44 *Nd* II (u)
99.65			.68 *Cr* I (u)	07.59	07.57	1	.59 *Ce* II (221)?
99.81			.87 β	07.73:	07.74		
4000.02		8:	.02 *Fe* I (360)	07.99	07.96	18	—.05 *Ti* I (187)
00.25		30:	.27 *Fe* I (556)	4008.17:	4008.1	1:	.17 *V* II (32)
00.45			***.47 Fe*** **I** (***426***); .45 *Dy* II .49 *Nd* II (64)	08.41	08.41	2	.41 *Sc* IIp (16)?
				08.61	08.66	3	.60 *Sc* IIp (16)?
00.62			.59 *Cr* I (295)?	08.75		0:	.77 *W* I (6)
00.80		6:		08.92	08.92	8	.93 *Ti* I (12)
00.93				4009.14	4009.14	4	.15 Sun
4001.14		15:	.18 *Mn* (M)?; .17 Sun	09.35	09.30	0:	
01.44		8:	.44 *Cr* I (268)	09.58	09.52	20w	—.54 *Fe* Ip (556)
01.69		12:	.67 *Fe* I (72)	09.70	09.71		***.71 Fe*** **I** (***72***); .65 *Ti* I (11)
01.98		2:	.91 *Mn* (M)?	09.97	09.99:	2	.98 *Ni* I (150)
4002.13		7:	.07 *Fe* II (29); .20 *Tb* II?	4010.17	4010.17	5	.18 *Fe* I (915)
02.46		11:	***.47 Ti*** **I** (***188***); .55 *Zr* I (46)	10.36	10.39	1	.41 β
02.66		7:	***.66 Fe*** **I** (***320, 655***); .60 *Tb* II	10.56	10.55	6	.59 Sun; .52 β
02.93		9:	.94 *V* II (9)	10.76	10.79	4	.77 *Fe* I (219, 320)
4003.21d		7w	.09 *Zr* (M)?; .26 *Mn* (M)?	10.93	10.93	3	.95 *Fe* I (M)?
03.54		8w	.60 *Co* I (130)?—	4011.10	4011.09	4	.09 *Co* I (2)
03.77		10:	***.76 Fe*** **I** (***728***); ***.79 Ti*** **I** (***188***) .77 *Ce* II (188)	11.42	11.42	9	.42 *Fe* I (218)—
					11.54	0:	.53 *Ti* I (10)
4004.00		5:	***.01 Nd*** **II** (***u***); .92 *Cr* I (268)	11.72	11.74	6	.71 *Fe* I (153)
04.20d?		4:		11.85	11.97	0	.89 *Fe* Ip (424)
04.42		2	.40 *Zr* (M)?	4012.01			
04.61	4004.56	8:		12.19	4012.19	5:	.16 *Fe* I (601); .25 *Nd* II (10)
04.95:	04.74:	10w	***.98 Fe*** **I** (***486, 557***); .83 *Fe* I (601)	12.41	12.42	9	***.37 Ti*** **II** (***11***); .39 *Ce* II (206) .49 *Cr* I (268)
4005.26w	4005.24w	20w	.25 *Fe* I (43)				
05.57			.55 *Tb* II	12.66r	12.72	7w	***.79 Ti*** **I** (***186***); .70 *Nd* II (u)
05.70	05.68w	9	.71 *V* II (32)	12.90		1:	
05.95	05.99:	6	.95 *Ti* I (187)	4013.07	4013.01	1	

TABLE 6—*Continued*

α Ser	α UMa	Int.	Identifications
4013.23	4013.23	3	.24 *Ti* IIp (186)
13.38	13.40	0	
13.60	13.60	8	***.64 Fe* I (*557*)**; .59 *Ti* I (187)
13.87d	13.84d	12w	***.82 Fe* I (*486*)**; ***.94 Co* I (*58*)** .80 *Fe* I (485)
4014.12			
14.26	4014.27	5	.28 *Fe* I (426, 427)
14.52	14.53	10	***.53 Fe* I (*802*)**; .49 *Sc* II (8)
14.71	14.70	1	.67 *Cr* I (268)
14.93	14.93	6	.90 *Ce* II (157)
4015.16	4015.17	3	.18 *Dy* (M)?
15.38	15.40	5	.38 *Ti* I (185)
15.60	15.60	6	.61 Sun; .60 β
15.78			
4016.00	15.90 4016.02	3w	
16.28	16.27	2:	.26 *Ti* I (186)
16.42	16.47	7	.43 *Fe* I (560)
16.57	16.60	0	.54 *Fe* I (277)
16.80	16.79	4	—.81 *Fe* IIp (428)
16.99	16.92	0	.94 *Ti* I (208)
4017.14	4017.14	11	.10 *Fe* I (279); .16 *Fe* IIp (527)
17.51	17.54	10	.47 Sun; .48 β; .56 *Ni* I (171)
17.77	17.80	6	.77 *Ti* I (185)
4018.10 18.28	4018.10 18.31	25w	.10 *Mn* I (5) .28 *Fe* I (560)
18.51	18.59:	0	.54 *Sm* II (M)?
18.64:			
18.84d?	18.84d?	4	.83 *Nd* II (19)—
4019.07	4019.09	8	.05 *Fe* I (219); .05 *Ni* I (72)
19.29	19.32	6	.29 *Co* I (16)
19.54	19.53	2	
19.80	19.81	2w	.81 β
4020.05	4020.04	6	.98 *Sm* II (16); .05 *Fe* IIp (556)
20.24	20.27	2:	.28 Sun
20.41	20.46	12	***.40 Sc* I (*7*)**; .49 *Fe* I (913)
20.90	20.91	12	***.90 Co* I (*16*)**; .87 *Nd* II (19)
4021.15	4021.18	0	
4021.34	4021.35 21.50	4	.33 *Nd* II (36)
21.61	21.63	6	.62 *Fe* I (120, 557)
21.85	21.89	10	.81 *Ti* I (185); .87 *Fe* I (278) .92 *V* I (96)
4022.05d?			.05 *Ni* I (238, 241)?
22.24	4022.24	7	—.26 *Cr* I (268)
22.46	22.46	4	.45 *Fe* I (173)
22.64 22.74	22.74	7	.66 *Cu* I (M) .74 *Fe* I (556, 654)—
22.99	4023.02	5	.00 *Nd* II (u)
4023.19	23.21	3	.23 *Sm* II (4)
23.40	23.42	8	***.39 V* II (*32*)**; .40 *Co* I (59)
23.69	23.71	9	***.69 Sc* I (*7*)**; .74 *Cr* I (268)
4024.06	4024.08d?	9w	***—.11 Fe* I (*277*)**; .99 *Zr* I (46)
24.32 24.45	24.38:	1:	.45 *Zr* II (54)?
24.58	24.54	10	.57 *Ti* I (12)
24.75	24.79	7	.74 *Fe* I (560)
24.99		1:	.92 *Zr* I (46)
4025.14	4025.11	10	.01 *Cr* I (37); .14 *Ti* II (11)
25.43	25.45	7	—.44 *Cr* I (37); .44 *Ni* I (117)?
25.63	25.61	0	
25.84	25.84	7	.83 Sun; .83 β
4026.18	4026.18	7	.17 *Cr* I (37)
26.49d?	26.50	10	***.54 Ti* I (*185*)**; .44 *Mn* I (u)
26.80	26.71 26.88	3w	
4027.08	4027.09 27.24	10	***.10 Cr* I (*37*)**; .03 *Co* I (3) .20 *Zr* I (46)
27.42	27.44	6	.43 *Ti* I (u)
27.66	27.66	6	.68 Sun; .66 β
27.96	27.99	7	.94 Sun; .94 β
4028.35	4028.35	9	***.33 Ti* II (*87*)**; .41 *Ce* II (47)
28.59	28.62	2	
28.77	28.78	5	.78 *Fe* (M)
4029.00	4029.06	1w	
29.25	29.27	1w	

TABLE 6—*Continued*

α Ser	α UMa	Int.	Identifications	α Ser	α UMa	Int.	Identifications
4029.45	4029.44	0		4036.95	4036.98	0	
	29.56			4037.14	4037.14	5	.12 Sun; .10 β
29.65	29.66	8	***.64 Fe* I (*556, 563*)**; .68 *Zr* II (41)	37.30	37.32	5	***.29 Cr* I (*36*)**; .33 *Gd* II (49)
29.88	29.90	3	.88 Sun; .87 β	37.55		0	
4030.03:	4030.08:	1	.03 *Zr* I (46)	37.70	37.68	6	.72 *Fe* I (118)
30.20	30.21	6	.19 ***Fe*** I (72)	37.92	37.89	2	.90 *Gd* II (49)
30.51	30.51	8:	***.50 Fe* I (*560*)**; ***.51 Ti* I (*185*)**; .47 *Nd* II (32)	4038.12	4038.12	4	.12 *Nd* II (31)—
				38.32	38.3	1w	.27 *Ni* Ip (150)
30.81w	30.81w	25w	.76 *Mn* I (2)	38.48	38.45	0	.43 β
4031.28	4031.31	8	***.24 Fe* I (*486*)**; .34 *Ce* II (108)	38.65	38.63	5	.62 *Fe* I (600, 728)
31.40:			.35 *Zr* II (42)?	38.79	38.79	7	.80 *Fe* (M)?
31.54	31.56	0		4039.08	4039.08	7	.10 *Cr* I (251)—
31.76	31.79	9	***.75 Ti* I (*185*)**; ***.81 Nd* II (*4*)**; .68 *La* II (40)	39.31	39.31d?	3	.30 *Cr* I (251)—
				39.58	39.56	3	.57 *V* II (32)
31.98	31.99	5	.97 *Fe* I (655)	39.75		1:	.83 *Y* I (5)
4032.25	4032.28:	1		39.92	39.93	6	.94 *Fe* I (276)
32.48	32.45	3	.46 *Fe* I (320)	4040.10	4040.10	4	.10 *Fe* (M)
32.65	32.64	6	***.64 Fe* I (*44*)**; .63 *Ti* I (297)	40.30	40.27	4	.31 *Ti* I (185)
32.89				40.50	40.46d?	0:	
4033.07	4033.07	20w	.07 *Mn* I (2)	40.65	40.63	5	.65 *Fe* I (655)
33.24	33.25	2:	.26 *Cr* I (36)	40.79	40.80	4	***.80 Nd* II (*30*)**; .76 *Ce* II (138)
33.64	33.68	7	.67 *Mn* (M)	4041.06	4041.06	3	.05 *Nd* II (β)?
33.93	33.87	5	***.88 Ti* I (*208*)**; .95 *Cr* I (36)	41.37	41.35	16	***.36 Mn* I (*5*)**; .29 *Fe* I (603, 654)
4034.07	4034.08	2	.10 *Zr* II (42)?	41.66	41.67	6	—.68 *Sm* II (22)
	34.28	1:	.23 Sun		41.80	0	.79 *Cr* I (36)
34.50	34.49	20w	.49 *Mn* I (2)	41.93	41.92	4w	.91 *Fe* I (602)
	34.58	0:		4042.07	4042.02	0	
34.89	34.87	3	.88 *Ti* I (208)	42.26	42.26	4	.25 *Cr* I (36)
4035.13	4035.10	2	.11 *Sm* II (33)	42.43	42.41:	1	
35.26	35.26	3	.25 *Fe* Ip (831)	42.63	42.60	4	***.58 Ce* II (*140*)**; .64 *V* I (96)
	35.58	1:	.54 *Co* I (173)	42.74	42.75	2	***.72 Sm* II (*4*)**; .75 *Fe* Ip (556)
35.71d?	35.72w	20w	***.73 Mn* I (*5*)**; .63 *V* II (32) .83 *Ti* I (208)	42.94	42.94	3	.90 *Sm* II (9); .91 *La* II (66)?
				4043.09			
35.99	35.96	2:	.98 *Fe* Ip (426)	43.33	4043.34	4	
4036.25	4036.16	0		43.62		0:	.57 *Zr* I (32)
36.40	36.36	6	.37 *Fe* Ip (279)	43.75	43.68	6w	***.78 Ti* I (*208*)**; .69 *Fe* Ip (122)
36.58	36.55	1		43.95	43.96	10w	.90 *Fe* I (276, 557); .98 *Fe* I p(559)
36.77	36.77	7	.78 *V* II (9)	4044.15	4044.15	8w	.14 *K* I (3)

TABLE 6—*Continued*

α Ser	α UMa	Int.	Identifications
	4044.29:		
4044.36:	44.39:	1	
	44.51:	0:	.49 *Fe* Ip (1073)
44.60:	44.64:	9	***.61 Fe*** **I** (***359***); .57 *Zr* I (46)
44.84:	44.82:		.82 *Pr* II (8)
4045.13:	4045.13:		***.14 Fe*** **I** (***425***); .13 *Mn* I (48)
45.41:	45.41:		.39 *Co* I (31)
45.91w	45.87w	60	***.82 Fe*** **I** (***43***) Rem
4046.48:	4046.42:		.46 *Fe* Ip (1075)?
46.76:			.76 *Cr* I (36)
46.97:			
4047.29	4047.30	10	***.21 K*** **I** (***3***); .32 *Fe* I (117, 853)
47.65	47.63	2	.64 *V* I (6)
47.82	47.79	7	.79 *Sc* I (7)
4048.08	4048.08	3	.08 Sun
48.36	48.35	3	
48.73	48.67	15w	.68 *Zr* II (43)
	48.78		***.76 Mn*** **I** (***5***); .78 *Cr* I (251)
4049.02	48.99	4	.00 *Mn* I (48)
49.14	4049.09	1:	
49.36	49.35	9	.34 *Fe* I (218); .40 *Ti* I (185); .43 *Gd* II (50)
49.56	49.57d	2	.57 Sun
49.78	49.78	6	***.86 Gd*** **II** (***u***); .78 *Cr* I (251)
4050.05	4050.08	3	***.02 Cr*** **I** (***36***); .08 *La* II (85)?
50.32	50.33	4	.32 *Zr* II (43)
50.52	50.51	2	***.58 Dy*** **II**; .48 *Zr* I (M)
50.68	50.66	4	.69 *Fe* (M)
50.96	4051.04	4	***.96 V*** **I** (***121***); .06 *V* II (32) Rem
4051.18	51.18	4	.14 *Nd* II (66) —
51.36	51.37	5	.35 *V* I (121)
51.72	51.69	1	.73 *Mn* (M)
51.93	51.95	11	.92 *Fe* I (700)
4052.04	4052.04	0	
	52.14		
52.28	52.29	6	.31 *Fe* I (700, 852)
52.48	52.46	8	***.47 Fe*** **I** (***563***); .47 *Mn* I (48)
52.68	52.70	7	.66 *Fe* I (524); .72 *Fe* Ip (557)
	4052.83:		
4052.95	52.94	5	.93 *Ti* I (208)
4053.27	4053.26	7	.27 *Fe* (M); .29 *Gd* II (u)
53.48	53.48	5	— ***.51 Ce*** **II** (***36***); .45 *Cr* II (19)
	53.63		
53.84	53.84v	7	***.81 Ti*** **II** (***87***); .82 *Fe* I (485)
4054.06		0	.11 *Cr* II (19)
54.19	4054.16	6w	.18 *Fe* I (557)
54.46	54.48	9w	.43 *Zr* (M)
54.56	54.61		.56 *Sc* I (6); .62 *Co* I (2)
54.83	54.80	8	***.83 Fe*** **I** (***698***); ***.88 Fe*** **I** (***698***) .84 *Pr* II (30)
4055.04	4055.01	7	***.01 Ti*** **I** (***80***); .03 *Zr* I (46); .05 *Fe* I (218)
55.23	55.18	1	.21 *Mn* I (48)
55.54	55.55	10	.54 *Mn* I (5)
55.66:		0:	
55.76:		0:	
55.85:		0:	
4056.01	55.98	4	.98 *Fe* I (914)
56.20	4056.23	4	***.21 Ti*** **II** (***11***); .27 *V* II (14)
56.40	56.47	6w	.35 Sun; .4 β
56.56			***.53 Fe*** **I** (***320***); .54 *Pr* II (26)
56.82w	56.84w	1w	.79 *Cr* I (306)?
4057.00	4057.03:	0:	.07 *V* I (121)
57.22	57.22w	6w	***.20 Co*** **I** (***3***); .19 *Cr* I (156)
57.35	57.42:	1	***.36 Fe*** **I** (***277***); .35 *Ni* I (89)
57.55	57.56	9w	***.50 Mg*** **I** (***16***); .61 *Ti* I (254)
57.90	57.86	10w	***.81 Pb*** **I** (***1***); .81 *Cr* I (251)
	57.98		.95 *Mn* I (29)
4058.21	4058.19	9	***.18 Co*** **I** (***16***); .23 *Fe* I (558); .14 *Ti* I (254)
58.45		1:	.46 *Fe* Ip (914)
58.60	58.56	6	.60 *Co* I (58)
58.78	58.76	6	***.77 Fe*** **I** (***120***); .77 *Cr* I (251)
58.93	58.97	9:	***.93 Mn*** **I** (***5***); .93 *Cb* I (1); .91 *Ca* I (40)
	4059.15	0:	

TABLE 6—*Continued*

α Ser	α UMa	Int.	Identifications
4059.37	4059.28	13w	.32 *Co* I (2)
	59.40		.39 *Mn* I (29)
59.73	59.72	7	.73 *Fe* I (767)
59.94	59.95	1	.96 *Nd* II (63)
4060.06	4060.04	2	— ***.09 Ti*** ***ip*** ***(254)***; .08 *Zr* (M)?
60.27	60.27	7	.26 *Ti* I (80)
60.50	60.52	2	.50 Sun; .56 *β*
60.62			.62 *Cr* I (156)
60.75	60.76	3	.77 *Fe* (Sun)?
60.93		0:	
4061.10	4061.10	7	— ***.08 Nd*** II ***(10)***
61.45	61.44	5	.45 Sun
61.73	61.73	8	.74 *Mn* I (29)
61.98	61.98	7	.96 *Fe* (M)
4062.23	4062.22	1	.22 *Ce* II (34)
62.45	62.46	8	.45 *Fe* I (359)
62.6	62.66	1:	.59 *Gd* II (u)?
	62.84	1:	.82 *Pr* II (26)
	4063.08	0:	
4063.27w	63.27w	8w	.29 *Fe* I (698)
	63.42:		.39 *Gd* II (u)
63.62w	63.71w	40w	***.60 Fe*** I ***(43)*** Rem
63.89w	63.98w	2w	.93 *V* I (121)
4064.18	4064.23	6w	***.20 Ti*** I ***(80)***; .16 *Zr* I (46)
64.44	64.47	7	.46 *Fe* I (44); .58 *Sm* II (24, 33)
	64.70	1:	
64.91:	64.91	0	.91 *Ce* II (M)?
4065.09	4065.09	8	***.09 Ti*** I ***(80)***; .07 *V* II (215)?
65.40	65.39	6	.40 *Fe* I (698)
65.68	65.62	3w	.60 *Ti* I (207)
	65.75		.72 *Cr* I (279)?
65.97	65.99	1	.02 *Fe* ip (695)
4066.13	4066.13	5	.12 Sun; .15 *β*
66.38	66.37	6	.36 *Co* I (30)
66.60	66.59	4	.60 *Fe* I (424)
66.77	66.78	1	.74 *Sm* II (28)
66.97	66.98	7	.98 *Fe* I (358); .93 *Cr* I (66)
4067.29	4067.30	8	***.28 Fe*** I ***(217)***; .28 *Ce* II (22)
4067.57	4067.56	2	.60 *Fe* ip (655); .49 *Fe* ip (422)
67.80	67.78	2	— .85 *Fe* ip (1103); .74 *V* I (M)
4068.00	4068.00	8	.98 *Fe* I (559); .00 *Mn* I (5)
68.34	68.32	0	.33 *Sm* II (42)
68.57	68.56	6	.54 *Co* I (58)
68.89	68.86	1:	.84 *Ce* II (82)
4069.06	4069.05	5	.08 *Fe* I (557)
69.28	69.29	3	.27 *Nd* II (20)
69.61	69.62	4	.61 Sun; .61 *β*
	69.74:		
	69.88	0	.88 *Mo* (M)
4070.01	4070.04	2w	.00 *Mo* (M)
70.27	70.29	8	.28 *Mn* I (5)
70.48		1	.45 *Fe* ip (525)
70.63:		0	
70.76	70.81	8	.77 *Fe* I (558)
	70.93:		.98 *Sm* II (M)?
4071.10	4071.09	6w	.09 *Zr* II (54)?
	71.57:		.52 *Fe* I (218); .54 *V* I (96)
71.79w	71.81w	30w	.74 *Fe* I (43)
4072.15	4072.05	7:	
72.33		2:	
72.52	72.52	6	.52 *Fe* I (698)
72.72	72.71	3	.71 *Zr* I (46)
72.92	72.92	3	.91 *Ni* I (197)
4073.15	4073.15	3	.20 *Gd* II (34); .11 *Dy* II
73.31	73.31	0	
73.52	73.50	4	.48 *Ce* II (4); .6 *AlH* (1, 0)Q?
73.77	73.77	9	***.76 Fe*** I ***(558)***; .76 *Gd* II (44)
4074.09	4074.05	4w	
	74.17		
74.35	74.36	4	— ***.36 Ti*** I ***(254)***; .37 *W* I (6)
74.80d	74.68	20w	— .70 *Fe* ip (912)?
	74.87		***.79 Fe*** I ***(524)***; .90 *Ni* I (28)
4075.11	4075.12	6	— .12 *Nd* II (62)
75.30	75.29	3	.27 *Nd* II (19)
75.46	75.48	1	
75.56			.54 *Mo* (M)?

TABLE 6—*Continued*

α Ser	α UMa	Int.	Identifications
4075.68	4075.67	4	***.71 Ce*** II (***57***); .66 *V* II (14)
75.93	75.92	8	.84 *Sm* II (51); .85 *Ce* II (206); .92 *Cr* I (66)
4076.06			.06 *Cr* I (279)?
76.17	4076.19	8	***.12 Co*** I (***16***); .23 *Fe* I (486)
76.38	76.38	1	.37 *Ti* I (9)
76.60	76.58	11	.64 *Fe* I (558)
76.84	76.83	7	.81 *Fe* I (557)
4077.11	4077.08	5	***.09 Cr*** I (***66***); .15 *Ti* I (207)
	77.24:		
77.35	77.38	7	***.38 Y*** I (***7***); .35 *La* II (41)
	77.57w		.47 *Ce* II (60)?
77.73w	77.77w	12w	.71 *Sr* II (1)
77.97w	77.96w	4w	.97 *Dy* II
4078.14	4078.11	0	
78.42d	78.33	15w	.36 *Fe* I (217)
	78.46		***.47 Ti*** I (***80***); .44 *Gd* II (15)
	78.66	0::	
78.82	78.82	4	— .9 *AlH* (1, 0)P, (1, 0)Q
4079.03	4079.02	1	.95 *SiH* (u)
79.23	79.23	11	***.24 Mn*** I (***5***); .18 *Fe* IP (700)
79.41	79.42	7	.42 *Mn* I (5)
79.71	79.69	4	.71 *Ti* I (207); .73 *Cb* I (1)
79.83	79.84	8	.85 *Fe* I (359) —
4080.22	4080.23	8	***.23 Fe*** I (***558***); .22 *Cr* I (66); .23 *Nd* II (18)
80.45	80.44	0	.44 *Hf* II (6)
80.60	80.59	3	***.60 Ru*** I (***7***); .56 *Cr* I (156)
80.88	80.90v	7	.89 *Fe* I (557)
4081.10:	4081.06	0:	.02 *Pr* II (14)
81.25	81.24	8	***.22 Zr*** I (***46***); .22 *Ce* II (4)
81.45	81.46	1	.44 *Mo* (M); .5 *AlH* (1, 0)Q?
81.58		0:	
81.73	81.72	4w	— .74 *Cr* I (66)
81.88	81.90	0	.90 *Pr* I (M)?
4082.12	4082.12	8	.12 *Fe* I (698) —
82.43	82.44	10	***.40 Sc*** I (***6***); ***.46 Ti*** I (***80***); .44 *Fe* I (906)
4082.58	4082.61	3	.59 *Co* (16)
82.94	82.95	10	.94 *Mn* I (5)
4083.22	4083.24	4	.23 *Ce* II (60)
83.58	83.56	20w	***.63 Mn*** I (***5***); .55 *Fe* I (117); .58 *Sm* II (24)
83.70	83.70		.71 *V* I (6); .78 *Fe* I (697)
4084.07d?	4084.12:	3w	
84.31	84.35	1	.39 *Mo* I (12)?
84.51	84.51	9	.50 *Fe* I (698)
84.74	84.74d?	2w	
4085.02	4085.02	8	.01 *Fe* I (358) —
85.30	85.29	9	***.31 Fe*** I (***559***); .23 *Ce* II (172); .26 *Fe* IP (276)
85.54	85.58	2	.56 *Gd* II (50)
85.75	85.75	1	.82 *Nd* II (16)
85.97	85.98	4	.98 *Fe* I (1073)
4086.12	4086.14	0	.14 *Cr* II (26)
86.33	86.33	9	.30 *Co* I (58)
86.70	86.72	7	.72 *La* II (10) —
86.97		0	.97 *SiH* (0, 0)R
4087.10	4087.11	7	.09 *Fe* I (694)
87.33	87.34	2	.30 *Ce* II (59) —
87.62	87.58	1:	.63 *Cr* II (19)?; .64 *Er* II (M)?
87.76	87.77	6	
87.99	87.98	1	.96 *AlH* (1, 0)Q (*β*)?
	4088.17	0:	
4088.29	88.28	5	.29 *Co* I (2)
88.57	88.57	6	.57 *Fe* I (906)
88.80	88.80	4	
88.99	4089.01	1	
4089.21	89.21	6	.22 *Fe* I (422)
89.52	89.44	2w	
	89.58		.63 *Cr* I (260)
4090.04	4090.06	10	.08 *Fe* I (700); .94 *Mn* (M)?
90.31	90.32	6	***.30 Cr*** I (***66***); .34 *Fe* IP (44)
90.55	90.55	9	.58 *V* I (41)
90.79	90.78	1	.75 *Fe* IP (943)?
90.96	90.96	7	***.98 Fe*** I (***695***); .99 *SiH* (0, 0)R

TABLE 6—*Continued*

a Ser	a UMa	Int.	Identifications
4091.26	4091.21	0	
91.55	91.57	8	.56 *Fe* I (357) —
91.83:			
91.98	4092.00	5	.94 *V* I (52)
4092.38w	92.36d?	14w	***.39 Co* I (*29*)**; .41 *V* I (52); .27 *Sm* II (1)
92.51		1:	.51 *Fe* I (18)
92.68	92.70w	13w	.63 *Ca* I (25); .69 *V* I (27)
92.84		2:	.85 *Co* I (59)
4093.04	4093.16	4w	.06 *Cr* I (260); .13 *Sc* I (M)
93.23			.16 *Hf* II (6)?
93.47	93.47	3	.50 *V* I (52)
93.62	93.61	3	.62 *Ni* IP (1)
93.78		0:	
93.99	93.98	2	.96 *Ce* II (160)?; .98 *β*
4094.23	4094.25:	2:	.27 *Zr* (M); .19 *Tm* I (u)?
94.40	94.41	6	.42 Sun; .43 *β*
94.63	94.63	4	.62 *β*
94.75:	94.78	0	
94.94d?	94.94d?	9	.93 *Ca* I (25)
4095.29	4095.27	7	— .25 *Mn* (M)?
95.47	95.46	6	.49 *V* I (41)
95.71	95.78	2	.71 *β*
4096.00	95.96	9	.98 *Fe* I (217)
96.19	4096.20	9	***.21 Fe* IP (*18*)**; .25 *SiH* (u)?
96.48	96.47	2w	.55 *SiH* (0, 0)R
96.66	96.66	7	— .63 *Zr* II (15); .71 *SiH* (u)
96.87		2:	***.80 SiH* (*0, 0*)*R*;** .82 *Pr* II (29)?
4097.05	4097.02	18w	— .10 *Fe* I (558); .02 *Fe* IP (700); *SiH* (*β*)?
97.22	97.26	1:	.22 *SiH* (0, 0)R
97.46	97.47	3	.45 *SiH* (0, 0)R
97.66	97.67	6	.65 *Cr* I (97)
	97.82	1:	.79 *Ru* I (9)?
97.98	97.97	4	.96 *Cr* I (97)
4098.18	4098.18	10	***.18 Fe* I (*558*)**; .18 *Cr* I (97)
	98.4	0:	.41 *Pr* II (M)?
98.55	98.55	10	***.53 Ca* I (*25*)**; .61 *Gd* II (49)
4098.84	4098.84	2:	.90 *Gd* II (49)
4099.06	98.99	7	***.08 Fe* I (*600, 651*)**; .02 *Cr* I (108); .19 *SiH* (0, 0)R
99.18	4099.18	3	.17 *Ti* I (207); .22 *SiH* (0, 0)R
99.43	99.46d?	4w	.42 *β*
99.80	99.80	10	.80 *V* I (27)
99.98	99.99	2	.99 *Fe* IP (698)
4100.19	4100.18r	11	***.17 Fe* I (*u*)**; .23 *SiH* (0, 0)R
00.31			***.33 SiH* (*0, 0*)*R*;** .24 *Nd* II (57); .35 *Fe* IP (320, 1103)
00.55	00.54	1:	
00.75w	00.73w	12	***.74 Fe* I (*18*)**; .75 *Pr* II (4)
00.92	00.93	4	***.92 Cb* I (*1*)**; .94 *SiH* (u)
4101.12	4101.10	3	.12 *SiH* (u); .16 *Cr* I (108)
01.27	01.29	9	.27 *Fe* I (698); *SiH* (*β*)
01.52	01.49	4	.49+.54 *SiH* (0, 0)R
01.69	01.70w	10w	***.74 Hδ* (*1*)**; .68 *Fe* I (120)
01.87			.88 *SiH* (u)?
4102.15	4102.15	8	***.16 V* I (*41*)**; .17 *SiH* (u)
02.38	02.38	4	.38 *V* I (7)
02.58	02.56	3w	.56 *SiH* (0, 0)R
02.71	02.69		.71 *W* I (2)?
02.94	02.94	10	***.93 Si* I (*2*)**; .94+.13 *SiH* (0, 0)R
4103.28	4103.30	6	— .31 *Dy* II; .22 *SiH* (0, 0)Q
03.59	03.58	7	.61 *Fe* IP (831); .63 *SiH* (0, 0)R
03.83	03.82	1	.82 *β*; .85 *Cr* I (180)?; .84 *Ho* I?
4104.12	4104.14	9	***.13 Fe* I (*356, 558*)**; .04 *SiH* (0, 0)R
04.41	04.42d	8	.32 *SiH* (0, 0)R —
04.74	04.74	6	.67 *SiH* (0, 0)Q; .78 *V* I (112)
04.93	04.94	8	***.97 Fe* I (*694*)**; .87 *Cr* I (108)
4105.16	4105.17	8	.17 *V* I (27)
05.38	05.38	2	.36 *Mn* I (47)
05.67	05.64	3	
05.82	05.79	3	***.82 SiH* (*0, 0*)*R*;** .84 *Tm* I (u)?
4106.03	4106.0	0:	.05 *Cr* I (180)?
06.24	06.24	7	***.18 SiH* (*0, 0*)*Q*; *.30 SiH* (*0, 0*)*R*;** .27 *Fe* I (217)
06.43	06.44	4	.44 *Fe* I (697)

TABLE 6—*Continued*

α Ser	α UMa	Int.	Identifications
4106.62	4106.63	5	.62 *SiH* (0, 0)R; .60 *Sm* II (M)?
06.95	06.94	3	.95 Sun; .96 β
4107.27	4107.23	1	.26 *SiH* (0, 0)Q
07.38			.39 *Sm* II (50)?
07.47	07.47	10	***.49 Fe*** **I** ***(354)***; ***.50 V*** **I** ***(52)***; .41 *SiH* (0, 0)R; .43 *Ce* II (138)
07.80	07.80	5	.75 *Fe* Ip (831) —
07.88			.88 *SiH* (0, 0)R
4108.11	4108.03	9w	.13 *Fe* Ip (559); .15 *SiH* (0, 0)R
	08.14		
	08.30		
08.49	08.50	9	.49 *Co* I (2); .55 *Ca* I (39)
08.70	08.74	0	
08.92	08.90	1	.91 Sun
4109.06	4109.05	7	***.05 SiH (0, 0)R; .07 Fe*** **I** ***(558)***; .07 *Nd* II (17)
09.45	09.44	5	***.41 SiH (0, 0)Q;*** .40 *Sm* II (28); .46 *Nd* II (10)
09.63:		0:	.58 *Cr* I (65); .60 *SiH* (0, 0)R
09.80	09.80	16	***.80 V*** **I** ***(27)***; .71 *Co* I (1); .81 *Fe* I (357)
09.99	4110.01	1:	***.98 Cr*** **I** ***(260)***; .05 *Zr* II (30)
4110.31	10.33	2	.38 *Ce* II (29)
10.52	10.53	9	.53 *Co* I (29)
10.86	10.87	7	***.87 Cr*** **I** ***(97)***; .90 *Mn* I (37, 47)
4111.03	4111.06	1:	.06 *Fe* Ip (689); .09 *SiH* (0, 0)Q
11.38	11.37	7	***.36 Cr*** **I** ***(97)***; .35 *Dy* II
11.76	11.75	10	***.78 V*** **I** ***(27)***; .67 *Cr* I (97)
4112.00	4112.06	5	— .02 *Os* I (5)?
12.31	12.30	7	.35 *Fe* I (695)
12.70	12.70	7	.71 *Ti* I (9)
12.95	12.95	8	.97 *Fe* I (1103)
4113.19	4113.20	4	— .24 *Mn* (M)
13.52	13.51	6	.52 *V* I (52)
13.63	13.67	1:	***.60 SiH (0, 0)R;*** .58 *Hf* II (24)
13.75			.73 *Ce* II (137)?
13.86	13.85	2	***.90 Sm*** **II** ***(16)***; .83 *Nd* II (25); .88 *Mn* I (47)
4114.08	4114.08	8	.11+.14 *SiH* (0, 0)R
14.46	14.45	10	***.45 Fe*** **I** ***(357)***; .49+.54 *SiH* (0, 0)Q
14.66	14.70	2:	
14.93	14.92	6	.96 *Fe* I (695)
4115.18	4115.18	8	.18 *V* I (27)
15.41	15.37	2:	.37 *Ce* II (22)
	15.61:		.54+68 *SiH* (0, 0)R
15.88	15.88	8	.80+.85 *SiH* (0, 0)R
4116.21	4116.15	4	.22+.28 *SiH* (0, 0)Q
	16.24		
16.49	16.50	9	.47 *V* I (27)
16.70	16.72	5	***.70 V*** **I** ***(27)***; *SiN* (0, 0)R Head
16.94	16.95	4	.97 *Fe* I (558)
	4117.12		
4117.28	17.26	0	.32 *Fe* I (484)
17.57	17.56	3:	.47 *SiH* (0, 0)R?
17.84	17.85	6	***.87 Fe*** **I** ***(700, 1103)***; .79+.91 *SiH* (0, 0)R
4118.19	4118.17	7	.14 *Ce* II (11); .18 *V* I (112)
	18.37		
18.56	18.53	9	***.55 Fe*** **I** ***(801)***; .48 *Pr* II (8); .55 *Sm* II (54)
			.64 *V* I (41)
18.70			
18.82	18.83	11	***.77 Co*** **I** ***(28)***; .90 *Fe* I (559)
4119.03	4119.00	0:	.02 *Ce* II (89); .08 *SiH* (u)?
19.27	19.1?	1:	
4119.40	4119.38v	9	***.44 Cr*** **I** ***(65)***; ***.46 V*** **I** ***(41)***; .48 *SiH* (0, 0)R Rem
19.64	19.60:	1	***.66 Fe*** **I** ***p (320)***; .64 *SiH* (u)
19.87	19.80	3	.83 *Zr* I (M)?; *SiN* (β)?
	19.91		.88 *Ce* II (83)
4120.07		0:	.04 *Ti* I (253)
20.20	4120.20	7	.18+.24 *SiH* (0, 0)R; .21 *Fe* I (423)
20.55	20.56	7	.54 *V* I (41); .61 *Cr* I (65)
20.81	20.81	3	— .83 *Ce* II (112); *SiN* (β)?
4121.07	4121.06	2:	
21.33	21.32r	10	***.32 Co*** **I** ***(28)***; .34 *SiH* (0, 0)R

TABLE 6—*Continued*

α Ser	α UMa	Int.	Identifications
4121.47:		0:	.45 *Zr* I (32)?
21.65	4121.63	2	.64 *Ti* I (u)
21.80	21.80	7	***.81 Fe* I (*356*)**; .82 *Cr* I (108)
4122.02		0	.00 *Fe* Ip (765)
22.19r	4122.19	8	***.14 Ti* I (*296*)**; .16 *Cr* I (65) —
22.51	22.51	5	.52 *Fe* I (356)
22.71d	22.65	3w	.64 *Fe* II (28)
	22.78		.76 *Mn* I (47); .72 *SiH* (0, 0)R
4123.00	4123.00	1	.02 *SiH* (0, 0)R
23.23	23.21	6	***.23 La* II (*41*)**; .19 *V* I (112); .28 *Mn* I (47)
23.49	23.47	9	***.56 Ti* I (*296*)**; ***.57 V* I (*27*)**; .39 *Cr* I (108)
23.76	23.76	9	***.75 Fe* I (*217, 422*)**; .81 *Cb* I (1)
	23.87		.87 *Ce* II (60); .96 *Sm* II (46) —
4124.10	4124.14	5	.07 *V* I (52) —
24.50	24.50	6	.50 Sun; .53 *β*
24.77	24.76	2	.73 *Lu* I (3)?
24.91	24.94	2	.91 *Y* II (14)
4125.18	4125.19	4	
25.39	25.39	3	.35 *SiH* (0, 0)R
25.64	25.64	7	.62 *Fe* I (1103)
25.88	25.89	6	.88 *Fe* I (354)
4126.17	4126.17	10	***.19 Fe* I (*695*)**; .10 *Cr* I (65)
26.54	26.54	10	.52 *Cr* I (35)
26.88	26.87	8	***.88 Fe* I (*354*)**; .92 *Cr* I (u)
4127.28	4127.31	5	***.30 Cr* I (*35*)**; .37 *Ce* II (4)
27.59	27.59	9	***.53 Ti* I (*296*)**; ***.61 Fe* I (*357*)**; .64 *Cr* I (65)
27.79	27.79	8	.81 *Fe* I (558, 727)
4128.06	4128.07	9	***.07 V* I (*27*)**; .06 *SiH* (0, 0)QR
28.32	28.30	5	.31 *Y* I (5)
28.54	28.5	0:	
28.73	28.73	3	.74 *Fe* II (27)
28.90	28.91	4	***.86 V* I (*112*)**; .93 *SiH* (0, 0)Q
4129.17	4129.17	8	***.21 Cr* I (*97*)**; .17 *Ti* I (u); .22 *Fe* I (698); .23 *Sm* II (24)
4129.46	4129.45	7	***.42 Dy* II**; .46 *Fe* Ip (695)
29.70	29.71	9	***.73 Eu* II (*1*)**; .81 *SiH* (0, 0)Q
4130.11	4130.04	11	.04 *Fe* I (44, 486) —
30.30	30.36d?	4w	.37 *Gd* II (19, 49)
30.66	30.68	5	***.65 Ba* II (*4*)**; ***.54 Co* I (*16*)**; .66 *SiH* (0, 0)Q; .71 *Ce* II (209)
4131.10	4131.09	8	***.12 SiH* (*0, 0*)*R*;** .10 *Ce* II (112)
31.32	31.34	3	.31+.37 *SiH* (0, 0)Q; .36 *Cr* I (261)
31.77	31.76	10:	— .74 *SiH* (*β*)?
4132.04w	4132.06w	18w	.06 *Fe* I (43) Rem
	32.25:		.28 *Gd* II (49)
32.53	32.54	6	— .54 *Fe* Ip (1103)
32.71	32.72	2:	.74 *SiH* (0, 0)Q
32.91	32.92	8	.90 *Fe* I (357)
	4133.15		.12 *SiH* (*β*)?
4133.34r	33.37d?	6	***.44 SiH* (*0, 0*)*Q*;** .36 *Nd* II (19)
33.65	33.64	4	.61 *Fe* (Sun)?
33.82	33.85	7	***.87 Fe* I (*698*)**; .80 *Ce* II (4)
4134.20	4134.16		***.17 SiH* (*0, 0*)*Q*;** .19 *Fe* Ip (217)
34.36d	34.41d	16w	***.34 Fe* I (*3*)**; ***.49 V* I (*27*)**; .43 *Fe* I (482, 697)
34.66	34.68	10w	.68 *Fe* I (357)
34.91	34.93	4w	.91 *SiH* (0, 0)Q
4135.03			.04 *Mn* (M)
35.30	4135.28	3	.32 *Nd* II (u) —
35.44	35.43	3	.46 Sun; .44 *β*; .44 *Ce* II (188)?
35.74	35.74	6	***.70 SiH* (*0, 0*)*Q*; *.77* *Fe* I (*1073*)**; .68 *Zr* I (50); .78 *Os* I (3)?
35.88	35.88	1:	.90 *SiN* (*β*)?
	4136.00:		
4136.11	36.12	2	.11 *V* I (M)
36.37	36.35d?	2:	.39 *V* I (26)
36.54	36.54	7	.51 *Fe* I (694); .53 *SiH* (0, 0)Q
	36.69:	0:	
	36.81:		.89 *Ti* I (221)?
4137.03	4137.00	8	***.00 Fe* I (*726*)**; .09 *Cb* I (1)
37.29	37.25		.28 *Ti* I (253) —

TABLE 6—*Continued*

α Ser	α UMa	Int.	Identifications
4137.40	4137.40	11w	***.40+.46 SiH (0, 0)Q;*** .42 *Fe* ip (1103)
37.67	37.65	4	.65 *Ce* II (2) —
37.93	37.94	5	—.97 *Fe* ip (320)
4138.07	4138.08	0:	
38.33	38.33	5	.35 *SiH* (0, 0)Q
38.44	38.46	0:	.46 *SiH* (0, 0)Q
38.74	38.75	6	
4139.05	4139.03	6	.09 *CN* (Sun)?; .05 *β*
39.23	39.25	2	.26 *V* I (M)?
39.47	39.47	7	***.45 Co* I (*94*)**; .40 *SiH* (0, 0)P; .40+.54 *SiH* (0, 0)Q
39.69:	39.62	1	.70 *Cb* I (1)
39.92	39.92	8	.93 *Fe* I (18)
4140.20	4140.21	5	.30 *Sc* I (20)—
40.44	40.44	7	.44 *Fe* I (694, 695); .54 *SiH* (0, 0)Q
40.75	40.76	7	.72 *SiH* (0, 0)Q
4141.06	4141.08	3	.06 *Mn* (M)
41.28	41.28	2	.28 *Pr* II (10)—
	41.40	0:	.35 *Fe* I (480)
41.59	41.59	3:	.54 (Sun)
41.84	41.83:	8	***.86 Fe* I (*422*)**; .80 *SiH* (0, 0)Q
4142.18	4142.18	1:	.19 *Cr* I (305)? Rem
42.28	42.33	1:	Rem .32 *Ni* I (u)
42.51	42.55	7:	Rem .48 *Ti* I (296)
42.84	42.80	5:	Rem .86 *Y* I (5)
4143.06	4143.07	4	Rem ***.05 Ti* I (*253*)**; .14 *Pr* II (4); .10 *Dy* II; *SiN* (1, 1)R Head
43.45	43.44	9	.42 *Fe* I (523)
43.85: w	43.92: w	17w	***.87 Fe* I (*43*)**; .83 *Fe* ip (354)
4144.20	4144.18	3	***.18 SiH (0, 0)Q;*** .16 *Ru* I (7)
	44.36:		.36 *SiH* (u)
44.51	44.52	3	.47 *Tb* II; .54 *SiH* (u); .55 *Nd* II (61)
44.76	44.74	6	.70 *SiH* (0, 0)Q
	44.84		.86 *SiH* (0, 0)Q
4145.03	4145.03	4	.00 *Ce* II (9); .05 *Ti* I (M)
45.23	45.21	5	.21 *Fe* I (274); .31 *SiH* (0, 0)Q
4145.49	4145.50	1	.44 (Sun); .56 (Sun)
45.74d?	45.76	3:	.68 *SiH* (0, 0)Q?; .74 *Ru* (M)?
45.88		0:	
4146.04	4146.03	9w	.07 *Fe* I (422)
46.22	46.22	2	.19 *SiH* (0, 0)Q; .20 *Cr* I (260)
46.50	46.46	0	.47 *Cr* I (108)
46.71	46.71	7	.70 *Cr* I (107); .62 *SiH* (0, 0)Q
46.98	46.99	3	.99 Sun; .98 *β*
4147.18	4147.17	4	.22 *SiH* (0, 0)Q
47.35	47.36	2	.37 *Zr* I (M)
47.67	47.65v	13w	***.67 Fe* I (*42*)**; .68 *SiH* (0, 0)Q
47.93	47.95	1	
4148.18	4148.17d?	4	.22 *SiH* (u)
48.45	48.43	5	.40 *SiH* (0, 0)Q
48.74	48.73	8w	.75 *Ni* ip (89)?
48.85	48.88		***.86 V* I (*26*)**; .91 *SiH* (0, 0)Q
4149.16	4149.19	7	.22 *Zr* II (42)
49.39	49.41	8	***.37 Fe* I (*694*)**; .40 *SiH* (0, 0)P; .44 *Ti* I (296)
49.77	49.76	8	***.76 Fe ip (3)***; .83 *Sm* II (8)
49.98:	49.95	0	.94 *Ce* II (158, 189)
4150.25	4150.27	5	***.26 Fe* I (*695*)**; .27 *SiH* (u)
50.45	50.42	3	.43 *Co* I (16)
50.60	50.53	0:	.56 *Ti* I (253)
50.71	50.71	6	***.70 CN; .78 CN;*** .72 *SiH* (u)?
50.99	4151.00	7	***.96 Ti* I (*206*)**; .97 *Zr* II (42); .03 *CN*
4151.30	51.3	1	.26 *SiH* (u)
51.43:			.49 *CN*?
51.59:			.56 *SiH* (u)?
51.75	51.7	1:	.71 *CN*
51.94	51.92:	3w	***.89 CN; .96 Fe* I (*764*)**; .97 *Ce* II (2); .98 *La* II (40); .87 *SiH* (0, 0)P
4152.18w	4152.16w	9w	***.17 Fe* I (*18*)**; .21 *Sm* II (16)
52.35		1:	***.30 CN (5, 6) Head;*** .36 *Sc* I (20)
52.56	52.58	5	.55 *CN;* .58 *Cb* I (1)
52.78	52.78	2	.78 *Cr* I (261); .77 *CN*
4153.08	4153.06	5	.07 *Cr* I (35)

TABLE 6—*Continued*

α Ser	α UMa	Int.	Identifications
4153.38	4153.40	7	.26 *CN*; .49 *CN*; .33 *V* I (26); .40 *Fe* I (M)
53.63	53.66	1	.66 *CN*; .67 *Ce* IIp (159)?
53.87	53.89	9	***.82 Cr* I (*35*)**; .90 *CN*; .91 *Fe* I (695)
4154.12	4154.14	5	***.11 Fe* I (*694*)**; .15 *CN*
54.49	54.48	8	***.50 Fe* I (*355*)**; .47 *CN*
54.80	54.82	7	.81 *Fe* I (694)
4155.03	4155.05	1	.96 *CN*; .06 *SiH* (u)
55.27	55.26	2:	.19 *CN*; .22 *Sm* II (8, 50); .30 *CN*
55.45	55.46	4	.43 *CN*
55.65	55.68	1:	.63 *SiH* (u); .66 *CN*; .72 *SiH* (0, 0)P
55.88	55.87	3	.83 *CN*
4156.06	4156.08	2:	***.08 Nd* II (*10*)**; .03 *CN*
56.27	56.27	5	***.28 CN;*** .26 *Nd* II (14)
56.49	56.47	2:	***.46 Fe* I (*693*)**; .43 *CN*; .56 *CN*
56.79	56.80w	17w	***.80 Fe* I (*354*)**; .67 *Fe* I (419); .81 *CN*
56.98:		1:	***.94 CN;*** .00 *SiH* (u); .01 *CN*
4157.20	4157.21	5	***.25 CN;*** .24 *SiH* (u)
57.48	57.45 57.59	4w	.43 *CN* .57 *CN*
57.78	57.80	9	***.79 Fe* I (*695*)** Rem
4158.08	4158.09	8	.06 *CN* (4, 5) Head
58.40	58.40	6	***.41 CN;*** .42 *Co* I (144)
58.79	58.80	8	.80 *Fe* I (695)
	4159.02	0:	
4159.19	59.19	6	.19 *CN*
59.42	59.44	1	.40 *SiH* (*β*)
59.66	59.66	5	.63 *Ti* I (206); .69 *V* I (25)
59.87	59.88	7	***.87 CN;*** .91 *SiH* (0, 0)P
4160.10	4160.09	1	.10 Sun
60.30	60.31	9	.26 *CN*
60.56	60.57	4	.56 *Fe* I (419)
60.79	60.81	6	.81 *CN*
4161.09 61.24	4161.18	11w	.08 *Fe* I (689) .20 *Zr* II (42); .28 *CN*
61.54	61.54w	15w	***.52 Ti* II (*21*)**; .49 *Fe* I (422); .64 *CN*
	4161.79		.80 ***Sr* II (3)**?
4161.96	61.99	3w	.95 *CN*; .03 *SiH* (0, 0)P
	4162.12:	0:	.05 *SiH* (*β*)?
4162.28	62.28	3	.28 *SiH* (0, 0)P; .29 *CN*
62.48	62.48	4	.47 *CN*
62.66	62.66	5	.67 *CN*
62.95	62.95	5	***.90 CN;*** .93 *Fe* Ip (476a)
	4163.28	0:	.28 *CN*
4163.41	63.44	9	.44 *CN*
63.64	63.65	8	***.62 Cr* I (*35*)**; .64 *Ti* II (105); .66 *Cb* I (1); .68 *Fe* I (274, 699)
	63.92:	1:	.90 *CN*
4164.04	4164.06	7w	***.05 CN; .13 Ti* I (*163*)**; .02 *Y* II (37)
64.26	64.26	6w	***.24 Fe* Ip (*694*); .25 *CN;*** .19 *Pr* II (8)
64.70r	64.66 64.78	10	***.64 Ni* I (*28*)**; .66 *Cb* I (1) ***.73 CN;*** .80 *Fe* I (418); .80 *SiH* (0, 0)P
4165.10	4165.10	9	***.15 CN;*** .18 *Sc* I (20); .20 *SiH* (0, 0)P
65.41	65.40	9	***.40 CN;*** .44 *CN*; .41 *SiH* (u)?
65.58	65.59	3:	.61 *Ce* II (10)
65.77	65.79	3	.78 *CN*
4166.06	4166.04	5	.99 *SiH* (1, 1)R; .00 *Ba* II (4); .08 *CN*
66.31	66.31	5	***.31 Ti* I (*163*)**; .35 *CN*; .37 *Zr* I (45)
66.73	66.66 66.89	9w	***.65 CN;*** .69 *SiH* (1, 1)R .83 *CN*
66.99		4:	.97 *CN*; .03 *CN* Rem
4167.27	4167.28	10	***.26*** + ***.27 Mg* I (*15*)**; .20 *CN*; .36 *CN*; .23 + .36 *SiH* (0, 0)P
67.62	67.57 67.75	5w	***.51 CN;*** .52 *V* I (7); .54 *SiH* (1, 1)R ***.70 CN (3, 4) Head;*** .79 *CN*
67.92	67.94	7:	***.98 CN;*** .86 *Fe* I (599); .97 *Dy* I?
4168.15d	4168.16	1:	.12 *Cb* I (1)
68.49	68.47	6	***.48 CN;*** .44 *SiH* (0, 0)P
68.62	68.62	6	.62 *Fe* I (689); .68 *CN*
	68.79:		.79 *CN*
68.94	68.94	5	.94 *Fe* I (694)
4169.09	4169.09	1	.09 *Fe* Ip (18)

TABLE 6—*Continued*

α Ser	α UMa	Int.	Identifications	α Ser	α UMa	Int.	Identifications
4169.28	4169.27	5	***.25 CN;*** .33 *Ti* I (163)	4177.36	4177.35	4:	.32 *Nd* II (10); .35 *CN;* .36 *Ti* I (163); .42 *CN*
69.48	69.46	2	.45 *CN;* .48 *Sm* II (24)	77.58	77.59	9	***.50 Fe*** I (***18***); .54 *Y* II (14); .59 *Co* I (2)
69.59	69.59	1	***.58 CN;*** .54 *SiH* (u)	77.87	77.88	4	.85 *CN*
69.79	69.79	6	***.78 Fe*** I (***693***); .84 *SiH* (0, 0)P	4178.05	4178.04	2	***.02 Sm*** II (***16, 50***); .00 *CH* (Sun); .05 *Fe* I (M)
4170.15	4170.14	7	***.12 CN; .22 CN;*** .20 *Cr* I (278)?	78.21	78.23	1	***.22 CN;*** .16+.25 *SiH* (0, 0)P
70.51	70.50 70.68	5	.50 *CN*	78.42 78.46		4	***.39 V*** II (***25***); .38 *CN;* .41 *SiH* (0, 0)P
70.96d?	70.96d?	11w	***.91 Fe*** I (***482***); ***.02 Ti*** I (***206***); .99 *CN*	78.56	78.62	3	***.60 CN;*** .52 *SiH* (0, 0)P
4171.43	4171.41	1:	.48 *Zr* (M)? Rem	78.89	78.89	7	***.94 CN;*** .86 *Fe* II (28)
71.69	71.68	7	.66 *SiH* (0, 0)P; .68 *Cr* I (261); .70 *Fe* I (941); .72 *CN*		4179.30	4:	***.25 CN; .39 CN;*** .23 *Co* I (144); .26 *Cr* I (179); .37 *SiH* (u)
71.90	71.88	3	***.90 Fe*** I (***650***); .90 *Ti* II (105)	4179.39ww	79.50	11	***.54 CN;*** .42 *V* I (25); .42 *Pr* II (4); .43 *Cr* II (26)
4172.09	4172.09	8	***.13 Fe*** I (***649***); .05 *Ga* I (1)?; *SiN* (2, 2) Head		79.63	3:	.58 *Nd* II (19); .66 *CN*
72.38 72.48	72.39 72.53	2: 1:	.43 *CN* .48 *CH* (Sun) Rem	79.82	79.83	4	***.81 Zr*** II (***99***); .80 *CN;* .86 *Ti* I (206)
72.72	72.71w	12	***.75 Fe*** I (***19***); .64 *Fe* I (689) Rem	4180.02	4180.04	4	.03 *CN*
72.97	72.97	2:	.97 *Fe* Ip (909, 1073)?; .88 *CN*?		80.21	1:	.22 *CN*
4173.10:	4173.11	0	.05 *CN;* .18 *Fe* Ip (698)	80.37v	80.37	8	***.38 CN;*** .41 *Fe* Ip (274)
73.32	73.31	7	***.32 Fe*** I (***355***); .31 *CN*		80.79	1:	.70 *CN*
73.49	73.49	7	.45 *Fe* II (27); .54 *Ti* II (21)	80.86v	80.91	8	.86 *CN* (2, 3) Head
73.70	73.69	1	***.70 CN;*** .76 *Y* II (23)	4181.17	4181.15	3	.20 *SiH* (0, 0)P
73.97	4174.00wr	12	***.93 Fe*** I (***19***); .04 *CN* .09 *Ti* I (55); .14 *Y* I (6)	81.37	81.38	3	***.34 CN;*** .40 *SiH* (1, 1)R
4174.13				81.54	81.54	3	.55 *SiH* (0, 0)P
74.36	74.38	7	.31 *CN;* .42 *Fe* I (799); .47 *Ti* I (220)	81.75	81.76	8	***.76 Fe*** I (***354***); .69+.85 *SiH* (0, 0)P
74.89	74.88	10	***.92 Fe*** I (***19***); .89 *CN;* .92 *SiH* (0, 0)P	81.96	81.98	3:	.98 Sun; .00 *β*
4175.17	4175.19	5	***.17 CN;*** .23 *Cr* I (261)	4182.32d?	4182.32w	10w	***.20 CN; .27 CN; .38 Fe*** I (***476a***); .35 *CN*
75.40	75.41	1	.36 *SiH* (0, 0)P; .45 *CN*	82.58	82.58	3	.59 *V* I (24)
75.62	75.64	7	***.64 Fe*** I (***354***); .60 *SiH* (0, 0)P .61 *Nd* II (39); .63 *CN*	82.79	82.80	5	.79 *Fe* I (694)
75.95	75.94r	7	***.89 Fe*** Ip (***694***); .94 *Cr* I (106); .98 *CN*	82.99	4183.00	3	.02 *Fe* I (697)
4176.36	4176.30	2:	***.26 CN; .40 CN;*** .32 *SiH* (u)	4183.25 83.41	83.23 83.42	4 4	***.29 Ti*** I (***220***); .19 *CN;* .31 *Zr* I (51) .44 *V* II (37)
76.57	76.56	8	***.57 Fe*** I (***695***); ***.49 CN;*** .57 *Fe* Ip (689)	83.63	83.64	4	***.62 CN;*** .67 *SiH* (u)
76.92 4177.06	76.89 4177.05	9w	.96 *CN* ***.12 CN;*** .07 *Fe* Ip (690); .11 *SiH* (u)	83.81 4184.01	83.77 4184.02	0: 7	.76 *Sm* II (4) .08 *CN*

TABLE 6—*Continued*

α Ser	α UMa	Int.	Identifications
4184.29	4184.30	6	***.25 Gd*** II (***15***); ***.33 Ti*** II (***21***); .22 *Fe* I (274); .27 *SiH* (0, 0)P
84.49	84.46	1:	.48 *Ni* I (89)
84.6	84.7	0:	.63 *SiH* (0, 0)P
84.92	84.93	10	***.90 Fe*** I (***355***); ***.92 CN; .98 CN;*** .90 *Cr* I (155)
4185.36	4185.36	3	.34 *Cr* I (106)—
	85.55:	0:	
85.70	85.73	6	.73 *CN*
4186.12	4186.11	5	***.12 Ti*** I (***129***); .15 *SiH* (1, 1)Q
86.33	86.35	4	***.31 CN;*** .36 *Cr* I (249); .37 *SiH* (u)
86.58	86.61	7	***.53 CN;*** .60 *Ce* II (1) .81 *Dy* I?
86.86:			
4187.03	4187.04	10	.01 *CN*; .04 *Fe* I (152)
87.30	87.31d	5	***.29 CN;*** .25 *Co* I (93); .31 *La* I (5); .32 *Ce* II (86)
87.60	87.62	7:	***.62 CN;*** .56 *Zr* I (45); .59 *Fe* I (694)
87.81	87.83	9	.80 *Fe* I (152)
4188.03	4188.07	4:	***.02 CN;*** .12 *Sm* II (50)
88.36	88.36	4	***.40 CN;*** .32 *Mo* (M)
88.74	88.74	7	***.69 Ti*** I (***220***); .78 *SiH* (1, 1)Q
88.95	88.94	6	***.91 CN;*** .97 *SiH* (u)?
4189.10	4189.12	2:	.11 Sun; .08 *β*
89.54	89.54	8	.49 *CN*; .50 *Co* I (2); .52 *Pr* II (8); .56 *Fe* I (940); .60 *CN*
89.86	89.84	5	.84 *V* I (24)
	89.97	0:	.96 *Cr* I (106)
4190.15	4190.17	7	***.13 CN; .16 Cr*** I (***84***); .24 *SiH* (1, 1)Q
90.40	90.42	0	.40 *V* II (25)
90.72	90.73	10	***.71 Co*** I (***1***); .70 *CN*; .66 *Cr* I (35)
90.87	90.9	0:	.85 *CN*; .89 *V* II (37)
4191.11r	4191.09r	1	***.07 Gd*** II (***34***); .27 *Cr* I (35)
91.43	91.42	14	***.44 Fe*** I (***152***); .27 *Cr* I (35); .31 *CN*; .36 *CN*
91.70	91.71	8	***.68 Fe*** I (***355***); .75 *Cr* I (35)
91.92	91.86	2:	.86 *CN*
4192.08	4192.06	3:	***.05 CN;*** .10 *Cr* I (273)
4192.43	4192.40	4	.39 *CN*
92.54	92.56	4	***.55 CN;*** .56+.57 *CH* (0, 0)R
92.93	92.93	5	***.90 CN;*** .86 *Co* I (94)
4193.17	4193.15	1	.21 *CN*
93.39	93.38	4	***.38 CN;*** .46 *SiH* (1, 1)Q
93.68	93.70	5	***.71 CN;*** .66 *Cr* I (248)
93.92	93.85	5	***.83 CN;*** .87 *Ce* II (85); .89 *Cr* I (248)
4194.09	4194.06	0:	.08 *SiH* (u)
94.26	94.28	5	.25 *CN*
94.48	94.47	2	***.45 CN;*** .50 *Fe* Ip (274)
94.68	94.70	4	***.65 CN;*** .63 *SiH* (u)? Rem
94.96	94.93	6w	***.88 CN;*** .95 *Cr* I (248) Rem
	4195.04		.01 *CN*
4195.34	95.34	7	.34 *Fe* I (693); .34 *CN*
95.62	95.63	7	.62 *Fe* I (478); .65 *CN*
95.95	95.95	6	.94 *CN*
4196.21	4196.21	6	.17 *CN*; .22 *Fe* I (693)
96.43	96.37	3:	***.39 CN;*** .34 *Ce* II (123)
96.64d	96.62	9w	***.53 Fe*** I (***418***); ***.58 CN; .74 CN;*** .55 *La* II (41)
96.91		0:	.87 *CN*
4197.08	4197.05	10	.06 *CN* (1, 2) Head; .10 *Fe* Ip (18)
97.32	97.32	1:	.23 *Cr* I (249); .38 *Fe* Ip (976)
97.67	97.67	6	***.65 CN;*** .62 *SiH* (u)?; .68 *Gd* II (u)?
4198.09	4198.05	7:	.08 *CN*
98.32w	98.31w	10w	***.31 Fe*** I (***152***); .27 *Fe* I (693)
98.64	98.66	7	***.61 V*** I (***24***); ***.64 Fe*** I (***693***); .63 *CH* (0, 0)R; .69 *CN*; .72 *Ce* II (3)
	98.97:	0:	.88 *Ru* I (M)?
4199.11	4199.11	9	.09 *CN*; .10 *Fe* I (522)
99.35	99.36	2:	.37 *Fe* Ip (416)
99.70	99.67	2:	.69 *CN*
99.98	99.98	10	.97 *Fe* I (3)
4200.14		1:	.09 *CN*; .10 *Cr* I (u)
00.49	4200.46	3	.46 *Ni* I (89)
00.73	00.74	7	***.75 Ti*** I (***220***); .67 *CN*; .67 *CH* (0, 0)R; .78 *Fe* Ip (44)
00.95	00.96	5	***.93 Fe*** I (***689***); .89 *V* I (6); .05 *CN*

TABLE 6—*Continued*

α Ser	α UMa	Int.	Identifications	α Ser	α UMa	Int.	Identifications
4201.26:	4201.27	0		4210.36	4210.36	10	***.35 Fe* I (*152*)**; .35 *Sm* II (8)
01.5	01.50	0	.45 *Zr* I (45)	10.67	10.67	4	.66 *CN*
01.70	01.71	4w	***.73 Fe* I (*799*)**; .72 *Ni* I (238); .63 *CN*?	10.92	10.92	5	.86 *CN*; .98 *CH* (0, 0)R
				4211.22			.21 *CN*
4202.05w	4202.05w	13w	***.03 Fe* I (*42*)**; .99 *CN*	11.32	4211.29	9	.29 *Nd* II (57); .35 *Cr* I (133); .39 *CN*
02.35	02.35	3:	.35 *V* II (25)				
02.54	02.57	3	.54 *CN*	11.75	11.84dr	10w	***.74 CN;*** .72 *Dy* I; .73 *Ti* I (279)
02.77	02.77	3	.76 *Fe* I (476a, 521)	11.89			.88 *Zr* II (15); .90 *CN*
02.92	02.96	2	.89 *CN*; .94 *Ce* II (186)	4212.05:		1	.00 *Gd* II (15); .06 *Fe* Ip (697)
4203.12	4203.14	2	.05 *Sm* II (42)?	12.25	4212.23	5	.24 *CN*
03.53	03.52	10	***.46 Ti* I (*220*)**; ***.59 Cr* I (*35*)**; .43 *CN*; .57 *Fe* I (19)	12.39	12.39	1	.39 *CN*
				12.68	12.66	6	***.70 CN;*** .58+.65 *CH* (0, 0)R
03.78	03.80:	0	.76 *CN*	12.88	12.92:	0	.85 *CN*
03.98	03.98	7	***.99 Fe* I (*355*)**; .95 *Fe* I (850); .03 *La* II (53)	4213.17	4213.15	7	***.14 CN; .26 CN;*** .18 *Cr* I (155)
				13.61v	13.61	9	***.54 CN; .66 CN;*** .65 *Fe* I (355)
4204.27	4204.24	6	***.29 CN;*** .19 *Cr* I (35); .20 *V* II (25)	13.93	13.94	7	***.92 CN; .02 CN;*** .86 *Zr* I (45)
04.50	04.44	1	.47 *Cr* I (272)—	4214.29	4214.29	6	.27 *CN*; .35 *CN*
04.71	04.70	5	***.76 CH (0, 0)R;*** .60 *CN*; .69 *V* II (1)	14.60	14.58	7	.61 *CN*; .66 *CN*
4205.06	4205.02	9	***.05 Eu* II (*1*)**; .08 *V* II (37); .12 *CN*	14.87	14.87	5	.88 *CN*; .93 *CN*
05.38	05.35	2	.42 *CN*	4215.12	4215.09	6	.07 *CN*; .16 *CN*
05.55	05.55	4	***.55 Fe* I (*689*)**; .60 *Nd* II (19)		15.33		.31 *CN*; .39 *CN*
05.94	05.90	4	***.91 CN;*** .91 *Zr* II (133)?	15.50w	15.52	18w	***.52 Sr* II (*1*)**; .43 *Fe* I (274, 419); .53 *CN*
	4206.14		.13 *Sm* II (38)?				
4206.25	06.27	3	.20 *CN*	15.93	15.93	8:	.97 *CN* (0, 1) Head; .98 *Fe* I (273)
06.70	06.69	11	***.70 Fe* (*3*)**; .61+.62 *CH* (0, 0)R; .68 *CN*; .74 *Pr* II (8)	4216.22	4216.20	13	***.19 Fe* I (*3*)**; .36 *Cr* I (132)
				16.60	16.58	4	.60 Sun
06.94		0	.95 *CN*	16.84:	16.79:	0	.84 *Mo* (M)?
4207.14	4207.13	6	.13 *Fe* I (352)	4217.03	4217.01	3	
07.43	07.42	6	***.43 CN;*** .35 *Cr* II (26); .51 *Cr* I (133)	17.22	17.22	4	.20 *Gd* II (49); .24 *CH* (0, 0)R
07.81	07.81	4	.82 Sun; .90; .81 *Pr* II (M)?	17.57	17.56	8	***.55 Fe* I (*693*)**; .63 *Cr* I (132)
4208.17	4208.19	5	.12 *CN*	4218.01	4218.01		
08.36	08.34	3	—.36 *Cr* I (249)	18.23	18.22	4	.21*B*; .26 *Sc* I (M)?
08.60	08.59	6	.61 *Fe* I (689, 696)	18.38	18.37	2	.40 Sun
08.82	08.81	4	.81 *CN*	18.70	18.71	5	***.72 CH (0, 0)R;*** .71 *V* I (24)
08.99	08.99	4	.99 *Zr* II (41)	18.94:	18.95	0:	
4209.43	4209.43	6	***.37 Cr* I (*248*)**; .46 *CN*	4219.21	4219.19	2:	.20 Sun; .20 *Fe* I (*B*)
09.83	09.81	8	***.86 V* I (*24*)**; .76 *Cr* I (155)	19.38	19.38	11	.36 *Fe* I (800); .41 *Fe* Ip (419)—
4210.09	4210.06	4	.08 *CN*	19.76	19.75	1	.74 *Fe* Ip (832)?

TABLE 6—*Continued*

α Ser	α UMa	Int.	Identifications	α Ser	α UMa	Int.	Identifications
4220.05	4220.05	5	—.05 *V* II (25)	4229.93	4229.92	2:	***.91 CH (0, 0)R;*** .96 *Co* I (1)
20.34	20.32	7	***.35 Fe* I (*482*)**; .26 *Nd* II (32)	4230.24	4230.24	4	—.29 *Cr* I (106)?
20.63	20.65	3	.66 *Sm* II (15.50)	30.52	30.53	6	.48 *Cr* I (132); .58 *Fe* I (478)
20.82	20.82	1	.86 *SiH* (β)	4231.01	4231.02	6	***.01 CH (0, 0)R; .04 Ni* I (*136*)**; .95 *La* II (83)
4221.22	4221.16d?	4	.18 *SiH* (β)				
21.52	21.51	6	.57 *Cr* I (155, 248)—	31.37	31.4	1	
21.68:	21.69	2:	.70 *Ni* I (86)	31.63	31.65	5	.64 *Zr* II (99)—
21.9	21.9	0		31.96	31.97	5	.96 Sun; .99
4222.22	4222.22	12	.22 *Fe* I (152)	4232.21		2	.22 *Cr* I (294)?
22.64	22.63	6	***.60 Ce* II (*36*)**; .73 *Cr* I (132)	32.42	4232.40	6	.38 *Nd* II (8); .46 *V* I (111); .43 *Hf* II (72)?
4223.01	22.98	7	—.98 *Pr* II (4)				
23.25	4223.25	4	.24 Sun; .23 β	32.74	32.73	8	.73 *Fe* I (3)
23.52	23.51	6	***.48+.57 CH (0, 0)R;*** .47 *Cr* I (132)	32.91	32.93	2	***.87 Cr* I (*132*)**; .93 *CH* (Sun); .95 *V* I (111)
23.73	23.73	3	.73 *Fe* Ip (417); .73 *SiH* (β)				
23.95	23.93	0	.01 β	4233.17	4233.17	7	.17 *Fe* II (27)
4224.18	4224.19	10	.18 *Fe* I (689)	33.60	33.61v	11	.61 *Fe* I (152)
24.52	24.50	9	***.51 Fe* I (*689*)**; .51 *V* II (25); .51 *Cr* I (155)	4234.01	4234.00	9	.00 *V* I (6, 111); .00 *Co* I (1)
				34.24	34.22	1	
24.84	24.85	7	.85+.87 *CH* (0, 0)R	34.55	34.55	6	***.52 V* I (*6*)**; .52 *Cr* I (178); .57 *Sm* II (42)
4225.27	4225.2	4:	***.23 V* II (*37*)**; .33 *Pr* II (8); .33 *Sm* II (22)		34.75		.73 *Ce* II (170)?
25.43	25.4	15:	.46 *Fe* I (693)	34.90:	34.88	0	
25.72	25.7	6:	***.79 Fe* Ip (*118*)**; .71 *Fe* Ip (1102)?	4235.14	4235.15	6	.14 *Mn* I (23)
25.98	4226.0	10:	.96 *Fe* I (521)	35.28	35.28	6	.29 *Mn* I (23)
4226.31	26.4		.43 *Fe* I (352)	35.70	35.70	4:	***.73 Y* II (*5*)**; .65 *Fe* Ip (215); .76 *V* I (111)
26.65			.57 *Ge* I (4)?				
26.95 ww	26.91 w	100w	.73 *Ca* I (2)	35.94	35.93	20w	***.94 Fe* I (*152*)**; .94 *V* I (5) Rem
4227.12:			.14 *Gd* II (43)	4236.27	4236.27	3:	.25 *CH* (0, 0)R
27.43	4227.4		.43 *Fe* I (693)	36.57	36.55	1	
27.71	27.7		***.75 Ce* II (*8*)**; ***.76 Zr* I (*45*)**; .65 *Ti* I (278); .72 *Nd* II (19)	36.78	36.79	4	***.76 Fe* I (*906*)**; .74 *Sm* II (53)
				4237.13	4237.12	11	***.16 Fe* I (*u*)**; .08 *Fe* I (19); .16+ .23 *CH* (0, 0)R
27.95	4228.0	7:	.95 Sun Rem				
4228.26	28.26	5w			37.51:	3	
28.71	28.72	5	—.71 *Fe* Ip (690)	37.70	37.69	5	***.71 Cr* I (*132*)**; .66 *Sm* II (8); .67 *Fe* Ip (418); .79 *Ti* I (252)
4229.04	4229.02	1					
	29.18:	0:		4238.00	4238.01	7	.03 *Fe* I (689, 696)
29.47	29.48	9	.52 *Fe* I (416, 649)—	38.37	38.36	5	.38 *La* II (41)—
29.77	29.77	11	***.76 Fe* I (*41*)**; ***.78 CH (0, 0)R;*** .70 *Sm* II (4)	38.64	38.61	0	.61 *Fe* Ip (849)
				38.82	38.82r	10	***.82 Fe* I (*693*)**; .78 *Gd* II (u)

TABLE 6—*Continued*

α Ser	α UMa	Int.	Identifications
4238.96		2:	.96 *Cr* I (131)
4239.34	4239.35	6	.31 *Zr* I (45)—
39.82	39.82w	15	***.72 Mn* I (*23*)**; ***.85 Fe* I (*18, 273*)**; .74 *Fe* I (416); .91 *Ce* II (2)
	4240.19	0	.20 Sun
4240.41	40.40	8	***.37 Fe* I (*764*)**; ***.46 Ca* I (*38*)**; .35 *Zr* I (45)
40.72	40.72	6	.70 *Cr* I (105, 178)—
4241.14	4241.13	6	***.11 Fe* I (*351*)**; ***.20 Zr* I (*45*)**; *AlH* (0, 0)R Head Rem
41.52	41.49	2	.57 *AlH* (0, 0)R
41.69	41.68	3	.64 *AlH* (0, 0)R; .68 *Zr* I (45)
41.88	41.95	1	
4242.11	4242.13	3	.17 *AlH* (0, 0)R; .15 *Tm* II (5)?
42.38	42.39	6	***.44 CH (0, 0)R;*** .38 *Cr* II (31); .44 *AlH* (0, 0)R
42.68	42.67	9	***.61 CH (0, 0)R;*** .59 *Fe* I (273); .73 *Fe* I (649); .82 *Cr* I (131)?
	4243.00:	0	.99 *AlH* (0, 0)R
4243.19	43.16	3:	.21 Sun
43.37	43.36	9	***.33+.45 CH (0, 0)R;*** .37 *Fe* I (906)
43.55	43.56	4:	.65 *AlH* (0, 0)R
43.81	43.82	4	.79 *Fe* I (994)—
43.99:	43.99:	0	.98 *AlH* (0, 0)R
4244.30	4244.29	3w	
44.73	44.72	1w	.70 *Sm* II (27)
	4245.01	0:	.15 *AlH* (0, 0)R
4245.29	45.30	9	.26 *Fe* I (352)
45.58	45.54	1	.51 *Ti* I (M)
	45.82		
4246.04	4246.04	7	***.09 Fe* I (*906*)**; .02 *Fe* Ip (649)
46.46	46.41	0	.48 *AlH* (0, 0)R; .41 *Cr* II (31)?
46.82	46.85	10	.83 *Sc* II (7)
	4247.11	0	
4247.39	47.40	11	***.43 Fe* I (*693*)**; .37 *Nd* II (8); .48 *AlH* (0, 0)R
47.72	47.70	2	.73 Sun; .66 *Pr* II (M)?
	47.9		.96 *AlH* (0, 0)R
4248.00	4248.05	1	.06 Sun
4248.32d	4248.27	12w	.23 *Fe* I (482)
	48.42		***.40 Fe* Ip (*19*)**; .34 *Cr* I (131)
48.71	48.71	4	***.68 Ce* II (*1*)**; .73 *Cr* I (105); .73 *CH* (0, 0)R
48.93	48.95	3	.94 *CH* (0, 0)R
4249.12	4249.11	2	.11 *Ti* I (252)
49.31		0	.32 *Fe* Ip (117)?
49.57	49.57	8	***.49+.64 CH (0, 0)R;*** .57 *AlH* (0, 0)R
4250.14	4250.12	14	.12 *Fe* I (152)
50.48	50.41	1:	.50 β; .3 *AlH* (0, 0)R?
	50.61	1:	
50.80	50.80	20	.79 *Fe* I (42)
4251.34	4251.31	2w	—.29 *AlH* (0, 0)R
51.65	51.68	6	***.63 Gd* II (*15*)**; .62 *Ti* I (162); .77 *Ti* I (254)
4252.06	4252.05	2:	.11 *Ni* I (136)
52.30	52.30	9	***.30 Co* I (*1*)**; .24 *Cr* I (131)
52.73d?	52.72	6	.65 *CH* (β)?; .76 *V* (β)?; .76 Sun
4253.00	4253.00	2	.97 *Cb* II (M)?
53.29	53.30d?	3	.15 *AlH* (0, 0)R; .36 *Ce* II (77); .37 *Gd* II (46)
53.51	53.54	4	***.52 Fe* Ip (*690*)**; .61 *Gd* II (u)
53.74	53.73	1	.72 *Sm* II (M)?
53.88	53.91	6	—.93 *Fe* Ip (905); .9 *AlH* (0, 0)R
4254.35	4254.34	20w	.35 *Cr* I (1)
54.95	54.96	7	***.94 Fe* I (*419, 477*)**; .99 *CH* (0, 0)R
4255.26	4255.25	4	.25 *CH* (0, 0)R
55.54	55.54	6	***.50 Cr* I (*105*)**; .50 *Fe* I (416); .63 *CH* (0, 0)R
55.84	55.84	5	***.82 CH (0, 0)R;*** .78 *Ce* II (81)
4256.04	4256.05	2:	.02 *Ti* I (252)
56.22	56.30v	9w	.21 *Fe* Ip (690); .39 *Sm* II (37)
56.64	56.60	2	.62 *Cr* I (131)
56.81	56.81	2	.79 *Fe* I (1102)?; .81 Sun; .83 β
4257.07	4257.10	1	.12 *Ce* II (123)
57.32	57.34	2	.37 *Cr* I (131)
57.64	57.65	5	.66 *Mn* I (23)
4258.09	4258.05	2:	***.05 Zr* II (*15*)**; .16 *Fe* II (28)

TABLE 6—*Continued*

α Ser	α UMa	Int.	Identifications
4258.30	4258.30	9	.32 *Fe* I (3)
58.61	58.61	7	***.62 Fe* I (*351*)**; .52 *Ti* I (252)
4259.03d	4259.02	1	***.96 Fe* I (*419*)**; .15 *Cr* I (131)
59.31	59.31	4	.31 *V* I (6) Rem
59.76	59.74	2	***.70 AlH (0, 0)Q;*** .75 *Ce* II (176)
4260.05	4260.06	11	.99 *Fe* I (689); .14 *Fe* I (476a)
60.49	60.47	15	.48 *Fe* I (152)
60.76	60.75	8	***.74 Ti* I (*251*)**; .73 *Fe* Ip (351); .75 *V* II (18); .85 *Os* I (1)
4261.28	4261.28	6	***.23 CH (0, 0)R;*** .35 *Cr* I (96)
61.59r	61.55	6	***.53 CH (0, 0)R; .61 Ti* I (*252*)**; .62 *Cr* I (u)
	61.75	1	***.75 CH (0, 0)R;*** .64 *AlH* (0, 0)Q
61.97	4262.02	4	***.99 CH (0, 0)R;*** .92 *Cr* II (31)
4262.12		3	***.09 Gd* II (*44*);** .16 *Cr* I (84, 178)
62.36	62.33	3	***.43 AlH (0, 0)Q;*** .36 *Cr* I (154)
	62.54		.58 Sun
62.67	62.67	4	.68 *Sm* II (37)
4263.15	4263.15	6	.13 *Ti* I (162); .14 *Cr* I (247)
63.63	63.59	2	.59 *La* II (84)?
63.95	63.94	2	.98 Sun
4264.23	4264.23	6	.21 *Fe* I (692)
64.48	64.47d	3	—.44 *AlH* (0, 0)Q
64.74	64.73	5	.74 *Fe* I (993)
	64.96:	0:	.91 *Zr* II (98)?
4265.24	4265.25	5	.26 *Fe* I (993, 994); .27 *Ti* I (252)
	65.53	0	.54 Sun
65.68	65.71	2	.68 *AlH* (0, 0)Q; .72 *Ti* I (162)
65.91	65.91	4	.92 *Mn* I (23)
4266.20	4266.21	2	.23 *Ti* I (252)
66.45:	66.41	0:	.44 *Cr* I (199)
66.72	66.71	3	.72 *Nd* II (58)—
66.96	66.96	6	***.97 Fe* I (*273*)**; .09 *AlH* (0, 0)Q
4267.36	4267.36	4	.38 *CH* (0, 0)R
67.81	67.80	7	***.76+.78 CH (0, 0)R;*** .83 *Fe* I (482)
4268.06	4268.06	5	.01 *Zr* I (45); .03 *Co* I (1)
68.38	68.30	1	.45 *Co* I (127)?
	68.41		
4268.69	4268.71	8	***.74 Fe* I (*649*)**; .64 *V* I (88); .73 *Gd* II (68); .70 *AlH* (0, 0)Q
68.99:	68.93	1	.93 *Ti* I (252)
4269.26	4269.26	4	.28 *Cr* II (31); .14 *AlH* (0, 0)P?
69.52	69.51	4	—.50 *La* II (76)?
69.71d	69.80d	8w	—.87 *Fe* Ip (690); .95 *Cr* I (154)
4270.18	4270.17	4	.14 *Ti* I (251)
70.35			***.31 Fe* Ip (*215*)**; .43 *Co* I (29)?
70.60	70.62	1w	.52 *AlH* (0, 0)Q; .64 *V* II (23)
4271.14	4271.15	10	***.16 Fe* I (*152*)**; .06 *Cr* I (154)
	71.54:	2:	.55 *V* I (88)
71.80w	71.77w	18w	.76 *Fe* I (42)
4272.02:	4272.03	1:	.95 *Fe* Ip (171)?
72.22:		0:	.27 *Pr* II (15)
72.46	72.47	7	.44 *Ti* I (44)
72.87	72.84	6	—.91 *Cr* I (96); .79 *Nd* II (11)?
	4273.13:		.10 β
4273.37r	73.39d	8w	.31 *Ti* I (251); .46 *CH* (0, 0)R
73.87	73.86	9	***.78+.92 CH (0, 0)R;*** .87 *Fe* I (478)
4274.19	4274.18	3	.18 *CH* (0, 0)R
74.39	74.39	2	.41 *Ti* I (252)
74.78	74.78w	20w	.80 *Cr* I (1)
4275.36d?	4275.32d?	2w	.26 *CH* (Sun); .27 β; .39 Sun
75.70	75.66	5	***.72 Fe* I (*215*)**; .64 *La* II (40)
4276.02	4276.02	3	.00 *Cr* (Sun); .07 β
76.24		1	.28 Sun
76.43	76.44	3	.44 *Ti* I (148)
76.70	76.69	7	***.68 Fe* I (*976*)**; .66 *Ti* I (252)
76.98	76.98	4	.96 *V* I (88)—
4277.24		1:	.24 *CH* (Sun); .25 β
77.40	4277.37	4	.37 *Zr* II (40)—
77.61	77.62	2:	***.68 Fe* I (*172*)**; .52 *AlH* (0, 0)P (0, 0)Q; .54 *CH* (Sun)
	77.92	0	
4278.21	4278.21	7	***.23 Ti* I (*291*)**; .23 *Fe* I (691)
78.48	78.48	0	.45 β; .54 *Tb* II?
	78.63	0:	.68 *Mn* (M)
78.80	78.83	5	—.83 *Ti* I (252)

TABLE 6—*Continued*

α Ser	α UMa	Int.	Identifications	α Ser	α UMa	Int.	Identifications
4279.06	4279.05	3	—.02 *Mo* II (3)?	4287.92	4287.93	8	***.89 Ti* II (*20*)**; .00 *Ni* I (178)—
79.48	79.48	4	.48 *Fe* I (993); .48 *CH* (0, 0)R	4288.16	4288.15	4	.15 *Fe* I (273); .16 *Ti* I (43, 79)
79.71	79.70	4	***.71 CH* (*0, 0*)*R*;** .68 *Sm* II (27)	88.40	88.40	0	.38 *Cr* (M)?
79.88	79.90	6	***.86 Fe* I (*351*)**; .93 *Sc* II (15); .02 *CH* (0, 0)R	88.6		0:	
				88.71	88.71	3	***.73 CH* (*0, 0*)*Q*; .78 *V* II (*17*)**; .78 *Ti* IP (45)
4280.20	4280.19	2:	***.21 CH* (*0, 0*)*R*;** .27 *La* I (5)	4289.03	4289.02	8	***.07 Ti* I (*44*)**; .02 *CH* (0, 0)Q
80.48	80.49	10	***.53 Fe* I (*598*)**; .40 *Cr* I (247); .49 *Gd* II (15)	89.37	89.37	8	.36 *Ca* I (5)
80.82	80.80	2	.79 *Sm* II (46)	89.74	89.77	16w	.72 *Cr* I (1)
4281.08	4281.07	7	.10 *Mn* I (23)	4290.28r	4290.26d?	7	.22 *Ti* II (41); .38 *Fe* I (416)
81.38	81.38	5	.37 *Ti* I (44)		90.62	3	.54 *AlH* (0, 0)P?
81.63	81.60	2	.60 *Fe* IP (171)—	90.93	90.91	8	***.93 Ti* I (*44*)**; .87 *Fe* I (351); .95 *CH* (0, 0)Q
81.98	4282.00	4	.97 *CH* (Sun)				
	82.22	0:	.20 *Zr* I (45)	4291.17	4291.17	4	***.12*+*.22 CH* (*0, 0*)*R*;** .05 *CH* (0, 0)Q; .21 *Ti* I (45, 147)
4282.41	82.41	9	***.41 Fe* I (*71*)**; .44 *Nd* II (u)				
82.69	82.71	7	.70 *Ti* I (162)	91.48	91.47	8	***.47 Fe* I (*3, 41*)**; .44 *Fe* IP (273)
4283.01	4283.01	9	.01 *Ca* I (5)	91.82	91.79	2	.82 *V* I (120); .88 *Ti* I (251)?
83.41	83.40	2	—.40 *Fe* IP (215)	4292.12	4292.09	7	***.04*+*.12 CH* (*0, 0*)*R*;** .13 *Fe* IP (70); .18 *Sm* II (32)
83.88	83.86	2	***.87 Fe* IP (*19*)**; .78 *AlH* (0, 0)P (0, 0)Q				
				92.28	92.29	3:	.29 *Fe* I (70)
4284.08	4284.10	4	.06 *V* I (88); .08 *Mn* I (23); .07 *CH* (Sun)	92.65	92.70	1	.68 *Ti* I (79); .75 *Gd* II (128)
				4293.10	4293.09	5	***.07 CH* (*0, 0*)*Q*; .11 CH* (*0, 0*)*Q*;** .14 *Zr* II (110)
84.25		0	.23 *CH* (0, 0)Q	93.55	93.54	2	.56 *Cr* I (96)
84.43	84.45	2	***.42 Fe* I (*417*)**; .52 *Nd* II (10)	93.81	93.81	3	.80 Sun; .80 *β*
84.71	84.72	3	***.68 Ni* I (*86*)**; .72 *Cr* I (96)	4294.12	4294.12	13	***.13 Fe* I (*41*)**; .10 *Ti* II (20)
84.9			.84 *CH*? (Sun)	94.59	94.60	1	.62 *W* I (6)
84.99	84.99	5	.99 *Ti* I (148)	94.79	94.79	4	.77 *Sc* II (15); .78 *Zr* I (45)
4285.44	4285.44	7	***.44 Fe* I (*597*)**; .37 *CH* (0, 0)R; .37 *Ce* II (11); .50 *Sm* II (27); .53 *CH* (0, 0)R	4295.07	4295.03	3	***.03 CH* (*0, 0*)*Q*; .05 CH* (*0, 0*)*Q*;** .94 *Fe* I (598)
85.81	85.79	5	.78 *Co* I (1)	95.21	95.20	2	.20+.22 *CH* (0, 0)Q
4286.02	4286.02	7	***.01 Ti* I (*44*)**; .03 *CH* (0, 0)R	95.44	95.46	0	
86.18	86.18	1:	.13 *V* II (23); .21 *CH* (0, 0)R	95.79	95.78	6	***.75 Ti* I (*44*)**; .76 *Cr* I (64)
86.49	86.49	6	***.44 Fe* I (*414*)**; .48 *CH* (0, 0)Q	4296.12	4296.09	3	***.11 V* I (*120*)**; .05 *La* II (53); .08 *Gd* II (46)
86.95	86.95	7	***.98 Fe* I (*976*)**; .96 *CH* (0, 0)Q; .97 *La* II (75)	96.27	96.32	0	.30 *Cr* I (176)
				96.65	96.65d?	6	***.58 Fe* II (*28*)**; *.73*+*.75 CH* (*0, 0*)*R*;** .68 *Ce* II (2); .74 *Zr* II (98)
4287.42	4287.42	6	.40 *Ti* I (44)				
	87.65:	0:	.71 *Ti* IP (45)				

TABLE 6—*Continued*

α Ser	α UMa	Int.	Identifications	α Ser	α UMa	Int.	Identifications
4297.00	4296.97	5	***.95*+*.96 CH* (*0, 0*)*Q*; .05 *Cr* I (64)	4305.17	4305.16	5	—.20 *Fe* I (760); .31 *CH* (0, 0)Q?
97.26	4297.25	4	***.21*+*.29 CH* (*0, 0*)*Q*; .17 *Gd* II (u)?	05.43	05.44	6	***.46 Fe* I (*476*)**; .45 *Cr* I (96); .45 *Sr* II (3); .45 *CH* (0, 0)Q; .47 *Ti* I (147)
97.52	97.51	2	.53 *CH* (Sun)				
97.73	97.74	5	***.74 Cr* I (*247*)**; .68 *V* I (120); .71 *Ru* I (5); .76 *Pr* II (7)	05.73	05.71	3:	***.72 Sc* II (*15*)**; .76 *Pr* II (8)
4298.04	4298.03	6	***.04 Fe* I (*520*)**; .99 *CH* (0, 0)R; .03 *V* I (120)	05.92	05.92	7	.91 *Ti* I (44); .91 *CH* (0, 0)Q
				4306.17	4306.17	4:	***.15 CH* (*0, 0*)*Q*;** .19 *AlH* (0, 0)P; ***.21 V* I (*5*)**
98.19:	98.19	1:	.21 *Fe* IP (476a)				
98.50:	98.47:	0:	.52 *Ni* I (178)?	06.66	06.67	4	***.68 CH* (*0, 0*)*Q*;** .72 *Ce* II (1)
98.70	98.71	8	***.66 Ti* I (*44*)**; .77 *Ni* I (28); .80 *CH* (0, 0)Q	06.88	06.85	4	***.85 CH* (*0, 0*)*Q*;** .94 *Ti* I (43)
				4307.21	4307.25	5	***.18 V* I (*5*)**; .31 *CH* (0, 0)Q
4299.00	98.99	7	***.99 Ca* I (*5*)**; .90 *CH* (0, 0)Q	07.56	07.54:	10:	.61 *CH* (0, 0)Q—
99.24	4299.24	11	***.24 Fe* I (*152*)**; .23 *Ti* I (148) Rem	07.87 w	07.90 w	20w	***.91 Fe* I (*42*)**; .90 *Ti* II (41) Rem
	99.4	0:	.36 *Ce* II (47); .49 *Fe* IP (648)	4308.2			***.17 CH* (*0, 0*)*Q*;** .23 *Gd* II (47)
99.65	99.66	6	***.64 Ti* I (*43*)**; .65 *Fe* I (416); .72 *Cr* I (96)	08.54	4308.56	8	***.51 Ti* I (*79*)**; ***.59 CH* (*0, 0*)*Q*;** .54 *Fe* IP (70); .62 *Dy* II
	99.83		.83 *CH*? (Sun)	08.89			***.90 CH* (*0, 0*)*Q*;** .94 *Zr* II (88)
4300.06	4300.05	7	.05 *Ti* II (41)	4309.04	4309.02 v	9w	***.04 Fe* I (*849*)**; .01 *Sm* II (15); .07 *Ti* I (235); .10 *CH* (0, 0)Q
	00.32	2	.33 *Ce* II (134); .32 *CH* (Sun)				
00.56	00.55	7	***.57 Ti* I (*44*)**; .58 *CH* (0, 0)Q	09.41	09.42	7	***.38 Fe* I (*414*)**; .37 *CH* (0, 0)Q; .46 *Fe* IP (478)
00.80	00.82	3	.83 *Fe* I (976)				
4301.10	4301.09	8	***.09 Ti* I (*44*)**; .00+.14 *CH* (0, 0)Q	09.73	09.70 d	10w	***.62 Y* II (*5*)**; ***.80 V* I (*5*)**; .70 *CH* (0, 0)Q; .74 *Ce* II (126)
01.52	01.53	0	.50 Sun				
01.90	01.89	7w	***.93 Ti* II (*41*)**; .97 *AlH* (0, 0)P	4310.13	4310.15	4	.10 *CH* (0, 0)Q
4302.21	4302.22	7	***.19 Fe* I (*520*)**; .26+.29 *CH* (0, 0)Q	10.46	10.45	5	***.46 CH* (*0, 0*)*Q*;** .37 *Ti* I (79)
02.54	02.55	8	.53 *Ca* I (5)	10.70	10.69	2	***.69 CH* (*0, 0*)*Q*;** .67 *AlH* (0, 0)P; .70 *Ce* II (133)
	02.73:		.75 *CH* (0, 0)Q				
02.89	02.94:	2:	.88 *Zr* I (45); .91 *CH* (0, 0)Q; .98 *Ti* I (79)	10.96	10.97	2	***.99 CH* (*0, 0*)*Q*;** .98 *Gd* II (15)
				4311.14	4311.16	2	.16 *CH* (0, 0)Q
4303.18	4303.19	6	.17 *Fe* II (27); .24 *Co* I (1) Rem	11.44	11.47	3	.44+.51 *CH* (0, 0)Q
03.61	03.60	4	.57 *Nd* II (10)	11.64	11.66	3	***.65 Ti* I (*205*)**; .72 *CH* (0, 0)Q
03.87	03.88	5	***.83*+*.94 CH* (*0, 0*)*Q*;** .94 *CH* (0, 0)R	4312.12	4312.10	3	.08+.16 *CH* (0, 0)Q
				12.26	12.27	2	***.20*+*.30 CH* (*0, 0*)*Q*;** .23 *Zr* II (99) Rem
4304.24	4304.28 d	1w	.39 *CH* (0, 0)Q?; .26 Sun				
04.57	04.55	5	***.55 Fe* I (*414*)**; .58 *CH* (0, 0)Q	12.55	12.56	3	***.55 Mn* I (*23*)**; .47 *Cr* I (177)
04.84	04.85	3	.90 *Gd* II (u); .87 *Fe* IP (598, 756)	12.87	12.89	9	***.86 Ti* II (*41*)**; .90 *CH* (0, 0)Q

TABLE 6—*Continued*

α Ser	α UMa	Int.	Identifications
4313.61	4313.62	4	Rem
4314.12	4314.10	7	***.08 Sc* II (*15*)**; .21 *CH* (0, 0)Q?
14.30	14.32	3	***.36 Ti* I (*45*)**; .30 *V* II (23); .29 *Fe* II (32)?
14.52:	14.50	0	.51 *Nd* II (9)
14.79	14.80	7	***.80 Ti* I (*43*)**; **.74** *Ti* Ip (43)
4315.05	4315.06	9	***.09 Fe* I (*71*)**; .98 *Ti* II (41)
15.44	15.45	1	.41 *AlH* (0, 0)P
4316.0	4316.03	1w	.05 *Gd* II (43)—
16.2			.26 *V* II (23)
16.79	16.80	3	.81 *Ti* II (94)
16.99	4317.02	3	.04 *Fe* Ip (762)?; .07 *TiO*?
4317.37	17.34	3	.32 *Zr* II (40)
17.70	17.74	0	.72 Sun
4318.27	4318.09	0:	.07 Sun
	18.34	0	
18.67	18.67	8	***.65 Ca* I (*5*)**; .63 *Ti* I (235)
18.94:	18.94	1	.94 *Sm* II (27)
4319.44	4319.42	2	.45 *Fe* Ip (214)?; .35 *TiO*?
19.64	19.62	2	.64 *Cr* I (96)
19.92:	19.91	0	.87 *Ru* I (M)?
4320.14:	4320.13	1	.13 *Fe* Ip (1170)?
20.40:	20.49	3w	***.36 Fe* Ip (*691*)**; .48 *AlH* (0, 0)P
20.53			***.52 Fe* I (*691*)**; .59 *Cr* I (96)
20.74	20.75	5	***.74 Sc* II (*15*)**; .72 *Ce* II (125)
20.95	20.96	3	.96 *Ti* II (41)
4321.21	4321.21	1	.24 *Cr* I (83)
21.40	21.38	1	
21.73d?	21.73	7	***.80 Fe* (*M*)**; .62 *Cr* I (177); .66 *Ti* I (235)
4322.07	4322.10	0	.02 *V* II (17)
	22.3		
22.45	22.50	1	.51 *La* II (25)
22.76	22.79	0	.70 *Fe* Ip (215)?
4323.02	4323.02	4w	.01 *CH*? (Sun)
23.41	23.37	7w	***.44 Ti* I (*79*)**; .37 *CH* (Sun); .52 *Cr* I (u)
23.87	23.91	3	.85 *CH* (Sun)
4324.13:	4324.12	1	.09 *CH*? (Sun); .06 *Gd* II (68)?
24.38	24.37	2	.41 Sun
24.64	24.62	1w	.62 Sun; .60 *β*
	24.77		
4325.05r	4325.04	10	***.01 Sc* II (*15*)**; .96 *Fe* I (70); .08 *Cr* I (104); .14 *Ti* I (235)
25.39	25.39	3:	***.36 Ni* I (*116*)**; .44 *Zr* I (M)?
25.81	25.80	25w	.76 *Fe* I (42)
4326.16			.14 *Mo* (M)
26.35	4326.36	5	.36 *Ti* I (43)
26.76	26.78	3	.76 *Fe* I (413)
26.92:	26.95	0	.99 *Ti* I (43)
4327.09	4327.11	4	.10 *Fe* I (761); .12 *Gd* II (15)
27.50	27.49	0	.52 *TiO*?
27.92	27.92	6	.92 *Fe* I (597)
	4328.27		
4328.60	28.61r	1	.61 Sun; .55 *TiO*? Rem
4329.02	4329.00:	2	.02 *Sm* II (15)
29.33	29.32	2	.40 Sun?; .34 *Mo* (M)?; .36 *Eu* (M)?
29.53	29.54	2	.54 *Fe* Ip (70)
4330.01	4330.01	6	***.02 V* I (*5*)**; .96+.00 *CH* (0, 0)P
30.25	30.25	1	.26 *Ti* II (94)
30.44	30.46	2	—.44 *Ce* II (82)
30.75	30.73	6	***.72 Ni* I (*149*)**; .61 *Gd* II (46); .71 *Ti* II (41)
30.96	30.96	3	.96 *Fe* I (597)
4331.17	4331.22	0	.23 *Co* I (168)?
31.41	31.41	3	.45 Sun; .36 *β*
31.65	31.65	5	.65 *Ni* I (52)
4332.06	4332.07d	1w	.94+.11 *TiO*
32.51d?	32.50	4	.57 *Cr* I (176)
32.85	32.84	7	.82 *V* I (5)
4333.23	4333.24	1	.28 *Zr* II (132)?
	33.50:		
33.78	33.78	4	***.76 La* II (*24*)**; .84 *CH* (0, 0)P
33.90			.91 *Pr* II (8)
4334.10	4334.10	2	***.15 Sm* II (*27*)**; .00 *CH* (0, 0)P
	34.46		

TABLE 6—*Continued*

α Ser	α UMa	Int.	Identifications
4334.67	4334.63	0	.66 *CH* (0, 0)P
34.83	34.85	4	***.84 Ti* I (*43*)**; .78 *CH* (0, 0)P
4335.29	4335.28	2	.28 Sun; .26 *TiO*
35.48	35.44	0	.46 *Fe* Ip (477)
35.70:	35.62:	0	
35.89	35.88	1	.89 *Fe* I (991)
	4336.08		.09 *TiO*
4336.27d?	36.26	1	.26 *Ce* II (89)
36.60	36.64	0	.66 *Hf* II (M)?; .63 *TiO?*
	36.85		.86 *Fe* Ip (692)
4337.05	4337.04	18	.05 *Fe* I (41)
37.23	37.25	1:	.33 *Ti* II (94)?; .27 *Cr* (M)?
37.56	37.54	8	***.57 Cr* I (*22*)**; .52 *Fe* Ip (214)?
37.92	37.90	7	***.92 Ti* II (*20*)**; .78 *Ce* II (82)
4338.27	4338.26	6	***.26 Fe* I (*70*)**; .2 *AlH* (0, 0)P?
38.44	38.45:	0	.48 *Ti* I (204)
38.74	38.72	6	.70 *Nd* II (68); .80 *Cr* I (198) Rem
4339.10	4339.10	2	.13 *Co* Ip (1)
39.27	39.26		Rem
39.45	39.46	9	***.45 Cr* I (*22*)**; .43 *CH* (0, 0)P
39.69	39.69	8	.72 *Cr* I (22)
4340.13	4340.13	4	***.13 Cr* I (*64*)**; .02 *Ti* I (174)
40.48w	40.45w	9w	.47 $H\gamma$ (1)
4341.00	4341.00	7	.01 *V* I (5)
41.37	41.35	7	.37 *Ti* II (32)
41.83	41.80	3	.83 Sun; .80 β
4342.19	4342.13	3	.18 *Gd* II (15)
42.48	42.44	0	.48 β
42.81	42.80	0	.83 *V* I (103)
4343.22	4343.22	8	***.26 Fe* I (*645*)**; .15 *CH* (0, 0)P; .16 *Cr* I (64)
43.50	43.50	2	.49 *CH* (0, 0)P
43.70	43.70	5	***.70 Fe* I (*517*)**; .69 *CH* (0, 0)P; .80 *Ti* I (204)
43.96	43.94	2	.96 *CH* (0, 0)P
4344.28	4344.28	3	.29 *Ti* II (20)
44.50	44.50	8	.51 *Cr* I (22)
44.90	44.88	2	.89 Sun; .89 β
4345.09	4345.09	1	.08 *Cr* I (198)
45.6	45.48	1w	
45.86	45.86	2	.86 *Sm* II (7)
4346.09	4346.06	2	.10 *Ti* I (234)
46.28	46.30	3	.30 Sun; .30 *TiO*
46.56	46.55	7	—.56 *Fe* I (598); .61 *Ti* I (204)
46.82	46.82	3	.83 *Cr* I (104)
4347.23	4347.23	7	.24 *Fe* I (2)—
47.53	47.51	3	***.54 CH* (*0, 0*)*P*;** .49 *Pr* II (30)
47.87	47.85	9	***.85 Fe* I (*828*)**; ***.96 CH* (*0, 0*)*P*;** .80 *Sm* II (37)
4348.34	4348.32	4	.34 *CH* (0, 0)P
48.61	48.59	1	
48.95	48.95	5	.94 *Fe* I (414)
4349.43	4349.40	0	
	49.62		
49.78	49.78	2	.79 *Ce* II (59)
49.94		0	.97 *V* II (36)?
4350.16	4350.18	4	.16 Sun; .17 *TiO?*
50.56	50.48	2w	***.46 Sm* II (*46*)**; .52 *Hf* II (72)?
50.78	50.78	4w	—.83 *Ti* II (94)
4351.04	4351.03	7	.05 *Cr* I (22)
51.29	51.30	3	.30 *Nd* II (10)—
51.54	51.54	4	.55 *Fe* I (413)
51.80	51.83	14	***.76 Fe* II (*27*)**; ***.77 Cr* I (*22*)**; .72 *CH* (0, 0)P; .85 *Pr* II (23)
51.98			***.89*+*.91 Mg* I (*14*)**; .07 *CH* (0, 0)P
4352.25	4352.24	1	.25 *CH* (0, 0)P
52.54	52.50	1	.55 *CH* (0, 0)P
52.80	52.78	13	.74 *Fe* I (71); .87 *V* I (5)
4353.17:	4353.2	0	***.27 AlH* (*1, 1*)*R Head;*** .19 *Tb* II
53.49	53.47	3	—.42 *AlH* (1, 1)R
53.96	53.93	4	***.98 Cr* I (*198*)**; .06 *Ti* I (204)?
4354.24	4354.23	0	.27 Sun
54.56	54.58v	8	***.54 Mg* I (*13*)**; .61 *Sc* II (14)
4355.06	4355.06	7	***.10 Ca* I (*37*)**; .98 *V* I (103)
55.32	55.33	2	.31 *Ti* I (174)
55.67	55.65	3	.71 *CH* (0, 0)P

TABLE 6—*Continued*

α Ser	α UMa	Int.	Identifications
4355.94	4355.94	7	***.94 V* I (*5*)**; .91 *Ni* I (149); .01 *CH* (0, 0)P
4356.34	4356.34	3	.37 *CH* (0, 0)P
56.71	56.66	5w	***.61 CH (0, 0)P;*** .76 *Cr* I (130)
56.93	56.94	0	.91 *Co*? (Sun)
4357.20	4357.22d	1	.17 *Co* (M)?
57.50	57.49	4	***.52 Cr* I (*198*)**; .50 *Fe* Ip (1170); .53 *Fe* Ip (994)?
	57.68		.73 *V* (M)?
57.92	57.90	4	.88 Sun; .87 *TiO*?
4358.16	4358.15	4	—.17 *Nd* II (10); .14 *AlH* (1, 1)R?
58.52	58.50	6	.50 *Fe* I (412)
58.71	58.71	7	***.73 Y* II (*5*)**; .66 *Cr* I (176); .70 *Nd* II (57)
58.90	58.90	1	—.95 *Fe* Ip (987)?
4359.19	4359.26d	0	.23 *TiO*
59.63	59.62	12	***.63 Cr* I (*22*)**; .58 *Ni* I (86) Rem
59.97	59.99	2	***.99 Cr* I (*198*)**; .93 *Tm* I (1)
4360.26	4360.27	2	.29 *CH* (0, 0)P
60.46	60.46	3	***.48 CH (0, 0)P;*** .49 *Ti* I (204); .48 *AlH* (1, 1)Q?
60.79	60.78	5	***.81 Fe* I (*903*)**; .72 *Sm* II (23); .80 *Zr* I (31)
4361.04:	4361.04	2	.03 *Co* I (1)
61.18	61.24	2	.17 β
61.37			.40 *V* (M)
61.68	61.65	0	.66 *Ce* II (157)?; .62 *TiO*?
4362.01	4362.03r	6w	.91 *Co* I (1); .04 *Sm* II (45)
62.17			.10 Sun
62.51	62.52	4	.54 Sun; .48 β
62.73	62.73	2	.75 Sun; .69 β
62.94			.95 *Cr* I (82)
4363.12	4363.11	5	***.09 CH (0, 0)P;*** .13 *Cr* I (103)
63.28	63.29	2	.31 *CH* (0, 0)P
63.52	63.52	6	.52 *V* I (23)
	63.84		
4364.10d	4364.11d	7w	***.07+.19 CH (0, 0)P;*** .14 *Cr* I (130)
64.65	64.64	3	.66 *Ce* II (135); .66 *La* II (53)
64.92	64.91	1	.87 *Cr* I (153)?; .04 *AlH* (1, 1)QP?
4365.20	4365.24	0	.24 *Mn* (M)
65.48	65.50	3	.54 Sun; .5 *TiO*?
65.90	65.90–	5	.90 *Fe* I (415)
4366.14			.06 *TiO*?
66.45	4366.49	6w	***.51 CH (0, 0)P;*** .45 *Zr* I (61)?
66.63			.68 *CH* (0, 0)P
4367.03	66.97	1	.07 *Fe* Ip (1170)?; .08 *AlH* (1, 1)Q?
67.28	4367.26d	1	.25 *TiO*?; .36 *Ni* I (88)?
67.60	67.60	10	***.58 Fe* I (*414*)**; .66 *Ti* II (104); .61+.73 *CH* (0, 0)P
67.94r	67.95	11	***.91 Fe* I (*41*)**; .04 *V* I (5)
4368.30	4368.30	4	***.33 Pr* II (*5*)**; .25 *Cr* I (130); .31 *Ni* I (102)
68.63	68.64	4	—.63 *Nd* II (11); .66 *Fe* Ip (644)
68.91	68.90	4	***.94 Ti* I (*245*)**; .89 *Cr* I (198)
	4369.18:		.17 *Gd* (M)?
4369.41	69.41	3	***.40 Fe* II (*28*)**; .52 *AlH* (1, 1)Q?
69.76	69.77	10	***.77 Fe* I (*518*)**; .68 *Ti* I (290) Rem
4370.06	4370.11	2	.04 *Ni* I (149)
70.35d?	70.29	2	.27 *V* II (31)
70.63	70.65	0	
70.99	4371.01	8	.96 *Zr* II (79); .00 *Fe* Ip (69); .03+.05 *CH* (0, 0)P
4371.27	71.28	9	.28 *Cr* I (22)
71.76	71.77	1	.80 Sun
4372.21	4372.32d	7	.21 *Ru* I (13)?; .3 *AlH* (1, 1)Q?
72.36			.38 *Ti* I (277)
72.78	72.79	4	.73+.85 *CH* (0, 0)P
72.97	72.97	4	.99 *Fe* I (473)
4373.24	4373.25	6	.25 *Cr* I (22)
73.57	73.57	6	.56 *Fe* I (214, 413)
73.81	73.81	3	—.82 *Ce* II (202)?; .83 *V* I (M)
4374.16	4374.18	7	***.22 CH (0, 0)P;*** .16 *Cr* I (104)
74.45	74.47	8	***.46 Sc* II (*14*)**; .50 *Fe* I (648)
74.90	74.92	9	***.94 Y* II (*13*)**; .82 *Ti* II (93); .92 *Co* I (150)
4375.30	4375.31	4	.33 *Cr* I (103)
75.54	75.56	4	***.57+.66 CH (0, 0)P;*** .54 *Co* I (143)
75.94	75.95	11	.93 *Fe* I (2)

TABLE 6—*Continued*

α Ser	α UMa	Int.	Identifications
4376.39r	4376.39	1	.42 Sun; .44 *Nd* (M)?
	76.77	0	.76 *Fe* I (471, 904)
4377.09	4377.13:	6	—.10 *TiO*?
77.28	77.27	7	***.24 CH (0, 0)P;*** .33 *Fe* I (990)
77.53	77.53	2	.55 *Cr* I (83)
77.80	77.79	5	.80 *Fe* I (645)
4378.25	4378.24	5	.23+.29 *CH* (0, 0)P; .24 *Sm* II (53)
78.51	78.56	1	.52 Sun; .49 *W* (M)
78.92	78.92	4	.92 Sun
4379.23	4379.23	10	.24 *V* I (22)
79.54	79.54	1	
79.76	79.77	3	***.78 Cr* I (130)**; .78 *Zr* II (88)
4380.07	4380.06	6	***.07 CH (0, 0)P;*** .06 *Ce* II (155)
80.46	80.46	6w	***.38 Mg* I (12)**; .55 *Cr* I (130)
80.72	80.73	5	.72 *CH* (0, 0)P
4381.08	4381.10	6	***.11 Cr* I (64)**; .04 *V* I (23)
	81.35:		.29 *Nd* II (56)?
	81.52		
81.67	81.71	3:	.64 *Mo* (M); .70 *Mn* (M)
81.88	81.90	2:	
4382.20	4382.16	2:	.17 *Ce* II (2)
82.49	82.49	3:	.52 Sun
82.76	82.75		.71+.73 *CH* (0, 0)P; .78 *Fe* I (799a); .85 *Cr* I (64)
4383.58 w	4383.52 w	60	.55 *Fe* I (41)
4384.22	4384.23		.29 *Sm* II (M)?
	84.50		.54 *Ni* I (86)
84.73	84.73	12:	***.72 V* I (5, 22)**; .68 *Fe* I (474); .81 *Sc* II (14)
4385.00	4385.00	7:	***.98 Cr* I (22)**; .10 *CH* (0, 0)P
85.29	85.31	7:	***.26 Fe* I (415)**; .21+.26 *CH* (0, 0)P; .38 *Fe* II (27)
85.65	85.66	4	—.66 *Nd* II (50); .65 *Ru* (M)?
85.8	85.87	0	
4386.07	4386.06	4	.06 Sun; .07 *Tb* (M)?
86.46	86.40	2	.43 *Tm* I (1); .46 *Ni* I (168)
86.62	86.61	1	.6 *Fe* I (899)?
86.83	86.81	4	***.84 Ce* II (57)**; .86 *Ti* II (104)
4387.02	4387.04	2	***.08 CH (0, 0)P;*** .91 *Ce* II (57)
4387.46	4387.46r	9	***.50 Cr* I (103)**; .38 *Cr* I (84); .54 *CH* (0, 0)P
87.91	87.91	5	.90 *Fe* I (476)
4388.07	4388.06:	2	.07 *Ti* I (219)
88.42	88.41	5	.41 *Fe* I (830)
88.79	88.79	3w	.88 *CH* (0, 0)P
4389.24	4389.25	8	.24 *Fe* I (2)
89.56	89.59	2	.64 *CH* (Sun); .72 *CH* (0, 0)P?
89.95	89.96	10	.97 *V* I (22)
4390.27	4390.25	1	.32 *Ni* I (136)
90.47:	90.48	6	***.46 Fe* I (413)**; .53 *CH* (0, 0)P
90.96	90.97	9	***.95 Fe* I (414)**; .98 *Ti* II (61); .86 *Sm* II (15)?
4391.26	4391.32	0	
	91.54		.57 *Co* I (150)
91.74	91.74	10	***.75 Cr* I (22)**; .66 *Ce* II (81); .74 *CH* (0, 0)P
4392.07	4392.07	4	.07 *V* I (23); .08 *CH* (0, 0)P
92.29	92.30	1	.26 *Cr* I (130)
92.57	92.59	3	.58 *Fe* I (973); .59 *TiO*?
92.99	92.98	2	—.03 *Fe* Ip (473); .90 *TiO*?
4393.30	4393.30	5	—.3 *AlH* (1, 1)P; .14 *TiO*?
93.54	93.53	2	.53 *Cr* I (102); .62 *CH* (0, 0)P
93.85	93.75		.70 *Fe* Ip (899)?; .71 *CH* (0, 0)P; .84 *V* I (40)
4394.03	4394.05v	7w	***.06 Ti* II (51)**; .92 *Ti* I (244)
94.49	94.54	0	.50 *Zr* I (M)
94.82	94.82	0	.82 *Ti* I (78); .83 *Cr* I (130)
4395.01	4395.03	5	.03 *Ti* II (19)
95.22	95.22	7	.23 *V* I (22); .29 *Fe* I (828)
95.49	95.49	6	***.51 Fe* I (991, 992)**; .42 *Cr* I (129)
95.84	95.85	5	***.85 Ti* II (61)**; .79 *Pr* II (29)?
4396.05:	4396.04:	1	.07 *CH* (Sun)?
96.34	96.33	2	.31 Sun; .35 *TiO*?
96.58	96.61	0	.58 *TiO*
96.93	96.95	2	.96 *CH* (Sun)
4397.24	4397.25	3	.25 *Cr* I (129)
97.70	97.67	1	.70 *β*
4398.02	4398.02	6	—.02 *Y* II (5)

TABLE 6—*Continued*

α Ser	α UMa	Int.	Identifications
4398.27	4398.28	3	.31 *Ti* II (61)
98.56	98.56	1	.52 *V* II (187); .62 *Ni* I (102); .56 *TiO*?
98.81	98.81	1	.79 *Ce* II (81)
4399.25	4399.24	2	.20 *Ce* II (81)
	99.56	0	.61 *Ni* I (196)
99.73v	99.74	7	.77 *Ti* II (51); .82 *Cr* I (129)
4400.16	4400.16	1	.14 *TiO*
00.38	00.41	5	.36 *Sc* II (14)
00.55	00.57	5	.58 *V* I (22)
00.85v	00.85v	3	.83 *Nd* II (10); .87 *Ni* I (149)
4401.04	4401.02	3	.03 Sun; .03 *TiO*
01.28	01.28	3	.29 *Fe* I (828)
01.49	01.50	7	***.55 Ni* I (*86*)**; .45 *Fe* I (350)
	01.87		.85 *Gd* (M); .83 *TiO*?
4402.3	4402.26	0	.24 *TiO*
02.66	02.67	1d	.56+.70 *TiO*?
4403.14	4403.14	4	.19 Sun; .14 *TiO*
03.39	03.38	4	***.35 Zr* II (*79*)**; .36 *Sm* II (22); .37 *Cr* I (128)
03.66	03.66	2	—.60 *Pr* II (34); .67 *V* I (M)
4404.00	4404.00	3	.98 Sun; .97 *TiO*
04.31	04.33		.28 *Ti* I (218, 219); .40 *Ti* I (78)
04.78 w	04.71 w	40w	.75 *Fe* I (41)
	4405.02		***.02 Fe* Ip (*2*)**; .01 *V* I (23); .91 *Ti* I (161)
4405.35	05.41	2:	.40 *Fe* Ip (991)?; .32 *TiO*?
05.68	05.72	5	.69 *Ti* I (78)—
4406.09	4406.10	5	.15 *V* I (40)—
06.62	06.63	9	.64 *V* I (22)
4407.00	4407.02	2	.07 *B*
07.22	07.23	3	—.28 *Ce* II (64)
07.65	07.66	10	***.64 V* I (*22*)**; ***.68 Ti* II (*51*)**; ***.71 Fe* I (*68*)**; .72 *Cr* I (129)
07.91	07.95	0	.91 *Be* I (4)?
4408.19	4408.20	7	***.20 V* I (*22*)**; .25 *Gd* II (44)
08.44	08.46	9	.42 *Fe* I (68); .51 *V* I (22)
08.84	08.81	2	.84 *Pr* II (4)
4409.18	4409.21	5	***.12 Fe* I (*645*)**; .22 *Ti* II (61)
	09.51	0	.52 *Ti* II (61)
09.70		2	.68 *Pr* II (M)?
09.78	09.8	0	
4410.01	4410.03d?	2	—.03 *Ru* I (5); .01 *TiO*?
10.24	10.27	2	.30 *Cr* I (129)
10.52	10.55	4	.52 *Ni* I (88)
10.77:	10.81	0	
4411.05	4411.07	6	***.05 Nd* II (*8*)**; ***.09 Cr* I (*129*)**; .97 *Cr* I (102); .08 *Ti* II (115)
11.28	11.29:	0	.21 *La* II (138)?
	11.60		
11.90	11.92	4	.90 *Mn* I (u); .94 *Ti* II (61)
4412.19	4412.22	7	***.25 Cr* I (*22*)**; .26 *Nd* II (9)?
12.41	12.47	1	.43 *Fe* Ip (69); .44 *Ti* I (54)
12.71	12.74	0	.67 *TiO*
4413.11	4413.11	1	.04 *Zr* I (61)?; .15 *TiO*?
13.36	13.31	0	.40 *Fe* Ip (1046)?
13.61	13.61	1	.60 *Fe* II (32)?
13.84	13.83	3	.87 *Cr* I (234)?
4414.15	4414.04	3	—.03 *Fe* Ip (825); .11 *Ti* (M)?
	14.19		.20 *Ni* I (88)
14.49	14.49	4	***.54 Zr* II (*79*)**; .47 *Fe* Ip (643)
	14.67:		
14.88:			.88 *Mn* I (22)
4415.13w	4415.10w	30	.12 *Fe* I (41)
15.54	15.54	7:	.56 *Sc* II (14)
4416.04:	15.94	1	
16.47	4416.48	8	***.47 V* I (*22*)**; .54 *Ti* I (161)
16.83	16.83	5	.82 *Fe* II (27)
4417.31	4417.29	7	***.27 Ti* I (*161*)**; .40 *Co* I (150)?
17.70	17.72	7	.72 *Ti* II (40)
4418.04:	4418.06	0	
18.36	18.35	7	***.43 Fe* I (*412*)**; .34 *Ti* II (51)
18.71	18.77	1	.78 *Ce* II (2)
4419.05	4419.02	1	.03 *Gd* II (15)
19.32	19.28	0	.30 *Fe* Ip (893)?; .29 *TiO*?
	19.54		.54 *Fe* (M)

TABLE 6—*Continued*

α Ser	α UMa	Int.	Identifications
4419.86	4419.88	7	.94 *V* I (21)
4420.27	4420.28	3	.29 Sun
20.53d	20.50	5w	.47 *Os* I (1); .53 *Sm* II (32)
	20.65		.66 *Sc* II (14)
4421.10	4421.16	2:	.14 *Sm* II (37)
21.34			.34 *Co* I (150)
21.56	21.55	7	***.57 V* I (*22*)**; *TiO* α (4, 0)Ra Head
	21.76		.75 *Ti* I (218)
21.99	21.97	3	.95 *Ti* II (93)
4422.55	4422.55	9	***.57 Fe* I (*350*)**; .59 *V* II (5)
22.88	22.86	7	***.82 Ti* I (*78*)**; .88 *Fe* I (646)
4423.20	4423.19	8	***.14 Fe* I (*412*)**; .21 *V* I (40); .22 *Ti* IIp (61)
	23.52		
23.83	23.83	4	***.86 Fe* I (*830*)**; *TiO* α (4, 0)Rc Head
4424.09	4424.10	1	.08 *Cr* I (82)
24.26	24.30	7	***.28 Cr* I (*129*)**; .34 *Sm* II (45)
24.57	24.55	2	.56 *V* (M)
24.86	24.84	0	.84 *Ni* I (262)?
4425.11	4425.08	1	.13 *Cr* I (152)?; .07 *TiO*
25.44	25.44	8	.44 *Ca* I (4)
25.73	25.73	6	—.66 *Fe* I (798); .75 *Fe* Ip (555); .71 *V* I (M)?
4426.01	4426.00	7	***.00 V* I (*22*)**; .05 *Ti* I (161)
26.63	26.66d	1	.66 *TiO*
4427.13	4427.12	15w	***.10 Ti* I (*128*)**
27.31	27.31		***.31 Fe* I (*2*)**; .30 *Fe* Ip (828)
	27.56		.58 *Sm* II (M)
27.85	27.86	4	***.90 Ti* II (*61*)**; .71 *Cr* I (129)
4428.2	4428.2	0	
28.52	28.51	8	***.51 V* I (*21*)**; .50 *Cr* I (129)
28.84	28.90	1	
4429.22	4429.22	5	—.24 *Pr* II (2, 4); .27 *Ce* II (19)
29.5	29.45	0	.44 *Cb* (M)?
29.81	29.89	10	.80 *V* I (22)
29.98:			.90 *La* II (38); .94 *Cr* I (234); .02 *Ti* I (267)
4430.18	4430.18	4:	.20 *Fe* I (472)
30.40	30.39	4:	***.37 Ti* I (*113*)**; .49 *Cr* I (234)
30.63	30.62	10	.62 *Fe* I (68)
4431.03	4431.02	2	.00 *TiO*
31.34	31.34	7	.28 *Ti* I (218); .37 *Sc* II (14)
31.59	31.54	1	.61 *Co* I (143)
31.83	31.82	3	.85 Sun; .82 *TiO*
4432.13	4432.13	6	***.18 Cr* I (*81*)**; .09 *Ti* II (51)
32.57	32.57	5	.57 *Fe* I (797)
32.92	32.94	1	.90 *Fe* Ip (271)?; .88 *TiO*?
4433.24	4433.24r	7	.22 *Fe* I (830)—
33.52		0	.58 *Ti* I (267)
33.80	33.80	6	***.79 Fe* I (*825*)**; .75 *TiO*
33.95	33.95	6	***.00 Ti* I (*161, 113*)**; .88 *Sm* II (41); .97 *Cr* I (128)
4434.39	4434.37	5	—.32 *Sm* II (36); .33 *TiO*
34.57	34.65:	1	.60 *V* (M); .57 *TiO*
34.97	34.97	7	.96 *Ca* I (4)
4435.15	4435.15	7	.15 *Fe* I (2)—
35.43:	35.40:	1	.45 β
35.66:	35.64	9	***.69 Ca* I (*4*)**; .58 *Eu* II (4)
4436.14	4436.15	6	.14 *V* I (21)
36.36	36.35	5	.35 *Mn* I (22)
36.64	36.63	3	***.59 Ti* I (*160*)**; .64 *Ti* I (267)
36.96	36.94	5	***.93 Fe* I (*516*)**; .98 *Ni* I (86)
4437.27	4437.30:	0	.28 *TiO*
37.61	37.60	1	.57 *Ni* I (168)?; .58 *TiO*
37.81	37.82	6	.84 *V* I (21)
4438.30	4438.32	6	***.23 Ti* I (*218*)**; .27 *Gd* II (44); .35 *Fe* I (828)
38.61	38.61	1	.65 *TiO*
4439.03	4439.00	3	.97 *V* (Sun)?
39.25	39.21	3	.17 Sun; .23 *TiO*?
39.63	39.63	3	.64 *Fe* I (515)
39.89	39.87	4	.88 *Fe* I (116)
4440.41	4440.42	7	***.34 Ti* I (*159*)**; ***.45 Zr* II (*79*)**; .48 *Fe* I (829)

TABLE 6—*Continued*

α Ser	α UMa	Int.	Identifications	α Ser	α UMa	Int.	Identifications
4440.84	4440.85	4	.84 *Fe* I (992)	4453.00	4452.99	4	.00 *Mn* I (22)
4441.01	4441.01	4	.97 *Fe* I (645)	53.31	4453.32	5	.31 *Ti* I (113)
41.24	41.26	1	.27 *Ti* I (160)	53.72	53.72	5	.71 *Ti* I (160)
41.70	41.69	8	.68 *V* I (21)		53.97		
41.96:			.95 *Co* (M)?; .97 *Fe* (Sun)?	4454.38	4454.39	5	***.38 Fe* I (*350*)**; .38 *Pr* II (5)
4442.35	4442.35	11	***.34 Fe* I (*68*)**; .27 *Cr* I (102)	54.76	54.75	10	***.78 Ca* I (*4*)** Rem
42.84	42.84	4	.84 *Fe* I (69)	4455.00	4455.01	4	***.01 Mn* I (*28*)**; .03 *Fe* I (974)
4443.00	4443.00:	1	.99 *Zr* II (88)	55.32	55.32	6	***.32 Mn* I (*28*)**; .32 *Ti* I (113)
43.19	43.19	5	.20 *Fe* I (350)	55.87	55.87	8	***.89 Ca* I (*4*)**; .82 *Mn* I (28)
	43.51:			4456.34	4456.36	5	.33 *Fe* I (516)
43.81	43.80	8	***.80 Ti* II (*19*)**; .71 *Cr* I (234)	56.61	56.62	5	***.61 Ca* I (*4*)**; .65 *Ti* II (115)
4444.22	4444.22	7	***.21 V* I (*2*)**; .27 *Ti* I (218)	4457.04	4457.04	4	.04 *Mn* I (28)
44.59	44.53	5	—.56 *Ti* II (31)	57.48	57.47	9	***.43 Ti* I (*113*)**; ***.48 V* I (*21*)**; .42 *Zr* II (79); .55 *Mn* I (28)
44.76:			.70 *Ce* II (u)?				
4445.04	4445.04	1	.04 *Co* (M); .00 *TiO*	57.78	57.76	2	.76 *V* I (101)
45.47	45.47	5	.48 *Fe* I (2)—	4458.18d	4458.08	7w	.10 *Fe* I (992)
45.79	45.78	1	.71 *Co* I (150); .84 *TiO*		58.24		.26 *Mn* I (28)
4446.35d	4446.38	2w	***.39 Nd* II (*49*)**; .21 *TiO?*	58.54	58.52	4	***.54 Cr* I (*127*)**; .52 *Sm* II (17)
46.85	46.85	5	.86 *Fe* I (828)		58.81		
4447.14	4447.13	5	.13 *Fe* I (69)	4459.11	4459.11	11	***.12 Fe* I (*68*)**; .04 *Ni* I (86)
47.39:	47.37	0	.37 *TiO*	59.34	59.35	3:	.34 *Cr* I (63)
	47.54			59.76	59.75	7	***.76 V* I (*21*)**; .74 *Cr* I (127)
47.73	47.72	10	.72 *Fe* I (68)	4460.29	4460.29	9	***.29 V* I (*21*)**; .21 *Ce* II (2); .38 *Mn* I (28)
4448.23	4448.16	1	.14 *TiO*				
48.6	48.51:		.53 *TiO*		60.54		.55 *Fe* Ip (1100)?
4449.14	4449.14	5	.14 *Ti* I (160)	60.77	60.79	2	.77 *Cr* I (63)
49.33	49.36	0	.34 *Ce* II (202)?; .34 *Ru* I (M)?	4461.12	4461.13	7	***.08 Mn* I (*28*)**; .20 *Fe* I (471)
49.68	49.72w	1w	***.70 Dy* II**; .57 *V* I (62)?	61.39	61.38	3	.37 *Fe* I (725)
4450.01	4450.01	1	.98 *Ti* I (159)	61.65	61.66	8	.65 *Fe* I (2)
50.31	50.31	4	***.32 Fe* I (*476*)**; .30 *Ni* I (236)	4462.05	4462.04	8	***.02 Mn* I (*28*)**; ***.10 Ti* I (*8*)**; .99 *Fe* I (471, 825, 902)
50.46	50.46	4	.49 *Ti* II (19)				
50.86	50.82	6	***.90 Ti* I (*160*)**; .73 *Ce* II (3)	62.41	62.41	5	.36 *V* I (87); .46 *Ni* I (86)
	4451.25	0	.23 *TiO*	62.74	62.72	2	.77 *Cr* I (127)
4451.60	51.59	6	***.59 Mn* I (*22*)**; .57 *Nd* II (50)	4463.06	4463.05d	3w	***.98 Nd* II (*50*)**; .16 *TiO*
4452.01	4452.02	5	.98 *Nd* II (6); .01 *V* I (87)	63.46	63.44	5	***.39 Ti* I (*160*)**; ***.54 Ti* I (*160*)**; .43 *Ni* I (102)
	52.25						
52.68	52.69	6w	—.62 *Fe* Ip (969)?; .73 *Sm* II (26); .70 *V* I (M)	63.94:	63.88	0	.81 *TiO*
					63.96		

TABLE 6—*Continued*

α Ser	α UMa	Int.	Identifications
4464.44	4464.45	4	.46 *Ti* II (40)
64.73	64.72	7	***.68 Mn* I (*22*)**; ***.77 Fe* I (*472*)**; .67 *Cr* I (127); .75 *V* I (110)
4465.10	4465.10	2	.15 *Cr* I (267)
65.36	65.36	3	.36 *Cr* I (127)
65.60:	65.60	0	.60 *Nd* II (13)?
65.81	65.81	3	.81 *Ti* I (146)
4466.12:	4466.16	1	***.16 Cr* I (*127*)**; .18 *Fe* I (901)
66.56	66.56	8	***.55 Fe* I (*350*)**; .55 *Gd* II (44); .57 *Fe* Ip (2)
66.91	66.91	4	.88 *Co* I (150); .94 *Fe* I (992)
4467.31	4467.35	2	.34 *Sm* II (53)
67.55	67.57	3	.56 *Cr* I (127)
67.92	67.90d	4w	—.01 *V* I (87); .84 *TiO*
4468.50	4468.52	7	.49 *Ti* II (31)
68.75	68.72	1	***.71 Pr* II (*20*)**; .76 *V* I (102)
4469.17	4469.17	3	.16 *Ti* II (18)
69.38	69.39	4	.38 *Fe* I (830)
69.62	69.62	3	***.55 Co* I (*150*)**; .71 *V* I (87)
4470.13	4470.14	4	.14 *Mn* I (22)
70.49	70.48	5	.48 *Ni* I (86)
70.86	70.86	4	.86 *Ti* II (40)
4471.25	4471.25	4	***.24 Ti* I (*146*)**; .24 *Ce* II (8); .29 *Gd* II (82)
71.67	71.68	6	***.68 Fe* Ip (*2*)**; .55 *Co* I (150)
	4472.13:		.13 *TiO*
4472.51:	72.46	1w	.52 *Fe* Ip (39)
72.79r	72.78	8	.72 *Fe* I (595, 900); .79 *Mn* I (22)
	72.97	1:	***.92 Fe* II (*37*)**; .02 *Sm* II (26)
	4473.6		.52 *TiO*?
4473.81	73.82	3	.78 *Cr* I (63)
4474.05	4474.08	3	.04 *V* I (110)
74.48	74.49	3	.53 *TiO*?; .56 *Mo* (M)?
74.80	74.80	6	***.71 V* I (*101*)**; .85 *Ti* I (113, 184)
4475.30	4475.29	4	.34 *Cr* I (95)—
75.57	75.62	1	***.52 Ti* I (*184*)**; .72 *V* I (14)
4476.04	4476.05	10	***.02 Fe* I (*350*)**; .08 *Fe* I (830)
76.58:	76.63d?	2w	—.61 *Ti* Ip (184)?; .57 *TiO*
4477.07	4477.08	3	.02 *Cr* I (63)
77.52:	77.46	1	.45 *V* I (14)
	77.72		.62 *TiO*?
4478.01	4478.02	3	.04 *Fe* I (69)
78.33	78.31	2	.32 *Co* I (150); .34 *TiO*
78.65	78.64	2	.66 *Sm* II (u)
78.97	78.95	1	.00 *Fe* Ip (987)?
	4479.2		.20 *TiO*?
4479.36	79.39	3	.36 *Ce* II (203)?; .40 *Mn* (M)?; .43 *Ce* II (124)?
79.66	79.65	5	***.61 Fe* I (*828, 848*)**; .72 *Ti* I (146)
4480.12d?	4480.13wv	8w	—***.14 Fe* I (*515*)**; .26 *Cr* I (197); .04 *V* I (M)?
80.60	80.60	4	***.60 Ti* I (*146*)**; .57 *Ni* I (211)
80.83	80.84	2	.83 Sun
4481.07	4481.06	1:	.06 *Gd* II (44)
81.27	81.27	5	***.26 Ti* I (*146*)**; .23 *Ni* I (168)
81.62	81.62	4	.62 *Fe* I (827)—
4482.23	4482.22	11	***.17 Fe* I (*2*)**; .26 *Fe* I (68)
82.76	82.75	6	***.69 Ti* I (*113*)**; ***.75 Fe* I (*828*)**; .88 *Cr* I (197)
4483.51:	4483.30	1:	.33 *Gd* II (62)?
	83.49		.43 β
83.85	83.85	3w	***.90 Ce* II (*3*)**; .92 *Co* I (150)
4484.23	4484.24	5	.23 *Fe* I (828)
84.54	84.52	2	.51 *Co* I (27); .54 *Ni* I (102)
84.8			.82 *Ce* (M)?; .76+.83 *TiO*?
4485.13	4485.18	1	.01 *Ti* I (184)? Rem
85.68	85.67	4	.68 *Fe* I (830)
4486.00	4486.01	2	—.97 *Fe* Ip (825)?
	86.33	0	.35 *Gd* II (135)?; .30 *TiO*
	86.64:	0	.71 *TiO*
86.96	86.93	4	.91 *Ce* II (57)
4487.32	4487.31	3w	—.28 *V* I (14); .22 *TiO*
87.5	87.52	0	.46 *Cr* I (63); .47 *V* I (14)
87.77	87.74:	2	.74 *Fe* Ip (594)
4488.13	4488.12	5	***.14 Fe* I (*819*)**; .05 *Cr* I (293)?
88.32	88.32	2:	.32 *Ti* II (115)

TABLE 6—*Continued*

α Ser	α UMa	Int.	Identifications
4488.93	4488.92	3	***.90 V*** **1** (***86, 110***); .92 *Fe* 1 (213, 827)
4489.12	4489.14	4	***.18 Fe*** **II** (***37***); .09 *Ti* 1 (146)
89.43	89.46	1	.47 *Cr* 1 (u)
89.76	89.76	6	.74 *Fe* 1 (2)
4490.12	4490.11	4	.08 *Mn* 1 (22); .08 *Fe* 1 (469)
90.59	90.59	2:	***.56 Cr*** **1** (***267***); .54 *Ni* 1 (134, 235)
90.77	90.79	3:	.77 *Fe* 1 (973, 974); .82 *V* 1 (86)
4491.14:	4491.12	0	.16 *V* 1 (62)
91.43	91.44	3	.40 *Fe* II (37)
91.71	91.68	2	.68 *Cr* 1 (95)
91.92	91.91	1:	.86 *Cr* 1 (83)
4492.31	4492.31	2	.31 *Cr* 1 (197)
92.52:			.54 *Ti* 1 (184)
92.65	92.65	3	***.69 Fe*** **1** (***969***); .64 *TiO*
4493.09:	4493.2	1	
93.49	93.50	3	.53 *Ti* II (18)
	93.76		.77 *TiO*
4494.00	4494.08d	5w	.97 *W* (M)?
94.18			—***.18 Na*** **1** (***15***); .15 *TiO*
94.57	94.57	10	.57 *Fe* 1 (68)
4495.02	4495.00	3	.01 *Ti* 1 (u)
95.46	95.50	4w	***.57 Fe*** **1** (***827***); .44 *Zr* II (79)
95.99	4496.00	2:	***.06 V*** **1** (***110***); .99 *Fe* 1 (825)
4496.18	96.19	6	.15 *Ti* 1 (146); .24 *Ti* 1 (8)
96.54	96.52	0	.43 *Pr* II (4, 25)
96.89	96.91	7	***.86 Cr*** **1** (***10***); .86 *V* 1 (86); .96 *Zr* II (40)
4497.30	4497.29	1	
97.68	97.66	5	***.71 Ti*** **1** (***184***); .66 *Na* 1 (15)
	97.89		
4498.27	4498.24	0	.28 *Gd* II (31)?; .30 *TiO*
98.72	98.67	2	.73 *Cr* 1 (81)
98.88	98.88	4	.90 *Mn* 1 (22)
4499.15	4499.14	2	.14 Sun; .12 β
99.44	99.46	1	.48 *Sm* II (23)
99.89	99.80	0	
	4500.06		.06 *TiO*
4500.30	00.30	4	.30 *Cr* 1 (150)
4500.65	4500.66	2	.64 Sun; .58+.75 *TiO*
	00.87:		.90 *TiO*
4501.09		1:-	.11 *Cr* 1 (81)
01.26	4501.26	7	.27 *Ti* II (31)
01.77	01.77r	4	***.79 Cr*** **1** (***81***); .69 *Ni* 1 (115); .81 *Nd* II (53)
01.96		1	.97 *V* 1 (62)
4502.22	4502.22	4	.22 ***Mn*** **1** (22)
02.60	02.60	3	.59 *Fe* 1 (796)—
	02.94		.85 *TiO*?
4503.22	4503.28d?	1w	.19 *TiO*
03.78	03.78	4	.76 *Ti* 1 (184)
4504.23	4504.23	1w	.20 *TiO*
	04.49		.43 *TiO*
04.81	04.81	5	.84 *Fe* 1 (555)
4505.1	4505.2		
05.4	05.5		
05.74	05.75	2	.72 *Ti* 1 (184)
4506.02	4506.00	0	.95 *V* 1 (14)
06.30	06.31	2	.30 *Ni* 1 (133)
06.72d	06.65r	4w	***.62 Ca*** **1** (***24***); .74 *Ti* IIp (30)
4507.15	4507.16	3:	.11 *Zr* 1 (31)
07.41	07.41	2:	.42 *Ca* 1 (24)
07.80	07.98d	3w	.85 *Ca* 1 (24)
4508.02			***.95 Cr*** **1** (***267***); .08 *Ce* II (153)?
08.28	4508.29	4	.28 *Fe* II (38)
08.71	08.71	2	.69 Sun; .70 β
4509.35d	4509.33	4w	***.31 Fe*** **1** (***514, 937***); .29 *V* 1 (110); .45 *Ca* 1 (24)
09.73	09.74	3	.74 *Ti* (M)
4510.11	4510.14d	2w	.10 *Ru* 1 (M); .16 *Pr* II (20)
	10.59		.52 *TiO*
10.84	10.84	2	.82 *Fe* IIp (823)—
4511.13	4511.11	3	.18 *Ti* 1 (u)
11.5	11.6	0	.56 Sun; .63 *TiO*
11.86	11.87	5	***.90 Cr*** **1** (***150***); .83 *Sm* II (14)
4512.27	4512.27	2	.28 *Ca* 1 (24)
12.72	12.73	6	.73 *Ti* 1 (42)

TABLE 6—*Continued*

α Ser	α UMa	Int.	Identifications
4513.00	4513.00	0	.00 *Ni* I (163)
13.39	13.37	2w	.44 Sun
13.67	13.70	2	.72 *Ti* I (112)
4514.19	4514.19	4	***.19 V*** I (***110***); .19 *Fe* I (514)
14.44	14.45	5	.43 Sun; .53 *Cr* I (95)?; .37 *Cr* I (287)?
14.78	14.82	1	.89 *TiO*?
4515.16	4515.15	2	***.09 Sm*** II (***u***); .17 *Fe* Ip (319)
15.37	15.36	4	***.34 Fe*** II (***37***); .44 *Cr* I (126)
15.90	15.90	1	.81 *TiO*?
4516.30	4516.31	3	.27 *Fe* Ip (819); .33 *TiO*
16.67	16.67:	1	.66 Sun; .65 *TiO*
	16.9		.81 *TiO*?
4517.12	4517.11	3	.09 *Co* I (150); .10 *TiO*
17.55	17.53	5	***.53 Fe*** I (***472***); .60 *Pr* II (2)
4518.02	4518.02	5	.02 *Ti* I (42)
18.37	18.37	3	.45 *Fe* I (593)
18.62	18.63	4	***.70 Ti*** I (***112***); .58 *Fe* Ip (69); .63 *Cr* I (34, 100)
4519.31	4519.30	0	.4 *TiO*
19.60	19.61	1	.63 *Sm* II (49)
19.97	19.99	3	***.99 Ni*** I (***51***); .07 *Gd* II (82)?
4520.20	4520.21	3	***.22 Fe*** II (***37***); .24 *Fe* Ip (471)
20.54	20.51	1	.49 *TiO*
20.80		0	.75 *TiO*
4521.11	4521.09	1	.14 *Cr* I (277, 287)
	21.62		.65 *Fe* Ip (641)
4522.01	21.98	1w	***.00 Cr*** I (***173***); .92 *Ni* I (116)
	4522.39		.37 *La* II (8, 74)
22.58	22.59	5	.59 *Eu* II (4); .63 *Fe* II (38)
22.77	22.78	5	.80 *Ti* I (42)
4523.07	4523.07	2	***.08 Ce*** II (***2***); .04 *Sm* II (3)
23.40	23.41	2	.40 *Fe* I (829)
	23.6		.53 *TiO*?
23.92	23.92	2	.91 *Sm* II (41)
4524.20	4524.21	1	.22 *V* I (99)
24.71	24.69	2	.73 *Ti* II (60)
24.95	24.93	1	.93 *Ba* II (3)?; .90 *TiO*
4525.16	4525.16	6	***.14 Fe*** I (***826***); ***.17 V*** I (***110***); .15 *Fe* I (819)
25.52	25.60	0	
25.87	25.86	3	.88 *Fe* I (319)
4526.10	4526.12	1	.11 *Cr* I (196)
26.47	26.47	8	***.47 Cr*** I (***33***); .37 *Ti* I (127, 184); .56 *Fe* I (471)
26.91	26.91	5	.94 *Ca* I (36)
4527.35	4527.35	7	***.30 Ti*** I (***42***); .34 *Cr* I (33, 82) Rem
27.81	27.81	3	***.80 Fe*** I (***641***); .80 *V* I (14)
4528.2	4528.22	0:	.26 *TiO*
28.61	28.62	15	.62 *Fe* I (68)
	4529.12:		.22 *TiO*?
4529.57	29.58	8	.56 *Fe* I (987)—
29.83	29.85	2:	.85 *Cr* I (33)
4530.2	4530.4 d?		.33 *TiO*
30.72	30.72	4:	***.76 Cr*** I (***33***); .69 *Cr* I (33)
30.92		2:	.95 *Co* I (150)
4531.13	4531.12	8	.15 *Fe* I (39)
31.62	31.62	4	.63 *Fe* I (555, 847, 992)
4532.23:w	4532.20	1	.19 *V* II (212)?; .10+.31 *TiO*
32.65:	32.65:	0	.58+.75 *TiO*
32.99	32.98	3:	.97 Sun; .98 β
4533.22	4533.23	6	***.24 Ti*** I (***42***); .14 *Fe* I (641)
33.54:	33.54:		
33.98r	33.98r	6	***.97 Ti*** II (***50***); .98 *Co* I (150); .15 *Pr* II (20); .17 *Fe* II (37)
4534.77	4534.77	6	.78 *Ti* I (42)
4535.15	4535.15	2	.15 *Cr* I (33)
35.64	35.63	10	***.57 Ti*** I (***42***); .72 *Cr* I (33)
35.95	35.96	11	***.92 Ti*** I (***42***); .92 *Pr* II (1); .05 *Ti* I (42)
4536.49	4536.49	2	***.51 Fe*** I (***896***); .55 *Cr* I (190)
4537.18	4537.13	1	.16 *TiO*
37.4			
37.69	37.68	3	***.68 Fe*** I (***594***); .66 *V* I (82)
4538.17	37.95	1w	.95 *Sm* II (45)
	4538.26		.25 *TiO*

TABLE 6—*Continued*

α Ser	α UMa	Int.	Identifications	α Ser	α UMa	Int.	Identifications
4538.77v	4538.78v	5	***.76 Fe*** **I** (***115***); .84 *Fe* I (969)	4553.08	4553.10	3w	***.01 Zr*** **I** (***31***); .18 *Ni* I (135)
4539.23	4539.09	1w	.10 *Ti* I (u)	53.46	53.44	1	.48 *Fe* IIp (472); .40 *TiO*
	39.30		.32 *TiO*		53.70		.69 *Ta* (M)?
39.75	39.74	4	***.79 Cr*** **I** (***33***); .76 *Ce* II (108)	4554.03	4554.03	8	.03 *Ba* II (1)
	4540.2		.18 *TiO*	54.48	54.47	4	***.47 Fe*** **I** (***319***); .51 *Ru* I (5)
4540.48	40.48	4	***.50 Cr*** **I** (***33***); .48 *Ti* I (8)	54.82:	54.83:	1:	.83 *Cr* I (173)
40.74	40.73	4	.72 *Cr* I (150)	4555.03	4555.02	3	***.02 Cr*** **II** (***44***); ***.07 Ti*** **I** (***266***); .09 *Cr* I (149)
4541.07	4541.05	3	.07 *Cr* I (33)				
41.32	41.29	1	.27 *Nd* II (58)	55.49	55.48	4	***.49 Ti*** **I** (***42***); .42 *Cs* I (2)?
41.57	41.51	2	***.52 Fe*** **II** (***38***); .51 *Cr* I (149)	55.88	55.88	2	.89 *Fe* II (37)
41.94	41.96	1	.95 *Fe* I (593)	4556.12	4556.12	1	***.13 Fe*** **I** (***410, 820, 974***); .17 *Cr* I (173)
4542.20	4542.18	0	.22 *Zr* I (49)				
42.45	42.42	2	.42 *Fe* I (894)		56.6	0	
42.64	42.64	3	***.62 Cr*** **I** (***149, 275***); .60 *Nd* II (u)	56.93	56.91	3	.94 *Fe* I (638)
4543.19d	4543.22d?	1w	.22 *Fe* Ip (893)?; .18 *TiO*	4557.28	4557.31	3	.24 *Sc* I (u)?
43.80	43.78	3	.74 *Cr* I (100); .81 *Co* I (142)	57.57	57.5	0	
43.99	43.98	2	***.01 Ti*** **II** (***60***); .95 *Sm* II (32)	57.80	57.77	2	.86 *Ti* I (270)
4544.65	4544.65	7	***.69 Ti*** **I** (***42***); .62 *Cr* I (33)	4558.13	4558.12	3	***.11 Fe*** **I** (***894, 974***); .08 *Gd* II (44); .09 *Ti* I (262, 263)
4545.15	4545.14	3	.14 *Ti* II (30)				
45.34	45.35	3	***.34 Cr*** **I** (***33***); .39 *V* I (109)	58.66	58.61	3	.66 *Cr* II (44)
45.96	45.95	6	***.96 Cr*** **I** (***10***); .98 *Co* I (142)	4559.3 d?	4559.11	1w	.28 *La* II (53)
4546.52d?	4546.53	0	.49 *W* (M)		59.40		
46.99	46.99	5	.02 *Fe* I (39)—	4560.00	4560.01	6	***.10 Fe*** **I** (***823***); .92 *Ti* I (112); .94 *Ni* I (115)
4547.23	4547.22	2:	.23 *Ni* I (146)				
47.84	47.84	4	***.85 Fe*** **I** (***755***); .85 *Ti* I (270)	60.31	60.29	1	.28 *Ce* II (8)
4548.17	4548.14	1	.09 *Ti* I (270); *TiO* α (7, 3)Rc Head	60.76d?	60.88	3w	.71 *V* I (109)
48.76	48.76	4	.76 *Ti* I (42)	4561.14:	4561.16	1	.20 *Cr* I (34)
	4549.25	1:	.24 *TiO*	61.42	61.42	2	.40 *TiO*
4549.62	49.62	11	***.62 Ti*** **II** (***80***); .47 *Fe* II (38); .66 *Co* I (150)	61.80	61.84	0	.84 *Tm* (M)?
				4562.33	4562.36	2	.36 *Ce* II (1)
4550.12	4550.16	1	.12 Sun; .09 *TiO*	62.63	62.62	3	.64 *Ti* I (7)
50.45:	50.40	0	.41 *Os* (M)?	62.91:	62.96:	0	.99 *TiO*
50.77	50.77	4	***.80 Fe*** (***M***); .74 *TiO*	4563.32	4563.30d	3w	.24 *Cr* I (246); .43 *Ti* I (266)
4551.25	4551.24	3	***.24 Ni*** **I** (***236***); .23 *TiO*	63.75	63.77	8	.76 *Ti* II (50)
	51.42			4564.19	4564.17	1	.22 *Ti* I (112)
51.66	51.65	3	***.67 Fe*** **I** (***972***); .62 *TiO*	64.72	64.74	5w	***.83 Fe*** **I** (***472***); .72 *Fe* I (823)
4552.18	4552.25	2:	.25 *Ti* IIp (30)	4565.54v	4565.53v	13	***.51 Cr*** **I** (***21***); .58 *Co* I (150); .68 *Fe* I (554)
52.48	52.46	8	.45 *Ti* I (42)—				

TABLE 6—*Continued*

α Ser	α UMa	Int.	Identifications
4566.21	4566.23	1	.21 *Sm* II (32)
66.53	66.52	3	***.52 Fe* I (*641*)**; .60 *Cr* I (125)
66.91	66.91	4	.99 *Fe* I (723)
	4567.39		.42 *Ni* I (102)
4567.6	67.68	1w	.90 *La* I (11)
67.9			
4568.34	4568.33	2	.31 *Ti* II (60)
68.78	68.78	5	***.79 Fe* I (*554*)**; .84 *Fe* I (894)
	4569.2 d?		*TiO*?
4569.57	69.57	4	.53 *Cr* I (173); .64 *Cr* I (173)
4570.00	4570.02	1	***.02 La* I (*11*)**; .24 *Co* I (178)
70.39	70.43	1	***.42 V* I (*109*)**; .30 *Cr* I (125, 190)
4571.07	4571.08	9	***.10 Mg* I (*1*)**; .98 *Cr* I (173); .10 *Cr* I (125)
71.44	71.42	1	.44 *Fe* Ip (319)
71.70	71.72	3	***.68 Cr* I (*32*)**; .78 *V* I (109)
71.95	71.97	6	.97 *Ti* II (82)
4572.28	4572.27	1	.28 *Ce* II (1)
72.83	72.84	2	.86 *Fe* Ip (819)
	4573.38:	0	.34 *TiO*
4574.20	4574.21	3	.24 *Fe* I (554); .22 *TiO*
	74.49		.45 *Cr* I (148)
74.75	74.78	5	***.72 Fe* I (*115*)**; .87 *La* II (23)?
4575.03	4575.08	1:	.12 *Cr* I (196)
75.50	75.51	3	.52 *Zr* I (5)
75.79	75.79	2	.80 *Fe* I (593, 970)
4576.34	4576.36	3	.33 *Fe* II (38)
76.56		0	.55 *Ti* I (262)
	76.67:		.76 *Cr* I (148)
4577.17	4577.16	6	.17 *V* I (4)
77.66	77.71	1	.69 *Sm* II (23)
4578.05	4578.00	2	.04 *Mn* (M)
78.59	78.58	5w	***.56 Ca* I (*23*)**; .73 *V* I (109)?
4579.05	4579.01	2	
79.31	79.32	2	***.34 Fe* I (*319, 936*)**; .20 *V* I (109)
79.77	79.81	2:	.82 *Fe* I (469)
4580.06	4580.07	6	***.06 Cr* I (*10*)**; .05 *La* II (53); .14 *Co* I (27)
4580.44d?	4580.44	5w	***.39 V* I (*4*)**; .46 *Ti* II (60)
	80.60		.60 *Fe* I (827); .62 *Ni* I (146)
4581.12	4581.12	0	.06 *Cr* I (148)
81.48	81.48	10	***.40 Ca* I (*23*)**; ***.52 Fe* I (*555*)**; .38 *Co* I (156); .60 *Co* I (150)
81.99:			.99 *TiO*?
4582.36	4582.44	2w	.38 *Gd* II (82)
82.88	82.86r	2	***.84 Fe* II (*37*)**; .94 *Fe* I (348)
4583.16	4583.18	1	.12 Sun; .12 β; .17 *Ta* (M)?
83.40	83.41	2	.44 *Ti* II (39)
83.81r	83.83	5	***.83 Fe* II (*38*)**; .78 *V* I (109); .89 *Cr* I (125)
	4584.03	1:	.10 *Cr* I (172)?; *TiO* α (3, 0)Ra Head
4584.4	84.37	0	.44 *Ru* I (6)?; *TiO* α (3, 0)Rb Head
84.78	84.78	5	***.82 Fe* I (*822*)**; .73 *Fe* I (820); .75 *Cr* I (125)
4585.33	4585.34	1	.35 Sun; .29 *TiO*
85.90	85.93	8	.87 *Ca* I (23); .92 *Ca* I (23)
4586.30	4586.32	7	.36 *V* I (4)
4587.07	4587.09v	5	***.13 Fe* I (*795*)**; .99 *Cr* I (u); *TiO* α (3, 0)Rc Head
87.70	87.74	2	.72 *Fe* Ip (971)?; .86 *Cr* I (125)?; .70 *TiO*
4588.16	4588.22	2	.22 *Cr* II (44)
88.70	88.70	3	.73 *Co* I (15)
4589.30d?	4589.32	1	.37 *Dy* I?; *TiO* α (8, 4)Ra Head?
89.95	89.95	4	.96 *Ti* II (50)
	4590.52:		.55 *Zr* (M)
4590.75	90.78	3	—.69 *Cr* I (125); .84 *TiO*
	4591.11:d		.12 β
4591.41	91.42	7	.39 *Cr* I (21)
4592.01	4592.04	1	.09 *Cr* II (44)
92.60	92.61	8	***.66 Fe* I (*39*)**; .53 *Ni* I (98)
4593.18	4593.15	0	.20 *Cs* I (2)?
93.53	93.51	2	.54 *Fe* I (971); .54 *Sm* II (36)
93.85	93.92	1:	.84 *Cr* I (190); .93 *Ce* II (6)
4594.09	4594.10	6	.10 *V* I (4)
94.58	94.59	1	.63 *Co* I (176)

TABLE 6—*Continued*

α Ser	α UMa	Int.	Identifications
4594.91	4594.92	2	***.96 Fe* I (*638*)**; .91 *Ni* I (u)
4595.35	4595.34	5	***.36 Fe* I (*594*)**; .29 *Sm* II (45)
95.64	95.65	1:	.59 *Cr* I (286)?; .62 *TiO*
4596.00	4596.02	6	***.06 Fe* I (*820*)**; .95 *Ni* I (101)
96.44	96.45	2	.38 *Fe* I (823)
96.94	96.96	3	.90 *Co* I (177); .98 *Gd* II (44); .98 *TiO*
4597.29	4597.26d?	2	.26 Sun; .20+.37 *TiO*
97.80	97.82	4	—.91 *Gd* II (44); .87 *TiO*
4598.12	4598.14	4	.12 *Fe* I (544)
98.36	98.37	3	.33 *Fe* Ip (17)
98.76	98.71	1	.74 *Fe* Ip (819)
	98.92:		.00 *Cr* I (171)?; .97 *TiO*
4599.22d	4599.23	1	.23 *Ti* I (u)
99.81	99.81	3	.84 *Fe*? (Sun)
4600.14	4600.22d?	6w	.10 *Cr* I (32)
00.34			***.37 Ni* I (*98*)**; .28 *Ti* IIp (60)
00.78	00.79	10w	.75 *Cr* I (21)
4601.00	4601.00		***.94 Fe* I (*591*)**; .02 *Cr* I (32); .05 *Gd* II (44)
01.50	01.42	1	.55 *TiO*
4602.00	4602.00	4	.00 *Fe* I (39)
02.6	02.50	0	.51 *Cr* I (210)?; .57 *Zr* I (M)?
02.94	02.94	8	.94 *Fe* I (39)
4603.32	4603.35	2	.34 *Fe* Ip (348); .33 *TiO*
03.89	03.89	2	.96 *Fe* I (410); .90 *TiO*
4604.20	4604.22	1	.23 *Fe* Ip (348)
04.56	04.54	2	***.58 Cr* I (*190*)**; .42 *Zr* I (29)?
04.99	04.98	5	.99 *Ni* I (98)
4605.49d	4605.55d?	5w	.60 Sun; .40+.61 *TiO*
05.82	05.81	0	.87 *TiO*
4606.17	4606.14r	5	.15 *V* I (4)
	06.56	1	.51 *Sm* II (1)
06.81	06.91		
4607.31	4607.34	3	.33 *Sr* I (2)
07.63	07.64	4	.66 *Fe* I (554, 969)
	07.98		
4608.2	4608.24	0	.26 *TiO*
4608.71:	4608.69	1	.71 *Mo* (M)?
4609.29	4609.30	2	.26 *Ti* IIp (39)?
	09.63:		.65 *V* I (61)?; .62 *TiO*
09.92	09.91	2	.90 *TiO*
4610.26	4610.23	1	.19 Sun
4611.24	4611.24	11	—***.28 Fe* I (*826*)**; .19 *Fe* Ip (319); .29 *Fe* Ip (819)
	11.65		.72 *TiO*
11.97	4612.02	2w	.97 *Cr* I (u)
	12.31		.27 *Dy* I?; .26 *TiO*
4612.57	12.56	2w	—.64 *Fe* Ip (349)
12.92	12.9		
4613.29	4613.29	8	.21 *Fe* I (554); .37 *Cr* I (21)
	13.64		.68 *TiO*
13.92	13.93	2	.95 *Zr* II (67)?; .92 *TiO*
4614.20	4614.19	3	***.22 Fe* I (*638*)**; .15 *Cr* I (148)
14.61	14.60	1	.52 *Cr* I (245)
4615.07:	14.93	0	.98 *TiO*
15.59	4615.59	4	***.69 Sm* II (*22*)**; .44 *Sm* II (49)
4616.12	4616.13	7	.14 *Cr* I (21)
16.64	16.65	3	—.64 *Cr* II (44); .57 *TiO*
4617.28	4617.26	5	.27 *Ti* I (145)
	17.61		
17.92	17.90	2	.94 *Ni* I (115); .87 *TiO*
4618.3	4618.24	1	.23 *TiO*
18.78	18.77	5	***.76 Fe* I (*409*)**; ***.83 Cr* II (*44*)**; .80 *V* I (39)
4619.30	4619.31	5	***.29 Fe* I (*821*)**; .33 *Co* I (27)
19.53	19.75d?	7w	.52 *Ti* I (261); .55 *Cr* I (81)
19.76			***.77 V* I (*4*)**; .65 *V* I (u)
			ZrO α (0, 0)Rc Head
4620.12	4620.13	0	
20.49	20.49	3	***.51 Fe* II (*38*)**; .38 *Ni* I (163)
4621.07:	4621.13	0	.00 *Cr* I (32)
21.51:	21.49	1	
21.91	21.91	7	.89 *Cr* I (32); .96 *Cr* I (32)
	4622.19:		.19 *TiO*
4622.48	22.49	4	.49 *Cr* I (233)

TABLE 6—*Continued*

α Ser	α UMa	Int.	Identifications
4622.76	4622.77	2	.76 *Cr* I (81)
4623.06	4623.08	6	***.10 Ti*** **I** ***(145)***; .02 *Co* I (156)
23.60	23.58	2	.54 *TiO*
4624.04	4624.08	1	.99 *TiO*?
24.44	24.43	3	.40 *V* I (39)
4625.04	4625.03	8	—.05 *Fe* I (554)
25.39	25.41	0	.30 *Cr* I (171); .38 *Mn* (M)
25.79	25.87	1	***.77 Co*** **I** ***(176)***; .92 *Cr* I (244)?
4626.17	4626.18	7	***.19 Cr*** **I** ***(21)***; *TiO* α (4, 1)Ra Head
26.50	26.54	4	***.48 V*** **I** ***(39)***; *TiO* α (4, 1)Rb Head
26.80	26.84	1	.76 *Fe* I (410)—
	4627.08		.02 *Fe* Ip (637)?
4627.49w	27.52v	5w	.37 Sun; .55 Sun; .53 *TiO*
4628.18	4628.16	2	.16 *Ce* II (1)
28.50:	28.5	1	.47 *Cr* I (186)
28.90	28.87	2	***.91 Co*** **I** ***(15)***; .75 *Pr* II (1)?
4629.36	4629.35	7	***.34 Fe*** **II** ***(37)***; ***.34 Ti*** **I** ***(145)***; .36 *Co* I (156)
	29.80		.81 *Zn* I (M)?
4630.12	4630.12	6	.12 *Fe* I (115)
30.54	30.61	1	.57 Sun; .63 *TiO*?
4631.05	4631.01	2	.04 *Fe* (Sun); .11 *TiO*?
31.50	31.51	1	.49 *Fe* I (1152); .43 *TiO*?
	31.83		.86 *TiO*
4632.11	4632.16	2	.18 *Cr* I (171)
32.91	32.90	10	***.92 Fe*** **I** ***(39)***; .83 *Fe* Ip (820)—
4633.26	4633.25	2:	.29 *Cr* I (186)
33.75	33.74	4	—.76 *Fe* I (410); .72 *TiO*
4634.06	4634.05	5	***.99 Zr*** **I** ***(5)***; .11 *Cr* II (44)
	34.37		
34.74	34.73	4	.74 *Ti* (M)?; .72 *Fe*? (Sun)
4635.18	4635.19	4	.18 *V* I (4)
35.58	35.58	4	.54 *Ti* I (261); .62 *Fe* Ip (319)
35.84	35.84	4	.85 *Fe* I (349)
4636.31	4636.34	3	.34 *Ti* II (38)
36.68	36.71	2	.66 *Fe* Ip (513)
4637.15	4637.17	4	***.18 Cr*** **I** ***(32)***; .21 *Ti* I (261)
37.51	37.52	6	.51 *Fe* I (554)—
4637.90d	4637.92d?	10	***.77 Cr*** **I** ***(32)***; .89 *Ti* I (261); .02 *Fe* I (822); *ZrO* α (0, 0)Rb Head
4638.57	4638.68	1	.68 *TiO*
38.90:	38.97	1	.01 *TiO*
4639.39	4639.39	5	.37 *Ti* I (145)
39.63	39.64	5	***.67 Ti*** **I** ***(145)***; .54 *Cr* I (186)
39.99	39.97	6	.94 *Ti* I (145); .06 *V* I (39)
4640.36d?	4640.31	4	.31 *V* I (94)
	40.48		***.43 Ti*** **I** ***(261)***; *ZrO* α (0, 0)Rc Head
40.79	40.88	4	***—.74 V*** **I** ***(39)***; .80 *Co* I (M)?
4641.27	4641.28	5	—.22 *Fe* Ip (347)
4642.14d?	41.64:	3w	.67 *TiO*
	4642.25		.24 *Sm* II (36)
42.60	42.72	2w	.70 *Mo* (M)?; .60 *TiO*
4643.21	4643.18	2	.20 *Fe* Ip (38)
43.48	43.48	5	.47 *Fe* I (820)
43.75	43.77	2:	.69 *Y* I (4)
4644.42	4644.38d?	2w	.43 *TiO*
44.79			.82 *Zr* I (64)?; *ZrO* α (1, 1)Rc Head
4645.18	4645.22	6	***.19 Ti*** **I** ***(145)***; .26 *Tb* II?
45.46	45.46:	1:	.50 Sun; .42 *TiO*
45.74:	45.75	0:	.76 *Nd* (M)?; .76 *TiO*
4646.16	4646.17	8	.17 *Cr* I (21)
46.44	46.41	5:	***.40 V*** **I** ***(39)***; .50 *Cr* I (147)
46.72	46.70	5	***.68 Sm*** **II** ***(26)***; .81 *Cr* I (186)—
4647.12	4647.21:	1:	.23 *Tb* (M)
47.41	47.42	9	.44 *Fe* I (409)
4648.00	4648.02	7w	***—.13 Cr*** **I** ***(132)***; .16 *Sm* II (1); .99 *TiO*
48.67	48.70	5	.66 *Ni* I (98)
48.90	48.94	5	***.87 Cr*** **I** ***(32)***; .93 *Fe* II (25)
4649.48	4649.47	4:	.46 *Cr* I (32)
49.75	49.74:	3:	.83 *Fe* I (592); .78 *TiO*
4650.03	49.96	4:	.02 *Ti* I (145)
50.31:	4650.27	1:	.32 Sun; .33 *La* I (M)
	50.63:		
4651.29	4651.30	8	.28 *Cr* I (21)
51.73	51.71	0	.75 *TiO*

TABLE 6—*Continued*

α Ser	α UMa	Int.	Identifications
4652.17	4652.18	8	.16 *Cr* I (21)
52.73:	52.87:	0	*TiO*
	4653.19		
4653.45	53.46	5	—.49 *Fe* Ip (17)
53.87:	53.84	0	.83 *TiO*
4654.15	4654.15	2	.16 Sun
54.58	54.57	11	***.50 Fe* I (*39*)**; ***.63 Fe* I (*554, 821*)**; .74 *Cr* I (186)
4655.27	4655.20	2	.19 *TiO*
	55.45		.49 *La* II (75)
55.72	55.70	5	***.66 Ni* I (*115*)**; ***.71 Ti* I (*261*)**; .75 *Ti* IIp (38)?
4656.09	4656.13	5	***.05 Ti* I (*145*)**; .19 *Cr* I (147)
56.49	56.48	7	.47 *Ti* I (6)
	56.94		.97 *Fe* II (43); .95 *TiO*
4657.24	4657.21	4	.21 *Ti* II (59)
57.58	57.62	3	.60 *Fe* I (346)
	4658.08		.09 *Pr* (M)?
4658.28	58.30	3	.29 *Fe* I (591)
58.87:	58.90	1w	.89 *Yt* I (M)?
4659.47	4659.45	1	.54 Sun; .48 *TiO*
59.9	59.90	1	.89 *TiO*
	4660.21		.24 *TiO*
4660.44	60.45	2	.43 Sun
60.89	60.91	2	.91 Sun; .93 *TiO*
4661.28		1	.33 *Fe* Ip (347)
61.51	4661.51v	2	.54 *Fe* I (1207)
4662.00	4662.00	6	.98 *Fe* I (409)—
	62.55	3w	.51 *La* II (8)
62.73d	62.77		—.71 *Ti* IIp (38); .74 *Ti* IIp (38)
4663.32	4663.34	9	***.33 Cr* I (*186*)**; .40 *Co* I (156)
63.84	63.84	6	.83 *Cr* I (186)
4664.37	4664.35:	0	*TiO*?
64.79	64.80	6	***.80 Cr* I (*186*)**; .81 *Na* I (12)
4665.22	4665.23	1	.24 *Fe* Ip (1115)?
65.57	65.56	0	.56 *Fe* Ip (1044)?
65.88	65.87	3	.90 *Cr* I (233)
4666.15	4666.18	4	***.22 Cr* I (*99*)**; .15 *V* I (94)
66.53	66.61d?	4	***.51 Cr* I (*186*)**; .75 *Fe* II (37)
4666.96	4666.95	3:	.99 *Ni* I (146)
4667.28	4667.27	1:	.18 *Cr* I (99)
67.57	67.55	10	.58 *Ti* I (6) Rem
4668.15	4668.15	7	.14 *Fe* I (554)
68.57	68.57	5	.56 *Na* I (12); *TiO* α (5, 2)Ra Head; C_2 (6, 5) Head
4669.26	4669.29	8	***.17 Fe* I (*821*)**; ***.34 Cr* I (*186*)**; .27 *V* I (4); .40 *Sm* II (7)
69.63	69.65	2	***.65 Sm* II (*26*)**; .67 *Cr* I (170)
4670.13	4670.20	1	.17 *Fe* II (25)
70.46	70.45	7	***.48 V* I (*39*)**; .40 *Sc* II (24)
70.96	4671.02	0	*TiO* α (5, 2)Rc Head
4671.40	71.44	2	.42 Sun; .40 *TiO*
71.68	71.75	2	.69 *Mn* I (21)
4672.0	4672.0	0	.08 *Pr* II (21)
72.32	72.34	3	***.34 Sun;*** .38 *TiO*
	72.61		.51 *TiO*?
72.84	72.84	3	.83 *Fe* Ip (40)
4673.20	4673.22	7	***.17 Fe* I (*820*)**; .28 *Fe* Ip (822)?
73.73	73.75	1w	.74 *TiO*
4674.16	4674.22	4	.10 Sun; .15+.26 *TiO*
74.70	74.69	7	.60 *Sm* II (14); .65 *Fe* Ip (40); .84 *Y* I (4)
4675.14	4675.13	4	.12 *Ti* I (77)—
75.61	75.65	2	.64 *Ni* I (115)
75.9	75.94	0	.89 *TiO*
4676.28	4676.30	2w	.37 *TiO*
76.88	76.93	2	.91 *Sm* II (3)
	4677.38		
4677.54	77.61	4	***.53 Co* I (*15*)**; .54 *TiO*
4678.15	4678.18	4	.18 Sun; .14 β
78.49	78.50	1:	.60 *TiO*?; C_2 (5, 4) Head
78.86	78.88	6	.85 *Fe* I (821)
4679.20	4679.22	4	.23 *Fe* I (688)
	79.56	0:	
	4680.03	0:	.91+.09 *TiO*
4680.39d	80.28	9	.30 *Fe* I (39)
	80.50		.48 *Fe* I (346); .49 *Cr* I (186)
80.87	80.85	5	***.87 Cr* I (*170*)**; .80 *TiO*

TABLE 6—*Continued*

α Ser	α UMa	Int.	Identifications
4681.43	4681.45	4	***.48 Fe* (*Sun*)**; .36 *TiO*
81.94	81.95	8	.91 *Ti* I (6)
4682.37	4682.31	4:	***.32 Y* II (*12*)**; .36 *Co* I (156)
	82.53		.58 *Fe* I (384)
	4683.09:		.07 *Gd* (M)?
4683.55	83.56	6	.56 *Fe* I (346)
	4684.04		.01 *TiO*
4684.21	84.27	2:	.25 *TiO*
84.58	84.57	3	.46 *V* I (94); .48 *Ti* I (203); .60 *Cr* I (146)
84.97	4685.19	3	.03 *Fe* Ip (347); .96 *TiO*; C_2 (4, 3) Head
4685.26		3	.26 *Ca* I (51)
85.89	85.86	2	.84 *Ge* I (3)?
4686.21	4686.22	5	—.22 *Ni* I (98)
86.89	86.86	2	***.93 V* I (*93*)**; .92 *Ti* I (203)
4687.33	4687.32	7	***.39 Fe* I (*347*)**; .30 *Fe* Ip (17); .18 *Sm* II (3)
87.76	87.81	4	.80 *Zr* I (43)
4688.18	4688.17	1:	***.19 Fe* (*Sun*)**; .14 *TiO*
88.48	88.45	6	.45 *Zr* I (5)
	4689.00	1:	.98 *TiO*
4689.41	89.44	5	.37 *Cr* I (186)
89.81			.78 *Yt* I (M)?
4690.17	4690.16	4	.15 *Fe* I (820)
90.43	90.43	3	.38 *Fe* Ip (17)—
90.79	90.79	4	.83 *Ti* I (76)
4691.40	4691.39	9	***.41 Fe* I (*409*)**; .34*Ti* I (75)
4692.03	4692.07	1	.99 *TiO*
92.59	92.61	5	—.50 *La* II (75); .64 *TiO*
4693.18	4693.18	3	.19 *Co* I (156)
93.67	93.66	5	***.67 Ti* I (*6*)**; .63 *Sm* II (14)
93.97	4694.00	3	.95 *Cr* I (99)
4694.4	94.3	1:	.34 *Gd* (M)
94.83	94.88	5	.87 *Fe* (Sun); .85 *TiO*
4695.10	4695.13	2:	.15 *Cr* I (99)
	95.40		.45 Sun; .50 *TiO*
95.80:	95.82	1w	.77 *Pr* (M)
4696.22:	4696.36:	0w	.38 *TiO*?
4697.01	4697.04r	5	***.06 Cr* I (*62*)**; .92 *Ti* I (203)
97.46		2:	.40 *Cr* I (195)?; .39 *TiO*
	97.68		C_2 (3, 2) Head
	4698.06		
4698.44	98.39	18w	***.46 Cr* I (*186*)**; .39 *Co* I (156); .41 *Ni* I (235)
98.70	98.68		.62 *Cr* I (62, 146); .77 *Ti* I (75)
4699.32	4699.33	5	.34 Sun
99.66	99.62	1:	.72 *Hf* II (71)?; .61 *TiO*
4700.16	4700.15	4	.17 *Fe* I (935)
00.58	00.58	3	.61 *Cr* I (62)
4701.10	4701.10	5	***.05 Fe* I (*820*)**; .16 *Mn* I (21)
01.46	01.45	3	***.54 Ni* I (*235*)**; .34 *Ni* I (101)
01.88	01.92:	1	***.92 Cr* I (*170*)**; .90 *Fe* Ip (688)
4702.27			.24 *TiO*
02.62	4702.53	0	.62 *TiO*
4703.00	4703.00	9	.98+.99 *Mg* I (11)
03.50:			.58 *Nd* II (55)?
03.79	03.79d?	4	.81 *Ni* I (133)
4704.12			.16 *TiO*
04.45	4704.44	3	***.40 Sm* II (*1*)**; .39 *Co* I (178)
04.97	04.96	5	.96 *Fe* I (821)
4705.47	4705.47	5	***.46 Fe* I (*752*)**; .50 *Ni* I (101)
4706.10d?	05.84	3	.93 *Ni* I (128)
	4706.13		***.10 Cr* I (*170*)**; .18 *V* I (94)
06.57	06.56	3	***.54 Nd* II (*3*)**; .57 *V* I (119)
	06.98		.97 *Sc* I (22)?
4707.36	4707.36	9	***.28 Fe* I (*554*)**; .48 *Fe* I (346)
4708.01	4708.02	4	.04 *Cr* I (186)
08.66	08.66	3	.66 *Ti* II (49)
4709.04	4709.04	7	***.09 Fe* I (*821*)**; .97 *Fe* I (889); .98 *Ti* I (203)
09.70	09.69	5	.72 *Mn* I (21)
4710.21	4710.23	9	***.19 Ti* I (*75, 203*)**; ***.29 Fe* I (*409*)**; .08 *Zr* I (43); .24 *Cr* I (145)
10.94:	4711.00	0	.93 *TiO*
4711.53	11.51	3	.49 *Fe* (Sun); .50 *TiO*

TABLE 6—*Continued*

α Ser	α UMa	Int.	Identifications
4712.10	4712.12	5	***.10 Fe*** **I (*467*)**; .07 *Ni* I (131)
12.67	12.63	3w	.71 Sun; .73 *TiO*
4713.16	4713.10	2w	.06 *Sm* II (49)
	13.79		*TiO* α (6, 3)Rc Head
4714.12	4714.12	5:	***.18 Fe*** **I (*591*)**; .11 *V* I (119); .07 *Fe* I (1206)
14.42	14.42	8	.42 *Ni* I (98)
14.94	14.95	1	.90 *TiO*
4715.30	4715.31	4	.30 *Ti* I (6); C_2 (2, 1) Head
15.80	15.76	6	—.78 *Ni* I (98); .78 *TiO*
	4716.47		.49 *TiO*
4716.79:	16.86	0:	.85 *Fe* Ip (634)?; .85 *TiO*
	4717.16		.08 *TiO*?
4717.64	17.65	5	***.69 Cr*** **I (*170*)**; .69 *V* I (119); .72 *Sm* II (41)
4718.43	4718.43	5	***.43 Cr*** **I (*186*)**; .33 *Sm* II (53)
4719.14	4719.11	0	.12 *Zr* I (66)?
	19.57		.52 *Ti* II (59)
19.62d	19.86	3w	.84 *Sm* II (3)
	4720.10		.13 *Sm* II (M)?
4720.5	20.41	0	.46 *TiO*
4721.01	4721.01	5	***.00 Fe*** **I (*409*)**; .01 *TiO*
21.56	21.51	0	.52 *V* I (108)
4722.16	4722.16	4	***.16 Zn*** **I (*2*)**; .28 *Sr* I (5)?
22.64	22.62	4	.60 *Ti* I (75)
4723.13	4723.14	6	***.17 Ti*** **I (*75*)**; .06 *Cr* I (145)
23.81:	23.86	1	.88 *Ni* Ip (167)
4724.45	4724.43	4	.42 *Cr* I (145)
4725.0	4725.1		.09 *Ce* II (153)?
25.5	25.4		
	25.63:		.67 *Cr* I (195)?; .65 *TiO*
4726.09	4726.08	4	***.16 Fe*** **I (*384*)**; .95 *Cr* I (99)
	26.45		.39 *TiO*
	26.71		.75 *TiO*
4727.12	4727.05	2	.15 *Cr* I (99)
27.39	27.34	9	***.40 Fe*** **I (*821*)**; .48 *Mn* I (21)
27.93	27.94d	5	***.94 Co*** **I (*15*)**; .85 *Ni* I (146)
4728.52	4728.51	5	***.56 Fe*** **I (*822*)**; .42 *Ni* I (115)
4729.14d	4729.07	4w	.03 *Fe* I (1043a)
	29.36		***.23 Sc*** **I (*14*)**; .29 *Ni* I (235)
29.68	29.67	4	.70 *Fe* I (688); .72 *Cr* I (169)
4730.03	4730.04	4	.03 *Mg* I (10)
30.37:	30.42	0	.39 *V* I (108)
30.73	30.72	3	.71 *Cr* I (145)
4731.06	4731.04	4	—.17 *Ti* I (202)
31.48	31.49	3	***.44 Fe*** **II (*43*)**; .50 *TiO*
31.85	31.83	2	***.81 Ni*** **I (*163*)**; .77 *Fe* Ip (67); .85 *Dy* (M)?
	4732.12	0	.05 *Co* I (15)
4732.41	32.44	2	.46 *Ni* I (235) Rem
32.86:		0	
4733.56	4733.58	8	***.60 Fe*** **I (*38*)**; .43 *Ti* I (202)?
4734.10	4734.08	5	***.09 Sc*** **I (*14*)**; .10 *Fe* I (1133)
	34.48	2	.43 *Gd* II (43)?
34.65	34.78	1	***.83 Co*** **I (*156*)**; .68 *Ti* I (233)
4735.30	4735.24	0	
35.87	35.91	5	.85 *Fe* I (1042)
	4736.16		.13 *Cr* I (195)?
4736.78	36.84	8	.78 *Fe* I (554)
4737.35	4737.31	4	***.35 Cr*** **I (*145*)**; C_2 (1, 0) Head
37.68	37.63	5	***.63 Fe*** **I (*590*)**; ***.64 Sc*** **I (*14*)**; .77 *Co* I (57)
	4738.40d		
4739.08	4739.08	5	.11 *Mn* I (21)
39.49	39.49	3	***.48 Zr*** **I (*43*)**; .49 *Ce* II (157)
4740.33	4740.34	7	***.34 Fe*** **I (*409*)**; .27 *La* II (8)
4741.02	4741.05	6	.02 *Sc* I (14); .08 *Fe* I (688)
41.53	41.57	5	.53 *Fe* I (346)
4742.18	4742.13	3w	.13 *Ti* I (202)
	42.40		.32 *Ti* Ip (111)?
42.93	42.86	5	.79 *Ti* I (233)—
4743.36:	4743.25:	0	.24 *TiO*
43.82	43.80	3	.81 *Sc* I (14)
4744.38	4744.39	3:	***.39 Fe*** **(*Sun*)**; .40 *TiO*
44.78	44.74	2:	.85 *TiO*?
4745.22	4745.20d	4:	.13 *Fe* I (67); .31 *Cr* I (61)

TABLE 6—*Continued*

α Ser	α UMa	Int.	Identifications
4745.77	4745.78	5	***.81 Fe*** **I** (***821, 1068***); .68 *Sm* II (7)
4746.24	4746.37	1	
	46.95		.00 *Cr* I (168)?; .02 *TiO*
4747.19d?	4747.24	2	.26 *Ti* I (75)
47.65	47.57	0	.68 *Ti* I (233)
4748.06:	4748.09	6	***.14 Sun;*** .94 *Na* I (11)
48.60	48.63	1	.52 *V* I (113)
	4749.08:		.13 β
4749.3			.25 *Fe* IP (1098)?
49.64	49.67	6	.68 *Co* I (156)
49.96	49.99	2:	.93 *Fe* I (1206)—
	4750.52		.52 *TiO*
4751.05	4751.12	4	—.99 *V* I (113); .12 *TiO;* .10 *Fe* (Sun)
	51.54		.57 *V* I (94)
51.80	51.83	1	.82 *Na* I (11)
4752.12	4752.14	3	.12 *Ni* I (165)
52.44	52.46	4	.43 *Ni* I (132)
52.81			.87 *Cr* I (194)
4753.17	4753.10	2	.15 *Sc* I (5)
	53.45		
4754.02	4754.04	8	***.04 Mn*** **I** (***16***); .96 *V* I (113)
	54.40	0	.36 *Co* I (156); .38 *Ti* I (202)
54.74	54.74	4	***.74 Cr*** **I** (***168***); .77 *Ni* I (141)
4755.16	4755.18	1	.14 *Cr* I (124)
55.74	55.73	2	.76 *TiO*
4756.14	4756.05	3	***.11 Cr*** **I** (***145***); *TiO* α (7, 4)Ra Head
56.49	56.53	4	***.52 Ni*** **I** (***98***); *TiO* α (7, 4)Rb Head
4757.52	4757.58v	5	***.58 Fe*** **I** (***634, 1115***); .37 *V* I (113); .50 *V* I (113); .59 *Cr* I (231)
4758.13	4758.13	4	.12 *Ti* I (233)
	58.46		.50 *Mo* (M)
58.84	58.81	4	***.91 Ti*** **I** (***41***); .74 *V* I (51); *TiO* α (7, 4)Rc Head
4759.26	4759.27	3	.27 *Ti* I (233)
59.73	59.69	1:	***.74 Ti*** **I** (***202***); .74 *Cr* I (124)
4760.07	4760.09	3	***.07 Fe*** **IP** (***384***); .91 *Cr* I (169)
	60.49:		
	60.72		.75 *Gd* (M)?
4761.11	4761.06	3	.98 *V* I (4); .24 *Cr* I (169); *TiO* α (2, 0)Ra Head
61.51	61.51	4	***.53 Mn*** **I** (***21***); *TiO* α (2, 0) Head
4762.40	4762.39	6	.38 *Mn* I (21)
62.67	62.66	5	.63 *Ni* I (71)
4763.4	4763.39d	1	.30 *TiO*
63.89	63.90	5	***.95 Ni*** **I** (***146***); .86 *Nd* II (6); .84 *Ti* IIp (48)?
4764.32	4764.31	4w	***.29 Cr*** **I** (***231***); *TiO* α (2, 0)Rc Head
64.58	64.56		***.54 Ti*** **II** (***48***); .64 *Cr* I (124)
4765.45	4765.46	7	.48 *Fe* IP (40)
65.85	65.84	4	.86 *Mn* I (21)
4766.41	4766.44	7	***.43 Mn*** **I** (***21***); .33 *Ti* I (233)
66.78	66.78	5	—.63 *Cr* I (231); .64 *V* I (113); .84 *TiO*
4767.24	4767.26	2	.28 *Cr* I (231)
67.90	67.83	2	.86 *Cr* I (231)
4768.34	4768.35	5	***.40 Fe*** **I** (***384***); .33 *Fe* I (821)
68.69	68.73:	2	.70 Sun
4769.2	4769.36	0	.4 *TiO?*
69.82	69.79	4	.78 *Ti* I (233); .80 *Cr* I (283); .83 *TiO*
	4770.08		
4770.62	70.60	1	.67 *Cr* I (124)
4771.12	4771.11	4	***.10 Ti*** **I** (***41***); .11 *Co* I (156)
71.60	71.63	6	***.70 Fe*** **I** (***67***); .57 *Cr* I (124)
4772.30	4772.32	1	.32 *Zr* I (43)
72.81	72.85	7	***.82 Fe*** **I** (***38, 467***); .89 *Ni* I (162)
4773.42	4773.44	2	.41 *Ni* I (167)
73.92	73.98	1	.94 *Ce* II (17)?
4774.50	4774.52	1	.56 *Cr* I (124)
4775.12	4775.09	1w	.14 *Cr* I (230)
	75.47		.53 *Cr* I (283)?; .39 *TiO*
4776.00	4776.10	1:	.07 *Fe* I (635)
76.35	76.42	6	***.31 Co*** **I** (***158***); ***.36 V*** **I** (***113***); .34 *Fe* I (1206)
4777.17:	4777.18	1	*TiO?*
77.66	77.74	2	.79 *TiO?*
4778.25	4778.18	3	***.26 Ti*** **I** (***232***); .23 *Co* I (186)

TABLE 6—*Continued*

α Ser	α UMa	Int.	Identifications
4778.7			.80 *Ti O*
	4778.97		.08 *Ti O*?
4779.37	4779.40	6	***.35 Sc* I (*5*)**; .44 *Fe* I (720)?
79.95	79.98	5	***.98 Co* I (*158*)**; ***.99 Ti* II (*92*)**; 87 *Cr* I (124)
4780.37			.28 *Ti O*
80.80	4780.60 80.94	2w	.64 *Ti O*
4781.40	4781.43	3	.81 *Fe* IP (633)?; .92 *Ti O*
81.68	81.74	4	.43 *Co* I (57)
4782.09	4782.20	1	.72 *Ti* I (41)
82.59	82.61	2	.04 *Ti O*?
82.98	82.98	1	.59 *Ti O*
			.94 *Mo* (M)?; .98 *Cr*? (Sun); .98 *Ti O*
4783.40	4783.42	9	***.42 Mn* I (*16*)**; .31 *Ti* I (41)
83.93	83.93	3	.00 Sun; .92 *Ti O*
4784.44	4784.40	2	.48 *V* I (3)
	84.71:		.78 *Ti O*
4785.06d?	4785.02	2w	***.07 Co* I (*186*)**; .94 *Zr* I (44)
85.60	85.73	1	.67 *Ti O*
85.93			.96 *Fe* I (1044)?; .84 *Ti O*?
	4786.21d?		.29 *Ni* I (50)
4786.53	86.54	2:	***.52 V* I (*113*)**; .54 *Ni* I (98)
86.80	86.82	6	.81 *Fe* I (467)
4787.37	4787.36:	3:	.46 *Ti O*?
87.80	87.81	5	—.74 *Cr* I (168); .84 *Fe* I (384); .88 *Ti O*
4788.23		0	.16+.32 *Ti O*
88.75	4788.74	5	.76 *Fe* I (588)
4789.35 89.64	4789.35 89.63	5 6	.35 *Cr* I (31) ***.65 Fe* I (*753*)**; .80 *Ti* I (41)?
4790.29	4790.34d?	1	.34 *Cr* I (31)
90.62			.64 *Ti O*
	90.82		.75 *Fe* IP (632)?
4791.15	4791.19	5	—.25 *Fe* I (633); .20 *Ti O*
	91.56		.50 *Sc* I (5); .58 *Sm* II (7)
4792.42	4792.44	7	***.48 Ti* I (*260*)**; ***.51 Cr* I (*168*)**; .39 *Ti* IIp (48)
4792.84	4792.88	3	.86 *Co* I (158)
4793.97	4793.96	1	***.96 Fe* Ip (*512*)**; .91 *Ti O*
4794.37	4794.39	2	.36 *Fe* Ip (115)
	94.83		.84 *Ti* IIp (29)?
4795.4	4795.4 d?	1w	.36 *Fe* (Sun); .53 *Ti O*
4796.22	4796.28	5	***.21 Ti* I (*260*)**; .17 *Cr* I (283)—
96.96	4797.00	4	.93 *V* I (113)
4797.62 97.99	97.70	2:	.69 *Cr* I (230) ***.98 Ti* I (*260*)**; .97 *V* I (93)
4798.31	4798.18	1:	.27 *Fe* I (1042)
98.66	98.62	4	***.74 Fe* I (*38*)**; .54 *Ti* II (17)
4799.34	4799.43	2	.41 *Fe* I (888)
99.82	99.82	5	***.80 Ti* I (*242*)**; .79 *V* I (3)
4800.17	4800.14	0	.14 *Fe* I (384)
00.62	00.63	5	***.65 Fe* I (*1042*)**; .55 *Fe* I (590)
4801.04	4801.02	3	.03 *Cr* I (168)
01.92	01.99	2	.90+.93 *Ti* Ip (40)
4802.49	4802.51	2	.53 *Fe* Ip (1206)
02.87	02.87	4	.88 *Fe* I (888, 934)
	4803.55	0	.62 *Ti O*
4803.99:	4804.00	1	.04 *Ti O*
4804.54	04.53	4	***.53 Fe* I (*794*)**; .64 *Cr* I (61); *Ti O* α (3, 1)Rab Head
4805.06	4805.06	5	.10 *Ti* II (92)
05.41	05.41	3:	.42 *Ti* I (260)
05.86:	05.86	1	.82 *Gd* II (60)?; .88 *Zr* I (43)?
4806.30	4806.29	2	.26 *Cr* I (61)
06.98	4807.03	4	.00 *Ni* I (163)
4807.62	07.66	4	.54 *V* I (113); .72 *Fe* I (688)
4808.14	4808.12	2	.16 *Fe* I (633)
08.63	08.62	4	.52 *Ni* I (114); .86 *Ni* I (160)
4809.20	4809.01 09.31	2w	.14 *Fe* I (933)— .32 *Cr* I (230)
	09.59:		.49 *Ti O*?
09.95	09.98	2	.94 *Fe* I (793)
4810.56	4810.56	3	***.53 Zn* I (*2*)**; .73 *Cr* I (144)
4811.01	4811.05	2	***.04 Fe* I (*467*)**; .07 *Ti* I (158)
11.38	11.39	2	.34 *Nd* II (3)

TABLE 6—*Continued*

α Ser	α UMa	Int.	Identifications
4811.91	4811.95	5w	***.00 Ni* 1 (*130*)**; .88 *Sr* 1 (5)?
4812.31	4812.32		.24 *Ti* 1 (260)
4813.00	4813.04	4	***.11 Fe* 1 (*630*)**; .91 *Ti* 1 (41)
13.48	13.47	3	.48 *Co* 1 (158)
13.92	13.84:	1	***.97 Co* 1 (*158*)**; .95 *V* II (197) Rem
4814.42	4814.28	3w	.26 *Cr* 1 (144)
	14.55		.62 *Ni* 1 (98)
4815.18	4815.19	2w	***.05 Zr* 1 (*44*)**; .22 *Fe* 1p (720); .14 *TiO*
15.88v	15.81	2w	***.90 Co* 1 (*142*)**; ***.92 Ni* 1 (*131*)**; .62 *Zr* 1 (43); .81 *Sm* II (14)
4816.48	4816.58	0	.41 *Cr* 1 (283)?; .47 *Ti* 1p (40)
	4817.32		.27 *TiO*
4817.84	17.84	5	***.77 Fe* 1 (*67*)**; .85 *Ni* 1 (254)?
	4818.39		.38 *Yb* (M)?
4819.09	4819.03	3	.02 *Ti*, *V* (Sun); .02 *TiO*
19.61	19.7 d?	0	.64 *V* 1 (13)?; .68 *TiO*
4820.39	4820.39	5	.41 *Ti* 1 (126)
4821.11	4821.12	4	.14 *Ni* 1 (254)?; .09 *TiO*
21.54	21.58	2	.59 *TiO*
21.92:	4822.08	0	.88+.07 *TiO*
4822.60	22.61	2	.66 *Fe* 1p (633); .50 *TiO*
	4823.3		.31 *V* II (22)?; .28 *TiO*
4823.48	23.46	9	.52 *Mn* 1 (16)
4824.14	4824.14	6	—.16 *Fe* 1 (888); .29 *Zr* 1 (43)?
24.83:	24.87	0	.87 *TiO*
4825.47	4825.44	6	***.44 Ti* 1 (*250*)**; .48 *Nd* II (3)
4826.2	4826.22	0	
26.86	26.84	2	.87 *La* II (22); .84 *TiO*
4827.49	4827.48	7	***.46 V* 1 (*3*)**; .60 *Ti* 1 (250); *ZrO* α (0, 1)Rc Head
4828.07:	4828.05	1	.05 *Zr* 1 (44)
28.52	28.61		.66 *Cr* 1 (31)
4829.03	4829.06	3	.03 *Ni* 1 (131)
29.37	29.39	5	.38 *Cr* 1 (31)
4830.50	4830.57	1	.53 *TiO*
4831.20	4831.19	3	.18 *Ni* 1 (111)
31.66	31.63	4	***.64 V* 1 (*3*)**; .63 *Cr* 1 (208)
4832.07		0	.06 *Ti* 1 (250)
4832.42	4832.42	4	.43 *V* 1 (3)
32.71	32.74	3	***.73 Fe* 1 (*888, 1098*)**; .70 *Ni* 1 (146)
4833.19	4833.28	0	.28 *TiO*
33.83	33.91	1w	.96 *Mo* (M)?
4834.54	4834.52	5	***.51 Fe* 1 (*115*)**; .62 *Sm* II (45)
	4835.28		.22+.42 *TiO*
4836.05	4836.02d	7w	***.86 Fe* 1 (*1068*)**; .98 *Nd* II (1); .12 *Ti* 1 (241)
36.85	36.91	2	.86 *Cr* 1 (144)
4837.52	4837.40		.42 *Ti* 1p (250)?
4838.09	4838.01	2	.09 *Fe* 1p (630)
38.56	38.56	7	—.52 *Fe* 1 (687); .50 *TiO*
4839.0	4839.16	0:	.25 *Ti* 1 (217)?; .18 *TiO*
39.55	39.56	4	.55 *Fe* 1 (588)
39.86:		1:	.87 *V* 1 (13)
4840.28	4840.28	6	.25 *Co* 1 (158); .33 *Fe* 1 (1068)
40.89	40.89	5	***.87 Ti* 1 (*53*)**; .89 *Fe* 1p (1070)
4841.34:			.36 *TiO*
41.76	4841.77	4	***.80 Fe* 1 (*1070*)**; .73 *Cr* 1 (266)?
4842.13			.19 *Fe* 1p (511)
42.77	4842.74	4	—.78 *Fe* 1 (1069); .71 *Fe* 1p (1098)? Rem
4843.18	4843.17	7w	***.16 Fe* 1 (*687*)**; .16 *Ni* 1 (50)
43.48	43.45		.45 *Co* 1 (158)
4844.11r	4844.09	5w	***.02 Fe* 1 (*750*)**; .21 *Sm* II (26); .99 *Ti I* (217)
	44.54		.56 *Ru* 1 (M)?
4845.10	4845.09	1	.17 *Ni* 1 (115)
45.65	45.65	3	***.66 Fe* 1 (*588, 888*)**; .67 *V* 1 (13)
4846.38	4846.44	4	.29 *Cr* 1 (208); .45 *Ta* (M)?
4847.31	4847.31	4	***.30 Ca* 1 (*50*)**; *TiO* α (4, 2)Ra Head; *ZrO* α (0, 1)Rb Head
47.65	47.67	1w	.76 *Sm* II (53)
4848.37	4848.35	4	.49 *Ti* 1 (201)?; .37 *Cb* (M)?
4849.04	4849.04	5w	—.90 *Fe* 1 (114); .12 *TiO*
49.62	49.64	3	—.67 *Fe* 1p (793); .66 *TiO*
	4850.21	1	*TiO* α (4, 2)Rc Head; *ZrO* α (0, 1) Ra Head
	50.71	1	

TABLE 6—*Continued*

α Ser	α UMa	Int.	Identifications
4851.49	4851.50	7	***.48 V* I (*3*)**; .46 *Cr* I (208)
51.94	4852.00	2	.96 *TiO*
4852.57	52.56	4	***.56 Ni* I (*130*)**; .69 *V* I (13)
4853.25	4853.23d?	1w	.12 *TiO*?
53.81	53.82	3	.74 *Ni* I (99)?
4854.34:	4854.25:		.36 *Sm* II (36)
54.82	54.83	4	***.87 Y* II (*22*)**; .73 *Ti* I (217)
4855.49	4855.52	7:	***.68 Fe* I (*687*)**; .41 *Ni* I (130)
4856.05	4856.02	5:	.01 *Ti* I (231)
56.66	4857.19	5	.66 *TiO*
4857.40			.34 *Cr* I (61); .38 *Ni* I (111)
4858.22	4858.23	5	.24 *Fe* Ip (1069)?; .27 *Fe* Ip (1098)?; .26 *TiO*
4859.10	4859.07	4	***.12 Fe* I (*1068*)**; .03 *Nd* II (3)
59.74	59.77	8	***.75 Fe* I (*318*)**; .84 *V* I (13)
4860.27	4860.42	1	.37 *Cr* I (31)
4861.28	4861.36	14w	.33 *Hβ* (1)
61.91	61.88	4	.84 *Cr* I (31)
4862.60	4862.56	3	.54 *Fe* Ip (1070)?; .60 *Fe* Ip (1069)?; .61 *V* (M)?
	4863.16		
4863.76	63.76	5	***.65 Fe* I (*687*)**; .75 *Ti* Ip (217)?
4864.26	4864.27	4	.19 *Ti* I (201); .28 *Ni* I (128)
64.78	64.74	5	.74 *V* I (3)
4865.17	4865.26:	0	.27 *TiO*
65.61	65.61	3	.62 *Ti* II (29)
4866.26	4866.28	4	.27 *Ni* I (111)
66.9 d?	66.82	1	.97 *TiO*?; .85 *Cb* (M)?
4867.48	4867.50	2:	.53 *Fe* Ip (38)
67.88	67.85	4	.87 *Co* I (158)
4868.32	4868.34	5	***.26 Ti* I (*231*)**; .38 *Fe* Ip (38)
4869.08			.15 *Ru* I (11)?
69.46	4869.44v	2	***.45 Fe* Ip (*751*)**; .52 *TiO*
4870.11	4870.10	4	.13 *Ti* I (231)
70.83	70.82	3	***.80 Cr* I (*143*)**; .84 *Ni* I (131)
	4871.0		
4871.35	4871.34	8	.32 *Fe* I (318)
4872.09	4872.09	9	***.14 Fe* I (*318*)**; .02 *Cr* I (30)
4872.93	4872.79	1	.91 *Fe* Ip (1097)?; .73 *TiO*
4873.37	4873.37	3	.44 *Ni* I (111)
73.82	73.9	0	.74 *Fe* Ip (633)?; .98 *TiO*?
4874.42:	4874.36:	1	.35 *Fe* Ip (467)
	74.75		***.81 Ni* I (*98*)**; .65 *Cr* I (167); .80
74.86		2w	*V* II (197)
	4875.06		.99 *TiO*
4875.48	75.48	4	.46 *V* I (3)
75.90	75.98	3	.89 *Fe* I (687)
4876.39r	4876.44	3	.46 *TiO*; .32 *Sr* I (5)?
4877.70	4877.63	2:	.61 *Fe* Ip (384); .72 *TiO*
4878.19	4878.19	8	***.22 Fe* I (*318*)**; .13 *Ca* I (35)
4880.12	4880.09	2	.06 *Cr* I (167)
80.50	80.56	3	.56 *V* I (50)
80.90	80.97	2	.92 *Ti* I (201)
4881.60	4881.62	8	***.55 V* I (*3*)**; .73 *Fe* I (588, 1041)
4882.21	4882.17	5	***.15 Fe* I (*687*)**; .18 *V* I (50)
82.79	82.79:	2	.70 *Co* I (158)
4883.66	4883.70	4	***.69 Y* II (*22*)**; .61 *Zr* I (44)?
4884.02	4884.11:	1:	.06 *V* II (197)
4885.04	4885.06	5	.08 *Ti* I (157)
85.45	85.47:	1	.44 *Fe* I (966)
85.83	85.79	3	***.78 Cr* I (*30*)**; .96 *Cr* I (143)
4886.30	4886.32	3	***.34 Fe* I (*1066*)**; .31 *TiO*
4887.07	4887.08r	7w	***.99 Ni* I (*141*)**; .01 *Cr* I (143)
87.76	87.93:	0	.73 *Cr* I (31)—
4888.62	4888.61	5	.53 *Cr* I (31); .65 *Fe* I (1066)
4889.04	4889.05	6	***.01 Fe* I (*67, 749*)**; .11 *Fe* I (985)
89.7			.73 *Cr* I (61)
4890.1	4890.22	1	.09 *β*
90.77	90.78	8	.76 *Fe* I (318)
4891.50	4891.51	9	.50 *Fe* I (318)
4892.4	4892.2		.26 *TiO*
92.91	92.90	4w	***.86 Fe* I (*1070*)**; .06 *Ti* I (231); *TiO* α (5, 3)Rab Head
4893.73	4893.80	2	.78 *Fe* II (36)
4894.48	4894.50	1	.43 *Zr* II (107)?
4895.55		0	.56 *TiO*

TABLE 6—*Continued*

α Ser	α UMa	Int.	Identifications
4896.49	4896.45	4	—.44 *Fe* I (984); .41 *TiO*
4897.05			.0 *TiO*
97.50d?	4897.49	2w	.44 *TiO*
4898.49		1w	.43 *TiO*
98.95			.00 *TiO*
4899.53	4899.51	3	.52 *Co* I (92)
99.99	4900.00	6	***.91 Ti* I (*157*)**; .92 *La* II (7); .13 *V* II (22)
4900.83	00.90	3w	***.97 Ni* I (*98*)**; .62 *V* I (118)?
4901.46	4901.44		.37 *TiO*
4902.18	4902.15	4	.02 *TiO*?
4903.28	4903.28	7	***.32 Fe* I (*318*)**; .24 *Cr* I (31)
4904.36	4904.36:	6	***.41 Ni* I (*129*)**; .28 *V* I (50); .35 *V* I (118); .45 *V* I (118)
4905.16	4905.13	5	.15 *Fe* I (986)
05.9			.92 *TiO*
4906.24	4906.21	1w	.35 *TiO*?
06.75	06.78	2w	.80 *Fe* Ip (1096)?
4907.13	4907.12	1:	.12 *Co* I (14)
07.82	07.84	6	—.74 *Fe* I (687); .89 *Ru* I (11)?
4908.59	4908.56	2	.61 *Fe* Ip (115)
4909.28d	4909.32d?	5	.10 *Ti* I (39); .39 *Fe* I (985)
4910.03	09.99	4	.03 *Fe* I (687)
10.48	4910.42	5	.33 *Fe* I (1068); .57 *Fe* I (1068)
4911.32	4911.25	3:	.20 *Ti* II (114)
11.89	11.82	4w	—.79 *Fe* I (984)
4912.51	4912.5	2	.52 *Fe* Ip (1040)?
4913.10	4913.10	1:	.25 *Sm* II (53)?; .14 Sun?
13.64	13.69	5	.62 *Ti* I (157)
13.97	13.96	2:	.97 *Ni* I (132)
4914.39	4914.45	1	.38 *Nd* II (52)?; .38 *TiO*
14.86			.89 *TiO*
4915.21	4915.23	3	.24 *Ti* I (157)
15.92	4916.29	1	.79 *TiO*
4916.60			.45+.80 *TiO*
4917.24	4917.26	4	.25 *Fe* I (1066)
17.98	4918.00	3	.03 *Fe* I (1070)
4918.40	18.38	3	.36 *Ni* I (177)
18.98v	18.98v	9	***.00 Fe* I (*318*)**; .71 *Ni* I (113)?
4919.84	4919.81	3	.87 *Ti* I (200)
4920.54	4920.54	11	.51 *Fe* I (318)
20.95	4921.02	2:	***.98 La* II (*7*)**; .94 *Cr* I (143)
4921.77	21.78	3	***.77 Ti* I (*200*)**; .80 *La* II (7)
4922.25	4922.17	6	.27 *Cr* I (143)
22.88	4923.10	1w	.84 *Sc* I (M); .84 *TiO*
4923.24			.16 *Fe* (Sun); .16 *TiO*
23.90	23.95	6	.92 *Fe* II (42)
4924.33	4924.3		.29 β
24.77	24.76	7	.78 *Fe* I (114)
4925.53	4925.52	7	***.66 V* I (*50*)**; .58 *Ni* I (141); .40 *Ti* I (157)
4926.17	4926.18	2	.15 *Ti* I (39)
26.72	26.75	1	.82 *Fe* Ip (844)?
4927.40	4927.44	5	.42 *Fe* I (792)
27.82	27.87	3	***.87 Fe* (*M*)**; .85 *TiO*
4928.36	4928.29	4	***.34 Ti* I (*200*)**; .29 *Ce* I (158)
28.9	28.89	0:	.90 *Ti* I (39)
4929.5	4929.38	0:	
4930.25	4930.29	7	.18 *Cr* I (259); .33 *Fe* I (985)—
30.92d?	30.87	2	.82 *Ni* I (193)?
4932.11	4932.02	4	.03 *V* I (50)
	32.90	0	.84 β
4933.27	4933.30	6	—.35 *Fe* I (1065); .30 *Sm* II (M)
4934.05	4934.03	9	***.09 Ba* II (*1*)**; .02 *Fe* I (1068)
4935.03	34.82	1	.89 *Cr* I (259)
35.83	4935.82	2	.83 *Ni* I (177)
4936.36	4936.36	3	.33 *Cr* I (166)
36.8	36.79	0	
4937.35	4937.35	4	.34 *Ni* I (114)
37.77	37.64	2:	.72 *Ti* I (39)
4938.21	4938.21	5	***.18 Fe* I (*966*)**; ***.28 Ti* I (*289*)**; .10 *Sm* II (23)
38.84	38.82	4	.82 *Fe* I (318)
4939.24	4939.27	2	.24 *Fe* I (1065, 1070)
39.71	39.71	5	.69 *Fe* I (16)
4941.26	4940.85	1w	—.02 *Ti* I (173)?
	4941.43		.32 *Ti* I (39); .56 *Ti* I (200)
41.91			.92 *Ni* I (114)

TABLE 6—*Continued*

α Ser	α UMa	Int.	Identifications
4942.51	4942.50	6	.50 *Cr* I (9)
	42.9	0:	.07 *Ti* I (52)?
	4943.48	0:	.46 *TiO*
	43.9	0:	.87 β
4944.37d	4944.30	2w	.39 *Ti* I (173); .59 *Cr* I (259)
4945.54	4945.55	5	.46 *Ni* I (145); .65 *Fe* I (1113)
4946.07	4946.06	0	.04 *Ni* I (148)
46.40	46.38	5	.39 *Fe* I (687)
4947.09	4947.44	1w	.05 *TiO*
47.60			.58 *V* II (197)
4948.16	4948.22	2w	.18 *Ti* I (200); .99 *Ti* I (39)?
4950.15	4950.09	5	.11 *Fe* I (687)—
	50.39		
50.60	50.93	0	.61 *TiO*
4951.41d?	4951.48	1w	.59 β
4952.28	4952.53	4	***.37 Sm* II (*32*)**; .33 *Ni* I (113)?
52.67			.65 *Fe* I (1068, 1111)
4953.21	4953.24	3	***.20 Ni* I (*111*)**; .18 *Co* I (14)
53.86	53.86	0	.71 *Cr* I (166)
4954.72	4954.73	4	.81 *Cr* I (166); *TiO* α (1, 0)Ra Head
4955.4			*TiO* α (1, 0)Rb Head
4956.00	4955.9	1	.07 *TiO*
56.61			*TiO* α (1, 0)Rc Head
4957.52w	4957.51w	15w	.30 *Fe* I (318); .60 *Fe* I (318)
4958.28	4958.22	3:	.26 *Ti* Ip (52)
4959.17	4959.12	3	***.13 Nd* II (*1*)**; .15 *TiO*
59.75	59.64	1	.68 *Co* I (14)
4960.32	4960.6	1	*TiO*?
4961.04	4961.09	2	*TiO*?
61.89	61.96	2	***.91 Fe* I (*845*)**; .94 *Sm* II (41)
4962.62	4962.60	2	.56 *Fe* I (1097)
4963.16			*TiO*?
63.58	4963.57	0	*TiO*?
4964.07	4964.14	1	*TiO*?
64.93	64.95	6w	***.93 Cr* I (*9*)**; .71 *Ti* I (173)
4966.06	4966.04	8	.10 *Fe* I (687)
66.67	66.72	1	.58 *Co* I (14); .80 *Cr* I (259)
4967.36	4967.36	2	.30 *Ti* I (5)
4967.89	4967.93	3	.90 *Fe* I (1067)
4968.58	4968.61	7	.57 *Ti* I (173); .46 *TiO*?
4969.36			*TiO*?
69.93	4969.93	4	***.93 Fe* I (*1066*)**; *TiO*?
4970.56	4970.56	5	.50 *Fe* I (883); *TiO*?
4971.41	4971.43	3	.35 *Ni* I (274)?; *TiO*?
4972.02d	71.94	1	.94 *Co* I (158)
4973.07	4973.09	6	***.05 Ti* I (*173*)**; .11 *Fe* I (984)
73.86			.82 *TiO*
4974.41	4974.36	3	.47 *Co* I (92)
4975.48	4975.40	4	.34 *Ti* I (283); .42 *Fe* I (586)
4976.26	4976.29	5	***.34 Ni* I (*49*)**; .16 *Ni* I (112)
76.9	4977.2	0w	*TiO*?
4977.68	77.72	3	***.65 Fe* I (*985*)**; .73 *Ti* I (173)
4978.16	4978.10	1:	.19 *Ti* I (173)
78.61	78.59	5	.54 *Na* I (9); .61 *Fe* I (966)
4979.66	4979.74	2:	—.58 *Fe* I (883); .60 *TiO*
4980.19	4980.24	5	***.16 Ni* I (*112*)**; .10 *TiO*
	80.74		*TiO*?
4981.03	4981.19		*TiO*?
81.33			
81.78	81.74	6	.73 *Ti* I (38)
4982.65	4982.61	6w	.51 *Fe* I (1067); .81 *Na* I (9)
4983.30	4983.30	4	.26 *Fe* I (1067)
83.96	83.96	5	.86 *Fe* I (1066)
4984.66	4984.57	1	.73 *TiO*?
4985.48	4985.44	8	***.55 Fe* I (*318*)**; .26 *Fe* I (984)
4986.20	4986.22	3	.24 *Fe* I (1070)
86.91	86.91	2	—.82 *La* II (22)
4987.91	4987.95	3	.85 *Co* I (14)
4989.05	4989.06	6	.96 *Fe* I (1066); .14 *Ti* I (173)
89.94d	89.94	1	.92 *TiO*
4990.43	4990.50	2	.46 *Fe* (M); .42 *TiO*
4991.15	4991.15	9	***.07 Ti* I (*38*)**; .28 *Fe* I (1065)
91.79	91.83	3	.86 *Fe* Ip (1094)?; *TiO*?
4992.31	4992.67	1	*TiO*?
92.84			
4993.34	4993.4	2	.36 *Fe* II (36)

TABLE 6—*Continued*

α Ser	α UMa	Int.	Identifications	α Ser	α UMa	Int.	Identifications
4993.71		1:	.69 *Fe* I (1111)	4997.72			*TiO*?
4994.12	4994.00	6	.13 *Fe* I (16)	4998.23	4998.27	4	.23 *Ni* I (111)
4995.02		0:	.06 *Ti* I (216)?; .09 *TiO*	98.99	4999.07	1:	.11 *Fe* I (1040)?; *TiO*?
95.52	4995.55	3	*TiO*?	4999.46	99.44	7	.50 *Ti* I (38); *TiO* α (2, 1) Rab Head
4996.0	4996.27	1	*TiO*?	5000.34	5000.34	6	.34 *Ni* I (145)
96.59				00.99	5001.00	4	.99 *Ti* I (173)
4997.03	96.94	7	.10 *Ti* I (5); .12 *TiO*	5001.90	01.86	6	.87 *Fe* I (965)

NOTES TO TABLE 6

4045.91 Secondary contributors, .07 *Fe* Ip (557); .59 *Fe* Ip (559).
4050.96 Possibly the wave lengths in α Ser and in α UMa do not refer to the same line; in α UMa there is a very faint line whose wave length coincides better with that of the line in α Ser.
4063.62 Secondary contributor, .53 *Mn* I (5).
4119.40 Atomic contributors are considered insufficient.
4132.04 Secondary contributors, .97 *Fe* Ip (558); .02 *V* I (27); .16 *Co* I (30); .05 *SiH* (0, 0)Q.
4142.18 to 4143.45 Several lines of *SiH* (0, 0)Q contribute to the observed lines and produce a general depression of the continuous background.
4157.78 Various *SiH* and *CN* lines contribute.
4166.99 Although not measurable, the line is present in α UMa.
4171.43 A faint line in the violet wing is .32 *CN*.
4172.48 and 4172.72 General background absorption due to *SiH* (0, 0)P.
4194.68 and 4194.96 Between these two lines there are two faint lines due to *CH* (0, 0)R.
4227.95 Enhanced in sunspots.
4235.94 Secondary contributors, .96 *Fe* Ip (692); .984 *Cr* I (132); .11 *CH* (0, 0)R.
4241.14 Various *AlH* (0, 0)R lines.
4259.31 General background absorption due to the *AlH* (0, 0)Q head.
4299.24 Secondary contributors, .25 *Fe* Ip (597); .14+.25 *CH* (0, 0)Q.
4303.18 General background absorption due to *CH* (0, 0)Q lines.
4307.87 Secondary contributors, .74 *Ca* I (5); .95 *CH* (0, 0)Q.
4312.26 Several indistinct *CH* (0, 0)Q lines.
4313.61 Several indistinct *CH* (0, 0)Q lines.
4328.60 A faint line to the red is .83+.87 *CH* (0, 0)P.
4338.74 Secondary contributors, .84 *Fe* Ip (117); .63+.84 *CH* (0, 0)P.
4339.27 See discussion apart.
4359.63 Secondary contributors, .74 *Zr* II (79); .50+.75 *CH* (0, 0)P.
4369.76 Secondary contributors, .77 *Gd* II (15); .72+.84 *CH* (0, 0)P.
4454.76 Secondary contributors, .66 *Fe* I (902); .80 *Zr* II (40); and, possibly, .63 *Sm* II (49).
4495.13 The observed wave length does not agree with that of the *Ti* line; this, however, ought to be present on the basis of multiplet intensities.
4527.35 Secondary contributors, .25 *Y* I (14); .35 *Ce* II (108); .46 *Ti* I (7).
4667.57 Secondary contributors, .46 *Fe* I (822); .77 *Ni* I (163).
4732.41 Secondary contributors, .34 *Zr* I (48); .60 *Gd* II (65).
4813.92 The observed wave length in α UMa is rather uncertain.
4842.77 Miss Davis indicates approximately at this position the head of the *AlO* (0, 0) band; the laboratory wave length is 4842.1, and, as the other heads of the *AlO* bands are absent, this identification cannot be accepted for the K giants.

The wave lengths in the column of identifications (only the decimal figures are given) are from the following sources:

The *MT*, to be distinguished by the number of the multiplet following the chemical symbols ("u" means that the line was unclassified).

The *Revised Rowland Table* (sun); only lines with intensity not less than 1 on the disk or 0 in sunspots were noted.

D. Davis' paper on the spectrum of β Pegasi (β); only lines with intensity not less than 2 were noted.

The wave length tables of the Massachusetts Institute of Technology (M).

Some lines of *Tb* II, *Dy* II, and *Ho* II are not followed by the indication of multiplet or of source; the wave lengths are from King's papers.[11]

The wave lengths of the molecular lines are from the papers quoted in Section VII, unless otherwise stated; those for *CN* are unpublished; and those for *TiO* are from D. Davis' paper.

The following symbols are used throughout:

In the columns of wave lengths and of the intensities:

d = Double line,
d? = Probably double line,
w = Wide or hazy line,
v = Unsymmetrical line, like that produced by a faint line on the violet wing of a strong one,
r = The same, but on the red wing,
} = Lines not well separated or a depression of the continuous background,
: = Uncertain wave length or intensity.

In the column of identifications a dash (—) preceding the identifications means that the main contributor is unknown or doubtful; a dash following the identifications means that the main contributor is probably that noted, but the observed line is too strong.

"Rem" corresponds to a note at the end of the table.

The observations for this investigation were made by the author at the McDonald Observatory while holding a fellowship from the Italian National Research Council. Thanks are due to Dr. Otto Struve and Dr. P. Jose for assistance during the observations. The measurements, reductions, and identifications were carried out at the Observatory of La Plata; Miss Vercesi of the computing staff helped in the computations.

VARIATIONS IN THE SPECTRUM OF SIGMA SCORPII

RICHARD D. LEVEE
Berkeley Astronomical Department, University of California
Received November 29, 1951

ABSTRACT

During 1950–1951, 225 three-prism spectrograms of σ Scorpii were obtained with the Mills spectrograph of the Lick Observatory. The radial velocities determined from the plates are connected by a period $P_2 = 0.246835$ day. There is also a variation in the line width, which has a period identical with that of the radial velocity. On some nights, double lines appear at maximum or minimum velocity; when they are not double, they are asymmetric, and there is little doubt that they are composed of the blended double lines. As in 12 Lacertae, it is the alternation of these lines which results in the measurement of a variable radial velocity.

There is a variation in the mean velocity with a period $P_3 \sim 33$ days. The amplitude of the radial velocity-curve also varies, but it is uncertain whether this variation is periodic. This latter variation is strongly correlated with a variation in the amplitude of the line-width curves.

Struve's recent hypothesis for the β Cephei stars is considered in the light of the present investigation. The effect of a turbulent spot (the presence of which is fundamental in the hypothesis) on the line profile is examined. If one takes (from the theory of the curve of growth) the equivalent line width in the turbulent spot to be three times that in the quiescent area (both per unit area), one finds that, for a symmetrical spot of radius half the radius of the star, the effect will be clearly marked.

I. INTRODUCTION

The variation in the radial velocity of σ Scorpii ($\alpha = 16^h15^m1$, $\delta = 25°21'$; $M_v = 3.08$) was discovered by V. M. Slipher[1] in 1904 from measurements of four spectrograms taken at the Lowell Observatory. He noted that the spectrum was of the Orion type; this star is now classified as B1 III on the Yerkes sysem. In 1909[2] he announced the presence of stationary H and K lines of calcium in its spectrum. In 1914 and 1915, M. Selga[3] found, from a study made at the Lowell and Lick Observatories, the very short period of 0.246829 day for the variation in the radial velocity. In 1918, F. Henroteau,[4] from observations with the Mills spectrograph of the Lick Observatory, determined the period of 0.246834 day, thus confirming Father Selga's work. He also found that the mean radial velocity varied, as had been suspected by Selga, with a period of about 34 days. Further, he noticed that the lines undergo a variation in width. He stated that the period of this variation was the same as that of the radial velocity. In later work, at Ottawa,[5] he found that the period of radial-velocity variation was variable. He also stated, in this work, that the amplitude of the mean velocity-curve is variable but that the amplitude of the short-period velocity-curve is constant. Henroteau's work at Ottawa, however, will not be considered in the present discussion.

Sigma Scorpii is now classified as a β Cephei or β Canis Majoris star.[6,7]

The present series of observations of σ Scorpii was initiated in 1950 by Dr. Struve with the Mills spectrograph of the Lick Observatory. These observations were carried on in the spring of 1951 by Dr. McNamara, and in the summer of 1951 by the writer.

[1] *Lowell Obs. Bull.*, **1**, 57, 1904.

[2] *Ibid.*, **2**, 1, 1909.

[3] *Rev. Soc. astr. d España y América*, **6**, 41, 1916.

[4] *Lick Obs. Bull.*, **9**, 177, 1918.

[5] *Pub. Dom. Obs. Ottawa*, **5**, 303, 1921; **8**, 45, 1922; **9**, 91, 1925.

[6] *Ap. J.*, **112**, 520, 1950.

[7] *Ap. J.*, **113**, 589, 1951.

II. THE OBSERVATIONS

During 1950 and 1951, twenty-one nights were spent in obtaining a total of 225 spectrograms, having a dispersion of 10 A/mm. The emulsion used was Eastman II*a*-O. The average exposure time was about 10 minutes in 1950 and about 16 minutes in 1951. Both maximum and minimum radial velocity were obtained on seven nights, and either maximum or minimum on nine nights. The remaining five nights, all in 1950, gave no satisfactory maxima or minima.

Photoelectric observations by D. M. Popper and M. Walker indicate only that, if there is a variation in light, it is extremely small.

III. THE RADIAL VELOCITIES

For one-third of the spectrograms, all of the fourteen lines listed in Table 1 were measured. For the remaining two-thirds, only the seven lines from *He* 4471 to *O* II 4596 were used. The omission of the seven lines causes no systematic differences in the radial velocities, nor does it appreciably affect the accuracy. The results are listed in column 3 of Table 2, and Figures 1–3 show the plotted radial velocities for the sixteen nights on which enough of the cycle was obtained to give either a maximum, a minimum, or both. The probable error of measurement of a single line is ± 4.0 km/sec, and the probable error of the arithmetic mean for one plate is ± 1.4 km/sec.

TABLE 1

LINES MEASURED IN σ SCORPII

Wave Length	Identification	Wave Length	Identification
4387.93	*He* I	4574.78	*Si* III
4414.90	*O* II	4590.97	*O* II
4416.98	*O* II	4596.18	*O* II
4471.48	*He* I	4638.86	*O* II
4481.23	*Mg* II	4641.87	*N* III
4552.65	*Si* III	4649.14	*O* II
4567.87	*Si* III	4650.84	*O* II

The curves are characterized by maxima which are, in general, much sharper than the minima. The sharpest maxima seem to occur on nights where $2K$ is large. A visual inspection of these curves shows immediately that there is a variation in both the amplitude of the velocity-curve and in the mean velocity (which we shall here designate as the "γ-velocity"). Drawing smooth curves through the plotted points, I determined the values of maximum and minimum velocity wherever possible. The difference, $2K$, is given in the third column of Table 3. For those nights on which only a maximum or a minimum was observed, $2K$ was determined by matching the slope and the minimum or the maximum of the incomplete curve with a complete curve. Values determined in this way are given in parentheses. $2K$, plotted as a function of time in Figure 4, shows a somewhat erratic behavior. The separation of the two deep minima is about 30 days, but it is uncertain whether this is related to the periodicity shown in Figure 3 (to be discussed below).

In all cases the γ-velocity was then estimated by a visual equalization of areas. The values obtained are given in Table 3. The parentheses indicate those values of the γ-velocity which depend on values of $2K$ determined by the matching procedure discussed above. The γ-velocity (plotted in Fig. 5) shows a periodicity of about 33 days, as found by Henroteau. In addition, it possibly shows a gradual change in amplitude. Such a

TABLE 2

Radial Velocities of σ Scorpii

Date	J.D. 243	Velocity	Si 4552	III 4568	Sum*
1950 July 16	3478.694	+ 18.5	146	116	262
	.709	+ 14.6	167	119	286
	.720	+ 9.4	153	162	315
	.731	+ 0.7	171	139	310
	.743	- 8.9	171	141	312
	.754	- 19.8	116	151	267
	.762	- 20.0	-	-	-
	.772	- 22.8	161	185	346
	.780	- 22.8	133	111	244
	.788	+ 14.5	82	82	164
	.797	- 9.5	74	92	166
	.806	- 4.8	78	72	150
	.815	+ 4.3	115	90	205
	.825	+ 14.0	-	-	-
July 24	3486.682	- 41.8			
	.691	- 37.0			
	.700	- 28.6			
	.714	- 17.5			
	.723	- 18.4			
	.733	- 5.3			
	.742	+ 4.2			
July 31	3493.667	- 2.5			
	.675	- 5.5			
	.683	+ 11.7			
	.690	+ 22.5			
	.698	+ 23.4			
Aug. 7	3500.670	- 7.3			
	.678	- 1.5			
	.685	- 15.9			
	.693	- 13.5			
	.701	- 25.1			
Aug. 14	3507.654	- 12.6			
	.662	- 14.6			
	.670	- 10.2			
Aug. 15	3508.650	- 17.8			
	.658	- 15.0			
	.666	- 9.0			
	.674	- 5.4			
1951 Apr. 18	3754.831	+ 2.9	119	78	197
	.849	+ 16.9	123	104	227
	.867	+ 32.7	105	114	219
1951 Apr. 18	3754.892	-	182	152	334

Date	J.D. 243	Velocity	Si 4552	III 4568	Sum*
1951 Apr. 18	3754.914	- 19.0	138	154	292
	.933	- 31.6	169	141	310
	.949	- 40.7	108	120	228
	.968	- 53.5	218	201	419
	.985	- 70.0	118	120	238
	3755.006	- 60.6	88	105	193
	.023	- 47.6	97	60	157
Apr. 27	3763.801	- 12.1	162	143	305
	.818	- 20.9	122	145	267
	.835	- 27.7	122	139	261
	.860	- 51.6	91	81	172
	.876	- 48.8	96	115	211
	.892	- 51.5	100	93	193
	.910	- 33.3	104	88	192
	.928	- 24.9	96	110	206
	.947	- 3.4	112	113	225
	.965	+ 17.0	111	94	205
	.983	+ 30.2	106	125	231
	3764.005	+ 54.5	153	125	278
May 16	3782.750	+ 29.1	-	-	-
	.765	+ 56.8	222	191	413
	.780	+ 36.3	239	197	436
	.801	+ 5.2	247	240	487
	.821	- 11.1	221	178	399
	.838	- 17.5	102	70	172
	.854	- 38.8	128	123	251
	.869	- 46.7	82	125	207
	.888	- 47.4	81	99	180
	.902	- 38.7	98	100	198
	.917	- 27.8	87	99	186
	.931	- 17.2	81	83	164
	.954	+ 3.0	86	96	182
	.969	+ 9.8	75	67	142
May 26	3792.722	- 54.1	118	121	239
	.733	- 61.3	135	130	265
	.744	- 71.8	128	150	278
	.761	- 71.5	118	86	204
	.770	- 70.8	152	100	252
	.783	- 58.3	100	70	170
	.794	- 55.5	87	103	190
	.807	- 39.9	115	82	197
1951 May 26	3792.819	- 32.8	73	96	169

TABLE 2 (continued)

Date	J.D. 243	Velocity	Si 4552	III 4568	Sum
1951 May 26	3792.830	- 23.1	104	115	219
	.854	+ 2.1	101	97	198
	.872	+ 16.9	115	134	249
	.892	+ 27.0	171	162	333
	.906	+ 25.7	227	193	420
	.922	+ 3.4	209	223	432
June 1	3798.699	- 15.0	127	113	240
	.726	+ 1.1	114	96	210
	.752	+ 21.7	110	115	225
	.772	+ 37.7	70	80	150
	.789	+ 55.8	104	103	207
	.803	+ 69.5	196	225	421
	.821	+ 56.1	271	253	524
	.837	+ 28.3	264	230	494
	.851	+ 11.9	208	194	402
	.869	+ 1.0	173	111	284
	3798.888	- 9.4	155	120	275
	.908	- 26.7	163	125	288
	.928	- 33.2	177	108	285
June 7	3804.691	+ 52.0	92	105	197
	.706	+ 68.1	126	135	261
	.726	+ 91.2	175	134	309
	.741	+115.2	235	292	527
	.758	+104.6	312	301	613
	.774	+ 43.6	240	223	463
	.790	+ 22.5	222	204	426
	.806	+ 16.5	188	194	382
	.822	+ 2.0	152	121	273
	.839	- 12.0	148	119	267
	.854	- 17.2	109	116	225
	.867	- 14.9	105	126	231
	.881	- 6.4	107	99	206
	.906	+ 19.1	95	93	188
	.919	+ 28.3	106	101	207
	.933	+ 44.6	142	124	266
June 14	3811.694	+ 10.9	130	135	265
	.717	- 7.9	158	142	300
	.732	- 19.9	118	115	233
	.746	- 28.9	151	127	278
	.776	- 34.6	163	159	322
	.793	- 25.7	144	126	270
1951 June 14	3811.808	- 19.4	124	114	238
	3811.822	- 5.8	117	78	195
	.836	+ 7.4	139	99	238
	.851	+ 23.5	158	124	282
	.865	+ 34.3	184	172	356
	.926	+ 37.6	-	-	-
June 15	3812.672	+ 12.8	196	222	418
	.687	- 2.4	231	188	419
	.700	- 6.8	142	457	299
	.713	- 13.1	155	135	290
	.726	- 26.4	109	104	213
	.738	- 34.5	122	109	231
	.756	- 41.0	140	117	257
	.770	- 36.0	137	120	257
	.783	- 31.3	139	144	283
	.794	- 24.0	123	108	231
	.828	+ 11.7	118	91	209
June 24	3821.691	- 36.4	125	94	219
	.702	- 21.9	79	81	160
	.714	- 14.6	90	93	183
	.725	- 5.0	135	116	251
	.736	+ 14.0	132	125	257
	.748	+ 23.1	142	126	268
	.757	+ 33.5	161	134	295
	.774	+ 53.8	182	148	330
	.785	+ 52.2	221	226	447
	.793	+ 30.0	289	245	534
	.801	- 5.3	280	269	549
	.834	- 31.9	162	180	342
	.844	- 47.0	156	130	286
	.860	- 61.3	120	116	236
	.867	- 68.2	126	107	233
	.881	- 74.9	110	103	213
	.894	- 75.6	125	96	221
	.906	- 67.3	132	114	246
June 25	3822.678	- 31.8	93	70	163
	.692	- 17.0	62	70	132
	.707	- 3.2	113	102	215
	.722	+ 14.5	125	127	252
	.736	+ 29.8	128	152	280
	.751	+ 42.0	154	135	289
	.765	+ 47.1	175	144	319
1951 July 1	3828.672	+ 28.4	112	109	221

TABLE 2 (continued)

Date	J.D. 243	Velocity	Si III 4552	Si III 4568	Sum
1951 July 1	3828.689	+ 47.1	171	132	303
	.706	+ 22.9	180	157	337
	.723	- 12.6	208	173	381
	.739	- 32.9	151	174	325
	.755	- 40.8	122	113	235
	.773	- 51.2	126	125	251
	.792	- 72.3	103	93	196
	.808	- 62.3	-	-	-
	.824	- 55.3	94	96	190
	.841	- 45.3	113	84	197
	.866	- 21.1	97	89	186
	.883	- 1.1	112	108	220
July 8	3835.676	+ 11.2	140	103	243
	.691	- 3.0	84	152	236
	.708	- 9.7	111	106	217
	.722	0.0	90	114	204
	.738	+ 3.8	114	76	190
	.751	+ 10.2	105	119	224
	.771	+ 24.9	84	79	163
	.785	+ 41.2	79	97	176
	.800	+ 51.3	113	120	233
	.815	+ 69.9	84	80	164
	.830	+ 80.4	108	110	218
	.850	+106.7	100	121	221
	.864	+112.1	-	-	-
July 15	3842.671	+ 3.3	79	102	181
	.686	+ 13.6	93	72	165
	.705	+ 33.9	82	81	163
	.724	+ 48.4	114	80	194
1951 July 15	3842.742	+ 61.6	112	89	201
1951 July 15	3842.758	+ 68.6	281	83	364
	.773	+ 48.4	284	231	515
	.789	+ 30.9	239	171	410
	.805	+ 19.5	300	170	470
	.820	+ 4.9	275	131	406
	.836	- 10.1	191	129	320
	.848	- 13.3	161	101	262
July 16	3843.667	+ 3.2	92	72	164
	.684	+ 15.9	76	73	149
	.701	+ 33.0	65	76	141
	.716	+ 39.4	82	89	171
	.733	+ 55.6	102	118	220
	.748	+ 51.7	173	97	270
	.765	+ 40.7	216	166	382
	.782	+ 14.8	211	191	402
	.799	- 0.5	129	151	280
	.816	- 7.7	143	114	257
	.829	- 19.3	134	130	264
	.844	- 22.6	111	113	224
July 30	3857.669	- 70.7	118	111	229
	.683	- 70.3	123	114	237
	.702	- 58.2	92	114	206
	.716	- 49.9	104	79	183
	.733	- 35.0	104	80	184
	.747	- 24.6	66	79	145
	.762	- 8.2	93	85	178
	.778	+ 10.7	118	124	242
	.792	+ 22.0	176	181	357
1951 July 30	3857.806	+ 33.2	200	158	358

*Units of measurement are microns

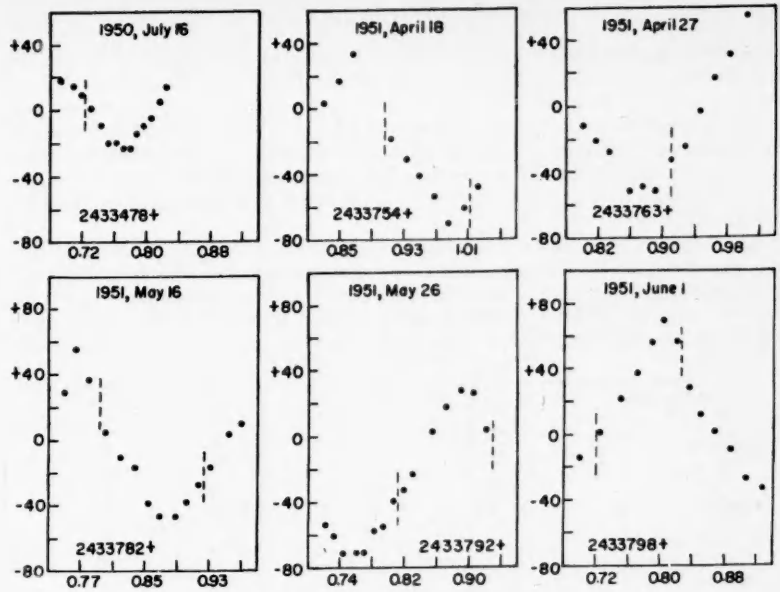

FIG. 1.—Radial velocity-curves of σ Scorpii

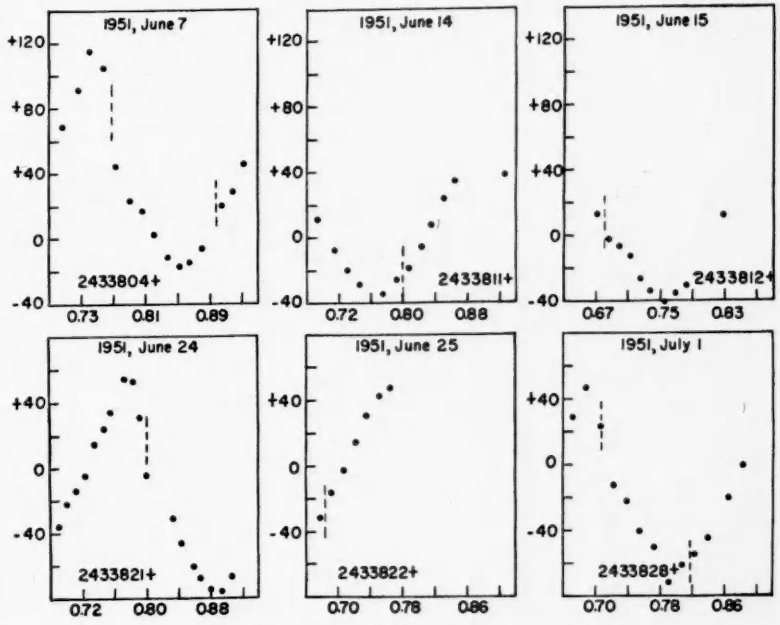

FIG. 2.—Radial velocity-curves of σ Scorpii

change was suspected by Henroteau. However, there are no observations between phases 9 and 28 days, and it is quite possible that the amplitude is really constant.

As mentioned above, the data are insufficient to permit conclusions as to whether a correlation exists between the values shown in Figures 4 and 5. However, if one assumes that the peaks at phase 44 days are in phase, there is a very slight indication that deep minima of the amplitudes fall somewhere between maximum and minimum γ-velocity and that the velocity amplitude may be a maximum at both maximum and minimum of the γ-velocity.

From the curves, the times of maximum and minimum velocity, as given in Tables 4 and 5, were determined. Only one radial velocity-curve was available from 1950, and this only at minimum; but it was well determined and should therefore give a good value of the period. 1321 cycles from this minimum until that of June 7, 1951, gave a new period of 0.246840 day; 1320 and 1322 cycles did not give satisfactory residuals. Using this peri-

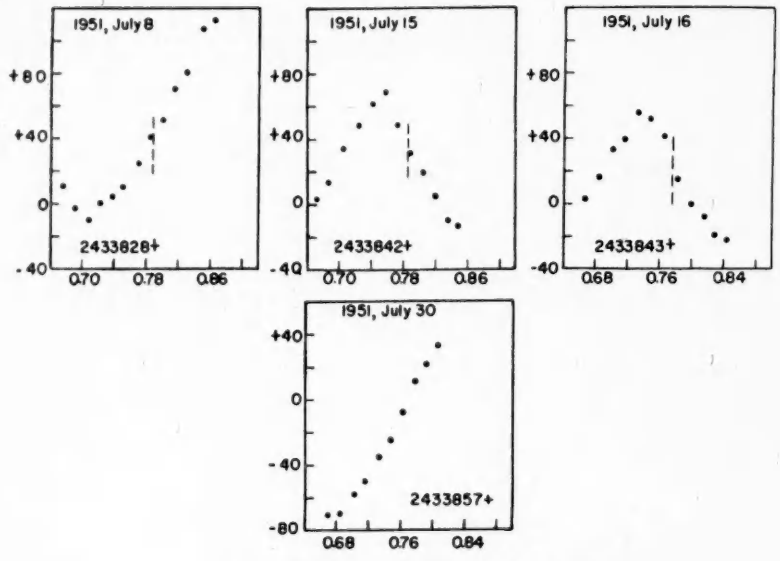

FIG. 3.—Radial velocity-curves of σ Scorpii

TABLE 3

VALUES OF $2K$ AND γ FROM INDIVIDUAL VELOCITY-CURVES

JD	Days	$2K$	γ	JD	Days	$2K$	γ
2433755	0	102	−21	2433822	67	130	−21
3764	9	(120)	(+ 8)	3823	68	(130)	(−20)
3783	28	106	− 9	3829	74	113	−22
3793	38	102	−28	3836	81	122?	+47
3799	44	104	+10	3843	88	78	+23
3805	50	126	+33	3844	89	80	+13
3812	57	81	+ 2	3858	103	(110)	(−16)
3813	58	(80)	(0)				

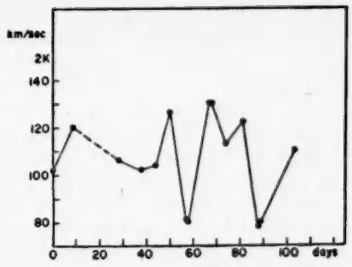

FIG. 4.—Variation in the amplitude of the radial velocity-curves

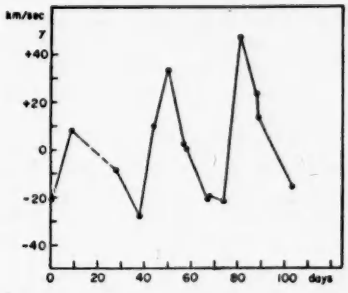

FIG. 5.—Variation in the mean radial velocity

TABLE 4

EPOCHS OF MAXIMUM RADIAL VELOCITY
(T_0 = 2433804.741; P = 0^{d}246840)

Observed	Computed	O−C	Observed	Computed	O−C
2433754.868.....	0.879	−0.011	2433821.777.....	0.773	+0.004
3782.765.....	.772	− .007	3822.767.....	.760	+ .007
3792.894.....	.893	+ .001	3828.688.....	.685	+ .003
3798.806.....	.817	− .011	3835.869?.....	.843	+ .026
3804.744.....	.741	+ .003	3842.751.....	.754	− .003
3811.886.....	0.899	−0.013	3843.740.....	0.742	−0.002

TABLE 5

EPOCHS OF MINIMUM RADIAL VELOCITY
(T_0 = 2433804.856; P = 0^{d}246840)

Observed	Computed	O−C	Observed	Computed	O−C
2433478.780.....	0.780	0.000	2433811.768.....	0.768	0.000
3754.990.....	.994	− .004	3812.760.....	.755	+ .005
3763.881.....	.881	.000	3821.888.....	.888	.000
3782.879.....	.887	− .008	3828.796.....	.799	− .003
3792.769.....	.761	+ .008	3835.710.....	.711	− .001
3798.934.....	.932	+ .002	3843.852.....	.857	− .005
3804.857.....	0.856	+0.001	3857.674.....	0.680	−0.006

od, epochs T_0(max.) = 2433804.741 and T_0(min.) = 2433804.856 were computed. The corresponding residuals are given in Tables 4 and 5. A plot of $(O-C)_{max}$ against $(O-C)_{min}$ shows no correlation. Henroteau's period of $P = 0.246834$ day fits the 1951 observations, since the periods differ by only 0.000006 day, and leaves a small residual of -0.008 in the minimum of 1950. Henroteau's epoch, T_0(max.) = 2421687.950 and the new epoch T_0(max.) = 2433804.856 are represented within 0.072 day by his period over about 50,000 cycles. This difference could be accounted for by an error of 0.0000014 day in Henroteau's period. My new period will not represent the old observations. The evidence indicates that the period of the radial-velocity variation may be slightly variable, but, until further observations are available, we shall assume that the period given by Henroteau is in error by a little over one unit in the last place, a better value being 0.246835 day.

One notes that the difference in the epochs given at the top of Tables 4 and 5 is 0.115 day, whereas half the period is 0.1234 day. The average interval from minimum to maximum of seven individual epochs given in Tables 4 and 5 is also 0.115 day. The velocity-curves are then asymmetric, and the interval from minimum to maximum is approximately 0.019 day shorter than the interval from maximum to minimum.

IV. THE LINE WIDTHS

A variation in the line widths is evident on all nights. Sometimes the lines are very shallow and broad, and sometimes they are quite narrow and deep. The equivalent widths do not change appreciably. The variation is much greater than in either β Canis Majoris or 12 Lacertae. The broadest lines appear on nights when $2K$ is a maximum and the narrowest lines when $2K$ is a minimum.

On the plates of June 7, 1951, double lines of *He* 4470 and 4387 were discovered by Dr. McNamara[8] and the writer. They are similar to those found in 12 Lacertae by Struve. (A re-examination of Henroteau's Lick plates shows, on several nights, lines which are probably double.) The two components are unequal in intensity, and it is the stronger which gives the same radial velocity as the other lines. The doubling does not appear in every cycle, but, when it does appear, the stronger is to the red of the weaker at maximum velocity, and to the violet of the weaker at minimum velocity. When the lines are not double, they are asymmetric, and there is little doubt that they are composed of the blended double lines. But the lines do not always look the same when they are double. On the nights of June 7 and 24, the strong component was very broad, as are all the lines in the spectrum. In fact, many lines are very nearly invisible. But on April 18 and July 8, all the lines, including the weak components, are relatively sharp, and the double components are of approximately the same width. On June 7, June 24, and July 8, when $2K$ was near a maximum, the weak component appeared near maximum velocity. The only night on which the weak component was found near minimum velocity was on April 18. On this night, $2K$ was neither a maximum nor a minimum.

I attempted to measure the weak component when it was well-seen, and the results are given in Table 6. The measurements may not be reliable because of the weakness of the lines and the blending with the strong components.

To make an objective test of the correlation of line width with velocity amplitude, I measured, on all the 1951 plates and on the plates of July 16, 1950, the widths of the lines *Si* III 4552 and 4568. The individual measurements are given in Table 2, columns 4 and 5, and the sums in column 6. The variations in the sums were then plotted for each night, and smooth curves were drawn through them. The maxima of these curves are, in general, similar to the corresponding maxima of the radial velocity-curve, but the minima are much more shallow.

The maximum and minimum values of the sums were then determined from the

[8] *Pub. A.S.P.*, **63**, 248, 1951.

curves and are given in Table 7. Since the minimum widths remain constant within the observational error, I plotted only the maxima in Figure 6. The correlation between Figures 4 and 6 is remarkable: the broadest lines appear on nights when $2K$ is a maximum and the narrowest lines when $2K$ is a minimum. Hence in σ Scorpii, as in 12 Lacertae, the major part of the variable radial velocity is caused by the alternation of strong and weak components. This oscillation corresponds to the wave with amplitude K_2 in 12 Lacertae.[7]

TABLE 6

MEASUREMENTS OF DOUBLE LINES*

JD	V_1	V_2	JD	V_1	V_2
2433754.914	− 19.0	+ 55.7	2433821.691	− 36.4	−190.0
.933	− 31.6	+ 81.4	.702	− 21.9	−156.3
.949	− 40.7	+ 81.5	.714	− 14.6	−133.6
.985	− 70.0	+ 82.8	.725	− 5.0	−118.8
755.023	− 47.6	+ 37.1	.748	+ 23.1	− 6.8
804.726	+ 91.2	+ 2.8	.774	+ 53.8	− 5.9
.741	+115.2	+ 85.3	.894	− 75.6	− 20.9
.758	+104.6	− 23.1	835.800	+ 51.3	− 46.2
.806	+ 16.5	− 96.0	.815	+ 69.9	− 84.5
.854	− 17.2	− 64.8	.830	+ 80.4	− 43.5
.906	+ 19.1	− 39.4	.850	+106.7	− 29.3
.933	+ 44.6	− 67.3	.864	+112.1	− 89.0

* V_1 = strong component; V_2 = weak component.

TABLE 7

MEASUREMENTS OF MAXIMA AND MINIMA OF THE LINE WIDTHS

JD	Days	Maxima	Minima	JD	Days	Maxima	Minima
2433755	0	370	190	2433822	67	555	210
764	9	.....	180	823	68	.....	150
783	28	490	170	829	74	385	180
793	38	450	170	836	81	.....	180
799	44	540	170	843	88	590	160
805	50	620	180	844	89	440	150
812	57	.....	200	858	103	.....	160
813	58	420	.....				

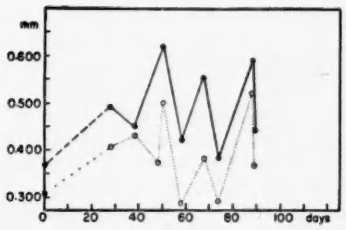

FIG. 6.—Variation in the line widths. The continuous curve with filled circles represents the maximum line width. The dotted line with open circles gives the widths of the lines appearing halfway between maximum and minimum radial velocity.

The positions of maximum and minimum line width, with respect to the velocity-curves, are indicated by the dotted lines in Figures 1–3. They do not fall at maximum or minimum radial velocity or at γ-velocity. Maximum line width falls 0.029 day after maximum radial velocity, and minimum line width 0.034 day after minimum radial velocity. The minima, however, are very poorly determined and should not be given much weight; apparently, the maximum and minimum line widths lag behind the maximum and minimum velocities by approximately 0.030 day. This lag probably has no physical reality. As will be discussed later, the broadest lines actually appear near γ-velocity, and the widest separation of the double lines occurs at maximum. But the observer measures the widest lines when the components are blended, somewhere between maximum and γ-velocity.

In σ Scorpii the dominant oscillation is K_2 (using the notation of Struve's paper on 12 Lacertae), but the existence of a small oscillation, corresponding to K_1 in β Canis Majoris, is not ruled out. Such an oscillation, with period P_1, slightly different from the period of oscillation with amplitude K_2, would cause the position of maximum and minimum

TABLE 8

EPOCHS FOR MAXIMUM AND MINIMUM WIDTHS OF LINES IN 1918
($P = 0^d.246834$)

T_0 (MAX.) = 2421207.973			T_0 (MIN.) = 2421707.880		
Observed	Computed	O−C	Observed	Computed	O−C
2421687.988	0.979	+0.009	2421687.896	0.886	+0.010
1688.969	.967	+ .002	1688.884	.874	+ .010
1707.979	.973	+ .006	1701.919	.956	− .037
1713.896	.897	− .001	1705.894	.905	− .011
1716.854	0.859	−0.005	1707.880	.880	.000
			1724.904	.912	− .008
			1726.878	0.886	−0.008

line width to slide slightly backward and forward along the velocity-curve. A test for such a phenomenon was made by taking the differences between the epochs of maximum velocity and maximum line width and between minimum velocity and minimum line width and plotting them against time. There is possibly a slight variation of this type. However, a plot of maxima against minima shows no correlation, and nothing can be concluded concerning such an oscillation.

Although Henroteau stated that the period of the variation in line width was the same as the period of variation in velocity, I tested this result independently by plotting the sums of his measurements of five lines for each night. The times of maxima and minima given in Table 8 were then determined. The residuals show that his radial-velocity period of 0.246834 day satisfies these epochs except for a small systematic trend. However, the period of velocity and line width cannot be different, since the positions of maximum and minimum widths fall at essentially the same place on his velocity-curves as they do in the present series of observations. Therefore, this small trend must be explained in another way. Such a trend might be the result of a wave with period P_1, as discussed above.

I then did the same for the observations of 1950 and 1951, as shown in Tables 9 and 10. Using the period of radial-velocity variation as determined above, $P_2 = 0^d.246835$, the epochs T_0(max.) = 2433804.770 and T_0(min.) = 2433804.902 were found. A plot of (O−C) minimum against (O−C) maximum shows no correlation. The period of variation in line width is therefore the same as that of radial-velocity variation. Since the

residuals are no longer systematic, there is no need here of introducing a wave with period P_1.

Since the velocity-curves are asymmetric and since there is a strong correlation of radial-velocity amplitude with line width, one would suspect that the curves of varying line width might also be asymmetric. This was investigated for both Henroteau's measures and my own. The epochs of Henroteau's maximum and minimum line widths show that the average time from minimum to maximum is 0.095 day. My own measures show that the average interval is 0.113 day from minimum to maximum. The difference may be significant. For my radial velocities the average interval from minimum to maximum was 0.115 day. The asymmetry was therefore identical in 1950–1951.

TABLE 9

EPOCHS FOR MAXIMUM LINE WIDTHS IN 1950–1951
(T_0 = 2433804.770; P = 0^{d}246835)

Observed	Computed	O−C	Observed	Computed	O−C
2433478.725	0.701	+0.024	2433812.680	0.669	+0.011
3754.906	.909	− .003	3821.802	.802	.000
3782.794	.802	− .008	3828.707	.713	− .006
3792.931	.922	+ .009	3842.786	.783	+ .003
3798.826	.846	− .020	3843.776	0.770	+0.006
3804.770	0.770	0.000			

TABLE 10

EPOCHS FOR MINIMUM LINE WIDTHS IN 1950–1951
(T_0 = 2433804.902; P = 0^{d}246835)

Observed	Computed	O−C	Observed	Computed	O−C
2433755.012	0.041	−0.029	2433804.900	0.902	−0.012
3763.910	.927	− .017	3811.800	.813	− .013
3782.924	.934	− .010	3822.683	.674	+ .009
3792.812	.807	+ .005	3828.818	.845	+ .027
3798.720	0.731	−0.011	3835.788	0.756	+0.032

V. SUMMARY OF OBSERVATIONAL RESULTS

1. The mean velocity varies with a period $P_5 \sim 33^d.9$

2. The radial velocity varies with a period $P_2 = 0^d2468$, which may be slightly variable.

3. The radial velocity-curves are asymmetric, the time from maximum to minimum being approximately 0.019 day greater than from minimum to maximum. They are also usually characterized by relatively narrow maxima.

[9] Following Struve's notation in 12 Lacertae, we shall use the following designations:

P_1 = Period of a hypothetical variation in velocity, not associated with a change in line width (not observed in σ Scorpii).

P_2 = Period of variation in line widths and of associated variation in velocity (this is the predominant period of σ Scorpii).

P_3 = Beat period of P_1 and P_2 (not observed in σ Scorpii).

P_4 = Period of hypothetical variation in the amplitude of the oscillations (P_2) of the line widths (probably irregular in σ Scorpii).

P_5 = Period of slow variation in mean velocity of individual oscillations in radial velocity (present in σ Scorpii, but probably not in β Canis Majoris and 12 Lacertae).

4. Double lines are often present at maximum and sometimes also at minimum radial velocity, and it is the alternation of these lines which results in the measurement of variable radial velocity.

5. The amplitude of the observed radial velocity-curve is correlated with the line widths and is therefore dependent on the amplitude of this variation, K_2.

6. There is a variation in the maximum line width and therefore in the amplitude of the radial velocity-curve; but it is uncertain whether this variation is periodic.

7. The period of change in line width is the same as the period of radial-velocity variation, $P_2 = 0^d2468$.

8. The curves of change in line width are asymmetric in exactly the same way as were the radial velocity-curves in 1950–1951.

9. The asymmetry of the curves of line-width variation may have changed since 1918, when the time from maximum to minimum was 0.057 day greater than the time from minimum to maximum.

10. There is some indication that there exists in σ Scorpii a wave with amplitude K_1 and period P_1, as in β Canis Majoris; but, if it is present, its amplitude is small, and therefore the beat period is indeterminate.

VI. DISCUSSION AND CONCLUSIONS

It is difficult to explain the 33-day variation in the mean velocity without the assumption of binary motion. The curves of Figure 5 are not quite symmetrical and indicate a small eccentricity of about 0.2. The rise to maximum is somewhat steeper than the decline to minimum and indicates that the longitude of periastron is about 270°.

The resulting elements are essentially the same as those given by Henroteau:

HENROTEAU	LEVEE
$K_1 = 33$ km/sec ,	$K_1 = 33$ km/sec ,
$e = 0.33$,	$e = 0.2$,
$P = 34.08$ days ,	$P = 33$ days ,
$\omega = 270°$,	$\omega = 270°$,
$\gamma = -3.2$ km/sec ,	$\gamma = +1$ km/sec
$T = 2421715.35$ J.D. ,	$T = 2433797.25$ J.D. ,
$f(m) = 0.107$,	$f(m) = 0.114$,
$a_1 \sin i = 14{,}600{,}000$ km.	$a_1 \sin i = 14{,}600{,}000$ km.

Recently, Struve[10] has put forward the following hypothesis for 12 Lacertae and β Canis Majoris:

Let us suppose that we have a B1 star, of which the atmosphere of one hemisphere is quiescent, whereas the atmosphere on a part of the other hemisphere is turbulent. Let us further suppose that these two areas are carried around the star so that we observe the following picture: When the quiescent hemisphere is pointing in the direction of the sun, the lines will come from this source alone and will be at their sharpest stage. When the turbulent hemisphere is pointing toward us, the lines will be at their broadest stage. When the axis of symmetry of the two hemispheres is at right angles to the line of sight, we see lines from both sources.

The areas may be carried around the star by rotation or by the motion of a small, dense companion. In the latter case, the cause of turbulence might be attributed to the companion itself.

Let us now consider this hypothesis as applied to σ Scorpii. If the areas are carried around by rotation, we should be able to measure the projected rotational velocity when

[10] *Loc. cit.*

the nonturbulent lines are observed alone. This stage occurs halfway between minimum and maximum radial velocity. I measured the *He* 4471 line at this epoch on a night when very good plates were obtained. The width was approximately 1.8 A, which corresponds to a projected rotational velocity, $V_0 \sin i = 50$ km/sec. Taking $i = 90°$, we find

$$R \text{ min.} = \frac{50 \times 0.2468 \times 24 \times 3600}{2\pi} = 1.7 \times 10^5 \text{ km},$$

which is much too small for the radius of a normal B1 star. A similar result was found by Struve for 12 Lacertae.

In σ Scorpii, the sharpest and deepest lines appear halfway between minimum and maximum velocity; the broadest and most shallow stage appears halfway between maximum and minimum. At maximum velocity the lines are double, with the deep component to the red; at minimum velocity it is to the violet. But the contours of the lines which appear halfway between maximum and minimum are not those of a turbulent atmosphere; they are the shallow, dish-shaped contours of a rotationally broadened line. Also, the lines appearing halfway between minimum and maximum velocity are probably not those of a quiescent atmosphere but those of a turbulent atmosphere. These observations have led Struve to revise his hypothesis in the following way.[11] We now suppose that the star is in rapid rotation and that the turbulent area covers a relatively small part of the star. The lines coming from the remainder of the star will be greatly broadened by the rotation. The following picture is then observed: When the turbulent area is in the direction of the sun, we observe sharp and intense lines from this area, superimposed on very shallow, rotationally broadened lines from the remainder of the hemisphere. When the turbulent area is away from us, we see only the very shallow, rotationally broadened lines. When the turbulent area is at the limb of the star, we see two components—one sharp and deep, the other wide and shallow. Since the turbulent area is probably carried around by the rotation of the star, the sharp component will actually lie inside the bounds of the wide component. However, one cannot determine by a visual inspection of the lines whether the components are separated.

The turbulent velocity, as inferred from the widths of the absorption lines when they are sharpest, cannot be much in excess of 10 km/sec. The velocity of rotation at the equator may be about 120 km/sec. If we compare the equivalent widths of the nonturbulent and the turbulent line profiles, both per unit area of the star's surface, the theory of the curve of growth leads us to expect that the former will be about three times smaller than the latter for those lines that are actually observable (they must lie on the intermediate branch of the curve of growth, where the slope is small). Adopting this ratio, we can, by a process of graphical integration, predict the combined profiles for turbulent areas of different sizes and for different orientations of the area on the visible hemisphere of the star. A few sample results are shown in Figure 7. (The area is, of course, not necessarily symmetrical; indeed, the more frequent appearance of double lines at maximum radial velocity would indicate that such is not the case.) It appears that if the radius of the turbulent area is $R_{\text{spot}} \sim \frac{1}{2} R_{\text{star}}$, the observed profiles will clearly show the indentation produced by the turbulent spot. We assume that, since the spectral type is constant, the surface brightness of the spot and the rest of the star are the same.

The hypothesis, as presented here, explains some of the salient results of observation:

a) The double lines cannot come from a binary and must therefore be produced on a single star.

b) The spectral types are similar, but the widths of the components differ greatly.

c) The maximum separation of the components is, within the precision of this work, similar to the equatorial rotational velocity of the star.

d) The period P_2 need not be the period of rotation but must be the period of the hypothetical companion which produces the turbulent area. (In β Canis Majoris, there is

[11] *Pub. A.S.P.*, **63**, 249, 1951.

some uncertainty as to whether P_1 or P_2 represents the orbital period; on the present hypothesis, the similarity of the two—observed in only a single object—is caused by an unexplained resonance phenomenon between the orbital period and a "natural" period of the star to respond to the turbulence-producing force of the companion.

e) The irregular variability of the velocity amplitudes suggests a physical phenomenon, such as prominence activity in a limited area of the star, rather than a purely mechanical effect.

On the other side of the picture are several objections that may be raised as the result of the present investigation.

1. Although the area of turbulence may change with time and therefore change the contours observed when this area is visible to us, the nonturbulent hemisphere should give the *same* picture at all times. This requires that the line widths halfway between maximum and minimum remain the same. These epochs were determined from the radial velocity-curves and the curves of varying line width, and the sums of the line widths measured at these epochs are given in Table 11. These sums, connected by a dotted line in Figure 4, show a very strong correlation with the maximum line widths, and we conclude that the lines at this phase are not constant in width but *vary* in the same manner as the maximum line widths.

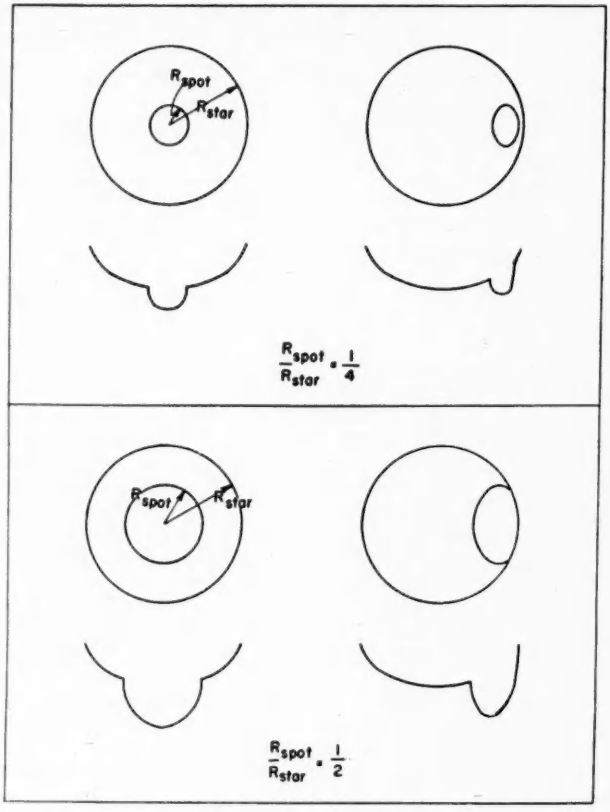

FIG. 7.—Theoretical profiles for a rotating star with a turbulent spot

2. A second test is to determine the rotational velocity from these same lines. The largest line widths with this phase were observed on June 7. A measurement of *He* 4472 gave a width of 3.6 A, which corresponds to a projected rotational velocity of at least 120 km/sec. We now find R max. $= 4.1 \times 10^6$ km, which is still small for the radius of a normal B1 star. But we have assumed here that the period of variable radial velocity and variation in line width is the period of rotation of the star. As mentioned above, this is not necessarily so.

3. The spectral lines of σ Scorpii at their sharpest are certainly not *strikingly* similar to the lines of other well-known turbulent B stars, for example, 55 Cygni.

Nor is there any noticeable absolute-magnitude effect, making the star *appear* more luminous than it really is (as is the case in shell-type spectra). Until a careful spectrophotometric study of the line profiles and the resulting curve of growth has been made, there will remain some uncertainty as to whether turbulence is present.

TABLE 11

SUMS OF THE MEASUREMENTS OF THE LINE WIDTHS APPEARING HALFWAY BETWEEN MAXIMUM AND MINIMUM RADIAL VELOCITY

JD	Days	Sum	JD	Days	Sum
2433755	0	310	2433813	58	290
3783	28	405	3823	68	385
3793	38	430	3829	74	295
3799	44	375	3843	88	520
3805	50	500	3844	89	370

4. As Struve has already pointed out, the period P_2 is so short that it places severe restrictions upon the maximum possible radius of the star, outside of which the companion is supposed to revolve.

5. As has been pointed out by H. Weaver, the velocity-curve should contain a horizontal portion, halfway down the descending branch; this would correspond to the interval when the turbulent area is hidden from sight. Although no such effect has been observed, the uncertainty of the measurements and the lengths of the exposure times would probably suffice to account for the discrepancy.

I am indebted to Dr. Struve and Dr. McNamara for turning over their plates to me for reduction and discussion. Also, I wish to thank Dr. Shane, for granting me permission to use the instruments of the Lick Observatory, and the staff of the Lick Observatory, for their assistance in the observational program. In conclusion, I wish to thank Dr. Struve for his encouragement, suggestions, and advice during the course of the work.

NOTE ADDED IN PROOF: Recent photoelectric observations by A. R. Hogg (*M.N.*, 111, 339, 1951) reveal a variation in light of 0.08 mag. with a period of 0.246841 day. Using Hogg's epochs of minimum light (JD 2432284.08 and 2433396.10) and the above period, the observed epoch of minimum radial velocity (JD 2433804.856) is represented with the following residuals:

$$\text{From JD } 2432284.08: \quad O - C = -0.005 \text{ day},$$

$$\text{From JD } 2433396.10: \quad O - C = -0.011 \text{ day}.$$

Thus minimum light occurs at minimum radial velocity.

THE SPECTRUM OF CHI OPHIUCHI*

E. MARGARET BURBIDGE
Yerkes and McDonald Observatories
Received December 24, 1951

ABSTRACT

Two high-dispersion spectrograms of χ Ophiuchi, one in the photographic and one in the infrared region, are described and wave-length measures are given.

A high-dispersion spectrogram of the photographic region of the B3e star χ Ophiuchi was obtained by W. A. Hiltner with the new coudé grating spectrograph of the McDonald Observatory. On this spectrogram, Dr. Hiltner observed that $H\beta$ appeared as an emission line with three maxima and two minima of intensity, while the rest of the Balmer lines appeared as double emissions. He therefore obtained a spectrogram of the infrared region of this star, using the same spectrograph, in order to see whether the Paschen lines of hydrogen showed the same structure as $H\beta$. Dr. Hiltner kindly lent these two spectrograms to the writer for study. Details of the plates are given in the accompanying tabulation. Descriptions and measures of the spectrum lines are divided

	Date	U.T.	Average Linear Dispersion (A/mm)	Range
1.....	1951, May 13	6^h	4.8	$H\beta$–λ 3450
2.....	May 14	$7\frac{1}{2}^h$	17	λ 8830–$H\alpha$

into separate sections for each element.

I. HYDROGEN LINES

The star χ Ophiuchi was listed by A. Slettebak[1] as a "pole-on" star, but spectra of moderate dispersion have shown[2] the emission lines of $H\gamma$, $H\delta$, and $H\epsilon$ to consist of two components which are subject to V/R variations.

On the first plate the Balmer lines, with the exception of $H\beta$, appear as fairly strong, but broad and ill-defined, double emission lines superimposed on very broad absorptions. The red components are slightly stronger than the violet, and the series can be traced in emission as far as $H21$. Only $H\beta$ has three definite emission maxima with nearly equal separations, the component with the longest wave length being slightly stronger than the other two, which are approximately equal. So far as the writer is aware, this structure has not been previously observed in any of the "normal" Be stars, where the accepted explanation of the emission lines is that they arise in a rotating equatorial ring. The second plate shows $H\alpha$ as a structureless, broad, and very intense emission line, and the Paschen series from $P12$ to $P20$ as rather ill-defined double emission lines, with the red components slightly stronger than the violet, similar in appearance to the Balmer

* *Contributions from the McDonald Observatory, University of Texas*, No. 210.

[1] *Ap. J.*, **110**, 498, 1949.

[2] D. B. McLaughlin, *Pub. Obs. U. Michigan*, **4**, 175, 1932.

lines. Previous spectrograms of the infrared region of this star[3] have not been of sufficiently high dispersion to resolve the Paschen lines into two components.

The wave lengths of the double hydrogen emissions were measured on both plates, and the separations, converted to velocities, are given in Table 1. The agreement between the Balmer and Paschen series, where a long range of wave length is available, provides striking confirmation of the proportionality of separation in angstroms to wave length of the lines and of the interpretation of this separation as a velocity difference.

The mean displacements of the red and violet components of the lines $H\gamma$–$H12$ are +37.2 and −71.9 km/sec, respectively; the three components of $H\beta$ have displacements of +40.7, −15.8, and −77.2 km/sec. It is clear that the two outer components agree in position with the two components of the other hydrogen lines, and their separation is the sum of the two separations given in Table 1, namely, 117.9 km/sec. The mean hydrogen velocity as given by both components of the Balmer and Paschen series together is −15.1 km/sec, which is in close agreement with the displacement of the central component of $H\beta$. The mean separation for all the Balmer and Paschen lines taken together is 110.0 km/sec, giving $v \sin i = 55$ km/sec, where v is the equatorial rotational velocity of the gas giving rise to these emission lines. Slettebak[1] gave the line-of-sight component of the equatorial velocity of the star itself, determined from the profile of *He* I 4026, as 100 km/sec—with some uncertainty. If angular momentum is conserved in the outer regions of the star,[4] then the mean radius of the emitting region would be of the order of twice the stellar radius. If we postulate that this star has a rotational velocity of the same order of magnitude as that which is presumed to cause the flat, dish-shaped absorption lines in other Be stars, namely, 300–400 km/sec, then the inclination of the axis of χ Ophiuchi to the line of sight will be of the order of 15° or 20°. It is difficult to see where the central component of $H\beta$ arises, and why it should not appear in the higher members of the Balmer series, although it may well be present in $H\alpha$, where the emission is too intense for any structure to be detected; i.e., it may arise in part of the gaseous envelope where the Balmer decrement is steeper than in the two lobes, which presumably give rise to the normal components. It will be interesting to see whether this third component is a permanent feature in the spectrum of χ Ophiuchi and whether it is present in any other Be stars.

TABLE 1

SEPARATIONS OF THE TWO EMISSION COMPONENTS OF THE BALMER AND PASCHEN SERIES

Line	Separation (Km/Sec)	Line	Separation (Km/Sec)	Line	Separation (Km/Sec)
$H\beta$	56.5+61.4	$H10$	122.7	$P15$	109.4
$H\gamma$	103.1	$H11$	107.3	$P16$	119.2
$H\delta$	101.9	$H12$	111.1	$P17$	109.6
$H\epsilon$	112.3	$P12$	104.0	$P18$	109.6
$H\zeta$	106.1	$P13$	110.6	$P19$	111.8
$H9$	108.6	$P14$	110.0	$P20$	104.5

II. IONIZED IRON LINES

The lines of *Fe* II were observed to consist of hazy double emissions, much weaker than the hydrogen lines. The separations of the two components of the observed lines are given in Table 2. The mean separation is 140.0 km/sec, which suggests that an effect of stratification is present, with the *Fe* II lines arising at a lower level than the *H* lines.

[3] W. A. Hiltner, *Ap. J.*, **105**, 212, 1947.

[4] E.g., O. Struve and K. Wurm, *Ap. J.*, **88**, 106, 1938.

O. Struve and P. Swings[5] found the same effect from measures of the total width of the emission lines in this star. The mean velocity from both components of all the *Fe* II lines is −12.8 km/sec.

III. HELIUM LINES

The *He* I lines appeared as very hazy, broad absorption lines, difficult to measure. Table 3 lists the observed wave lengths, with the tabular wave lengths in parentheses.

TABLE 2

SEPARATIONS OF THE EMISSION COMPONENTS OF *Fe* II

Tabular Wave Length	Separation (Km/Sec)	Tabular Wave Length	Separation (Km/Sec)
4629.34	136.1	4508.28	156.3
4583.83	139.5	4233.17	129.5
4549.47	135.9	4173.45	151.9
4515.34	131.0		

TABLE 3

OBSERVED WAVE LENGTHS OF THE *He* I LINES

4712.68 (3.14)	4387.90 (7.93)	4120.33 (0.81)	4009.02 (9.27)
4471.31 (1.48)	4143.54 (3.76)	4025.92 (6.19)	3819.35 (9.61)

The mean velocity from the *He* I lines is −19.2 km/sec, with considerable scatter because of the poor quality of the lines.

IV. INTERSTELLAR LINES

In his study of the structure of the interstellar *Ca* II lines, W. S. Adams[6] was able to resolve the H and K lines in χ Ophiuchi into two components, the stronger having a displacement of −11.1 km/sec, and the weaker and broader one of −27.5 km/sec. The dispersion he used was 2.9 A/mm. These lines were not resolved in the McDonald spectrogram but were clearly unsymmetrical, with a sharp red edge and a shaded violet edge. Most of the other interstellar lines observed by Adams in this star could be seen, but the lines of *CH* II and *CN* I were extremely faint. Table 4 gives the interstellar lines observed, an estimate of their intensities, and their displacements, which may be compared with the observations by Adams. The tabular wave lengths used for the *CH* I, *CH* II, and *CN* I lines are those determined by Adams.

TABLE 4

OBSERVED WAVE LENGTHS AND DISPLACEMENTS OF THE INTERSTELLAR LINES

Element	Observed Wave Length	Int.	Displacement (Km/Sec)	Element	Observed Wave Length	Int.	Displacement (Km/Sec)
Ca II (H)	3968.29	7	−14.1	*CH* II	4232.32	1	−18.1
Ca II (K)	3933.47	5	−15.4	*CH* II	3957.48	0	−18.1
CH I	4300.14	3	−13.4	CN I	3874.48	0	−11.2

[5] *Ap. J.*, **75**, 161, 1932.

[6] *Ap. J.*, **97**, 105, 1943.

V. OXYGEN LINES

W. A. Hiltner[3] observed the two groups of *O* I lines at λ 8446 and λ 7773 to be single emission lines, the blend at λ 8446 being very much stronger than that at λ 7773. This anomaly, which has been observed in several Be stars,[3, 7, 8] was explained by I. S. Bowen[9] as being due to overpopulation of the 3^3D° state of *O* I by absorption of Lyman-β radiation and subsequent cascading; and Slettebak[8] pointed out that, if the relative strengths in the Lyman series are similar to those in the Balmer series, then stars with strong $H\beta$ emission, such as χ Ophiuchi, would be expected to show this effect.

The second plate shows *O* I λ 8446 to have two emission maxima, with the red component very much stronger than the violet. The tabular wave lengths and intensities of the three *O* I lines contributing to this blend are λλ 8446.35 (25), 8446.35 (25), and 8446.76 (23).[10] The adopted mean wave length was that given for the blend in the *Revision of Rowland's Preliminary Table of Solar Wavelengths;* with this value, the displacements of the two components are +23.8 and −60.7 km/sec, the separation is 84.5 km/sec, and the mean of the two displacements is −18.5 km/sec, in agreement with the mean velocities given by the other elements. The fact that the separation of the two components is smaller than that given by the hydrogen lines suggests stratification again, with the region giving rise to the oxygen emission lying farther out from the star than the region where the hydrogen lines arise.

The *O* I blend at λ 7773 was not resolved; the tabular wave lengths of the lines giving rise to this are λλ 7771.96 (27), 7774.18 (26), 7775.40 (25),[10] and the spacing of these would mask any structure that was present. The appearance of the blend was a flat, rather weak emission band with a total width of 8.7 A.

VI. CALCIUM LINES

The members of the infrared *Ca* II triplet, λλ 8662.14 (1000), 8542.09 (1500), and 8498.02 (300)[10] fall near the Paschen lines *P*13 at λ 8665.02, *P*15 at λ 8545.38, and *P*16 at λ 8502.49; and it is therefore difficult to tell whether they are present or not when the Paschen lines are strong, as in χ Ophiuchi. They have not been detected on infrared spectrograms of this star previously obtained,[3] but on the present spectrogram there appeared to be a faint emission extension to the violet of *P*13, and possibly a faint emission alongside an absorption line on the violet side of *P*15. Nothing was observed near *P*16. This evidence is inconclusive, and it is not certain yet whether *Ca* II emission is present in this star or not. The appearance of emission in the infrared *Ca* II triplet in stars where the H and K lines are in absorption has been discussed by several workers.[3, 11] Wyse has suggested that the mechanism is the depopulation of the ^2D state of *Ca* II by ionization by Lyman-α quanta; but other factors may be involved.

VII. CONCLUSION

χ Ophiuchi is not such a striking example of a "pole-on" star as, for example, 11 Camelopardalis; it is likely that the axis is inclined to the line of sight by about 15° or 20°. This angle is small enough, however, for the broad *H* absorptions underlying the emission lines to show a "pole-on" effect. The region giving rise to the emission lines shows stratification, the *H* emission arising on the average farther out from the star than the *Fe* II emission, and *O* I λ 8446, which presumably arises through fluorescence involving absorption of Lβ, comes from a region still farther out than the *H* region.

[7] P. W. Merrill, *Ap. J.*, **79**, 183, 1934; P. Swings, *Pub. A.S.P.*, **56**, 238, 1944; P. C. Keenan and J. A. Hynek, *Ap. J.*, **111**, 1, 1950.

[8] A. Slettebak, *Ap. J.*, **113**, 436, 1951.

[9] *Pub. A.S.P.*, **59**, 196, 1947.

[10] Charlotte E. Moore, *Revised Multiplet Table* (*Contr. Princeton U. Obs.*, No. 20 [1945]).

[11] A. B. Wyse, *Pub. A.S.P.*, **53**, 184, 1941; J. L. Greenstein and P. W. Merrill, *Ap. J.*, **104**, 188, 1946.

The mean velocities given by the different elements do not, in view of the scatter which is present, show significant differences from one another.

The two most striking unexplained features in the spectrum are, first, the presence of a third emission component between the two normal components of $H\beta$ and, second, the strength of the red component of the double emission of *O* I λ 8446 as compared to the violet component, when the *H* and *Fe* II lines have the red component only slightly stronger than the violet.

I am indebted to the International Astronomical Union for a grant which has enabled me to work at Yerkes Observatory. I also wish to express my gratitude to Professor B. Strömgren for extending to me the facilities of the Yerkes Observatory, and to Dr. Hiltner for the loan of the plates.

MEAN DISTANCES IN SINGLE-LINE BINARIES

VICTOR M. BLANCO
Warner and Swasey Observatory, Case Institute of Technology*
Received January 30, 1952

ABSTRACT

The distribution of mean distances is determined for a group of single-line spectroscopic binaries with primaries within the spectral-type interval B8–A5. The masses of the primaries are evaluated from the mass-luminosity relation, and the distribution of mass ratios is obtained from the mass functions by assuming random inclinations. The distribution of mass ratios and Kepler's third law are then used to determine the distribution of mean distances. The effects of incompleteness of the observational data are allowed for. The systems studied show a marked drop in number with decreasing mean distances at $a = 7 \times 10^6$ km. The frequency of mass ratios is found to increase with decreasing mass ratios.

From the definition of the mass function f we may write

$$\left(\frac{f}{m_1}\right)^{1/3} = \frac{\mu \sin i}{(1+\mu)^{2/3}} \qquad \text{or} \qquad T = X \sin i\,, \tag{1}$$

where m_1 is the mass of the primary and $\mu = m_2/m_1$ is the mass ratio. If f is known and m_1 is evaluated from the mass-luminosity relation, one can obtain the distribution of the quantity T for a group of stars.

The distributions of T, X, and sin i are connected by an integral equation which may be readily solved if one assumes random inclinations. Kuiper[1] and Colacevich[2] have investigated the distributions of mass ratios for various groups of binary systems with this method. More recently, Chandrasekhar and Münch[3] have shown that for random inclinations the moments of X can be found directly from the observed moments of T. With a suitable interpolation formula, one can then reconstruct the distribution of X. Furthermore, from the distribution of X that of μ can be obtained by transforming variables.

We may write Kepler's third law in the form

$$C m_1^{1/3} P^{2/3} = \frac{a}{(1+\mu)^{1/3}} \equiv A\,. \tag{2}$$

The constant $C = 2.94 \times 10^6$ when a is in kilometers, P in days, and m_1 in solar units. Since the quantity A may be evaluated for each of the systems in the group considered above, one can establish the distributions of mass ratios for different values of A. In effect this yields the bivariate distribution of A and μ, from which one may interpolate the distribution of a with respect to μ.

In practice the application of this method has the following difficulties.

1. The masses of the primaries can be estimated only when the correct spectral and luminosity classifications are known. For this reason the present study was limited to early spectral classes, and supergiants were eliminated when known.

2. The observed spectroscopic binary systems suffer from observational selection. Selection according to apparent magnitudes does not affect the distributions except in the

* A major portion of this study was carried out at the Leuschner Observatory, University of California, Berkeley, Calif.

[1] *Pub. A.S.P.*, **47**, 15, 1935.

[2] *Mem. Soc. astr. italiana*, Nuova Serie, **11**, 132, 1938.

[3] *Ap. J.*, **111**, 142, 1950.

case of eclipsing binaries, where it is found that the fainter systems studied tend to be eclipsing stars and hence systems with high inclinations. Since random inclinations are essential, in this study those faint binaries were eliminated whose orbits were determined primarily because they were known to eclipse. A much more serious selection effect is the selection according to the semiamplitude K_1 of the velocity-curve, which favors the higher values of the mass functions. Struve[4] has suggested the use of factors of incompleteness equal to $75/K_1$ to correct the distributions for those early-type stars where $K_1 < 75$ km/sec. This method was followed in the present study.

In order to correct the populations, a plot of the quantity $\frac{1}{2} \log A$ against $\log T$ was prepared. It may be readily shown[5] that

$$\log T - \tfrac{1}{2} \log A - \log K_1 = \tfrac{1}{2} \log \frac{(1 - e^2)}{m_1} + \text{constant}. \qquad (3)$$

If the systems are selected so that the primaries are of nearly the same mass, the right-hand side of the above expression is approximately a constant. Given a value of K_1, the

TABLE 1

OBSERVED DISTRIBUTIONS

log A:					
8.0					
	4	3	2	0	
7.6					
	5	9	2	2	
7.2					
	11	15	8	3	
6.8					
	1	4	1	1	
6.4					
log T	−0.30	−0.52	−0.74	−0.96	−1.18

resulting linearity between $\log T$ and $\frac{1}{2} \log A$ allows the division of the ($\log T$, $\frac{1}{2} \log A$) plane into regions with different degrees of incompleteness, where the populations can be increased by the appropriate factors.

The method outlined above was followed with a group of 71 systems with orbital elements listed in Moore and Neubauer's *Fifth Catalogue of Spectroscopic Binaries*.[6] When determining the values of T and A, m_1 was obtained as follows: If a parallax value was available and it was greater than 0".035, the absolute bolometric magnitude was computed and the mass was estimated from Kuiper's mass-luminosity relation.[7] For parallaxes in the range 0".020 to 0".035 the above procedure was followed, but the resulting mass was averaged with one estimated directly from the spectral class with the help of a diagram given by Russell and Moore.[8] For parallaxes less than 0".020 and in those cases where no parallaxes were available the mass derived from the spectral class was used. After correction for incompleteness the 71 cases were found to represent an effective population of 172 binaries. Tables 1 and 2 show the observed and corrected distributions, respectively.

[4] *Pop. Astr.*, **58**, 7, 1950.

[5] From eq. (2) of Moore and Neubauer, *Fifth Catalogue of Spectroscopic Binaries* (*Lick Obs. Bull.*, No. 521 [1948]).

[6] *Ibid.*

[7] *Ap. J.*, **88**, 472, 1938.

[8] *Masses of the Stars* (Chicago: University of Chicago Press, 1939).

In these tables the upper limit of log T coincides with the value of T obtained from equation (1) by setting $i = 90°$ and $\mu = 0.7$. This value of the mass ratio follows from the mass-luminosity relation, if the difference in magnitude of the two components in single-line systems is taken to be at least 1 mag. The observed lower limit of log A is a little higher than the limit of 6.1, which results if we let $a = 2.2$ solar radii, corresponding to contact between an A5 primary and a dwarf M0 secondary. The other limits of log T and log A were set by lack of data. It should be noticed that the numbers of stars added in correcting for incompleteness increase toward the right side and upward in the tables; hence, the uncertainty in Table 2 increases in the same sense.

Because there were few stars, the application of incompleteness corrections was limited to systems with $K_1 > 15$ km/sec. For a given row in the tables this limitation tends to eliminate systems with small inclinations and mass ratios, the number with low inclinations being small, since the frequency function of random inclinations equals sin i. In the derivation of the distribution of log X from the data in each row, the missing systems do not affect the results seriously, as may be appreciated if the effect of random inclinations on the distribution of log T is considered. If the distributions of log X were known, the

TABLE 2

CORRECTED DISTRIBUTIONS

log A:					
8.0					
	10	12	15	0	
7.6					
	7	22	9	17	
7.2					
	12	23	21	14	
6.8					
	1	4	2	3	
6.4					
log T	−0.30	−0.52	−0.74	−0.96	−1.18

distributions in Table 2 could be derived by "smearing" the populations in such a way that 80 per cent of the stars in a given interval were left in the same place, 13 per cent were shifted one interval to the right, 4 per cent were shifted two intervals to the right, and so forth, satisfying the condition $T \leqslant X$. Hence the lack of data for $K_1 < 15$ km/sec does not seriously affect the derivation of the distribution of log X, inasmuch as only 20 per cent of the systems missed will be absent in our final distributions for the lowest values of X and 7 per cent or less in the rest of the intervals. The "smearing" procedure outlined above is, in fact, the method by which the distribution of X is obtained if one uses numerical integration.

In order to derive the distribution of X, the moments of T are necessary. These are presented in Table 3. Sheppard's corrections, although small, have been applied. From these moments, the moments of X were obtained directly by use of Chandrasekhar and Münch's formulae. A Gram-Charlier distribution that satisfied the required moments was then computed for each row. The resulting distributions of X are given in Table 4. In this table, for each value of X the corresponding value of μ is indicated. By estimating the mean value of log $(1 + \mu)^{1/3}$ in each interval, the ordinates were changed to log a. Owing to the varying mass ratios, the set of new ordinates in successive rows did not agree, and uniformity was obtained by interpolations. The actual interpolations involved only very slight shifts in the populations. The final results show that the total distribution of log a is very similar to the observed total distribution of log A after correction for

incompleteness, except for the change in the values of the interval limits. In fact, the observed total distribution of log A even before correction shows the essential features of the final total distribution of log a.

Table 5 presents the final results. The marginal distributions in this table indicate the total distributions of log a and μ. Because of the incompleteness in the original data, the parts of this table that can best be trusted are downward and toward the left.

Of particular interest is the drop, observed below log $a = 6.846$, in the distributions of

TABLE 3

MOMENTS OF T AND THEIR PROBABLE ERRORS

log A	$\overline{T}$	$\overline{T^2}$	$\overline{T^3}$
8.0	0.24±0.01	0.064±0.006	0.019±0.003
7.6	0.19±0.01	0.044±0.004	0.011±0.002
7.2	0.20±0.01	0.048±0.004	0.013±0.002
6.8	0.19±0.02	0.040±0.003	0.010±0.003
6.4			

TABLE 4

COMPUTED DISTRIBUTION OF X OR μ

log A:						
8.0	2	7	17	11	0	
7.6	1	6	17	22	9	
7.2	2	9	22	27	10	
6.8	0	1	3	4	2	
6.4						
X	0.55	0.45	0.35	0.25	0.15	0.05
μ	0.82	0.62	0.45	0.30	0.17	0.05

log a, regardless of the mass ratios. This mean distance, 7×10^6 km, is from six to twelve times the radii of the primaries for the spectral classes studied here and shows that the number of systems drops sharply well before physical contact is possible. Of interest also is the increase, with decreasing mass ratios, shown by the fraction of the total in each column formed by those systems that fall in the lower two intervals of log a. This result agrees with the supposition that stable systems are more likely if the secondary has a small mass.[9]

The total frequency of the mass ratios increases with decreasing μ. In the last interval the drop in frequency may be explained by the omission of systems with $K_1 < 15$ km/sec and by the higher uncertainty of this part of the distribution. In the interval 0.62–0.82 the small numbers obtained are undoubtedly due in part to the exclusion of systems with double lines, but for the other intervals this selection effect is not believed to be of im-

[9] I am indebted to Dr. Struve for this observation.

portance. Since the derived distribution of the mass ratios depends on the method adopted in correcting for incompleteness, another solution was made with a different set of correction factors. The new factors were obtained by comparing the distribution of K_1 for systems with primaries of spectral types later than F0 with the corresponding distribution for earlier types and assuming the first group to be complete. This procedure is based on the assumption that the binaries with early types are incomplete solely because their spectra do not admit the same precision of measurement as the later types.

TABLE 5

DISTRIBUTION OF LOG a AND μ

All a's	5	23	59	64	21	172
log a:						
8.046	2	7	17	10	0	36
7.646	1	6	17	22	8	54
7.246	2	9	22	27	10	70
6.846	0	1	3	5	3	12
6.446						

Mass ratios μ	0.82	0.62	0.45	0.30	0.17	0.05	All μ's

As a matter of fact, the resulting corrections are known to be too small. The factors of incompleteness were found necessary below $K_1 = 24$ km/sec and equaled about one-fourth of those recommended by Struve. In this solution the features of the distribution of log a discussed above were found unchanged. The total distribution of mass ratios, however, was approximately constant. These considerations show that the number of systems definitely increases with decreasing mass ratios for the group of stars studied here.

Although the method of moments employed here reduces the effect of most of the accidental fluctuations in the observed distributions in comparison with solutions based on numerical integrations, it may suffer from the appreciable effects that those fluctuations occurring near the limits of the population have on the higher moments. The resulting over-all features may then be spurious. In view of this, I should point out that a parallel analysis based on numerical integrations yielded essentially the results that were presented above.

I wish to acknowledge my gratitude to Dr. Trumpler for suggesting this problem and for his counsel during its development.

THE SPACE DISTRIBUTION OF INTERSTELLAR MATERIAL IN THE MILKY WAY

L. BINNENDIJK
Sproul and Goodsell Observatories
Received November 13, 1951

ABSTRACT

Several catalogues of intersellar intensities of the H and K doublet of *Ca* II, the D1 and D2 doublet of *Na* I, and the λ 4430 band were reduced to one system of equivalent widths expressed in angstrom units. Probable errors were determined from the external agreement, and the results are very close to the internal probable errors. The photoelectric colors of Stebbins, Huffer, and Whitford and the Yerkes spectral classification were used to derive the interstellar reddening, corrected for zero point. The Morgan system was adopted for the spectroscopic distances of the B stars.

The observed doublet ratios were studied in some detail, and curves of growth were derived in the usual way by shifting line segments. Small areas in the Milky Way were chosen, and the distance relations were established for the intensities, reddening, and polarization. The galactic-rotation effect in the equivalent widths was found to be small, at least within a distance of 1.8 kpc. The average density of *Ca* II and *Na* I in successive distance intervals of 100 psc in each area was found with the help of the distance relations and the curves of growth. Figures were plotted, giving the average distribution of the gas and the smoke (or solid particles) in the plane of the Milky Way. Within a radius of 1 kpc in the plane, average numbers of 3×10^{-9} calcium ions and 11×10^{-9} sodium atoms/cm^3 were found; the numbers for the continuum and the gas concentrations were 0.8×10^{-9} and 6×10^{-9} for calcium and 2×10^{-9} and 32×10^{-9} for sodium, respectively. An indication was found of some structure, especially in the general direction of Cygnus, 90° from the direction of the center of the Milky Way.

The general relations between interstellar-line intensities and reddening for successive distance intervals of 300 psc were discussed for all observed stars in the Milky Way having accurate data. For unreddened stars the K and D intensities continue to increase for more distance intervals. It is found that for small areas the near-by stars and the distant stars give two almost parallel relations. The line intensity is a function both of the distance of the star and of the reddening; the first approximation yields $K = 0.18\,r + 0.7\,E_{1c}$. Reasons are given for the poor relations found by some authors. The relation between the λ 4430 band and the reddening is a simple one and holds for all distance intervals.

The interpretation of observations of interstellar material is intermediate between the uniform distribution and the other extreme, namely, all gas and smoke concentrated in discrete clouds. In general, the clouds consist of gas and smoke (or solid particles); between the smoke clouds a rarefied gas continuum is still observable, but the smoke continuum is either still more rarefied or cannot be observed. Reasons are given why in some places deviations may occur from this general behavior.

The calcium and sodium gases seem to be well mixed. They indicate the galactic-rotation effect; they show small-scale turbulence effects; and in some places larger-scale currents introduce the multiplicity of the interstellar lines. No decisive result could be found as to whether there is a flow of the gas out of the Milky Way.

I. INTRODUCTION

The subject of the present study is the relation between the interstellar gases and interstellar smoke. The former are atoms and ions, giving absorption lines. Smoke or dust consists of grains or solid particles, giving absorption and reddening effects.

The sharp interstellar H and K doublet of *Ca* II was discovered by J. Hartmann[1] as early as 1904. The sharp interstellar D1 and D2 doublet of *Na* I was discovered by M. L. Heger.[2] The unidentified λ 4430 band was discovered by P. W. Merrill.[3]

Many authors find a poorly defined relation between the intensities of the sharp interstellar lines and reddening. Since most of these publications deal with stars spread out over the whole Milky Way, it seems worth while to study the same relation in small areas

[1] *Ap. J.*, **19**, 268, 1904.
[2] *Lick Obs. Bull.*, **10**, 59, 1919.
[3] *Ap. J.*, **83**, 126, 1936; *Mt. W. Contr.*, No. 536.

and for stars over a certain distance interval in such an area. Enough accurate material is now available for such a regional study.

First, it is necessary to combine into one uniform system all observations given in the different catalogues. Since the area of an absorption line has more physical meaning than the depth of the line, we chose the equivalent widths in angstrom units as a desirable standard. We will have to consider the three following groups of lines separately after the combination: the H and K lines, the D lines, and the λ 4430 band, each of them consistent in itself. C. S. Beals measured all principal interstellar lines, but his measurements show unexplained scale differences from those of other authors.

Next we must establish a uniform weight system, because most authors give only symbols or number of plates and some indication of the internal probable error. After an intercomparison of the different catalogues, the percentage probable error has to be found in each case. Then we have to compute the probable error in angstrom units for each star. Thus, after combining all data, we can get an idea of the accuracy of the line intensity of a star. Moreover, the reddenings and the distances of the B stars concerned should be of as high quality as possible.

A definition is necessary of what we mean by a "cloud." By "cloud" we will understand a discrete unit, and we will use it mostly in the case of a smoke cloud. There is evidence that in the Milky Way the density of the gas is more continuous than that of the smoke. The terminology used here in the case of gas is therefore "continuum" and "concentration." The continuum is defined as the more transparent part of the gas distribution in the line of sight; the concentration, as the more opaque part of higher density. We will use the term "current" for local stream motion with respect to the general mean motion of the gas. This term is thus the equivalent of the peculiar velocity of the gas clouds.

II. CATALOGUES OF INTERSTELLAR LINES

Table 1 contains the most important observing data: the interstellar line, the author, the number of stars observed, the observatory with aperture of the telescope in inches, the focal length of the camera in inches, the dispersion in angstrom units per millimeter near the given line, and the emulsion used.

THE CALCIUM DOUBLET (*Ca* II)

The following measurements are given of the H and K lines:

a) R. F. Sanford published the measurements for the K line in a more general Mount Wilson publication[4] but discussed the material elsewhere.[5] R. F. Sanford and O. C. Wilson[6] gave a list of intensities for the H and K lines. Recently, Sanford[7] published another list of the K-line intensities for stars in open clusters. A total of 148 star data could be used. There are no systematic differences between the three catalogues of Sanford, which have been reduced to one system. This system, given in equivalent widths in angstrom units, was taken as our standard system. The effective dispersion is 25 A/mm. For the weights the symbols A, B, and C are given in these catalogues and sometimes the number of plates.

b) L. Spitzer, I. Epstein, and L. Hen[8] measured intensities for 141 stars of the Mount Wilson material for which Adams had given estimates (see later). The spectra were taken at the coudé focus of the 100-inch reflector. Most of them were made with a Schmidt camera of focal length 114 inches, having a dispersion of 2.9 A/mm; but part of the material was taken with a Schmidt camera of focal length 32 inches, having a dispersion of

[4] *Ap. J.*, **86**, 274, 1937; *Mt. W. Contr.*, No. 576.

[5] *Ibid.*, p. 136; *Mt. W. Contr.*, No. 573.

[6] *Ap. J.*, **90**, 235, 1939.

[7] *Ap. J.*, **110**, 117, 1949.

[8] *Ann. d'ap.*, **13**, 147, 1950.

10.3 A/mm. Fortunately, this was noted in the catalogue. For stars showing double or multiple lines, the sum of the equivalent widths was taken as most representative for our purpose.

Spitzer has already noted by comparison with other catalogues that there seems to be a systematic difference between these two sets of data. We found by intercomparison a similar effect. In the following pages we will use the symbol I, with index, for the intensity of the interstellar line, as given in the system of the author mentioned. The scale factors were always derived directly from the graphs, where a straight line was drawn, which fitted the weighted observations in the best way:

$$I_{Sa} = 1.10\, I_{Sp,\,2.9}\,; \qquad I_{Sa} = 1.00\, I_{Sp,\,10.3}\,.$$

TABLE 1

DATA OF OBSERVATIONS

Line	Author	Number of Stars	Obs.†	Telescope (Inches)	Camera (Inches)	Dispersion (A/mm)	Emulsion
K, (H)	Sanford, Wilson	148, (40)‡	MtW	60	10	23	Imperial Eclipse
				60	15	15	Imperial Eclipse
				100	32	10	Imperial Eclipse
				100	10	48	Imperial Eclipse
	Spitzer, Epstein	141, (141)	MtW	100	114	2.9	Eastman Kodak 103-O
				100	32	10.3	Eastman Kodak 103-O
	Williams	62, (43)	MtW	60	15	16.6	Imperial Eclipse
				60	10	23.5	Imperial Eclipse
	Beals	123, (32)	V	72	17	33.5	Eastman Kodak 33
				72	28	20	Eastman Kodak 33
	Struve*	295	Y	40	24	30	.....
			MtW	60	18	45	.....
	Plaskett, Pearce*	153	V	72	28	29	.....
				72	16	49	.....
	Adams*	300, (50)	MtW	100	114	2.9	Eastman Kodak 103-O
				100	32	10.3	Eastman Kodak 103-O
D2, D1	Merrill, Wilson	213	MtW	100	18	34	Eastman Kodak IIIc
				100	10	66	Eastman Kodak IIIc
	Spitzer	37	MtW	100	18	34	Eastman Kodak IIIc
				100	32	20	Eastman Kodak 103a-D
				100	72	8.9	Eastman Kodak 103a-D
	Beals	90	V	72	28	30.7	Ilford Panchromatic
				72	38	22	Ilford Panchromatic
				72	38	66	Ilford Panchromatic
λ 5780	Merrill, Wilson	117	MtW	100	18	34	Eastman Kodak IIIc
5797	.....	61		100	10	66	Eastman Kodak IIIc
6284	.....	129					
λ 4430	Greenstein, Aller	36	McD	82	7	70	Eastman Kodak IIa-O
				82	20	30	Eastman Kodak IIa-O
	Beals, Blanchet	42	V	72	17	33.5	Eastman Kodak 30
				72	28	20	Eastman Kodak 30
	Duke	346	Y	40	6	123	Eastman Kodak IIa-O
	Baker	7	E	36	20	32	Ilford Astra VIII
	Sherman*	22	Y	40	3	225	Ilford Process

* Author gives only estimates.

† MtW = Mount Wilson, V = Victoria, Y = Yerkes, McD = McDonald, E = Edinburgh.

‡ The numbers in parentheses correspond to the H line.

For the weights the symbols A, B, C, and D were used. Spitzer did not take into account the scale differences of 10 per cent in the computation of the external probable error and therefore found too high values for the percentage probable errors.

c) E. G. Williams[9] gave a list of line intensities of 62 stars and found that the emission Be stars are intrinsically somewhat redder. The line intensities are given in units of a tenth wave number, so we first have to multiply by a factor of 0.0155 for the K line and a factor of 0.0157 for the H line. The intercomparison showed that the scale agrees but that there is a zero-point difference in the material of Williams. The relation between the intensities of the K line is given by

$$I_{\mathrm{Sa}} = 1.00 \times 0.0155 I_{\mathrm{Wi}} - 0.05 .$$

The weights published are between 1 and 6.

d) C. S. Beals[10] published several lists of measurements and kindly sent a more extensive and revised list concerning 123 stars. The equivalent widths are expressed in km/sec and were therefore multiplied by a factor of 0.0131 for the K line and a factor of 0.0132 for the H line to convert into angstrom units. An intercomparison shows that the relation between the intensities of the K line is

$$I_{\mathrm{Sa}} = 0.80 \times 0.0131 I_{\mathrm{Be}} = 0.0105 I_{\mathrm{Be}} .$$

The large difference had been noted already by several authors and may be ascribed partly to a dispersion effect (see later). The number of plates is given and sometimes the internal probable error.

The following catalogues give only estimates of the K line:

e) O. Struve[11] gave a list for 295 bright B stars, observed mostly with the Yerkes refractor. His estimates are on a scale for which the unit is an absorption of 0.1 mag. For the relation with Sanford's system we find

$$I_{\mathrm{Sa}} = 0.043 I_{\mathrm{St}} .$$

From much more material Struve found a distance relation for the K line, showing that line intensities can be used as a distance criterion.

f) J. S. Plaskett and J. A. Pearce[12] published a list of K line radial velocities with estimates of line intensities for 153 stars. As E. G. Williams[9] has already pointed out, there is a magnitude effect; the fainter stars are assigned too low an intensity. The lack of data on the different cameras used in the observation for a certain star makes it impossible to find out whether this is, in reality, a dispersion effect. For the stars brighter than 6.5 mag. we find the following relation:

$$I_{\mathrm{Sa}} = 0.040 I_{\mathrm{PP}} .$$

The estimates are in a scale for which the unit corresponds to an absorption of 0.1 mag. There is thus only very little scale difference between Struve's system and this system, as follows from the close agreement between the two coefficients. The authors find a criterion for the distance in the linear relation between intensities and galactic-rotation term.

g) W. S. Adams[13] gave a list of radial velocities and estimates of intensities of 300 stars. This list supersedes an older list of 50 stars by the same author,[14] in which the intensity

[9] *Ap. J.*, **79**, 280, 1934; *Mt. W. Contr.*, No. 487.
[10] *M.N.*, **93**, 585, 1933; **94**, 663, 1934; **96**, 661, 1936.
[11] *M.N.*, **89**, 567, 1929; *Ap. J.*, **67**, 353, 1928; **65**, 163, 1927.
[12] *Pub. Dom. Ap. Obs. Victoria*, **5**, 167, 1935.
[13] *Ap. J.*, **109**, 354, 1949; *Mt. W. Contr.*, No. 760.
[14] *Ap. J.*, **97**, 105, 1943; *Mt. W. Contr.*, No. 673.

scale is four-thirds the new one. The material was divided according to the two dispersions used, and a considerable systematic deviation was found. The relations are

$$I_{Sa} = 0.014 I_{Ad,2.9} ; \qquad I_{Sa} = 0.027 I_{Ad,10.3} .$$

The two sets of estimates have a scale difference by a factor of 2; compare herewith the measurements of the same two sets by Spitzer. If we take this systematic error into account, we find an accidental error in the estimates of Adams in close agreement with those of the other estimates.

THE SODIUM DOUBLET (*Na* I)

The following measurements are given of the D1 and D2 lines:

h) P. W. Merrill, R. F. Sanford, O. C. Wilson, and C. G. Burwell[4] published an extensive list of 213 stars, discussed by Wilson and Merrill[15] and once more by the last author.[16] The system of equivalent widths in angstrom units given by Merrill is taken as standard. The effective dispersion is 34 A/mm. The authors use the symbols A, B, and C for the weight.

Merrill and his co-workers also included the measurements of the unidentified shallow lines with the wave lengths λλ 5780, 5797, and 6284 in the same units. It may be assumed, therefore, that the scale is the same as for the D lines.

i) L. Spitzer[17] published a list of 37 stars observed at Mount Wilson. This system also is given in equivalent widths in angstrom units but has only 4 stars in common with Merrill's system. However, both systems show the same relation with the following system, so that we may safely conclude that there is no scale difference. For the weights the symbols A, B, C, and D were used.

j) C. S. Beals[10] sent us revised data of 90 stars for the D lines. The equivalent widths are given in km/sec, so we first have to multiply by a factor of 0.0197 to convert into angstrom units. A comparison with the other systems shows that there is a scale difference of 30 per cent, as was already found by the previous authors:

$$I_{Me} = 0.70 \times 0.0197 I_B = 0.0138 I_{Be} .$$

The large-scale difference is very unsatisfactory and cannot be ascribed to a dispersion effect. Several tests at Victoria and Mount Wilson did not clarify the real source of the differences. According to Merrill, two factors may be responsible for this systematic deviation: differences in scattered light in the two spectrographs and personal differences in treating the edges of the lines.

THE λ 4430 BAND

The following measurements of this broad band are available:

k) J. L. Greenstein and L. H. Aller[18] gave a list of equivalent widths in angstrom units of 36 stars observed at McDonald Observatory. We therefore chose it as our standard system. For the weights the numbers of spectra are given.

l) C. S. Beals and G. H. Blanchet[19] published data of 42 stars. Their data for this band are given in km/sec and a factor of 0.0148 was applied first to get equivalent widths in angstrom units. It is impossible to find a direct relation with the previous catalogue, because the catalogues have only 2 stars in common. Two diagrams in Greenstein's paper, namely, the correlation between the λ 4430 band and reddening and the correlation between the λ 4430 band and the λ 6284 line, suggest that there may be a slight scale difference. However, no conclusion can be drawn, since completely different stars are in-

[15] *Ap. J.*, **86**, 44, 1937; *Mt. W. Contr.*, No. 573.

[16] *Ap. J.*, **86**, 28, 1937; *Mt. W. Contr.*, No. 569.

[17] *Ap. J.*, **108**, 276, 1948.

[18] *Ap. J.*, **111**, 328, 1950.

[19] *M.N.*, **98**, 398, 1938.

volved and the intrinsic spread in the measurements of this band is large. The comparison of both catalogues with the next one shows an identical relation in both cases, and we conclude that the scale difference between the catalogues of Greenstein and Beals is very small. For the weights the sums of the weights of the individual tracings are given.

m) D. Duke[20] published an extensive list of measurements of 346 stars observed with the Yerkes refractor. He measured the depth of the band, which is more accurate in this case than the equivalent width and gives the percentage absorption expressed in the continuum at the same wave length. Unfortunately, he does not give additional measurements in equivalent widths for stars in both previous catalogues, which would have given a direct scale comparison. Now we can give only the empirical relation:

$$I_{Gr} = 0.23\, I_{Du}\,.$$

For the weights the symbols A, B, C, D, and F are used.

n) E. A. Baker[21] included this band for 7 stars in a more general study. The published errors indicate a high precision. The small number of stars prevents any definite conclusions, but there seems to be good agreement with Duke's results.

o) F. Sherman[22] published a list of 22 estimates.

III. RELATION BETWEEN LINE INTENSITY AND DISPERSION

There is a relation between the intensity measurement of a line and the dispersion used in the sense that high dispersion tends to give a smaller intensity measurement. The scale differences found between the catalogues of the same lines can be ascribed to this effect. Whatever its cause the effect seems to be real, and therefore each observer should give the dispersion used for each observation. The K line of average intensity has an equivalent width of 0.3 A in the standard system of Sanford (25 A/mm); the other data given in the accompanying tabulation are the corresponding intensities measured by other observers

Author	Dispersion (A/mm)	K Value (A)	Author	Dispersion (A/mm)	K Value (A)
Spitzer	2.9	0.27	Sanford	25	0.30
Sanford	10	.24	Beals	33.5	.38
Spitzer	10.3	.30	Sanford	50	0.36
Williams	20	0.35			

arranged according to the dispersion used. Three values of Sanford for different dispersion are given according to his published reduction formulae. The value of Beals may be affected by an unknown source, as we saw, and therefore has to be considered of low weight in this connection.

The same effect was found by P. Th. Shajn[23] but is not well confirmed by the results of A. D. Thackeray.[24] Laboratory measurements could determine whether the photographic Eberhard effect or some other effect plays a role.

IV. WEIGHTS AND PROBABLE ERRORS

The different catalogues can now be reduced to one system from the information given in the previous pages. We now have to introduce a uniform weight system.

In the publications one sometimes finds the internal percentage probable error as found

[20] *Ap. J.*, **113**, 100, 1951.

[21] *Edinburgh Pub.*, **1**, 15, 1949.

[22] *Ap. J.*, **90**, 630, 1939.

[23] *Bull. Poulkovo*, Vol. **13**, No. 4, 1934.

[24] *M.N.*, **94**, 99, 1933.

by the author. We have determined the external percentage probable error for the best data by comparing the different catalogues and found very little difference between the two kinds of errors. For the measurements of the sharp K and D lines we find a percentage probable error of 6 per cent for the best data, increasing to about 14 per cent for the data with the lowest weight. For the K line the average intensity is about 0.3 A and for the D lines 0.4 A, so that these lines of average intensity have a probable error in one catalogue of the order of ± 0.03 A for average weight. For the estimates of the K line we find percentage probable error of 17 per cent. This means that estimates from two or three catalogues combined for the fainter lines still give rather accurate values and can be used.

The percentage probable error for the measurements of the λ 4430 band is of the order of 7 per cent for the best data and increases to 30 per cent for the data with lowest weight. The difficulty in measuring this broad band is thus shown. The average intensity of the λ 4430 band is about 1.5 A, so that a band of this average intensity has a probable error in one catalogue of the order of ± 0.3 A for average weight.

In Table 2 are to be found the lines, author, symbol, and weight given, internal per-

TABLE 2

WEIGHTS AND PERCENTAGE PROBABLE ERRORS

Line	Author	Symbol	Weight	Internal Percentage p.e.	External Percentage p.e.	Adopted Percentage p.e.	Average p.e.
K, D	Sanford, Merrill	A	6, 5	.....	5	6	±0.02 A
		B	4, 3	7	8	8	± .03
		C	2, 1	12	.....	12	± .04
K, D	Spitzer, Epstein	A	2	6	5	5	± .02
		B	1	6	7	7	± .03
		C	½	14	.....	10	± .04
		D	¼	.....	.....	14	± .04
K	Williams	.....	6, 5	6	8	8	± .03
		.....	4, 3	.....	.....	11	± .04
		.....	2	.....	.....	13	± .04
		.....	1	.....	.....	15	± .05
K, D	Beals	.....	8, 7, 6	4	5	5	± .02
		.....	5, 4, 3	7	9	8	± .03
		.....	2	11	.....	11	± 04
		.....	1	14	.....	14	±0 04
λ 4430	Greenstein, Aller	.....	6, 5	.....	.....	9	±0.2 A
		.....	4, 3	.....	12	11	± .2
		.....	2	.....	.....	14	± .3
		.....	1	.....	.....	20	± .4
λ 4430	Beals, Blanchet	.....	18–9	.....	9	9	± .2
		.....	8, 7, 6	.....	.....	11	± 2
		.....	5, 4, 3	.....	.....	15	± .3
		.....	2	.....	.....	21	± .4
		.....	1	.....	.....	30	± .6
λ 4430	Duke	A	.....	.....	9	7	± .2
		B	.....	.....	.....	13	± .3
		C	.....	22	.....	20	± .4
		D	.....	.....	.....	26	± .5
		F	.....	.....	.....	30	± 6
λ 4430	Baker	.....	.....	.....	.....	5	±0.1

centage probable error given by the authors, external percentage probable error, adopted percentage probable error, and the average probable error for a line of average intensity corresponding to the weight symbol.

Authors who measure the depth of the line or band usually give probable errors; those who measure equivalent width (area of the absorption line) usually give percentage probable errors. The comparison of the equivalent widths shows that the percentage probable error of the fainter lines is somewhat larger than for the very strong lines. For each line of each star we converted the adopted percentage probable error into probable error and rounded off upward for faint lines and downward for very strong lines. For each star we combined the data of different catalogues for each line and found an average value in angstrom units with the corresponding probable error.

V. DOUBLET RATIOS AND CURVES OF GROWTH

In the upper part of Figure 1 the relation is given between the H and K lines of *Ca* II for all material. In case more than one component of the K line was observed, the sum of the intensities was taken; the same was done for the H line. For the strong lines the relation is K = 1.58 H. In the left-hand side of Table 3 are given the intensities of the K and H lines, their ratio, and the number of stars. These normal points were computed after arranging the data according to the K (respectively, D2) intensity.

The stars in the Milky Way were also divided according to the longitude difference from the zero points of the galactic-rotation effect. The doublet ratio in the straight part

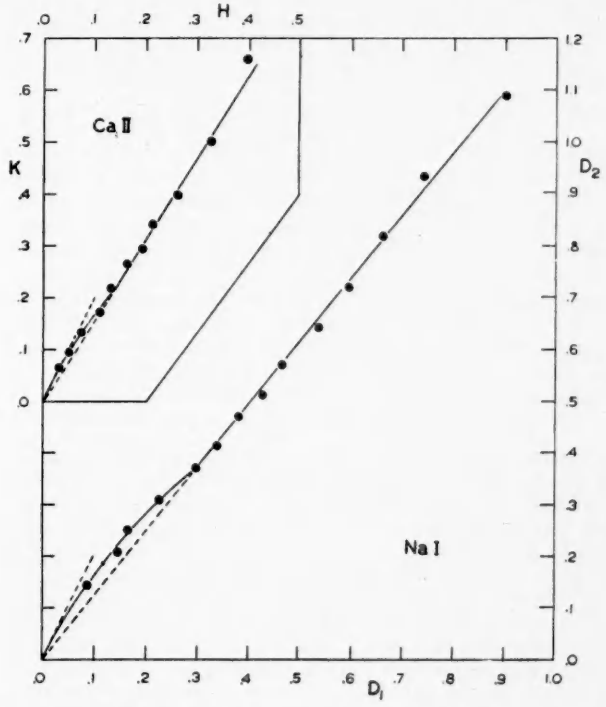

FIG. 1.—Relation between intensities of the H and K lines of *Ca* II (*upper part*) and of the D1 and D2 lines of *Na* I (*lower part*).

for the *Ca* II lines was found to be 1.57 for those stars for which the longitude difference from the zero points is less than 15° and 1.60 for the stars near the extremes of the galactic-rotation effect.

It is of interest to know that the ratio came out to be 1.50 from the data in Table 4 for those H and K components in each spectrum which show the greatest equivalent width. The residual radial velocities of these deepest components show the galactic-rotation effect.

TABLE 3

DOUBLET RATIOS

K	H	K/H	*n*	D2	D1	D2/D1	*n*
0.061	0.033	1.85	20	0.143	0.087	1.64	20
.085	.050	1.70	20	0.206	.148	1.39	20
.132	.074	1.78	20	0.252	.169	1.49	20
.168	.109	1.54	20	0.308	.228	1.35	20
.217	.131	1.66	20	0.368	.302	1.22	20
.258	.162	1.59	20	0.415	.342	1.21	20
.295	.194	1.52	20	0.465	.383	1.21	20
.346	.215	1.61	20	0.511	.428	1.19	20
.402	.262	1.53	17	0.570	.466	1.22	20
.507	.326	1.56	10	0.640	.536	1.19	20
0.662	0.395	1.67	10	0.720	598	1.20	20
				0.814	.665	1.22	20
				0.931	.744	1.25	15
				1.087	0.909	1.20	15

TABLE 4

DEEPEST COMPONENT OF MULTIPLE H AND K

K	H	K/H	*n*
0.054	0.032	1.69	20
.089	.051	1.75	20
.130	.074	1.76	20
.174	.114	1.52	20
.231	.153	1.51	20
.291	.195	1.49	20
0.399	0.273	1.46	17

In the lower part of Figure 1 the relation between the D1 and D2 lines of *Na* I is given. For the faint lines the ratio is again 2, but for the stronger lines the relation is D2 = 1.21 D1. The right-hand side of Table 3 contains the information for the D lines. A subdivision according to the longitude difference from the zero points of the galactic-rotation effect yields for the ratio 1.20 near the zero points and 1.23 near the extremes. The influence of the galactic-rotation effect on the doublet ratio is thus small.

The H line is situated on the wing of the $H\epsilon$ stellar-absorption line and therefore is more difficult to measure than the K line. The H line was given half-weight, and from Figure 1 the corresponding K value was read off. The weighted mean value was taken as the representative K value for *Ca* II. For the other doublet the average $D = \frac{1}{2}(D1 + D2)$ was taken as the D value of *Na* I. We have now available 542 stars with a K value, 271 stars with a D value, and 367 stars with a value for the λ 4430 band.

Our observed curves of growth for *Ca* II and *Na* I in Figure 2 were determined from the observed doublet ratios in the usual way by shifting line segments, where use is made of the fact that any pair of values of the doublet intensities corresponds to effective numbers of atoms in the ratio 1:2. The oscillator strengths for the H and K lines are 0.36 and 0.72, respectively, and for the D1 and D2 lines 0.33 and 0.66, respectively. Using these values, we give in Figure 2 the relation between the logarithms of the line intensity and the number of atoms N (and not the number of effective atoms, as is usually done). The broken line has been derived from the deepest component of the multiple H and K. The curves of growth for stars near the zero points and for stars near the extremes of the galactic-rotation effect are only slightly different from the average curve, and the differences are negligible for distances smaller than 1 kpc.

A. Unsöld, O. Struve, and C. T. Elvey[25] published a theoretical curve of growth for the

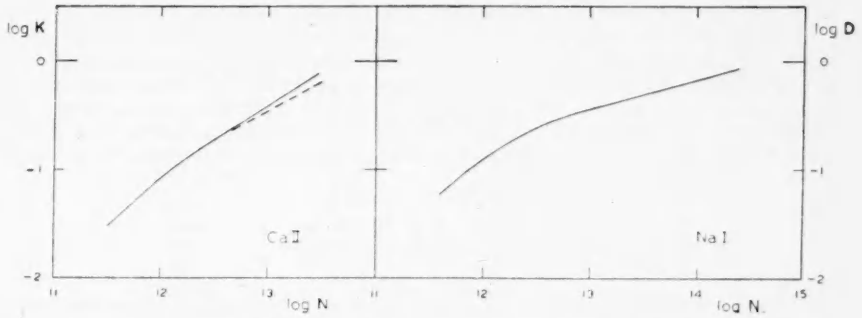

FIG. 2.—The observed curves of growth for *Ca* II (*left*) and *Na* I (*right*). The broken line has been derived from the deepest component of the multiple H and K.

Ca II lines. O. C. Wilson and P. W. Merrill[15] discussed the curve for *Na* I. They found that they had to introduce large clouds having linear dimensions of 700 psc to explain the observed curve. However, recent results show that these clouds will have much smaller diameters. More recent discussions are the following: B. Strömgren[26] computed a theoretical curve of growth for one calcium or sodium cloud, assuming that only Doppler motion played a role. He considered also the case of two clouds. L. Spitzer[17] gave formulae for the curve of growth for a single cloud and for the statistical curve of growth for many clouds. C. Jentzsch and A. Unsöld[27] gave a discussion of the influence of the turbulence and galactic-rotation effect upon the curves of growth. It is found theoretically that this galactic-rotation effect in the equivalent widths must be small, in agreement with the observations but in contradiction to Spitzer's theory. Furthermore, the work of O. A. Melnikov[28] has to be mentioned.

We compared our observed curves of growth with the theoretical ones for a homogeneous medium, which can be derived from Strömgren's data, where the Doppler constants are taken as 0.09 A for *Ca* II and 0.11 A for *Na* I. The agreement in the linear part of the curve for the faint lines is satisfactory up to the point where saturation sets in. For the strong lines we have the well-known disagreement between observation and simple theory, because the doublet ratio does not decrease toward unity but stays constant. This can be explained by large currents in the gas continuum (or large peculiar velocities of the gas clouds). Another remarkable fact first discovered by O. C. Wilson[29] is the different be-

[25] *Zs. f. Ap.*, **1**, 314, 1930.
[26] *Ap. J.*, **108**, 242, 1948.
[27] *Zs. f. Phys.*, **125**, 370, 1948.
[28] *A.J. U.S.S.R.*, **24**, 73, 1947.
[29] *Ap. J.*, **90**, 244, 1939.

havior of the curves of growth for the stronger lines of *Ca* II and *Na* I, because the doublet ratios are observed to be different, namely, 1.58 and 1.21, respectively. This can be accounted for by different distribution laws of the radial-velocity components, the *Ca* II velocities having a larger spread than those of *Na* I. Recently P. M. Routly and L. Spitzer[30] found from a detailed study that, in regions in space with low radial velocity, *Na* I tends to be more abundant, while in regions with high velocities the reverse is true.

The theoretical curve of growth is rather satisfactory except perhaps for the very strong lines, and it was decided, therefore, to use the observed curves of growth only for the faint and the strong lines in the following discussion.

VI. RADIAL VELOCITIES

W. S. Adams[13] has given accurate radial velocities and residual velocities for the components of the multiple K line; the latter have been corrected for a linear solar motion of 20 km/sec but not for galactic-rotation effect in the radial velocities. The probable error is of the order of ± 1 km/sec.

We will consider, first, the deepest component, which shows the galactic-rotation effect in the radial velocities. We take the stars in the Milky Way for which the longitude difference with the zero points is less than 10°, and we omit the supergiants. By this choice we are sure that the galactic-rotation effect does not play a role. We find, for the mean residual radial velocities, the values given in the accompanying tabulation. In the

Center region	$+1.1 \pm 0.4$ km/sec	22 stars
Cygnus region	$+1.4 \pm 0.5$ km/sec	32 stars
Anticenter region	$+5.0 \pm 0.5$ km/sec	20 stars

anticenter region the residuals systematically exceed those in the other regions by about 3.7 km/sec. This fact is caused by the peculiar outward motion of the gas in the Orion and Pleiades regions rather than by a general outflow of gas from our Milky Way. It was noted first by P. W. Merrill and R. F. Sanford.[31] We find that the residual radial velocities of open clusters measured by Sanford[7] do not show this effect. For the probable error of one star, ± 2.2 km/sec was found in this computation, more than twice the probable error of Adams' measurements. It shows that the small-scale turbulence effect in the deepest component of the multiple K is of the order of ± 2 km/sec. We have to realize here that the high dispersion used by Adams is still not enough to separate all components and that very close ones can never be resolved at all, even with still higher dispersion. If one considers all observed components of multiple K combined, one finds naturally much more for the large-scale turbulence effect. This combined effect is found if the observations are made with lower dispersion than Adams used, because one can then observe only one K line per star.

This turbulence effect in the interstellar gas is of the same order in the radial velocity as is the galactic-rotation effect for the normal B stars. It is not surprising that J. W. Evans[32] gets several negative distances, with the rotation effect of the interstellar lines as a distance criterion. We conclude that these distances of the stars are reliable only for supergiant B stars and very distant open clusters situated near the extremes of the galactic-rotation effect.

VII. REDDENING AND SPECTROSCOPIC DISTANCES

For the reddening of the stars, only photoelectric color measurements were used, namely, the list of J. Stebbins, C. M. Huffer, and A. E. Whitford;[33] this gives the color

[30] *Ap. J.*, **115**, 227, 1952.
[31] *Ap. J.*, **87**, 118, 1938.
[32] *Ap. J.*, **93**, 275, 1941.
[33] *Ap. J.*, **91**, 20, 1940; *Mt. W. Contr.*, No. 621.

C_1 and the color excess E_1, which is related to the International System by $E = 1.5\ E_1$. Zero-point corrections to this system were suggested by J. H. Oort[34] and P. J. van Rhijn.[35] We adopted their conclusion that the normal colors for stars of types O–B3 are 0.04 mag. bluer than those used by the authors and that smaller corrections are applied between B5 and B8 for the normal stars. The Yerkes system of spectral classification was adopted, and our corrected reddenings E_{1c} are essentially the same as those used at that observatory.

We adopted spectroscopic distances for the B stars. W. W. Morgan kindly sent us his unpublished data, while the lists of his associates, J. Ramsey[36] and D. Duke,[20] were also used. At this point it was decided to use only the data of those stars in the following discussion for which the accurate Yerkes distances are available at the moment. Also a number of emission-line stars and shell stars were rejected because circumstellar material is a cause of inaccurate interstellar data and also gives inaccurate distances. This leaves us 421 stars with a K value, 211 stars with a D value, and 348 stars with a value of the λ 4430 band. In these spectroscopic distances corrected for space absorption, systematic errors are introduced by the adopted absolute magnitude and by the adopted ratio of general to selective absorption. The probable error in the distance modulus may be estimated to be of the order of ± 0.3 mag.

For stars which are members of clusters, the average distance was introduced and the membership data taken from the following authors: Orion, W. Markowitz;[37] *h* and χ Persei, W. P. Bidelman;[38] Pleiades, L. Binnendijk;[39] ζ Persei, A. Blaauw;[40] Scorpius-Centaurus, A. Blaauw;[41] and other clusters, R. F. Sanford.[7]

VIII. DISTANCE RELATIONS

A map of the Milky Way was made on a large scale, giving all stars for which Adams and other authors had measured the radial velocities of the interstellar lines. In three regions—Orion, Cygnus, and Ophiuchus—there are several stars with multiple K lines. In these directions there may be currents in a rather continuous medium having different radial velocities, or there may be more calcium clouds behind one another. Another map was made on the same scale, in which the absorption of the smoke clouds was drawn in. The Harvard material on star counts and the reddening gave most of the data for this map. The maps and data in the Milky Way constellations given by the following authors were used: Monoceros, B. J. Bok and J. M. Rendall-Arons;[42] Orion, B. J. Bok, M. Olmsted, and B. D. Boutell;[43] Taurus, S. W. McCuskey;[44] Auriga, L. Kiefer and R. H. Baker;[45] Perseus, D. S. Heeschen;[46] Cassiopeia, R. H. Baker and E. Nantkes;[47] Cepheus, A. M. Risley;[48] Cygnus, F. D. Miller,[49] F. D. Miller and J. A. Hynek,[50] J. J. Nassau and

[34] *B.A.N.*, **8**, 233, 1938.

[35] *Groningen Pub.*, No. 51, 1946.

[36] *Ap. J.*, **111**, 434, 1950.

[37] *A.J.*, **54**,, 111, 1949.

[38] *Ap. J.*, **98**, 68, 1943.

[39] *Leiden Ann.*, Vol. **19**, Part 2, 1946.

[40] *B.A.N.*, **10**, 29, 1944.

[41] *Groningen Pub.*, No. 52, 1946.

[42] *Ap. J.*, **101**, 281, 1945.

[43] *Ap. J.*, **110**, 21, 1949.

[44] *Ap. J.*, **88**, 209, 1938; **89**, 568, 1939; **94**, 468, 1941.

[45] *Ap. J.*, **94**, 482, 1944.

[46] *Ap. J.*, **114**, 132, 1951.

[47] *Ap. J.*, **99**, 126, 1944.

[48] *Ap. J.*, **97**, 277, 1943.

[49] *Harvard Ann.*, **105**, 297, 1937.

[50] *Perkins Contr.*, Vol. **1**, No. 13, 1939.

D. A. MacRae;[51] Aquila, R. H. Baker,[52] H. F. Weaver,[53] and R. L. Calvert;[54] and Ophiuchus, R. H. Baker and L. Kiefer.[55]

The areas in the Milky Way were now chosen in such a way that the gas and smoke seemed to be as uniform as possible in each area. Some areas, like the Orion group, Cygnus star cloud, and Scorpius cluster, are well defined by the grouping of the B stars in these parts of the Milky Way. However, the boundaries of the other areas were chosen by trial and error and may indicate a personal preference. The number of observed stars naturally plays a role. In Figure 3 the areas are given where the name of the main constellation

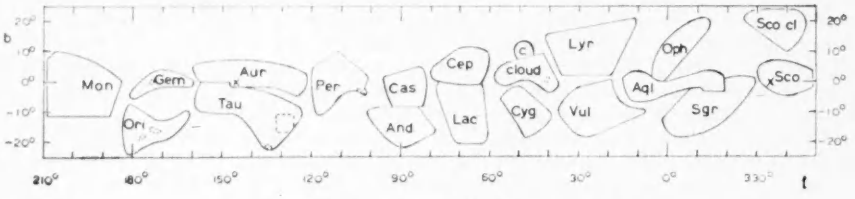

FIG. 3.—The adopted areas in the Milky Way

is used to indicate the area, but the boundaries of the areas are not at all related to those of the constellations. When possible, two areas were chosen in a particular longitude interval.

Near the anticenter not enough observations are made in the Milky Way north of +10° latitude. The reason is that the material depends so heavily on observations made with the 100-inch telescope at Mount Wilson. The northern limit of declination for the telescope is +64°, while that of the coudé spectrograph is about +52°. The 60-inch telescope at Mount Wilson will turn to the north pole of the equatorial system. To a certain extent, however, the H and K observations were planned to parallel those of the D lines. Thus the 60-inch was not used for northern stars quite so much as might otherwise have been the case. No data are available between longitude 210° and 310°, this being the Milky Way in the Southern Hemisphere, where almost no large telescopes are available.

For each star the weighted observing data were written on a card. For each area the intensities of the K and D lines and the λ 4430 bands, respectively, were then plotted against the spectroscopic distance of the stars and normal points formed in distance intervals. Also the polarization was studied from the data of W. A. Hiltner.[56] The plane of polarization is the plane defined by the electrical vector and the line of sight. The position angle θ' of this plane with respect to the direction normal to the galactic system is given. The data of J. S. Hall and A. H. Mikesell[57] give the plane defined by the magnetic vector and the line of sight, and their position angle is therefore 90° different. Further on, a zero-point correction of 3° was subtracted, to reduce their position angle to Hiltner's system.

Table 5 gives the name of the main constellation and sometimes that of the cluster, the interval in galactic longitude and latitude, the spectroscopic distance r in kiloparsecs, the corrected reddening in the scale of Stebbins, the polarization and its direction with respect to the direction of the galactic north pole as defined above, the intensities in angstrom units of the lines K, D, and the λ 4430 band, and the number of stars used for the K value.

[51] *Ap. J.*, **110**, 40, 1949.
[52] *Ap. J.*, **94**, 493, 1941.
[53] *Ap. J.*, **110**, 190, 1949; *Contr. Lick Obs.*, Vol. **2**, No. 24, 1949.
[54] *Ap. J.*, **114**, 123, 1951.
[55] *Ap. J.*, **96**, 224, 1942.
[56] *Ap. J.*, **114**, 241, 1951.
[57] *Pub. Naval Obs.*, Vol. **17**, Part 1, 1950.

TABLE 5

DISTANCE RELATIONS

Area	Interval	r	E_{1c}	P (Per Cent)	θ'	K	D	λ 4430	n
Polar caps	$\|b\|$ = 45° to 90°	0.13	0m03	.....	.....	0.05	.....	0.5	2
		0.34	.05	.....	.....	.07	0.19	0.5	3
		0.89	.06	.....	.....	.15	.16	0.7	3
Intermediate latitudes	$\|b\|$ = 25 to 45	0.13	.07	.....	.....	.09	.....	1.0	6
		0.16	.03	.....	.....	.08	.....	.....	6
		0.25	.05	.....	.....	.09	.....	0.8	6
		1.02	.09	.....	.....	.21	.....	1.2	3
Monoceros	l = 210 to 185	0.20	.08	0.5	98°	.05	.....	1.0	5
	b = − 13 to + 10	0.39	.06	0.8	150	.12	.27	0.7	5
		0.72	.10	0.2	.....	.15	.25	0.8	5
		1.15	.08	0.4	77	.17	.24	0.9	4
Orion	l = 185 to 160	0.29	.06	.....	.....	.11	.23	0.3	9
	b = − 25 to − 8	0.32	.04	.....	.....	.10	.16	0.2	10
Belt	l = 173 b = −16	0.32	.06	.....	.....	.10	.....	.....	6
Nebula	l = 177 b = −18	0.32	.09	0.6	66	.13	.19	0.6	10
		0.42	.05	.....	.....	.13	.25	0.5	11
Gemini	l = 185 to 160	0.17	.02	.....	.....	.10	.....	.....	4
	b = − 6 to + 4	0.64	.10	1.4	104	.19	.....	1.6	5
		1.19	.16	1.1	95	.31	.48	1.4	4
NGC 2244	l = 174 b = − 1	1.53	.20	1.1	110	.32	.40	2.3	6
Pleiades	l = 135 b = −22	0.18	.03	0.3	109	.05	.....	0.2	8
Taurus	l = 160 to 120	0.20	.06	1.0	90	.09	.11	0.8	8
	b = − 23 to − 2	0.40	.10	1.4	87	.16	.27	1.5	9
ζ Persei	l = 128 b = −15	0.26	.16	0.9	111	.12	.....	1.0	10
Auriga	l = 160 to 120	0.17	.06	0.9	123	.09	.....	0.6	5
	b = − 2 to + 6	0.59	.16	1.7	103	.18	.43	1.6	5
		1.01	.21	2.3	105	.32	.50	2.1	4
		1.65	.20	2.4	110	.30	.54	1.8	4
Perseus	l = 120 to 102	0.18	.08	0.5	127	.07	.24	.....	6
	b = − 11 to + 9	0.59	.26	3.2	93	.25	.44	3.2	5
		0.88	.32	4.6	93	.31	.65	2.4	4
		1.18	.34	3.7	89	.41	.57	2.5	4
χ Persei	l = 103 b = − 2	1.91	.31	3.7	91	.61	.88	2.1	8
h Persei	l = 102 b = − 3	1.91	.22	3.7	92	.66	.85	1.9	10
Andromeda	l = 100 to 80	0.17	.04	.....	.....	.08	.....	0.4	4
	b = − 22 to − 8	0.43	.07	.....	.....	.25	.....	0.6	5
Cassiopeia	l = 98 to 82	0.61	.14	1.8	97	.26	.35	1.6	6
	b = − 8 to +5	1.15	.23	1.8	77	.41	.76	2.1	5
		1.43	.29	2.2	76	.56	.85	2.3	4
		2.72	.26	3.2	90	.60	.87	2.4	5
Lacerta	l = 80 to 60	0.22	.09	.....	.....	.14	.....	0.4	5
	b = − 20 to 0	0.39	.09	.....	.....	.17	.....	0.9	5
		0.51	.08	.....	.....	.13	.32	0.7	4
		0.69	0.06	.....	.....	0.16	0.20	0.4	4

TABLE 5—*Continued*

Area	Interval	r	E_{1c}	P (Per Cent)	θ′	K	D	λ 4430	n
Cepheus	$l=$ 80° to 60°	0.31	0m17	2.5	58°	0.23	0.43	1.6	6
	$b=$ 0 to + 13	0.53	.24	1.4	71	.27	.50	1.7	6
		0.68	.21	1.9	63	.26	.48	1.7	6
		0.98	.21	1.8	89	.24	.46	1.6	6
Cygnus	$l=$ 58 to 40	0.21	.06	.....	.....	.09	.12	1.6	5
	$b=-$ 18 to − 1	0.62	.08	0.6	91	.20	.40	0.9	5
		1.00	.10	.....	.....	.20	.....	0.9	5
		1.70	.09	0.4	84	.28	.47	0.8	4
Cygnus star cloud	$l=$ 58 to 38	0.24	.06	.....	.....	.10	.....	0.6	5
	$b=-$ 33 to + 8	0.40	.05	.....	.....	.15	.....	0.6	5
		0.57	.19	1.2	61	.25	.46	1.0	5
		0.81	.24	1.8	86	.29	.44	1.5	5
		1.11	.29	0.7	92	.39	.56	1.8	6
NGC 6871	$l=$ 40 $b=+$ 1	1.28	.24	0.8	58	.45	.69	1.7	5
		1.72	.21	1.3	31	.41	.71	1.9	6
Vulpecula	$l=$ 35 to 9	0.19	.06	.....	.....	.06	.....	0.7	5
	$b=-$ 16 to 0	0.49	.11	1.5	78	.20	.30	1.0	5
		1.11	.17	2.1	71	.43	.38	1.6	4
Lyra	$l=$ 40 to 14	0.20	.05	0.8	64	.09	.....	0.8	5
	$b=+$ 2 to + 19	0.28	.04	.....	.....	.11	.....	0.8	5
		0.38	.09	0.8	94	.12	.24	1.1	5
		0.50	.07	1.3	89	.17	.....	1.0	4
		0.99	.11	2.2	80	.22	.39	0.7	4
Ophiuchus	$l=$ 2 to 346	0.29	.15	3.3	131	.12	.24	1.4	4
	$b=$ 0 to 22	0.57	.11	2.4	134	.23	.37	1.2	3
Aquila	$l=$ 16 to 341	0.86	.39	1.3	95	.40	.68	2.4	2
	$b=-$ 4 to 2	2.54	.32	1.6	84	.72	.81	2.9	2
Sagittarius	$l=$ 0 to 330	0.20	.16	1.8	84	.18	.....	1.3	4
	$b=-$ 15 to 0	0.76	.18	2.0	65	.19	.21	2.2	4
clu.	$l=$ 334 $b=-$ 3	0.98	.14	0.4	65	.24	.31	.....	5
		1.34	.19	1.0	67	.30	.31	1.9	4
		1.68	.14	0.7	120	.34	.34	1.7	4
Scorpius cluster	$l=$ 334 to 314	0.17	.15	2.5	59	.07	.19	2.1	5
	$b=+$ 10 to + 25	0.19	.13	.....	.....	.05	.18	2.3	7
Scorpius	$l=$ 330 to 310	0.75:	0.11	4.3	60	.35	.67	.....	5
	$b=-$ 2 to + 5	1.37:	.....	.....	.....	0.43	0.60	.....	5

Figure 4 shows the distance relation for the reddening for the stars concerned. It shows the known fact that the reddening often remains constant over a considerable distance interval. In Figure 5 the distance relations for the K line are collected for all areas. Now we find that the average intensity usually increases with increasing distance. The few exceptions can be explained by the saturation effect for the very strong lines. This behavior is important for a later explanation.

We see that the distance relation for the K line in the direction of the polar cap is very similar to the distance relation for the Monoceros area. In the general anticenter direction, two areas in one longitude interval always agree very well. There is a pronounced

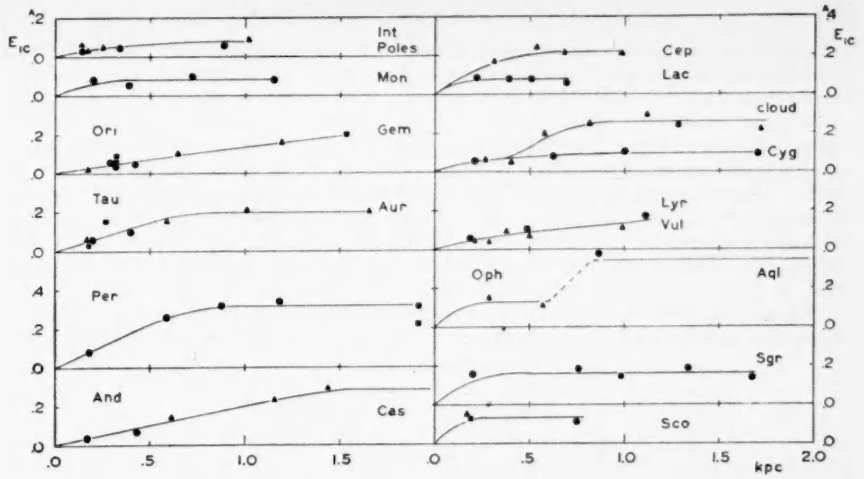

FIG. 4.—Distance relations for the reddening in the different areas. Normal points are average dat[a] of about five stars. Dots correspond to southern areas, triangles to northern areas, squares to stars in open clusters.

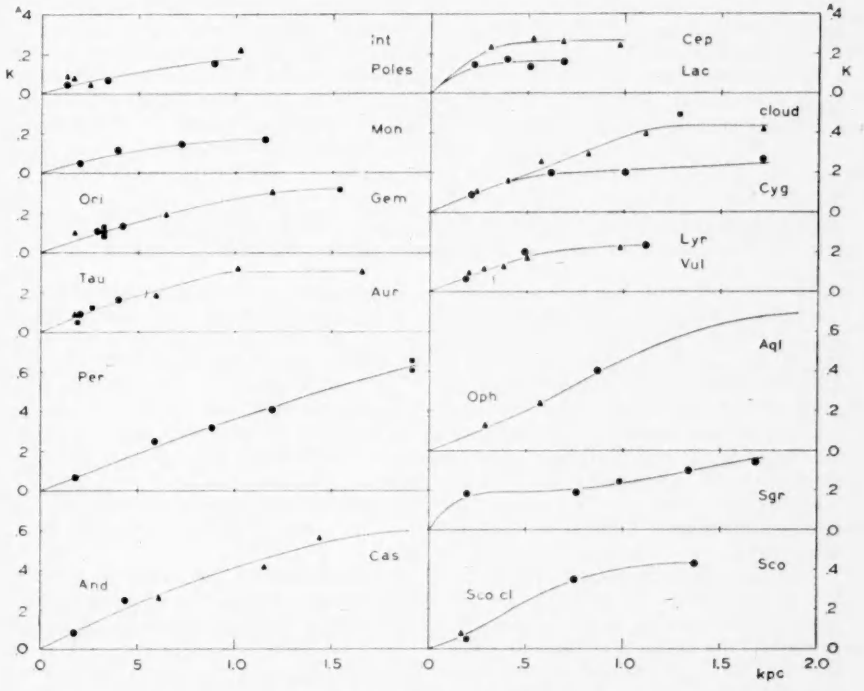

FIG. 5.—Distance relation for *Ca* II in the different areas. For further explanation see legend to Fig. 4.

difference between them, however, when we look at the areas which are about 90° from the center in the general direction of Cygnus. Both the K and the D line material confirm each other. This can never be explained by a galactic-rotation effect in the equivalent widths but has to be a difference in densities. However, W. W. Morgan's[58] recent discovery of the spiral arm of our Milky Way system makes this understandable. In the direction of the center of the Milky Way such a division is not easily made. The different curves at once reveal the large differences between them, showing that *Ca* II does not have the same density in each direction. We now have to consider whether this is a latitude effect caused by the relatively thin layer of interstellar gas on both sides of the Milky Way plane or whether this is a difference in densities in the Milky Way plane itself.

We can also make another graphic representation in the plane of the Milky Way. For every 100 psc, the interstellar line intensity was read off from the graphs of the distance

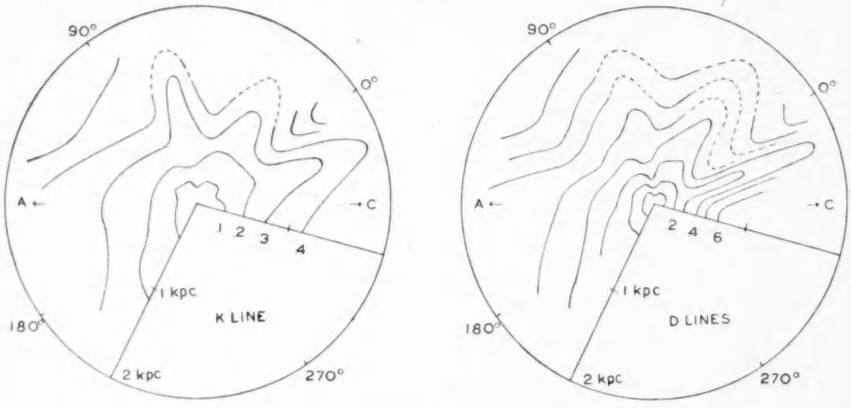

FIG. 6.—The plane of the Milky Way is shown within a radius of 2 kpc from the sun at the origin. The curves of equal observed intensity for *Ca* II (*left*) and *Na* I (*right*) show how far one has to travel from the sun in a certain direction to reach the same intensity. *C* is the direction toward the center.

relation in each area. The areas Monoceros, Gemini, Auriga, Perseus, and Cassiopeia in the general anticenter direction have latitudes between $+10°$ and $-10°$ and have well-defined distance relations. Weighted values were taken for the two pairs of areas in the general direction of Cygnus, namely, Cepheus and Lacerta, Cygnus and star cloud. In fact, the weights were chosen in such a way that the resulting distance relation is the same as that found from those stars in the longitude interval which have latitudes between $+10°$ and $-10°$. The areas Lyra and Vulpecula have the same distance relations. The areas Aquila and Scorpius are representative for the Milky Way plane in the center direction, while it is found that the Sagittarius area has the same distance relation if we omit the stars south of $-10°$. By choosing the areas in this latitude interval, the stars having a distance of 1 kpc from the sun will be less than 175 psc away from the Milky Way plane.

In a drawing in the plane of the Milky Way, these intensities were now placed in the longitude concerned. The left-hand side of Figure 6 shows curves of equal observed intensity for *Ca* II, showing how far one has to travel from the sun in the origin in different directions in the Milky Way plane to reach the same intensity. The right-hand side shows the same for *Na* I. The open sector represents the missing observations in the Southern Hemisphere.

[58] *A.J.*, in press.

The similar behavior of the curves for the K and D lines proves that the gases *Ca* II and *Na* I are well mixed in the Milky Way plane, but in detail there are differences. Also the radial velocities are found to be of the same order in general, but also here there are differences in detail.

Our observed curves are not circles at all, as the case would be for uniform distribution of the gases and if the galactic-rotation effect in the equivalent widths is negligible. If this effect were more serious, these circles would be deformed in such a way that the distance to the origin would become larger in the zero points. According to Spitzer's[17] theory, for example, the curve D = 0.5 would have to go through $r = 1.0$ kpc in the zero points and $r = 0.6$ kpc in the extremes. These computed curves do not agree at all with the observed ones; in fact, the latter do not seem to show any definite relation to the zero points. Obviously, Spitzer's working model is too simple, and we again find evidence that the galactic-rotation effect in the equivalent widths is small but that differences in gas and smoke densities are important.

IX. SPACE DISTRIBUTION

In all our following discussions the analysis of the data of line intensities and reddening suggests a working model intermediate between the uniform distribution and the other extreme, namely, all gas and smoke concentrated in discrete clouds. We add to the last model a rarefied gas continuum. Observations do not decide whether this is a rather homogeneous medium or a large number of almost transparent clouds of small size.

We will first try to find the density distribution of the gases in the Milky Way plane. From the distance relation in an area and the observed curve of growth, one knows the number of atoms situated between the sun and 400 psc, for example, and also in the same manner between the sun and 300 psc. Thus one knows how many atoms there are between 300 and 400 psc by simple subtraction. This was done for successive intervals of 100 psc in all areas near the plane of the Milky Way. We can write down all these absolute densities per square centimeter per 100 psc in a drawing of the plane of the Milky Way, where the areas are represented as sectors.

Table 6 shows the number, respectively, of *Ca* II ions and *Na* I atoms per square centimeter per 100 psc for successive intervals in the areas. Within the radius of 1 kpc around the sun in the plane of the Milky Way, we find, on the average, 8×10^{11} calcium ions/cm^2/100 psc or 3×10^{-9} ions/cm^3, corresponding to a density of about 2×10^{-31} gm/cm^3.

The value for the continuum can be estimated as an average value of the small and rather uniform densities in the table; that for the concentrations, as an average value of larger densities, which are quite distinct from the previous ones. The data in the accompanying tabulation give an idea of the range in densities and may be compared with the

Calcium	Ions per Cm^3	Jentzsch and Unsöld
Continuum	0.8×10^{-9}	.....
Average	3×10^{-9}	1.0×10^{-9}
Concentration	6×10^{-9}	.....

average result of C. Jentzsch and A. Unsöld.[27]

For the *Na* I within the same radius of 1 kpc, we find, on the average, 33×10^{11} atoms/cm^2/100 psc or 11×10^{-9} atoms/cm^3, corresponding to a density of about 4×10^{-31} gm/cm^3. We may compare here our results with those of O. C. Wilson and P. W. Merrill[15] and those of L. Spitzer[17] and B. Strömgren[26] (see accompanying tabulation).

Sodium	Atoms per Cm^2	Wilson and Merrill	Spitzer	Strömgren	Jentzsch and Unsöld
Continuum	2×10^{-9}	.....	2×10^{-9}	.....	.....
Average	11×10^{-9}	3×10^{-9}	7×10^{-9}	2×10^{-9}	3.6×10^{-9}
Concentration	32×10^{-9}	.....	50×10^{-9}	40×10^{-9}	.....

Spitzer's values for his transparent clouds, when averaged over all space near the galactic plane, and opaque clouds agree very favorably with our values for the continuum and concentration, respectively. If we take the radius smaller than 1 kpc, our results for the density come out somewhat smaller.

The left-hand side of Figure 7 is an attempt to visualize the distribution of the calcium and sodium gases in the plane of the Milky Way within a radius of 1 kpc from the sun in the origin. Each point corresponds to the same arbitrary number of gas particles. It gives an indication of the distance at which the concentration in the gas starts and shows some evidence of certain structure, especially in the direction 90° from the center. Table 6 and

TABLE 6

NUMBER OF GAS PARTICLES PER SQUARE CENTIMETER PER 100 PSC IN THE DIFFERENT AREAS
(The Unit Is 10^{11})

Area (In Kpc)	Galactic Longitude										
	200°	170°	140°	110°	90°	70°	50°	20°	350°	340°	320°
	Ca II										
0.0-0.1	3	4	5	4	6	9	5	4	3	13	3
.1-0.2	3	4	5	5	7	11	5	4	5	13	5
.2-0.3	3	5	6	6	7	10	6	6	7	3	9
.3-0.4	3	5	7	7	10	6	7	7	8	2	12
.4-0.5	3	5	7	8	13	4	7	6	10	1	16
.5-0.6	3	6	7	10	14	2	8	5	16	1	17
.6-0.7	2	7	7	12	15	1	8	4	20	2	18
.7-0.8	2	7	8	13	17	1	9	3	25	2	16
.8-0.9	2	7	9	15	17	1	9	2	27	4	10
0.9-1.0	2	6	6	14	13	1	9	1	20	4	9
	Na I										
0.0-0.1	8	6	6	12	5	18	7	6	5	2	9
.1-0.2	8	6	9	21	7	27	8	7	7	2	13
.2-0.3	9	8	14	25	11	35	14	10	13	3	20
.3-0.4	8	11	22	30	16	41	21	12	24	3	27
.4-0.5	3	12	32	47	26	26	30	14	36	4	47
.5-0.6	2	13	53	58	37	20	38	12	65	6	60
.6-0.7	.....	14	64	60	58	13	43	10	124	7	73
.7-0.8	.....	17	56	62	90	7	46	10	186	6	80
.8-0.9	.....	24	28	70	130	5	47	10	180	6	85
0.9-1.0	.....	33	24	98	180	5	49	11	160	6	78

Figure 7 are given only to 1 kpc for four reasons: the distances of the stars are more inaccurate at larger distances; the probable errors of the interstellar intensities increase for the stronger lines; the material would no longer be complete in all directions; and for larger distances we are mostly on that part of the curve of growth which deviates from the theoretical curve of growth for a homogeneous medium and where also the influence of the galactic-rotation effect in the equivalent widths would perhaps become more serious.

The data for the λ 4430 band show that there are much larger deviations between a northern and a southern area in the same longitude interval than in the case of the gases. The right-hand side of Figure 7 gives the distribution of the smoke clouds, derived from

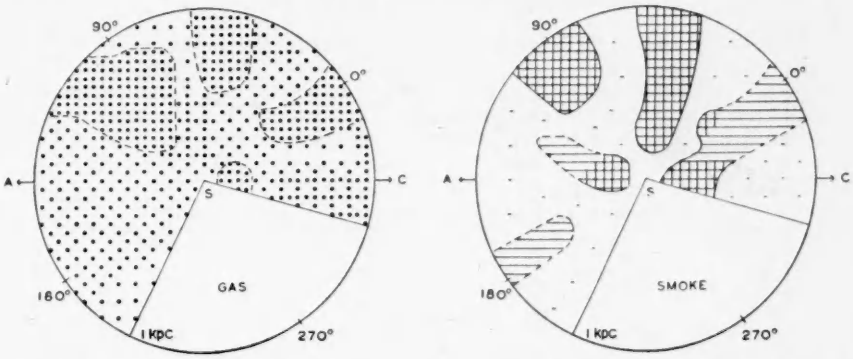

FIG. 7.—*Left:* distribution of the calcium and sodium gases in the plane of the Milky Way within a radius of 1 kpc from the sun. *Right:* distribution of the smoke clouds. *C* is the direction toward the center.

the Harvard star counts, and the reddening given by Stebbins and his co-workers. The main features agree with the diagram published in W. Becker's[59] textbook, but the details differ, as could be expected. In three dimensions one could make a much more accurate representation. Also fluctuations in the gas and smoke densities having a size smaller than 100 psc will not appear.

If we consider the distribution of the gas and smoke together, we see that in the upper part of the figure there seems to be a tendency for the smoke clouds to occur where there is a concentration of the gas. The smoke clouds are more pronounced with respect to the smoke continuum than the gas concentrations are with respect to the gas continuum. The lower part of the figure seems to contradict this statement, but this is very probably a selection effect. Toward the center the data for the gas are rather scarce beyond 0.5 kpc from the sun. Toward the anticenter we have the dense near-by Taurus cloud. Only supergiant B stars would be visible through the densest part of the cloud, but they are uncommon in this region of the Milky Way.

With increasing distance, the amount of polarization increases in some areas but decreases in other areas. This last effect may be expected if starlight passes through two clouds having different planes of polarization.

X. RELATION BETWEEN INTENSITY, REDDENING, AND DISTANCE

We will now consider more accurately the relation between gas and smoke in the Milky Way and study the relation between intensity and reddening as it is dependent upon the distance. First, the data of the stars in the Milky Way with latitudes between

[59] *Sterne und Sternsysteme* (Dresden and Leipzig: Steinkopff, 1950), p. 197.

+25° and −25° were divided into six equal distance intervals, each 300 psc long. Further, we subdivided into two groups: (1) the stars whose longitude difference with the zero points was smaller than 15°; (2) the stars near the extremes of the galactic-rotation effect. The scattering in each of the diagrams showing the individual data is naturally considerable because stars of the whole Milky Way are included, but it is more pronounced for the reddening than for the intensities. The data were then arranged according to reddening, and normal points were formed, as given in Figure 8 and Table 7, where

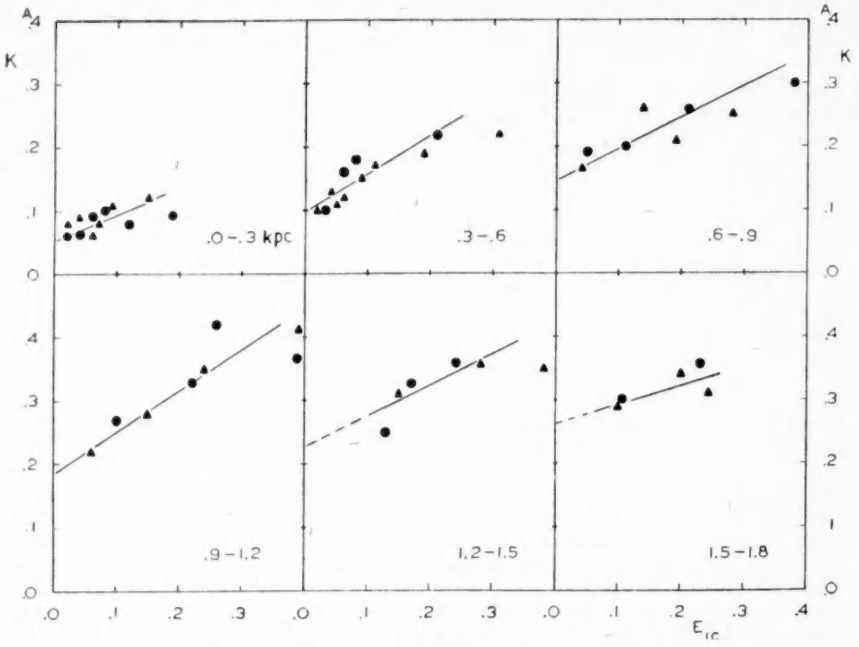

FIG. 8.—General relation between the K line intensity and reddening for distance intervals in the Milky Way. Normal points are average data of about eight stars for the nearest intervals and about four stars for the distant intervals. Dots correspond to stars near the zero points, triangles to stars near the extremes of the galactic-rotation effect.

n is the number of stars used for the K line.

The result of these figures for the K and D line data is rather decisive. They show a similar relation between intensity and reddening depending on distance and with the dispersion of the same order. There is no systematic difference in the intensities between observations near the zero points and near the extremes. We find again that the galactic-rotation effect in the equivalent widths is small for the distances concerned.

For unreddened stars the K and D (but not the λ 4430 band) intensities keep increasing for more distant distance intervals, showing the effect of the gas continuum. For the nearest distance interval one could argue that the authors of the catalogues could have had a tendency to omit those B stars which do not show any interstellar line. For this limit a K value of 0.03 A can be taken. This argument certainly does not hold for the more distant intervals, where the unreddened stars have an appreciable line intensity. We count 20 stars having $E_{1c} \leqslant 0.10$ and a distance larger than 1 kpc. For no reddening and

a distance of 1 kpc, we find for the calcium a K value of 0.18 A, which corresponds to $N = 28 \times 10^{11}$ ions/cm^2/kpc, or 0.9×10^{-9} ions/cm^3. For the sodium we find a D value of 0.27 A, which corresponds to $N = 41 \times 10^{11}$ atoms/cm^2/kpc, or 1.3×10^{-9} atoms/cm^3. This agrees very well with the values of the continuum found earlier, and we thus find only little or no smoke in the gas continuum.

We also see a definite slope in the relations, showing that between a more reddened star and the observer there is usually more gas also. We find thus that the K and D line intensities are functions both of distance and of reddening. For unsaturated line intensities we can write in a first approximation:

$$K = 0.18\,r + 0.7E_{1c}\,, \qquad D = 0.27\,r + 1.0E_{1c}\,,$$

where the intensities are in angstrom units, the distance r in kiloparsecs and the reddening E_{1c} in Stebbins' system.

The strongly reddened stars show only a slow increase in reddening for more distant intervals, indicating the selection effect. At a certain distance the normal B stars which happen to be strongly reddened will be the first to become so faint that they cannot be

TABLE 7

INTENSITY-REDDENING RELATIONS FOR DISTANCE INTERVALS

Distance Intervals (In Kpc)	Zero Points					Extremes				
	E_{1c}	K	D	λ 4430	n	E_{1c}	K	D	λ 4430	n
0.0–0.3	0^{m}02	0.06	.....	0.3	8	0^{m}02	0.08	.....	0.4	10
	.04	.06	0.16	.....	8	.04	.09	.....	1.4	10
	.06	.09	.12	0.3	7	.06	.06	0.11	0.7	10
	.08	.10	.18	0.8	7	.07	.08	.....	0.9	10
	.12	.08	.21	1.3	7	.09	.11	.15	1.0	10
	.19	.09	.19	1.5	7	.15	.12	.23	1.3	10
0.3–0.6	.03	.10	.....	0.4	7	.02	.10	.....	.....	10
	.06	.16	.....	0.7	7	.04	.13	.15	0.2	10
	.08	.18	.....	0.9	7	.05	.11	.19	0.4	10
	.21	.22	.41	1.7	6	.06	.12	.20	.....	10
	.....	.....	.....	.....	.....	.09	.15	.30	0.6	10
	.....	.....	.....	.....	.....	.11	.17	.26	0.7	10
	.....	.....	.....	.....	.....	.19	.19	.33	1.3	10
	.....	.....	.....	.....	.....	.31	.32	.51	2.1	9
0.6–0.9	.05	.19	.....	0.4	6	.04	.17	.24	0.6	6
	.11	.20	.31	1.1	6	.14	.26	.44	1.5	6
	.21	.26	.50	1.8	6	.19	.21	.36	1.5	5
	.38	.30	.45	1.9	6	.28	.25	.....	1.9	5
0.9–1.2	.10	.27	.35	1.1	5	.06	.22	.31	0.9	6
	.22	.33	.46	1.6	5	.15	.28	.44	1.6	6
	.26	.42	.....	1.8	5	.24	.35	.51	1.8	6
	.39	.37	.46	2.0	5	.40	.41	.54	2.7	5
1.2–1.5	.13	.25	.34	1.3	4	.15	.31*	.....	1.5	4
	.17	.33	.36	2.0	4	.28	.36	.65	2.0	3
	.24	.36	.52	2.0	3	.38	.35	.56	3.0	3
1.5–1.8	.11	.30	0.37	1.1	3	.10	.29	.39	1.2	4
	0.23	0.36	.....	1.7	3	.20	.34	.....	2.3	4
	.....	.....	.....	.....	.....	0.24	0.31	0.45	2.5	3

observed any longer, while the unreddened stars are still bright enough to give accurate data. With increasing distance the less reddened B stars will gradually become too faint also. If the distance is increased still more, the same selection effect will repeat itself with the supergiant B stars. We can certainly expect that the data of the strongly reddened distant stars are missing.

In Figure 9 is shown what can be expected for the relation between line intensity and reddening in one area in a somewhat idealized case, using the information we already have. The dotted curves show the general relations for the distance intervals. The points and open circles show the information we found from Figures 4 and 5, namely, that the average intensity always increases for successive distance intervals but the average reddening sometimes remains constant over a considerable distance interval. The heavy parts of the dotted lines show the expected deviation in the reddening, being much more pronounced than the deviation in the intensities. The smoke distribution is known to be very spotty in some areas, so that stars at the same distance may have very different reddening. It is better to arrange the data of the stars in each area according to reddening and then determine the normal points. The two nearly parallel lines in Figure 9 show that one

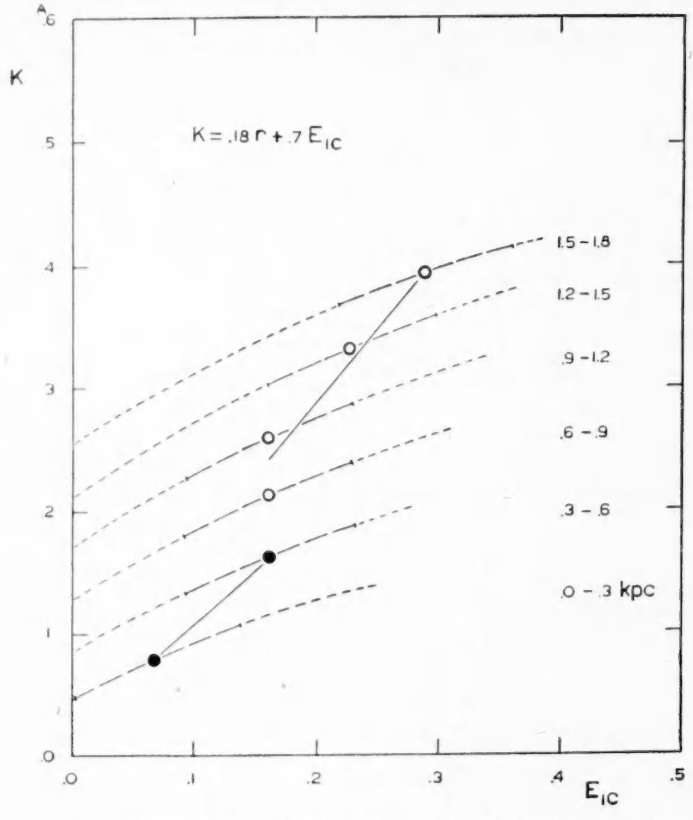

FIG. 9.—The expected relation between the K line intensity and reddening for one area in a somewhat idealized case.

can expect two relations, one for the near-by stars and one for the distant stars. We expect to find small differences from area to area, depending on the situation in space in the direction of this area.

XI. INTENSITY-REDDENING RELATIONS IN THE AREAS

If one plots the intensity-reddening diagram for a certain area in the Milky Way and writes in the distances of the individual stars, one finds that for constant reddening the distant stars have the strongest intensities. In other words, the near-by stars are found in the lower part of the diagram, the distant stars in the upper part. For the relations between the K and D line intensities with respect to reddening, it was necessary to choose two distance intervals. All that we need to know at the moment is whether the star is near by or distant. However, it is very helpful to know the accuracy of the intensities.

In Table 8 the data are arranged according to reddening in the two distance intervals; the columns give the names of the area, the reddening, the K value, the D value, the intensity of the λ 4430 band, the number of stars used for the K value, the mean distance, and the distance interval in kiloparsecs.

Figure 10 shows the relation between the K line intensity and reddening in the different areas, where the distance intervals are given in kiloparsecs. A first glance shows that it is not easily possible to draw only one relation. The scatter of the normal points would be mainly cosmic and much larger than expected. The two relations drawn fit the observations much better; the highest relation always corresponds to the most distant distance interval. The figure for the D lines is very similar and confirms these properties.

Let us first consider the stars in an open cluster, because we know that they have the same distances. The Scorpius cluster gives an excellent relation even for the single stars, showing a definite slope. The result for the *h* and χ Persei clusters is confirmed by the stronger D line material. Note the two open squares at the top of the figure for the Perseus area. We see that a large increase in reddening corresponds with a rather small increase in line intensity. The slope of the relation for the Orion cluster is larger than for the other clusters. Note the two squares at the left corner of the figure for the Orion area. There is a deviation from the general $1/\lambda$ reddening law in this region, as found by W. Baade and R. Minkowski[60] and confirmed by J. Stebbins and A. E. Whitford.[61] The slopes found in these three cases are important because they prove that a more reddened star in the cluster also has a stronger line intensity, so that more smoke in front of the star also means more gas in front of the same star. This agrees with our result in the previous pages, that smoke clouds occur, in general, where there is a concentration of the gas.

The Pleiades cluster shows the same effect as the other clusters; however, the values are rather small and inaccurate. Eight of the ten members of the ζ Persei group for which we have data give the expected relation with very small deviation, but two stars deviate considerably. These last two stars have a radial velocity which deviates 7 km/sec from the averaged group motion. Besides the cluster stars and perhaps a few not yet recognized as members of these clusters, it is usually impossible to find enough B stars in an area which have even approximately the same distance.

We now consider the relation belonging to the near-by stars and see that, in general, the slope is larger if we include greater distance intervals. The relation belonging to the distant stars has again a different slope. These stars are, in general, somewhat more reddened and have considerably stronger line intensity. Both relations can be explained with the help of Figure 9. The normal points of the two areas in the same longitude interval agree rather well.

The only possible interpretation for two relations in one area seems to be the continuum

[60] *Ap. J.*, **86**, 119 and 123, 1937; *Mt. W. Contr.*, Nos. 571 and 572, 1937.

[61] *Ap. J.*, **102**, 318, 1945.

TABLE 8

INTENSITY-REDDENING RELATIONS

Area	E_{1c}	K	D	λ 4430	n	r	Interval
Polar caps	0^{m}02	0.05	.....	.....	3	0.23	0.1–0.6
	.07	.09	0.17	0.7	3	0.41	0.1–0.6
Intermediate latitudes	.01	.07	.....	0.5	6	0.18	0.1–0.3
	.04	.10	.....	0.6	6	0.18	0.1–0.3
	.09	.10	.....	1.0	7	0.25	0.1–0.3
	.08	.24	.....	1.2	3	1.32	1.0–1.6
Monoceros	.05	.05	.....	.....	3	0.26	0.2–0.5
	.08	.06	.....	.....	3	0.23	0.2–0.5
	.05	.15	.21	0.4	4	0.95	0.6–1.4
	.14	.21	.36	1.3	3	1.07	0.6–1.4
Orion clu.	.04	.11	.11	.....	6	0.32	0.3
clu.	.09	.15	.21	0.3	5	0.32	0.3
	.02	.09	.....	.....	7	0.35	0.2–0.5
	.04	.12	.15	0.2	7	0.30	0.2–0.5
	.05	.13	.23	0.3	7	0.41	0.2–0.5
	.07	.11	.23	0.3	8	0.34	0.2–0.5
Gemini	.02	.10	.....	.....	4	0.17	0.1–0.2
	.05	.20	.36	.....	4	0.63	0.5–1.7
	.19	.28	.50	1.6	5	1.13	0.5–1.7
clu.	.21	.32	.40	2.3	6	1.53	1.5
Taurus clu.	.03	.05	.....	0.2	8	0.18	0.2
	.05	.11	.....	0.9	8	0.22	0.1–0.6
	.11	.14	.26	1.4	8	.....	0.1–0.6
clu.	.16	.12	.18	1.0	10	0.26	0.3
Auriga	.05	.08	.14	0.5	4	0.18	0.1–0.7
	.15	.15	.40	1.3	5	0.47	0.1–0.7
	.17	.29	.42	1.3	4	1.22	0.7–1.9
	.24	.34	.47	2.1	4	0.94	0.7–1.9
Perseus	.08	.07	.24	.....	7	0.18	0.1–0.2
	.23	.25	.49	1.6	4	0.72	0.4–1.8
	.31	.38	.55	2.3	4	0.74	0.4–1.8
	.38	.38	.65	2.8	5	0.98	0.4–1.8
clu.	.17	.62	.76	1.8	9	1.91	1.9
clu.	.32	.65	.88	2.1	9	1.91	1.9
Andromeda	.03	.07	.12	0.3	4	0.18	0.1–0.5
	.07	.09	.....	0.6	5	0.25	0.1–0.5
	.09	.35	.48	0.5	3	1.39	0.8–2.3
Cassiopeia	.06	.12	.14	.....	3	0.34	0.1–0.5
	.16	.34	.52	1.7	5	0.98	0.5–2.2
	.21	.41	.69	1.7	5	1.63	0.5–2.2
	.32	.50	.89	2.5	5	1.28	0.5–2.2
Lacerta	.04	.14	.24	0.4	6	0.46	0.1–0.8
	.07	.15	.....	0.6	6	0.40	0.1–0.8
	.11	.17	.....	0.7	6	0.45	0.1–0.8
	.30	.56	.72	2.3	2	2.30	1.9–2.2
Cepheus	.12	.20	.40	1.4	5	0.54	0.2–1.3
	.17	.23	.50	1.4	6	0.69	0.2–1.3
	.25	.30	.49	1.8	6	0.58	0.2–1.3
	0.30	0.27	0.47	1.9	6	0.67	0.2–1.3

TABLE 8—*Continued*

Area	E_{ic}	K	D	λ 4430	n	r	Interval
Cygnus	0^{m}05	0.11	0.14	0.4	6	0.38	0.1–0.9
	.09	.20	.34	1.2	6	0.58	0.1–0.9
	.04	.24	.39	.....	5	1.51	1.0–2.1
	.10	.36	.55	1.0	4	1.46	1.0–2.1
Cygnus star cloud	.02	.09	.....	0.5	6	0.35	0.2–1.4
	.08	.15	.....	0.6	6	0.41	0.2–1.4
	.19	.33	.58	1.5	6	0.88	0.2–1.4
	.28	.40	.48	1.7	6	0.87	0.2–1.4
	.39	.44	.62	2.1	5	0.96	0.2–1.4
	.17	.40	.77	1.8	5	1.64	1.4–2.0
	.25	.45	.....	2.0	4	1.74	1.4–2.0
Vulpecula	.04	.06	.....	.....	4	0.21	0.2–0.4
	.09	.12	.....	0.8	4	0.26	0.2–0.4
	.17	.31	.38	1.5	6	0.99	0.7–1.3
Lyra	.03	.10	.19	0.5	7	0.44	0.1–0.6
	.05	.13	.....	0.7	7	0.30	0.1–0.6
	.11	.13	.24	1.1	7	0.34	1.0–1.8
	.13	.28	.37	0.9	3	1.28	1.0–1.8
Ophiuchus	.09	.15	.26	1.1	3	0.35	0.1–0.7
	.14	.18	.35	1.4	4	0.45	0.1–0.7
Aquila	.34	.66	.80	2.8	5	1.82	1.1–2.9
Sagittarius	.09	.17	.....	1.1	5	0.62	0.1–1.1
	.19	.21	.32	1.4	5	0.57	0.1–1.1
	.10	.31	.32	1.1	4	1.66	1.1–2.0
	.19	.32	.31	2.0	4	1.40	1.1–2.0
Scorpius cluster clu.	.03	.03	.16	.....	2	0.19	0.2
clu.	.09	.05	.18	1.4	2	0.19	0.2
	.09	.06	.17	.....	2	0.17	0.2
clu.	.14	.06	.19	1.2	2	0.19	0.2
	.20	.07	0.20	1.8	2	0.18	0.2
clu.	0.24	0.08	.....	1.9	2	0.19	0.2

effect. There must be a large part of space filled with a rarefied gas continuum but without observable smoke. Suppose this is the case between a cluster and a number of distant stars behind the cluster, the latter group all having about the same distance. One then expects a parallel relation situated higher in the figure, because all line intensities will increase by the same amount. Because in space this condition may not be exactly fulfilled, one can expect in practice a nearly parallel relation, situated higher and somewhat more to the right in the figure. The fact that we have to work in most cases with stars in distance intervals changes only the slope of the relation somewhat.

Three other possible interpretations seem unlikely. First, the two relations could be caused by differences in normal colors for a normal B star and a supergiant B star of the same spectral class. However, these corrections for the reddening are taken into account as far as they are known at the moment. Moreover, we will find for the λ 4430 band only one relation. Second, it is unlikely that these two relations are caused by the galactic-rotation effect in the equivalent widths, because this effect was found to be small. The areas around the zero points show two relations as well. In the third place, we have to

consider the selection effect. This cannot be the cause of the phenomenon found for rather near-by intervals in several areas, but it could be the reason for the data found in very distant distance intervals. But even there we find a rather clear separation between the two relations if we use the individual points, a situation one would not expect if this effect were the only reason. It is more likely that more powerful instruments giving more complete data would make it possible to draw extensions of both relations.

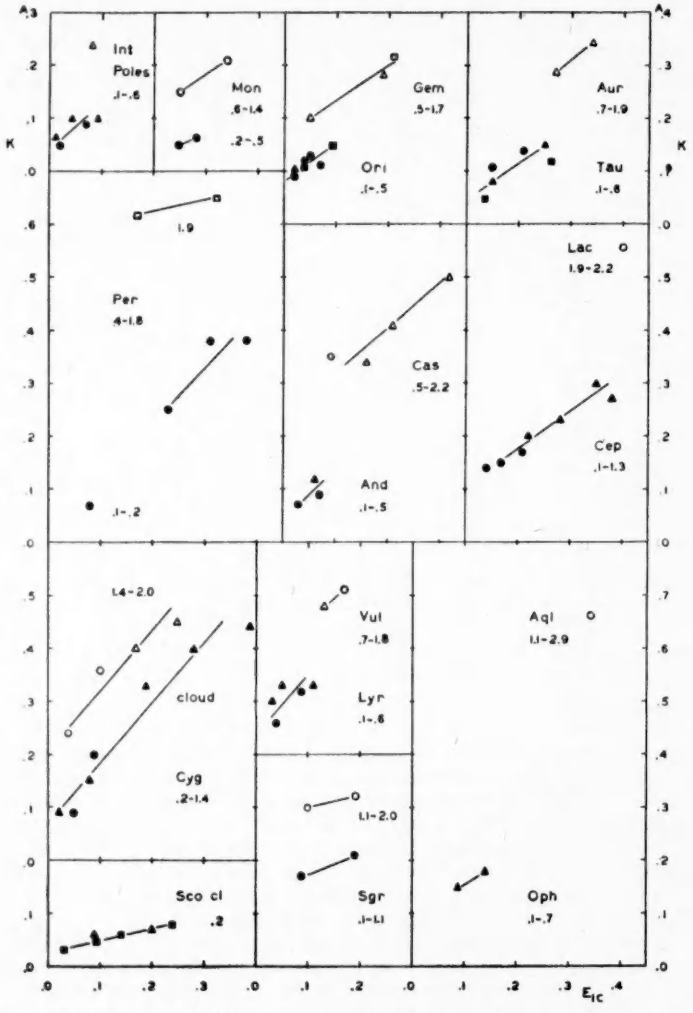

FIG. 10.—Relation between the K line intensity and reddening in the different areas. Normal points are average data of about four stars. Dots correspond to southern areas, triangles to northern areas, squares to stars in open clusters. Open symbols refer to distant stars; the distance intervals are given in kiloparsecs.

There are not enough observed stars in one area to divide into more than two distance intervals. In several areas we would expect even more than two relations in that case. We can make only one other check. For each star with known accurate distance, we determined that part of the line intensity caused by a uniform gas continuum. Stars with distances larger than 2 kpc were excluded, because the distances of the stars are no longer accurate. The remaining or corrected line intensity, $K_c = K - 0.18\,r$, should now show a close relation with the reddening if our working model is correct. It will mainly correspond with the discrete clouds containing both a gas concentration and smoke. The data

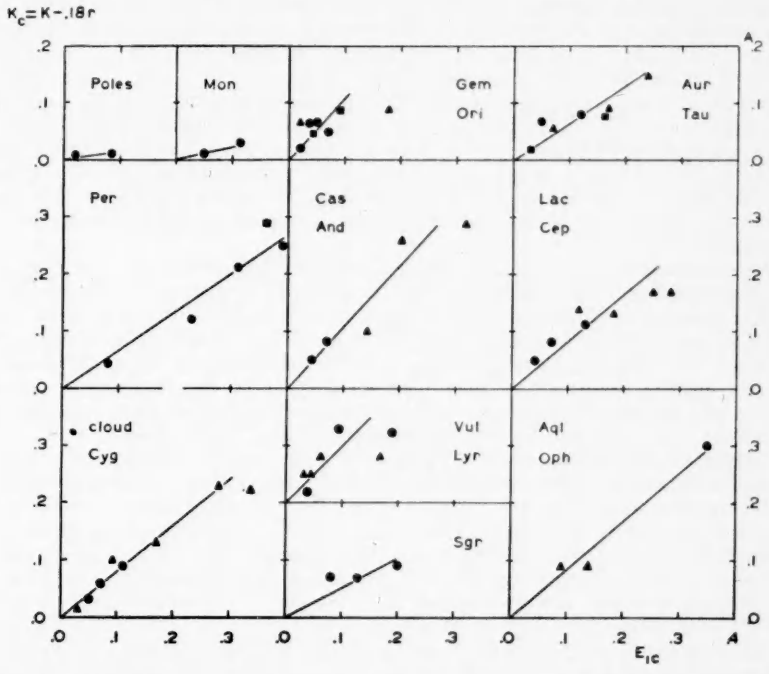

FIG. 11.—Relation between the line intensity $K_c = K - 0.18r$, corrected for the effect of a uniform gas continuum, and the reddening in the different areas. Normal points are average data of about four stars. Dots correspond to southern areas, triangles to northern areas, squares to stars in open clusters.

of the stars in one area were arranged according to reddening and normal points formed. Figure 11 gives this corrected K_c line intensity as a function of the reddening. Indeed, we now find a single relation with only small dispersion. The slope of the relation is not the same in each area. One reason will be that we have already found considerable density fluctuations in the continuum for which it is difficult to apply corrections. Therefore, it is not possible at the moment to decide whether the relation between gas and smoke in the discrete clouds is exactly the same in each area—but it is certainly not very different.

We can now explain why other authors often found such a considerable scatter in their intensity-reddening diagrams. Often all B stars in the Milky Way were considered together, and many authors did not divide the material into distance intervals.

The measurements of R. F. Sanford[5] for the K line and P. W. Merrill[16] for the D lines were used by the authors for plotting a general diagram for the whole Milky Way, where

one normal point is the average for one of their regions. By doing the same for our areas, we would get the same reasonable scatter they get. The latter author also gives figures showing the relation for the D lines in several of his regions. J. W. Evans[32] included all stars together in one diagram, which exhibits considerable scatter.

The estimates are too inaccurate for any analysis except those of the faintest lines. Furthermore, as we saw before, in the estimates of J. S. Plaskett and J. A. Pearce[12] a magnitude error exists. This explains why J. Stebbins and C. M. Huffer[62] found no relation at all. Also, it makes plausible why W. Becker[63] found a negative result. He reduced the K line intensities to a distance of 500 psc, which would be permissible only in the case of a strictly uniform distribution of the gas. The estimates of O. Struve[11] have no magnitude error, which explains why C. Westgate[64] and A. Colacevich[65] got at least some result. Struve's estimates in the Cepheus region were also discussed by C. T. Elvey and T. G. Mehlin[66] without yielding any relation at all.

L. Spitzer[17] finds definite relations between the D line intensity and reddening, but the first one is found to be affected by a galactic-rotation effect in the equivalent widths. He used his simple working model, namely, all gas and smoke concentrated in discrete clouds. A constant reddening then means a constant number of sodium atoms in the line of sight. His four distance intervals are 0.25–0.63, 0.63–1.0, 1.0–1.6, and 1.6–2.5 kpc. His figures for the two most distant distance intervals are most convincing with respect to the galactic-rotation effect.

We did not find such an effect by taking equal distance intervals, and the same result was obtained from the doublet ratios and the behavior of the curves in Figure 6. The same conclusions were reached by O. C. Wilson and P. W. Merrill[15] and by O. A. Melnikov.[28] It is clear that Spitzer's two most distant distance intervals, 0.6 and 0.9 kpc, were too large. The continuum effect, together with the preference for clustering among the B stars, must be the reason for the systematic effect in his figures. Our result demonstrates that Spitzer's working model is too simple and that a continuum of rarefied gas (or a large number of transparent clouds) must be added to his model.

Another check was made by P. J. van Rhijn,[67] who studied a possible discrepancy between the distance of stars derived from interstellar lines and from photometric distances in the system of W. W. Morgan. No such differences were found which depended on the positions of the stars with respect to the zero points. This agrees with our result.

Another remark of van Rhijn needs comment. He finds no variations of the mean reddening with longitude at any specified distance and latitude. This is undoubtedly because his intervals were too large in longitude and were not chosen according to any special properties of the area. We found marked differences both in line intensity and in reddening between our areas, depending on the longitude and the latitude and caused by differences in space distribution rather than by the galactic-rotation effect in the equivalent widths.

Figure 12 gives the relations between the intensity of the λ 4430 band and the reddening for the different areas and the result for all areas combined. Obviously, here we have a simpler relation which is satisfied within the accuracy of the observations. It strongly suggests that the λ 4430 band may be produced by the main compound of the smoke particles, and it would be very interesting if one could succeed in identifying this band. Some deviations of the usual relation observed in a few stars may be caused by an unusual mixing with other compounds of the smoke particles.

[62] *Pub. Washburn Obs.*, **15**, 252, 1934.

[63] *Zs. f. Ap.*, **11**, 98, 1935.

[64] *Ap. J.*, **78**, 65, 1933.

[65] *Rend. Accad. Nat. dei Lincei*, **17**, ser. 6, 1065, 1933.

[66] *Ap. J.*, **75**, 354, 1932.

[67] *Groningen Pub.*, No. 53, 1949.

According to the theory of J. H. Oort and H. C. van de Hulst,[68] the following occurs in interstellar space: A smoke nucleus will grow through encounters with ions and atoms of gases other than hydrogen and helium, which will then condense against the nucleus. The gas has to have a high enough concentration to give enough encounters that the nucleus will grow to a certain critical size, above which it can be observed through absorption and reddening effects. The minimum total gas density is given as 10^{-24} gm/cm^3. In our part of the Milky Way, we are most concerned with this minimum total gas density, because the mean density is about 3×10^{-24} gm/cm^3. It explains why one can expect places in space where gases exist but where no smoke is observable. Their estimate that

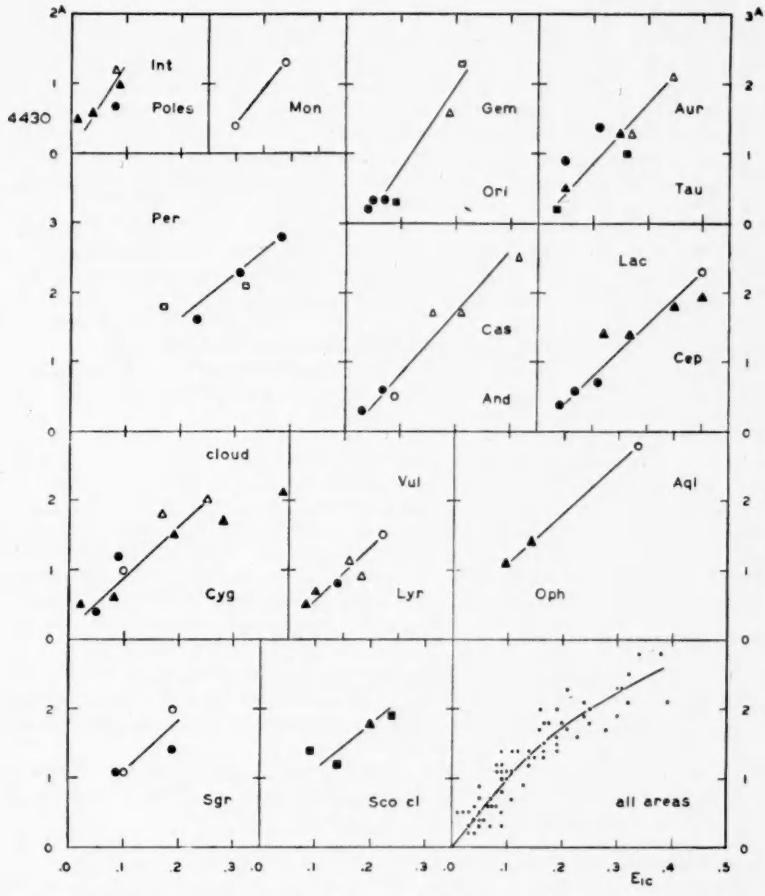

FIG. 12.—Relation between the intensity of the λ 4430 band and the reddening in the different areas. Normal points are average data for about four stars. Dots correspond to southern areas, triangles to northern areas, squares to open clusters. Open symbols refer to distant stars.

[68] *B.A.N.*, **10**, 187, 1946.

14 per cent of space near the galactic plane is occupied by interstellar clouds is consistent with our results.

Some deviations of the usual relation observed in a few stars, where we are reasonably sure that they are not caused by circumstellar material or by the selection effect, may have the following explanation: Too low a line intensity for certain reddening and distance may mean an exhaustion of the gas. Too high a line intensity for certain reddening and distance may mean that most of the smoke particles are rather recently formed and did not have time enough to reach the critical size in large enough numbers.

XII. MOTION OF INTERSTELLAR MATERIAL

It was pointed out long ago by the Mount Wilson and Victoria observers that the interstellar gas follows galactic rotation, while L. Spitzer[69] found theoretically that the smoke must follow the motion of the gas. The gas continuum, together with the concentrations at large, will produce the deepest interstellar component, which will thus show the differential galactic-rotation effect in its radial velocity. Local currents will give one or more additional faint components, as observed for *Ca* II and in some cases for *Na* I, if they are of the right size and amount. It is estimated that this size has to be of the order of 20 psc. A study by B. Donn[70] on the velocity distribution reaches the same result, and it seems to be justified to call them "currents" instead of "gas clouds."

It may be of theoretical interest to give the formulae for a possible radial outflow of gas from the Milky Way, the practical results not being decisive at the moment. Let the outflow of the gas in the sun's neighborhood be F km/sec in the anticenter direction. As long as the distance of the sun is small, the outflow may be considered as a parallel beam and the effect on the radial velocities will be $-F\cos(l-325°)$. For larger distances we have to take into account that the outflow at the center of the Milky Way has to be zero, and thus we take this outflow now in a radial direction away from the center and as a function of the distance R toward the center. We get two correction terms with constants analogous to the constants of galactic rotation:

$$B' = -\frac{1}{2}\left(\frac{F}{R}+\frac{\partial F}{\partial R}\right), \qquad A' = \frac{1}{2}\left(\frac{F}{R}-\frac{\partial F}{\partial R}\right).$$

Further, let the effective distance of the gas be $r' = fr$, where r is the distance of the star from the sun and f is a weighting factor that we can find from the distribution of the gas in the Milky Way. In the case of uniform distribution we have $f = \frac{1}{2}$. The formula for the outflow as it will affect the radial velocities of stars in the Milky Way plane will be:

$$\text{Outflow} = -\{F\cos(l-325°) + B'r' + A'r'\cos 2(l-325°)\}.$$

The quantity B' will be negative according to this definition. The quantity A' will be very small. The result has to be a somewhat distorted cosine curve in the radial velocities, after the latter have been corrected for linear solar motion and galactic-rotation effect.

I wish to express my gratitude to Dr. W. W. Morgan and Dr. C. S. Beals for sending me their unpublished catalogues. I am particularly indebted to Dr. L. Spitzer, Jr., and Dr. A. Blaauw for a number of useful comments.

[69] *Ap. J.*, **93**, 369, 1941; **94**, 232, 1941; **95**, 329, 1942.

[70] Unpublished.

OB STARS IN THE P CYGNI REGION

J. J. NASSAU AND DANIEL HARRIS III*

Warner and Swasey Observatory, Case Institute of Technology

Received January 25, 1952

ABSTRACT

A region of 89 square degrees around P Cygni was examined for faint OB stars. The 4° objective prism in conjunction with the Burrell Schmidt-type telescope was used for this purpose. Within this area, 249 OB stars are present; of these, 136 were published in a previous survey and the rest are given in the present paper. The greatest number of stars of the latter group are faint (limiting photographic magnitude 12.2). The surface distributions of the stars of the two groups are approximately the same.

The photoelectric colors of 140 OB stars were available for the present discussion; of these, the colors of 90 stars were determined at Case. A number of highly reddened stars were found, 9 of which have C_1 color between 0.40 and 0.65 mag.

The two groups of stars appear to be at the same distance, with a distance modulus of 11.1 mag.

The concentration of highly luminous early-type stars near and around P Cygni has been the subject of several investigations.[1] A recent survey by Nassau and Morgan[2] lists some 146 such stars in a galactic belt 12° in width, from longitude 35° to longitude 50°. The list includes stars of the following types to about the tenth photographic magnitude: (1) O and early B stars and (2) high-luminosity stars from B2 to A3. Stars of these types are designated as OB.

In order to ascertain the extent of clustering of OB stars and the effect of absorption due to the Great Rift, long-exposed plates were examined. The area of the sky on which the present survey was made is roughly in the form of a rectangle with its center at $l = 42°$ and $b = +2°$. Two sides of the rectangle are parallel to the galactic equator. Its boundaries are $l = 36°$ to 49° and $b = +4°.0$ to $-2°.75$, with an area of about 89 square degrees. Within this rectangle, 249 OB stars are present; of these, 136 were included in the previous survey[2] and the rest are the stars given in the present paper. The two groups show the same surface distribution, with one significant difference. While only a dozen or so stars of the first group are situated in the area of the Great Rift, about 50 per cent of the fainter stars, that is, the stars of the second group, are in the area of obscuration.

Stars of the two groups show the same high concentration near P Cygni; 75 per cent are distributed within 3° of this star. The greatest concentration (about 80 per cent) lies in a belt 1° on either side of the galactic equator.

If we are to assume that the OB stars in the region form a group, Figure 1 shows that the limits of the survey were not too narrowly chosen. The marked absence of OB stars in the region with center at $l = 42°$ and $b = +3°$, which is known to be free of excessive interstellar absorption, is noteworthy. While a number of OB stars are present west and south of P Cygni, many of them are highly reddened.

Figure 2 shows the distribution in apparent photographic magnitude of the 113 OB stars (crosshatched) listed in the paper and the 136 stars (hatched) already published. The column at the twelfth magnitude includes 16 stars with magnitudes 11.8–12.2. No effort was made, however, to attain completeness to this limit. Stars which were too faint to classify with certainty were omitted. At first sight, the range in magnitude of all the 249 stars appears too large for a group of stars of not too great difference in luminosity and, as we wish to propose, at the same distance. This, as will be shown later, is due to the variation in the interstellar absorption in the region.

* Now at the Yerkes Observatory.

[1] Bok, *The Distribution of the Stars in Space* (Chicago: University of Chicago Press, 1937), p. 117.

[2] *Ap. J.*, **113**, 141, 1951.

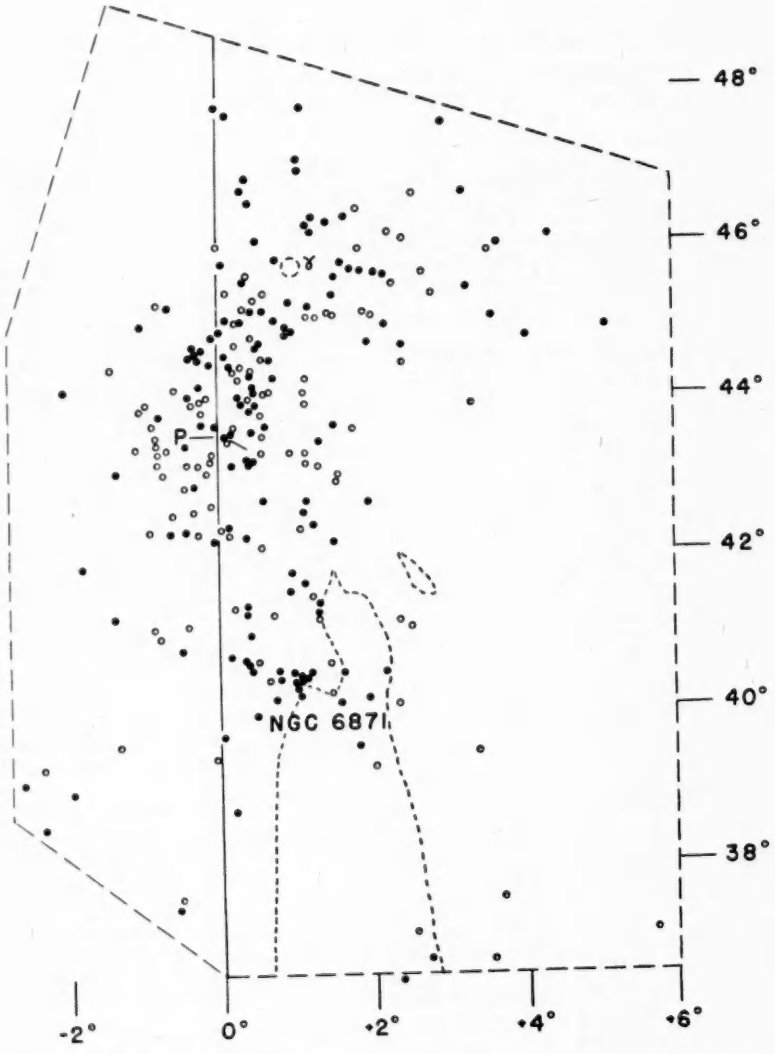

FIG. 1.—OB stars in the region of P Cygni. The open circles refer to stars in the present survey

Figures 3–8 are reproductions from a plate (Kodak IIa-O) centered on P Cygni. Seventy-five of the 113 stars in the region of the survey are marked by serial numbers. Stellar images between two bars indicate stars in the previous paper, and 6 stars which were given in the same paper by co-ordinates only are shown by circled numbers.

DETERMINATION OF COLORS

In the region of our survey the photoelectric colors of 140 OB stars were available for the present discussion. Of these, the colors of 90 stars were determined at Case. In the present paper we give the colors of 50 stars situated mostly in the neighborhood of P Cygni, of which 38 are new (Tables 1 and 2). All our colors are based on the C_1 system of

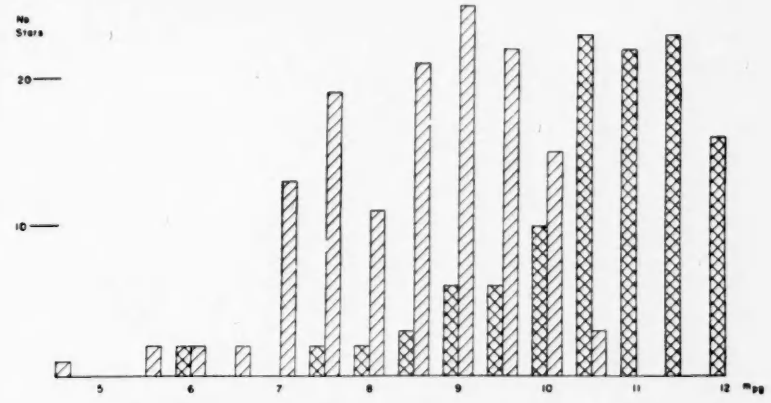

FIG. 2.—The apparent-magnitude distribution of OB stars

Stebbins, Huffer, and Whitford[3] and reduced to their system in the following manner: From the six-color photometry of Stebbins and Whitford[4] we have found, for the space-reddened stars, the following relation between C_1 and the violet (V) and green (G) colors:

$$C_1 = 0^m23 + 0.42\,(V - G)\,. \tag{1}$$

From 14 stars observed by us and present in their list we obtained the relation

$$V - G = -0^m40 + 1.26C_0\,, \tag{2}$$

where C_0 represents our observed colors reduced to outside the atmosphere. Hence

$$C_1 = 0^m06 + 0.53C_0\,. \tag{3}$$

Comparing the values of C_1 for the 14 common stars computed from equations (1) and (3), we find, for the probable error of a single difference, ± 0.011 mag. On the other hand, the published values of C_1 compared with the computed values for the same stars give, for the corresponding probable errors, ± 0.016 mag. and ± 0.018 mag. Further comparison of 37 stars on the C_1 list which were observed by us gave a probable error of ± 0.018 mag.

The catalogue of the stars in this investigation is divided into three parts, as follows:

Table 1 gives all the stars marked in Figures 3–8. The numbers of the first column correspond to the numbers in these figures. The second column gives the BD number

[3] *Ap. J.*, **91**, 20, 1940. [4] *Ap. J.*, **102**, 318, 1945.

FIGS. 3–8.—Identification of new OB stars (denoted by numbers). Stellar images between two bars indicate OB stars found in previous survey. Circled numbers refer to OB stars not in BD found in previous survey.

FIG. 4

FIG. 5

11
12
46
38
32
33
52
44
41
42
39
36
30
29
43
31
45
48
47
40
34
51
49
37
35
50
74
73
66
64
72
70
68

FIG. 6

FIG. 7

FIG. 8

TABLE 1

OB STARS IN P CYGNI REGION IDENTIFIED IN FIGURES 3–8

No.	BD	Pg	Pv	Ci	Remarks
1		11^m.9	11^m.6	+0^m.10	
2	+39° 4076	10.3		+ .01	Popper*
3		11.9			
4		11.2			
5		11.5			
6	+39 4117	10.7	9.8	+ .34	
7		11.8			
8		10.6			
9	+38 4002	9.4	9.1	+ .09	
10		11.6			
11	+38 4017	10.1	9.9	+ .03	
12	+38 4044	10.4	10.0	+ .17	
13		11.5	10.7	+ .34	
14		11.6	10.6	+ .43	
15	+38 4054	10.6	9.7	+ .36	
16		11.6	10.6	+ .41	
17		10.9	9.8	+ .46	
18	+39 4168	10.9	9.9	+ .43	
19		12.0	10.6	+ .65	
20		12.2			
21		11.6			
22	+36 3925	9.6	9.6	− .07	
23	+37 3828	9.1			
24	+38 3958	8.6			
25		11.1	10.5	+ .22	
26	+37 3837	9.6		+ .08	Popper*
27	+37 3844	8.8			
28		12.2			
29		11.4			
30		10.6			
31		11.4			
32		12.2			
33		12.0			
34	+37 3877	10.1	9.9	+ .04	
35	+36 4004	10.3	9.6	+ .25	
36	+37 3887	10.6	10.2	+ .10	
37		11.3			
38		11.4	11.0	+ .12	
39		11.7	10.9	+ .29	
40	+37 3901	10.5	9.8	+ .28	
41		11.9	11.4	+ .18	
42	+38 4034	10.2	9.9	+ .09	
43	+37 3902	10.8	9.8	+ .39	
44	+38 4036	9.1	8.6	+ .16	
45		11.6	10.6	+ .39	
46	+38 4043	9.5	9.0	+ .19	
47		12.0	11.0	+ .39	
48	+37 3917	10.8	9.8	+ .41	
49	+37 3927	11.3	10.2	+ .47	
50	+36 4063	10.8	9.7	+ .45	
51		11.4	10.5	+ .36	
52		11.8	10.8	+ .40	
53	+36 3882	10.2			
54	+35 4006	7.8	7.8	− .11	SHW†
55		10.5	10.4	−0.05	

* *Ap. J.*, **111**, 495, 1950.

† Stebbins, Huffer, and Whitford, *Ap. J.*, **91**, 20, 1940.

TABLE 1—*Continued*

No.	BD	Pg	Pv	C_1	Remarks
56		11.5			
57		11.4			
58		10.7			
59		11.4			
60		11.4			
61		10.8			
62		11.7			
63		11.1			
64	+36° 4000	10.2	$9^m.6$	$+0^m.25$	
65		11.0			
66		11.0			
67		11.9	11.2	+ .26	
68		11.9			
69	+36 4022	10.6	9.9	+ .27	
70		11.6			
71		11.6			
72		11.9			
73		11.2			
74		12.1			
75	+36 4049	9.2	8.6	+0.21	

when available. The third and fourth columns give the photographic (Pg) and the photovisual (Pv) magnitudes as indicated. The latter were derived from our measures with the yellow filter and are reduced to the system at the North Pole as defined by Stebbins, Whitford, and Johnson.[5] The photographic magnitudes were derived in the same manner. The reductions were carried out to two decimals and then rounded to the nearest tenth of a magnitude. Since the probable error in color is ± 0.02 mag. and the ratio of seven is used for the total to the selective absorption, two-decimal magnitudes are superfluous in this discussion. Where photovisual magnitudes are not given, the photographic magnitudes for these stars were based on measures made on plates taken with the Schmidt telescope. Mrs. Virginia Knight determined their magnitudes with the astrophotometer, using sequences generously provided by Drs. John Irwin and Gerald Kron. The fifth column gives the value of C_1. When this value was obtained from other sources, the "Remarks" column gives the source.

Table 2 gives the stars which are not included in Figures 3–8. The BD number given in the first column identifies them. Several stars not measured by us appear in the *Henry Draper Extension*,[6] and their photographic magnitudes, diminished by 0.2 mag., are indicated (second col.) by an "E." The magnitudes in parentheses (third col.) are from the BD catalogue. The "Remarks" column gives the source from which the colors were obtained.

Table 3 includes 7 stars not in Figures 3–8 or present in the BD. Their identification is given in Figure 9.

SOME HIGHLY REDDENED STARS

Table 1 includes three stars of unusually high color: No. 19 with $C_1 = 0.65$ mag., No. 49 with $C_1 = 0.47$ mag., and No. 50 with $C_1 = 0.45$ mag. Also in the same region the OB star HD 229059, brought to our attention by W. W. Morgan, has $C_1 = 0.61$ mag. All four stars are located in the direction of a narrow and very dense obscuring cloud shown in a beautiful reproduction of this region by Duncan,[7] which indicates a total absorption of at least 5 mag.

[5] *Ap. J.*, **112**, 469, 1950. [6] *Harvard Ann.*, Vol. **100**, 1925. [7] *Ap. J.*, **109**, 478, 1950.

TABLE 2

OB STARS IN P CYGNI REGION NOT IDENTIFIED IN FIGURES 3–8

BD No.	Pg	Pv*	C_1	Remarks
+34°3631	.....	(9^{m}5)	.....	
+34 3707	10^{m}8E	(9.5)	.....	
+33 3618	10.3E	(9.2)	.....	
+35 3899	9.1E	(9.2)	−0^{m}02	Popper
+36 3827	10.6	(9.5)	.....	
+33 3717	10.4	10.2	+ .06	
+31 3925	6.0	5.6	+ .13	SHW
+35 3955	7.4	7.3	− .04	SHW
+35 3961	9.9	(9.2)	.....	
+35 3964	8.3	8.3	− .04	SHW
+35 3969	8.7	8.9	− .14	SHW
+40 4032	10.6	(9.5)	.....	
+35 3986	.....	(9.4)	.....	
+35 3987	.....	(8.3)	− .11	SHW
+35 3993	9.5	(9.2)	− .10	SHW
+35 3994	7.3	7.4	− .05	SHW
+41 3644	8.8	8.7	−0.03	SHW
+40 4061	10.1	(9.3)	.....	
+34 3929	10.4E	(9.4)	.....	
+32 3752	10.7E	(9.4)	.....	
+40 4072	9.7E	(9.9)	.....	
+41 3670	10.7E	(9.4)	.....	
+32 3761	.....	(9.3)	.....	
+40 4082	9.9E	(9.1)	.....	
+34 3952	10.8E	(9.5)	.....	
+40 4091	9.8E	(9.1)	.....	
+41 3689	9.9	(9.1)	.....	
+40 4102	9.8	(9.1)	.....	
+40 4112	11.4	(9.5)	.....	
+40 4124	11.3	(9.5)	.....	
+40 4220	.....	(9.1)	.....	

* Values in parentheses are from the BD catalogue.

TABLE 3

OB STARS NOT INCLUDED IN BD

No.	Pg	No.	Pg	No.	Pg
1	10^{m}3E	4	11^{m}7	6	10^{m}9
2	12.5	5	11.3	7	10.7
3	11.2				

THE VALUE OF m_0

The reduction due to interstellar absorption in the apparent visual magnitudes of the OB stars in the region of the survey was made by means of the equation

$$m_0 = m - 7\,(C_1 + 0^m25)\,.$$

The value of the normal C_1 colors of the OB stars was estimated from Popper's[8] values. Stebbins, Huffer, and Whitford's[3] value for the ratio of absorption to color excess was used. Of the 141 stars with C_1 colors available, 91 were included in the published list.[2] The remaining 50 stars are among those given in Tables 1 and 2. The distributions of m_0

[8] *Ap. J.*, 111, 495, 1950.

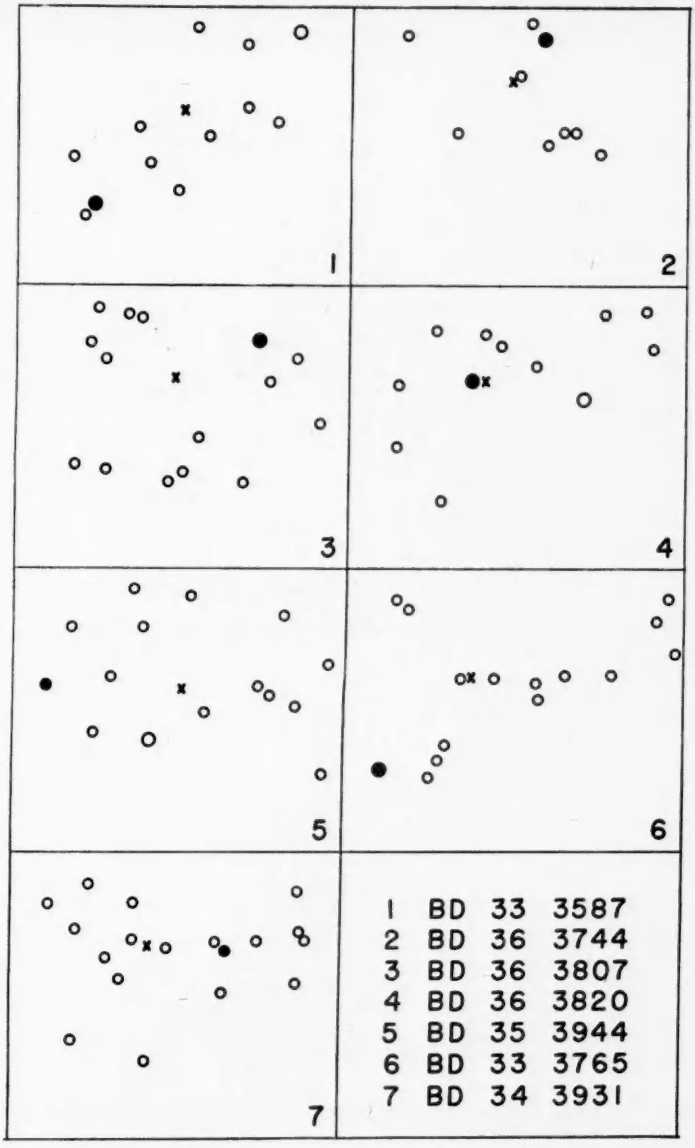

FIG. 9.—The filled circles designate BD stars for which the numbers are given in this figure. The cross in each of the fields designates OB stars, while the open circles are other stars in the field.

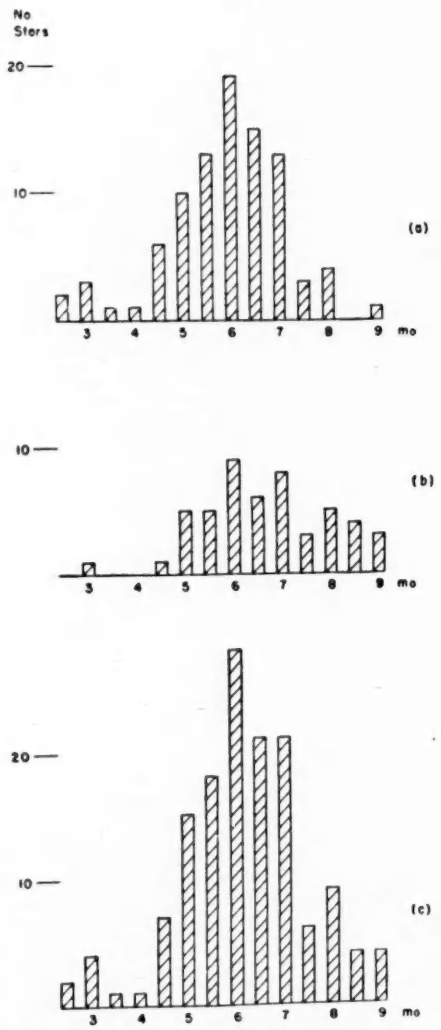

FIG. 10.—Distribution of OB stars in m_0: *a*, for stars previously published; *b*, for stars given in Tables 1 and 2; *c*, for the two groups combined.

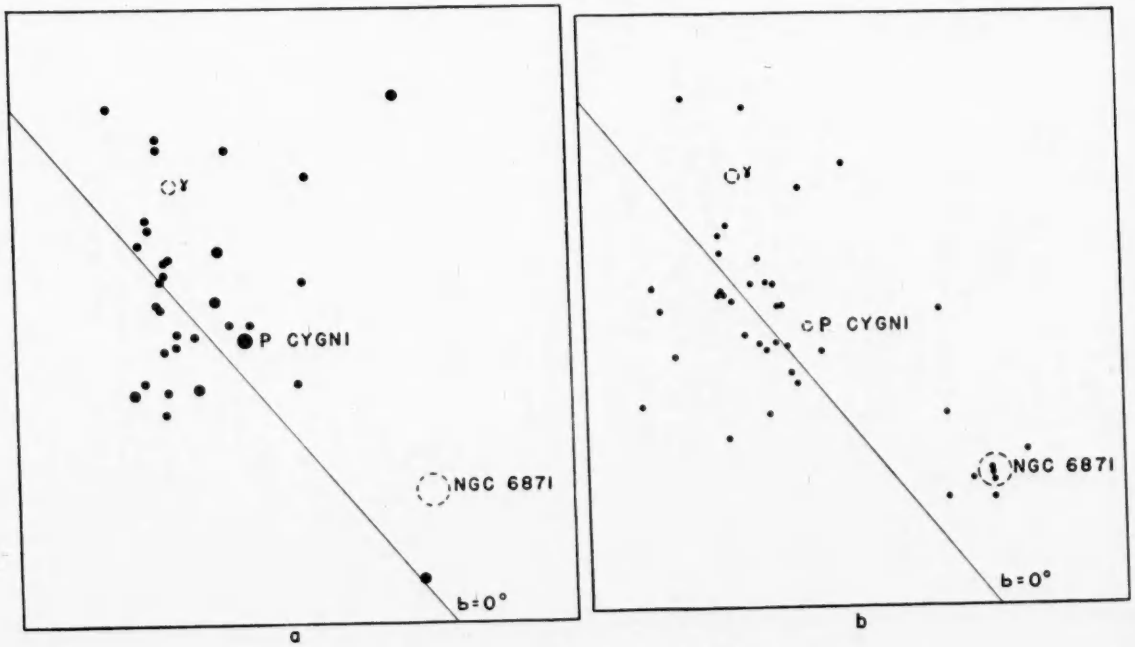

FIG. 11.—*a*, stars with $m_0 < 5.4$ mag.; *b*, stars with m_0 between 5.5 and 6.4 mag.

on half-magnitude intervals for the two groups, separately and combined, are shown in Figure 10. Although the number of stars is small, particularly in the case of Figure 10, *b*, some tentative conclusions are possible.

Since the surface distributions of the bright and faint stars appear to be the same, we may assume provisionally that they are at the same distance. Hence the maximum frequency of m_0 should occur at the same value of m_0 for both groups. This is the case, although the two distributions show dissimilarities which are mostly due to observational selection. Since the first group was selected on the basis of apparent magnitude, it is bound to contain a number of stars of higher luminosity than the average luminosity of the OB stars considered. Also, it is appropriate to point out here that our faint-star survey did not reach the highly reddened OB stars of low luminosity which might be present. The absolute visual magnitude -3.0 is taken as the low-luminosity limit.[9]

Figure 10, *c*, gives the combined distribution of the two groups and suggests that all the stars are at the same distance. The computed mean value of m_0 is equal to 6.3 ± 0.86 mag. (m.e.). Also, the range in m_0 does not differ materially from the range in absolute magnitude of the OB stars obtained from slit spectra by Morgan and his associates at the Yerkes Observatory.[9] In this discussion we omit the 7 stars which have values of m_0 less than 3.8 mag. They appear to form an isolated group, perhaps at the same distance as the rest but much more luminous. In the paper by Nassau and Morgan[9] the suggested mean absolute visual magnitude of OB stars is about -4.8, which gives 11.1 for the distance modulus.

Miss Nancy G. Roman,[10] working with some of the stars in the same aggregate, obtained a distance modulus of 11.0. Her result is based on slit spectra and photoelectric magnitudes (range 6.5–10.5) and colors of 75 stars. If the luminosity distributions for the bright and faint stars are the same, the distance moduli obtained in the two determinations are in good agreement.

NGC 6871

This cluster is less than 2° south of P Cygni. It includes OB stars for which we have obtained values of m_0. In order to examine a possible difference in the luminosity distribution of the cluster stars as compared to the rest of the OB stars in the region we have plotted in Figure 11, *a*, the stars with $m_0 < 5.4$ mag. and in Figure 11, *b*, the stars with m_0 between 5.5 and 6.4 mag. These figures include all stars with known C_1, except, in each case, 3 stars which were omitted because they fell outside the marked boundaries of the figures. The lack of stars with $m_0 < 5.4$ mag. in the cluster is the conspicuous feature in Figure 11, *a*, while stars of the two m_0 groups are present in about the same numbers near P Cygni.

In order to strengthen our data, we include in the following discussion stars for which C_1 colors were not available. Within $\frac{1}{2}$° of the nucleus of the cluster we have 27 stars, of which 15 have known colors. The mean value of C_1 for these stars is 0.04 ± 0.01 mag. (m.e.). If we assume this as the C_1 color of the remaining stars, we obtain, for the 27 stars, $m_0 = 6.9 \pm 0.8$ mag. (m.e.). Within a circle of radius 1° at the point of the greatest concentration near P Cygni we have 83 stars. If we assume that within this circle C_1 varies as a smooth function of position, we are able to secure m_0 for all these stars, from which we obtain $m_0 = 6.2 \pm 1.2$ mag. (m.e.). For these two groups of stars both m_0 and σ are significantly different. The larger spread in m_0 for the stars near P Cygni may be due partly to the assumed colors and partly to a greater spread in absolute magnitude.

It appears either that the stars in NGC 6871 are at a greater distance than the rest of the OB stars in the region or that they are less luminous. To arrive at a definite conclusion on this matter, it seems best to wait until slit spectra are made available, although the objective-prism spectra seem to indicate that many of the cluster stars are not very luminous.

[9] Nassau and Morgan, *Pub. Obs. U. Michigan*, **10**, 43, 1951.

[10] *A.J.*, **56**, 46, 1951.

A FINDING LIST OF F STARS OF HIGH LUMINOSITY

J. J. NASSAU AND W. W. MORGAN
Warner and Swasey and Yerkes Observatories
Received February 4, 1952

ABSTRACT

A list of 111 stars which are probably F-type supergiants is given for a galactic belt 12° wide and extending over the northern sky from $l = 333°$ to $l = 202°$. The classification was made from objective-prism plates of the Warner and Swasey Observatory.

The objective-prism plates obtained for the Case survey for early-type stars of high luminosity have now been used for a survey of F0–G2 stars of luminosity classes I and II on the system of the Yerkes spectral atlas. The area covered is a belt extending in galactic latitude from +6° to −6° and between galactic longitudes 333° and 202°.[1] For the sake of completeness, all objects found to be within this range of spectral type and luminosity have been included; cepheids and known F-type supergiants are therefore listed.[2] The data are given in Table 1. When two spectral types are listed for the same star, they refer to estimates on plates of different exposure; the range in the types gives an idea of their uncertainty, except in the case of the cepheids, where spectral variations occur.

The classification of low-dispersion objective-prism spectra near F0 is especially difficult, because of the occurrence of peculiar stars similar to β Coronae Borealis. The segregation of high-luminosity stars should be most definite in the range F5–F8, since peculiar objects are not often encountered and some complications met with in the G and K stars are not present.

It should be emphasized that the types are, of necessity, only approximate; slit-spectrograms are now being obtained for all of the stars with the 40-inch refractor at Yerkes by Dr. W. P. Bidelman.

[1] J. J. Nassau and W. W. Morgan, *Ap. J.*, **113**, 141, 1951.

[2] Spectra of hopelessly overexposed bright stars have not been considered.

TABLE 1

A FINDING LIST OF F-TYPE SUPERGIANTS

HD or BD No.	α (1900)	δ (1900)	m	HD Sp.	Case Sp.	Name
371	$0^h\ 3^m3$	+62° 39′	6.59	G5	G2 II, cG+A:	.....
611	0 5.4	+60 15	8.56	K0	G0 *Ib*:	.....
725	0 6.5	+56 43	7.12	F5	F0 *Ib* or F0p	.....
1142	0 10.6	+60 27	6.62	G5	G0 II:	.....
4362	0 40.9	+59 2	6.49	G5	G2 I: or G2p:	HR 207
5851	0 55.0	+59 49	8.0	F5	F5 II	.....
6474	1 0.7	+63 15	8.4	K2p	G0 I	.....
7927	1 13.8	+57 42	5.25	F5p	F5 *Ia*:, F2 *Ia*	φ Cas
8906	1 22.7	+59 31	7.24	F5	F0 I:, F2 II:	.....
8992	1 23.5	+58 15	7.6	G5	F5 I:	.....
9250	1 25.9	+63 4	7.30	K0	G0 I:, G0 I	.....
9973	1 32.4	+60 34	7.11	G0	F2 I, F2 *Ia*	.....
10494	1 37.3	+61 21	7.46	G5	F2 I–comp.:, cF+A:	.....
11544	1 48.3	+56 5	6.99	G5	G2 II:	.....
12399	1 56.5	+63 46	7.8	K5	G0 I	.....
14662	2 16.9	+54 55	6.46	G0p	F5 I	HR 690
17306	2 41.6	+53 44	7.8	K0	G0 I: +B:	.....
17971	2 48.2	+59 59	7.81	F5	F2 *Ib*:, F2 I	.....
18391	2 52.2	+57 16	7.46	K5	G0 *Ia*	.....
22451	3 31.6	+52 30	7.96	G5	F5 *Ib*, F5 II	.....
23359	3 39.5	+48 29	8.4	F5	F8 *Ib*:	.....
25056	3 53.8	+53 35	7.35	G5p	G0 I, G0 *Ib*	.....
26673–4	4 8.1	+40 14	4.89	G0 A5	G2 I+B	52 Per
31913	4 54.5	+39 49	Var.	G5	G0 I, F5p	RX Aur
32655	4 59.7	+43 2	6.21	F2	F2 II	HR 1644
33503	5 5.6	+32 47	7.58	F5	F2 II	.....
36891	5 29.8	+40 7	6.18	K0	G0 *Ib*:	HR 1884
38232	5 39.2	+29 16	7.40	F2	F2 II	.....
38503	5 41.2	+35 7	6.60	G0	F8 II, F5 I	.....
39455	5 47.6	+18 8	7.4	F5	F2 II	.....
39949	5 50.8	+27 18	7.7	G5	G0 II	.....
43210	6 9.9	+12 8	8.5	F8	F2 II	.....
E 254429	6 11.2	+12 7	9.3*	G5	F8 II	.....
44990	6 19.8	+ 7 8	Var.	G5p	G0 *Ib*, G5 Ip	T Mon
48616	6 39.2	+ 3 15	7.3	G0	F2 II	.....
−19°1823	7 15.8	−19 16	9.7	.....	F2 *Ib*	.....
58526	7 20.9	− 5 35	6.08	G0	G0 I	HR 2833
59693	7 26.0	− 9 34	Var.	G5	G0p or G0 I	U Mon
165405	18 0.7	−19 5	9.1	G0	F5 I	.....
165553	18 1.4	−21 12	8.3	G5	G0 I:	.....
167516	18 10.5	+ 1 20	8.4	F8	F5 *Ib*:	.....
168393	18 14.3	−11 20	7.45	F8	F0 I	.....
168608	18 15.5	−18 54	Var.	F5p	F8 I	Y Sgr
170764	18 26.0	−19 12	Var.	F8	F5 *Ia*	U Sgr
172365	18 34.7	+ 5 10	6.30	G0p	F8 *Iap*	HR 7008
175580	18 50.9	+ 7 3	6.76	G5	G2 I	.....
176155	18 53.8	+17 14	5.37	F5	F8 *Ia*, F5 *Ia*	FF Aql
178332	19 3.1	+15 21	8.3	F8	F8 *Ib*:	.....
178359	19 3.2	+ 1 9	Var.	G5	F5 I	TT Aql
178695	19 4.5	+10 23	8.5	K0	F2 I	.....
180028	19 9.8	+ 5 52	7.24	F8p	F5 I, F2 *Ia*	.....
180583	19 12.0	+27 45	6.06	F8p	F5 *Iab*, F5 *Ia*	HR 7308
181214	19 14.5	+ 6 58	7.7	F5	F2 I	.....

TABLE 1—*Continued*

HD or BD No.	α (1900)	δ (1900)	m	HD Sp.	Case Sp.	Name
E 231195	19h16m1	+14°14′	9.2*	G0p	F8 I	
182101	19 18.0	+ 9 43	6.25	F8	F2 II	HR 7354
182296	19 18.9	+ 8 28	7.08	K0	G2 *Ib*:	
182900	19 21.8	+12 49	5.77	F5	F5 *Ib*	HR 7389
+20°4166	19 26.0	+21 5	9.3		F5 I	
183864	19 26.5	+24 54	8.1	G0	G0 *Ib*	
185059	19 32.3	+20 7	Var.	G5	F2 I, F8 I	U Vul
185353	19 33.6	+22 34	7.7	G0	G2 II	
185758	19 35.6	+17 47	4.37	G0	G0 *Ib*	α Sge
186688	19 40.8	+29 1	Var.	F2p	F5 *Ib*, F2 I, F5 II	SU Cyg
187321–2	19 44.3	+18 37	7.05	G0 A	G0 I+B8:, G2 I+B	
187428	19 44.8	+19 33	7.9	G5	F8 I or F8p	
187505	19 45.2	+16 8	7.8	G5	G2 *Ib*:	
187921	19 47.4	+27 12	Var.	K0	F8 I	SV Vul
E 226223	19 48.1	+38 30	9.8*	G0	F2 I:	
188121	19 48.5	+28 17	8.6	G0	F8 I	
189378	19 54.6	+33 0	7.12	A5	F2 I–II:	
190004	19 57.8	+24 39	5.32	F0	F2 *Ib* or F0p	16 Vul
+31°3907	19 59.3	+31 38	8.0		G0 I	
190446	19 59.9	+39 59	8.44	F2	F2 *Ib*:	
+24°4008	20 3.4	+24 19	8.7		F2 II	
191546	20 5.4	+43 46	8.5	G0	F2 *Ib*:	
191897	20 7.1	+36 45	8.0	G5	F8 I, G0 I–II	
E 228380	20 9.6	+34 45	9.9*	F8	F5 I:	
193370	20 14.8	+34 40	5.18	F5p	F2 I:	35 Cyg
193701	20 16.6	+45 2	7.02	F5	F2 *Ib*:	
194069	20 18.5	+40 48	6.43	G5	G2 I:, G0 I–II	HR 7795
194708	20 22.0	+42 17	6.79	F5	F2 II	
195100	20 24.2	+42 44	7.54	K0	G2 *Ib*:	
195405	20 26.0	+41 59	8.2	G5	G0p, G0 I	
195593	20 27.2	+36 36	6.30	F8p	F2 Ip, F2 I, F2p	44 Cyg
197376	20 38.2	+41 39	8.1	G0	F5 II	
+46°3014	20 38.9	+46 50	8.5		F5 II	
198797	20 47.7	+39 1	8.0	F2	F2 I:	
200031	20 55.8	+38 25	6.69	G5	G2 *Ib*:	
200102	20 56.3	+44 36	6.79	G5	G2 *Ib*, G2 II	
200406	20 58.2	+47 6	7.7	F8	F5 II	
203918	21 20.1	+50 4	8.17	F8	F8 II	
204022	21 20.7	+50 1	7.77	K0	G0 *Ib*	
205114–5	21 28.1	+52 11	6.20	K0 A3	G2 I: +B9:	HR 8242
206121	21 34.9	+49 20	7.07	G5	G2 *Ib*: or G2p	
209329	21 57.5	+47 49	7.9	F5	F0 *Ib* or F0p	
213482	22 26.6	+56 20	8.6	G5	F8 *Ib*	
214847	22 35.9	+55 38	8.7	K	F8 *Ib*:	
214975	22 36.9	+56 19	Var.	F5	G2 I	Z Lac
215807	22 42.7	+53 25	8.7	F5	F2 II	
217476	22 55.9	+56 24	5.48	G0p	G0 *Ia*	HR 8752
218375	23 2.4	+60 55	6.74	F5	F2 II	
218600	23 4.2	+56 23	8.7	G5	F2 *Ib*	
219135	23 8.5	+56 0	7.6	G5	G0 I:	
+61°2575	23 53.1	+62 4	9.0		F8 *Ib*:	

* Photographic magnitude.

For the stars having slit spectra available, there are six of unusual interest because of high luminosity; these stars are listed in Table 2, together with 44 Cygni, which had

TABLE 2

NEW F5–G0 STARS OF LUMINOSITY CLASS *Ia*

HD or BD No.	α (1900)	δ (1900)	m	Sp.	Remarks
6474.....	$1^h\ 0^m.7$	+63° 15′	8.4	G0 *Ia*	1
10494.....	1 37.3	+61 21	7.46	F5 *Ia*	
17971.....	2 48.2	+59 59	7.81	F5 *Ia*	
18391.....	2 52.2	+57 16	7.46	G0 *Ia*	
E 231195.....	19 16.1	+14 14	8.1	F5 *Ia*	2
+31°3907.....	19 59.3	+31 38	8.0	F8 *Ia*	
195593.....	20 27.2	+36 36	6.30	F5 *Iab*	44 Cyg

NOTES TO TABLE 2

1. See W. P. Bidelman, *Ap. J.*, **113**, 304, 1951.
2. See A. J. Cannon, *Pub. A.A.S.*, **5**, 6, 1922.

been classified as F5 *Ia* by Morgan and Roman.[3] Since three other objects of the same spectral type have now been found whose luminosity appears definitely higher than 44 Cygni, the classification of the latter has been changed from F5 *Ia* to F5 *Iab*.

We are indebted to Dr. W. P. Bidelman for discussions and some unpublished data. This work was supported by a grant from the Office of Naval Research.

[3] *Ap. J.*, 112, 362, 1950.

VARIATIONS IN THE STELLAR LUMINOSITY FUNCTION V. A REGION IN CAMELOPARDALIS

S. W. McCuskey
Warner and Swasey Observatory, Case Institute of Technology
Received January 18, 1952

ABSTRACT

Spectral types and colors for 881 stars have been observed in an area of 16.2 square degrees located at R.A. 3^h51^m; Dec. $+56°.8$ (1945). An analysis of the red color excesses and of some photoelectric color measures indicates that the region is covered by an obscuring cloud which sets in at a distance of 200 parsecs and extends to 500 parsecs from the sun. The total absorption in this cloud is 2.0 mag. at 500 parsecs. Thereafter the absorption increases uniformly to 3 mag. at 2500 parsecs.

Space-density analyses indicate a condensation of B8–A0 stars and of giant F8–K3 stars at distances between 200 and 300 parsecs. In this region the density of the former is four times the density in the solar neighborhood; the density of giants is two to three times that near the sun. Beyond this clustering, the density functions decrease to values somewhat less than the density near the sun. The B5 stars and the F0–F5 stars diminish rapidly in number with distance.

A general luminosity function computed from these data shows an excess of 0.4 in $\log \phi(M)$ for stars with $-1 < M < 2$, as compared to the standard van Rhijn function.

The Milky Way in the Perseus-Camelopardalis–northern Auriga region presents many complexities of structure. Dark clouds of interstellar matter confuse the picture of stellar surface features in negative galactic latitudes. To the north of the galactic plane, however, the intense dark markings are less pronounced. It is in this area that spectral types, magnitudes, and colors have been determined. The following discussion presents an analysis of the galactic structure in the region and a determination of the general luminosity function.

As in former papers of this series,[1] we shall designate the region by a number, LF6. Its center is R.A. 3^h51^m; Dec. $+56°.8$ (1945); $l = 114°$, $b = +4°$, and it covers 16.2 square degrees. The area was selected, in the earlier stages of this program, for the relative smoothness of the surface density of stars. The choice was not fortunate, for, as will appear later, the area is affected by a heavy cloud of interstellar matter.

OBSERVATIONAL DATA

A statistical summary of the distribution of spectral type as a function of apparent photographic magnitude is given in Table 1. All the spectra were taken with the 4° or the 2° prisms attached to the Schmidt-type 24–36-inch telescope of the Warner and Swasey Observatory. The spectral-type data for the brighter stars ($m_{pg} < 11.0$) depend on estimates, and direct comparison with standard spectra, on at least four plates. For the fainter stars, in general, estimates on three plates were made.

The nomenclature for luminosity classification is that of Morgan, Keenan, and Kellman.[2] Criteria for classification appropriate to our spectra have been published by Nassau and van Albada.[3] In many cases, particularly among the fainter stars, it was impossible to assign a luminosity classification. As Table 1 indicates, the number of completely unclassified objects does not become appreciable until the faintest magnitude group is reached.

The photographic magnitudes are based on measures of four Kodak IIa-O plates taken

[1] *Ap. J.*, **106**, 1, 1947; **109**, 139 and **414**, 1949; **110**, 40, 1949; **113**, 672, 1951.

[2] *An Atlas of Stellar Spectra* (Chicago: University of Chicago Press, 1943).

[3] *Ap. J.*, **106**, 20, 1947.

with the 24–36-inch telescope. A sequence for this work was established by direct comparison with the North Polar Sequence on four pairs of plates. It was then observed, more recently, with the photoelectric photometer attached to the same telescope. A zero point for these measures was established by observation of stars 1, 4, 6, 10, 2r, and 4r in the North Polar Sequence. The probable error of a tabulated magnitude for a field star is ± 0.04 mag. All measures on the plates were made with our iris-diaphragm astrophotometer, described recently by Cameron.[4]

In a similar way, photored magnitudes were determined for the majority of the stars in the field. Kodak 103*a*-E plates and a No. 22 Wratten filter were used. Colors on the

TABLE 1

DISTRIBUTION OF OBSERVED SPECTRAL TYPES IN LF6
(Area 16.2 Square Degrees)

m_{pg}*	Spectral Type																							
	B0, 1	B2	B3	B5	B8	B9	A0	A2, 3	A5	F0†			F2			F5			F8			G0		
										III	IV	V	III	IV	V	III	IV	V	III	IV	V	III	IV	V
≤ 6.0	0	0	0	0	0	1	0	1	0	0	0	0	0	0	0	0	0	0	0	0	0	0	0	0
6.25	0	0	0	0	1	0	1	0	0	0	0	0	0	0	0	0	0	0	0	0	0	0	0	0
6.75	0	0	0	0	0	0	0	0	0	0	0	0	0	0	0	0	0	0	0	0	0	0	0	0
7.25	0	0	0	1	0	1	0	2	0	0	0	0	0	0	0	0	0	0	0	0	0	0	0	0
7.75	0	0	0	0	0	0	1	0	1	0	0	0	0	0	0	0	0	1	0	0	0	0	0	0
8.25	0	0	0	1	0	0	0	1	0	1	0	0	0	0	0	0	0	0	0	0	0	0	0	0
8.75	0	1	0	0	1	0	1	1	0	0	0	0	1	0	0	0	0	1	0	1	2	0	0	0
9.25	1	1	0	1	2	2	0	2	0	0	1	1	0	0	0	0	0	0	0	0	0	1	0	0
9.75	0	0	0	3	3	0	0	3	0	0	0	2	0	0	1	0	0	0	0	1	0	0	0	1
10.25	2	1	0	3	1	6	1	5	0	0	0	1	0	1	3	1	0	1	0	0	2	1	1	4
10.75	0	0	0	2	10	6	3	5	0	0	1	2	0	0	1	0	0	1	0	0	2	1	1	4
11.25	4	1	1	2	10	9	8	9	1	2	(3)	3	1	1	0	2	0	2	1	0	1	2	2(3)	4
11.75	3	0	1	9	13	25	20	16	2	3	(7)	2	0	(3)	0	0	(1)	1	0	(3)	1	3	1(23)	0
12.25	0	0	1	11	25	20	50	15	8	1	(11)	1	0	(2)	0	0	(3)	1	0	(1)	0	0	(39)	0
>12.5	0	0	0	3	13	17	48	13	1	0	(2)	0	0	0	0	0	0	0	0	0	0	0	(12)	1
Total	10	4	3	36	79	87	133	73	13	7	25	12	2	7	5	3	4	8	1	6	8	8	82	14

* The entries under m_{pg} refer to half-magnitude intervals, e.g., 7.01–7.5, 7.51–8.0, etc.

† Parentheses around entries for the fainter stars of spectral class F0 and later indicate those for which no luminosity class could be assigned.

TABLE 1—*Continued*

m_{pg}*	Spectral Type																		Unclassified	All Stars
	G2			G5			G8			K0			K2, 3			K5–M8†				
	III	IV	V	III	IV	V	III	IV	V	III	IV	V	III	IV	V	III	IV	V		
≤ 6.0	0	0	0	0	0	0	0	0	0	0	0	0	0	0	0	0	0	0	0	2
6.25	0	0	0	0	0	0	0	0	0	0	0	0	0	0	0	0	0	0	0	2
6.75	0	0	0	0	0	0	0	0	0	0	0	0	0	0	0	0	0	0	0	0
7.25	0	0	0	0	0	0	0	0	0	0	0	0	0	0	0	0	0	0	0	4
7.75	0	0	0	0	0	0	0	0	0	0	1	0	0	0	0	0	0	0	0	4
8.25	0	0	0	0	0	0	0	0	0	0	0	0	0	0	0	0	0	0	2	5
8.75	0	1	0	1	0	0	0	0	0	0	0	0	0	0	0	0	0	0	0	11
9.25	0	0	1	2	0	1	1	0	1	0	0	0	0	0	0	0	0	0	1	18
9.75	0	0	0	0	1	0	1	1	0	3	0	0	0	0	0	1	0	0	1	22
10.25	1	0	0	3	1	0	1	0	1	0	1	0	1	0	0	1	0	0	2	46
10.75	0	0	1	2	1(1)	0	2	1	1	2	0	0	1	0	0	1	0	0	2	54
11.25	0	(1)	2	2	3(1)	1	0	(1)	0	3	1	0	5	0	2	0	0	0	2	96
11.75	2	0	3	5	2	7	3	(1)	2	3	(2)	1	1	(1)	0	1	0	0	12	183
12.25	1	(3)	1	8	1(3)	0	5	(6)	5	8	(11)	0	2	(2)	0	0	0	0	43	288
>12.5	0	(2)	0	1	(6)	0	1	(2)	0	1	(16)	0	0	0	0	0	7	0	.....	146
Total	4	7	8	24	20	9	14	12	9	20	32	1	10	3	2	4	7	0	65	881

[4] *A.J.*, **56**, 92, 1951.

International yellow System obtained for the sequence stars with the photoelectric cell were used to strengthen the red sequence determined photographically.

An R.C.A. type 1P21 photomultiplier was used for this work.[5] GG13 and BG12 filters provide a blue-magnitude measure with effective wave length slightly to the yellow of the International Photographic. A GG11 filter provides a yellow point a little to the blue of the International Photovisual. The relationship to the International Photovisual System is given by $V = Y_0 - 0.054\,C_0 +$ constant, where Y_0 is our measured yellow magnitude and C_0 is our color index reduced to outside the atmosphere. The relationship of our colors, C_0, to the International System is $P - V = 0.335 + 1.137\,C_0$. Blue-yellow color indices were converted into blue-red indices by the relation R.I. $= 1.33\,(P - V)$. Four plates were measured to obtain the magnitudes of the field stars. These, too, were measured with the astrophotometer. The probable error of a final red magnitude for a field star is ± 0.05.

Faint-star counts to $m_{pg} = 18$ were made in four small areas totaling 1.15 square degrees near the center of LF6. A sequence for this work was established by intercomparison on three plates, taken in series with the North Polar Sequence. The sequence magnitudes were measured with a graduated scale of stellar images. They have a probable error of ± 0.1 mag. The total number of stars counted was 1973.

Counts, according to spectral type in the *Henry Draper Catalogue* for an area of 100 square degrees surrounding LF6, are presented in Table 2. These have been used to strengthen the statistical analysis for the brighter stars.

Table 3 gives the average red color index (R.I.) as a function of apparent photographic

TABLE 2

DISTRIBUTION OF SPECTRAL TYPES FROM THE *Henry Draper Catalogue* FOR THE REGION SURROUNDING LF6
(Area 100 Square Degrees)

m_{pg}	Spectral Type									All Stars
	B0–B2	B5	B8–A0	A2–A5	F0–F5	F8–G0	G5	K0–K2	K5–M	
6.51–7.00	4	0	6	3	5	0	0	3	0	21
7.01–7.50	0	1	9	0	5	1	0	2	0	18
7.51–8.00	3	0	17	3	1	1	0	1	0	26
8.01–8.50	1	1	14	7	7	10	0	6	0	46
8.51–9.00	0	0	38	17	10	8	9	8	4	94
9.01–9.50	0	0	24	7	12	12	10	9	1	75

TABLE 3

AVERAGE OBSERVED RED INDICES IN LF6

Spectrum	R.I. Norm.	$\bar{M}$	m_{pg}							
			9.01–9.50	9.51–10.00	10.01–10.50	10.51–11.00	11.01–11.50	11.51–12.00	12.01–12.50	12.51–13.00
B5	−0.50	−1.4	.....	+0.11 (2)	+0.51 (2)	.....	.....	+0.50 (5)	+0.41 (9)	+0.66 (2)
B8	− .40	−0.4	.....	+ .26 (2)	+ .26 (1)	+0.41 (6)	+0.49 (5)	+ .46 (7)	+ .46 (15)	+ .46 (6)
B9	− .33	0.0	+0.49 (2)	.....	+ .52 (5)	+ .57 (3)	+ .49 (4)	+ .45 (16)	+ .45 (12)	+ .46 (10)
A0	− .20	+0.4	.....	.....	+ .76 (1)	+ .60 (2)	+ .55 (4)	+ .55 (13)	+ .51 (34)	+ .51 (29)
A2	− .08	+1.0	.....	+0.39 (1)	.....	+ .66 (2)	+ .50 (3)	+ .69 (3)	+ .44 (5)	+ .68 (4)
A3	− .05	+1.2	.....	.....	+0.51 (1)	+0.68 (2)	+0.66 (3)	+ .73 (6)	+ .49 (3)	+ .65 (3)
A5	0.00	+1.7	.....	.....	.....	.....	.....	+0.70 (1)	+0.61 (4)	+0.52 (1)

[5] See the Report by MacRae, Harris, and Rogerson, Cleveland Meeting, American Astronomical Society, December, 1951 (*A.J.*, abstract, in press).

magnitude and spectral type for the stars earlier than F0. The normal red indices and mean absolute photographic magnitudes required in the analysis of these colors are listed in the second and third columns. These have been taken from the paper by Nassau and MacRae.[6] Numbers in parentheses indicate the number of colors entering into the average. The probable error of a red index is ± 0.06 mag. Photoelectric observations of a few field stars have been made to assure a consistent color system over the whole area of the plate.

INTERSTELLAR ABSORPTION IN LF6

The predominance of positive red indices in Table 3 even for the bright early-type stars indicates that the interstellar matter in LF6 must be strongly absorbing and relatively close by. This is brought out clearly by the plot of red color excesses, E_r, against uncor-

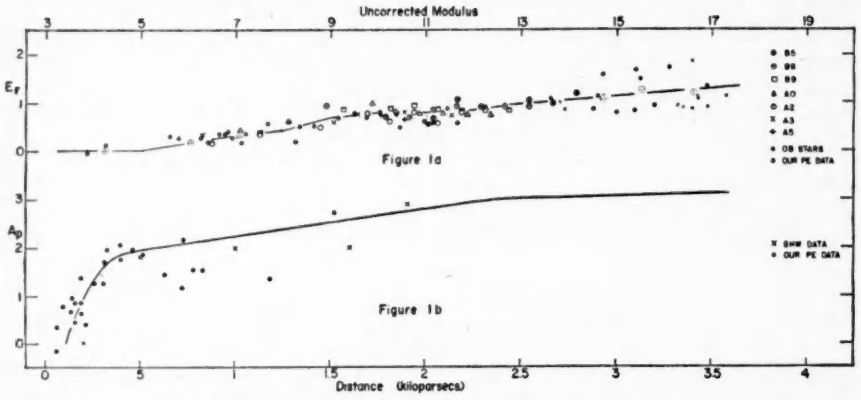

FIG. 1.—*a*: Color-excess–distance modulus relation for LF6. A legend indicating the significance of the symbols is at the right. The average color excess for groups of late-type dwarf stars is indicated by a dotted cross within a circle in the left-hand part of the curve. Similar symbols on the right end of the curve denote average values of E_r for the OB stars. Small filled circles and crosses in the right end of the plot designate, respectively, OB stars classified by Nassau and Morgan and by me.

b: Absorption-distance relation in LF6. Ordinates are absorption in magnitudes for photographic light; abscissas are distances in kiloparsecs. The crosses are based upon photoelectric colors measured by Stebbins, Huffer, and Whitford for a large region surrounding LF6. The dots refer to our photoelectric measures. The curve was deduced from that of Fig. 1 *a*.

rected distance modulus shown in Figure 1, *a*. Average color excesses for the late-type dwarfs (indicated in Fig. 1, *a*, by dotted crosses in circles between $m - M = 4$ and 7) show that for distances less than 150 parsecs no appreciable reddening occurs.

The points indicated for the early-type stars are obtained from the mean values and the normal indices of Table 3. It is interesting to note that the average deviation in the observed color indices from the mean for each of the groups plotted in Figure 1, *a*, is about 0.1 mag. This small dispersion, not much greater than the accidental error in a color index, would indicate a high degree of uniformity of the interstellar material over the field.

In addition to the data from Table 3, we have the photoelectric colors of the sequence stars and of a few field stars, to strengthen the color-excess–distance relation. Color excesses E_y on the blue-yellow International System for these individual stars, converted to red color excesses E_r by use of the factor $E_r = 1.33\ E_y$, are also plotted in Figure 1, *a*. These are indicated by small open circles.

[6] *Ap. J.*, **110**, 45, 1949.

Furthermore, in LF6 there are 10 early O- and B-type stars classified by Nassau and Morgan[7] as OB. I have added 10 stars, mostly fainter than those in Nassau and Morgan's list. These 20 stars have been assumed to have an $\bar{M}_{pg} = -5.3$ and a normal R.I. $= -0^m65$. Red color excesses for them, determined photographically, are plotted in Figure 1, *a*, as small filled circles and crosses. These points help to strengthen the $E_r \sim m - M$ curve in the modulus range 14–17. The great scatter in the red excesses of these stars may be a reflection of the spottiness of the absorption here, or it may reflect the large dispersion in absolute magnitude among the stars concerned. Photoelectric observations are now being planned to study the matter further.

We may conclude from the figure that the absorption sets in very near the sun, is very heavy, and therefore shields from our view many distant galactic features in this area. Figure 1, *b*, presents the photographic absorption A_{pg} as a function of corrected distance. A ratio $A_{pg}/E_r = 2.6$ has been used to convert the red excesses into absorption of photographic light. This is in conformity with the ratio adopted in previous investigations of this series.

The color of early B stars observed photoelectrically by Stebbins, Huffer, and Whitford[8] furnishes additional evidence of high reddening in this region of the galaxy. The E_1 color excesses found by them average about $+0.2$ for this longitude. An independent color-excess–distance relation derived on the basis of these data for the interval $l = 107°$–$120°$ and $b = 0°$ to $+10°$ was made. The values of E_1, multiplied by 9, for selected points on this curve are indicated by crosses in Figure 1, *b*. The agreement between these values and the results of our color observations is reasonably good.

In order to indicate how the photoelectric colors of 27 stars in LF6, determined here, fit individually on this curve, I have replotted the same data as those used in Figure 1, *a*. They bracket very well the steep shoulder of the curve and indicate how abruptly the absorption sets in.

A recent analysis of the galactic structure in Perseus by Heeschen[9] includes the region of LF6. His analysis, based upon observed color excesses in S.A. 9 and other data, indicates an absorption of about 1.0 mag. at 200–300 parsecs and 2.3 mag. at 800 parsecs. This is in good accord with our values.

The corrections for absorption in the density analyses that follow will be based on the absorption-distance relation shown in Figure 1, *b*.

PERCENTAGE OF DWARFS AMONG LATE-TYPE STARS

We assume in the statistical analysis for space density that the dwarf stars are distributed uniformly within the volume of space encompassed by the spectral-type data. Of these intrinsically faint stars, none is likely to be farther than 200 or 250 parsecs from the sun. On the basis of this assumption and from the observed numbers of dwarf stars with $m_{pg} = 9$–11, we can compute the percentage of dwarfs among the brighter stars. These percentages are exhibited in Table 4, together with similar percentages indicated by proper-motion studies of the past. The greatest uncertainty in these figures occurs for the F8–G2 group, where the separation of giants and dwarfs at $m_{pg} = 10$ and 11 becomes difficult.

ADOPTED VALUES OF LOG $A'(m)$ FOR ANALYSIS

Table 5 gives the values of log $A'(m)$ adopted for density analyses in LF6. Here $A'(m)$ is the number of stars per 100 square degrees with magnitude $m - \frac{1}{4}$ to $m + \frac{1}{4}$. These data are obtained from smoothed curves of log $A'(m)$ as a function of m for the regrouped data of Table 1, supplemented by the *Henry Draper Catalogue* material (Table 2) and by

[7] *Ap. J.*, **113**, 141, 1951.

[8] *Ap. J.*, **91**, 20, 1940.

[9] *Ap. J.*, **114**, 132, 1951.

the counts made by Seydl[10] of the bright stars in the *Henry Draper Catalogue*. For these bright stars ($m \leq 7.0$), log $A'(m)$ has been computed for the galactic-latitude zones 0° to ±10°. The number of K5–M8 stars was too small to warrant their inclusion in the analysis.

SPACE-DENSITY FUNCTIONS IN LF6

The number of stars per 1000 cubic parsecs as a function of the distance has been calculated according to a method described by Malmquist[11] and modified slightly by Nassau

TABLE 4

PERCENTAGE OF DWARFS AMONG LATE-TYPE STARS

m_{pg}	F8–G2		G5		G8–K3	
	Adopted	P.M.*	Adopted	P.M.	Adopted	P.M.
5	23	32	10	20	2	4
6	28		10		2	
7	35		10		2	
8	42		11		3	
9	49	45	20	25	5	8
10	58		29		9	
11	81	.....	50	.....	16	.....
12	98	.....	63	.....	29	.....

* "P.M." indicates the percentages of dwarf stars found from proper-motion data.

TABLE 5

ADOPTED LOG $A'(m)$ FOR LF6

m_{pg}	SPECTRAL TYPE									
	B5	B8–A0	A2–A5	F0–F5	F8–G2		G5		G8–K3	
					g	*d*	*g*	*d*	*g*	*d*
4.0	9.17	9.20	9.26	8.83	8.28	7.64	8.05	.....	7.70	.....
4.5	9.34	9.54	9.48	9.10	8.50	7.94	8.33	.....	8.10	.....
5.0	9.51	9.90	9.70	9.37	8.76	8.24	8.64	7.66	8.46	7.40
5.5	9.70	0.23	9.91	9.62	9.00	8.54	8.91	7.96	8.80	7.70
6.0	9.86	0.55	0.13	9.90	9.23	8.84	9.21	8.26	9.17	8.00
6.5	0.02	0.79	0.35	0.17	9.46	9.14	9.50	8.56	9.49	8.30
7.0	0.20	0.90	0.57	0.41	9.70	9.44	9.80	8.86	9.80	8.60
7.5	0.34	0.96	0.74	0.64	9.94	9.74	0.07	9.16	0.12	8.90
8.0	0.48	1.00	0.80	0.80	0.18	0.04	0.30	9.46	0.48	9.20
8.5	0.61	1.10	0.84	0.91	0.40	0.34	0.53	9.76	0.77	9.50
9.0	0.86	1.22	0.98	1.04	0.65	0.64	0.71	0.06	1.00	9.80
9.5	0.90	1.38	1.18	1.20	0.90	0.94	0.88	0.36	1.22	0.10
10.0	1.04	1.60	1.35	1.40	1.10	1.24	1.00	0.66	1.40	0.40
10.5	1.20	1.87	1.52	1.59	1.20	1.54	1.15	0.96	1.55	0.70
11.0	1.37	2.13	1.70	1.76	1.26	1.84	1.27	1.26	1.70	1.00
11.5	1.54	2.40	1.90	1.93	1.32	2.14	1.36	1.49	1.82	1.30
12.0	1.70	2.65	2.09	2.11	1.40	2.40	1.43	1.70	1.93	1.60
12.5	1.86	2.90	2.27	2.30	1.42	2.73	1.50	1.90	2.00	1.90

[10] *Pub. Obs. Nat. Prague*, No. 6, 1929.

[11] *Uppsala Medd.*, No. 84, 1942.

and MacRae.[12] The densities were first computed without regard to the absorption and then were corrected by the Seeliger method[13] for the effects of the latter. No significant differences between values of the density computed according to Malmquist's method and according to the more usual (m, log π) method were found in tests made for this purpose. The mean absolute magnitudes per unit volume of space and the dispersions used in these calculations are taken from the paper by Nassau and MacRae.[14]

Table 6 summarizes the density functions, corrected for the absorption according to Figure 1, *b*.

TABLE 6

DENSITY FUNCTIONS IN LF6
(Number of Stars per 1000 Cubic Parsecs)

DISTANCE r (PARSECS)	SPECTRAL GROUP									
	B5	B8–A0	A2–A5	F0–F5	dF8–G2	dG5	dG8–K3	gF8–G2	gG5	gG8–K3
50	.....	0.085	(0.64)	2.1	1.62	1.48	4.68	(0.04)	(0.05)	(0.18)
100	0.028	.163	.41	1.60	1.62	1.48	4.68	.098	.100	.280
150	.027	.435	.26	1.35	1.62	1.48	4.68	.140	.160	.370
200	.026	.310	.32	1.20	1.62	1.48	.....	.163	.191	.440
300	.021	.138	.33	1.02	1.62	.....	.....	.165	.138	.359
400	.013	.109	.25	0.92	.....	.....	.....	.058	.083	.198
500	.0085	.100	.17	0.83	.....	.....	.....	.033	.044	.139
600	.0056	.100	0.09	(0.80)	.....	.....	.....	.028	.028	.092
800	.0042	.100	.....	.....	.....	.....	.....	(0.024)	(0.019)	(0.025)
1000	0.0040	0.100	.....	.....	.....	.....	.....	.....	.....	.....

Several aspects of the structure of the galaxy in LF6 are worthy of note. Foremost, perhaps, is the concentration of B8–A0 stars and of giant stars of the later spectral groups at distances of 100–300 parsecs from the sun. To some extent, the A2–A5 stars also show this concentration. Even without the effect of the absorption, the high density of B8–A0 stars is present. To remove the peak effect in the density functions for the giant stars would require a very gradual onset of absorption in the area. This does not seem to be justified by the color data.

A second feature of this region is the rapidly diminishing density of F0–F5 stars. At 400 parsecs the number of these stars is only one-third that near the sun. The B5 stars also decrease in number with increasing distance. It may be noted that, in LF7 at $l = 133°$, $b = +2°$, only 19° from LF6, there was a similar negative density gradient among the F stars. It was not so steep, however, the density at 400 parsecs being 0.6 that of the solar neighborhood.

VARIATIONS IN THE LUMINOSITY FUNCTION

The density functions listed in Table 6 have been used to derive a luminosity function, log $\phi(M)$, at distances of 100, 200, 400, and 600 parsecs. Here $\phi(M)$ is the number of stars per cubic parsec with absolute magnitude $M - \frac{1}{2}$ to $M + \frac{1}{2}$. In view of the large absorption in this area and the consequent uncertainty in the numbers of stars per unit volume for the intrinsically fainter stars, the log $\phi(M)$ functions are fragmentary at 400 and 600 parsecs. We have assumed in computing log $\phi(M)$ that the stars of each spectral group at a given distance are distributed in a Gaussian fashion about the same mean absolute magnitude, M_0, with dispersion σ_0, that was used in obtaining the density functions.

[12] *Op. cit.*, p. 51.

[13] See Bok, *The Distribution of the Stars in Space* (Chicago: University of Chicago Press, 1937), p. 14.

[14] *Op. cit.*, p. 45.

No account of the highly luminous OB stars has been taken in forming the luminosity functions. They are so distant in general that their inclusion would not materially alter the values of log $\phi(M)$ for $r < 600$ parsecs.

Table 7 gives the resulting functions, together with the standard van Rhijn luminosity function for the solar neighborhood. These are also plotted in Figure 2. As in the other areas studied in this program, the stars with M between -1 and $+2$ exceed in number those predicted by the standard function. There appears to be a deficit of dwarf stars, $M > +4$, in LF6. This also has been found in other LF regions and may be due to an uncertainty of 0.5 in the mean absolute magnitude adopted for these stars.[15]

We conclude that the shape of the luminosity function is sensibly the same within 500 parsecs of the sun in this direction. In absolute value, however, there is first an increase and then a diminution in log $\phi(M)$ with increasing distance, which amounts to a factor of about 3 in the stellar population.

TABLE 7

LUMINOSITY FUNCTIONS IN LF6
(Entries Are log $\phi(M) + 10$)

M_{PR}	DISTANCE (PARSECS)				STANDARD
	100	200	400	600	
−2	4.81	4.82	4.49	4.19	4.75
−1	5.48	5.62	5.23	5.07	5.07
0	5.96	6.19	5.78	5.67	5.68
+1	6.43	6.59	6.26	5.99	6.34
+2	6.78	6.84	6.59	6.31	6.77
+3	7.00	6.95	.....	.....	6.86
+4	7.13	7.08	.....	.....	7.19
+5	7.06	7.05	.....	.....	7.35
+6	7.17	7.17	.....	.....	7.50
+7	7.32	7.32	.....	.....	7.53

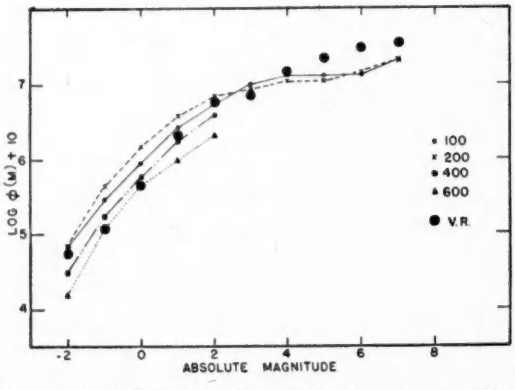

FIG. 2.—Luminosity functions in LF6. Large filled circles refer to the van Rhijn luminosity function (GP. 47). Ordinates are log $\phi(M) + 10$, where $\phi(M)$ is the number of stars per cubic parsec with $M - 1/2$ to $M + 1/2$. Absolute photographic magnitudes are plotted as abscissas.

[15] See *Ap. J.*, **109**, 423, 1949, for a discussion of this point.

GENERAL STAR COUNTS IN LF6

In spite of their limitations, counts of faint stars without regard to spectral type give a first approximation to the galactic structure in a given area. Counts of this type in LF6 to $m_{pg} = 17$ have been made in a small area about the center of the region. For the brighter stars, a summation of the spectral-type data (Table 1) suffices. The star-count data are given in Table 8. For comparison, the results of counts by Heeschen[16] and by van

TABLE 8

GENERAL STAR COUNT IN LF6
(log $N(m)$ per Square Degree)

m_{pg}	LF6	Heeschen	GP 43 Zone	m_{pg}	LF6	Heeschen	GP 43 Zone
8	9.84	.....	9.93	13	1.90	1.87	1.76
9	0.24	0.35	0.36	14	2.30	2.19	2.11
10	0.68	0.75	0.76	15	2.72	2.49	2.50
11	1.08	1.15	1.13	16	3.12	.....	2.87
12	1.50	1.53	1.44	17	3.50	.....	3.26

Rhijn[17] are also indicated. The counts by Heeschen cover a much larger area than that of LF6, while the data from *Groningen Publications*, No. 43, are smoothed results based upon counts in the Selected Areas.

An analysis of the data for LF6, based upon the m, log π, table given by Bok and MacRae[18] for $b = 4°$, is shown in Table 9. The absorption was included in the numerical

TABLE 9

RELATIVE DENSITY FUNCTIONS IN LF6

DISTANCE r (PARSECS)	$D(r)$		DISTANCE r (PARSECS)	$D(r)$	
	Counts LF6	Heeschen ($T+2°.5$)		Counts LF6	Heeschen ($T+2°.5$)
100	1.2	1.5	600	2.0	.....
200	1.5	2.0	800	1.5	0.8
300	2.0	1.8	1000	1.5	.....
400	2.5	1.5	1500	1.1	.....
500	2.5	1.3	2000	0.9	0.1

table. Since the absorption sets in abruptly close to the sun and the spread in luminosity of the stars is large, the solution for the density function is very sensitive to the correction for absorption. The density function is therefore somewhat uncertain. For comparison, the density function computed by Heeschen for his area $T + 2°.5$ is included. It is apparent that the excess density of A stars and giants is reflected in the excess in general density at 200–300 parsecs from the sun.

[16] *Ap. J.*, **114**, 132, 1951.

[17] *Groningen Pub.*, No. 43, Table 10, 1929.

[18] *Ann. New York Acad. Sci.*, **42**, 252 ff., 1941.

SUNSPOT PROMINENCES AND THE YELLOW CORONAL LINE

WALTER ORR ROBERTS

High Altitude Observatory of Harvard University and University of Colorado,
Boulder, Colorado

Received January 28, 1952

ABSTRACT

A study of twenty-five cases of bright emission of the yellow coronal line λ 5694, from 1946 through 1951 revealed close association between this emission and fast-moving prominences of the "sunspot" type. It also showed that unusually sharp discontinuities and intensifications of the red coronal line λ 6374 occurred at the regions where the yellow coronal line was seen. In a few cases small Doppler effects in λ 6374 also appeared at the solar-limb position of the λ 5694 emission. The observations lead to the preliminary speculation that the source of the emission corona lies in a few, relatively small, active regions scattered over the solar disk.

INTRODUCTION

For many years astronomers have been aware of the nearly complete independence of the solar corona and the prominences seen at the limb of the sun. This independence was one of the surprising facts discovered from day-to-day observations of the corona made possible in 1930 by Lyot's new coronagraphic techniques.[1] Lyot's earliest birefringent-filter photographs of the corona, taken over a decade ago in the monochromatic light of the emission lines λ 5303 and λ 6374, revealed further how completely different were the changes and motions of coronal gases from those of prominences.[2]

In 1937, at about the time he started his work of photographing the corona in monochromatic light, Lyot discovered a new line of the coronal-emission spectrum at 5694 A. This yellow coronal line, recent studies have shown, displays a striking association with certain types of prominences and with active solar regions. The results have been described by Waldmeier, who made extensive observations of λ 5694 at Arosa, Switzerland,[3] and by Roberts.[4] The yellow coronal line is generally visible only over regions of marked solar activity as evidenced by sunspots and by the small, sharply curved, and highly changeable "sunspot" prominences of the types classified as III*a*, III*b*, and III*c* by Pettit.[5] The yellow-coronal-line emission probably arises from *Ca* XV,[6] the atom of highest ionization potential in the corona, and its association with them suggests that prominences of this "sunspot" type differ markedly in their physical conditions from the other forms of prominences that are often more brilliant, more massive, and more spectacular in evolution.

RESULTS

The yellow coronal line λ 5694 can be detected only relatively infrequently with the coronagraphs at Climax and at Sacramento Peak. Thus the occasions when it appears are unusual ones. For the line to show on the coronal spectra, which are taken daily (or more often) when weather permits, two conditions must be fulfilled: (1) a region of unusually intense emission of λ 5694 must be present near the solar limb, and (2) the air

[1] *M.N.*, **99**, 580, 1939.

[2] L. d'Azambuja, *Trans. I.A.U.*, **7**, 118, 1950.

[3] *Zs. f. Ap.*, **20**, 172, 1940, and **26**, 312, 1949; *Astr. Mitt. Eidgenössischen Sternw. Zürich*, No. 146; *Zs. f. Ap.* **27**, 73, 1950.

[4] *Ap. J.*, **108**, 523, 1947.

[5] *Ap. J.*, **98**, 309, 1943.

[6] B. Edlén, *Zs. f. Ap.*, **22**, 30, 1940 (or summary by P. Swings, *Ap. J.*, **98**, 116, 1943).

above the coronagraph must be very free from dust or other contaminants—more so than is necessary for observation of other coronal lines.

To date I have isolated and examined twenty-five different occurrences of the yellow coronal line when the line was bright enough on coronagraph spectra to be clearly perceived against the background of scattered light from the photosphere of the sun. There are additional instances to be studied later. In several of the cases there were ten or fifteen separate spectra available for examination and, in addition, numbers of photographs of the prominences in *Hα* at the same location taken within a short time of the spectra.

Table 1 lists the twenty-five cases and gives the dates of the observations of the yellow-

TABLE 1

REGIONS OF EMISSION OF THE YELLOW CORONAL LINE

Case No.	Date	Position Angle (Heliographic)	Case No.	Date	Position Angle (Heliographic)
1	Feb. 27, 1946	60°–65°	13	July 24, 1949	110°–115°
2	July 27, 1946	122°	14	Aug. 7, 1949	253°
3	Nov. 27, 1946	250°–255°	15	Sept. 16, 1949	260°
4	Nov. 30, 1946	280°	16	Nov. 7, 1949	293°
5	Feb. 12, 1947	255°–260°	17	Nov. 19, 1949	271°
6	Mar. 19, 1947	75°	18	Nov. 21, 1949	80°
7	Apr. 14, 1947	255°	19	Feb. 2–3, 1950	290°
8	June 14, 1947	90°–95°	20	Feb. 13, 1950	80°–95°
9	July 24–26, 1947	280°–290°	21	May 6, 1950	85°–90°
			22	Dec. 6, 1950	80°
10	Aug. 14, 1947	260°–265°	23	Feb. 4, 1951	283°
11	Aug. 20, 1947	280°–285°	24	Apr. 10, 1951	80°
12	Aug. 24, 1947	70°–75°	25	Apr. 25, 1951	285°

coronal-line emission at the solar limb and the position angles at which the emission occurred, measured from the north of solar rotation, with angles increasing to the east.

In twenty-three of the twenty-five cases there is strong evidence that centers of great activity of sunspot-type prominences were present within a few degrees of the positions of the maxima of the yellow-line emission, and the other two cases are not certainly negative. In twenty-two out of the twenty-five cases the line-of-sight velocities in the sunspot-type prominences were significantly greater than the usual velocities for prominences in general.

For example, on February 3, 1950, at 290° (case 19 in Table 1) small features of the associated active-region prominences showed a range of line-of-sight velocities up to 100 km/sec, typical of such active-region prominences, whereas prominences in general do not usually show velocities in the line of sight exceeding 40 km/sec. Sunspot prominences of this type, on the other hand, generally show velocities like this even when the yellow coronal line is absent. This absence can be attributed to the difficulty of observing the yellow line, and it is probable that in most instances better observations would reveal the line. For this reason, spectra with a higher-resolution coronagraph, allowing observations closer to the solar limb, are important. The prominence velocities were judged qualitatively from the Doppler displacements visible in the emission spectra of *Hα* and of D3 of helium on the spectrograms containing the yellow-line emission.

The results reveal the clear relationship between the yellow coronal line and the appearance of these sunspot-type prominences with their high-velocity surges, down-flowing arches, and loops; prominences of the sunspot type are not sufficiently common to show any similar association with regions chosen at random on the solar surface, even within the sunspot latitude belt alone.

At the points where the yellow-line emission shows, it also appears that unusually sharp discontinuities in and intensifications of the intensity of the red coronal line λ 6374 are likely. In twenty-three out of the twenty-five cases listed in Table 1, the red coronal line exhibited maxima that appeared to be unusually sharp for the red line, as compared with its appearance over most solar regions. In many of these cases the red-line emission rose from a minimum to a maximum in less than 5°. This behavior is typical only in active regions that include sunspot-type prominences.

In at least three cases a phenomenon far more rare than the occurrence of yellow-line emission was evident: a definite broadening or asymmetry in the red coronal line, which it seems reasonable to attribute to Doppler displacement from large-scale motions, showed just at the position of the yellow-line emission. Probably less than a dozen cases of any discernible Doppler effects in coronal lines appear in the entire decade of coronal observations from Climax.

For most of the cases the green coronal line λ 5303 (*Fe* XIV) was relatively bright at the point of emission of the yellow line, but the green line showed neither sharp discontinuities nor any association that would have been viewed as particularly significant in the absence of the other phenomena.

Figure 1 (top) contains examples of the phenomena under investigation and corresponds to cases 1 and 17 in Table 1. At the top, in this figure, are shown prominence photographs in *Hα*, surmounting polar diagrams giving the intensity distributions (on independent, arbitrary scales) for the three coronal lines. The slit of the spectrograph in each case was placed directly on the region shown in the photograph, and the spectra were obtained for positions corresponding to the photographs, at a single height close to the solar limb.

Figure 1, *a*, shows a typical case of the phenomena associated with yellow-coronal-line emission. In this case, the center of activity toward which the small high-velocity sunspot streamers converged was at about 63°. At the time of this photograph the converging sunspot prominences were not particularly evident, but examination of other parts of the film records showed them to be present and constantly changing in typical fashion. The large, relatively stable prominence from 70° to 85° continued to shoot streamers toward the point of convergence.

In many cases the point of maximum yellow-line emission is not at the location of the brightest parts of the associated prominences but rather at the center of symmetry or convergent point for continuing spurts of high-velocity prominence streams. In many cases intense flarelike prominences frequently formed at or very near the center of activity, and in some cases the emission spectra of these exhibited large line broadening so characteristic of solar flares on the disk,[7] though it is possible that none of the cases yet examined shows a limb feature of sufficient brightness to be called a typical flare. It may also be that the spectrograph slit was placed too high above the limb, in these cases, to record flares if they were present, or it may be that the spectra were never taken at precisely the time and place where a full-fledged flare occurred at the limb.

Several of the cases given in this list have been associated with outstanding regions of solar activity. One case, that of June 14, 1947, was the subject of an earlier paper.[4] Most notable, perhaps, was the case of November 19, 1949. On this date an outstanding outburst of activity took place on the sun. This event, by a fortunate series of circumstances, has been very extensively observed with many types of recording devices. The solar activity was unambiguously associated with the largest changes of cosmic-ray[8] and neutron[9] counts yet recorded and with other terrestrial disturbances.

Figure 1 (bottom) shows the yellow-line and related observations of November 19, 1949.

[7] M. A. Ellison, *Pub. R. Obs. Edinburgh*, **1**, No. 4, 53, 1950 (see also p. 64); *M.N.*, **109**, 37, 1949.

[8] S. E. Forbush, T. B. Stinchcomb, and M. Schein, *Phys. Rev.*, **79**, 501, 1950.

[9] Unpublished result of H. J. J. Braddick, of Manchester, England, reported by Ellison and Conway, *Observatory*, **70**, 77, 1950.

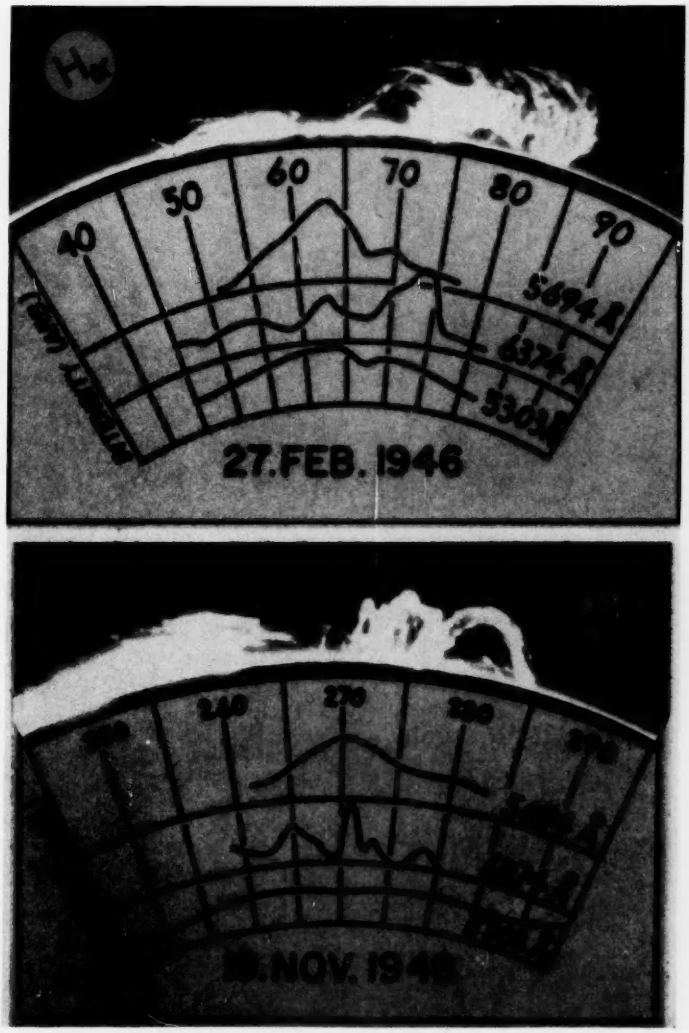

FIG. 1.—Association between sunspot-type prominences and coronal-emission lines. *Hα* prominences shown at the top, with the yellow, red, and green coronal lines plotted below on independent arbitrary line-intensity scales. Positions shown are heliographic position angles. The maxima of the yellow line coincide with centers of sunspot-type prominence activity.

At about 270°, where the yellow line peaked at 16:34 U.T., there was a decided center of prominence activity. Loops and knots from the prominence shown at the right, from 270° to 280°, continued to "rain" down toward the center located at about 268°. The large, relatively quiescent prominence shown at the left, which extended to about 265°, showed little activity, except that at its right extremity it also "rained" prominence material toward the center.

Independent evidence shows that the outstanding solar phenomenon recorded on this date was a chromospheric flare that occurred a short distance inside the disk, below the center of activity visible at the limb. The flare was recorded at Wendelstein Observatory in Bavaria and at the Royal Observatory in Edinburgh[10] before sunrise in Colorado, and thus several hours before our observations at Climax. It appeared at approximately 10^h30^m U.T. very near the solar equator and well toward the west limb of the sun (268° heliographic latitude and 70° west from the central meridian) at the center of activity shown in Figure 1 (bottom). The flare increased rapidly in intensity, peaking at about 10^h32^m U.T., at which time the *Hα* line reached the greatest line width yet recorded at the Royal Observatory. By 10^h36^m U.T. the peak had passed, showing that the flare was a very rapid one both in rise and in fall. By 12^h09^m U.T. no appreciable *Hα* emission remained to be seen. All these phenomena took place before 16^h34^m U.T., the time of the first spectrogram at Climax, on which the graphical material of Figure 1 (bottom) is based.

Ellison and Conway also report that prominence material was ejected across the limb with the extremely high line-of-sight velocity of 550 km/sec and an average velocity in the plane perpendicular to the line of sight of about 300 km/sec. The prominence, too, was invisible after about 11^h00^m U.T. Associated with the flare, Ellison and Conway reported bright helium λ 6678 emission and a short-lived outbreak of continuous emission from the flare.

A complete ionospheric fade-out occurred at 10^h29^m from about 5 Mc/sec to about 20 Mc/sec, and atmospheric noise at 22 kc/sec was suddenly enhanced at the same moment as the flare, both phenomena testifying to the enormous and sudden increase in the D-region ionization at the instant of the flare. The fade-out lasted about 5 hours. At the same time, sudden breaks (crochets) in the geomagnetic intensity took place.

Mr. Fleming, the observer at Climax, who first noted the unusual activity of this solar region, initiated a program of special spectra and photographs of the region, co-ordinated by radio with similar photographs taken at the Sacramento Peak Station of Harvard College Observatory in New Mexico. We can assume that, had the phenomena of the disk been located somewhat closer to the limb on this date, we would have observed the yellow line as being more brilliant. But in this case the disk phenomena probably would not have been observed, and one does not know whether the terrestrial phenomena would have been detected with such magnitude. It may also be that the yellow-line intensity had already declined from an earlier peak by the time of our first Climax observation.

The behavior of the regions of yellow-line emission is under continuing scrutiny; I hope to be able to study the rate of decline of line intensity following outbursts for the yellow and red coronal lines from new observations taken at closer intervals and to make more detailed studies of associated solar activity for dates surrounding those of yellow-line occurrence, using existing observational materials. The present work, however, leads to some speculative conclusions and ideas that rest on admittedly shaky observational ground but that perhaps merit tentative mention now and further observational test as soon as possible.

CONCLUSIONS AND SPECULATIONS

Waldmeier has already suggested that the yellow coronal line is intensified over solar flares.[3] The present work seems entirely consistent with this observation, though I have

[10] M. A. Ellison and M. Conway, *Observatory*, **70**, 77, 1950.

not, in most cases, specifically studied in this paper the effect of individual flares on the yellow-line emission. Most of the active regions identified here with the yellow-line emission were, however, highly productive of flares.

It seems probable that prominence activity can be divided sharply into two types, depending on whether or not the prominences are identified with centers of great activity near the solar surface.[11] Furthermore, it seems likely that active-region prominences are clearly associated with emission of the yellow coronal line and the related phenomena here described. The largest and brightest prominences, on the other hand, are frequently quiet-region prominences, totally unrelated to coronal maxima. Thus the inclusion of all prominences in studies of corona-prominence correlations failed to reveal significant positive association to Lyot and other earlier workers. For the same reason, efforts to correlate observed prominence areas with terrestrial magnetic and radio disturbances have been relatively unproductive. The correlation between the typical active-region prominences associated with yellow-coronal-line emission should reveal a very different result.

The association of the active-region prominences with emission of λ 5694 radiation probably originating in *Ca* XV[6, 12] further suggests that prominences of the two types are sharply differentiated in physical conditions such as temperatures, pressures, strength of associated magnetic fields, etc. Waldmeier's recent findings confirm this supposition.[13]

The behavior of λλ 5303, 6374, and 5694 suggests that the emission corona may find its source in relatively few active centers of the sun that are usually the seat of well-defined sunspots, bright plages, sunspot-type prominences, etc. The gases that radiate the emission lines of the corona, according to this speculation, emanate from these sources and spread gradually over the surface of the sun, moving perhaps 200,000 km in a time of the order of a week, and decline in brightness of emission the farther they move away from the point of origin.

Obvious difficulties stand in the way of this idea and suggest that it must be viewed with caution. If the process by which the coronal gases move from the localized sources is one of atomic diffusion, even granting nonisotropic diffusion controlled, perhaps, by magnetic conditions of the solar atmosphere near the active regions, it is troublesome to think of recombination times for the emitting ions of the order of weeks.

Other obstacles arise from the fact that the lines λλ 5303, 6374, and 5694 exhibit systematic differences in behavior as they move, according to this concept, from their localized sources. The brightness of λ 5694 declines sharply with distance from the source, λ 6374 declines at an intermediate rate, and λ 5303 declines slowly with distance.

Yet the shape and location of the emission regions of the different coronal lines suggest the concept, as does the character of the day-to-day changes of coronal intensities at the solar limb. And the excellent motion pictures of Lyot, taken in the light of emission lines of the corona, agree with the assignment of extremely low velocities of motion to clouds of emitting coronal ions. Figure 2 shows a typical example of the isophotal contours for λ 5303, corresponding to cases 24 and 25 in Table 1.

Further study of these active solar regions is most important. It seems likely to me that they bear close relationship not only to some of the better-known geophysical effects of solar activity but also to the production of solar radio noise and to changes in cosmic-ray intensities. Piddington and Minnett,[14] for example, have discussed hypothetical "hot" regions of the sun's atmosphere, which they hold responsible for the slowly varying component of the sun's radio spectrum (in the range 600 mc/sec and above). There seems a fair chance that their "hot" regions are the same active centers discussed in this

[11] D. H. Menzel, W. O. Roberts, and J. W. Evans, "A New Prominence Classification System" (in preparation).

[12] M. Waldmeier, *Zs. f. Ap.*, **29**, 29, 1951.

[13] *Ibid.*, **28**, 208, 1951.

[14] *Australian Jour. Sci. Res.*, *A*, **4**, 131, 1951.

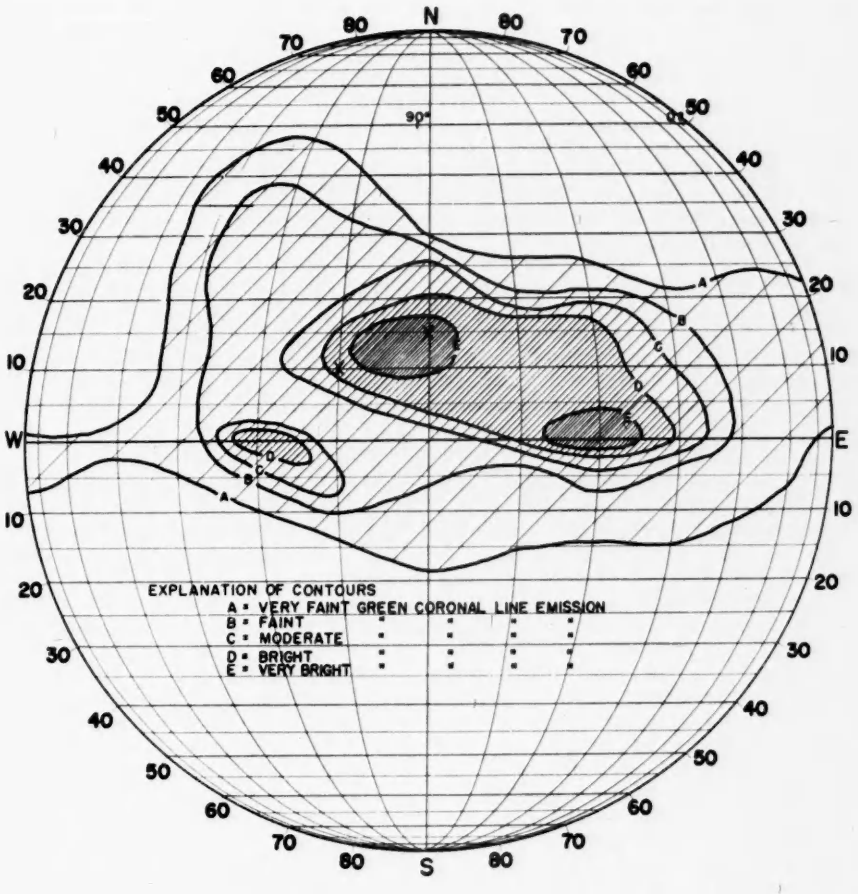

FIG. 2.—Isophotal contours of the green coronal-emission line for April 18, 1951, based on east- and west-limb observations for a 2-week period centered on April 18, 1951. Bright emission of the yellow coronal line occurred during the east- and west-limb passages of the principal center of activity shown in the Northern Hemisphere.

paper. Furthermore, Simpson[15] has found day-to-day changes of cosmic-ray intensities that seem to be correlated with the solar location of active centers like these. We hope, therefore, to be able soon to undertake work of a more quantitative sort on these solar regions.

My thanks are due to the many observers at Climax and at Sacramento Peak for their part in the observations reported here and to Mrs. Kathryn Virnelson, who assisted in the reduction work reported. Also I wish to express my gratitude to my associate, John W. Evans, as well as to Richard N. Thomas and Donald H. Menzel, for their help and criticism during this work. From Alan H. Shapley and Roger Moore, of the National Bureau of Standards, I have had helpful comments and discussions which I gratefully acknowledge. To Harvard College Observatory I express appreciation for the opportunity to examine spectra and to use data obtained from its solar station at Sacramento Peak, operated under Contract W19-122ac-17 with the Geophysical Research Division of the Air Force Cambridge Research Center. I wish, finally, to acknowledge support of certain phases of this work by the Research Corporation, the Office of Naval Research, and the National Bureau of Standards.

[15] *Phys. Rev.*, **85**, 366, 1952.

REFLECTION FROM METEORITIC SURFACES*

F. A. KLOVERSTROM AND W. A. RENSE
Department of Physics, University of Colorado
Received October 4, 1951

ABSTRACT

Observational data are presented pertaining to the polarization of light diffusely reflected by several meteoritic samples. Comparison of results with theory indicates that the polarization may be explained by a combination of molecular-like scattering and metallic-like reflection, even in the case of stony meteorites. Directional and total albedos for the samples are also listed.

INTRODUCTION

Light diffusely reflected from meteoritic particles is believed to be a contributing factor in the origin of several types of astronomical glows, including certain bright nebulae, the rings of Saturn, and the zodiacal light. Very few firsthand data have been obtained by measurement of light reflected by laboratory specimens of meteorites.[1, 2, 3] The present work concerns studies of the amount of polarization introduced into unpolarized light when the latter is diffusely reflected from each of several meteoritic samples, including both stony and iron types. Albedos were also obtained for some of the samples.

PREPARATION OF SPECIMENS AND EXPERIMENTAL PROCEDURE

Five small specimens, all from different falls, were studied, including four stony and one iron meteoritic fragments. In each case a portion of the sample was ground with No. 240 carborundum to a flat surface of about 1 cm^2 in area. All measurements presented in this paper apply to such surfaces. No effort was made to attempt to duplicate the roughness of a meteoritic surface as it might exist in interstellar space (such as by shattering the samples). Curves run for one sample ground to different degrees of smoothness indicated no noticeable change in the polarization effects present in the diffusely reflected light.

A sample was mounted as in Figure 1. The setup is equivalent to that used by Rense[4] in studying diffuse reflection, except that a photomultiplier and amplifier-galvanometer arrangement was used to detect the light. In the figure, *OR* is the normal to the ground surface. The direction of the incident beam is indicated by the angle i, and that of the diffusely reflected beam by the angle ϵ. The angles are both measured with respect to the normal to the ground surface. For theoretical reasons it is helpful to consider also the angle j, which is half the angle between the incident and the reflected beams (which form a plane referred to as the "plane of incidence") and would correspond to the angle of incidence, were true reflection from elemental mirrors on the surface of the sample responsible for the diffuse reflection. ψ is the angle between the normal to the elemental mirrors and the normal to the surface. One obtains galvanometer deflections for various j's by keeping i and ψ constant.[4] A polaroid placed between the sample and the photo-

* The research reported in this paper has been sponsored by the Geophysics Research Division of Air Force Cambridge Research Center under Contract W19-122 ac-9.

[1] H. N. Russell, *Ap. J.*, **43**, 101, 173, 1916.

[2] F. G. Watson, *Proc. Nat. Acad. Sci.*, **24**, 532, 1938.

[3] Schniederhohn and Ramdohr, *Lehrbuch der Eramikroskopie*, 2, 39, 1931.

[4] *J. Opt. Soc. America*, **40**, 1, 55–59, 1950.

cell enables the observer to obtain the depolarization, γ, defined by

$$\gamma = \text{Intensity of component vibrating parallel to the plane of incidence} \div \text{Intensity of component vibrating perpendicular to plane of incidence} . \quad (1)$$

A graph showing how γ varies with j for the range of j permitted by the setup constitutes the polarization data for a given sample.

Albedo measurements were made as follows: The sample was mounted as in Figure 1, except that ϕ was made 90° and i, 0° for convenience (assuming azimuthal symmetry). Deflections were obtained for various j's; and, from the geometry of the setup, the reflected flux per unit area of the surface per unit solid angle in the directions corresponding to the j's could be computed. These values divided by the deflection produced by the collimated incident beam of unit cross-section when allowed to fall on the photocell make up the albedo data. Total albedos were obtained by graphically integrating the reflected flux over a hemisphere and dividing by the incident flux (in terms of galvanometer deflections).

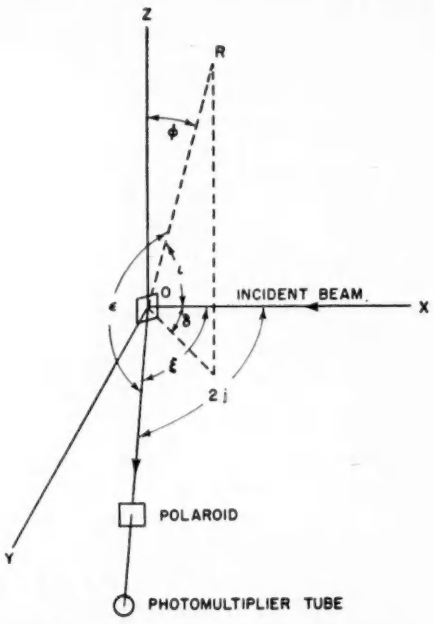

FIG. 1.—Arrangement for studying diffuse reflection from sample surface. *OR* is the normal to the surface; i is the angle of incidence; and ϵ is the angle of diffuse reflection for light striking the photocell.

A 108-watt General Electric lamp (18AT10, C-8 filament) served as a source for both polarization and albedo studies. No filters were used.

OBSERVATIONAL DATA

The polarization studies are summarized in Table 1. The first column identifies the meteoritic samples; the second and third give, respectively, the angle of incidence, i,

TABLE 1

Sample	i	ψ	j	Observed γ
No. 77.113, stony	45°	45°	16°	0.83
			24	.73
			32	.63
			40	.55
			50	.56
			60	.65
Alamogordo, New Mexico	20°	20°	16	.80
			24	.69
			32	.56
			40	.43
			50	.43
			60	.59
No. 373.10, stony	45°	45°	16	.85
			24	.75
			32	.65
			40	.56
			50	.57
			60	.68
Grady, New Mexico	20°	20°	16	.82
			24	.71
			32	.58
			40	.46
			50	.47
			60	.61
No. 414.152, stony	45°	45°	16	.89
			24	.85
			32	.80
			40	.75
			50	.74
			60	.81
Beenham, New Mexico	20°	20°	16	.90
			24	.84
			32	.77
			40	.70
			50	.70
			60	.79
No. 464.151, stony	45°	45°	16	.86
			24	.75
			32	.66
			40	.58
			50	.58
			60	.68
La Lande, New Mexico	20°	20°	16	.82
			24	.71
			32	.47
			40	.45
			50	.46
			60	.59
"O," metallic	45°	45°	16	.91
			24	.83
			32	.74
			40	.66
			50	.67
			60	.76
Odessa, Texas	20°	20°	16	.86
			24	.77
			32	.68
			40	.57
			50	.57
			60	0.70

of the collimated illuminating beam and the angle, ψ, between the normal to the surface and the normal to the small mirrors assumed to deflect the light by regular reflection through the angle $2j$; the fourth gives the angles j; the fifth gives the observed values of γ. Observational difficulties prevented accurate observations at high values of j.

The albedo measurements are presented in Table 2. The first column identifies the

TABLE 2

Sample	ϵ	σ	Total Albedo
No. 373.10, stony	32°	0.10	0.27
	40	.09	
	48	.08	
	56	.06	
	64	.05	
	72	.03	
No. 414.152, stony	32	.20	.62
	40	.18	
	48	.16	
	56	.13	
	64	.10	
	72	.07	
No. 464.151, stony	32	.11	.38
	40	.10	
	48	.08	
	56	.07	
	64	.06	
	72	.04	
"O," metallic	32	.20	0.58
	40	.18	
	48	.14	
	56	.11	
	64	.08	
	72	0.06	

sample; the second gives the values of the angle ϵ, between the normal to the surface and the reflected beam; the third gives σ, the values of the reflected flux per unit solid angle per square centimeter of surface divided by the total incident flux on 1 cm^2 of surface; the fourth gives the total albedo, or the ratio of the total flux reflected to that incident on the surface. In all cases the angle of incidence of the beam illuminating the sample was 0°. Further experiments indicated that the values of Table 2 are little affected by a change in the angle of incidence.

DISCUSSION OF RESULTS

The observed variation of γ with j can be anticipated on the basis of certain assumptions concerning the nature of the meteoritic surfaces. One can write:

$$\gamma = \frac{I_p + i_p + U}{I_s + i_s + U}, \tag{2}$$

where the subscripts refer to the parallel and perpendicular polarization components of the light. The intensities, I, refer to the contributions of the dielectric mirrors (following Fresnel's equations), and the i's refer to the contributions of molecular-like scattering.

The U refers to a possible nonplane-polarized component. Equation (2) can be written in terms of dielectric constants and scattering polarizabilities;[4] one finally gets:

$$\gamma = \frac{k_r p + k_u + k_s \cos^2 2J}{k_r s + k_u + k_s}, \tag{3}$$

where the subscripts of the constants (for a given i and ψ), namely, r, u, and s, refer, respectively, to the contributions of (1) regular reflection from dielectrics, (2) scattering or reflection involving no polarization other than circular polarization, and (3) molecular-like scattering. The terms p and s are the two Fresnel reflection coefficients for parallel and perpendicular polarization, computed on the basis of an assumed average dielectric constant.

When equation (3) is used to explain the observed variation of γ with j for the stony specimens, the surprising fact is found that, for good agreement with theory, the contributions of the r-term must be negligible compared to the u- and s-terms. Nonhomogeneity on a microscopic scale in the crystalline structure of the meteoritic surface probably accounts for this result. In Figure 2, *a*, are shown the observed and predicted curves (with $\psi = i = 45°$) of γ versus j for a typical stony sample. In Figure 2, *b*, are

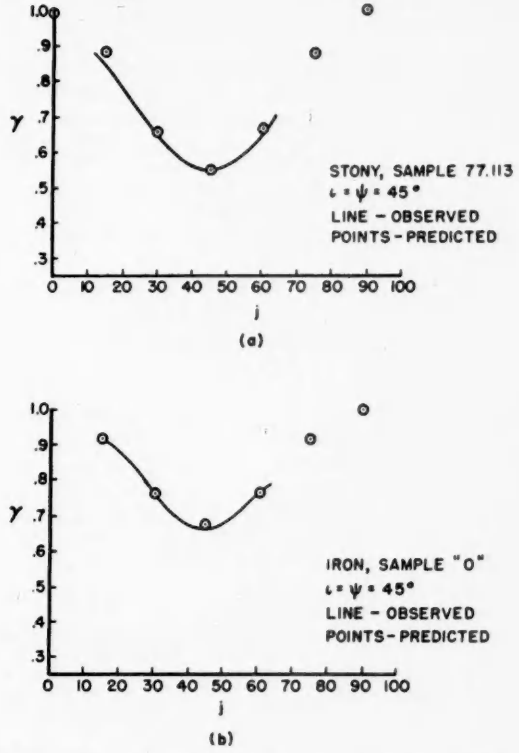

FIG. 2.—Observed curves of depolarization, γ, as a function of j for (*a*) stony sample, (*b*) iron sample. The small circles refer to points predicted from eq. (3).

corresponding curves for the iron sample. Here the best predicted curve required that k_r again be zero, but this result is now to be expected because of the metallic nature of the surface. The irregularities in the structure of the surface probably account for the scattering term.

The albedos obtained for the samples (Table 2) run slightly higher than those for samples studied by Watson,[2] whose values range from 0.1 to 0.5 for both types of meteoritic surfaces. The latter surfaces were prepared by fracture, however, rather than by grinding, so that the presence of shadows caused by rough irregularities could easily account for the difference.

To summarize, the polarization present (Table 1) in light diffusely reflected from four stony and one iron meteoritic surfaces (ground flat with No. 240 carborundum) resembles that for a combination of molecular-like scattering and regular metallic reflection, with regular dielectric reflection contributing but a small part. The total albedos (Table 2) of the surfaces were found to be in line with, although slightly higher than, values obtained by other observers who used freshly fractured surfaces rather than ground surfaces. Reflection factors (Table 2) for different angles of reflection (illuminating beam at normal incidence) were also obtained for the five samples and indicate a gradual dropping-off in reflecting power as the angle of diffuse reflection is increased. The variation approximately follows a cosine law and indicates that the brightness is independent of the angle of view.

The authors are greatly indebted to the Institute of Meteoritics, University of New Mexico, and in particular to Dr. Lincoln LaPaz, for his enthusiastic and kind cooperation in providing the meteoritic specimens used for the study.

THE ORIGIN OF ZODIACAL LIGHT*

W. A. RENSE
Department of Physics, University of Colorado
Received October 4, 1951

ABSTRACT

On the assumption that the zodiacal glow is caused by reflection from stony and metallic particles which make up an interplanetary cloud whose density falls off inversely with distance from the sun, predicted values of polarization and intensity variations along the glow are made. Diffuse-reflection studies of laboratory specimens of meteoritic surfaces were utilized. The results compare favorably with available observations of the glow.

THEORIES OF ZODIACAL LIGHT

The several theories of the origin of the zodiacal light may be divided into two categories: those theories that attribute the origin to a lens-shaped cloud of scattering particles immediately surrounding the earth's "inner" atmosphere[1, 2, 3] and those theories that are concerned with reflection or scattering from interplanetary particles surrounding the sun.[4, 5, 6] Both atmospheric- and planet-dust theories can explain the general aspects of the zodiacal light, but many details are left unaccounted for. In this article, currently available polarization and intensity observations of the zodiacal light as a function of angular distance from the sun are compared with values of these quantities predicted on the basis of the interplanetary-dust theory. For the first time, reflection and polarization data obtained from studies of laboratory specimens of meteoritic surfaces were used in such calculations. The results cover the angles 30°–90° from the sun and are not confined simply to an explanation of the observed maximum polarization in the region of $\theta = 55°$.

OBSERVATIONS OF THE ZODIACAL LIGHT

The light of the zodiacal glow is white in appearance, and its spectrum reveals the Fraunhofer lines, consistent with the belief that it is mostly reflected sunlight. Several observers have detected polarization in the light. Dufay[7] has made careful observations of the polarization of the light from that part of the zodiacal glow extending from about 30° to 90° from the sun. Average values of Dufay's measurements of the polarization of zodiacal light are plotted as squares in Figure 1. These observations have not been corrected for the influence of night-sky light. The ordinate is the depolarization factor, γ, which is the value of the intensity of the light vibrating in the plane determined by the line of sight and the sun, divided by the intensity of the light vibrating perpendicular to this plane. The abscissa is the angular distance, θ, of the observed region of the zodiacal light along the ecliptic from the sun. The aspects of Dufay's observations that

* The research reported in this paper has been sponsored by the Geophysics Research Division of Air Force Cambridge Research Center under Contract W19-122 ac-9.

[1] S. K. Mitra, *The Upper Atmosphere* ("Royal Asiatic Society of Bengal Monograph Series," Vol. 5 [Calcutta, 1947]), p. 460, Schmid's theory.

[2] E. O. Hulburt, *Phys. Rev.*, **35**, 1098, 1930.

[3] L. Vegard, *Ergebn. der exakt. Naturwiss.*, **17**, 229, 1938.

[4] V. G. Fessenkoff, *Ap. J.*, **98**, 129, 1943.

[5] H. C. van de Hulst, *Ap. J.*, **105**, 471, 1947.

[6] F. L. Whipple and J. L. Gossner, *Ap. J.*, **109**, 380, 1949.

[7] *J. d. phys.*, **10**, 219, 1929.

stand out are (1) the shallow minimum between $\theta = 50°$ and $\theta = 60°$; (2) the rapid rise as $\theta \to 90°$ from 60°; and (3) the very slight rise as $\theta \to 30°$ from 50°.

Elvey and Roach[8] have made measurements of the surface brightness of the night sky, including the zodiacal glow. Figure 2 shows a curve, the points of which have been obtained from some of their averaged data, giving the variation of zodiacal light-intensity (in arbitrary units), night-sky light excluded, with angular distance from the sun.

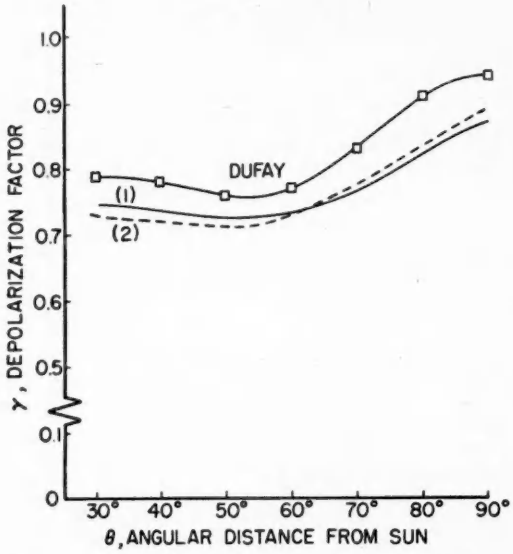

FIG. 1.—Observed and predicted values of polarization in the zodiacal light. θ is the angular distance from the sun along the zodiacal glow, γ is the depolarization factor. Averaged observations (Dufay's) are indicated by squares; curve *1* is predicted curve on basis of diffuse reflection from stony and metallic particles; curve *2* represents observed data corrected for dilution by night-sky light.

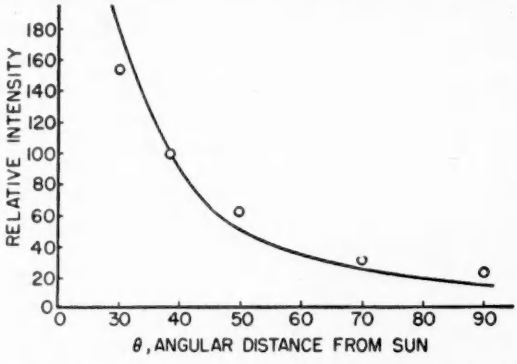

FIG. 2.—Expected variations with angular distances from the sun of zodiacal light-intensity (arbitrary units), as seen above the earth's atmosphere. The curve is drawn from observations by Elvey and Roach, after allowing for atmospheric extinction. The circles refer to predicted values of relative brightness on the basis of reflection from interplanetary particles.

[8] *Ap. J.*, **85**, 213, 1937.

The original data have been corrected by the present writer for atmospheric extinction. Values listed by van de Hulst[9] for the optical thickness of the earth's atmosphere were utilized. The exact position of the sun below the horizon was not given for the times of the zodiacal light-intensity measurements, so that for this and other reasons the extinction correction is to be regarded as a rough approximation, especially for the lower θ's. One may regard the curve of Figure 2, therefore, as giving an indication of the brightness of the zodiacal glow as viewed above the earth's atmosphere.

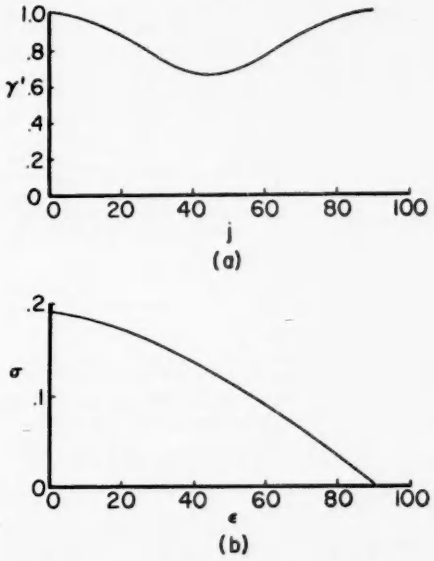

FIG. 3.—Reflection-curves for an "average" meteoritic surface (roughly polished) taken from laboratory measurements of meteoritic specimens, both stony and metallic. Curve *a* shows how the depolarization γ' varies with the angle of regular reflection, *j*. Curve *b*, which shows the variation of reflectance with angle of view ϵ, closely follows a cosine law, indicating that brightness is constant with ϵ. Neither curve is sensitive to the angle of incidence of the illuminating beam or to the degree of polish of the surface.

PREDICTED POLARIZATION AND INTENSITY OF ZODIACAL GLOW

If one adheres to the idea that the zodiacal glow is caused mainly by reflection from interplanetary particles, one might make the following two assumptions: (1) the density of the lenticular cloud falls off from the sun inversely as the distance; (2) the glow consists mostly of light diffusely reflected from meteoritic particles. In regard to the first assumption, there is some evidence that a cloud might exist for which the simple density-inverse-with-distance law holds.[4] In regard to the second assumption, because of the known evidence for significant meteoric densities around the earth's orbit, it is not unlikely that the particles consist in part of small fragments of stony and metallic materials of sizes large enough to produce diffuse or regular reflection.

Calculations can be made which predict, on the basis of the above two broad assumptions, what the depolarization factor should be for the zodiacal light as viewed from the earth at any angle of elongation from the sun. The data from observations[10] on meteoritic surfaces which were utilized in making the computations are shown in Figure 3. The

[9] G. P. Kuiper (ed.), *The Atmospheres of the Earth and Planets* (Chicago: University of Chicago Press, 1949), pp. 51, 55.

[10] K. Kloverstrom and W. A. Rense, *Ap. J.*, **115**, 495, 1952.

upper curve (*a*) is the assumed variation of depolarization, γ', with angle j (half the angle between the incident and the diffusely reflected rays). This curve is found by averaging the results for five meteoritic surfaces, including stony and metallic types (both types reflect similarly). Extension over the entire range of j was found by assuming a variation of the form:[10]

$$\gamma' = \frac{\kappa + \cos^2 2j}{\kappa + 1}.$$

The lower curve (*b*) shows the variation of reflectance, σ, of a meteoritic surface, with angle ϵ from the normal to the surface. The curve approximately follows a cosine law, indicating that the brightness is nearly constant with ϵ.

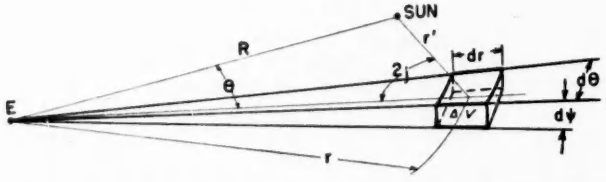

FIG. 4.—Geometry of light-reflection from particles in elementary volume of interplanetary dust cloud.

The value of γ for a given θ was determined as follows: Considering an element of volume in space, as shown in Figure 4, one can set up the following relationship for the total intensity of the volume element as viewed from the earth:

$$\Delta I \propto \frac{P(j, \epsilon)\, r^2 d\psi\, d\theta\, dr}{r^2 r'^2 r'}. \tag{1}$$

In the numerator, $P(j, \epsilon)$ is a function accounting for light lost because of the phase of the particles and for the dependence of reflectance on average angle of view for the particle surfaces; the remainder is the volume of the element. In the denominator, r^2 accounts for the fall in intensity of the reflected light because of the distance of the earth from the elementary volume; r'^2 for the drop in intensity of the incident light because of the distance of the elementary volume from the sun. The r' accounts for the variation in density of the cloud with distance from the sun.

If it is assumed that the brightness is independent of the angle of view (Fig. 3, *b*) and that the phase function is the same as for a spherical planet, namely, $(1 + \cos 2j)/2$, one obtains

$$\Delta I_s \propto \frac{(1 + \cos 2j)\, dr}{r'^3 (\gamma' + 1)}, \tag{2}$$

$$\Delta I_p = \gamma' \Delta I_s,$$

where γ' can be found from curve *a* in Figure 3 and where ΔI_p and ΔI_s are the intensities of the parallel and perpendicular components, respectively. Assuming that the cloud is thick enough to accommodate the volume elements at distances for which the intensity contribution becomes negligible, one can integrate from the earth along $\theta =$ Constant, through the cloud, to obtain I_p and I_s; then

$$\gamma(\theta) = \frac{I_p}{I_s}. \tag{3}$$

The integration was performed graphically for various values of θ. The results for γ are shown by the curve marked *1* in Figure 1.

The variation of surface brightness of the zodiacal light with angular distance from the sun may also be found. By adding the intensity numbers for the two components for a given θ as determined above, one can plot predicted relative intensities, such as those indicated by circles in Figure 2. The curve in the figure is from the observations of Elvey and Roach.[8] The scale was chosen so that the computed point at $\theta = 40°$ was made to fall on the observed curve; no effort was made to estimate absolute intensities.

CONCLUSIONS

The predicted variation of γ with θ (Fig. 1) parallels the observed points (Dufay) rather closely. The maximum polarization occurs at about 55° for both curves. A still better check can be effected by correcting Dufay's observation for dilution by the little-polarized night-sky light.[11] The average intensity of the latter in terms of the zodiacal light-intensity for various altitudes was obtained from the data of Elvey and Roach.[8] Assuming, for our purposes, negligible polarization of the sky light, the corrections for the values of γ can be found. The corrected γ versus θ relationship is shown by curve *2* of Figure 1. The agreement with the predicted curve is now quite good along the whole range of θ. The predicted curve to some extent depends on the validity of the assumption that the curves of Figure 3 are applicable to the meteoritic surfaces of the reflecting cloud. These curves were determined in their detail by averaging the results of four stony and one metallic meteoritic surfaces. However, the variation of γ with j was very similar for all surfaces, both stony and metallic, differing only in the range of γ between $j = 0°$ and $j = 90°$. For this reason and in view of the lack of information concerning the relative amounts in space of stony and metallic meteorites and of the relative amounts of the various types of stony meteorites, a simple average is justified for a first approximation. The second curve of Figure 3, which was typical for all surfaces, was utilized only in so far as it indicated no appreciable variation in brightness with angle of view—a result well known to hold for many diffusely reflecting surfaces.

No correction for atmospheric effects need be allowed for in examining Figure 2, because both the curve and the predicted points correspond to the expected intensity as viewed just outside the earth's atmosphere. Agreement between the observed and the predicted points for the relative intensity of the zodiacal light as a function of θ is quite good, especially in view of the fact that the assumption regarding the variation of density of the reflecting cloud with distance from the sun was made on independent grounds.

The writer wishes to express his gratitude to Mr. James Jackson, of the University of Colorado, for his kind aid and co-operation concerning many details of the preparation of this paper.

[11] E. O. Hulburt, *J. Opt. Soc. America*, **39**, 211, 1949.

MULTIPLET INTENSITIES FOR THE LINES $^4S-^2D$ OF *S* II, *O* II, AND *N* I*

R. H. GARSTANG
Yerkes Observatory
Received October 30, 1951

ABSTRACT

The transition probabilities and intensity ratio of the doublet $^4S-^2D$ of *S* II are computed, including the effect of spin-spin interaction. Revised transition probabilities and intensity ratios are also given for the $^4S-^2D$ doublets of *N* I and *O* II.

The effect of the spin-other-orbit and spin-spin interactions on the transition probabilities of the forbidden lines within the configuration $2p^3$ ($^4S-^2D$ only) has been studied for *N* I[1] and *O* II.[2] The effect has also been studied within the $2p^2$ and $2p^4$ configurations for a number of ions.[3] Examination of the results for the $2p^2$, $2p^3$, and $2p^4$ configurations indicates that spin-other-orbit and spin-spin interactions would have a negligible effect in the $3p^2$ and $3p^4$ configurations, but further study is required before anything can be said about the $3p^3$ configuration (spin-spin interactions might be important here, owing to the vanishing of the conventional spin-orbit interaction in the half-closed shell). We shall investigate the $3p^3$ configuration in *S* II.

We use without modification the formulae of AUV.[2] Estimates of the integrals s_q, ζ, and η are required. Self-consistent field wave functions, without exchange, have been computed for *S* II by A. S. Douglas,[4] using the electronic computer ("EDSAC") at the Cambridge University Mathematical Laboratory. Using these wave functions, we obtain, by numerical integration,

$$s_q = 2.10\, e a_H^2 , \qquad \zeta = 459 \text{ cm}^{-1} , \qquad \eta = 0.23 \text{ cm}^{-1} .$$

The values of s_q and η given here will be adopted. The value of ζ requires further investigation. Using AUV formulae (16), we try to fit the observed energy levels[5] by the method of least squares. Taking (i) $\eta = 0$ and (ii) $\eta = 0.23$ cm^{-1}, we obtain in case (i) $\zeta = 521$ cm^{-1}, the sum of the squares of residuals being 9.5 cm^{-2}, and in case (ii) $\zeta = 538$ cm^{-1}, with sum of squares of residuals 2.2 cm^{-2}. The inclusion of η ($\neq 0$) appreciably improves the representation of the observations (even though η has not been treated as an unknown parameter), and we shall adopt $\zeta = 538$ cm^{-1} and $\eta = 0.23$ cm^{-1} in our further work. It is a happy coincidence that our value of ζ agrees with that suggested by Robinson and Shortley.[6] The value $\zeta = 459$ cm^{-1} from the wave functions gives an appreciably worse fit of the observations. The remaining parameters [case (ii)] are $E(^4S) = 11.8$ cm^{-1}, $E(^2D) = 14{,}885.9$ cm^{-1}, and $E(^2P) = 24{,}523.6$ cm^{-1}.

* These calculations were begun during the author's tenure of an Isaac Newton Studentship at the University of Cambridge, England.

[1] C. W. Ufford and R. M. Gilmour, *Ap. J.*, **111**, 580, 1950.

[2] L. H. Aller, C. W. Ufford, and J. H. Van Vleck, *Ap. J.*, **109**, 42, 1949. Hereafter abbreviated "AUV."

[3] R. H. Garstang, *M.N.*, **111**, 115, 1951. Some similar calculations have been reported by A. M. Naqvi, *A.J.*, **56**, 45, 1951.

[4] Unpublished.

[5] Charlotte E. Moore, *Circ. Nat. Bur. Stand.*, No. 467, 1949.

[6] *Phys. Rev.*, **52**, 713, 1937.

The doublet splittings may now be calculated. We find

$$\Delta^2\mathrm{D} = 33.2\ \mathrm{cm}^{-1}\,, \qquad \Delta^2\mathrm{P} = 47.6\ \mathrm{cm}^{-1}\,,$$

whereas the experimental values are

$$\Delta^2\mathrm{D} = 31.5\ \mathrm{cm}^{-1}\,, \qquad \Delta^2\mathrm{P} = 48.6\ \mathrm{cm}^{-1}\,.$$

The agreement is excellent, considering the uncertainties in ζ and η and the neglect of ζ^3 in the formulae given by AUV. Formulae (18), (19), and (20) of AUV may now be used to obtain the line strengths and thence the transition probabilities for the doublet $^4\mathrm{S}-^2\mathrm{D}$. Expressing the transition probabilities in the form

$$A = a\, s_q^2 \zeta^2 + \beta\zeta^4 + \gamma\zeta^2\eta + \delta\eta^2\,,$$

we find in our case

$$A\,(^2\mathrm{D}_{5/2} \rightarrow {}^4\mathrm{S}_{3/2}) = (5.99+0.29+0.03+0.00) \times 10^{-4}\ \mathrm{sec}^{-1} = \ 6.31 \times 10^{-4}\ \mathrm{sec}^{-1}\,;$$

$$A\,(^2\mathrm{D}_{3/2} \rightarrow {}^4\mathrm{S}_{3/2}) = (3.81+12.90+0.64+0.01) \times 10^{-4}\ \mathrm{sec}^{-1} = 17.36 \times 10^{-4}\ \mathrm{sec}^{-1}\,.$$

The intensity ratio, assuming a Boltzmann distribution in the ^{2}D levels, is

$$r = \frac{I\,(^2\mathrm{D}_{5/2} \rightarrow {}^4\mathrm{S}_{3/2})}{I\,(^2\mathrm{D}_{3/2} \rightarrow {}^4\mathrm{S}_{3/2})} = 0.55\,.$$

If η is omitted, we find $r = 0.56$. From this it is seen that the value of r does not depend appreciably on η. This is in contrast to O II and N I, where the inclusion of η is the critical step in the calculations. We may safely conclude that spin-other-orbit and spin-spin interactions may be omitted in calculations of line strengths in shells of equivalent p-electrons if the principal quantum number is not less than 3. It is just worth retaining η when fitting the theory to the observed energy levels in atoms with $3p^3$ shells.

It should be noted, however, that the ratio of the intensities of the lines is fairly sensitive to the value of s_q adopted. If we use the value of s_q adopted by Pasternack,[7] we obtain $r = 0.79$, while his transition probabilities give $r = 0.86$. Thus the major part of the difference $(0.86 - 0.55)$ between Pasternack's and our results is explained by the choice of the new s_q. If wave functions calculated with the inclusion of exchange were available, we would obtain a still smaller value of s_q and a still smaller ratio r.

Observations of the intensity of the S II lines have been made for several planetary nebulae.[8] Dr. L. H. Aller gives a mean value of $r = 0.74$ from unpublished measures of NGC 7662 made by him in collaboration with Dr. R. Minkowski at Mount Wilson, and the measures of Swings and Jose indicate a similar value. Since observational uncertainties are appreciable and we do not know the target areas for collisional excitation, a satisfactory comparison between theory and observation is impossible.

The previous calculations on N I[9] and O II[10] used values of s_q obtained from self-consistent field wave functions calculated without exchange. It is of interest to use wave functions calculated with exchange for N I[9] and O II[10] to obtain improved values of s_q. We might use the formula

$$s_q = \frac{2}{5}\int_0^\infty r^2\mathrm{P}^2\,(2\mathrm{p})\,d\,r\,, \tag{1}$$

[7] *Ap. J.*, **92**, 129, 1940.

[8] L. H. Aller and R. Minkowski, *Pub. A.S.P.*, **58**, 258, 1946; P. Swings and P. D. Jose, *Pub. A.S.P.*, **61**, 181, 1949; L. H. Aller and R. Minkowski, unpublished.

[9] D. R. Hartree and W. Hartree, *Proc. R. Soc. London, A*, **193**, 299, 1948.

[10] D. R. Hartree, W. Hartree, and B. Swirles, *Phil. Trans. R. Soc. London, A*, **238**, 229, 1939.

where P(2p) is the radial wave function for the ground state of the ion. I am indebted to Dr. C. W. Ufford[11] for pointing out that we should use the formula

$$s_q = \frac{2}{5}\int_0^\infty r^2 \mathrm{P}(2\mathrm{p}, {}^4\mathrm{S})\,\mathrm{P}(2\mathrm{p}, {}^2\mathrm{D})\,dr, \tag{2}$$

where P(2p,^{4}S) and P(2p,^{2}D) are the radial wave functions for the ^{4}S and ^{2}D states, respectively, of the 2p^3 ion. Using the same values of ζ and η, we obtain the results in Table 1. Comparing these results with those obtained by other authors,[1,2] we see that the

TABLE 1

	N I		*O* II	
	Formula (1)	Formula (2)	Formula (1)	Formula (2)
s_q	1.027	1.055	0.584	0.596
r (our results)	0.62	0.64	0.45	0.47
r (previous results)	0.83	.....	0.58	.....
$A(^2D_{5/2}\rightarrow{}^4S_{3/2})$ sec^{-1}	6.65×10^{-6}	6.95×10^{-6}	3.94×10^{-5}	4.08×10^{-5}
$A(^2D_{3/2}\rightarrow{}^4S_{3/2})$ sec^{-1},	16.06×10^{-6}	16.25×10^{-6}	13.06×10^{-5}	13.15×10^{-5}

inclusion of exchange has an appreciable effect on the transition probabilities and intensity ratio (r) but that the change from formula (1) to formula (2) is not of much importance.

The value of r(0.47) obtained for *O* II is quite close to the observational value of AUV[2] ($r = 0.49$), but, owing to the uncertainties in the calculations (especially in the choice of ζ and η and the assumption of a Boltzmann distribution in the ^{2}D levels), this agreement may be fortuitous.

It will be interesting to repeat these calculations for *S* II, using exchange wave functions when these become available.

It is a pleasure to thank Professor D. R. Hartree and Dr. B. Jeffreys for their advice and encouragement during this work. I am especially grateful to Mr. A. S. Douglas for his kindness in supplying me with his unpublished wave functions. I am also indebted to Dr. L. H. Aller for informing me of his unpublished intensity measures and to him and Dr. R. Minkowski for permission to quote them here.

[11] Private conversation.

FORMATION OF ABSORPTION LINES BY NONCOHERENT SCATTERING

MALCOLM P. SAVEDOFF*
Princeton University Observatory
Received January 5, 1952

ABSTRACT

The problem of noncoherent scattering, with and without selective absorption, has been solved by iterating the exact integral equation for $J - B$, for the case where ϵ and η_ν are independent of depth. The first iteration introduces a correction which is of the order of 15 per cent of the zero-order solution for $\epsilon = 0$ and $\tau > 0.01$ and is less than 4 per cent for $\epsilon = 0.01$ and $\tau > 0.001$. The differences from pure absorption are therefore secure. Line contours, even for $\epsilon = 0$, lie very close to the pure absorption solution except for the line center and for small μ. Exact values of $J - B$ are given for $\epsilon = 1$. Deviations from pure absorption are shown to be proportional to $\epsilon\eta_0^{1/2} + (1 - \epsilon)(\eta_0/1 + \eta_0)^{1/2}$, which measures the coupling with the thermal emission. Tables are given from which the zero-order solutions for any ϵ, η_0, and β can be obtained.

In stellar atmospheres, there are many processes which act within a spectral line to couple together radiation of different frequencies. The center-limb variations of spectral lines on the sun led J. Houtgast[1] to investigate noncoherent scattering as the dominant process of line formation. H. Zanstra[2] found that the observed low polarization of spectral lines near the limb of the sun would result if the scattering were 90 per cent noncoherent. He showed that a classical oscillator damped by collisions and radiation acts partly as a noncoherent scatterer.

L. Spitzer[3] gave a quantal description for the extremes of statistical and collisional broadening. For both processes he predicts that the noncoherent emission completely redistributes the absorbed energy, the emission being proportional to the line-absorption coefficient. It is noncoherence from these processes which is probably dominant in the sun. In the absence of material perturbers, noncoherence results from the complex interlocking of lines broadened by natural width or radiation perturbations. This case has been discussed by L. Spitzer[4] and R. van der R. Woolley.[5]

L. Henyey[6] has shown that the Maxwellian velocity distribution of the atoms and ions leads to noncoherence, because of the angular dependence of the Doppler shifts.

Observational evidence for the importance of noncoherent scattering was obtained by J. Houtgast.[1] Both Houtgast and G. Münch[7] discuss the results of noncoherent scattering by substituting the coherent solution in computing the emission terms in the transfer equation. Since, for frequencies and depths important in the discussion of the line wings, the coherently computed emission is identical to that in thermodynamic equilibrium, these methods do not permit estimates of the deviations from pure absorption. D. Labs[8] and Z. Suemoto[9] use a step profile for the line-absorption coefficient; however, it is diffi-

* National Research Council Fellow, 1951–1952, at the Mount Wilson Observatory.

[1] *The Variations in the Profiles of Strong Fraunhofer Lines along a Radius of the Solar Disc* (Diss.; Utrecht, 1942).

[2] *M.N.*, **101**, 273, 1941.

[3] *Ap. J.*, **99**, 1, 1944.

[4] *M.N.*, **96**, 794, 1936.

[5] *M.N.*, **98**, 624, 1938.

[6] *Proc. Nat. Acad. Sci.*, **26**, 50, 1940.

[7] *Ap. J.*, **109**, 275, 1949.

[8] *Zs. f. Ap.*, **28**, 150, 1951.

[9] *Pub. Astr. Soc. Japan*, **1**, 78, 1949.

cult to relate the constants of the step profile to actual physical conditions. Sobolev's[10] procedure (based on the invariance principle) seems to be too cumbersome in its present form to permit an understanding of all the properties of a noncoherently scattering atmosphere. A more complete description of these papers will be given later.

Accordingly, a new solution of the transfer equation for noncoherent scattering was undertaken. Tables are given from which an estimate of the deviations from pure absorption can be computed for any values of the parameters. Here, complete redistribution of the absorbed light is assumed. The emission terms contain some dependence on the local kinetic temperature represented by $\epsilon \neq 0$. A linear form for the Planck function $B(\tau)$ is also assumed. The run of $\bar{J}(\tau)$ and line profiles are computed. In these computations, however, ϵ and η_ν were assumed independent of τ, and a dispersion profile for η_ν was used.

EQUATION OF TRANSFER

The equation of transfer relates the change in the intensity of the light to the difference between the energy absorbed and that emitted in a given volume. The energy absorbed, in the case of an atmosphere containing both continuous absorption and line absorption, can be written $(1 + \eta_\nu)I_\nu$, where I_ν is the light-intensity and η_ν is the ratio of the line to the continuous absorption coefficient. Part of the emitted energy may be written as $(1 + \epsilon\eta_\nu)B$, where $B(\tau)$ is the Planck function for the local temperature. This term gives formal recognition to the fact that the occupancy of the excited state depends partly on the local kinetic temperature, ϵ being the ratio of the number of excited atoms resulting from either cascade from above or collisional excitations to the number present in thermodynamic equilibrium. Under usual conditions in stellar atmospheres, collisional excitation and de-excitation are less efficient than coupling with the high excited states and the continuum.

When either statistical or collisional broadening is dominant, the scattering becomes completely noncoherent. In the case of statistical broadening, the energy of a particular atomic state is considered to be time-dependent and may be computed from the sum of the effects of the perturbing atoms and ions. The line-absorption coefficient is computed from the probability of the perturbation. In this case, since the changes in the perturbation are significant within the mean life of the atomic state, one may say that there is no relation between the environment at the time of the absorption of energy and at the time of the subsequent re-emission. Thus both the absorption and the emission are proportional to η_ν. For collisional broadening, the coupling between the electronic structure and the kinetic energy of the colliding particles permits redistribution of the energy within the line. For both these cases the emission may be written $\eta_\nu\bar{J}$, where $\bar{J}$ is the integral of $\eta^{-1}\eta_\nu J_\nu$ over frequency. Since J_ν is the radiation density and η is the integral of η_ν over frequency, $\bar{J}$ is a weighted mean radiation density.

The equation of transfer becomes

$$-\frac{\mu}{\kappa\rho}\frac{dI_\nu}{dX} = (1+\eta_\nu)\,I_\nu - (1+\epsilon\eta_\nu)B - (1-\epsilon)\,\eta_\nu\bar{J}\,, \tag{1}$$

where μ is the cosine of the angle between the direction of the light-ray and the normal to the atmosphere, κ is the continuous absorption coefficient per unit density, and ρ is the density.

INTEGRAL EQUATION FOR $\bar{J} - B$

In the case of the resonance lines of *Ca* II (H and K lines), the observed damping constant far exceeds the natural width. Since calcium is predominantly singly ionized on the sun, the relative abundance of *Ca* II ions is independent of electron pressure. Further-

[10] *A.J.U.S.S.R.*, **26**, 129, 1949.

more, in the solar atmosphere, the H^- ion is the major source of the continuous absorption, which is therefore proportional to the electron pressure. Nevertheless, since in the wings of strong absorption lines the absorption coefficient is proportional to the damping constant, which is proportional to the electron pressure, the ratio of these coefficients is independent of depth.

The differential equation (1) is equivalent to the inhomogeneous integral equation

$$J_\nu(\tau) = \frac{1}{2}\int_0^\infty [(1+\epsilon\eta_\nu)B(\tau') + (1-\epsilon)\eta_\nu \bar{J}(\tau')]E_1[|\tau-\tau'|(1+\eta_\nu)]\,d\tau', \quad (2)$$

which can be obtained in a manner similar to that used in deriving the Schwarzschild-Milne integral equation.[11] Here E_1 is the exponential integral,

$$E_1(\omega) = \int_1^\infty e^{-z\omega}\frac{dz}{z}. \quad (3)$$

In writing equation (2), η_ν and ϵ have been assumed to be independent of τ. Multiplying through by $\eta^{-1}\eta_\nu$ and integrating over all frequencies, we obtain the following inhomogeneous linear integral equation for $\bar{J}$:

$$\bar{J} = \tfrac{1}{2}\eta^{-1}\int_{-\infty}^{+\infty} d\nu \int_0^\infty [(\eta_\nu + \epsilon\eta_\nu^2)B(\tau') + (1-\epsilon)\eta_\nu^2\bar{J}(\tau')]E_1[|\tau-\tau'|(1+\eta_\nu)]\,d\tau'. \quad (4)$$

Substituting $G = \bar{J} - B$ and inverting the order of integration, we may write equation (4) as

$$G(\tau) = -B(\tau) + \int_0^\infty B(\tau')K_1(|\tau-\tau'|)\,d\tau' + (1-\epsilon)\int_0^\infty G(\tau')K_0(|\tau-\tau'|)\,d\tau', \quad (5)$$

where

$$K_0(u) = \tfrac{1}{2}\eta^{-1}\int_1^\infty \frac{dz}{z}\int_{-\infty}^{+\infty}\eta_\nu^2 e^{-(1+\eta_\nu)zu}d\nu \quad (6)$$

and

$$K_1(u) = \tfrac{1}{2}\eta^{-1}\int_1^\infty \frac{dz}{z}\int_{-\infty}^{+\infty}(\eta_\nu+\eta_\nu^2)\,e^{-(1+\eta_\nu)zu}d\nu. \quad (7)$$

The K functions defined above will be recognized as related to the exponential integral.

In solutions of problems of this type, $B(\tau)$ is usually chosen as a linear function of the depth. Although equation (5) could be solved for any given $B(\tau)$, it does not seem wise to use more accurate forms for $B(\tau)$ because of the increased computational labor in obtaining a solution and the uncertainties of the correct form to choose. In addition, a dispersion profile will be used for η_ν, the justification for which will be given below. When $B(\tau) = B_0(1+\beta\tau)$ is introduced into equation (5), the inhomogeneous part may be written $B_0({}_I\boldsymbol{B} + \beta_L\boldsymbol{B})$, where

$${}_I\boldsymbol{B}(\tau) = -1 + 2\int_0^\infty K_1(u)\,du - \int_\tau^\infty K_1(u)\,du \quad (8)$$

and

$${}_L\boldsymbol{B}(\tau) = \tau\,{}_I\boldsymbol{B}(\tau) + \int_\tau^\infty K_1(u)\,u\,du. \quad (9)$$

Since equation (5) is a linear inhomogeneous integral equation, we may solve separately for the isothermal (using ${}_I\boldsymbol{B}$) and for the linear atmosphere (using ${}_L\boldsymbol{B}$). For, if G is the

[11] S. Chandrasekhar, *Radiative Transfer* (Oxford: Clarendon Press, 1950), chap. xiii, eq. (16).

solution of an equation of this form with arbitrary inhomogeneous part $\boldsymbol{B}$, and G' is the solution corresponding to $\boldsymbol{B}'$, then $G + G'$ is the solution of the equation with inhomogeneous part $\boldsymbol{B} + \boldsymbol{B}'$.

Some understanding of the η_ν dependence of the K functions may be gained through examination of their Laplace transforms. By reversing the order of integration once more, we obtain, for the Laplace transforms,

$$\int_0^\infty e^{-\lambda u} K_0(u)\, du = \frac{1}{2\eta\lambda}\int_{-\infty}^{+\infty} \eta_\nu^2 \log\left(1 + \frac{\lambda}{1+\eta_\nu}\right) d\nu; \tag{10}$$

$$\int_0^\infty e^{-\lambda u} K_1(u)\, du = \frac{1}{2\eta\lambda}\int_{-\infty}^{+\infty} (\eta_\nu + \eta_\nu^2) \log\left(1 + \frac{\lambda}{1+\eta_\nu}\right) d\nu. \tag{11}$$

For small λ, the Laplace transform can be expanded in a Taylor series in λ whose coefficients are the moments of the original function. For the functions K_0 and K_1, we find

$$\int_0^\infty K_0(u)\, du = \frac{1}{2}\left(1 - \eta^{-1}\int_{-\infty}^{+\infty} \frac{\eta_\nu}{1+\eta_\nu}\, d\nu\right); \tag{12}$$

$$\int_0^\infty K_1(u)\, du = \tfrac{1}{2}. \tag{13}$$

Thus the zero moment of K_1 is independent of the shape of η_ν, while the zero moment of K_0 depends only on the shape of η_ν in the frequency range where η_ν is of the order unity. Similarly,

$$\int_0^\infty K_0(u)\, u\, du = \tfrac{1}{4}\eta^{-1}\int_{-\infty}^{+\infty} \frac{\eta_\nu^2}{(1+\eta_\nu)^2}\, d\nu, \tag{14}$$

while

$$\int_0^\infty K_1(u)\, u\, du = \tfrac{1}{4}\eta^{-1}\int_{-\infty}^{+\infty} \frac{\eta_\nu}{1+\eta_\nu}\, d\nu. \tag{15}$$

Since the moments of the K functions are independent of the shape of the peak, one may infer that $K(u)$ for large u is nearly independent of the shape of the peak of η_ν.

In this paper the dispersion profile has been used in calculating the functions K_0 and K_1. Although solutions based on the Voigt profile may some day be available, it seems that any difference which will occur will affect only the cores of strong lines and the behavior of lines near the extreme limb of the sun, both of which depend on the values of $K_1(u)$ and $K_0(u)$ near $u = 0$.

Introducing the dispersion profile,

$$\eta_\nu = \frac{\eta_0}{1 + (\Delta\nu^2/\gamma^2)}, \tag{16}$$

we carry out the integration over ν in equations (6) and (7), using the transformation $\tan\phi/2 = \Delta\nu/\gamma$ and noting the properties of the Bessel functions,

$$I_0(x) = J_0(ix) = \frac{1}{\pi}\int_0^\pi e^{-x\cos\phi} d\phi, \tag{17}$$

$$I_1(x) = -iJ_1(ix) = -\frac{1}{\pi}\int_0^\pi e^{-x\cos\phi}\cos\phi\, d\phi, \tag{18}$$

$$\frac{dI_0(x)}{dx} = I_1(x). \tag{19}$$

Thus we can obtain

$$K_0(u) = \tfrac{1}{4}\eta_0 \int_u^\infty \exp\left(-u - \tfrac{1}{2}u\eta_0\right)\left[I_0\left(\tfrac{1}{2}u\eta_0\right) - I_1\left(\tfrac{1}{2}u\eta_0\right)\right]\frac{du}{u}, \tag{20}$$

and

$$K_1(u) = \frac{1}{2}\int_u^\infty \exp\left(-u - \tfrac{1}{2}u\eta_0\right)\left[\left(1 + \tfrac{1}{2}\eta_0\right) I_0\left(\tfrac{1}{2}u\eta_0\right) - \tfrac{1}{2}\eta_0 I_1\left(\tfrac{1}{2}u\eta_0\right)\right]\frac{du}{u}. \tag{21}$$

The asymptotic expansion

$$I_0\left(\tfrac{1}{2}u\eta_0\right) = \frac{\exp\left(\tfrac{1}{2}u\eta_0\right)}{(\pi u\eta_0)^{1/2}}\left\{1 + \sum_{m=1}^{\infty}\frac{(u\eta_0)^{-m}}{2^{+4m-2}m!}\left[\frac{(2m-1)!}{(m-1)!}\right]^2\right\} \tag{22}$$

is valid for $u\eta_0 \gg 1$.

The following are the asymptotic forms for K_0, K_1, and certain related integrals used in this paper, which were obtained by substituting equation (22) (see also eq. [19]) in equations (20) and (21) and by performing the indicated integrations.

$$\begin{aligned} K_0(u) = \frac{1}{4}\left(\frac{1}{\pi\eta_0}\right)^{1/2}\Bigg\{\Bigg(\int_{\sqrt{u}}^\infty e^{-x^2}dx - \tfrac{1}{2}e^{-u}u^{-1/2} + \tfrac{1}{4}e^{-u}u^{-3/2}\Bigg)\left(\tfrac{8}{3} - \tfrac{4}{5}\eta_0^{-1} + \tfrac{3}{7}\eta_0^{-2}\right. \\ \left. - \tfrac{5}{18}\eta_0^{-3} + \ldots\right) + e^{-u}u^{-5/2}\left(\tfrac{3}{10}\eta_0^{-1} - \tfrac{9}{56}\eta_0^{-2} + \tfrac{5}{48}\eta_0^{-3} - \ldots\right) + e^{-u}u^{-7/2}\left(\tfrac{45}{112}\eta_0^{-2}\right. \\ \left. - \tfrac{25}{96}\eta_0^{-3} + \ldots\right) + e^{-u}u^{-9/2}\left(\tfrac{175}{192}\eta_0^{-3} - \ldots\right) + \ldots\Bigg\}; \end{aligned} \tag{23}$$

$$\begin{aligned} \int_u^\infty K_0(u)\,du = \frac{1}{4}\left(\frac{1}{\pi\eta_0}\right)^{1/2}\Bigg\{\int_{\sqrt{u}}^\infty (x^2 - u)\,e^{-x^2}dx\left(\tfrac{8}{3} - \tfrac{4}{5}\eta_0^{-1} + \tfrac{3}{7}\eta_0^{-2} - \tfrac{5}{18}\eta_0^{-3} + \ldots\right) \\ + \int_{\sqrt{u}}^\infty e^{-x^2}dx\left(-\tfrac{16}{3} + \tfrac{12}{5}\eta_0^{-1} - \tfrac{12}{7}\eta_0^{-2} + \tfrac{25}{18}\eta_0^{-3} - \ldots\right) + e^{-u}u^{-1/2}\left(\tfrac{4}{3} - \tfrac{4}{5}\eta_0^{-1}\right. \\ \left. + \tfrac{9}{14}\eta_0^{-2} - \tfrac{5}{9}\eta_0^{-3} + \ldots\right) + e^{-u}u^{-3/2}\left(\tfrac{1}{5}\eta_0^{-1} - \tfrac{3}{14}\eta_0^{-2} + \tfrac{5}{24}\eta_0^{-3} - \ldots\right) \\ + e^{-u}u^{-5/2}\left(\tfrac{9}{56}\eta_0^{-2} - \tfrac{5}{24}\eta_0^{-3} + \ldots\right) + e^{-u}u^{-7/2}\left(\tfrac{25}{96}\eta_0^{-3} - \ldots\right) + \ldots\Bigg\}; \end{aligned} \tag{24}$$

$$\begin{aligned} \int_u^\infty K_0(u)\,u\,du = \frac{1}{4}\left(\frac{1}{\pi\eta_0}\right)^{1/2}\Bigg\{\int_{\sqrt{u}}^\infty \left(\tfrac{1}{2}x^4 - \tfrac{1}{2}u^2 - x^2\right) e^{-x^2}dx\left(\tfrac{8}{3} - \tfrac{4}{5}\eta_0^{-1}\right. \\ \left. + \tfrac{3}{7}\eta_0^{-2} - \tfrac{5}{18}\eta_0^{-3} + \ldots\right) + \int_{\sqrt{u}}^\infty e^{-x^2}dx\left(\tfrac{4}{3} - \tfrac{8}{5}\eta_0^{-1} + \tfrac{27}{14}\eta_0^{-2} - \tfrac{20}{9}\eta_0^{-3} + \ldots\right) \\ + e^{-u}u^{-1/2}\left(\tfrac{3}{5}\eta_0^{-1} - \tfrac{6}{7}\eta_0^{-2} + \tfrac{25}{24}\eta_0^{-3} - \ldots\right) + e^{-u}u^{-3/2}\left(\tfrac{15}{56}\eta_0^{-2} - \tfrac{5}{12}\eta_0^{-3} + \ldots\right) \\ + e^{-u}u^{-5/2}\left(\tfrac{35}{96}\eta_0^{-3} - \ldots\right) + \ldots\Bigg\}; \end{aligned} \tag{25}$$

$$K_1(u)=\frac{1}{4}\left(\frac{1}{\pi\eta_0}\right)^{1/2}\left\{\left(\int_{\sqrt{u}}^{\infty}e^{-x^2}dx-\tfrac{1}{2}e^{-u}u^{-1/2}\right)\left(-\tfrac{16}{3}+\tfrac{8}{15}\eta_0^{-1}-\tfrac{6}{35}\eta_0^{-2}+\tfrac{5}{63}\eta_0^{-3}-\ldots\right)\right.$$
$$+e^{-u}u^{-3/2}\left(\tfrac{2}{3}+\tfrac{2}{15}\eta_0^{-1}-\tfrac{3}{70}\eta_0^{-2}+\tfrac{5}{252}\eta_0^{-3}-\ldots\right)+e^{-u}u^{-5/2}\left(\tfrac{3}{10}\eta_0^{-1}\right.$$
$$\left.+\tfrac{9}{140}\eta_0^{-2}-\tfrac{5}{168}\eta_0^{-3}+\ldots\right)+e^{-u}u^{-7/2}\left(\tfrac{45}{112}\eta_0^{-2}+\tfrac{25}{336}\eta_0^{-3}-\ldots\right)$$
$$\left.+e^{-u}u^{-9/2}\left(\tfrac{175}{192}\eta_0^{-3}-\ldots\right)+\ldots\right\}; \tag{26}$$

$$\int_u^{\infty}K_1(u)\,du=\frac{1}{4}\left(\frac{1}{\pi\eta_0}\right)^{1/2}\left\{\int_{\sqrt{u}}^{\infty}(x^2-u)\,e^{-x^2}dx\left(-\tfrac{16}{3}+\tfrac{8}{15}\eta_0^{-1}-\tfrac{6}{35}\eta_0^{-2}+\tfrac{5}{63}\eta_0^{-3}-\ldots\right)\right.$$
$$+\int_{\sqrt{u}}^{\infty}e^{-x^2}dx\left(+\tfrac{8}{3}-\tfrac{4}{15}\eta_0^{-1}+\tfrac{3}{35}\eta_0^{-2}-\tfrac{5}{126}\eta_0^{-3}+\ldots\right)+e^{-u}u^{-1/2}\left(\tfrac{4}{3}-\tfrac{2}{15}\eta_0^{-1}\right.$$
$$\left.+\tfrac{3}{70}\eta_0^{-2}-\tfrac{5}{252}\eta_0^{-3}+\ldots\right)+e^{-u}u^{-3/2}\left(\tfrac{1}{5}\eta_0^{-1}-\tfrac{9}{140}\eta_0^{-2}+\tfrac{5}{168}\eta_0^{-3}-\ldots\right)$$
$$\left.+e^{-u}u^{-5/2}\left(\tfrac{9}{56}\eta_0^{-2}-\tfrac{25}{336}\eta_0^{-3}-\ldots\right)+e^{-u}u^{-7/2}\left(\tfrac{25}{96}\eta_0^{-3}-\ldots\right)+\ldots\right\}; \tag{27}$$

$$\int_u^{\infty}K_1(u)\,u\,du=\frac{1}{4}\left(\frac{1}{\pi\eta_0}\right)^{1/2}\left\{\int_{\sqrt{u}}^{\infty}\left(\tfrac{1}{2}x^4-\tfrac{1}{2}u^2-x^2\right)e^{-x^2}dx\left(-\tfrac{16}{3}+\tfrac{8}{15}\eta_0^{-1}\right.\right.$$
$$\left.-\tfrac{6}{35}\eta_0^{-2}+\tfrac{5}{63}\eta_0^{-3}-\ldots\right)\int_{\sqrt{u}}^{\infty}e^{-x^2}dx\left(\tfrac{4}{3}-\tfrac{14}{15}\eta_0^{-1}+\tfrac{51}{70}\eta_0^{-2}-\tfrac{155}{252}\eta_0^{-3}+\ldots\right)$$
$$+e^{-u}u^{-1/2}\left(\tfrac{3}{5}\eta_0^{-1}-\tfrac{57}{140}\eta_0^{-2}+\tfrac{55}{168}\eta_0^{-3}-\ldots\right)+e^{-u}u^{-3/2}\left(\tfrac{15}{56}\eta_0^{-2}-\tfrac{65}{336}\eta_0^{-3}+\ldots\right)$$
$$\left.+e^{-u}u^{-5/2}\left(\tfrac{35}{96}\eta_0^{-3}-\ldots\right)+\ldots\right\}. \tag{28}$$

With the explicit form for η_ν (eq. [16]), the moments of K_0 and K_1 can be obtained, thus:

$$\int_0^{\infty}K_0(u)\,du=\tfrac{1}{2}\left[1-(1+\eta_0)^{-1/2}\right]; \tag{29}$$

$$\int_0^{\infty}K_0(u)\,u\,du=\tfrac{1}{8}\eta_0(1+\eta_0)^{-3/2}; \tag{30}$$

$$\int_0^{\infty}K_1(u)\,du=\tfrac{1}{2}; \tag{31}$$

$$\int_0^{\infty}K_1(u)\,u\,du=\tfrac{1}{4}(1+\eta_0)^{-1/2}. \tag{32}$$

Although these integrals and the expansions above are dependent only on η_0 (the line strength of the dispersion profile at the line center), for Voigt profiles the proper η_0 is that pertaining to a dispersion profile fitting the true profile in the neighborhood of $\eta_\nu = 1$.

Substituting equations (31) and (32) in the definitions of ${}_I\boldsymbol{B}$ and ${}_L\boldsymbol{B}$ (eqs. [8] and [9]),

we obtain

$$ {}_{I}\boldsymbol{B}(\tau) = -\int_{\tau}^{\infty} K_1(u)\,du\,, \tag{33} $$

$$ {}_{L}\boldsymbol{B}(\tau) = \tau\,{}_{I}\boldsymbol{B}(\tau) + \int_{\tau}^{\infty} K_1(u)\,u\,du\,. \tag{34} $$

The form of these functions for moderate τ is almost independent of η_0. It is estimated that, for *Ca* II, the appropriate value of η_0 is of the order of 10^6 to 10^8. Calculations have been carried out for $\eta_0 = 4 \times 10^6$. Values of ${}_{I}\boldsymbol{B}$, ${}_{L}\boldsymbol{B}$, and $\int_{\tau}^{\infty} K_0(u)du$ may be found in Table 1. The exponents in Table 1, as well as in the other tables, are the powers of 10 by which the tabular entries are to be multiplied.

SOLUTION OF INTEGRAL EQUATION

The integral equation (5) can be readily solved by direct iteration, provided that the procedure converges. Writing the equation symbolically as $G = \boldsymbol{B} + \lambda G$, we see that the solution for G is $G = \boldsymbol{B} + \lambda\boldsymbol{B} + \lambda^2\boldsymbol{B} + \ldots$. In order to estimate the rate of convergence of this solution for G, we must estimate the ratio between successive terms in the expansion. Referring to equation (5), we find that the explicit form of λ contains an integral whose value may be estimated by using the inequality

$$ \int K_0 F \leqslant \text{max. } F \int K_0\,, \tag{35} $$

where K_0 and F are both nonnegative and where F is otherwise arbitrary. From the properties of K_0, we find that the expansion for G converges more rapidly than the power series with argument $(1-\epsilon)[1-(1+\eta_0)^{-1/2}]$. This method of calculating is useful for $\epsilon > 0.9$ or for η_0 small. For strong resonance lines, however, η_0 is large, and one expects $\epsilon = 0.01$ in order of magnitude.[12] For these lines, the procedure certainly converges, but too slowly for computational use. However, ${}_{I}\boldsymbol{B}$ and ${}_{L}\boldsymbol{B}$ are the solutions of equation (5) for $\epsilon = 1.0$.

In order to make use of the peakedness of the function K_0 in the iterations, we subtract

$$ G(\tau)(1-\epsilon)\int_0^{\infty} K_0(|\tau-\tau'|)\,d\tau' \tag{36} $$

from both sides of equation (5), and, transposing, we obtain

$$ (1-\epsilon)\int_0^{\infty} K_0(|\tau-\tau'|)[G(\tau') - G(\tau)]\,d\tau' = -\boldsymbol{B}(\tau) + G(\tau) \times\left[1-(1-\epsilon)\int_0^{\infty} K_0(|\tau-\tau'|)\,d\tau'\right]. \tag{37} $$

Here $\boldsymbol{B}$ represents any linear combination of ${}_{I}\boldsymbol{B}$ or ${}_{L}\boldsymbol{B}$.

If we consider the diffusion of photons, equations identical with equations (4), (5), and (37) can be obtained. In terms of photon diffusion, equation (4) states that the number of photons absorbed at τ equals the sum of the number emitted by all elements $d\tau'$, weighted by the probability of reaching τ and the probability of absorption. Therefore $K_0(|\tau-\tau'|)$ is the probability that a photon absorbed at τ' will be re-emitted and subsequently absorbed at τ. Since most photons do not travel far (mean free path of 6.25×10^{-5} for $\eta_0 = 4 \times 10^6$) compared to the distance in which G changes appreciably, one may neglect the left-hand term of equation (37) and obtain a first approximation to G. This solution can then be used to compute corrections to the first approximations.

[12] B. Strömgren, *Zs. f. Ap.*, **10**, 237, 1935.

TABLE I

Solution for $\epsilon = 1$, With Integral of Kernel

τ	$-_I B$	$_L B$	$\int_u^\infty K_0(u)\,du$	τ	$-_I B$	$_L B$	$\int_u^\infty K_0(u)\,du$
.0001	9.40391 $^{-3}$	1.23120 $^{-4}$	9.15950 $^{-3}$	.0066	1.13666 $^{-3}$	1.09816 $^{-4}$	9.29298 $^{-4}$
.0002	6.64636 $^{-3}$	1.22341 $^{-4}$	6.40424 $^{-3}$	.0068	1.11923 $^{-3}$	1.09590 $^{-4}$	9.12462 $^{-4}$
.0003	5.42481 $^{-3}$	1.21744 $^{-4}$	5.18443 $^{-3}$	.0070	1.10255 $^{-3}$	1.09368 $^{-4}$	8.96361 $^{-4}$
.0004	4.69651 $^{-3}$	1.21241 $^{-4}$	4.45760 $^{-3}$	.0072	1.08656 $^{-3}$	1.09149 $^{-4}$	8.80944 $^{-4}$
.0005	4.19939 $^{-3}$	1.20797 $^{-4}$	3.96176 $^{-3}$	.0074	1.07121 $^{-3}$	1.08933 $^{-4}$	8.66164 $^{-4}$
.0006	3.83235 $^{-3}$	1.20396 $^{-4}$	3.59587 $^{-3}$	.0076	1.05647 $^{-3}$	1.08720 $^{-4}$	8.51978 $^{-4}$
.0007	3.54702 $^{-3}$	1.20028 $^{-4}$	3.31160 $^{-3}$	.0078	1.04229 $^{-3}$	1.08510 $^{-4}$	8.38349 $^{-4}$
.0008	3.31696 $^{-3}$	1.19685 $^{-4}$	3.08252 $^{-3}$	.0080	1.02864 $^{-3}$	1.08303 $^{-4}$	8.25242 $^{-4}$
.0009	3.12635 $^{-3}$	1.19363 $^{-4}$	2.89283 $^{-3}$	.0085	9.96635 $^{-4}$	1.07797 $^{-4}$	7.94548 $^{-4}$
.0010	2.96506 $^{-3}$	1.19059 $^{-4}$	2.73241 $^{-3}$	.0090	9.67302 $^{-4}$	1.07306 $^{-4}$	7.66486 $^{-4}$
.0011	2.82626 $^{-3}$	1.18770 $^{-4}$	2.59443 $^{-3}$	.0095	9.40289 $^{-4}$	1.06830 $^{-4}$	7.40703 $^{-4}$
.0012	2.70517 $^{-3}$	1.18493 $^{-4}$	2.47412 $^{-3}$	.0100	9.15302 $^{-4}$	1.06366 $^{-4}$	7.16909 $^{-4}$
.0013	2.59830 $^{-3}$	1.18228 $^{-4}$	2.36800 $^{-3}$	.0105	8.92100 $^{-4}$	1.05914 $^{-4}$	6.94864 $^{-4}$
.0014	2.50307 $^{-3}$	1.17973 $^{-4}$	2.27349 $^{-3}$	.0110	8.70477 $^{-4}$	1.05473 $^{-4}$	6.74366 $^{-4}$
.0015	2.41751 $^{-3}$	1.17727 $^{-4}$	2.18862 $^{-3}$	.0115	8.50260 $^{-4}$	1.05043 $^{-4}$	6.55245 $^{-4}$
.0016	2.34009 $^{-3}$	1.17489 $^{-4}$	2.11186 $^{-3}$	.0120	8.31303 $^{-4}$	1.04623 $^{-4}$	6.37353 $^{-4}$
.0017	2.26958 $^{-3}$	1.17259 $^{-4}$	2.04200 $^{-3}$	.0130	7.96675 $^{-4}$	1.03809 $^{-4}$	6.04781 $^{-4}$
.0018	2.20501 $^{-3}$	1.17035 $^{-4}$	1.97806 $^{-3}$	.0140	7.65770 $^{-4}$	1.03028 $^{-4}$	5.75836 $^{-4}$
.0019	2.14561 $^{-3}$	1.16818 $^{-4}$	1.91926 $^{-3}$	.0150	7.37959 $^{-4}$	1.02277 $^{-4}$	5.49902 $^{-4}$
.0020	2.09069 $^{-3}$	1.16606 $^{-4}$	1.86494 $^{-3}$	.0160	7.12753 $^{-4}$	1.01551 $^{-4}$	5.26498 $^{-4}$
.0022	1.99228 $^{-3}$	1.16198 $^{-4}$	1.76766 $^{-3}$	.0170	6.89765 $^{-4}$	1.00850 $^{-4}$	5.05242 $^{-4}$
.0024	1.90641 $^{-3}$	1.15808 $^{-4}$	1.68287 $^{-3}$	.0180	6.68685 $^{-4}$	1.00171 $^{-4}$	4.85832 $^{-4}$
.0026	1.83060 $^{-3}$	1.15435 $^{-4}$	1.60809 $^{-3}$	.0190	6.49259 $^{-4}$	9.95125 $^{-5}$	4.68019 $^{-4}$
.0028	1.76304 $^{-3}$	1.15075 $^{-4}$	1.54152 $^{-3}$	.0200	6.31279 $^{-4}$	9.88723 $^{-5}$	4.51599 $^{-4}$
.0030	1.70232 $^{-3}$	1.14729 $^{-4}$	1.48175 $^{-3}$	.0220	5.98995 $^{-4}$	9.76428 $^{-5}$	4.22290 $^{-4}$
.0032	1.64736 $^{-3}$	1.14394 $^{-4}$	1.42771 $^{-3}$	.0240	5.70747 $^{-4}$	9.64737 $^{-5}$	3.96849 $^{-4}$
.0034	1.59730 $^{-3}$	1.14070 $^{-4}$	1.37854 $^{-3}$	.0260	5.45751 $^{-4}$	9.53577 $^{-5}$	3.74510 $^{-4}$
.0036	1.55145 $^{-3}$	1.13755 $^{-4}$	1.33355 $^{-3}$	.0280	5.23418 $^{-4}$	9.42889 $^{-5}$	3.54704 $^{-4}$
.0038	1.50925 $^{-3}$	1.13449 $^{-4}$	1.29218 $^{-3}$	.0300	5.03302 $^{-4}$	9.32625 $^{-5}$	3.36996 $^{-4}$
.0040	1.47024 $^{-3}$	1.13151 $^{-4}$	1.25397 $^{-3}$	.0320	4.85053 $^{-4}$	9.22744 $^{-5}$	3.21051 $^{-4}$
.0042	1.43403 $^{-3}$	1.12861 $^{-4}$	1.21855 $^{-3}$	.0340	4.68395 $^{-4}$	9.13212 $^{-5}$	3.06602 $^{-4}$
.0044	1.40031 $^{-3}$	1.12577 $^{-4}$	1.18558 $^{-3}$	.0360	4.53107 $^{-4}$	9.03999 $^{-5}$	2.93435 $^{-4}$
.0046	1.36879 $^{-3}$	1.12300 $^{-4}$	1.15481 $^{-3}$	.0380	4.39008 $^{-4}$	8.95080 $^{-5}$	2.81377 $^{-4}$
.0048	1.33925 $^{-3}$	1.12029 $^{-4}$	1.12600 $^{-3}$	.0400	4.25949 $^{-4}$	8.86432 $^{-5}$	2.70286 $^{-4}$
.0050	1.31149 $^{-3}$	1.11764 $^{-4}$	1.09895 $^{-3}$	.0450	3.97088 $^{-4}$	8.65877 $^{-5}$	2.46058 $^{-4}$
.0052	1.28533 $^{-3}$	1.11505 $^{-4}$	1.07349 $^{-3}$	.0500	3.72542 $^{-4}$	8.46652 $^{-5}$	2.25791 $^{-4}$
.0054	1.26063 $^{-3}$	1.11250 $^{-4}$	1.04947 $^{-3}$	.0550	3.51320 $^{-4}$	8.28567 $^{-5}$	2.08547 $^{-4}$
.0056	1.23726 $^{-3}$	1.11000 $^{-4}$	1.02675 $^{-3}$	.0600	3.32725 $^{-4}$	8.11476 $^{-5}$	1.93670 $^{-4}$
.0058	1.21509 $^{-3}$	1.10755 $^{-4}$	1.00524 $^{-3}$	.0650	3.16248 $^{-4}$	7.95260 $^{-5}$	1.80685 $^{-4}$
.0060	1.19403 $^{-3}$	1.10514 $^{-4}$	9.84823 $^{-4}$	.0700	3.01512 $^{-4}$	7.79822 $^{-5}$	1.69241 $^{-4}$
.0062	1.17400 $^{-3}$	1.10278 $^{-4}$	9.65411 $^{-4}$	.0750	2.88227 $^{-4}$	7.65084 $^{-5}$	1.59071 $^{-4}$
.0064	1.15490 $^{-3}$	1.10045 $^{-4}$	9.46927 $^{-4}$	.0800	2.76167 $^{-4}$	7.50797 $^{-5}$	1.49965 $^{-4}$

TABLE I (cont'd)

τ	$^{-}{}_{I}B$	$_{L}B$	$\int_{u}^{\infty} K_0(u)\,du$	τ	$^{-}{}_{I}B$	$_{L}B$	$\int_{u}^{\infty} K_0(u)\,du$
.0800	2.76167 $^{-4}$	7.50797 $^{-5}$	1.49965 $^{-4}$	.76	2.88998 $^{-5}$	1.62205 $^{-5}$	6.81014 $^{-6}$
.0850	2.65152 $^{-4}$	7.37450 $^{-5}$	1.41762 $^{-4}$	.78	2.77014 $^{-5}$	1.56546 $^{-5}$	6.44262 $^{-6}$
.0900	2.55040 $^{-4}$	7.24449 $^{-5}$	1.34329 $^{-4}$	.80	2.65646 $^{-5}$	1.51121 $^{-5}$	6.09917 $^{-6}$
.0950	2.45711 $^{-4}$	7.11933 $^{-5}$	1.27561 $^{-4}$	.85	2.39667 $^{-5}$	1.38502 $^{-5}$	5.33375 $^{-6}$
.10	2.37070 $^{-4}$	6.99866 $^{-5}$	1.21371 $^{-4}$	.90	2.16751 $^{-5}$	1.27103 $^{-5}$	4.68191 $^{-6}$
.11	2.21538 $^{-4}$	6.76954 $^{-5}$	1.10446 $^{-4}$	.95	1.96453 $^{-5}$	1.16783 $^{-5}$	4.12369 $^{-6}$
.12	2.07939 $^{-4}$	6.55494 $^{-5}$	1.01105 $^{-4}$	1.00	1.78408 $^{-5}$	1.07420 $^{-5}$	3.64325 $^{-6}$
.13	1.95902 $^{-4}$	6.35314 $^{-5}$	9.30257 $^{-5}$	1.05	1.62313 $^{-5}$	9.89097 $^{-6}$	3.22786 $^{-6}$
.14	1.85151 $^{-4}$	6.16271 $^{-5}$	8.59671 $^{-5}$	1.10	1.47914 $^{-5}$	9.11605 $^{-6}$	2.86725 $^{-6}$
.15	1.75473 $^{-4}$	5.98248 $^{-5}$	7.97479 $^{-5}$	1.15	1.34998 $^{-5}$	8.40935 $^{-6}$	2.55300 $^{-6}$
.16	1.66704 $^{-4}$	5.81146 $^{-5}$	7.42277 $^{-5}$	1.20	1.23383 $^{-5}$	7.76392 $^{-6}$	2.27821 $^{-6}$
.17	1.58712 $^{-4}$	5.64882 $^{-5}$	6.92963 $^{-5}$	1.30	1.03460 $^{-5}$	6.63307 $^{-6}$	1.82510 $^{-6}$
.18	1.51390 $^{-4}$	5.49382 $^{-5}$	6.48655 $^{-5}$	1.40	8.71476 $^{-6}$	5.68271 $^{-6}$	1.47258 $^{-6}$
.19	1.44653 $^{-4}$	5.34584 $^{-5}$	6.08644 $^{-5}$	1.50	7.36997 $^{-6}$	4.88059 $^{-6}$	1.19561 $^{-6}$
.20	1.38428 $^{-4}$	5.20434 $^{-5}$	5.72347 $^{-5}$	1.60	6.25464 $^{-6}$	4.20108 $^{-6}$	9.76142 $^{-7}$
.22	1.27285 $^{-4}$	4.93890 $^{-5}$	5.09056 $^{-5}$	1.70	5.32478 $^{-6}$	3.62350 $^{-6}$	8.00921 $^{-7}$
.24	1.17587 $^{-4}$	4.69424 $^{-5}$	4.55805 $^{-5}$	1.80	4.54595 $^{-6}$	3.13109 $^{-6}$	6.60093 $^{-7}$
.26	1.09058 $^{-4}$	4.46777 $^{-5}$	4.10465 $^{-5}$	1.90	3.89094 $^{-6}$	2.71019 $^{-6}$	5.46224 $^{-7}$
.28	1.01492 $^{-4}$	4.25737 $^{-5}$	3.71466 $^{-5}$	2.00	3.33803 $^{-6}$	2.34951 $^{-6}$	4.53661 $^{-7}$
.30	9.47305 $^{-5}$	4.06127 $^{-5}$	3.37629 $^{-5}$	2.10	2.86975 $^{-6}$	2.03976 $^{-6}$	3.78053 $^{-7}$
.32	8.86496 $^{-5}$	3.87799 $^{-5}$	3.08048 $^{-5}$	2.20	2.47196 $^{-6}$	1.77321 $^{-6}$	3.16017 $^{-7}$
.34	8.31501 $^{-5}$	3.70628 $^{-5}$	2.82015 $^{-5}$	2.30	2.13312 $^{-6}$	1.54341 $^{-6}$	2.64914 $^{-7}$
.36	7.81523 $^{-5}$	3.54506 $^{-5}$	2.58969 $^{-5}$	2.40	1.84378 $^{-6}$	1.34494 $^{-6}$	2.22659 $^{-7}$
.38	7.35907 $^{-5}$	3.39338 $^{-5}$	2.38462 $^{-5}$	2.50	1.59612 $^{-6}$	1.17327 $^{-6}$	1.87602 $^{-7}$
.40	6.94114 $^{-5}$	3.25044 $^{-5}$	2.20128 $^{-5}$	2.60	1.38370 $^{-6}$	1.02456 $^{-6}$	1.58423 $^{-7}$
.42	6.55689 $^{-5}$	3.11551 $^{-5}$	2.03666 $^{-5}$	2.80	1.04400 $^{-6}$	7.83462 $^{-7}$	1.13680 $^{-7}$
.44	6.20253 $^{-5}$	2.98797 $^{-5}$	1.88829 $^{-5}$	3.00	7.91385 $^{-7}$	6.01159 $^{-7}$	8.21848 $^{-8}$
.46	5.87480 $^{-5}$	2.86723 $^{-5}$	1.75409 $^{-5}$	3.20	6.02390 $^{-7}$	4.62680 $^{-7}$	5.98101 $^{-8}$
.48	5.57092 $^{-5}$	2.75281 $^{-5}$	1.63233 $^{-5}$	3.40	4.60226 $^{-7}$	3.57090 $^{-7}$	4.37844 $^{-8}$
.50	5.28851 $^{-5}$	2.64425 $^{-5}$	1.52152 $^{-5}$	3.60	3.52806 $^{-7}$	2.7625 $^{-7}$	3.22077 $^{-8}$
.52	5.02547 $^{-5}$	2.54115 $^{-5}$	1.42040 $^{-5}$	3.80	2.71237 $^{-7}$	2.1426 $^{-7}$	2.38289 $^{-8}$
.54	4.78001 $^{-5}$	2.44312 $^{-5}$	1.32790 $^{-5}$	4.00	2.09109 $^{-7}$	1.6650 $^{-7}$	1.76981 $^{-8}$
.56	4.55051 $^{-5}$	2.34984 $^{-5}$	1.24308 $^{-5}$	4.20	1.61614 $^{-7}$	1.2964 $^{-7}$	1.31972 $^{-8}$
.58	4.33558 $^{-5}$	2.26100 $^{-5}$	1.16513 $^{-5}$	4.40	1.25191 $^{-7}$	1.0112 $^{-7}$	9.87713 $^{-9}$
.60	4.13398 $^{-5}$	2.17633 $^{-5}$	1.09336 $^{-5}$	4.60	9.71816 $^{-8}$	7.9002 $^{-8}$	7.41719 $^{-9}$
.62	3.94461 $^{-5}$	2.09556 $^{-5}$	1.02714 $^{-5}$	4.80	7.55852 $^{-8}$	6.1817 $^{-8}$	5.58724 $^{-9}$
.64	3.76647 $^{-5}$	2.01847 $^{-5}$	9.65942 $^{-6}$	5.00	5.88937 $^{-8}$	4.8442 $^{-8}$	4.22098 $^{-9}$
.66	3.59869 $^{-5}$	1.94483 $^{-5}$	9.09288 $^{-6}$	5.20	4.59651 $^{-8}$	3.8010 $^{-8}$	3.19726 $^{-9}$
.68	3.44048 $^{-5}$	1.87446 $^{-5}$	8.56759 $^{-6}$	5.40	3.59306 $^{-8}$	2.9862 $^{-8}$	2.42799 $^{-9}$
.70	3.29112 $^{-5}$	1.80715 $^{-5}$	8.07981 $^{-6}$	5.60	2.81277 $^{-8}$	2.3489 $^{-8}$	1.84800 $^{-9}$
.72	3.14996 $^{-5}$	1.74276 $^{-5}$	7.62623 $^{-6}$	5.80	2.20495 $^{-8}$	1.8496 $^{-8}$	1.40978 $^{-9}$
.74	3.01642 $^{-5}$	1.68110 $^{-5}$	7.20389 $^{-6}$	6.00	1.73068 $^{-8}$	1.4580 $^{-8}$	1.07761 $^{-9}$

Thus the solution of equation (37) can be written

$$G = \Sigma\, {}^{n}G\,, \tag{38}$$

where

$${}^{0}G(\tau) = \frac{\boldsymbol{B}(\tau)}{\epsilon + (1-\epsilon)(1+\eta_0)^{-1/2} + (1-\epsilon)\int_{\tau}^{\infty} K_0(u)\,du} \tag{39}$$

and

$${}^{n+1}G(\tau) = \frac{1-\epsilon}{\epsilon + (1-\epsilon)(1+\eta_0)^{-1/2} + (1-\epsilon)\int_{\tau}^{\infty} K_0(u)\,du} \times \int_0^{\infty} K_0(|\tau-\tau'|)[{}^{n}G(\tau') - {}^{n}G(\tau)]\,d\tau'\,. \tag{40}$$

The denominator in equations (39) and (40) is obtained from

$$1 - (1-\epsilon)\int_0^{\infty} K_0(|\tau-\tau'|)\,d\tau' \tag{41}$$

through the use of equation (29). This procedure is equivalent to iterating the linear equation

$$G(\tau) = \frac{\boldsymbol{B}(\tau)}{\epsilon + (1-\epsilon)(1+\eta_0)^{-1/2} + (1-\epsilon)\int_{\tau}^{\infty} K_0(u)\,du} + (1-\epsilon)\int_0^{\infty} \tilde{K}_0(|\tau-\tau'|)G(\tau')\,d\tau'\,, \tag{42}$$

where

$$\tilde{K}_0(|\tau-\tau'|) = \frac{1}{\epsilon + (1-\epsilon)(1+\eta_0)^{-1/2} + (1-\epsilon)\int_{\tau}^{\infty} K_0(u)\,du} \times \left[K_0(|\tau-\tau'|) - \delta(\tau-\tau')\int_0^{\infty} K_0(|\tau-\tau'|)\,d\tau'\right] \tag{43}$$

and where $\delta(\tau-\tau')$ is the Dirac δ function.

In Table 2 the functions ${}^{0}G(\tau)$ for the isothermal and linear atmospheres are tabulated for different ϵ. Since $\boldsymbol{B}$ is approximately proportional to $\eta_0^{-1/2}$, ${}^{0}G$ is inversely proportional to $\epsilon\eta_0^{1/2} + (1-\epsilon)(\eta_0/1+\eta_0)^{1/2}$ for sufficiently large τ. The first and second iterations were performed for values of this parameter of about 1 and 21. For larger values of this parameter, the difference between the noncoherent and pure absorption solutions is small, and the parameter may be taken as a measure of the effect of the inclusion of noncoherent scattering on phenomena dependent on $\tau \gg \eta_0^{-1/2}$. The dependence of these functions on ϵ is shown in Figures 1 and 2. Here ${}_{I}G$ and ${}_{L}G$ are the solutions of equation (5) for $B=1$ and $B=\tau$ respectively.

The quantities ${}^{1}G$ and ${}^{2}G$ were obtained by numerical integration. For these calculations, the kernel K_0 is given in Table 3. For $\epsilon = 0$, ${}^{1}G$ provides an appreciable correction for all τ, while for $\epsilon = 0.01$ these corrections are almost negligible. ${}^{1}G$ may be found from Figure 3, while the effect of including ${}^{1}G_0$ is also shown in Figures 1 and 2. The few values of ${}^{2}G$ obtained indicate that the sequence is sufficiently convergent, provided that $\tau > 0.01$ for $\epsilon = 0$ and $\tau > 0.001$ for $\epsilon = 0.01$.

TABLE 2

${}^{0}G$, First Approximation to $\bar{J}-B$

τ	$-{}^{0}_{I}G_{0}$	${}^{0}_{L}G_{0}$	$-{}^{0}_{I}G_{.001}$	${}^{0}_{L}G_{.001}$	$-{}^{0}_{I}G_{.01}$	${}^{0}_{L}G_{.01}$	$-{}^{0}_{I}G_{.1}$	${}^{0}_{L}G_{.1}$
.0000	9.995 $^{-1}$	2.499 $^{-4}$	9.985 $^{-1}$	2.496 $^{-4}$	9.896 $^{-1}$	2.474 $^{-4}$	9.087 $^{-1}$	2.272 $^{-4}$
.0001	9.735 $^{-1}$	1.275 $^{-2}$	8.830 $^{-1}$	1.156 $^{-2}$	4.807 $^{-1}$	6.294 $^{-3}$	8.652 $^{-2}$	1.133 $^{-3}$
.0002	9.627 $^{-1}$	1.772 $^{-2}$	8.416 $^{-1}$	1.549 $^{-2}$	3.948 $^{-1}$	7.267 $^{-3}$	6.258 $^{-2}$	1.152 $^{-3}$
.0003	9.543 $^{-1}$	2.142 $^{-2}$	8.122 $^{-1}$	1.823 $^{-2}$	3.471 $^{-1}$	7.790 $^{-3}$	5.161 $^{-2}$	1.158 $^{-3}$
.0004	9.473 $^{-1}$	2.446 $^{-2}$	7.890 $^{-1}$	2.037 $^{-2}$	3.150 $^{-1}$	8.133 $^{-3}$	4.496 $^{-2}$	1.161 $^{-3}$
.0005	9.412 $^{-1}$	2.707 $^{-2}$	7.695 $^{-1}$	2.213 $^{-2}$	2.913 $^{-1}$	8.379 $^{-3}$	4.037 $^{-2}$	1.161 $^{-3}$
.0006	9.357 $^{-1}$	2.939 $^{-2}$	7.527 $^{-1}$	2.365 $^{-2}$	2.727 $^{-1}$	8.566 $^{-3}$	3.696 $^{-2}$	1.161 $^{-3}$
.0008	9.259 $^{-1}$	3.341 $^{-2}$	7.244 $^{-1}$	2.614 $^{-2}$	2.449 $^{-1}$	8.835 $^{-3}$	3.213 $^{-2}$	1.159 $^{-3}$
.0010	9.173 $^{-1}$	3.683 $^{-2}$	7.011 $^{-1}$	2.815 $^{-2}$	2.246 $^{-1}$	9.020 $^{-3}$	2.881 $^{-2}$	1.157 $^{-3}$
.0015	8.992 $^{-1}$	4.379 $^{-2}$	6.559 $^{-1}$	3.194 $^{-2}$	1.909 $^{-1}$	9.298 $^{-3}$	2.360 $^{-2}$	1.149 $^{-3}$
.0020	8.840 $^{-1}$	4.931 $^{-2}$	6.218 $^{-1}$	3.468 $^{-2}$	1.694 $^{-1}$	9.448 $^{-3}$	2.047 $^{-2}$	1.142 $^{-3}$
.0025	8.708 $^{-1}$	5.392 $^{-2}$	5.943 $^{-1}$	3.680 $^{-2}$	1.540 $^{-1}$	9.537 $^{-3}$	1.832 $^{-2}$	1.134 $^{-3}$
.0030	8.590 $^{-1}$	5.789 $^{-2}$	5.713 $^{-1}$	3.850 $^{-2}$	1.423 $^{-1}$	9.591 $^{-3}$	1.672 $^{-2}$	1.127 $^{-3}$
.0040	8.382 $^{-1}$	6.451 $^{-2}$	5.342 $^{-1}$	4.111 $^{-2}$	1.253 $^{-1}$	9.641 $^{-3}$	1.447 $^{-2}$	1.114 $^{-3}$
.0050	8.202 $^{-1}$	6.990 $^{-2}$	5.049 $^{-1}$	4.303 $^{-2}$	1.132 $^{-1}$	9.649 $^{-3}$	1.293 $^{-2}$	1.102 $^{-3}$
.0060	8.042 $^{-1}$	7.443 $^{-2}$	4.808 $^{-1}$	4.450 $^{-2}$	1.041 $^{-1}$	9.635 $^{-3}$	1.178 $^{-2}$	1.091 $^{-3}$
.0080	7.762 $^{-1}$	8.172 $^{-2}$	4.426 $^{-1}$	4.660 $^{-2}$	9.093 $^{-2}$	9.574 $^{-3}$	1.017 $^{-2}$	1.070 $^{-3}$
.0100	7.741 $^{-1}$	8.741 $^{-2}$	4.131 $^{-1}$	4.801 $^{-2}$	8.169 $^{-2}$	9.493 $^{-3}$	9.054 $^{-3}$	1.052 $^{-3}$
.0150	7.029 $^{-1}$	9.742 $^{-2}$	3.602 $^{-1}$	4.992 $^{-2}$	6.685 $^{-2}$	9.265 $^{-3}$	7.311 $^{-3}$	1.013 $^{-3}$
.0200	6.634 $^{-1}$	1.039 $^{-1}$	3.236 $^{-1}$	5.069 $^{-2}$	5.769 $^{-2}$	9.036 $^{-3}$	6.259 $^{-3}$	9.803 $^{-4}$
.0250	6.301 $^{-1}$	1.083 $^{-1}$	2.960 $^{-1}$	5.090 $^{-2}$	5.129 $^{-2}$	8.818 $^{-3}$	5.535 $^{-3}$	9.515 $^{-4}$
.0300	6.013 $^{-1}$	1.114 $^{-1}$	2.741 $^{-1}$	5.079 $^{-2}$	4.648 $^{-2}$	8.613 $^{-3}$	4.995 $^{-3}$	9.257 $^{-4}$
.0400	5.530 $^{-1}$	1.151 $^{-1}$	2.407 $^{-1}$	5.009 $^{-2}$	3.958 $^{-2}$	8.236 $^{-3}$	4.230 $^{-3}$	8.803 $^{-4}$
.0500	5.133 $^{-1}$	1.167 $^{-1}$	2.160 $^{-1}$	4.908 $^{-2}$	3.476 $^{-2}$	7.899 $^{-3}$	3.701 $^{-3}$	8.412 $^{-4}$
.0600	4.797 $^{-1}$	1.170 $^{-1}$	1.965 $^{-1}$	4.793 $^{-2}$	3.113 $^{-2}$	7.593 $^{-3}$	3.307 $^{-3}$	8.064 $^{-4}$
.0800	4.249 $^{-1}$	1.155 $^{-1}$	1.674 $^{-1}$	4.552 $^{-2}$	2.595 $^{-2}$	7.056 $^{-3}$	2.746 $^{-3}$	7.464 $^{-4}$
.1000	3.815 $^{-1}$	1.126 $^{-1}$	1.463 $^{-1}$	4.318 $^{-2}$	2.233 $^{-2}$	6.593 $^{-3}$	2.358 $^{-3}$	6.960 $^{-4}$
.1500	3.027 $^{-1}$	1.032 $^{-1}$	1.111 $^{-1}$	3.788 $^{-2}$	1.659 $^{-2}$	5.658 $^{-3}$	1.746 $^{-3}$	5.951 $^{-4}$
.2000	2.484 $^{-1}$	9.340 $^{-2}$	8.893 $^{-2}$	3.343 $^{-2}$	1.312 $^{-2}$	4.932 $^{-3}$	1.377 $^{-3}$	5.178 $^{-4}$
.2500	2.084 $^{-1}$	8.429 $^{-2}$	7.337 $^{-2}$	2.968 $^{-2}$	1.074 $^{-2}$	4.345 $^{-3}$	1.126 $^{-3}$	4.557 $^{-4}$
.3000	1.775 $^{-1}$	7.609 $^{-2}$	6.179 $^{-2}$	2.649 $^{-2}$	8.998 $^{-3}$	3.857 $^{-3}$	9.428 $^{-4}$	4.042 $^{-4}$
.4000	1.330 $^{-1}$	6.227 $^{-2}$	4.562 $^{-2}$	2.136 $^{-2}$	6.600 $^{-3}$	3.091 $^{-3}$	6.909 $^{-4}$	3.235 $^{-4}$
.5000	1.026 $^{-1}$	5.132 $^{-2}$	3.491 $^{-2}$	1.746 $^{-2}$	5.032 $^{-3}$	2.516 $^{-3}$	5.264 $^{-4}$	2.632 $^{-4}$
.6000	8.091 $^{-2}$	4.260 $^{-2}$	2.737 $^{-2}$	1.441 $^{-2}$	3.935 $^{-3}$	2.072 $^{-3}$	4.115 $^{-4}$	2.166 $^{-4}$
.8000	5.249 $^{-2}$	2.986 $^{-2}$	1.764 $^{-2}$	1.004 $^{-2}$	2.530 $^{-3}$	1.439 $^{-3}$	2.644 $^{-4}$	1.504 $^{-4}$
1.0000	3.542 $^{-2}$	2.133 $^{-2}$	1.187 $^{-2}$	7.146 $^{-3}$	1.699 $^{-3}$	1.023 $^{-3}$	1.776 $^{-4}$	1.069 $^{-4}$
1.5000	1.470 $^{-2}$	9.738 $^{-3}$	4.911 $^{-3}$	3.252 $^{-3}$	7.022 $^{-4}$	4.650 $^{-4}$	7.337 $^{-5}$	4.859 $^{-5}$
2.0000	6.670 $^{-3}$	4.695 $^{-3}$	2.225 $^{-3}$	1.566 $^{-3}$	3.180 $^{-4}$	2.239 $^{-4}$	3.323 $^{-5}$	2.339 $^{-5}$
2.5000	3.191 $^{-3}$	2.346 $^{-3}$	1.064 $^{-3}$	7.823 $^{-4}$	1.521 $^{-4}$	1.118 $^{-4}$	1.589 $^{-5}$	1.168 $^{-5}$
3.0000	1.583 $^{-3}$	1.202 $^{-3}$	5.277 $^{-4}$	4.009 $^{-4}$	7.541 $^{-5}$	5.728 $^{-5}$	7.878 $^{-6}$	5.985 $^{-6}$
4.0000	4.182 $^{-4}$	3.330 $^{-4}$	1.395 $^{-4}$	1.110 $^{-4}$	1.992 $^{-5}$	1.586 $^{-5}$	2.082 $^{-6}$	1.658 $^{-6}$
5.0000	1.178 $^{-4}$	9.688 $^{-5}$	3.928 $^{-5}$	3.231 $^{-5}$	5.612 $^{-6}$	4.616 $^{-6}$	5.863 $^{-7}$	4.822 $^{-7}$
6.0000	3.461 $^{-5}$	2.916 $^{-5}$	1.154 $^{-5}$	9.723 $^{-6}$	1.649 $^{-6}$	1.389 $^{-6}$	1.723 $^{-7}$	1.451 $^{-7}$

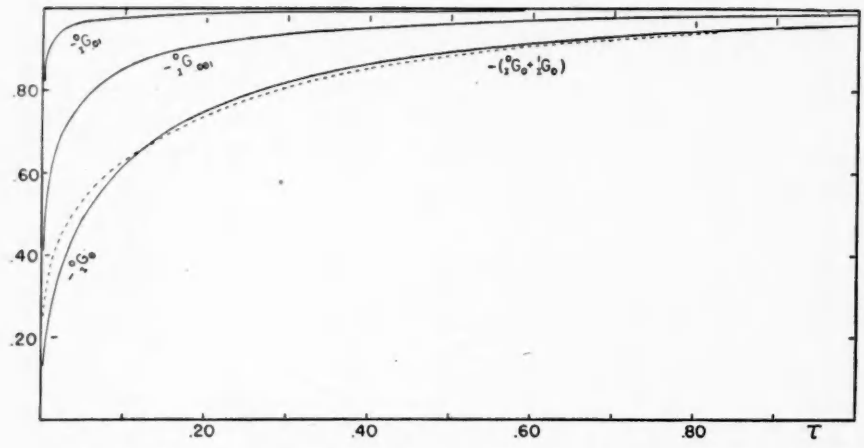

FIG. 1.—First approximation for isothermal atmosphere. The dashed curve represents the final $\bar{J}$ for $\epsilon = 0$.

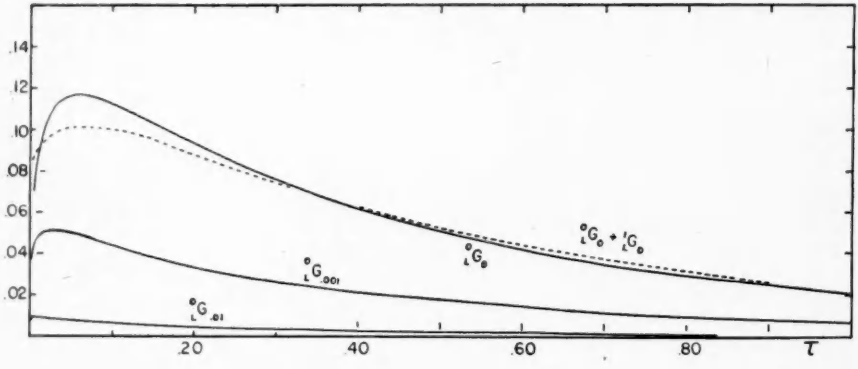

FIG. 2.—First approximation to $\bar{J} - B$ for purely linear temperature gradient. The dashed curve represents the final $\bar{J} - B$ for $\epsilon = 0$.

TABLE 3

Kernel of Integral Equation

τ	$K_0(u)$	τ	$K_0(u)$	τ	$K_0(u)$	τ	$K_0(u)$
.0001	4.70549^{+1}	.0040	1.83784^{-1}	.0360	6.29317^{-3}	.60	3.44499^{-5}
.0002	1.66222^{+1}	.0044	1.59128^{-1}	.0400	5.32438^{-3}	.70	2.35080^{-5}
.0003	9.04361^{0}	.0048	1.39507^{-1}	.0500	3.72543^{-3}	.80	1.66029^{-5}
.0004	5.87174^{0}	.0050	1.31151^{-1}	.0600	2.77271^{-3}	.90	1.20417^{-5}
.0005	4.20002^{0}	.0052	1.23591^{-1}	.0700	2.15366^{-3}	1.00	8.92039^{-6}
.0006	3.19403^{0}	.0056	1.10471^{-1}	.0800	1.72604^{-3}	1.20	5.14097^{-6}
.0007	2.53386^{0}	.0060	9.95041^{-2}	.0900	1.41689^{-3}	1.40	3.11242^{-6}
.0008	2.07329^{0}	.0070	7.87542^{-2}	.1000	1.18535^{-3}	1.60	1.95457^{-6}
.0009	1.73701^{0}	.0080	6.42909^{-2}	.1200	8.66413^{-4}	1.80	1.26276^{-6}
.0010	1.48264^{0}	.0090	5.37395^{-2}	.1400	6.61252^{-4}	2.00	8.34506^{-7}
.0012	1.12722^{0}	.0100	4.57655^{-2}	.1600	5.20951^{-4}	2.40	3.84120^{-7}
.0014	8.94002^{-1}	.0120	3.46378^{-2}	.1800	4.20529^{-4}	2.80	1.86428^{-7}
.0016	7.31311^{-1}	.0140	2.73491^{-2}	.2000	3.46069^{-4}	3.00	1.31898^{-7}
.0018	6.12529^{-1}	.0160	2.22736^{-2}	.2400	2.44972^{-4}	3.20	9.41233^{-8}
.0020	5.22692^{-1}	.0180	1.85747^{-2}	.2800	1.81236^{-4}	3.60	4.90009^{-8}
.0024	3.97180^{-1}	.0200	1.57820^{-2}	.3000	1.57884^{-4}	4.00	2.61386^{-8}
.0028	3.14837^{-1}	.0240	1.18906^{-2}	.3200	1.38515^{-4}	4.50	1.22526^{-8}
.0030	2.83727^{-1}	.0280	9.34678^{-3}	.3600	1.08545^{-4}	5.00	5.88938^{-9}
.0032	2.57406^{-1}	.0300	8.38838^{-3}	.4000	8.67642^{-5}	5.50	2.88956^{-9}
.0036	2.15484^{-1}	.0320	7.57897^{-3}	.5000	5.28851^{-5}	6.00	1.44224^{-9}

TABLE 4

Transform of $\bar{J} - B$

y	${}_{-1}L_0$	${}_{-1}L_{0.01}$	${}_{1}L_0$	${}_{1}L_{0.01}$	y	${}_{-1}L_0$	${}_{-1}L_{0.01}$	${}_{1}L_0$	${}_{1}L_{0.01}$
.95	.125	.006	.049	.003	.125	.393	.030	.093	.007
.90	.131	.006	.050	.003	.10	.422	.034	.094	.007
.85	.137	.007	.052	.003	.09	.436	.036	.095	.007
.80	.144	.007	.054	.003	.08	.451	.038	.096	.007
.70	.160	.008	.057	.003	.07	.468	.041	.096	.008
.60	.179	.009	.061	.003	.06	.487	.045	.096	.008
.50	.202	.011	.066	.004	.05	.508	.050	.096	.008
.40	.232	.013	.072	.004	.04	.534	.056	.096	.008
.30	.271	.016	.078	.005	.03	.563	.065	.094	.009
.25	.296	.019	.083	.005	.02	.603	.079	.091	.009
.20	.327	.022	.086	.006	.01	.663	.109	.085	.009
.15	.368	.026	.091	.006					

LINE PROFILES

Once $G(\tau)$ has been obtained, the residual intensity, r, can be obtained by simple integration. Since the emission term of equation (1) can be written as

$$j_\nu = (1+\eta_\nu) B_0 (1+\beta\tau) + (1-\epsilon)\,\eta_\nu G(\tau)\,, \tag{44}$$

and

$$I_\nu = \int_0^\infty j_\nu\, e^{-(1+\eta_\nu)\tau/\mu}\,\frac{d\tau}{\mu}\,, \tag{45}$$

the residual intensity for noncoherent scattering becomes

$$r_N = \frac{I_\nu}{I_c} = 1 - \frac{\eta_\nu}{1+\eta_\nu}\,\frac{1}{1+\beta\mu}\left[\beta\mu - {}_1L\left(\frac{\mu}{1+\eta_\nu}\right) - \beta\,{}_1L\left(\frac{\mu}{1+\eta_\nu}\right)\right], \tag{46}$$

where

$$B_0 L(y) = (1-\epsilon)\int_0^\infty e^{-\tau} G(\tau y)\, d\tau\,. \tag{47}$$

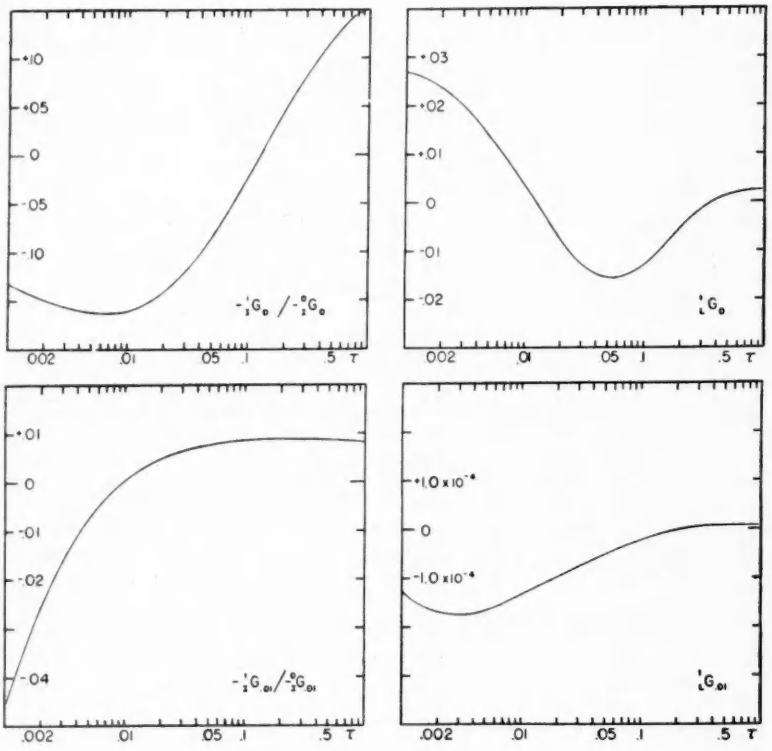

FIG. 3.—Results of first iteration

The integral $L(y)$ has been found by using a five-point integration formula. The representative points and weights were taken from the table quoted by S. Chandrasekhar.[13] The values in Table 4, obtained by this means, are certainly correct to 0.01, except possibly for small $\mu/(1+\eta_\nu)$ for which $G(\tau)$ near $\tau = 0$ has not been determined. $L(y)$ is given in Table 4 and in Figure 4. Residual intensities have also been computed for pure absorption and coherent scattering. For pure absorption,

$$r_A = 1 - \frac{\eta_\nu}{1+\eta_\nu}\frac{\beta\mu}{1+\beta\mu}. \tag{48}$$

For coherent scattering,[14]

$$r_C = \frac{H(\mu)}{1+\beta\mu}\frac{1}{1+\eta_\nu}\left[\left(\frac{1+\epsilon\eta_\nu}{1+\eta_\nu}\right)^{1/2}(1+\beta\mu+\eta_\nu) + \tfrac{1}{2}\beta a_1(1-\epsilon)\frac{\eta_\nu}{1+\eta_\nu}\right], \tag{49}$$

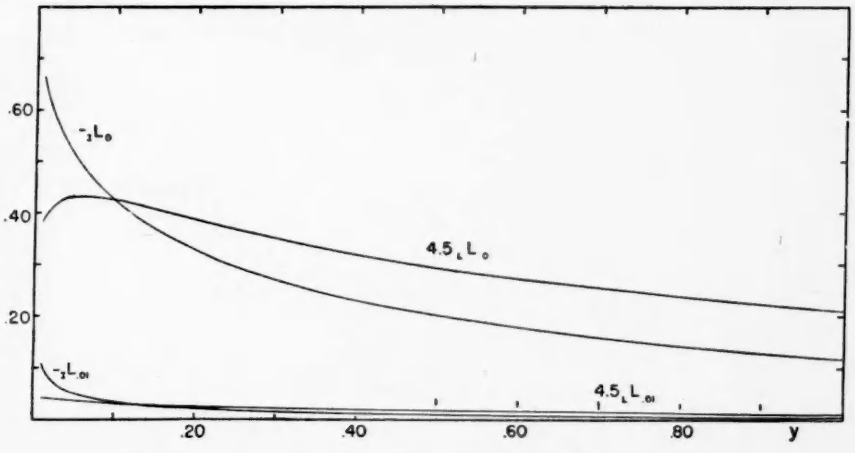

FIG. 4.—Transform of $G = \bar{J} - B$ for linear and isothermal atmosphere

where $H(\mu)$ is the Chandrasekhar H function for isotropic scattering with the albedo $\varpi_0 = (1-\epsilon)\eta_\nu(1+\eta_\nu)^{-1}$, and a_1 is the first moment of $H(\mu)$. In Figures 5 and 6, r_A, r_C, and r_N are represented. For the center of the disk, these solutions lie very close to one another. As μ decreases, the noncoherent scattering solution remains close to that for pure absorption, while that for coherent scattering departs rapidly from r_A. These profiles have been computed for $\beta = 4.5$, which represents the solar gradient in the vicinity of the H and K lines.

In the far wings, $1 - r$ becomes nearly proportional to η_ν. Thus, a single parameter C can be used to describe the shape of the line wing, where

$$C = \lim_{\eta_\nu \to 0} \frac{1-r}{r\eta_\nu}. \tag{50}$$

[13] Chandrasekhar, *op. cit.*, chap. ii, p. 65, Table V.

[14] *Ibid.*, chap. xii, eq. (66).

Houtgast's C, determined from

$$C = \lim_{\Delta\lambda\to\infty} \frac{1-r}{r}\Delta\lambda^2, \tag{51}$$

differs from the one defined above only by a constant which is the ratio between η_ν^{-1} and $\Delta\lambda^2$. We obtain $C(\mu)$ by carrying out the limiting process for the different solutions r_A, r_C, and r_N. Using similar subscripts for identification, we obtain

$$C_A(\mu) = \frac{\beta\mu}{1+\beta\mu}, \tag{52}$$

$$C_C(\mu) = (\tfrac{3}{2}-\tfrac{1}{2}\epsilon) + \tfrac{1}{2}(1-\epsilon)\,\mu \log\left(\frac{\mu}{1+\mu}\right) - \frac{1}{1+\beta\mu}\left[1+\frac{\beta}{4}(1-\epsilon)\right], \tag{53}$$

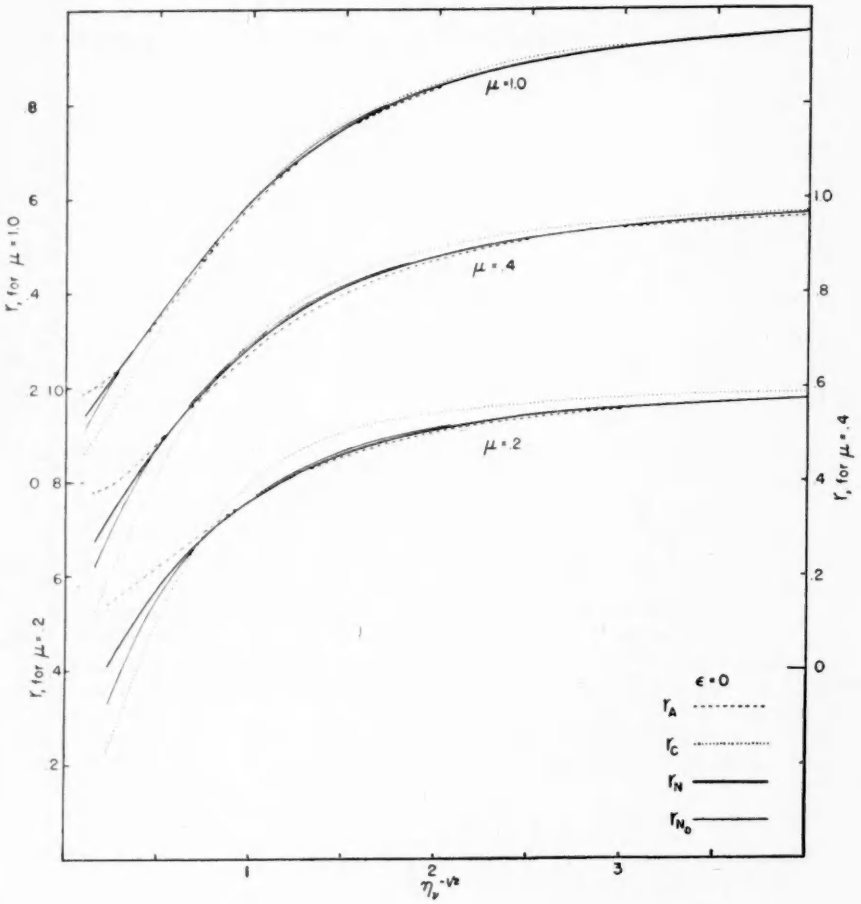

FIG. 5.—Line profiles for $\epsilon = 0$. r_{N_0} is the profile computed by using first approximation to $\bar{J} - B$.

$$C_N(\mu) = \frac{1}{1+\beta\mu}[\beta\mu - {}_IL(\mu) - \beta\,{}_LL(\mu)]. \tag{54}$$

In the derivation of $C_C(\mu)$, the expansion of $H(\mu)$ for low albedos, small ϖ_0, was needed. From the defining equation,[15]

$$H(\mu) = 1 + \tfrac{1}{2}\mu H(\mu)\varpi_0 \int_0^1 \frac{H(\mu')}{\mu+\mu'}\,d\mu', \tag{55}$$

we obtain

$$H(\mu) = 1 + \tfrac{1}{2}\mu\varpi_0 \log\frac{1+\mu}{\mu}. \tag{56}$$

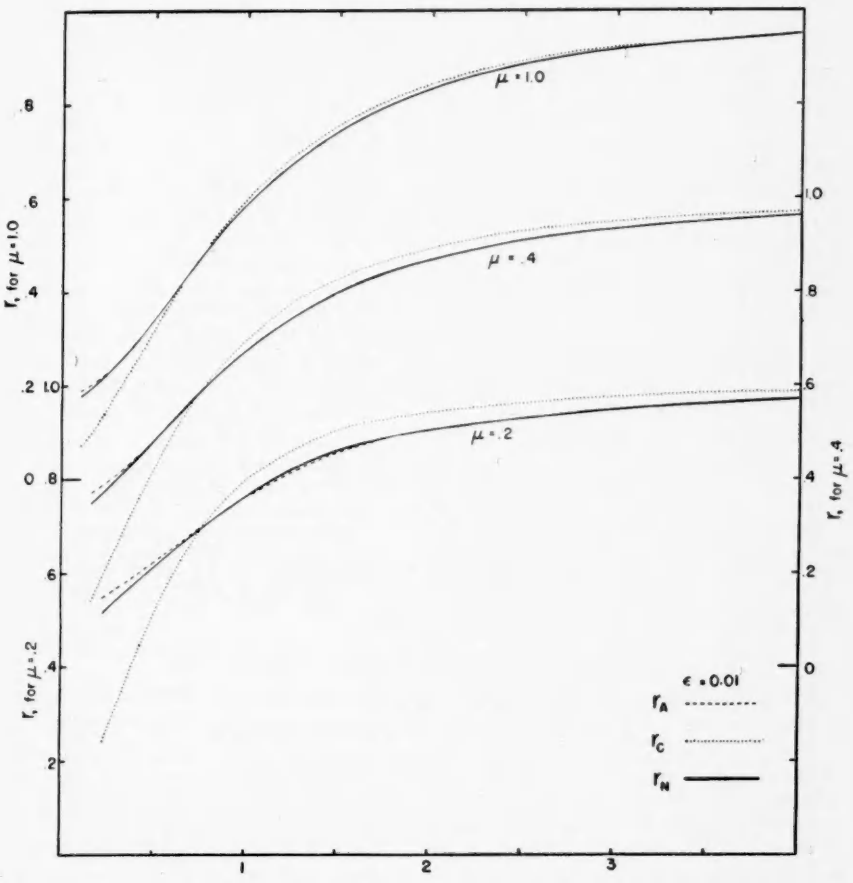

FIG. 6.—Line profiles for $\epsilon = 0.01$. In this figure, r_{N_0} was omitted, since it does not deviate appreciably from r_N.

[15] *Ibid.*, chap. v, eq. (1).

The center-limb variation of the far wings is described by $C(\mu)/C(1)$. The theoretical and observed values of $C(\mu)/C(1)$ are represented graphically in Figure 7. In this figure are plotted the observed values of $C(\mu)/C(1)$ obtained by Houtgast[1] for the K line of *Ca* II. The representation of these points with physically reasonable values of ϵ is improved, but it is not possible to reach this part of the curve without some change in the physical model, independent of any change in the parameters.

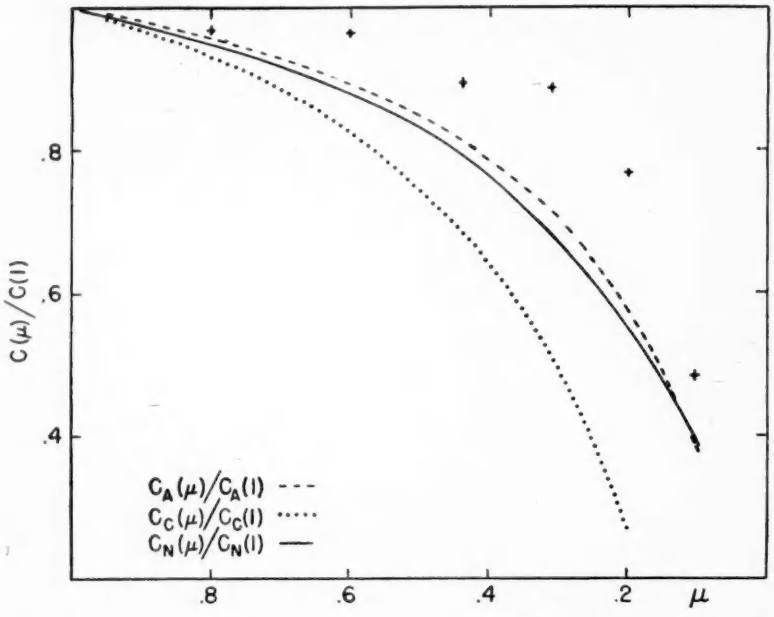

FIG. 7.—Relative strength of line wings computed for pure absorption, coherent scattering, and noncoherent scattering. For coherent scattering, the mean of the two curves for $\epsilon = 0$ and $\epsilon = 0.01$ is plotted, since the differences between the solutions are too small to be indicated. The C_N curve is computed for $\epsilon = 0$. The $\epsilon = 0.01$ curve for C_N almost coincides with C_A. The crosses represent observed measures of relative line strengths for the K line of *Ca* II measured by Houtgast.

COMPARISON OF RESULTS WITH OTHER INVESTIGATIONS

J. Houtgast[1] has interpreted the variations of line profiles across the solar disk by describing $\bar{J}$ in terms of B and the J computed by coherent scattering. Thus, for the wings of lines, $\bar{J} = B$ for those regions where wings of lines are formed, while $\bar{J}$ equals the coherent J_ν in the higher layers. Therefore, he uses pure absorption in computing the wings of lines, employs coherent scattering in computing the line center, and introduces an extinction coefficient (allowing nonconservation of energy) to represent deviations from coherent scattering or pure absorption. Comparing the observations with these computed line profiles, he explains the observations by noting the probable relations between $\bar{J}$, B, and J_ν. No attempt at a quantitative theory is made.

L. Spitzer[3] has solved the transfer equation under the assumption that both $\bar{J}$ and B are linear functions of the depth $\eta_\nu \tau$. The constants were not determined, as the author

considered the remarks exploratory. L. Spitzer[4] obtained dependence of the solution on $\epsilon\eta_0^{1/2}$ from an approximate treatment.

Z. Suemoto[9] has used a five-step function to approximate η_ν in the calculation of $\bar{J}$. The transfer equation is simplified through the use of Eddington's approximate relations between the radiation pressure, flux, and density. A solution of the five simultaneous differential equations for $J(\tau)$ was obtained through the use of the coherent solutions for the line wings in the equation for the line center and through the use of this corrected line-center solution in redetermining $J(\tau)$ in the wings. This procedure was repeated and is said to have converged satisfactorily. The observations of Houtgast for H and K are incorrectly plotted in Figure 6, *a*, of Suemoto's paper. It should be pointed out that, for H and K, Suemoto finds that $C_N(\mu)/C_N(1)$ lies above the curve $C_A(\mu)/C_A(1)$, while in this paper $C_N(\mu)/C_N(1)$ lies slightly below the absorption-curve. Since the use of iterations beginning with $J(\tau)$ should be more slowly convergent than those starting with B, this difference is partially understandable.

D. Labs[8] also uses a step function for η_ν and the Eddington approximate relations in solving the transfer problem. Only a two-step or a three-step function is used. The resulting simultaneous equations are solved directly rather than through iteration. Labs finds that, for $\beta = 4.5$, $J(\tau)$ exceeds $B(\tau)$ for a considerable range of τ and that the difference $\bar{J} - B$ decreases rapidly with ϵ for moderate τ. His figure for $r(\cos\theta)/r(\cos\theta = 1)$ with $\beta = 4.5$ and $i_2/x = 0.1$ is similar to Figure 7. One difficulty in comparing the two solutions is the impossibility of deciding which parameters to use for the step function representing η_ν. In both the Gaussian approximation and the analogous scheme used in the five-point integration formula for $L(y)$, integrals are represented by sums. The moments of these weight functions are finite, and these representations are known to be accurate for polynomials up to a certain order. Since no systematic method of determining the step function representing η_ν has been proposed, it is difficult to relate these solutions of Labs and Suemoto to the exact solution.

G. Münch[7] computed the correction to the coherent solutions by replacing $\bar{J}$ with the corresponding integral for coherent scattering. In this computation, he makes a further approximation, using, for the coherent J_ν, the J_ν computed in the Chandrasekhar two-point approximation. By this procedure, the integral $\bar{J}$ is effectively replaced by B for all τ much larger than η_0^{-1}. Further, Münch uses $\lambda_c = 0.01$ or $\eta_0 \sim 100$, which implies an extremely large damping constant, in order to have reasonable line strengths in the wings of the K line. This is introduced to fit the observed intensity in the line center. Usually it is assumed that this residual intensity in the line center is produced by selective absorption. A comparison of Münch's results with the profiles of Figures 5 and 6 shows that there is good agreement. The profiles of Figures 5 and 6, however, were computed with physically reasonable parameters.

From the principle of invariance, Sobolev[10] obtained a solution for the problem of diffuse noncoherent reflection from a semi-infinite atmosphere. This solution is applied to compute profiles for the D lines of sodium, with $\epsilon = 0$. Since the procedure is extremely complicated and the physical meaning of the mathematical approximations is unclear, it is difficult to understand the meaning of the results.

VARIATION OF ϵ, η_0, AND β

Although the tables have been computed for only two values of ϵ and for $\eta_0 = 4 \times 10^6$, it is possible to estimate, in at least the first approximation, the effect of changes in these parameters. From Table 1, ${}^0G$ can be computed for any ϵ, η_0, β, if one uses

$$ {}^0G(\tau) = \frac{2 \times 10^3 \eta_0^{-1/2} B}{\epsilon + (1-\epsilon)(1+\eta_0)^{-1/2} + 2 \times 10^3 \eta_0^{-1/2}(1-\epsilon)\int_\tau^\infty K_0(u)\,du}, \tag{57} $$

which is correct for $\tau > \eta_0^{-1/2}$. From this expression, $L(y)$ can be computed by any convenient method. A further simplification can be made, when the contribution of the integral in the denominator to $L(y)$ is negligible, in which case

$$L_{\epsilon_1} = L_{\epsilon_2} 2 \times 10^3 \eta_0^{-1/2} \frac{\epsilon_2 + 5 \times 10^{-4}(1-\epsilon_2)}{\epsilon_1 + (1+\eta_0)^{-1/2}(1-\epsilon_1)} . \tag{58}$$

Thus, for $\epsilon = 0$, the solutions are very insensitive to η_0 unless $\eta_0 \sim 1$, in which case the approximations break down. For $\epsilon = 0$, ${}^0G$ will increase approximately one part in 10^7 in going from $\eta_0 = 4 \times 10^6$ to infinite η_0.

For the best fit to the K line of calcium, an η_0 around 4.1×10^8 is indicated, for a damping constant about 6.5 times the natural width. If the damping constant were increased by a factor of about 10, the η_0 used in the previous computations would be valid. As has already been pointed out, a change of this amount in η_0 alters the solutions for $\epsilon = 0$ only for $\tau < 0.0001$. For $\epsilon \neq 0$, the change in η_0 from 4×10^6 to 4×10^8 can be simulated by considering results for $\epsilon = 0.01$ to apply to $\epsilon = 0.001$. This change invalidates none of the conclusions of this paper.

SUMMARY

Noncoherent scattering is a process which is known to occur in the atmosphere of the sun. The solutions of the purely noncoherent scattering equation approach those of the pure absorption equation, provided that $\epsilon\eta_0^{1/2} + (1-\epsilon)(\eta_0/1+\eta_0)^{1/2}$ exceeds 10. For smaller values, measurable deviations from pure absorption are found. The character of these corrections depends strongly on β. Although the agreement with observations is improved, compared to coherent solutions with physically reasonable ϵ, the observations cannot be represented by any choice of the parameters ϵ and η_0 upon which the solutions depend.

I wish to thank Lyman Spitzer, Jr., who suggested this problem, for all his assistance and encouragement. I also wish to express my appreciation for the William Charles Peyton Advanced Fellowship in Astronomy, which I have held for the past year.

ON THE CURVE-OF-GROWTH METHOD

SU-SHU HUANG*
Berkeley Astronomical Department, University of California
Received September 26, 1951

ABSTRACT

In the calculation of the theoretical curve of growth, physical parameters, such as the Doppler velocity, the damping constant, etc., are supposed to be constant for the entire atmosphere. Investigations have therefore been made in this paper to show, in the first place, what is the meaning, if any, of the values determined for such parameters by the curve of growth, when, as a matter of fact, all these parameters vary with depth in real stellar atmospheres; and, second, among many theoretical curves of growth so far computed by various authors, what particular one should be used in order to have the best approximation. For lines formed according to the mechanism of local thermodynamic equilibrium we conclude that the observationally determined value can be regarded as a certain mean value properly weighted according to the formula given by equation (22) in the present paper. And the theoretical curve of growth computed independently by Unsöld and by Menzel is one of the best for practical use. The temperature, the turbulent velocity, and the damping constant in stellar atmospheres derived from the curve of growth are individually discussed in the light of the present analysis. The observationally determined values for these quantities are, on the whole, consistent with the predicted values as given by the proposed averaging formula.

I. INTRODUCTION

The curve-of-growth idea had its origin in H. N. Russell and his associates' classical work[1] on the calibration of the Rowland intensities of the Fraunhofer lines. Since then the method has become one of the most powerful ones employed in astrophysical research.

The other one of the two fundamental principles from which the method of the curve of growth evolved is W. Schütz's theory[2] of the broadening of spectral lines, which combines the Doppler effect with the radiation damping. The first application of Schütz's theory to astronomical spectra was made by A. Unsöld, O. Struve, and C. T. Elvey[3] in a discussion of the intensities of interstellar calcium lines. But M. Minnaert and G. F. W. Mulders[4] and M. Minnaert and C. Slob[5] were the first who gave a comprehensive discussion of the problem and brought the curve-of-growth method to its present form of perfection. Together with A. Pannekoek,[6] they made it directly applicable to stellar spectra.

The later development of the theory was due to many investigators,[7] and we can only refer to some standard source.[8] The theoretical curves of growth which we now use frequently as the standards for comparison were computed by A. Unsöld and by D. H. Menzel.[9] More recently, A. Pannekoek and G. B. van Albada[10] computed a curve of

* John Simon Guggenheim Memorial Foundation Fellow.

[1] H. N. Russell, W. S. Adams, and C. E. Moore, *Ap. J.*, **68**, 1, 1928; W. S. Adams and H. N. Russell, *Ap. J.*, **68**, 9, 1928.

[2] *Zs. f. Ap* , **1**, 300, 1930; *Zs. f. Phys.*, **64**, 682, 1930.

[3] *Zs. f. Ap.*, **1**, 314, 1930.

[4] *Zs. f. Ap.*, **1**, 192, 1930; **2**, 165, 1931.

[5] *Proc. Amsterdam Acad.*, Vol. **34**, No. 4, 1931.

[6] *M.N.*, **91**, 139, 1930.

[7] E.g., C. W. Allen, *Mem. Commonwealth Solar Obs. Canberra*, Vol. **1**, No. 5, 1934.

[8] A. Unsöld, *Physik der Sternatmosphären* (Berlin: J. Springer, 1938). A recent review of the curve-of-growth method can be found also in a paper by B. Bell: *Special Report No. 35* (AMC Contract W19-122ac-17) (1951).

[9] *Ap. J.*, **84**, 462, 1936.

[10] *Pub. Astr. Inst. Amsterdam*, No. 6, Part 2, 1946.

growth based on a series expansion of the solution for the Milne-Eddington model. This was soon superseded by a more elaborate computation by M. H. Wrubel,[11] who used, as the basis of his calculation, S. Chandrasekhar's exact solution[12] for the same model. It is, however, interesting to note that Unsöld's and also Menzel's curves of growth, based on an interpolation formula first introduced by M. Minnaert,[13] still have their special value for actual use, particularly when the ratio of the line absorption to the continuous absorption in stellar atmospheres is known to vary with depth. This is due to the fact that the interpolation formula is true, as a first approximation, in an atmosphere with varying absorption, if we properly interpret the ratio of the line absorption to the continuous absorption as a certain mean value. We shall come to this point in Section II.

In studying interstellar lines, C. Jentzsch and A. Unsöld[14] and later the present author[15] have computed a set of curves of growth for the case of a velocity distribution different from the normal Gaussian one. Although these calculations are limited to the case of absorption without re-emission, the general features of the effect of the velocity distribution on the form of curves of growth is worth noticing.

Important information on the physical nature of stellar atmospheres has been obtained by applying the curve-of-growth method. Besides the original purpose of determining the chemical abundances in stellar atmospheres, two important discoveries were established with the help of this method. First, the collisional damping in dwarf stars was made known to us through the large damping constants observed.[16] Second, through a systematic study of Struve and Elvey,[17] the existence of turbulent motions in certain supergiant stars was discovered. More recently, K. O. Wright's relation[18] between turbulent velocities and excitation potentials has led to a suggestion[19] that turbulent velocity varies with the optical depth. Each time an anomaly in the observed curve of growth was noticed, a new fact about stellar atmospheres was subsequently discovered and the anomaly explained. We may well believe that more facts will still be found in this way.

Despite its power, the curve-of-growth method has its difficulties. In the calculation of the theoretical curve of growth, physical parameters, such as the turbulent velocity, the damping constant, etc., are supposed to be constant for the entire atmosphere. Actually, as is well known, no single physical quantity is constant over a considerable range of depth in stellar atmospheres. The question therefore arises: What is the meaning of the values of physical quantities derived from the curve of growth? Evidently, the values derived must be a sort of mean value, and it is the purpose of the present paper to investigate fully the mathematical averaging process which is consistent with the process involved in the plotting of the curve of growth.

The material presented here is a general presentation of the meaning of the curve-of-growth method for deriving values of physical quantities in stellar atmospheres. Hence the formulae we derived in the previous paper[19] are a first approximation to those presented in Section III of the present paper.

[11] *Ap. J.*, **109**, 66, 1949; **111**, 157, 1950.

[12] S. Chandrasekhar, *Radiative Transfer* (Oxford: Clarendon Press, 1950).

[13] *Zs. f. Ap.*, **10**, 40, 1935.

[14] *Zs. f. Phys.*, **125**, 370, 1948.

[15] *Ap. J.*, **112**, 399, 1950.

[16] M. Minnaert and G. F. W. Mulders, *Zs. f. Ap.*, **2**, 165, 1931; A. Unsöld, *Zs. f. Ap.*, **12**, 56, 1936; B. Strömgren, *Physica*, **12**, 701, 1946.

[17] O. Struve, *Proc. Nat. Acad. Sci.*, **18**, 585, 1932; *Ap. J.*, **79**, 409, 1934.

[18] *J.R.A.S. Canada*, **40**, 183, 1946; **41**, 49, 1947.

[19] A. Unsöld and O. Struve, *Ap. J.*, **110**, 455, 1949; S. S. Huang, *Ap. J.*, **114**, 287, 1951.

II. GENERAL DISCUSSION ON THE CURVE OF GROWTH IN AN ATMOSPHERE WITH ABSORPTION DEPENDING ON DEPTH

As has been mentioned in Section I, none of the theoretical curves of growth computed to date takes into account the variation of the absorption with depth. Actually, all physical parameters in stellar atmospheres and consequently the absorption itself change with the depth. But we use these theoretical curves of growth as a standard of comparison anyway. What, then, is the justification of such a process? In order to clarify this point, it is of importance to investigate first what the theoretical curve of growth will be, if the variation of the ratio of the line absorption to the continuous absorption is taken into account. For this purpose let us consider, as usual, a semi-plane-parallel atmosphere.

Following the standard notation, we define σ_ν as the line-scattering coefficient, l_ν as the line-absorption coefficient, and κ as the continuous absorption coefficient. If τ is the optical depth in the continuum and t the optical depth in the line, we have

$$t = \int_0^\tau \left(1 + \frac{l_\nu + \sigma_\nu}{\kappa}\right) d\tau = \tau + \int_0^\tau N(\tau)\, a_\nu(\tau)\, d\tau, \tag{1}$$

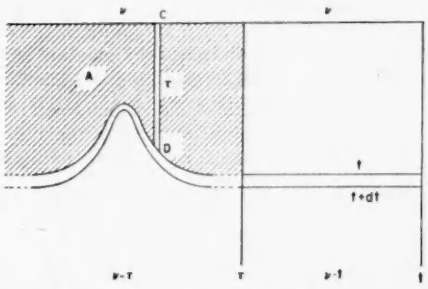

FIG. 1.—The relative dependence on frequency ν of the optical depth t in the line, and of the optical depth of τ in the continuum. The parallel strip in the $\nu - t$ plane transforms into a curved strip in the $\nu - \tau$ plane (shown in the figure). And a parallel strip in the $\nu - \tau$ plane transforms into a curved strip in the $\nu - t$ plane (not shown).

where $a_\nu(\tau)$ stands for the atomic line-absorption coefficient and $N(\tau)$ for the number of effective absorbing atoms per unit optical thickness in the continuum.

Using t as the independent variable (the t-representation), we have the equation of transfer and the formal solution, respectively, as follows:

$$\mu \frac{dI}{dt} = I - J \tag{2}$$

and

$$I_\nu(0, \mu) = \int_0^\infty J(t)\, e^{-t/\mu} \frac{dt}{\mu}. \tag{3}$$

The equation of transfer and the formal solution assume their simplest forms in the t-representation. But all the physical parameters, in a certain approximation, are functions of τ directly (i.e., independent of frequency); as a consequence of equation (1), the same value of τ will correspond to a wide range of values of t, depending on the frequency chosen. Hence t is not a good variable to use to describe the physical nature of a stellar atmosphere. For this latter purpose it is better to use τ as the independent vari-

able (the τ-representation). We can transform the t-representation to the τ-representation or vice versa according to equation (1). Thus Figure 1 shows graphically the transformation between t and τ and its dependence on frequency ν. A parallel strip in the ν-t plane is transformed into a curved strip in the ν-τ plane.

Let ν_0 be the frequency at the center of the line; then at $\nu - \nu_0$ the optical depth τ, which corresponds to a definite value of t, is a function of frequency ν. Further, it is obvious that

$$\lim_{\nu-\nu_0\to\pm\infty} \tau = t \,. \tag{4}$$

Now we consider the emission between the layers t and $t + dt$, regarding temporarily all the other layers as a pure absorbing medium without emission. The difference of emission at a point ν inside the line and at a point in the continuum is

$$[J(t) - J(\tau)]\, dt \,, \tag{5}$$

where t and τ are related by equation (1). The amount of radiation removed from the emergent continuous background between ν and $\nu + d\nu$ due to the existence of the absorption line is therefore

$$[J(t) - J(\tau)]\, e^{-t/\mu} \frac{dt}{\mu}\, d\nu \,, \tag{6}$$

because the total optical depth is t at any frequency whether in the line or in the continuum. Summing over the emission of all layers in the atmosphere, we find the contribution to the equivalent width dW_μ between ν and $\nu + d\nu$ derived from intensity observations in the direction μ to be

$$dW_\mu = d\nu \frac{\int_0^\infty [J(t) - J(\tau)]\, e^{-t/\mu}(dt/\mu)}{\int_0^\infty J(t)\, e^{-t/\mu}(dt/\mu)} \,. \tag{7}$$

Also, the differential equivalent width dW_f derived from flux observations is

$$dW_f = d\nu \frac{\int_0^1 \mu\, d\mu \int_0^\infty [J(t) - J(\tau)]\, e^{-t/\mu}(dt/\mu)}{\int_0^1 \mu\, d\mu \int_0^\infty J(t)\, e^{-t/\mu}(dt/\mu)} \,. \tag{8}$$

Hereafter we shall follow the idea of local thermodynamical equilibrium and set, as usual,

$$J(\tau) = a + b\tau \,. \tag{9}$$

Equations (1) and (9) combine to give

$$J(t) - J(\tau) = b \int_0^\tau N a_\nu d\tau = b\tau \overline{N a_\nu}(\tau) \,. \tag{10}$$

Hence $\overline{N a_\nu}(\tau)$ is evidently the average value of $N(\tau)a_\nu(\tau)$ over a thickness τ of the uppermost layers in the atmosphere. With this definition, equation (1) can be written as

$$\tau = \frac{t}{1 + \overline{N a_\nu}(\tau)} \,. \tag{11}$$

From equations (7), (9), and (10) we can write the equivalent width,

$$W_\mu = \frac{b}{a + b\mu} \int_{-\infty}^\infty d\nu \int_0^\infty e^{-t/\mu} \frac{dt}{\mu} \int_0^\tau N(\tau)\, a_\nu(\tau)\, d\tau \,. \tag{12}$$

If we exchange the order of integration over t and over τ, equation (12) reduces to the following form:

$$W_\mu = \frac{b}{a+b\mu}\int_{-\infty}^{\infty} d\nu \int_0^{\infty} N(\tau)\, a_\nu(\tau) \exp\left\{-\frac{1}{\mu}\left[\tau + \int_0^{\tau} N(\tau)\, a_\nu(\tau)\, d\tau\right]\right\} d\tau . \quad (13)$$

After carrying out the integration over μ, we have

$$W_f = \frac{6b}{3a+2b}\int_{-\infty}^{\infty} d\nu \int_0^{\infty} N(\tau)\, a_\nu(\tau) E_3\left[\tau + \int_0^{\tau} N(\tau)\, a_\nu(\tau)\, d\tau\right] d\tau , \quad (14)$$

where E_3 is the usual exponential integral of index 3.

Equation (12) may also be written, as a consequence of equations (10) and (11), in the form

$$W_\mu = \frac{b}{a+b\mu}\int_{-\infty}^{\infty} d\nu \int_0^{\infty} \frac{\overline{Na_\nu}(\tau)}{1+\overline{Na_\nu}(\tau)}\, t e^{-t/\mu}\frac{dt}{\mu} . \quad (15)$$

If Na_ν were independent of τ, we would have, simply,

$$W_\mu = \frac{b\mu}{a+b\mu}\int_{-\infty}^{\infty} \frac{Na_\nu}{1+Na_\nu}\, d\nu . \quad (16)$$

Equation (16) gives the formula on which Unsöld and Menzel based their calculations of the theoretical curve of growth. Even when Na_ν is a function of τ, $\overline{Na_\nu}(\tau)/[1+\overline{Na_\nu}(\tau)]$ is a slowly varying function of t as compared with $te^{-t/\mu}$, and we can therefore find a mean value of t—call it $\bar{t}$—such that

$$\bar{t} = \frac{\int_0^{\infty} t^2 e^{-t/\mu}(dt/\mu)}{\int_0^{\infty} t e^{-t/\mu}(dt/\mu)} = 2\mu , \quad (17)$$

and substitute $\bar{t}$ for t in $\overline{Na_\nu}(\tau)$. Hence we have

$$W_\mu = \frac{b\mu}{a+b\mu}\int_{-\infty}^{\infty} d\nu \frac{\overline{Na_\nu}(\tau')}{1+\overline{Na_\nu}(\tau')} , \quad (18)$$

where τ' is given by

$$\tau' = \frac{2\mu}{1+\overline{Na_\nu}(\tau')} . \quad (19)$$

Equation (18) is in a form similar to equation (16), only with the averaged quantity $\overline{Na_\nu}(\tau')$ replacing the constant quantity Na_ν. This shows that the curve of growth based upon equation (16) can be used even for an atmosphere with varying absorption, and thus proves our statement in Section I. It is also evident that the value derived by the curve-of-growth method for the physical parameter will be, within the approximation introduced here, a certain mean value over the depth τ'. For a given function Na_ν of τ, a curve of growth can be computed easily according to equation (18).

The same argument and reduction can, of course, be carried out for W_f.

III. THE AVERAGING PROCESS FOR PHYSICAL VARIABLES

Now we can consider the meaning of physical quantities as derived from the curve of growth. Following the methods presented in Section II, we assume, for the time being, that the emission occurs only in layers between t and $t+dt$, while the rest of the atmosphere does not emit but does absorb. Under this assumption a spectral line would

be formed because of the absorption between the layers $t = 0$ and $t = t$, and this line would therefore bear the mark which characterizes the physical properties between these layers. In the τ-representation this layer is the shaded area A in Figure 1. Now let $X(\tau, \mu)$ be a physical parameter, such as turbulent velocity, the mean value of which can be determined by the curve-of-growth method. The average value of X over the column CD at frequency ν as shown in Figure 1 will be

$$\langle X(\tau, \mu) \rangle_{\tau(\nu)} = \frac{\int_0^{\tau(\nu)} X(\tau, \mu) N(\tau) d\tau}{\int_0^{\tau(\nu)} N(\tau) d\tau}. \tag{20}$$

In order to distinguish the running index τ and the τ given by equation (1), the latter has been denoted by $\tau(\nu)$ in equation (20). The value $\langle X(\tau, \mu) \rangle_{\tau(\nu)}$ should further be averaged over ν, because we consider the total absorption of a line, and also over t, because every layer in the atmosphere emits radiation which is absorbed by the overlying layers. Because we are concerned with the equivalent widths, the weighting factor should be the amount of radiation intensity depleted from the continuous background at different frequency ν and at different depth t. This is evidently the expression given by equation (6). If we consider the flux, the corresponding weight factor is

$$[J(t) - J(\tau)] e^{-t/\mu} dt d\nu d\mu . \tag{21}$$

Hence the value of X derived from a curve of growth will be

$$\langle X(\tau, \mu) \rangle_{\tau(\nu), \nu, t} = \frac{\int_0^\infty e^{-t/\mu} (dt/\mu) \int_{-\infty}^\infty [\overline{N a_\nu}(\tau_\nu) / \bar{N}(\tau_\nu)] d\nu \int_0^{\tau_\nu} N(\tau) X(\tau, \mu) d\tau}{\int_0^\infty e^{-t/\mu} (dt/\mu) \int_{-\infty}^\infty [\overline{N a_\nu}(\tau_\nu) / \bar{N}(\tau_\nu)] d\nu \int_0^{\tau_\nu} N(\tau) d\tau}, \tag{22}$$

where $\bar{N}(\tau_\nu)$ is defined as $(1/\tau_\nu) \int_0^{\tau_\nu} N(\tau) d\tau$.

In order to make the integrations involved in equation (22) manageable, we introduce an approximation for τ_ν as follows:

$$\tau_\nu = \frac{t}{1 + m\overline{N a_0}} = \frac{t}{1 + \beta} \equiv \tau_0 , \qquad \text{with} \qquad \beta = m\overline{N a_0} , \tag{23}$$

where a_0 represents the central atomic absorption coefficient. Hence τ_0 is no longer a function of ν. We shall discuss this approximation in a more detailed way at the end of the present section. As in most cases $\int_{-\infty}^\infty a_\nu d\nu$ is an atomic constant independent of the macroscopic properties of the absorbing medium, the approximation (23) reduces equation (22) to the following simplified form:

$$\langle X(\tau, \mu) \rangle_{\tau(\nu), \nu, t} = \frac{\int_0^\infty e^{-t/\mu} (dt/\mu) \int_0^{\tau_0} N(\tau) X(\tau, \mu) d\tau}{\int_0^\infty e^{-t/\mu} (dt/\mu) \int_0^{\tau_0} N(\tau) d\tau}. \tag{24}$$

The expression for the value of $X(\tau, \mu)$ derived from an analysis of the flux, i.e., $\langle X(\tau, \mu) \rangle_{\tau(\nu), \nu, t, \mu}$ is simply a further integration over μ in the numerator as well as

in the denominator after both are multiplied by a factor $\mu d\mu$. If we now introduce the approximation

$$\int_0^\infty e^{-x} f(x)\, dx = f(1),$$

equation (24) and the corresponding equation for $\langle X(\tau, \mu)\rangle_{\tau(\nu), \nu, t, \mu}$ reduce to the forms given previously (eqs. [18] and [19] of the paper[19] cited).

As the variation of $1/(1+\beta)$ with t in equation (23) is not so important as that of t itself, we may neglect altogether the dependence of β on t in equation (23), to simplify the expression.[20] Thus equation (24) reduces to

$$\langle X(\tau, \mu)\rangle_{\tau(\nu), \nu, t} = \frac{\int_0^\infty N(\tau)\, X(\tau, \mu)\, e^{-(1+\beta)\tau/\mu} d\tau}{\int_0^\infty N(\tau)\, e^{-(1+\beta)\tau/\mu} d\tau}, \tag{25}$$

after we have interchanged the order of integration and effected the integration over t. In most cases $X(\tau)$ is not a function of μ; hence it is easy to show that

$$\langle X(\tau)\rangle_{\tau(\nu), \nu, t, \mu} = \frac{\int_0^\infty N(\tau)\, X(\tau) E_3([1+\beta]\tau)\, d\tau}{\int_0^\infty N(\tau) E_3([1+\beta]\tau)\, d\tau}. \tag{26}$$

Integrals of the form which occurs in equations (25) and (26) can be most conveniently evaluated by the Gaussian quadrature formula.[21] Thus

$$\langle X(\tau, \mu)\rangle_{\tau(\nu), \nu, t} = \frac{\sum_{j=1}^{m} a_j N\left(\frac{\mu x_j}{1+\beta}\right) X\left(\frac{\mu x_j}{1+\beta}, \mu\right)}{\sum_{j=1}^{m} a_j N\left(\frac{\mu x_j}{1+\beta}\right)}, \tag{27}$$

where the x_j's are the zero of the Laguerre polynomials and the a_j's the corresponding Christoffel numbers. As a first approximation we have

$$\langle X(\tau, \mu)\rangle_{\tau(\nu), \nu, t} = X\left(\frac{\mu}{1+\beta}, \mu\right), \tag{28}$$

which does not depend on $N(\tau)$.

Now we are going to discuss the approximation introduced into equation (23). Consider the integral

$$I = \int_{-\infty}^{\infty} \frac{\overline{N a_\nu}(\tau_\nu)}{\bar{N}(\tau_\nu)}\, d\nu \int_0^{\tau_\nu} X(\tau, \mu)\, N(\tau)\, d\tau. \tag{29}$$

[20] This assumption, which may not be good for certain lines such as those involving very high levels, is introduced only to simplify the calculation and is obviously not a necessary condition to the validity of the theory so far formulated. Calculations which take care of the dependence of β on τ can be carried out, but it seems to us that such elaborate calculations (which will eventually introduce more adjustable parameters) may not be necessary, because, owing to observational difficulties and uncertainties, the curve-of-growth method involves certain intrinsic approximations of a statistical nature. A compromise for the matching with depths of the $\overline{Na_0}$'s which are responsible for the formation of different lines has therefore been adopted here.

[21] A. Reiz, *Ark. f. mat. astr. o. fys.*, Vol. **29A**, No. 29, 1943. Further references can be found in this paper.

So far as the linear branch and the flat branch of the curve of growth are concerned, it is necessary only to investigate the Doppler core. Thus

$$\frac{\overline{N a_\nu}(\tau)}{N(\tau)} = \frac{C}{\Delta\nu_D(\tau)} \exp\left[-\left(\frac{\nu-\nu_0}{\Delta\nu_D}\right)^2\right], \tag{30}$$

where $\Delta\nu_D$ is the Doppler width and C may be regarded as constant. Substitute equation (30) in equation (29) and change the variable from ν to y,

$$y = \frac{\nu-\nu_0}{\Delta\nu_D}, \qquad \tau(\nu) = \tau(y), \tag{31}$$

and we have

$$\begin{aligned} I &= C\int_{-\infty}^{\infty} e^{-y^2} dy \int_0^{\tau(y)} X(\tau, \mu) N(\tau) d\tau \\ &= C\sum_{j=1}^{m} p_j \int_0^{\tau(y_j)} X(\tau, \mu) N(\tau) d\tau, \end{aligned} \tag{32}$$

where y_j is the zero of the Hermite polynomial and p_j its corresponding Christoffel number.[21] For the second approximation we have

$$y_1 = -y_2 = 0.7071, \qquad p_j = 0.5, \qquad j = 1, 2,$$

and τ is a symmetrical function of y; hence

$$I = C\int_0^{\tau(0.7071)} X(\tau, \mu) N(\tau) d\tau,$$

where

$$\tau(0.7071) = \frac{t}{1+0.606\overline{N a_0}[\tau(0.7071)]}. \tag{33}$$

Comparing equation (33) with equation (23), we obtain

$$m = 0.606.$$

If damping is included, the previous argument fails. The weight of the averaging process gradually goes toward the wing as N increases. Hence m in equation (23) is no longer a constant but decreases as N increases. The variation of m more or less compensates for the variation of N, and we may therefore regard β as practically constant for the damping branch of the curve of growth.

We have seen that the physical quantities derived from the curve of growth depend on the number of effective absorbing atoms, the absorption coefficient, and the manner in which they vary with depth. Hence no two lines will give exactly the same value of the physical quantities, because the domain of averaging involved and its weighting factor are not strictly the same for any two lines. This is one of the reasons why the points in the observed curve of growth always show scatter. But, on the other hand, the domains mostly overlap; so we can still find a general regularity among the scattered points. This makes the curve-of-growth method applicable to stellar spectra.

In the following sections we shall consider separately the turbulent velocity, the temperature, and the damping constant, as derived from observations in comparison with those derived from the present theory.

IV. THE TURBULENT VELOCITIES

Soon after the relation between the turbulent velocities and the excitation potential had been discovered by Wright,[18] Unsöld and Struve[19] suggested the idea of the variation

of turbulent velocities with depth as a possible explanation. Developing their idea into a quantitative form, the present author[19] suggested an exponential relation between the turbulent velocity v of the small eddies[22] and the optical depth τ as follows:

$$v = v_0 e^{-a\tau} . \tag{34}$$

The calculated result of the velocity-excitation (v-χ) relation based on equation (34) agrees very well with Wright's observed results for all supergiant stars. Hence we may well believe equation (34) gives a good description of the state of turbulence in the atmospheres of supergiant stars.

In presenting this section we have two purposes in mind. First, it is necessary to recalculate the v-χ relation from assumption (34) with the refined theory presented in Section III, and thus to redetermine the values of v_0 and a for those stars which have been investigated by Wright. The second purpose is to present our results in a suitable form so that they can be used directly as a standard for comparison with the observational v-χ curves yet to be obtained.

Consider, now, the square of the velocity,

$$X(\tau) = v^2 = v_0^2 e^{-2a\tau} . \tag{35}$$

If $X(\tau)$ varies exponentially, the variation of $N(\tau)$ can be neglected in averaging the integrals. In fact, for neutral *Fe* atoms in any excited state there is a wide range of τ over which $N(\tau)$ does not vary much.[23] It therefore follows from equation (25) for intensity observations and from a corresponding equation for flux observations that

$$\frac{\langle v^2 \rangle_{\tau(\nu),\nu,l}}{v_0^2} = \frac{1}{1+\lambda\mu} , \tag{36}$$

and

$$\frac{\langle v^2 \rangle_{\tau(\nu),\nu,l,\mu}}{v_0^2} = 3\left[\frac{1}{2}\frac{1}{\lambda} - \frac{1}{\lambda^2} + \frac{1}{\lambda^3}\ln(1+\lambda)\right] = f(\lambda) , \qquad \text{say} , \tag{37}$$

where

$$\lambda = \frac{2a}{1+\beta} . \tag{38}$$

For small λ,

$$f(\lambda) = 1 - \tfrac{3}{4}\lambda + \tfrac{3}{5}\lambda^2 + O(\lambda^3) . \tag{39}$$

From equation (23), the definition of β, we have

$$\log \beta = \log \beta_0 - \theta\chi , \tag{40}[24]$$

where

$$\beta_0 = m\overline{N_0 a_0}\,\frac{g_i}{u} f \qquad \text{and} \qquad \theta = \frac{5040}{T} ,$$

where u is the partition function, and χ is expressed in units of electron volts. Considering a definite species of atoms at a definite stage of ionization, we now divide the spectral lines into groups according to the excitation potential of the lower level. And if each group consists of a sufficient number of lines, $\log \bar{\beta}_0$ can be regarded as constant for all the groups. (Differences of β_0 are due to the different gf-values of each line and to the

[22] E.g., S. S. Huang, *Ap. J.*, **112**, 418, 1950.

[23] P. ten Bruggencate and J. Houtgast, *Zs. f. Ap.*, **20**, 149, 1940.

[24] In this paper we shall consistently use ln x to denote the natural logarithm of x and log x to denote the common logarithm of x.

continuous opacity at the point where that line is located. We shall discuss this in a more detailed way at the end of the section.) Now plot v against $\log \beta$ for a definite value of a according to equations (37) and (38). By translating this single curve along the $\log \beta$ axis we obtain a family of curves which are the v-$\theta\chi$ relations for different values of $\log \beta_0$. In Figure 2 we have plotted (v/v_0)-$\log \beta$ curves for different values of a.

Given an observed v-χ relation, we can first determine a in the following way: $f(\lambda)$, as defined by equation (37), is monotonically decreasing for the relevant domain of $\lambda \geqq 0$; and, for a given a, λ takes the highest possible value when $\beta = 0$, i.e., $\lambda = 2a$. Hence $f(2a)$ is the lowest possible value of v^2/v_0^2 for a given value of a. Estimate values for v_0 and for the lowest value v_1 from the observed result; then

$$\frac{v_1^2}{v_0^2} = f(2a) \tag{41}$$

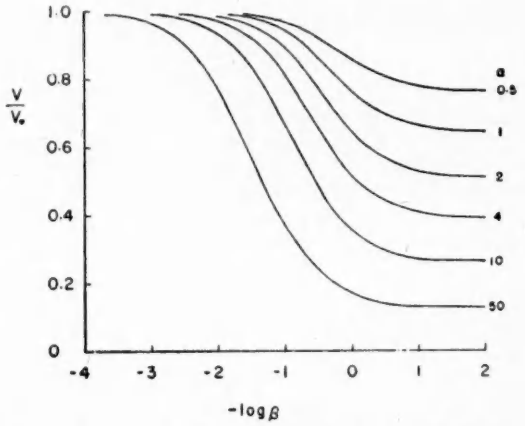

FIG. 2.—The relations between the velocity v measured in the curve of growth and the abundance of absorbing atoms for different values of a.

will determine a. We say "estimate v_0 and v_1" because the observed points will always be scattered and a smooth curve to represent these points should first be drawn in order to get values for v_1 and for v_0. After a is determined, a theoretical v-$\log \beta$ curve for this particular value of a can be obtained either by interpolation in Figure 2 or by direct calculation according to equations (37) and (38). Next plot the observed results in a (v/v_0)-$\theta\chi$ curve in the same scale as that in Figure 2. Slide the observed curve onto the theoretical curve along the abscissa, i.e., $\log \beta$ axis, in order to find a best fit with the theoretical curve for that particular value of a. If the agreement is not good, we can try another set of values of v_0 and of v_1 and repeat the process until a good agreement between the observed and the theoretical curves is obtained. The relative shift along the $\log \beta$ axis between the theoretical and the observed curves will be $\log \bar{\beta}_0$. The method and the procedure are, therefore, very much like the curve-of-growth method itself.

It should be noticed that this simplified procedure becomes possible only when we omit in the averaging integrals the variation of the factor $e^{-\chi/kT(\tau)}$ in $N(\tau)$. Otherwise, $\langle v^2 \rangle_{\tau(\nu),\, \nu,\, t,\, \mu}$ will be a function not only of β but also explicitly of χ, and the invariant property of the relation (v/v_0)-$\log \beta$ under translations parallel to the $\log \beta$ axis will be lost.

We can now compare Wright's results with the present calculation by the procedure just described. The theoretical curve, the observed points, and the values of a and v_0 thus determined for each star are all shown in Figure 3. The agreement between the calculation and the observation is very good, as before. The value a derived from the present analysis differs appreciably from the previous approximate determination, because here we not only have made a better approximation in the calculation than that in the previous paper but also have taken into account the individual temperature for each star concerned. It is interesting to note, however, that, whether in a first approximation, as in the previous paper, or in a better approximation presented here, the calculated curves always give the same form for the v-χ relation. This is due to the fact that the form of the calculated curve is intrinsically related to assumption (34).

Before leaving this section we should like to discuss the effect of the continuous absorption on the final results, such as v-χ curves, etc. The continuous opacity r enters into our discussion in equation (1). Hence $N(\tau)$ as defined there and consequently β_0 as defined by equation (40) involve a factor $1/r$, which has the same effect on β_0 as that of the gf-value of the line. Now if we have lines scattered along a wide range of frequencies in each subgroup, $\bar{\beta}_0$ will be constant for all such subgroups, and no question will arise. But if, owing to the limitation of circumstances, we must select lines for each subgroup in a certain narrow range of spectrum where $1/r$ is consistently higher or lower than the average, then a correction for the variation of $\log \bar{\beta}_0$ for each subgroup becomes necessary. The correction will be small, because $\log \bar{\beta}_0$, instead of $\bar{\beta}_0$ itself, is involved here. Moreover, no correction will be required for the determined velocities, as can easily be seen from our formulation. Hence, by taking into account the continuous opacity, we shall not alter the v-$\theta\chi$ relation in an appreciable way.

V. THE EXCITATION TEMPERATURE

In an atmosphere in radiative equilibrium the radiation temperature has been investigated very thoroughly, and its variation with optical depth τ can be represented by the well-known formula

$$T^4 = \tfrac{3}{4} T_e^4 [\tau + q(\tau)], \tag{42}$$

where $q(\tau)$ has been given numerically.[12] As we are concerned with temperature radiation, the gas temperature and consequently the excitation temperature at each layer in the atmosphere should be the same as that given by equation (42). Therefore, the temperature as determined from the curve of growth is a certain average of T given by equation (42) over the domain as implied in the integrals in equation (25). With $X(\tau) = T(\tau)$, the first approximation of the Gaussian quadrature for equation (25) is simply

$$\langle T(\tau) \rangle_{\tau(\nu),\nu,t} = T_e \left(\tfrac{3}{4}\right)^{1/4} \left[\frac{\mu}{1+\beta} + q\left(\frac{\mu}{1+\beta}\right)\right]^{1/4}. \tag{43}$$

The second approximation can be correspondingly written out. We have computed $\langle T(\tau) \rangle_{\tau(\nu),\nu,t}$ for five cases: $\beta = 0$, 1, 4, 9, and ∞; and we have plotted the results in Figure 4, with $T_e = 5700°$ K. For the cases $\beta = 0$ and $\beta = 1$ the second approximation to the quadrature formula is used, while the others are computed from the first approximation (43). The variation of $N(\tau)$ required in the second approximation has been given by P. ten Bruggencate and J. Houtgast[23] for neutral iron atoms. An average excitation potential, 2.4 eV of the two multiplets which ten Bruggencate and Houtgast[23] used for determining the variation of tempteratures with μ in the solar disk, has been used in this calculation. The three observed points in Figure 4 are also taken from their paper. The calculation predicts that the observed points should lie in an area bounded by the T-μ curves for $\beta = 0$ and for $\beta \to \infty$ and a straight line $\mu = 1$. Hence the

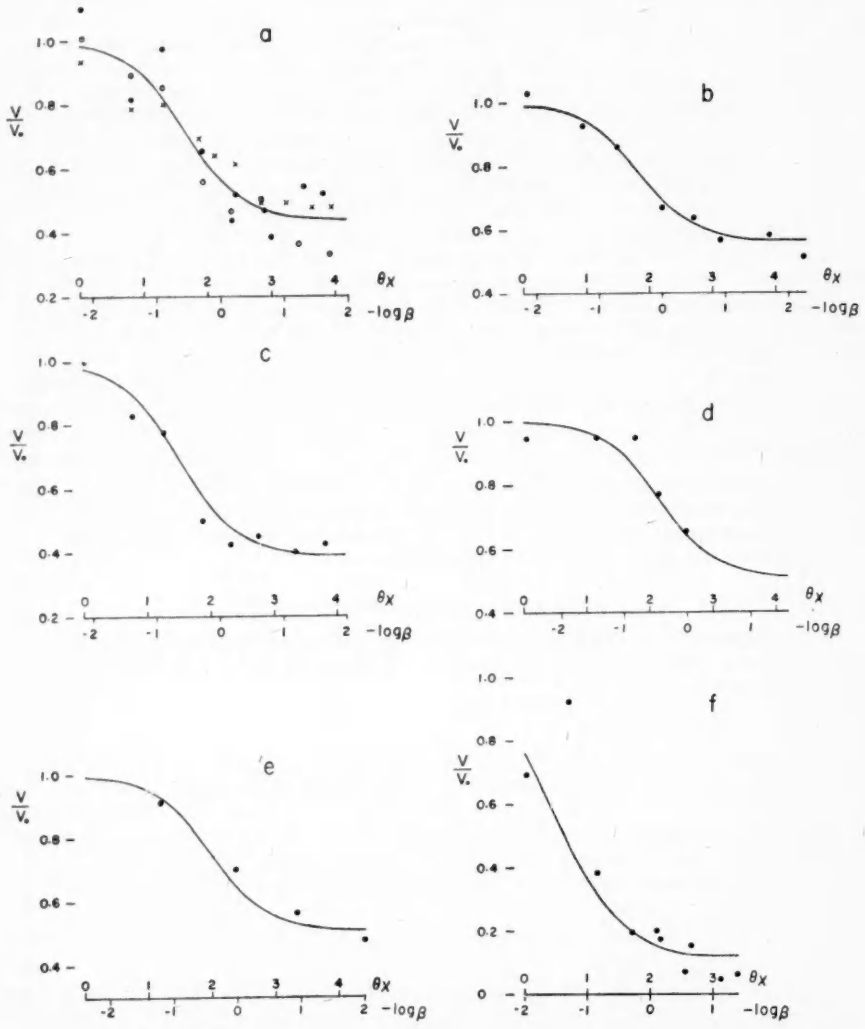

FIG. 3.—Comparison of the theoretical curve with observations. The theoretical curve is of the same nature as those illustrated in Figure 2, but has been translated along the $\theta\chi$ axis until it fits into the observed points. Curve *a*: α Persei, $v_0 = 7.5$, $\alpha = 3$; curve *b*: γ Cygni, $v_0 = 7.8$, $\alpha = 1.5$; curve *c*: α Canis Minoris, $v_0 = 4.0$, $\alpha = 4$; curve *d*: α Carinae, $v_0 = 3.5$, $\alpha = 2$; curve *e*: δ Canis Majoris, $v_0 = 9.0$, $\alpha = 2$; curve *f*: ϵ Aurigae, $v_0 = 24$, $\alpha = 50$. The observed points are due to Wright. Dr. Struve pointed out that the high-dispersion spectrograms of α Canis Minoris show a much smaller turbulent velocity than those used here. The determination of the constants v_0 and α for this star is therefore only tentative.

agreement is only fair—but well within the empirical errors—because enough spectral lines were not used in plotting the curve of growth from which the temperature was determined.

Next we consider the temperature as derived from the flux observations. For the two extreme cases of $\beta = 0$ and $\beta \to \infty$, we computed $\langle T \rangle_{\tau(\nu),\nu,t,\mu}$ by numerical integration over μ. Plotting T/T_e againt T_e, we obtain two straight lines, as shown in Figure 5. Evidently, all observed points should lie between these two straight lines, for they are the two limiting cases. Now let us examine the results of the observations: Wright found that different values for the excitation temperature are obtained for each star according to whether or not the effect of the velocity variation with the excitation potential was taken into account. When we plot Wright's results[25] derived from the assumption of varying velocities in Figure 5, they nearly all fall in between the parallel strips (bounded by two parallel lines $T/T_e = 0.968$ and $T/T_e = 0.810$), as we predicted. These points are denoted in the figure by circles, with the attached vertical lines representing the probable error of the determined temperature, also given by Wright. But if we plot the excitation temperature derived from the assumption of constant velocity, the observed

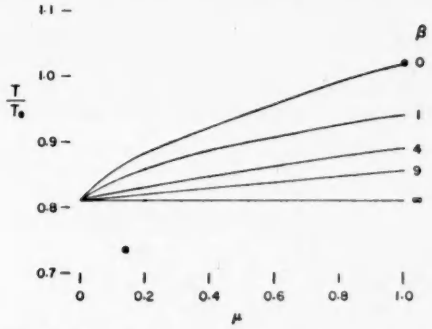

FIG. 4.—The center-limb variation of the temperature T, determined by the curve-of-growth method for different values of β. We expect the observed points to be lying in the area between two curves $\beta = 0$ and $\beta \to \infty$. The three observed points are due to ten Bruggencate and Houtgast.

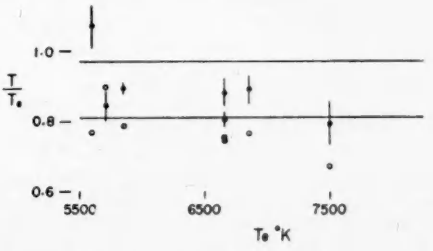

FIG. 5.—The temperature, as derived from the flux observation. According to the calculation, the region where observed points should be found is the parallel strip in the figure. The observed temperature given in the figure consists of two sets of different determinations (the black dot and the circle) using the same observed material. The black dot is obtained when the variation of turbulent velocity with excitation potential has been taken into account, while the circle is obtained when no such variation is allowed. The line attached to each black dot represents the amount of probable error occurring in the determination. All these determinations are due to Wright.

[25] *J.R.A.S. Canada*, **41**, 49, Table 4, 1947.

points will be well below the smallest possible value, i.e., the surface temperature. These are represented by the black dots in Figure 5. Their values are taken from the same table of Wright.[25] Evidently, the excitation temperature cannot be below the surface temperature. This gives us another independent proof of the correctness of the conclusion that we drew in equation (34) about the variation of turbulent velocities with optical depth.

VI. THE DAMPING CONSTANT

We shall conclude the present paper by considering the variation of the damping constant across the solar disk. Unlike the case of the temperature, we are not going to investigate the absolute value of the damping constant. Instead, only the relative values observed in different directions μ from the solar surface will be discussed. Now we have, for the damping constant γ_e due to electron collisions,[8]

$$\gamma_e = \gamma_{e0} T^{-5/6} P_e \,, \tag{44}$$

and, for the damping constant γ_H due to collisions with hydrogen atoms,

$$\gamma_H = \gamma_{H0} T^{-7/10} P_g \,, \tag{45}$$

where P_e is the electron pressure and P_g should be the partial pressure of hydrogen atoms. As hydrogen atoms are the dominant constituent in the solar atmosphere, we may take P_g as the total gas pressure. Finally, γ_{e0} and γ_{H0} are two constants which are independent of the macroscopic nature of the absorbing medium.

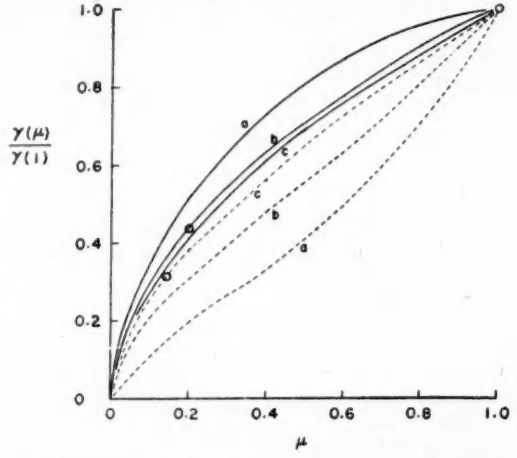

FIG. 6.—The center-limb variation of the damping constant. The full-line (*dotted*) curves represent the variation of damping constant if the latter is caused by collisions with hydrogen atoms (electrons). The three observed points shown in the figure are due to ten Bruggencate and Houtgast. Curve *a*: $\beta = 0$; curve *b*: $\beta = 1$; curve *c*: $\beta = 4$.

Using the first approximation (28), we have computed the relative values of γ_e and of γ_H at different μ's for different values of $\beta(\beta = 0, 1, \text{and } 4)$. In the course of the computation, use has been made of G. Münch's revised table[26] on the model solar atmosphere formerly calculated by B. Strömgren.[27] We have adopted $\log A = 3.8$, where A

[26] *Ap. J.*, **106**, 217, 1947.

[27] *Pub. mind. med. Kobenhavns Obs.*, No. 138, 1944.

represents, as usual, the ratio of the number of both the neutral and the ionized hydrogen atoms to the corresponding number for all metals taken together. It is quite evident that the following results will not change much if other values are adopted for log A. The computed results are plotted in Figure 6. The full-line curves represent the variation of γ_H across the disk and the dotted curves that of γ_e. Three observed points obtained by ten Bruggencate and Houtgast[23] are also shown in the figure. It may be noticed that, no matter what values β assumes, the computed curve for γ_H does not change much. And, moreover, the three observed points lie on or very near these curves. Hence the variation of damping constants can be fully accounted for by the present calculation. At the same time, it seems to indicate that the damping is mainly due to the collision of hydrogen atoms.

At this point we may raise the following question: Using the same number of spectral lines, why did ten Bruggencate and Houtgast obtain a better determination of the damping constant than of the temperature? The answer lies in the fact that, for the damping branch, β, as mentioned in Section III, is practically a constant for different lines. Hence a few lines are enough to make a good determination. Another important fact is that the determination of the damping constant (as well as of the turbulent velocities) from the curve of growth is a direct one, while the temperature is indirectly determined through the numbers of the effective absorbing atoms at two stages of excitation. As the number of effective absorbing atoms varies with depth, the temperature determined from the curve of growth does not have such a clear-cut meaning as those of the turbulent velocity and of the damping constant.

I wish to express my obligation and cordial thanks to Professor O. Struve, who has encouraged and helped me in various ways and who has read the manuscript of this paper. My thanks are also due to Mr. D. E. Osterbrock for profitable discussions he and I had when we both were at the Yerkes Observatory.

SUPERTHERMIC PHENOMENA IN STELLAR ATMOSPHERES

VII. COLLISIONAL EXCITATION FROM LEVELS OTHER THAN THE LOWEST*

SATOSHI MATSUSHIMA
University of Utah
Received October 19, 1951

ABSTRACT

The effect on the chromospheric b_n values of collisional excitation from other than the ground level is computed. The principal effect occurs in b_1 and b_2. The collisional terms place an upper limit on b_2 over the case where radiative terms only were included. The resulting prediction on the population of the Balmer ground state agrees well with the value inferred from eclipse observations.

In the second and third papers of this series[1, 2] the departure from thermodynamic equilibrium in an idealized hydrogen chromosphere is treated. The chromosphere was considered to be illuminated by a radiation field of intensity $I(\nu)$ and characterized by a kinetic temperature $T_r < T_e$, where T_r is a reference temperature approximating the continuum of the radiation field $I(\nu)$. Detailed numerical calculations were carried out for the case $T_e = 35{,}000°$, $T_r = 6000°$; and approximate calculations for several other T_e and N_e values.

While collisional excitations may be predominantly important in the case of high kinetic temperature, the values of collisional cross-sections for relatively low energies seem to be rather obscure in the literature. In Paper II, Thomas has included only the collisional transitions from the ground level by adopting the Born first-order approximation for relative cross-sections and using some empirical formulae derived from experimental data on ionization cross-sections. One might question the error introduced by this approximation. Giovanelli has carried out similar computations,[3] wherein collisional excitation from states other than the lowest were included, but he dropped from the equations of statistically steady state all states higher than the third. A further difference between Thomas' and Giovanelli's work lies in Thomas' ignoring of the azimuthal splitting. Even with these differences, however, the gross results of the two sets of calculations were very similar.

It is of some interest to investigate the details of the error arising from Thomas' neglect of collisional excitation from states other than the ground while he yet retained all energy levels. As Thomas has pointed out,[2] and as Giovanelli's further calculations show,[4] the central intensity of $H\alpha$ depends directly on these collisional terms. Hence it is important to have the details of the problem as clear as possible, even though we may not have available the exact collision cross-sections.

In the present paper we shall recompute the problem, including all these collisional effects. Because the $2S$ state is not, as Giovanelli assumed, metastable, the azimuthal splitting does not seem critical. Hence we neglect it. We shall follow the general method applied in Papers II and III. For the collision cross-sections for various transitions from

* Work supported in part by the University of Utah Research Fund and in part by Air Research and Development Contract AF 33-038-20067.

[1] *Ap. J.*, **108**, 142, 1948; hereafter called "Paper II."

[2] *Ap. J.*, **109**, 480, 1949; hereafter called "Paper III."

[3] *Australian J. Sci. Res.*, **1**, 275, 289, 1948.

[4] *M.N.*, **109**, 298, 1949.

levels higher than the first, we assume them proportional to the corresponding optical transition probabilities. We shall consider shortly a comparison of this assumption to that introduced by Giovanelli.

a) FORMULATION OF EQUATIONS

We adopt the notation used in Paper II except for a few conventional constant terms which become obviously distinguishable. For spontaneous and radiation-induced transitions, no alteration is needed for the equations given in Paper II, namely, equations (1)-(12).

We rewrite equation (11*a*) in Paper II, which gives the number of collisions per second per cubic centimeter which raise the atoms from level n to n'', in the form:

$$C_{nn''}=\frac{4\pi^2 a_0^2}{m^2} N_i N_e^2 \left(\frac{h}{2\pi kT_e}\right)^3 b_n\left(1-\frac{b_{n''}}{b_n}\right)\varpi_n \ (\exp X_n) \int_E^\infty EQ_{nn''} \exp\left(-\frac{E}{kT_e}\right)dE \qquad (1)$$
$$(n''>n>n').$$

We proceed to consider the cross-sections $Q_{nn''}$. Giovanelli has suggested that an assumption setting the value of $Q_{nn''}$ proportional to the corresponding transition probabilities, $B_{nn''}$, is valid for collisions by electrons whose energies are slightly above the corresponding excitation potential.[3] He further assumed that, for high-energy electrons, the value of $Q_{nn''}$ varies as $E^{-1/2}$ and derived the general expression for $Q_{nn''}$ as a function of E. The integration in equation (1) was approximated by separating into two cases, $1 \ll E/kT_e$ and $E/kT_e \ll 1$. In the present case the values of $E/kT_e = X_{nn''}$ are very close to unity for the Lyman and Balmer series. Therefore, we rather assume that $Q_{nn''}$ is constant and set it proportional to $B_{nn''}$ throughout the whole range of possible energies of electrons. Thus we write,

$$Q_{nn''} = \mu B_{nn''} = \mu \frac{n''^2}{n^2} \frac{A_{n''n}}{8\pi hR^3([1/n^2]-[1/n''^2])^3}. \qquad (2)$$

The value of the proportionality constant, μ, may be evaluated by introducing the appropriate value for certain definite transitions, say, Q_{12}. Thus

$$\mu = \frac{Q_{12}}{B_{12}} = \frac{Q_{12}}{2.02\times 10^{19}}.$$

Since $Q_{nn''}$ is measured in atomic units, we simply assume that $Q_{12} = 1$. Substituting the numerical values, equation (2) can be expressed as

$$Q_{nn''} = 2.25\times 10^{-10} \frac{n''^2}{n^2} \frac{A_{n''n}}{([1/n^2]-[1/n''^2])^3}, \qquad (3)$$

where the spontaneous transition probabilities $A_{nn''}$ are given by Menzel and Pekeris.[5]

Integrating equation (2) and arranging the constant factors, we obtain

$$C_{nn''} = C_0 \frac{N_i N_e^2}{T_e} b_n\left(1-\frac{b_{n''}}{b_n}\right)\varpi_n (\exp X_{n''}) \ (X_{nn''}+1) Q_{nn''}, \qquad (4)$$

where

$$C_0 = \frac{a_0^2 h^3}{2\pi m^2 k} = 1.163\times 10^{-26}.$$

We consider the value of C_{ni}.

An expression similar to equation (1) results for C_{ni}, the number of ionizations from

[5] *M.N.*, **96**, 77, 1936.

level n by collisions with electrons (in the present paper the notation C_{ni} is used instead of $C_{n\kappa}$ as in Paper II, because, for ionizations, C_{ni} denotes the integration over transition to the whole range of continuum rather than to a certain state, κ, in continuum):

$$C_{ni} = C_0 \frac{N_i N_e^2}{T_e} b_n \left(1 - \frac{1}{b_n}\right) \varpi_n (X_n + 1) Q_{ni} . \tag{5}$$

For the value of Q_{ni}, Giovanelli has also adopted a theoretical formula.[3] On the other hand, in Paper II, Thomas gives an empirical expression for $Q_{nn'}$ evaluated from experimental data. We may compare the values from these expressions with experimental data in the accompanying tabulation. Thus we see that for the more important, low-

	20 ev	25 ev	30 ev	50 ev	100 ev
Giovanelli	1.79	2.03	2.03	1.61	0.96
Thomas	0.18	0.32	0.45	1.00	0.95
Experiment*	0.4	0.6	0.8	1.2	1.2

*Mott and Massey, *Theory of Atomic Collisions* (2d ed.; Oxford: Clarendon Press, 1949), p. 244.

energy values, Thomas' empirical formula agrees better with experiments. Therefore, we adopt this empirical cross-section for ionization from the ground level, and for the ionizations from the higher level we again assume proportionality to the optical transition probabilities, B_{ni}. Thus:

$$Q_{ni} = \frac{B_{ni}}{B_{1i}} Q_{1i} = 0.096 \frac{B_{ni}}{B_{1i}} , \tag{6}$$

from equations (17a) and (17b) in Paper II.

$B_{n\kappa}$ may be expressed as

$$B_{n\kappa} = \frac{c^3}{8\pi h \nu_{n\kappa}^3} \frac{\varpi_i}{\varpi_n} A_{\kappa n} = \frac{\pi e^2}{m h \nu_{n\kappa}} f_{\kappa n} , \tag{7}$$

where the oscillator strength, $f_{\kappa n}$, can be given by the formula,[5]

$$f_{ni} = \int d f_{\kappa n} = \int_{R/n^2}^{\infty} \frac{m c}{\pi e^2} \frac{32\pi^2 e^6}{3\sqrt{3}\, c h^3 \nu_{n\kappa}^3} \frac{g_{II}}{n^5} d\nu_{n\kappa} , \tag{8}$$

in which g_{II} is the Gaunt factor, tabulated by Menzel and Pekeris.[5] For our present calculations we set g_{II} equal to unity.

Integrating equation (8) and substituting it in equation (7), we have

$$B_{ni} = \frac{32\pi^2 e^6}{3\sqrt{3} h^3} \frac{n}{3R^3} = 3.67 \times 10^{-11} n . \tag{9}$$

Thus we obtain from equation (6)

$$Q_{ni} = 0.096 n . \tag{10}$$

Substituting the values of the cross-sections in the collisional terms (1) and (5), we may write the cyclic equations (corresponding to eq. [19] of Paper II) thus:

$$\frac{2N_1N_e K \exp X_n}{T_e^{3/2}n^3}\left[\sum_{n+1}^{\infty}\left\{\left(b_{n''}-S_\nu\frac{b_n \exp X_{nn''}-b_{n''}}{\exp Y_{nn''}-1}\right)\frac{g_{nn''}}{n''^3}\frac{\exp(-X_{nn''})}{(1/n^2)-(1/n''^2)}\right.\right.$$

$$\left.-b_n\left(1-\frac{b_{n''}}{b_n}\right)J_{nn''}\right\}-\sum_{1}^{n-1}\left\{\left(b_n-S_\nu\frac{b_{n'}\exp X_{n'n}-b_n}{\exp Y_{n'n}-1}\right)\frac{g_{n'n}}{n'^3}\frac{1}{(1/n'^2)-(1/n^2)}\right. \tag{11}$$

$$\left.-b_{n'}\left(1-\frac{b_n}{b_{n'}}\right)J_{n'n}\right\}+\tfrac{1}{2}\{-E_i(-X_n)\}-\frac{\bar{S}_\nu}{2}\sum_{a=1}^{\infty}\left\{b_n[-E_i(-aY_n)]\right.$$

$$\left.\left.-\left[-E_i\left(-Y_n\left\{a+\frac{T_1}{T_e}\right\}\right)\right]\right\}-\left\{b_n\left(1-\frac{1}{b_n}\right)J_{n\kappa}\right\}\right]=0,$$

where

$$J_{nn''}=\frac{C_0}{2K}T_e^{1/2}N_e n^3\varpi_n(\exp-X_{nn''})\,(X_{nn''}+1)\,Q_{nn''},$$

$$J_{n'n}=\frac{C_0}{2K}T_e^{1/2}N_e n^3\varpi_{n'}(X_{n'n}+1)\,Q_{n'n}, \tag{12}$$

$$J_{n\kappa}=\frac{C_0}{2K}T_e^{1/2}N_e n^3\varpi_n(\exp-X_n)\,(X_n+1)\,Q_{n\kappa}.$$

For computing purposes, we may rewrite these equations in the following form:

$$b_n\left[\sum_{n''=n+1}^{\infty}\left\{\frac{S_\nu}{\exp Y_{nn''}-1}\frac{g_{nn''}}{n''^3}\frac{1}{(1/n^2)-(1/n''^2)}+J_{nn''}\right\}\right.$$

$$+\sum_{n'=1}^{n-1}\left\{\left(1+\frac{S_\nu}{\exp Y_{n'n}-1}\right)\frac{g_{n'n}}{n'^3}\frac{1}{(1/n'^2)-(1/n^2)}+J_{n'n}\right\}$$

$$\left.+\frac{\bar{S}_\nu}{2}\sum_{a=1}^{\infty}\{-E_i(-aY_n)\}+J_{n\kappa}\right]=\sum_{n''=n+1}^{\infty}b_{n''}\left\{\left(1+\frac{S_\nu}{\exp Y_{nn''}-1}\right)\right. \tag{11a}$$

$$\left.\frac{g_{nn''}}{n''^3}\frac{\exp-X_{nn''}}{(1/n^2)-(1/n''^2)}+J_{nn''}\right\}+\sum_{n'=1}^{n-1}b_{n'}\left\{\frac{S_\nu}{\exp Y_{n'n}-1}\frac{g_{n'n}}{n'^3}\frac{\exp X_{n'n}}{1/n'^2-1/n^2}\right.$$

$$\left.+J_{n'n}\right\}+\tfrac{1}{2}\{-E_i(-X_n)\}+\frac{\bar{S}_\nu}{2}\sum_{a=1}^{\infty}\left\{-E_i\left(-Y_n\left\{a+\frac{T_1}{T_e}\right\}\right)\right\}+J_{n\kappa}.$$

We obtain the values of b_n by solving the above set of equations by successive approximation.

b) NUMERICAL RESULTS, NEGLECTING THE CHROMOSPHERIC RADIATION FIELD

As in Paper II, we treat the problem for $T_e = 35{,}000°$, $T_r = 6000°$, by assuming the existence of constant kinetic temperature throughout the region of the chromosphere. We set $N_e = 2 \times 10^{11}$. (In Paper II, the Boltzmann constant k is taken as 1.4×10^{-16}; however, we take the exact value 1.376×10^{-16}.) We consider, first, the cases $S_\nu = 1$ and $S_\nu = 0$.

Numerical solutions for b_n are shown in Table 1 in comparison with those from Paper II.

We see from Table 1 that there are no great differences in the numerical results of b_n between the two calculations. The higher-level terms are altered the most, relatively, as was, of course, to be expected. Any great differences, then, must arise from the effect of the chromospheric radiation field.

c) CONSIDERATION OF THE CHROMOSPHERIC RADIATION FIELD

If we add the chromospheric absorption and emission to the radiation field from the photosphere, S_ν may or may not be greater than unity. For the Lyman lines, whose chromospheric opacity is so high, this consideration is particularly important. In Paper

TABLE 1

b_n FOR NO CHROMOSPHERIC RADIATION FIELD

S	b_1	b_2	b_3	b_4	b_5	b_6	b_7	b_8	b_9	b_{10}
1.....	1.61×10^6	9.08	3.82	2.80	2.31	2.01	1.75	1.54	1.38	1.20
	$2.1\times10^{6*}$	10.9*	4.67*	3.45*	2.93*	2.62*	2.42*	2.27*	2.17*	2.08*
0.....	1.85×10^6	10.3	4.41	3.24	2.72	2.43	2.17	1.90	1.61	1.43
	$2.3\times10^{6*}$	12.3*	5.33*	3.92*	3.31*	2.96*	2.75*	2.60*	2.47*	2.36*

* Denotes Paper II solution.

TABLE 2

b_n INCLUDING THE CHROMOSPHERIC EMISSION

	b_1	b_2	b_3	b_4	b_5	b_6	b_7	b_8	b_9	b_{10}
${}_nS=1$ $(1<n)$ ...	4.24×10^4	1.18×10^3	57.4	19.0	11.2	8.14	6.54	5.57	4.87	4.41
${}_nS=0$ $(n=2)$	2.41×10^5	2.36×10^5	71.9	26.6	15.9	11.34	8.60	6.75	5.53	4.59
${}_nS=1$ $(2<n)$ ...										

III, Thomas has discussed the problem and has shown that the essential perturbation to the radiation field by the chromosphere is in the Lyman region, with a small effect also in the center of the early Balmer lines. In Paper III he obtained, for S_ν in the Lyman lines,

$$S_\nu = b_n b_1^{-1} (\exp Y_{1n} - 1) \exp(-X_{1n}) \ . \tag{13}$$

In a private communication Thomas has mentioned that equation (13) is in error because of the faulty inclusion of the induced emissions, and the correct expression—which follows from his Paper V[6] in the present series under conditions of large values[7] for $(n_n \cdot \alpha/\beta)$, where β is the atmospheric logarithmic density gradient—is

$$S_\nu = (\exp Y_{1n} - 1)\left(\frac{b_1}{b_n} \exp X_{1n} - 1\right)^{-1} . \tag{14}$$

With this expression for S_ν, the bracket in equation (11) involving the Lyman-line radiative transitions vanishes. In the following solutions we neglect the chromospheric emission outside the Lyman lines. As in the earlier results of Paper III, the significant parameter is ${}_2S$, the residual intensity in the Balmer lines. We tabulate the solution for the b_n in Table 2 for two extreme values of ${}_2S$.

[6] *Ap. J.*, **110**, 12, 1949.

[7] Cf. a forthcoming paper by Thomas.

From the results in Table 2 we see that b_n has a larger value for the higher n, compared with the solution for the case without chromospheric emission. Especially, b_2 has almost the same value as b_1. We find considerably different values for the case ${}_nS = 1$ (for $1 < n$) and ${}_2S = 0$, ${}_nS = 1$ $(2 < n)$.

As a check on these results, we may compare the value of b_2 with the population of the Balmer ground state, N_2, which is obtained by Thomas[8] from the effect of Balmer decrement in the flash spectrum. Thomas obtained the result for N_2—the total number cm^{-2} along the line of sight—as 1.20×10^{16} and 0.26×10^{16}, respectively, at the height of 670 and 1500 km in the chromosphere. We may evaluate the values of b_2 from these results, assuming an isothermal chromosphere at $T_e = 35{,}000°$ and $N_e = 2 \times 10^{11}$. We obtain the following:

$$\text{At } 670 \text{ km:} \quad b_2 = 5.72 \times 10^4 ;$$

$$\text{At } 1500 \text{ km:} \quad b_2 = 1.24 \times 10^4 .$$

These results agree well with those in Table 2, if we note that the most likely value of ${}_2S$ is near 0.15–0.20.

It is a pleasure to acknowledge the extended discussions with and suggestions by Dr. R. N. Thomas on the investigation reported here.

[8] *Ap. J.*, 111, 165, 1950.

SUPERTHERMIC PHENOMENA IN STELLAR ATMOSPHERES
VIII. COMMENT ON THE CHROMOSPHERIC MODEL*

RICHARD N. THOMAS
University of Utah
Received October 19, 1951

ABSTRACT

The analytic structure for a model solar chromosphere in a statistically steady state is summarized. The dependence of the structure upon chromospheric eclipse observations is exhibited, and several checks upon the internal consistency of the model are discussed.

The earlier papers in this series represent an attempt to gain physical insight into the spectroscopically steady state of a hydrogen atmosphere whose energy supply is not solely radiation. The preceding solutions have been numerical successive approximations. It is desirable on two accounts to investigate the possibility of more explicit algebraic solutions. First, in this series of papers we are primarily concerned with obtaining some insight into the problem of extended atmospheres. We have earlier proposed[1, 2] that such atmospheres are supported by the dissipation into atmospheric thermal energy of, and/or the direct momentum-transfer from, a system of jet ejections akin to some types of the solar prominences. Thus we need to know the implication of any observed spectrum in terms of the mechanical energy supply required to supplement the conventionally discussed radiation field. Second, plans for observations of the (February, 1952), eclipse indicated a need for as explicit an indication as possible of the relation between the electron density and kinetic temperature, on the one hand, and the population of the atomic levels, on the other. The earlier numerical calculations have indicated that probably only the lowest two energy levels depart by much more than one order of magnitude from the thermodynamic equilibrium value.[2] Because of the strong dependence of the Balmer series, eclipse results,[3] and the ultraviolet radiation in the Lyman region upon the populations of these two levels, we shall consider them in detail.

I. GENERAL DISCUSSION

From Paper IV[2] of this series we have the following equations for the statistically steady state of the energy level in question (the following summary deals with hydrogen, and we consider only the principal quantum number; thus we neglect the splitting of levels according to azimuthal quantum number; because the 2s level is not metastable, a neglect of this splitting does not seem to be serious):

$$b_n\left\{\Phi N_e\sum_{n''}U_{nn''}\left(1-\frac{b_{n''}}{b_n}\right)\varpi_n\exp X_n+\sum_{n'}\left[1-S_\nu\frac{(b_{n'}/b_n)\exp X_{n'n}-1}{\exp Y_{n'n}-1}\right]\right.$$

$$\left.\times\varpi_{n'}f_{n'n}\nu^3\exp X_n\right\}=\left\{\sum_{n''}b_{n''}\varpi_n f_{nn''}\nu^2\exp(X_{n''})\left[1-S_\nu\frac{(b_n/b_{n''})\exp X_{nn''}-1}{\exp Y_{nn''}-1}\right]\right.$$

$$+\frac{1}{2R}\int_{\nu_n}^{\infty}\varpi_n f_{n\kappa}\nu^2\kappa^3\exp\left[\frac{-h\nu}{kT_e}\right]\exp(X_n)\left[1-S_\nu\frac{b_n\exp X_{n\kappa}-1}{\exp Y_{n\kappa}-1}\right]d\nu+\Phi N_e\Sigma b_{n'}U_{n'n}$$

$$\left.\times\left(1-\frac{b_n}{b_{n'}}\right)\varpi_{n'}\exp X_{n'}\right\}, \tag{1}$$

* Work supported by Air Research and Development Contract AF 33-038-20067.

[1] R. N. Thomas, *A.J.*, **52**, 158, 1947.

[2] R. N. Thomas, *Ap. J.*, **109**, 500, 1949. Hereafter cited as "Paper IV."

[3] R. N. Thomas, *Ap. J.*, **111**, 165, 1950.

where

$$U_{nn''} = \int_{q_0}^{\infty} Q_{n\,n''} q \exp(-q)\, dq$$

and $Q_{nn''}$ is the cross-section for collisional excitation from n to n''.

$$X_n = \frac{h\nu_n}{kT_e}; \qquad Y_n = \frac{h\nu_n}{kT_e}; \qquad X_{nn''} = X_n - X_{n''};$$

$$\Phi = \left[\left(\frac{2\pi k}{m}\right)^{1/2} a_0^2 \frac{m c^3}{4\pi^2 \epsilon^2}\right] T_e^{1/2} = C_1 T_e^{1/2};$$

$S_\nu B_\nu (T_r) = I_\nu$, where I_ν is the incident radiation intensity.

$$b_n = N_n \left[N_i N_e T_e^{-3/2} \frac{\varpi_n}{2\varpi_i} \left(\frac{h^2}{2\pi m k}\right)^{3/2} \exp X_n\right]^{-1},$$

where N_n is the population of the nth energy state, with N_i and N_e the ion and electron density. The $f_{nn''}$ are the oscillator strengths.

Assuming the radiation and collision cross-section as known, the above set of equations can be solved, once one knows the value of N_e, T_e, and S_ν. The critical part of S_ν is that representing the radiation field from the chromosphere itself. This radiation field can, in general, be found only by means of successive approximations. We may formulate the problem in the following manner: Surround the particular region in the chromosphere under question by a sphere of optical thickness $\tau_{0\nu}$. Incident on this sphere assume radiation field I_0 (with, of course, I_0 and τ_0 possibly depending upon the angle). Then the radiation field at the center of this sphere may be written:

$$I'_\nu = I'_{0\nu} \exp - \tau_{0\nu} + \int_0^{\tau_{0\nu}} \exp(-\tau) \left[\frac{b_{n'}}{b_n} \exp X_{n'n} - 1\right]^{-1} d\tau, \tag{2}$$

where

$$I'_\nu = \frac{c^2}{2h\nu^3} I_\nu.$$

Thus, a knowledge of I'_0 as well as of the bracket in the integrand is required before a solution may be carried through completely. We have actually two extreme ways of considering the solution. In the first, we regard the whole chromosphere as included within the spherical boundary. In such a case I'_0 is a combination of the radiation field from the "classical photosphere" and that from the outside of the star. τ_0 is the optical depth from the bottom of the photosphere and from the outside of the star. In such a case the essential aspect is the value of the bracket term in the integrand of equation (2). That is, we must know the variation of the b_n and T_e throughout the chromosphere.

The second method of approach regards the sphere as inclosing a region of the atmosphere over which the variation of T_e, N_e, and hence b_n is essentially negligible. Then I'_0 is the radiation within the chromosphere incident on the boundary of this homogeneous region. Each case is of use in a particular region of the spectrum. For those spectral regions in which the optical depth of the chromosphere is very large—and, in particular, where the depth is large compared to the distance over which the thermodynamic parameters vary significantly—the second method of approach is the more useful. In those regions of the spectrum to which the chromosphere is essentially transparent, the first method of approach is the more useful. If for T_r we have chosen the radiation field characteristic of the solar continuum, we may in this last case choose S_ν essentially equal to 1. In the other case the value of S_ν must be computed from other considerations.

In the case where the chromosphere is optically very thick, we may proceed systematically to consider the value of S_ν. It is apparent that the critical parameter is the value of τ_0 as compared with the distance over which the thermodynamic parameters vary appreciably. Making reference to Figure 1, we may write the expression for τ_0 as follows, assuming an exponential density gradient:

$$\tau_{0\nu} = N_n' a_\nu \int_0^\infty \exp(-\beta w)\, d\sigma = N_n' a_\nu \exp\left[\frac{r}{2}\beta \cot^2\phi\right] \sqrt{\frac{2r}{\beta}} \int_{V_0}^\infty \exp(-V^2)\, dV;$$

$$\tau_{0\nu} = \frac{N_n' a_\nu}{\beta} \sec\phi \left[1 - \frac{1}{2V_0^2} + \frac{3}{4V_0^4} - \dots\right]; \tag{3}$$

$$V_0 = \sqrt{\frac{\beta r}{2}} \cot\phi \sim 18 \cos\phi.$$

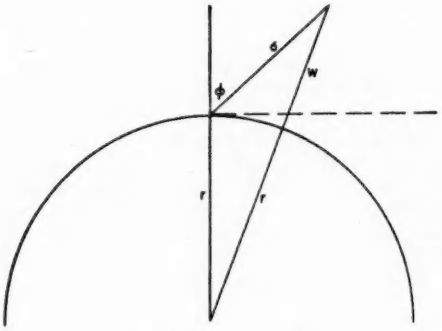

FIG. 1.—Geometry of τ_0

The above expression applies to the optical depth above a given level, and the optical depth down from the level to another level, at which the density is ${}_L N_n'$, is

$$\tau_{1\nu} = \left(\frac{{}_L N_n'}{N_n'} - 1\right) \tau_{0\nu}. \tag{3.1}$$

Thus, if the ratio $N_n' a/\beta$ is considerably greater than 1, the second method of approach above is the more useful one. That is, we may regard $(N_n' a)^{-1}$ as the length characterizing the optical opacity of the medium and β^{-1} as the length characterizing the homogeneity of the atmosphere with respect to thermodynamic parameters (so long as the temperature variation is less than that of the density). With the ratio $N_n' a/\beta$ greater than 1, the atmosphere essentially behaves as though it is homogeneous so far as the local radiation field is concerned. Again, we emphasize, this computation must be made for each region of the spectrum—and its validity in one region does not imply that in the other. As we shall see later, neglect of this very obvious remark has led to unrealistic results.

In order to evaluate the parameter S_ν, it is necessary first to have an approximate solution to the set of equations (1). To solve these equations, one must assume some value of S_ν and know N_e and T_e. Papers II and III[4] in this series carried out such solutions, in which the first trial solution placed $S_\nu = 1$. Various other solutions were based upon computations of the values of S_ν and their use in the equations. In brief, we may

[4] R. N. Thomas, *Ap. J.*, **108**, 142, 1948, and **109**, 480, 1949.

summarize the situation by stating that the solar chromosphere is optically opaque only for the Lyman-line region; is partially opaque for the Lyman continuum and the Balmer lines and continuum; and is essentially transparent for the remainder of the spectrum. The case of high opacity, i.e., $1 \ll N_{n'}\alpha/\beta$, results in a relatively simple form for S_ν—as may be seen from the solution of equation (2) under the assumption that, in the regions for which $\tau_0 \leq 1$, the bracketed integrand of equation (2) does not vary greatly. We have, then, for the integral of equation (2), and hence for I' and S_ν:

$$I'_\nu = \left[\frac{b_{n'}}{b_n} \exp X_{n'n} - 1\right]^{-1}, \tag{4}$$

$$S_\nu = I'_\nu [\exp Y_{n'n} - 1]. \tag{5}$$

Inserting this value for S_ν in equations (1), the term involving the radiative transitions connecting level 1 and other levels vanishes. It should be noted here that the computation on this S_ν used in Paper III is erroneous, owing to a faulty manner of including the induced transitions. The method there adopted resulted in a term remaining—of very small numerical value—in these optical transitions connecting levels 1 and n; hence any results in Paper III depending upon this residual term are invalid. However, the first set of calculations in Paper III placed this term equal to zero and so are valid.

The difficult terms to include are those for spectral regions at which the optical depth of the chromosphere is not considerably greater than 1; hence both terms in equation (2) must be included, in order to compute the value for S_ν. Some of these spectral regions are critical in the solution for the b_n, and some are essentially irrelevant. We consider the point in detail.

II. SOLUTION FOR b_1

Because of the detailed balancing in the Lyman lines, caused by the opacity of the chromosphere in this region, we see from equation (1) that b_1 is directly proportional to the term involving the Lyman continuum. Thus it is extremely important to have the correct value for S_ν in this region. Consider equation (2). The first term, the part $I'_0 e^{-\tau_0}$, had the value 0 because of the vanishing of $e^{-\tau_0}$ when we considered the model of the chromosphere, where we drew our boundary at a distance equal to the scale height of the atmosphere. Now, however, when we place our boundaries at the base of the chromosphere and outside the atmosphere of the star, the term $e^{-\tau_0}$ has some value which is neither 1 nor 0. The factor I'_0 has a value depending on the direction. I'_0 from the outward radial direction has the value 0, since no radiation is incident from outside the star. For that radiation coming from the photosphere, I_0 is not that of the black body which represents the continuum in the optical part of the spectrum, but rather takes on a value somewhat near that to be expected for a black body at the so-called "boundary temperature" of the sun, i.e., the temperature of the classical reversing layer, about 4700°. (For example, refer to the calculations[5] by Greenstein.) Thus we may write the expression for the S in the Lyman region as follows:

$$S_\nu = \frac{1}{2}\frac{B_\nu(4700°)}{B_\nu(6000°)} \exp(-\tau_0) + (\exp Y_{1\kappa} - 1) \times \int\int_0^{\tau_0} (b_1 \exp X_{1\kappa} - 1)^{-1} \exp(-\tau)\, d\tau \frac{d\omega}{4\pi}, \tag{6}$$

where the integral over the solid angle fixes the average value for S_ν at the point in question and has been replaced by $\frac{1}{2}$ for the first term. Thus the contribution to S_ν coming from the regions outside the chromosphere gives an additive factor, coming from

[5] J. L. Greenstein, *The Atmospheres of the Earth and Planets* (Chicago: University of Chicago Press, 1949), p. 118.

the first term of the above equation, of about 10^{-3}. Hence the majority of the contribution comes from the second term in equation (6) above. We note the contrast to the preceding case, where we considered the contribution to the Lyman lines from such expressions as the above. In the Lyman-line expression, the contribution to the above integrand came from regions so close to the point in question that the bracketed part of the integrand did not have a chance to vary appreciably. Hence we could remove the bracket from the integral, and we obtained the detailed balancing in the Lyman lines. If, now, the atmosphere were homogeneous, we could write the above expression in the form

$$S_\nu = (\exp\ Y_{1\kappa} - 1)\,(b_1 \exp\ X_{1\kappa} - 1)^{-1}\,[\,1 - \exp\,(-\tau_0)\,]\,. \tag{7}$$

For reference we write the equation for b_1 as follows:

$$b_1\left[C_1 T_e^{1/2} N_e \Sigma U_{1n}\left(1 - \frac{b_n}{b_1}\right)\right] = \frac{1}{2R}\int_{\nu_1}^{\infty} f_{1\kappa}\nu^2\kappa^3 \exp\left(\frac{-h\nu}{kT_e}\right) \times\left[1 - S_\nu \frac{b_1 \exp\ X_{1\kappa} - 1}{\exp\ Y_{1\kappa} - 1}\right] \tag{8}$$

and, using equation (7),

$$= \frac{1}{2R}\int_{\nu_1}^{\infty} \varpi_1 f_{1\kappa}\nu^2\kappa^3 \exp\left[\frac{-h\nu}{kT_e}\right] \exp\,(-\tau_0)\,d\nu\,. \tag{8.1}$$

Thus we see that, had the integrand a constant value, we would find in the expression (8.1) for b_1 simply $e^{-\tau_0}$. This value of τ_0 is, of course, an average over the directions in the chromosphere, and so it is necessary to form some kind of estimate of this mean value of the optical depth. There are several remarks that we may make on this expression (8).

We must realize in these remarks that our removal of the bracketed part of the integrand from the integral sign is not justified; thus the following remarks are simply by way of a guide to the physical situation. We note now the practice found in the literature[5] of forming some estimate of the contribution from the solar Lyman continuum to the value of the radiation needed to form the terrestrial ionosphere. Then a "temperature" is ascribed to the chromosphere by equating this energy needed for the terrestrial ionosphere to the black-body expression. This procedure is justified by the remark found equally often in the literature, that an optically thick gaseous atmosphere, no matter what its thermodynamic state, will mimic a state of thermodynamic equilibrium in so far as the radiation field is concerned. The arguments justifying such a result are essentially those which have led us to the result of detailed balancing in the Lyman-line region. That is, since the atmosphere is optically thick, each region sees only the emission from the atmosphere, and we obtain exactly that result which we obtain with the Lyman lines. The difficulty is, however, that the observer sees only the radiation which can escape the atmosphere, and, conversely, that region of the atmosphere which contributes to the emission actually emerging from the atmosphere can "see" the observer. Hence that portion of the atmosphere that contributes directly to the emission does not lie in a region that is optically opaque—i.e., shielded from the outside. Therefore, the above remarks used to justify the assumption of the equivalence of the radiation to black-body emission at the kinetic temperature of the atmosphere are not valid. Instead, we must write the emission from the atmosphere as follows:

$$I_\nu = \frac{2h\nu^3}{c^2}\int_0^{\infty} (b_1 \exp\ X_{1\kappa} - 1)^{-1} \exp\,(-\tau)\,d\tau\,, \tag{9}$$

where, even though the above upper limit of the integral is infinity, only the lesser-optical-depth regions of the atmosphere contribute to the emission. Hence the interest-

ing portions of the atmosphere are those within which b_1 is determined by using an S_ν fixed by equations (6). As we have seen, if the atmosphere does remain homogeneous, we have an expression something like that in equation (7) for S_ν. Thus the value of b_1 is directly proportional to $e^{-\tau_0}$, where τ_0 is the optical depth down to the emitting layer in question. We see that the emission from the atmosphere is essentially that from a black body at the atmospheric kinetic temperature, divided by the value of b_1. Thus, thinking back on the results on b_1 for the chromosphere as determined in the earlier papers of the series—where values ranging between 10^5 and 10^6 were found—we see that quite an appreciable error may be made if one simply interprets the emission to be that from a black body at the kinetic temperature of the atmosphere. Thus we are forced to reject the results found, for example, by Wooley and Allen[6] in so far as they relate to discussions of the Lyman continuum.

Returning now to the solution of equation (6), we see that actually we must solve equations (6) and (8) as simultaneous equations. That is, equation (8) specifies the value of b_1 at any particular point of the atmosphere in terms of the value of S_ν there. Equation (6) gives the value of S_ν in terms of the integral over b_1 at all points of the atmosphere. The parameter of the solution is the value of the optical depth between the two points. Consequently, prior to the discussion of the two equations simultaneously, we must consider the value of τ_0, which is given by equation (3) with $n' = 1$. (As discussed in Paper III, the bound-free exceed the free-free absorptions.) Thus, from the numerical value of V_0 we see that for all values of ϕ except those of $\phi \sim \pi/2$ we are justified in dropping all except the first terms of the expression for τ_0 (specifically, for angles less than about 87°). Actually, we wish the mean value of the exponential term $e^{-\tau_0}$ and can estimate it as follows:

$$\overline{\exp\ -\tau_0} \sim \frac{1}{2\pi}\int_0^{2\pi}\int_0^{\pi/2} \exp(-\tau_0)\sin\phi\, d\phi\, d\psi = \int_0^{\pi/2} \exp(-a\sec\phi)\, d\cos\phi$$
$$= a\int_a^\infty \exp(-y)\,\frac{dy}{y^2}, \tag{10}$$

where

$$a = \frac{N_1 a}{\beta} \qquad y = a\sec\phi;$$

for large a:

$$\overline{\exp -\tau_0} \sim \frac{\exp(-a)}{a}\left[1 - \frac{2}{a} + \frac{3!}{a^2} - \ldots\right]; \tag{10.1}$$

for small a:

$$\overline{\exp -\tau_0} = \exp(-a) - a\left[-\gamma - \ln a + \frac{a}{1\cdot 1!} - \frac{a^2}{2\cdot 2!} + \ldots\right]. \tag{10.2}$$

We see that the maximum value of the quantity a, using the results from Paper III with $b_1 = 2\cdot 10^6$, is about 0.35 at the head of the Lyman series. For greater frequencies, of course, the value of a decreases as ν^{-3}. Hence the expansion (10.2) is the appropriate one. Returning to equation (6), we see that we may express the equation in its dependence on polar angle as

$$S_\nu = \frac{1}{2}\frac{B_\nu(4700°)}{B_\nu(6000°)}\exp(-\tau_1) + \left\{\frac{1}{2}\int_{\pi/2}^{\pi}\int_0^{-\tau_1\sec\phi}[b_1(\tau)\exp X_{1\kappa} - 1]^{-1}\right.$$
$$\left.\times\exp(-\tau)\, d\tau\, d\omega' + \frac{1}{2}\int_0^{\pi/2}\int_0^{\tau_2\sec\phi}[b_1(\tau)\exp X_{1\kappa} - 1]^{-1}\exp(-\tau)\, d\tau\, d\omega'\right\} \tag{11}$$
$$\times\,[\exp Y_{1\kappa} - 1],$$

[6] R. Wooley and C. W. Allen, *M.N.*, **110**, 358, 1950.

where τ_1 is the radial optical depth downward to some region where the first term of equation (11) represents S_ν and τ_2 is the outward radial optical depth. In the Lyman region, of course, the exponential term multiplied by b_1 is much greater than the term 1, and so the term 1 may be dropped.

We see that we cannot proceed further with a solution unless we know the variation of T_e and N_e throughout the atmosphere. With the knowledge of this variation, we may solve the two equations (8) and (11) by successive approximation. As indicated earlier by the author,[3] eclipse observations from the Balmer decrement can provide just such values of N_e and T_e as are needed to solve these equations. Having solved these equations, one can use equation (9) to calculate the emission from the chromosphere in the Lyman region. Then, and only then, can one make a rigorous comparison between this high-temperature chromosphere and reality as regards a judgment on the basis of the Lyman emission. We may remark on the solution of equations (8) and (11) for an isothermal atmosphere, which leads to conclusions of interest for the actual atmosphere.

If the atmosphere is isothermal, the optical depth and temperature terms are not related—the $X_{1\kappa}$'s do not depend upon τ. Hence, b_1 varies only with the electron density, and expressions (8) and (11) may be somewhat simplified.

If we introduce:

$$I_\nu'' = \frac{1}{2}\left\{\frac{B_\nu(4700°)}{B_\nu(6000°)}\exp(-\tau_1)\,\exp\,(X_{1\kappa}-Y_{1\kappa}) + \int_{\pi/2}^{\pi}\int_0^{\tau_1\sec\phi} b_1^{-1}\exp(-\tau)\,d\tau\,d\omega' + \int_0^{\pi/2}\int_0^{\tau_2\sec\phi} b_1^{-1}\exp(-\tau)\,d\tau\,d\omega'\right\}, \tag{12}$$

so that equation (11) becomes

$$S_\nu = \exp\,(Y_{1\kappa}-X_{1\kappa})\,I_\nu'', \tag{13}$$

then equation (8) becomes

$$b_1 = \left[C_1 N_e T_e^{1/2}\Sigma U_{1n}\left(1-\frac{b_n}{b_1}\right)\right]^{-1}\frac{1}{2R}\int_{\nu_1}^{\infty} f_{1\kappa}\nu^2\kappa^3\exp\left[-\frac{h\nu}{kT_e}\right]\{1-b_1 I''\}\,d\nu. \tag{14}$$

With the exception of the first term in equation (12) (which is obviously negligible), the frequency dependence of I_ν'' is that of $e^{-\tau_0}$ (where τ_0 is τ_1 or τ_2) and so as $\exp(-\#\nu^{-3})$, where # is about $0.15\cdot 10^{-6}b_1$. Since the upper limit of b_1 is $2\cdot 10^6$ for the lower chromosphere, the influence of $e^{-\tau_0}$ upon the integrand in equation (14) is then quite small, particularly since we note that we may write:

$$f_{1\kappa} = k_{1\kappa} g_{II}\nu^{-3}\kappa^{-3}\varpi_1^{-1}, \tag{15}$$

where $k_{1\kappa}$ is a numerical constant and g_{II} is the Gaunt factor, which has a maximum value near 1 for $\kappa = 1$ and decreases on either side. Thus the integrand in equation (14) becomes:

$$\frac{k_{1\kappa}}{\varpi_1}\int_{X_1}^{\infty}\frac{\exp(-X)}{X}\,g_{II}[1-b_1 I'']\,dx,$$

with $X_1 = 4.4$ for $T_e = 35{,}000$ (hence a *lower* limit for X_1 in the current discussion of the true value of T_e). Thus the integrand has essentially its value at X_1, and we may write equation (14) thus:

$$b_1 \sim \left[C_1 N_e T_e^{1/2}\Sigma U_{1n}\left(1-\frac{b_n}{b_1}\right)\right]^{-1}\frac{k_{1\kappa}g_{II}(\nu_1)}{2R\varpi_1}\frac{\exp(-X_1)}{X_1}(1-b_1 I''), \tag{14.1}$$

where the uncertainty is of the order of the departure from unity of the factor $(1 - 1/X + 2/X^2 \ldots)$, or about 50 per cent. The b_1 dependence of equation (14.1) is somewhat illusory, as we note that the factor $b_1 X''$ actually does not vary directly with b_1. If we write ${}_0b_1$ to denote the value of b_1 at the point of the atmosphere under investigation, we may write equation (12) (dropping the first term) thus:

$$I_\nu'' = {}_0b_1^{-1} I_\nu''' ,$$

$$I_\nu''' = \int_{\pi/2}^{\pi} \int_0^{-\tau_1 \sec\phi} \frac{{}_0b_1}{b_1} \exp - \tau \, d\omega' + \int_0^{\pi/2} \int_0^{\tau_2 \sec\phi} \frac{{}_0b_1}{b_1} \exp(-\tau) \, d\tau \, d\omega' ; \qquad (16)$$

and equation (14) becomes

$${}_0b_1 \sim \left[C_1 N_e T_e^{1/2} \Sigma U_{1n} \left(1 - \frac{b_n}{b_1}\right) \right]^{-1} \frac{k_{1\kappa} g_{11}(\nu_1)}{4R} \frac{\exp(-X_1)}{X_1} (1 - I''') . \qquad (14.2)$$

For a uniform atmosphere, I''' is $(1 - e^{-\tau_0})$, and so we see that the last bracket of expression (14.2) is essentially $e^{-\tau_0}$ (where $e^{-\tau_0}$ is a kind of weighted average of $e^{-\tau_1}$ and $e^{-\tau_2}$, with the weight factor being b_1^{-1}). Thus, with the chief uncertainty being $e^{-\tau_0}$, we see that its effect on the possible range of value of b_1 (for fixed N_e) is only that from $1 (\tau_0 = 0)$ to $e^{-\tau_0}$. From Paper III we have an estimate of τ_1 maximum to be 0.35. From equation (10.2) this gives an average value of $e^{-\tau_1}$ of

$$\exp(-\tau_1) - \tau_1 \left[-0.58 - \ln \tau_1 + \frac{\tau_1}{1 \cdot 1!} \ldots \right].$$

Thus, if we solve equations (16) and (14.2) by iteration and assume for the first iteration that τ_0 is 0, we see that the first approximation overestimates the value of b_1, and hence the second approximation—based on this value of b_1 in the computation of τ_0—overestimates τ_0 and hence underestimates b_1. Thus a successive approximation gives, on the first two approximations, an upper and a lower limit for the value of b_1. Based on the value of 0.35 as the maximum of τ_0, we see that the values differ by only something like the cube root of e. Hence the procedure is fairly rapidly convergent.

We note a further remark on the value of b_1 from the form of equation (14.2). The values of the b_n, $n > 2$, enter equation (14.2) only through the factors $(1 - b_n/b_1)$. Because of the rapid decrease in energy difference between levels, the departure from thermodynamic equilibrium is far more serious in the first and second levels than in the higher. Hence only for b_2 does the above factor depart appreciably from unity. If we assume that the collision cross-sections are in nearly the same ratio as the optical absorption cross-sections (the Born approximation), the coefficient of the b_2 term in equation (14.2) exceeds the coefficient of the b_3 term by a factor of 10 for $T_e = 35{,}000$. Thus we see that the maximum range in the value of b_1 due to the uncertainty in b_n is a factor of 10 (between the two extremes: $b_2/b_1 \leqslant 0.1$ and $b_2/b_1 \sim 1$). If we substitute numerical values in equation (14.2), we have (assuming $Q_{12} = 1$ and the Born result for the ratio)

$${}_0b_1 \sim 0.75 \cdot 10^{15} N_e^{-1} T_e^{1/2} \exp(-\tau_0) \left[(X_{12} + 1)(\exp X_2)\left(1 - \frac{b_2}{b_1}\right) + \frac{(X_{13} + 1)}{6.25} (\exp X_3)\left(1 - \frac{b_3}{b_1}\right) + \ldots \right]^{-1}.$$

Thus, for the lower limit at the chromospheric level defined by an N_e of $2 \cdot 10^{11}$ we have, for the case $b_2/b_1 \leqslant 0.1$,

$${}_0b_1 \sim 5 \cdot 10^4 \exp(-\tau_0), \qquad \text{for} \qquad T_e = 35{,}000 .$$

For the case $b_2/b_1 \sim 1$, the above value increases by about a factor of 10. Thus we see that the value of b_1 is fixed within about a factor of 10 without further computation, as soon as we know the value of N_e. For this isothermal atmosphere, the critical factor is then the value of N_e. For a column of gas in the laboratory, where there is no gravitational field and hence a constant density, N_e should vary rather slowly. For the astronomical case, where N_e is fixed by the gravitational field as much as by the spectroscopic conditions, we require the value of N_e as a function of optical depth. This, as mentioned, can come only from a study of the chromospheric eclipse results.

We see that there is not actually a very great deal of difference between the case of the isothermal and the nonisothermal chromosphere; for the logarithmic electron density gradient is considerably greater than that of the kinetic temperature if the values obtained by the author are at all correct. Thus we may say that the problem of the emission in the Lyman continuum is a fairly straightforward one, depending only upon a final evaluation of the electron density (and, of course, kinetic temperature) as a function of height in the atmosphere. The algebraic process for the computation of conditions upon the population of the ground level of hydrogen and the emission in the Lyman continuum and Lyman lines is fairly well established.

III. CONSIDERATION OF THE POPULATION OF THE BALMER GROUND STATE AND THE BALMER REGION OF THE SPECTRUM

The solution for the b_n with $n > 1$ assumes a different aspect from the solutions in the Lyman region. As mentioned above, this difference in solution arises from the much smaller contribution of the chromosphere to the emission in the regions other than the Lyman—that is, from the much smaller opacity of the chromosphere to radiation outside the Lyman region. The sole exception to this statement lies in the central regions of the Balmer lines, particularly in $H\alpha$ and $H\beta$. Here the opacity is sufficiently great that the chromosphere essentially fixes the central-line intensity. Consequently, the solution for the b_n, $n \geq 2$, contains as a parameter the value S_2.

We note that the formulation adopted tacitly assumes square-profile lines. The assumption is valid in the computations on the Lyman region; for, as we have seen, the Lyman lines are essentially formed in the immediate neighborhood of the point in question. However, we note that the Balmer lines actually are a composite formed in all parts of the atmosphere. Consequently, there is not much point in attaching a rigorous meaning to a value S_2 relating to the Balmer lines as a whole, but one must use a kind of weighted average of S_2 over the line and over the atmosphere. The formation of such a weighted average is somewhat difficult. One may, however, inquire just how sensitively the solution for the b_n depends upon the value of S_2. To answer such a question, we may review the approximations for the solution of these equations to date.

These solutions are contained in Papers II and III and in a paper[7] by Matsushima. As discussed in Section (II) above, the value of b_1 is not particularly sensitive to the values of the higher b_n because of the detailed balancing in the Lyman lines. As already mentioned, in Paper III—owing to an erroneous method of including the induced emissions—this conclusion on b_1 just stated was not reached. Rather, in Paper III the result was obtained that the ratio b_1/b_2 was fixed—rather than the value of b_1 itself—if the value of b_2 were sufficiently high. Further, in Papers II and III two serious approximations were made. First, only collisional excitations from the ground level were included. Second, the term representing the collisional de-excitations was ignored; that is, the factor $(1 - b_n/b_1)$ in equation (1) was taken as 1, based on the realization that b_n/b_1 was very small. We have already recognized the smallness of this quantity, but the essential point is that in the equation for b_2, if S_2 is small and if no collisional excitations from level 2 are included, the only remaining coefficient of b_2 is this term represent-

[7] S. Matsushima, *Ap. J.*, **115**, 544, 1952.

ing the collisional de-excitations. That is, for small photoelectric excitations from level 2 and for detailed balancing in the Lyman-line transitions, the only means of exit from level 2 are the collisional de-excitations. Consequently, with these two assumptions of no collisional excitations from level 2 and the absence of collisional de-excitations from level 2 to level 1, the value of b_2 was fixed entirely by—that is, directly proportional to—the quantity $\bar{S}_2$. That is, quoting the result from Paper III, we had the following equation for b_2:

$$b_2 \cdot {}_2\bar{S} = c_2 + \sum_3^\infty c_i b_i , \tag{17}$$

where the c_i's are constants.

Thus we see that the actual value of S_2 was indeed critical in the solution for b_2. Actually, because the product $b_2 \bar{S}_2$ may be removed from the equation for the other b_n, $2 < n$, the solution for b_n, $2 < n$, does not depend upon S_2 under the two assumptions stated. If one now includes *all* collisional terms, the coefficient of b_2 contains collision terms in addition to ${}_2S$. Evaluating these terms—under the assumptions already stated on the relative collision cross-sections—we find the ratios for the various terms, for T_e and N_e of $3.5 \cdot 10^4$ and $2 \cdot 10^{11}$, respectively: Collisions up from level 2:collisions down from level 2:photoelectric transitions up from level 2: $= 1 : \frac{1}{2} : 2 \cdot 10^2$.

Thus the range of solution for b_2 is a factor of 100—from about 10^3 to 10^5 based on the results in Paper III for ${}_2S = 1$. (In the paper referred to, Matsushima obtains specifically $1.2 \cdot 10^3$ and $2.4 \cdot 10^5$.) Actually, since the earlier Balmer lines are formed in the reversing layer even in the strictly classical atmospheric model, we recognize that

$${}_2S = \leq \frac{B_\nu (4830°)}{B_\nu (6000°)} \sim 0.41$$

at the base of the chromosphere. Hence, unless the chromosphere itself builds up the Balmer radiation field, this value of ${}_2S$ will be an upper limit. Some insight into the problem of the observed central intensity of $H\alpha$ results from elaborating on this last point.

By considering the net emission at a given point, we have the necessary condition[8] for the chromosphere to build up the intensity in a line:

$$\frac{b_{n'}}{b_n} < (\exp\, Y_{n'n} - 1 + S) \exp(-X_{n'n})\, S^{-1} . \tag{18}$$

If we use Matsushima's latest results, we have numerically for $H\alpha$ (and $T_r = 6000°$, $T_e = 35{,}000°$):

$$\begin{aligned} S = 1{:}\ \frac{b_2}{b_3} &= \frac{1.18 \cdot 10^3}{57.4} = 20.6 > 20.4 , \\ S = 0{:}\ \frac{b_2}{b_3} &= \frac{2.36 \cdot 10^5}{71.9} = 3.28 \cdot 10^3 < \frac{19.8}{S(\to 0)} . \end{aligned} \tag{19}$$

Since the right-hand side of expression (18) is essentially proportional to S^{-1} and b_2 is essentially proportional to $(0.005 + S)^{-1}$ by the remarks of the last paragraph, the direction of the inequality is that of the first of equations (19) until S becomes small. That is, the chromosphere will further decrease the central intensity of $H\alpha$ until S reaches such a value that (18) is just satisfied. Strictly, one should solve the cyclic equations to find the value of S_c for which the inequality (18) just holds; but, assuming b_2/b_3 to vary directly as $(0.006 + S)^{-1}$, one interpolates a value $S_c \sim 0.15$. We note that if N_e and T_e

[8] R. N. Thomas, *Ap. J.*, **110**, 12, 1949.

remained constant throughout the atmosphere, we would expect S_c to be the observed central intensity of the line; for from the foregoing it is apparent that the atmosphere would "adjust" its absorption and emission until the intensity reaches this value. Because N_e and T_e do vary, we cannot take the 0.15 value literally as the expected central intensity of $H\alpha$. We note, however, that the b_2 value corresponding to this $S_c = 0.15$ is $8 \cdot 10^3$, and the corresponding value of the optical depth term $(n_2 a/\beta)$ is 7. Thus the observed central intensity is fixed by the S_c somewhat higher in the atmosphere. Because the collision-term part of the b_2 coefficient varies as $N_e T_e^{1/2}$, and N_e decreases faster than $T_e^{1/2}$ rises, we expect that at $(n_2 a/\beta) \sim 1$, $S_c < 0.15$ but not by too great a factor, since the optical depth varies as N_e^2 while the b_2 coefficient varies as N_e. Thus, by these rough quantitative calculations on the coefficient of b_2 in the cyclic equations, we reach a central intensity of $H\alpha$ in good agreement with Allen's[9] observed value of 0.12. Because of the uncertainties in the adopted collision cross-section, N_e, and T_e, detailed calculations are not in order until the detailed information on N_e and T_e sought at the 1952 eclipse becomes available. As in the discussion on b_1, we note, however, the small range of uncertainty on the physical conditions obtainable from a minimum of detailed computations, and the accompanying clarity of the physical picture.

Using the above value $b_2 \sim 8 \cdot 10^3$, we compute a value $0.8 \cdot 10^{15}$ for the total number of atoms, ${}_7N_2$, in the Balmer ground level along the line of sight. This number may be compared with that obtained by the author[3] from the eclipse data:

Eclipse Height	${}_7N_2$
670 km	$12 \cdot 10^{15}$
1500 km	$2.6 \cdot 10^{15}$

Again, in view of the uncertainty in N_e and T_e already mentioned, the agreement between the N_2 values is not unsatisfactory.

The essential point here, however, is that the foregoing discussion demonstrates that the central intensity of $H\alpha$ furnishes another observational parameter for use in inferring the structure of the solar chromosphere. From the results of this section and of the eclipse paper,[3] we see that the chromospheric model must satisfy—from the standpoint of direct optical observations—(1) the observed Balmer decrement (which depends on N_2); (2) the difference between emission and null-height gradients (which depends on the departure from thermodynamic equilibrium among the higher members); and (3) the central intensity of $H\alpha$ (which measures b_2). Section II provides an indirect condition (4) on b_1, if the Lyman continuum can be inferred from ionospheric measures. All these conditions depend, of course, on the (N_e, T_e) structure of the chromosphere, and the optical observations giving directly T_e (line profiles) and N_e (merging of lines at the series head) give evidence of the structure directly. The above points 1–4 provide, however, the important supplemental checks on the analytical structure adopted to construct the model chromosphere.

We note in this connection the earlier paper[10] in the series by Giovanelli which has paralleled this series on the hydrogen chromosphere. There are several differences in the formal structure of the analytic approach, chiefly because we have discussed the problem in terms of the departures of populations from thermodynamic equilibrium, while Giovanelli has dealt with absolute populations. Consequently, the direction of emphasis has been somewhat shifted, although the physically significant results are necessarily similar. Giovanelli has, however, adopted a lower T_e of $2.5 \cdot 10^4$, and finally concluded that the more nearly correct model consists of a network of high ($\sim$25,000°) and low ($\sim$5000°) temperature radial columns rather than a uniform chromosphere. Of the points listed in the preceding paragraph, Giovanelli has considered only the central intensity of $H\alpha$ as

[9] C. W. Allen, *Mem. Comm. Solar Obs.*, Vol. 1, No. 5, 1934.

[10] R. G. Giovanelli, *M.N.*, **109**, 298, 1949.

an observational check on the calculations. We note that his results give an $S_c \sim 0.19$, somewhat larger than ours, and an $\tau_5 N_2 = 1.1 \cdot 10^{14}$ for the level at which $N_e = 2 \cdot 10^{11}$. Without considering the merits of the network versus uniform models, it would seem that our somewhat higher temperature is preferable on the basis of these results. However, it is also probable that not much weight should be attached to this last remark as such but that it should rather be taken to illustrate once more the uncertainty in the chromospheric model resulting from the lack of application of all possible self-consistency checks. These self-consistency checks should now be fairly clear from both a physical and an algebraic standpoint, and the 1952 eclipse data should permit their specific application.

ON THE RADIUS OF GYRATION OF STARS

LLOYD MOTZ
Rutherfurd Observatory, Columbia University
Received December 26, 1951

ABSTRACT

A comparison of the radius of gyration of a star, which is defined by the integral

$$H = \left(\frac{8\pi}{3M}\int_0^R \rho r^4 dr\right)^{1/2},$$

with the apsidal-motion constant for various stellar models shows that, for polytropes and various main-sequence stars, there is a linear relationship between $-\log (H/R)$ and $-\log k$, where k is the apsidal-motion constant. Giant models, however, do not fall on this line.

The apsidal-motion constant for the Epstein two-source (proton-proton reaction and the carbon cycle) model for the sun is found to be 0.00599, which is equivalent to an effective polytropic index of 3.38. This result is used to draw some conclusions concerning the point along the main sequence where the proton-proton process gives way to the carbon cycle.

I. INTRODUCTION

In carrying out investigations into the constitution of stars, one has to deal with internal physical parameters that cannot be measured directly but must be inferred from the solution of the equations of equilibrium. It is important, therefore, to seek confirmation of these inferred results by investigating other parameters that can be obtained from the theory and that can at the same time be observed directly for various groups of stars.

Although it is a general practice to use the mass-luminosity and mass-radius relations for comparing theory with observations, other criteria have from time to time been investigated. Thus apsidal motions and radial pulsations[1] have been considered in some detail, and recently H. Bondi[2] has used the Hertzsprung-Russell diagram and the luminosity–surface-temperature relation to evaluate the theoretical results.

Since the apsidal-motion constant has proved to be quite sensitive to variations of the stellar model and since it is amenable to a direct observational check, it appears to be useful to try to find some physical parameter that can serve as a good functional argument for the apsidal-motion constant and that is easy to calculate. H. N. Russell has suggested that the apsidal-motion constant might depend in a simple way on the radius of gyration of a star.[3] One purpose of this paper is to see whether this is so.

The other purpose of this paper is to determine the apsidal-motion constant for the model of the sun recently calculated by I. Epstein[4] in which two energy sources are used, namely, the proton-proton reaction and the carbon cycle.

II. THE RADIUS OF GYRATION

If we define the radius of gyration of a stellar model by means of the relation

$$H = \left(\frac{8\pi}{3M}\int_0^R \rho r^4 dr\right)^{1/2}, \tag{1}$$

[1] L. Motz, *Ap. J.*, **94**, 253, 1941, and **112**, 434, 1950; G. Keller, *Ap. J.*, **108**, 347, 1948; I. Epstein, *Ap. J.*, **112**, 6, 1950.

[2] *M.N.*, **110**, 595, 1950.

[3] Private communication from Professor M. Schwarzschild. This calculation was undertaken after a discussion with Professor Schwarzschild.

[4] *Ap. J.*, **114**, 438, 1951.

in which ρ is the density at a distance r from the center and M and R are the total mass and radius of the model, then the dimensionless quantity $(H/R)^2$ can be calculated for various stellar models with the aid of the following formulae:

1. For a polytrope of index n,

$$\left(\frac{H}{R}\right)^2 = \frac{2}{3}\left[1 + \frac{6}{\xi_1^4 (d\theta_n/d\xi)_{\xi=\xi_1}} \int_0^{\xi_1} \xi^2 \theta_n d\xi\right], \tag{2}$$

where ξ_1 is the first root of the equation $\theta_n(\xi) = 0$, and ξ and θ have their usual meanings.

2. For a two-zone model (convective core and radiative envelope),

$$\left(\frac{H}{R}\right)^2 = \frac{2}{3}\left[1 + \frac{2(2.5)^{5/2}}{p_c^{3/2}} t_c^4 \xi_f^3 \theta_{3/2}(\xi_f) - \frac{6(2.5)^{5/2}}{p_c^{3/2}} t_c^4 \int_0^{\xi_f} \xi^2 \theta_{3/2} d\xi - 2\int_{x_f}^1 qx\,dx\right], \tag{3}$$

where the subscript c refers to the central values of a quantity and the subscript f to the values at the core-envelope interface. The quantities q, t, p, and x are defined in terms of the mass $M(r)$, the temperature T, the pressure P, and the radial distance r by means of the relations

$$P = p\left(\frac{GM^2}{4\pi R^4}\right); \qquad T = t\left(\frac{GM\mu\mathfrak{H}}{kR}\right); \qquad M(r) = qM; \qquad r = xR,$$

where k is Boltzmann's constant, μ is the mean molecular weight, and $\mathfrak{H}$ is the mass of the hydrogen atom in grams.

3. For a three-zone model (convective core, isothermal zone, radiative zone),

$$\left(\frac{H}{R}\right)^2 = \frac{2}{3}\left[1 + \frac{2(2.5)^{5/2} t_c^4 \xi_1^3 \theta_{3/2}(\xi_1)}{p_c^{3/2}} - 6(2.5)^{5/2} t_c^4 p_c^{-3/2} \int_0^{\xi_1} \xi^2 \theta_{3/2} d\xi + 2t_1^4 p_1^{-3/2} \int_{\chi_1}^{\chi_2} \chi^{-3}\left(-\frac{d\psi}{d\chi}\right) d\chi - 2\int_{x_2}^1 qx\,dx\right], \tag{4}$$

where the subscripts 1 and 2 refer to the values of the quantities at the two interfaces and ψ and χ are the dependent and independent variables in the isothermal zone which obey the equations

$$\frac{d^2\psi}{d\chi^2} = \chi^{-4} e^{-\psi}, \qquad \chi = t_1 p_1^{-1/2} x^{-1}.$$

4. For a three-zone model with chemical inhomogeneities (convective core and two radiative zones with different mean molecular weights),

$$\left(\frac{H}{R}\right)^2 = \frac{2}{3}\left[1 + 2(2.5)^{5/2} t_c^4 p_c^{-3/2} \xi_1 \theta_{3/2}(\xi_1) - 6(2.5)^{5/2} p_c^{-3/2} t_c^4 \int_0^{\xi_1} \xi^2 \theta_{3/2} d\xi - 2\int_{x_1}^{x_2} qx\,dx - 2\int_{x_2}^1 qx\,dx\right], \tag{5}$$

where the subscripts 1 and 2 refer to values at the two interfaces.

The above forms for $(H/R)^2$ were used rather than equation (1) directly, because the integrations for the various models are given in terms of q, θ, ψ, etc., and not in terms of ρ.

Formula (2) was used to obtain values of $(H/R)^2$ for the polytropes $n = 1$, 1.5, 2, 2.5, 3, 3.5, and 4. Formula (3) was used to find values of $(H/R)^2$ for Schwarzschild's[5] Russell-mixture (RM), for Keller's pure oxygen model,[1] and for Epstein's[4] two-source

[5] *Ap. J.*, **104**, 203, 1946.

model. Formulae (4) and (5) were used to calculate $(H/R)^2$ for the red giant noise-zone model of Richardson and Schwarzschild[6] and the red giant chemically inhomogeneous model of Li Hen and Schwarzschild, respectively.[7]

The results of the calculations are given in Table 1. In Figure 1 the logarithm of the apsidal-motion constant k is plotted against the logarithm of H/R. We see that all the points except those for the giant models lie on or very close to a straight line.

That the two points for the giant models do not lie on the plotted line need not be surprising, since the structure of these models is considerably different from that of the main-sequence stars. This is at once obvious from the values of the mass-luminosity parameter C (defined by Schwarzschild)[5] which one obtains for the main-sequence models and the giant models. This parameter is about ten times larger for the giant models than it is for the main-sequence models.

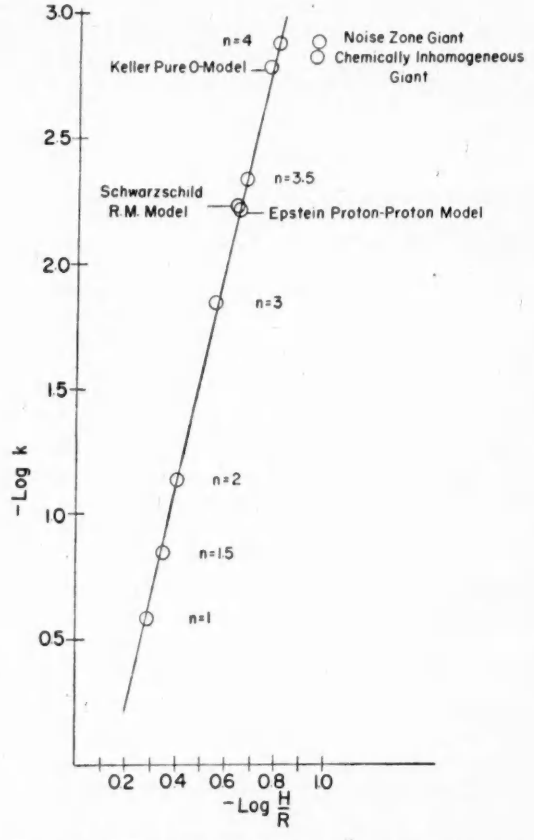

FIG. 1.—The linear relationship between log (H/R) and log k is clearly shown for polytropes and main-sequence models. The two points in the upper right-hand part represent red giants.

[6] *Ap. J.*, **108**, 373, 1948.
[7] *M.N.*, **109**, 631, 1949.

III. THE APSIDAL-MOTION CONSTANT FOR EPSTEIN'S TWO-SOURCE MODEL

In a recent paper, I. Epstein[4] has shown that the central temperatures in stars like the sun are sufficiently low ($\sim$15,000,000°) that the proton-proton reaction plays the dominant role in the generation of energy rather than the carbon cycle. Epstein's results are based on the new cross-sections for the nuclear reactions in the carbon cycle, but they do not take into account the recent revisions in the theoretical value of the proton-proton cross-section.

The calculations of Frieman and Motz[5] on the proton-proton capture cross-section

TABLE 1

Model	$(H/R)^2$	Apsidal-Motion Constant k	Effective Polytropic Index from Apsidal Motion
Polytrope $n=1$	0.26138	0.25992	.....
Polytrope $n=1.5$	.20502	.14460	.....
Polytrope $n=2$	.15704	.07410	.....
Polytrope $n=2.5$	.11203	.....	.....
Polytrope $n=3$	.07583	.01440	.....
Epstein proton-proton model	.04935	.00599	3.38
Schwarzschild Russell-mixture model	.05203	.00585	3.40
Polytrope $n=3.5$	.04558	.00470	.....
Keller pure oxygen model	.02908	.00174	3.91
Polytrope $n=4$	.02358	.00134	.....
Noise-zone giant model	.01200	.00153	3.94
Chemically inhomogeneous model	0.01177	0.00123	4.01

strengthen the evidence in favor of the proton-proton chain reaction. In these calculations the correct Fermi g-factor and improved deuteron wave functions were used, with the result that the cross-section was found to be considerably larger than that used by Epstein.

As one moves up the main sequence toward stars of type earlier than the sun, the higher central temperatures in these stars will favor the carbon cycle as against the proton-proton reaction. This follows from the fact that the nuclear reactions in the carbon cycle are much more dependent on the relative velocities of the interacting nuclei than are the reactions in the proton-proton chain.

The work of Epstein indicates that the carbon cycle is of negligible importance for G0 or later-type stars. Although the exact point on the main sequence where the carbon cycle and the proton-proton chain become of equal importance cannot be determined without detailed integrations of the equations of stellar structure, it is possible to obtain some estimate of where this occurs by indirect means.

Bondi[2] has approached this problem by considering the difference in the slopes of the upper and lower portions of the main-sequence branch in the Hertzsprung-Russell diagram. Using general power laws for the energy generation and the opacity, he obtains relationships between the luminosity and the effective temperature which enable him to determine where on the main sequence the proton-proton reaction gives way to the carbon cycle. He concludes that this occurs for stars of $M_{bol} = 6.5$. Since this corresponds to a central temperature of 1.3×10^7 degrees, this is in distinct disagreement with Epstein's conclusions. It is therefore of interest to establish other criteria for determining where this change occurs. If we compare the observed apsidal motion of binaries of

[5] *Phys. Rev.*, **83**, 202, 1951. A detailed account of this work will soon be published.

various spectral classes with that calculated for a given stellar model, we should be able to use this as a criterion for determining where a change occurs.

The apsidal-motion constant for Epstein's two-source model was obtained by integrating numerically the differential equation for the distortion as described by Motz and Keller.[1] The value of this constant was found to be 0.00599, giving an effective polytropic index of 3.38. For a model having approximately the same hydrogen and helium content but using only the carbon cycle, the apsidal-motion constant is found to be considerably smaller. Thus Keller[1] obtains the value $k = 0.0035$, corresponding to an effective index of 3.7 for a carbon-cycle model having approximately the same chemical composition as Epstein's model.

The observational material obtained from actual binaries is unfortunately rather meager and, except for few cases, not too reliable. A critical review of the available data has been given by Russell[9] and has been re-examined by Keller,[1] who concludes that for only seven stars is the material sufficiently reliable to be compared with theory.

Unfortunately, seventeen of the eighteen stars analyzed by Russell are of spectral class F or earlier (except for CO Lacertae, which is an F star, they are all earlier than A2). The one G0-type star included is 13 Ceti A, for which the apsidal motion is uncertain because of unexplained discordances in radial velocities. Nevertheless, the tentative k value for this star is so much larger than that for the early-type stars as to indicate a distinct change of model in going from G0 to early-type stars.

If, following Keller, we take the seven most reliable determinations of the apsidal motion, we find that these apply to stars earlier than F0, and five of them have values smaller than that found for Epstein's model. Keller assumes an average value of k corresponding to an effective polytropic index of 3.7. This, of course, is what we would expect for these stars, since the carbon cycle is surely dominant for the early main-sequence stars.

The need for more observational data in this field, particularly for binary stars of spectral class G0 and later, is quite evident. If the observational data show a definite increase in the k values of the apsidal motion for the G0 and later stars, as compared to those of the earlier-type stars, one may be justified in concluding that a change of model occurs at this point corresponding to a transition from the carbon cycle to the proton-proton reaction.

[9] *Ap. J.*, **90**, 641, 1939.

NOTES

NOTE ON THE IDENTIFICATION OF THE GROUND STATE OF THE *TiO* MOLECULE

Up to the present time, five band systems have been positively identified in the spectrum of the *TiO* molecule.[1,2] Three systems result from transitions between triplet electronic states, and two are produced by transitions between singlet states. The lowest observed triplet and singlet electronic states are a $^3\Pi$ and a $^1\Delta$ state, respectively. Since no intercombination system is at present known, there has been some doubt as to which of these two states is the ground state of the molecule.

A decision may be made as to the relative electronic energies of the lowest triplet and singlet states, by studying the changes, with temperature, of the relative intensities of representative triplet and singlet bands, using a source of radiation in which it can be assumed that thermodynamic equilibrium prevails. Under these conditions, the intensity of a spectral feature in emission is represented by the well-known formula

$$I_{em}^{nm} \sim \nu_{nm}^4 \left| R^{nm} \right|^2 e^{-\nu_n hc/kT} ,$$

in which R^{nm} is the corresponding matrix element of the electric dipole moment, and ν_n is the energy in wave members of the initial state. In thermodynamic equilibrium the population of the initial state is proportional to $\exp(-\nu_n hc/kT)$.

The ratio of the intensities in emission of a singlet and a triplet band at temperature T_1 will be

$$R(T_1) = \left(\frac{\nu_s}{\nu_t}\right)^4 \left(\frac{|R_s|^2}{|R_t|^2}\right) \exp - \left[\frac{(\nu_s - \nu_t)\, h\, c}{kT}\right],$$

where the subscripts s and t refer to the singlet and triplet bands, respectively. A similar ratio may be obtained at a second temperature, T_2. Finally, the ratio of $R(T_1)$ to $R(T_2)$ becomes

$$\frac{R(T_1)}{R(T_2)} = \exp - \left[(\nu_s - \nu_t)\left(\frac{h\, c}{kT_1} - \frac{h\, c}{kT_2}\right)\right].$$

If T_1 and T_2 are known, the measurement of the band intensities at the two temperatures will result in the determination of the energy difference, $(\nu_s - \nu_t)$, in wave numbers, of the respective upper states. Of course, as soon as the energy of any singlet state relative to the energy of any triplet state is known, it is immediately possible to locate correctly all known singlet and triplet levels on the same energy-level diagram and to make a decision as to which electronic state is the ground state of the molecule.

In 1950 the entire emission spectrum of the *TiO* molecule, from 4500 A to 8000 A, was photographed at the Yerkes Observatory, using as a source a carbon-resistance electric furnace of the King type. The furnace was operated at three different temperatures, 1900°, 2100°, and 2300° C. Below 1900° C the *TiO* spectrum was too faint for observation; at 2500° C the spectrum of C_2 became prominent. A partial atmosphere of argon was introduced into the furnace in order to reduce diffusion of the *TiO* molecules from the ends of the carbon tube and to insure conditions of thermodynamic equilibrium. The spectrum was photographed with a plane-grating spectrograph, with a dispersion of 50 A/mm. Plate calibration was accomplished through the use of a rotating sector, and plates were standardized by photographing the radiation from a solid carbon plug midway in the furnace tube. The furnace will be described in a later publication.

[1] G. Herzberg, *Spectra of Diatomic Molecules* (New York: D. Van Nostrand Co., Inc., 1950), p. 576.

[2] F. P. Coheur, *Bull. Soc. R. Sci., Liége*, **12**, 98, 1943.

The bands chosen for study were the (0–0) band of the β system ($c^1\Phi$–$a^1\Delta$) at 5597 A, and the (0–1) band of the α system ($C^3\Pi$–$X^3\Pi$) at 5448 A. At each of the three temperatures, measurements were made of the radiation emitted in these two bands, in the wavelength interval between their heads and the heads of the succeeding bands in the respective band sequences. The background emission in each case was assumed constant with wave length and equal to the emission found immediately to the violet of the respective heads. This simplifying assumption as to the intensity of the background undoubtedly introduced systematic errors into the determination of the intensity of an individual band, but, by carrying out the same procedure at each temperature, the effects of these errors would have a minor effect on the final ratio $R(T_1)/R(T_2)$. The ratios $R(T)$ are presented on the left side of Table 1. As can be seen, the singlet band steadily decreased in

TABLE 1

RATIO OF INTENSITIES OF THE λ 5598 AND THE λ 5448 BANDS OF THE *TiO* MOLECULE

Temperature (° C)	$R(T) = I_s(5598)/I_t(5448)$	Ratio	$(\nu_s - \nu_t)$ (Cm^{-1})
1900	0.58	$R(1900)/R(2300)$	−840
2100	0.56	$R(1900)/R(2100)$	−700
2300	0.53	$R(2100)/R(2300)$	−1230

intensity, relative to the triplet band, as the temperature was raised.

The ratios $R(T)$ were then combined in three different ways to find the energy difference, $(\nu_s - \nu_t)$. The results are listed on the right side of Table 1. The negative signs of $(\nu_s - \nu_t)$ indicate that the upper state of the singlet band is below the upper state of the triplet band.

The relative energies of the lowest known triplet and singlet electronic states could then be found, since the electronic energies of the initial states of the two bands, above their respective lowest states, were known. The upper state of the 5448 A band is the unresolved triplet vibrational level, $v' = 0$, of the excited $C^3\Pi$ state. The three triplet components of the vibrational energy, ν_{00}, are very similar: their mean is 19,345.1 cm^{-1}. Similarly, the upper state of the 5598 A band is the $v' = 0$ vibrational level of the $c^1\Phi$ state, which is 17,840.6 cm^{-1} above the $v'' = 0$ level of the $a^1\Delta$ state. By combining these quantities with the results presented in Table 1, it was found that the $v'' = 0$ level of the $X^3\Pi$ state was definitely lower than the corresponding level of the $a^1\Delta$ state, the energy difference ranging from 274 to 804 cm^{-1}, depending upon the particular value of $(\nu_s - \nu_t)$, of Table 1, that was used. The average $(\nu_s - \nu_t)$ gave a difference of 581 cm^{-1}.

While the method thus led to a poor determination of the excitation energy of the $a^1\Delta$ state, it did provide conclusive evidence that the $X^3\Pi$ state is the lowest observed state of the *TiO* molecule. The $X^3\Pi$ state can therefore be regarded as the ground state, although the possibility always remains that the analysis of additional band systems in the complex spectrum of the molecule may lead to the discovery of an electronic state that is even lower.

The author wishes to express his thanks to Dr. George Herbig, and to the Lick Observatory, for making it possible for him to obtain the tracings used in this study. The electric furnace was constructed on a contract with the Office of Naval Research.

JOHN G. PHILLIPS

LEUSCHNER OBSERVATORY
UNIVERSITY OF CALIFORNIA
December 26, 1951

ON THE CORONAL LINES λλ 5445, 5694, AND 4086

Edlén[1] tentatively attributed the coronal line λ 5694 to the transition $2p^2\ {}^3P_1-{}^3P_0$ in *Ca* XV; and Waldmeier[2] has suggested that the coronal line λ 5445 be ascribed to the corresponding ${}^3P_2-{}^3P_1$. Naqvi[3] has, however, proposed the identification of one or the other of the lines λ 4567 and λ 4586 as the ${}^3P_2-{}^3P_1$ transition in *Ca* XV. Shklovskii[4] examined the *Ca* XV transitions theoretically and has shown that the proposed identifications of λ 5445 and λ 5694 are probably incorrect. Extrapolation of the data given by Garstang[5] for the $2p^2$ configurations enable these calculations to be refined. We find, for the relevant parameters in *Ca* XV (in cm^{-1}),

$$\zeta = 24{,}210\,, \qquad \eta = 91\,,$$

$$(SP) = 162{,}700\,, \qquad (DP) = 76{,}400\,.$$

Using these and solving the secular determinant exactly (instead of an expansion in powers of ζ), the triplet intervals are

$${}^3P_2 - {}^3P_1 = 18{,}580\ cm^{-1} = 5380A\,,$$

$${}^3P_1 - {}^3P_0 = 18{,}240\ cm^{-1} = 5480A\,.$$

Although the extrapolation is a large one, it seems quite probable that these wave lengths are accurate to ±50 A. The differences between the theoretical and the observed wave lengths are greater than would thus be expected and support the conclusion that the identification of any of the lines λλ 5445, 5694, 4586, and 4567 as due to *Ca* XV is incorrect. Revised theoretical transition probabilities for *Ca* XV $2p^2$ are given in Table 1.

TABLE 1

TRANSITION PROBABILITIES FOR *Ca* XV AND *Ca* XIII (SEC^{-1})*

Transition	Type	*Ca* XV	*Ca* XIII	Transition	Type	*Ca* XV	*Ca* XIII
${}^1S_0-{}^1D_2$	*e*	6.84	11.0	${}^1D_2-{}^3P_1$	*m*	610	107
${}^1S_0-{}^3P_2$	*e*	17.1	1.6		*e*	0.065	0.0071
${}^1S_0-{}^3P_1$	*m*	9680	8560	${}^3P_2-{}^3P_1$	*m*	81	330
${}^1D_2-{}^3P_2$	*m*	880	840		*e*	0.00035	0.0033
	e	0.14	0.25	${}^3P_2-{}^3P_0$	*e*	0.0038	0.011
${}^1D_2-{}^3P_0$	*e*	0.41	0.0042	${}^3P_1-{}^3P_0$	*m*	105	3.6

* *m* = magnetic dipole; *e* = electric quadrupole, s_q (atomic units) *Ca* XIII = 0.0416, s_q (atomic units) *Ca* XV = 0.0365.

The calculations of Shklovskii on the ratio ($r = I[5694]/I[5445]$) of the intensities of the *Ca* XV lines are essentially unaltered by these revised values. It should, however, be emphasized that, owing to the serious uncertainties in our knowledge of electron-collision cross-sections, the calculated intensity ratio may be appreciably in error. Notwithstanding this, the differences between theoretical [r = 1.0–1.5 on Shklovskii's assumption (*a*)] and observed ($r = 6$) intensity ratios are such as to leave little doubt of the correctness of Shklovskii's conclusions.

It is of interest to examine the corresponding transitions in *Ca* XIII ($2p^4$). We find in this case (in cm^{-1})

$$\zeta = 21{,}690\,, \qquad \eta = 56\,, \qquad (SP) = 158{,}600\,, \qquad (DP) = 72{,}300\,.$$

[1] *Zs. f. Ap.*, **22**, 30, 1943.
[2] *Zs. f. Ap.*, **29**, 29, 1951.
[3] *A.J.*, **56**, 135, 1951.
[4] *Izv. Crimean Ap. Obs.*, **5**, 109, 1950.
[5] *M.N.*, **111**, 115, 1951.

The triplet intervals are

$$^3P_0 - {}^3P_1 = \quad 4110\ \text{cm}^{-1} = 24{,}330\text{A}\,,$$

$$^3P_1 - {}^3P_2 = 24{,}900\ \text{cm}^{-1} = \quad 4016\text{A}\,.$$

The extrapolation is rather more uncertain than for *Ca* XV, and the identification of a line λ 4086 with *Ca* XIII $2p^4\ {}^3P_1 - {}^3P_2$ is consistent with the above calculations. Transition probabilities for *Ca* XIII are given in Table 1. The case of *Ca* XIII is of special interest, because we can compare our parameters with those obtained from a self-consistent field, with exchange, calculated by Davis.[6] He obtained $\zeta = 22{,}240\ \text{cm}^{-1}$, and the writer finds $\eta = 62\ \text{cm}^{-1}$. The agreement is excellent and can be regarded as confirming our extrapolations.

R. H. GARSTANG

YERKES OBSERVATORY
December 1, 1951

ABSOLUTE ABSORPTION OF THE H_2 CONTINUUM*

The absorption coefficients of molecular nitrogen and oxygen[1] and of neon[2] for ultraviolet radiation have been studied experimentally with a grazing-incidence vacuum spectrograph in the range from 300 A to 1300 A, using photometric techniques in conjunction with a constant-intensity emission-line source.[3] Preliminary results on the absorption coefficients in H_2 were obtained in the same way and are presented in Figure 1. The coefficient k_λ is defined by $I = I_0 \exp(-k_\lambda x)$, where I_0 and I are the relative inten-

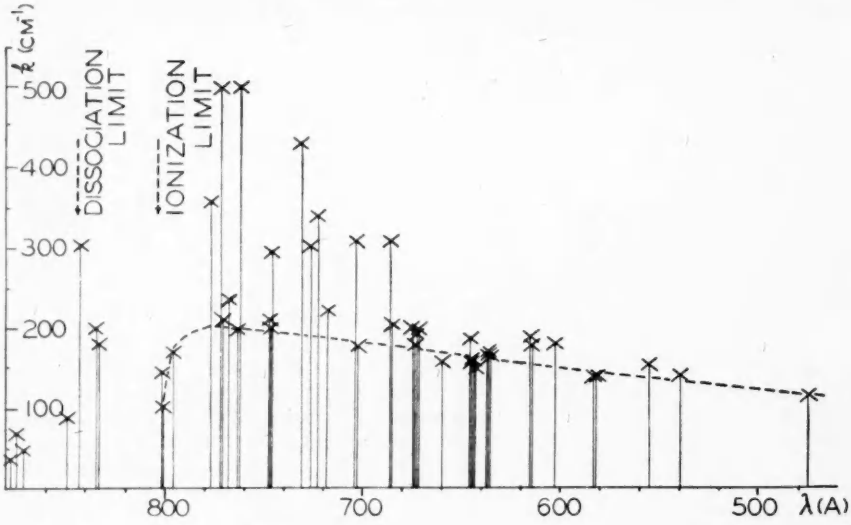

FIG. 1.—Absorption coefficients in H_2 versus wave length. The crosses represent measured values of the absorption coefficients $k(\text{cm}^{-1})$. The dashed line is an estimate of the H_2 ionization continuum.

[6] *Ap. J.*, **110**, 17, 1949.

* The help of ONR is gratefully acknowledged.

[1] G. L. Weissler, Po Lee, and E. I. Mohr, *J. Opt. Soc. America* (in press).

[2] Po Lee and G. L. Weissler, *J. Opt. Soc. America*, to be published as a Letter to the Editor.

[3] Po Lee and G. L. Weissler, *op. cit.* (in press).

sities of radiation before and after passing through a length x (at N.T.P.) of the absorbing H_2. The experimental points were obtained from one photographic plate in the following manner. If, for a given source emission line, the linear relationship $\ln I_0 - \ln I = \alpha p$ was found to hold for various pressures of the absorbing gas, then the k value was calculated from the slope $\alpha = (LT_0k)/(p_0T)$ and was plotted as a single point. A dashed line has been drawn in the figure roughly connecting the lowest absorption coefficients for wave lengths shorter than 803.7A (the ionization limit, $H_2^+X^2\Sigma_g^+$).

The absorption spectrum of H_2, which was studied by Tanaka[4] with a Lyman continuum, revealed strong absorption bands between 838 A and 770 A, the $D \leftarrow A$ band system,[5] and a dissociation continuum starting at 849.4 A,[6] together with other diffuse bands, all overlapping the ionization limit at 803.7 A. This makes it extremely difficult to identify clearly the hydrogen ionization continuum which is presumably represented by the dashed line in Figure 1. The high k values above this line are known to fall within the strong $D \leftarrow A$ bands and other unidentified diffuse bands in this region. It is to be noted that the large coefficients around 735 A lie close to the dissociation limit of the D state ($H_2D^1\Pi_u$), namely, 748.6 A. At 303 A the k value was measured to be less than 20 cm^{-1}. The integrated area under the dashed curve yields an effective oscillator strength $f = 0.79$ which is somewhat larger than the value obtained from the equation fitting the index of refraction measurements,[7] $f_1 = 0.69$ at $\lambda_1 = 734.5$ A. The error of the measurements of k values presented here is estimated to be about 15 per cent. More work over a more extended wave-length range is in progress.

Po Lee
G. L. Weissler

Physics Department
University of Southern California
December 22, 1951

ABSOLUTE OSCILLATOR STRENGTHS OF CHROMIUM

The *Cr* vapor-pressure measurements of Speiser, Johnston, and Blackburn[1] make possible a new computation of the absolute f-values of the *Cr* resonance triplet $a^7S_3 - z^7P^\circ_{2,3,4}$ (respectively, λλ 4290, 4275, 4254), using the previously reported spectroscopic nf-values for these transitions.[2]

These authors report two vapor-pressure equations for *Cr:* the first (I) results from a least-squares treatment of their experimental results, while the second (II) results from their experimental value of ΔH_0^0 combined with the free-energy computations of K. K. Kelley.[3] Equations (I) and (II) are both given in the usual form: $\log P = -A/T + B$, having values for A, respectively, of 20,473 and 20,434. The older work of Baur and Brunner, which this new work definitely supersedes, had $A = 10{,}220$. If the spectroscopic data are plotted in the form $\log nfT$ versus $1/T$, the slope of the curve roughly indicates $A = 14{,}000$. Hence the spectroscopic data still do not agree too well; the three f-values computed from the nf-values at the lowest temperature (1410°.5 K) in particular being about 10 per cent larger than the average f-values. It may be, however, that this system-

[4] *Sci. Pap. Inst. Phys. Chem. Res., Tokyo*, **42**, 49, 1944; contains fifty-three references.

[5] J. J. Hopfield, *Nature*, **125**, 927, 1930; *Phys. Rev.*, **47**, 788, 1935; H. Beutler, A. Deubner, and H. O. Jünger, *Zs.f. Phys.*, **98**, 181, 1936; **100**, 80, 1936.

[6] G. H. Dieke and J. J. Hopfield, *Phys. Rev.*, **30**, 400, 1927.

[7] K. L. Wolf and K. F. Herzfeld, *Handb. d. Phys.*, **20**, 49s; S. A. Korff and G. Breit, *Rev. Mod. Phys.*, **4**, 471, 1932.

[1] *J. Amer. Chem. Soc.*, **72**, 4142, 1950.

[2] F. B. Estabrook, *Ap. J.*, **113**, 684, 1951.

[3] *Contributions to the Data on Theoretical Metallurgy*, Part III (U.S. Bureau of Mines Bull. 383 [1935]).

atic deviation is spurious, as the equivalent width determinations of the weak absorption lines at 1410°.5 K were particularly difficult.

The magnitudes of the *f*-values calculated from the new data are over seven times those tentatively reported previously (using Kelley's work). The new averaged absolute *f*-values for *Cr* are, using equation (I): $f(4290) = 0.047$, $f(4275) = 0.067$, $f(4254) = 0.084$. Using equation (II), they are but slightly different: $f(4290) = 0.050$, $f(4275) = 0.071$, $f(4254) = 0.089$. The probable error of these values is about 10 per cent.

I would like to thank Professor Leo Brewer, of the University of California, for calling my attention to the publication of these new data and for several private communications on the subject.

FRANK B. ESTABROOK

MIAMI UNIVERSITY
OXFORD, OHIO
December 8, 1951

HERBIG'S NEBULOUS OBJECTS NEAR NGC 1999

In a recently published note G. H. Herbig[1] reports the discovery of three peculiar nebulous objects near NGC 1999 and gives the spectroscopic description of the two brightest. The writer had independently discovered these peculiar objects,[2] finding *Hα* and the [*O* I] lines at λ 6300 and λ 6363 in emission in the spectra of the three. In the same region of the sky, covering an area of 20 square degrees, four additional, similar objects were found. It is of interest to point out that these seven peculiar objects are the only ones that were found in an investigation over Milky Way regions which cover approximately 1000 square degrees.

The emphasis of this note, however, is upon the stars that Herbig found in his nebulous objects Nos. 1 and 2 and what he suggests about them.

Herbig is faced with the alternative of postulating either (1) the existence of faint blue, high-temperature stars in the NGC 1999 objects or (2) the interaction of a late-type dwarf star with the nebular material. The latter seems more plausible to him.

In order to prove whether the stars associated with the nebulous objects are faint blue dwarfs or whether they are late-type dwarf stars, the writer took with the Tonantzintla Schmidt camera several direct infrared plates (hypersensitized I-N plates behind a filter that cuts approximately at λ 7200) over the NGC 1999 region. It is assumed that on the long-exposure infrared plates all stars later than type G and with photographic magnitudes as faint as 19 must appear. Thus, all the stars that are in the surroundings of the three nebulous objects and that appear on 103*a*-O plates with photographic magnitudes as faint as 19 also are easily visible on the infrared plates (Fig. 1). However, and in spite of what has been mentioned, the stars found by Herbig in his objects Nos. 1 and 2, with visual magnitudes 16 and 17.5, do not appear on the infrared plates.

This clearly indicates that the stars associated with the three peculiar nebulous objects cannot be late K or early M-type dwarfs. If any star is associated with these nebulous objects, it must be a faint, very blue, hot star.

GUILLERMO HARO

OBSERVATORIO DE TONANTZINTLA
MEXICO
January 5, 1952

[1] *Ap. J.*, 113, 697, 1951.

[2] In personal letters dated May 31, 1950, which were written to Drs. Shapley and Minkowski, the writer pointed out the peculiarity of these objects.

FIG. 1.—The centers of the circles mark the positions of Herbig's nebulous objects. Hypersensitized I-N plate.

THE SHELL SPECTRUM OF OMICRON ANDROMEDAE

The spectrum of *o* Andromedae[1] at the present time is that of a shell surrounding a rapidly rotating star of type B6.5. The star was discovered by Irene Hansen and W. W. Morgan, on the basis of an examination of spectrograms taken at Yerkes and McDonald Observatories in 1946, to be of the shell type and to have *Hα* in emission.[2]

The star has evidently changed back and forth between a shell-type and a normal B-type star a number of times since it was first observed spectroscopically. It was classified as composite by Miss Maury,[3] on the basis of a one-prism plate taken with the 11-inch Draper telescope of the Harvard College Observatory in February, 1890. According to Miss Maury, the spectrum combined the features of an *α* Cygni–type spectrum with those of a normal B5 spectrum at that time. Two-prism plates taken in September and October, 1893, revealed only the B5 spectrum, and the change was attributed by Miss Maury to the difference in the dispersions employed. A re-examination of the above plates plus additional plates led Miss Emma T. R. Williams[4] to conclude that the changes noted were probably real. She also pointed out that plates taken in 1927 and 1928 showed only the B5 spectrum. It seems certain, therefore, that *o* Andromedae was in the shell stage in 1890 but resembled a normal B-type star in 1893, 1927, and 1928.

Perkins spectrograms of 1937 and 1940 do not reveal the narrow metallic lines characteristic of the developed shell spectrum, but sharp hydrogen-absorption cores were present, indicating at least a thin shell. During this same period, there was no visible emission at *Hα*. In 1946, both *Hα* emission and shell-type spectrum were present, as was noted above. Spectrograms of the blue region taken at the Perkins Observatory from 1949 to date have shown no change. The spectrum of *o* Andromedae at present is shown in Figure 1, *a*, as obtained with the two-prism spectrograph attached to the 69-inch reflector of the Perkins Observatory, giving a dispersion of 30 A/mm at *Hγ*. The narrow hydrogen-absorption cores and lines of *Fe* II, *Ni* II, and other metals which arise from the shell are seen superposed on the rotationally broadened spectrum of the underlying star. *Hα*, however, has changed somewhat in the past few years. In 1949 it was a weak absorption line with no visible emission edges, while emission can be clearly seen on either side of the central absorption core on a recent spectrogram, as is shown in Figure 1, *c*. Evidently, the increase in the size of the shell surrounding *o* Andromedae in recent years did not appreciably change the amount of material as seen projected against the disk of the star, since the shell absorption lines showed no detectable change in this interval.

The spectrum of *o* Andromedae at present resembles most closely the spectrum of the shell-type star HD 217050, which has been described by Baldwin[5] and others.[6,7] In Figure 1 the blue and red spectra of the two stars are compared.

The spectral types of the underlying stars appear to be slightly different: *o* Andromedae is of type B6.5, while HD 217050 is a B5-type star. Spectral types of the B-type absorption shell stars are difficult to assign with any certainty, however, because of the tremendous rotational broadening of the underlying stellar lines. The stars *o* Andromedae and HD 217050 are among the most rapidly rotating known, the former having an equatorial rotational velocity of 360 km/sec and the latter having one of 380 km/sec.[2]

A comparison of the shells of these two stars shows first that the shell of *o* Andromedae is optically the thinner of the two. Although both stars feature sharp and deep cores of the Balmer series, due to absorption in the shell, the Balmer wings, which are due to Stark broadening in the underlying star, are much stronger in the spectrum of *o* Androm-

[1] $\alpha(1900) = 22^h57^m3$; $\delta(1900) = +41°47'$; $m_v = 3.63$.

[2] *Ap. J.*, **110**, 498, 1949.

[3] *Harvard Ann.*, **28**, 100, 1897.

[4] *Harvard Circ.*, No. 348, p. 13, 1930.

[5] *Ap. J.*, **97**, 388, 1943.

[6] O. Struve, *Ap. J.*, **99**, 205, 1944.

[7] W. A. Hiltner, *Ap. J.*, **105**, 212, 1947.

edae. This is also true, to a lesser extent, of the *He* I lines. An examination of the red spectra of the two stars brings this out even more clearly: in HD 217050, only lines arising from the shell are easily visible, while the Paschen series of hydrogen arising from the underlying star is strong in the spectrum of *o* Andromedae.

The two shells differ strongly with respect to emission. *Hα*, the only line which shows any emission in *o* Andromedae, is very much weaker than the corresponding line in HD 217050. In addition, the latter shell has *Hβ* and *Hγ*, several lines of *Fe* II, the infrared *Ca* II triplet, and *O* I λ8446 in emission. This would point to a larger shell, relative to the size of the star, in HD 217050 as compared to *o* Andromedae.

A comparison of the metallic absorption lines arising from the two shells is of interest. The lines of *Fe* II, the principal contributor to the shell spectrum of *o* Andromedae, are about equal in strength in the two stars. Perhaps the most striking difference is the weakness of *Ti* II in *o* Andromedae relative to HD 217050. Though nearly as strong as *Fe* II in the latter star, the lines of *Ti* II are considerably weaker than those of *Fe* II in *o* Andromedae. A number of other elements, including *Sr* II, *Sc* II, *Ca* I, and *Fe* I, are also much stronger in the shell of HD 217050. The *Ca* II K line (which probably arises from the shell in both stars) appears to be slightly stronger in the spectrum of HD 217050.

In view of the ionization potentials of the above elements, it would seem that the degree of ionization is somewhat higher in the shell of *o* Andromedae than in that of HD 217050. The relatively great strength of *Fe* II in the latter shell might then be a result of the greater amount of material contained in the shell.

An examination of the widths of the lines in Figure 1, *a*, shows that the shell of *o* Andromedae is stratified. The lines of *He* I, which arise entirely from the underlying star, suffer the greatest rotational broadening. From the lower strata of the shell come the *Mg* II and *Si* II lines, which are nebulous but not so broad as the lines of *He* I. Next are the many lines of *Fe* II, probably arising at various places in the shell, since they vary somewhat in degree of sharpness. The stratification of the shell of *o* Andromedae is similar to that previously announced by Struve and Wurm[8] for *ζ* Tauri and by Struve[9] for 48 Librae.

It is impossible to determine the luminosity class spectroscopically, for the reasons given above. The broad wings of the hydrogen lines visible in Figure 1, *a*, suggest an object which is close to the main sequence, however.

It is interesting to note that both *o* Andromedae and HD 217050 have exhibited light-variations. The former star was shown to be variable by Emberson,[10] who found a variation of 0.5 mag. or more in radiometric measures made with a thermoelectric photometer in 1939. An examination of Harvard patrol plates by Miss Hoffleit[10] indicated variability in photographic light of about 1 mag. She found the star to be photographically faint when the K line was very weak or invisible, that is, when the spectrum was that of a normal B-type star. Light-variations in HD 217050 were pointed out by Walker,[11] who found fluctuations up to 0.20 mag. in a few hours during the night of August 27/28, 1950.

In view of the recent changes in the *Hα* emission in the spectrum of *o* Andromedae, it will be of interest to observe the star spectroscopically in the future. If more material is passing into the shell, the degree of ionization will probably change, with corresponding changes in the intensities of *Fe* II, *Ti* II, and other elements. On the other hand, if the increased *Hα* emission simply means a slowly expanding shell dissipating into space, the spectrum may return to that of a normal B-type star once more.

[8] *Ap. J.*, **88**, 105, 1938.

[9] *Ap. J.*, **98**, 112, 1943.

[10] *Harvard Announcement Card* No. 499, 1939.

[11] *Pub. A.S.P.*, **63**, 36, 1951.

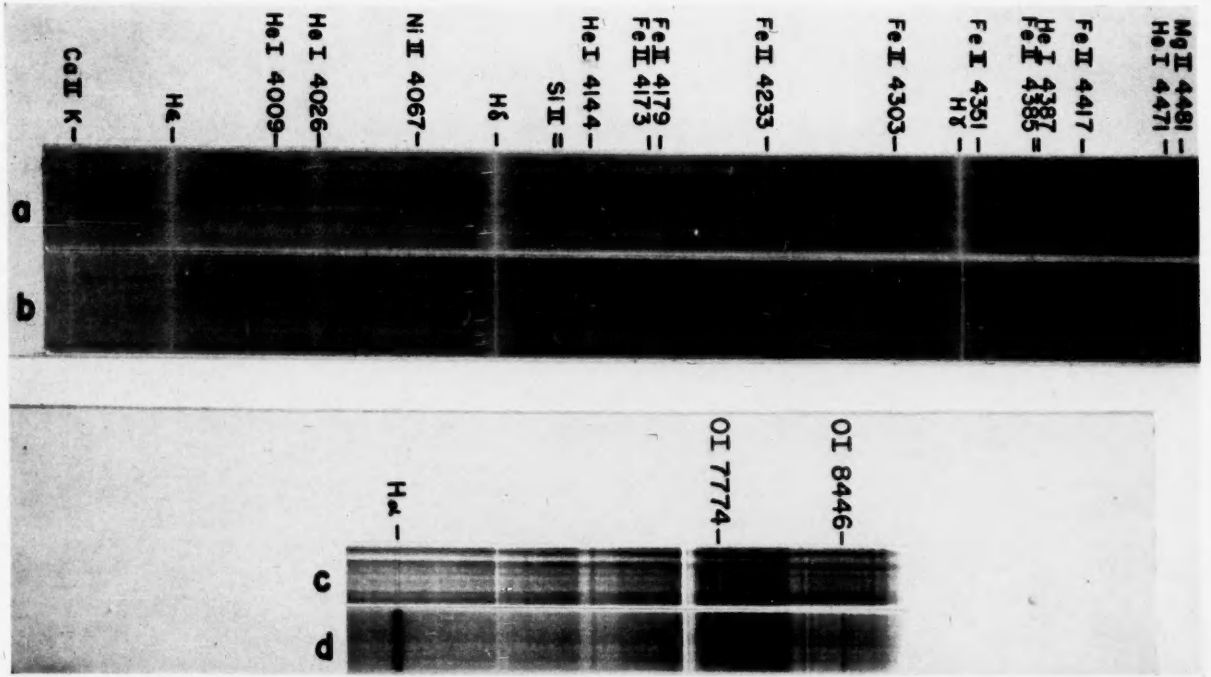

FIG. 1.—Comparison of the blue and red spectra of the shell-type stars *o* Andromedae, and HD 217050. *a*, *o* Andromedae, process plate (August 29, 1951); *b*, HD 217050, 103-O plate (July 21, 1951); *c*, *o* Andromedae, 1–N plate focused on *Hα* (September 12, 1951); *d*, HD 217050, 1-N plate focused on λ 7774 (September 19, 1951).

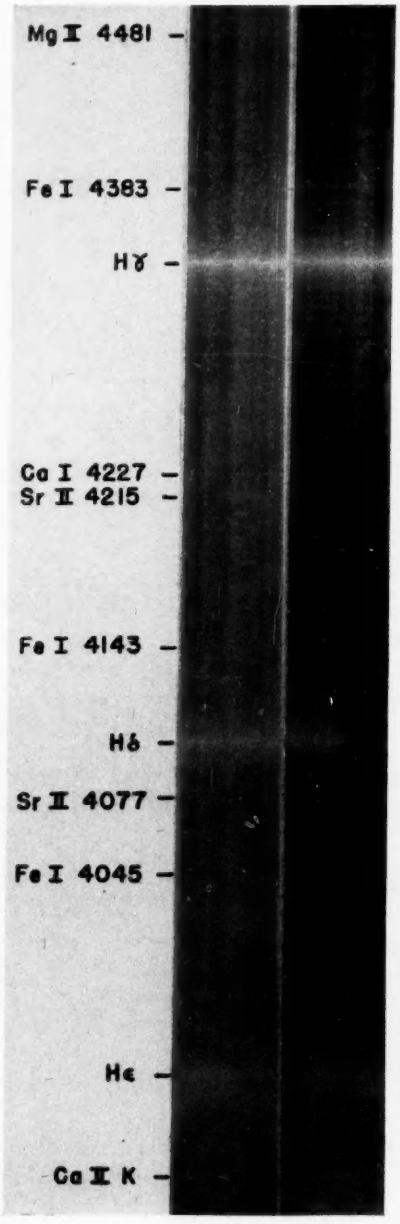

FIG. 1.—The spectrum of 29 Cygni *(top)* with the spectrum of the standard A2 main-sequence star η Ophiuchi for comparison. Both spectrograms were taken on 103-O emulsion.

It is a pleasure to thank Dr. W. W. Morgan for calling my attention to this star. I am also indebted to Dr. Morgan and Dr. Otto Struve for a critical reading of this paper.

ARNE SLETTEBAK

PERKINS OBSERVATORY
September 1951

THE SPECTRUM OF 29 CYGNI

In the course of an investigation of the rotational velocities of the B8–A2 stars brighter than the fifth magnitude, some 150 spectra have been examined. Of these, two stars were found to be characterized by a general weakening of the spectral lines.[1] One of these, λ Bootis, was previously announced by Morgan, Keenan, and Kellman.[2] The spectral type is A0, as determined by the Balmer lines of hydrogen and the *Ca* II K line, the only spectral lines which can be clearly seen. The *Mg* II λ 4481 line and the *Fe* I λ 4045 line are the only other lines visible, and these are just on the threshold of visibility on Perkins spectrograms, which are greatly widened to aid in the detection of faint features. Morgan points out that λ Bootis is probably located below the main sequence, as indicated by its trigonometric parallax. The other star with weakened spectral lines is 29 Cygni,[3] which will be briefly described in this note.

Figure 1 shows the spectrum of 29 Cygni (top spectrum) with the spectrum of the standard A2 main-sequence star η Ophiuchi for comparison, both taken with the two-prism spectrograph attached to the 69-inch reflector of the Perkins Observatory, giving a dispersion of 30 A/mm at $H\gamma$. The metallic lines in the spectrum of 29 Cygni are seen to be much more shallow, but no wider, than the corresponding lines in the comparison star. The weakening is therefore not an effect of axial rotation. It is interesting to note that some lines suffer more than others: in general, the lines of ionized atoms are weakened the most, and those of neutral atoms the least. Thus the lines of *Fe* II, *Ti* II, *Ni* II, and *Mg* II are conspicuously weakened, while the lines of *Fe* I and *Ca* I are among the most prominent in the spectrum of 29 Cygni. An exception to this is *Sr* II, the lines of which are relatively strong in this star. *Sr* II shows a negative absolute-magnitude effect in the early A-type stars, however.[4] The Balmer series of hydrogen in 29 Cygni may be somewhat weaker than that of the A2 standard star, although this is uncertain.

A 1-N plate of 29 Cygni shows the infrared portion of the spectrum to be similar to that of an early A-type main-sequence star. The infrared *O* I lines, which show a positive absolute-magnitude effect in the early A-type stars,[5] are not conspicuously weakened, indicating that 29 Cygni is evidently not too far from the main sequence.

It appears probable from the spectroscopic data that 29 Cygni is a star of spectral type near A2 which is somewhat below the main sequence. Its spectral peculiarities are not so striking as those of a true subdwarf, but they tend in that direction. The trigonometric parallax of this star ($+0''.033 \pm 0''.006$)[6] would seem to confirm this; it locates the star about 1 mag. below the main sequence.

ARNE SLETTEBAK

PERKINS OBSERVATORY
September 1951

[1] A third star, ξ Aurigae [$\alpha(1900) = 5^h46^m5$, $\delta(1900) = +55°41'$, $m_v = 4.92$, spectral type A2], also appears to have weakened lines and shows some spectroscopic evidence of low luminosity, but the effect is not nearly so pronounced as in λ Bootis and 29 Cygni.

[2] *An Atlas of Stellar Spectra* (Chicago: University of Chicago Press, 1943).

[3] $\alpha(1900) = 20^h10^m8$; $\delta(1900) = +36°30'$; $m_v = 4.98$.

[4] W. W. Morgan, *Ap. J.*, **77**, 291, 1933.

[5] P. C. Keenan and J. A. Hynek, *Ap. J.*, **111**, 1, 1950.

[6] I am indebted to Miss Louise F. Jenkins, of the Yale Observatory, for this value.

THE SPECTRUM OF THE HIGH-VELOCITY A-TYPE STAR HD 161817

The A-type star HD 161817[1] was found by Albitzky,[2] at the Simeis Observatory, to have the very high velocity of −360 km/sec. This result was confirmed by Merrill,[3] who obtained a radial velocity of −363.1 km/sec from measures of 60 lines on a plate of dispersion 10 A/mm. He found the velocities from various lines to be in excellent agreement. The writer obtains a radial velocity of -362.5 ± 0.8 km/sec from measures of 68 lines on a plate of 30 A/mm dispersion, taken with the two-prism spectrograph attached to the 69-inch reflector of the Perkins Observatory.

Svetlova[4] determined the proper motion of HD 161817, obtaining $\mu_\alpha = -0''.050 \pm 0''.007$ and $\mu_\delta = -0''.064 \pm 0''.005$. She points out that the parallax of this star is badly needed and suggests that the star is probably an intermediate white dwarf ($M \simeq +5$). Merrill,[3] however, states that "the spectrum photographed with dispersion 10 A/mm resembles that of a sharp-line main-sequence A4 star ($M = +1$) more closely than it does that of the intermediate white dwarfs." Miczaika[5] finds HD 161817 to have an A0 spectrum with sharp Balmer lines which have weak, broad wings. He observes the Balmer series to be visible to *H*18 or *H*19, concluding that HD 161817 is a normal main-sequence star ($M \simeq 0$) and may even be located somewhat above the main sequence.

Figure 1 shows the spectrum of HD 161817 with the spectrum of the A2 main-sequence star η Ophiuchi for comparison. Although the two spectra appear roughly similar, there are distinct differences which lead to the conclusion that the spectrum of HD 161817 is peculiar. Considering first the metallic lines, *Fe* II, *Cr* II, *Ni* II, *Mg* II, and *Si* II are somewhat weaker in HD 161817; *Fe* I, *Ti* II, *Sr* II, and *Ca* II are of about the same strength in the two stars; and *Ca* I and *Sc* II appear to be somewhat stronger in HD 161817. Second, the Balmer lines are slightly weaker in the spectrum of HD 161817, as seen in Figure 1. These differences cannot be reconciled in terms of the normal H-R diagram. Thus, if the spectral type were in the neighborhood of A5, the Balmer line intensities might be normal but the lines of *Ca* II, *Ti* II, *Fe* I, and *Ca* I would be too weak. If the spectral type were placed at A0, the lines of *Ca* II, *Ti* II, *Fe* I, and *Ca* I would be too strong and the Balmer lines too weak. If HD 161817 were above the main sequence at A2, the weakness of the Balmer lines would be explained but the lines of *Fe* II, *Cr* II, *Ni* II, and *Si* II would then be too weak and the lines of *Ca* I and *Fe* I too strong. The spectrum of HD 161817 therefore appears to be peculiar; the approximate spectral type of A2 assigned is a compromise of various criteria.

The peculiarities of the spectrum of HD 161817 are similar to those of the high-velocity A-type subdwarf HD 140283,[6] though not nearly so extreme. The *Ca* II K line of the latter star would suggest a spectral type near A5, but the Balmer lines are very much too weak for this type. All the metallic lines are weak, with the exception of *Ca* I λ 4227 and the *Fe* I lines. HD 140283 has an absolute magnitude of +4.7, placing it about 2.5 mag. below the main sequence at A5.

The spectroscopic data suggest that HD 161817 is a star with spectral peculiarities which place it somewhere between a normal main-sequence star and a subdwarf. In view of the similarities of the spectrum of HD 161817 to a subdwarf spectrum, the criterion of the visibility of Balmer lines to determine the absolute magnitude of this star seems questionable. The trigonometric parallax of HD 161817 is still badly needed.

ARNE SLETTEBAK

PERKINS OBSERVATORY
October 1951

[1] α (1900) = 17h42m6; δ(1900) = +25°48′; m_v = 6.87.

[2] *Poulkovo Obs. Circ.*, No. 7, 1933.

[3] *Pub. A.S.P.*, **59**, 256, 1947.

[4] *A.J.U.S.S.R.*, **23**, 148, 1946.

[5] *Zs. f. Ap.*, **26**, 13, 1949.

[6] α(1900) = 15h37m7; δ(1900) = −10°36′; m_v = 7.26. See Morgan, Keenan, and Kellman, *An Atlas of Stellar Spectra* (Chicago: University of Chicago Press, 1943), Pl. 33.

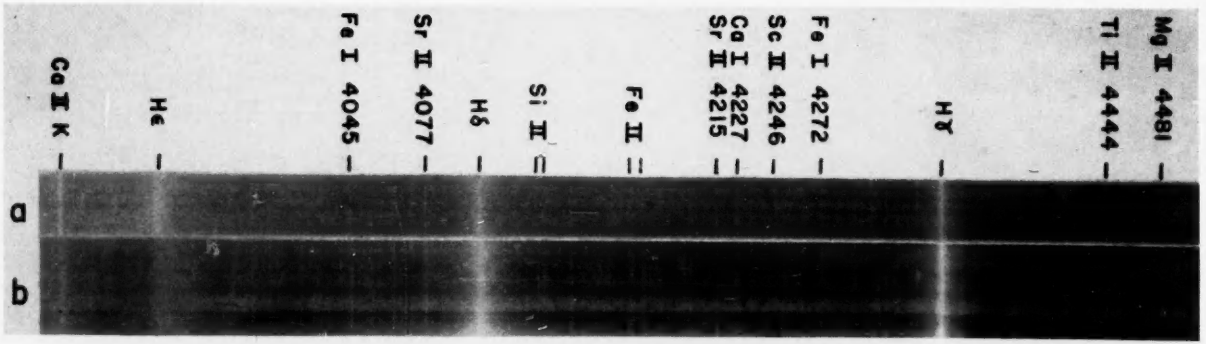

FIG. 1.—*a*, the blue spectrum of the high-velocity A-type star HD 161817, July 21, 1951. Eastman 103-O emulsion. *b*, the blue spectrum of the standard main-sequence A2 star η Ophiuchi, August 22, 1950. Eastman 103-O emulsion.

ON THE BOLOMETRIC CORRECTION FOR EARLY-TYPE STARS

Recently J. C. Pecker,[1] from model-atmosphere computations for B-type stars, has determined the bolometric correction for spectral types B1 and B1.5. Since it is of interest to obtain a sound theoretical estimate of the bolometric correction for the early-type stars, we have computed this quantity for three early-type model atmospheres,[2] using the visual sensitivity-curve given by Nutting.[3] The main characteristics of these model atmospheres and the bolometric correction, B.C., are given in Table 1, together with the

TABLE 1

PROPERTIES OF THE MODEL ATMOSPHERES

	Author				
	A. B. Underhill		J. K. McDonald	J. C. Pecker	
T_e from flux	44,600°	36,800°	22,700°	27,300°	26,360°
T_0	35,000°	25,200°	16,800°	17,700°	17,300°
log g	4.20	4.20	3.80	4.48	4.48
H:He by number	85:15	85:15	83:17	100:0	100:0
Spectral type	O5 V	O9.5 V	(B2)	B1 V	B1.5 V
B.C.	− 4.31	− 3.68	− 2.63	− 3.00	− 2.83

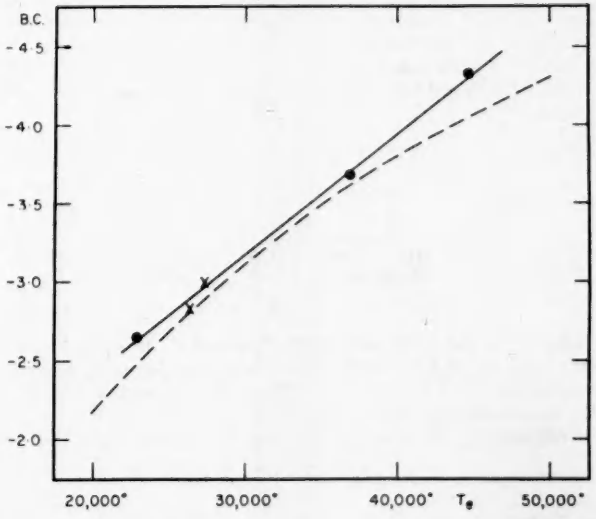

FIG. 1.—The relationship between T_e and the B.C. established by our model-atmosphere computations. The broken line gives the relationship suggested by Kuiper, and Pecker's results are indicated by X's.

[1] *Ann. d'ap.*, **13**, 433, 1950; *Contr. Inst. Ap. de Paris*, Ser. B, No. 65, p. 68.

[2] A. B. Underhill, *Pub. Dom. Ap. Obs. Victoria*, Vol. **8**, No. 12, 1951; A. B. Underhill, *Pub. Copenhagen Obs.*, No. 151, 1950; J. K. McDonald, unpublished.

[3] *Phil. Mag.*, **29**, 304, 1915.

results by Pecker.[1] The bolometric corrections are adjusted to a scale giving B.C. = −0.11 for the sun; hence we have

$$\text{B.C.} = 2.5 \log \frac{\int p_\lambda F_\lambda d\lambda}{\int p_\lambda F_\lambda (\odot)\, d\lambda} - 10 \log \frac{T_e}{T_e(\odot)} - 0.11 ,$$

where p_λ is the normalized visual sensitivity function and F_λ is the emergent monochromatic flux from the model atmosphere. We have used the $F_\lambda(\odot)$ given by Unsöld,[4] and we took $T_e(\odot) = 5713°$.

The results are displayed in Figure 1. It is seen that they are in fair accord with the scale of bolometric corrections based on effective temperatures, suggested some years ago by Kuiper.[5] An extrapolation of the curve relating B.C. to θ_e, given by E. Vitense,[6] suggests values about 0.5 mag. less negative than we find.

JEAN K. MCDONALD
ANNE B. UNDERHILL

DOMINION ASTROPHYSICAL OBSERVATORY
VICTORIA, B.C.
November 28, 1951

THE SPECTRUM OF CPD−60°3278

As early as August 10, 1950, Father O'Connell, S.J., called the writer's attention to "a very interesting eclipsing binary with a very long minimum . . . CPD−60°3278[1] . . ." for which "it would be interesting to know the spectrum at minimum." "The star was at maximum from JD 2426500 (the date of our earliest plates) to about 2430000, when the eclipse began. The middle of the eclipse was at JD 2433200 (pg. mag. 10.25). The magnitude is now about 10.2 and it is changing very slowly. The magnitude at maximum is 9.549. The eclipse is partial, though a short totality is not positively excluded."[2]

On account of O'Connell's discovery, S. Gaposchkin[3] has recently published a light-curve of CPD−60°3278 based on 1090 estimations on Harvard plates, which cover the interval 1890–1949.

Plate	Date (1951)	U.T.	Projected Slit-Width (Mm)	Exposure Time (Min.)
I 1652	June 29	0:36	0.038	288
1673	August 17	0:07	0.046	177

Two spectrograms of the star have been obtained at Bosque Alegre on Eastman 103*a*-O emulsion with the 154-cm reflector and the Wood-grating spectrograph, which gives a dispersion of about 42 A/mm. The relevant data corresponding to the two plates are given in the accompanying tabulation.

According to O'Connell,[4] the star "has remained at substantially the same brightness

[4] *Physik der Sternatmosphären* (Berlin: J. Springer, 1937), p. 32.

[5] *Ap. J.*, **88**, 429, 1938.

[6] *Zs. f. Ap.*, **29**, 73, 1951.

[1] $\alpha = 11^h40^m.8$; $\delta = -60°27'$ (1950.0). CD−60°3704.

[2] Some of the preliminary data in O'Connell's letter have been modified according to those published in his paper in *M.N.*, **111**, 111, 1951.

[3] *Pub. A.S.P.*, **63**, 80, 1951.

[4] Private communication of October 3, 1951.

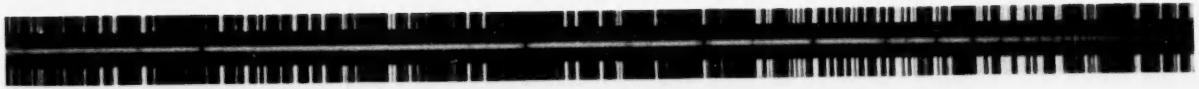

FIG. 1.—Spectrum of CPD−60°3278 taken on June 29.025ᴅ, 1951 (U.T.) (positive enlargement)

since about JD 2433000 until the latest observations JD 2433864." Therefore, at the times our plates were taken the star was at about 10.2 mag.

The spectrum of June 29, which was very kindly taken for me by Dr. J. Landi Dessy, shows a shell spectrum (Fig. 1) displaying sharp absorption of *H*, *He* I, and *Ca* II, with *H* the most outstanding and *He* I very faint. The radial velocity from that plate was determined by measuring the *H* lines from *H*20 to *Hγ*; *He* I λλ 3820, 4026, and 4471; and *Ca* II H and K. The value obtained is -20 ± 1.3 (p.e.) km/sec, the plate being measured twice.

The plate of August 17 is underexposed; nevertheless, one can readily see that the character of the spectrum is the same as on the June plate. The radial velocity, measured twice, as a mean from six *H* lines and *Ca* II K is $+10 \pm 4.2$ (p.e.) km/sec.

The spectrum of the star, taken at maximum light, was classified as B5: by Becker[5] and as B3 in the *Henry Draper Extension*,[6] where it is assigned the HD number 306989.

The star will be observed again in the next season.

JORGE SAHADE

OBSERVATORIO ASTRONÓMICO
CÓRDOBA, ARGENTINA
December 26, 1951

THE SPECTRUM OF NOVA SCORPII 1950 II ON AUGUST 16, 1950

Two slit-spectrograms of Nova Scorpii 1950 II[1] were obtained with the Wood-grating spectrograph attached to the 154-cm reflector at Bosque Alegre, on August 16 and 21, 1950, the dispersion being about 42 A/mm. The spectrograms were taken on Eastman 103*a*-F emulsion, with a projected slit-width of 0.038 mm and exposure times of 94 and 84 minutes, respectively. The plate of August 21 was secured under unfavorable weather conditions and is underexposed; nevertheless, the strongest lines present on August 16 are also present on this plate, and the impression is that the spectrum of the nova had not appreciably changed in the interval between the two exposures.

The spectrum of August 16 (Fig. 1) is characterized by the presence of several very broad emission features, which can be identified as due to *H*, *Ca* II, *Si* II, *Sc* II, *Ti* II, and *Fe* II. The *H* emission clearly shows a complex structure. Centered at about λλ 3825, 3877, 3918, and 3953 there are some broad absorption features. Furthermore, the emissions of *Ca* II H and K are crossed by relatively narrow absorptions, which yield, in the mean, a radial velocity of -24 km/sec. The edges of the complex *H* emission structure correspond to velocities of the order of -700, $+200$, $+1000$, and $+1500$ km/sec, respectively. Our observations suggest that, at the time they were made, the nova was in the "Q3" stage, according to the classification scheme proposed at the Seventh General Assembly of the I.A.U.[2] The exposure time was such that no features between λ 5320 and *Hα* appear on the plate.

Table 1 lists the measured wave lengths at the center of the emission features, their width, and their identification. The widths of the *H* emission—except at *Hα*—are prob-

[5] *Pub. Ap. Obs. Potsdam*, **27**, No. 89, Part II, 59, 1930.

[6] A. J. Cannon and M. W. Mayall, *Harvard Ann.*, **112**, 160, 1949 (Chart 140).

[1] $\alpha = 17^h48^m6$; $\delta = -35°22'$ (1950.0); discovered by Haro, who found the star at magnitude 7.5 on August 7 (*Harvard Announcement Card* No. 1091), and independently by Herzog (*Pub. A.S.P.*, **63**, 121, 1951). Light-curves of this nova have been published by Herzog and Zwicky (*Pub. A.S.P.*, **63**, 121, 1951) and by N. Tapia (*Circ. Obs. La Plata*, No. 8, p. 15, 1951). Results from objective-prism spectra have been reported by McLaughlin (*Pub. A.S.P.*, **63**, 129, 1951), covering the interval August 8–August 17, and by Henize and McLaughlin (*A.J.*, **56**, 74, 1951), covering the interval July 27–August 16.

[2] *Trans. I.A.U.*, **7**, 305, 1950.

TABLE 1

THE SPECTRUM OF NOVA SCORPII 1950 II ON AUGUST 16, 1950
(Emission Features)

λ	Width (A)	Identification*
3768	23	*Ti* II 3759.29 (200), 61.32 (200); *H* 70.63
3800	19	*H* 3797.90
3837	16	*H* 3835.39
3863	10	*Si* II 3856.02 (8), 62.59 (6)
3896	15	*H* 3889.05; *Ti* II 3900.55 (70)
3934	16	*Ca* II 3933.66 (400)
3972	23	*Ca* II 3968.47 (350); *H* 3970.07
4104	22	*H* 4101.74
4124	18	*Si* II 4128.05 (8), 30.88 (10)
4176	18	*Fe* II 4173.45 (8), 78.86 (8)
4236	21	*Fe* II 4233.17 (11)
4259	24	*Sc* II 4246.83 (100)
4303	24	*Ti* II 4300.05 (60); *Fe* II 03.17 (8)
4343	22	*Ti* II 4337.92 (50); *H* 4340.47
4396	10	*Ti* II 4395.03 (60)
4414	9	*Fe* II 4416.82 (7)
4446	13	*Ti* II 4443.80 (50)
4520	18	*Fe* II 4515.34 (7), 20.22 (7), 22.63 (9)
4552	18	*Fe* II 4549.47 (10), 55.89 (8); *Ti* II 49.62 (60n)
4585	20	*Fe* II 4583.83 (11)
4636	27	*Fe* II 4629.34 (7)
4864	27	*H* 4861.33
4925	22	*Fe* II 4923.92 (12)
5020	22	*Fe* II 5018.43 (12)
5174	27	*Fe* II 5169.03 (12)
5320	24	*Fe* II 5316.61 (8)
6572	48	*H* 6562.82

* The figures in parentheses are laboratory intensities as quoted in Mrs. Moore Sitterly's *Revised Multiplet Table* (*Contr. Princeton U. Obs.*, No. 20, 1945).

ably too small because of underestimation of the outer red edge of the complex structure. The contrary is probably true for *Hα* because of exposure effect.

JORGE SAHADE
JORGE LANDI DESSY

OBSERVATORIO ASTRONÓMICO
CÓRDOBA, ARGENTINA
January 5, 1952

A NOTE ON THE CONCEPT OF EFFECTIVE WAVE LENGTH

The response of a light-measuring instrument to starlight is a complicated function of the distribution of energy in the spectrum of the star, the transmission of the atmosphere and the telescope, and the sensitivity of the light-receiving device. In the difficult problem of interpreting the resulting magnitudes, a frequent line of attack has been the attempt to characterize a magnitude system by an effective wave length. Much has been written on the subject of effective wave lengths, and some of the conflicting ideas set forth in the literature may come to impede progress in fundamental photometry.

The meaning of the term "effective wave length" for fundamental photometry should

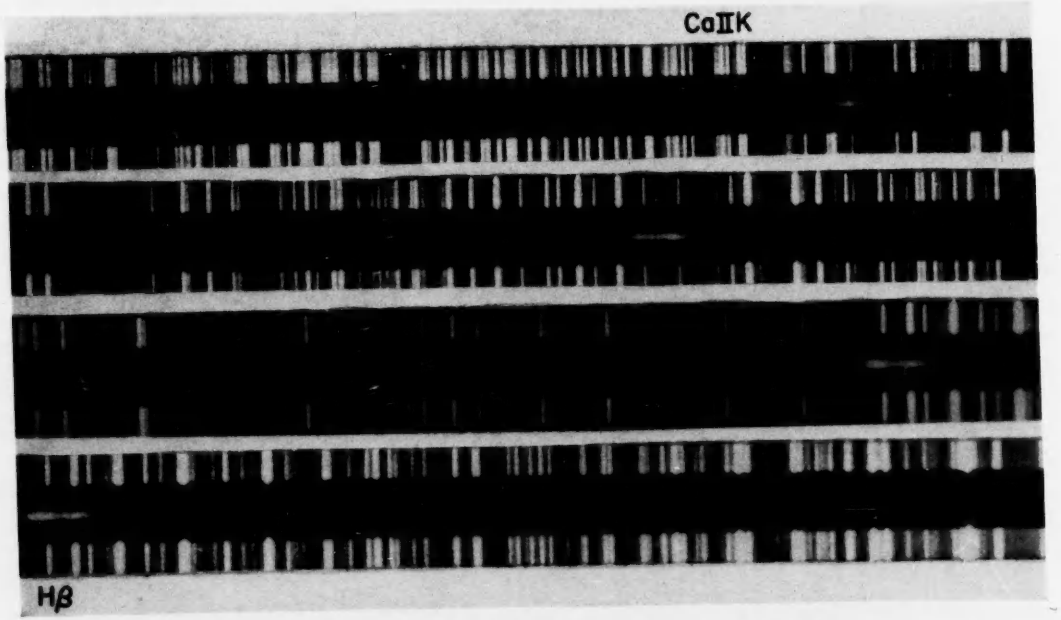

FIG. 1.—The spectrum of Nova Scorpii 1950 II on August 16, 1950 (positive enlargement)

be clear: the instrument acts effectively as if all the light were concentrated at this wave length. More exactly, the effective wave length of a comparison of two stars by a given instrument is that wave length at which a monochromatic light-receiver would register the same magnitude difference as does the actual instrument. (Note the necessary qualification that the word "monochromatic" is not used here in the strictest sense but refers to stellar energy distributions in which the absorption lines have been smoothed out.) This definition is essentially the same as that of Brill's "isophotal wave length."[1] It is in no way arbitrary but follows directly from our intuitive understanding of the word "effective."

The above definition of effective wave length requires the specification of two stars. There is no meaningful way of defining the effective wave length (in this sense) of a single star, unless the definition tacitly specifies a second star with which the comparison is to be made. Moreover, since the properties of the stars appear in the definition, a photometric system is, in general, characterized not by a single effective wave length but by a double infinity of wave lengths, one for each pair of stars compared.

There may, however, be some wave length which to a first approximation acts as an effective wave length for all stars. B. Strömgren[2] and Wesselink[3] have independently shown that such a wave length is given by

$$\lambda_0 = \frac{\int_0^\infty \lambda \phi(\lambda)\, d\lambda}{\int_0^\infty \phi(\lambda)\, d\lambda},$$

where $\phi(\lambda)$ is the sensitivity of the instrument at wave length λ. Strömgren, in an illuminating but little-read discussion, goes on to derive the theoretical form of the correction term which converts heterochromatic magnitudes to monochromatic magnitudes at wave length λ_0.

Unfortunately, the name "effective wave length" has at the same time been applied to a very different quantity, which may be defined in the present notation as

$$\lambda_s = \frac{\int_0^\infty \lambda S(\lambda)\phi(\lambda)\, d\lambda}{\int_0^\infty S(\lambda)\phi(\lambda)\, d\lambda},$$

where $S(\lambda)$ is the intensity of a star's light at wave length λ. (This definition is prominent in the writings of Seares.)[4] The application of the name "effective wave length" to the quantity λ_s is highly misleading. For the name "effective wave length" carries with it such definite connotations that the choice of a mathematical definition is a task not of picking the most convenient arbitrary definition but simply of giving exact expression to the meaning that we already attach to the term. If, in spite of this difficulty, the quantity λ_s continues to bear the name "effective wave length," it will be only too easy to err in attributing to λ_s properties which its name, but not its definition, implies.

For example, misuse of Seares's definition of effective wave length might lead us to criticize the retention of the International photographic system, using arguments which involve just this error. The reasoning can be broken down into several successive steps: (1) If the effective wave length of a magnitude system varies greatly with spectral

[1] *Veröff. d. U.-Sternw. Berlin-Babelsberg*, Vol. **7**, No. 5, 1929.

[2] *Handbuch der Experimentalphysik* (Leipzig: Akademische Verlagsgesellschaft, 1937), **26**, 392.

[3] *Trans. I.A.U.*, **7**, 269, 1950.

[4] Seares and Joyner, *Ap. J.*, **98**, 302, 1943.

type, then the system is a bad one. (2) The quantity λ_e for the International System varies greatly with spectral type. (3) Therefore, the International System is a bad one. The argument involves the tacit assumption that the bestowal of the name "effective wave length" on the quantity λ_e automatically endows λ_e with all the properties of a true effective wave length. As a matter of fact, calculations by Seares and Joyner[5] show that Brill's isophotal wave length (which is a true effective wave length) varies much less with spectral type than does λ_e. The inadequacies of the International System are therefore smaller than we might lead ourselves to believe.

It is a pleasure to acknowledge the value of discussions with Dr. A. J. Wesselink and Dr. R. H. Stoy.

IVAN KING

HARVARD COLLEGE OBSERVATORY
August 29, 1951

SEARCH FOR FLARES OF dM STARS ON THE SPROUL ASTROMETRIC PROGRAM

During the last fifteen years a number of late M dwarf stars have been observed to increase their luminosity considerably in a very short time and slowly return to normal brightness. These outbursts, or flare-ups, may be similar to the flares on the larger, dG0 star, our sun.[1,2] All the known flare stars show relatively strong H and K lines of *Ca* II in emission,[2,3] and it is thought that these lines vary in intensity during the visual flare-ups. "Spectral flares" have been observed for L 726-8 and Proxima Centauri.[3,4] It is not the purpose of this note to describe in detail or to offer explanations for these phenomena, which have been described elsewhere in the literature, viz., *Harvard Reprint* No. 344 and other references listed with this paper. Table 1 lists those stars for which flares have been observed, together with apparent and absolute visual magnitudes, and spectra.

TABLE 1

KNOWN FLARE STARS

STAR	1900		m_v	SP.	M_v	NOTES
	α	δ				
L 726-8B	1^h34^m0	$-18°28'$	13.5	dM5.5	16.6	1, 2
Ross 882	7 39.4	+ 3 48	11.6	dM4.5e	12.4	3
BD+20°2465	10 14.2	+20 22	9.4	dM4e	11.1	4
Lal. 21258B	11 0.5	+44 2	14.8	dM5.5e	16.0	5
Proxima Centauri	14 22.8	−62 15	11.3	dM–e	15.4	6, 7
Krüger 60B	22 24.4	+57 12	11.3	dM4.5e	13.3	8

NOTES TO TABLE 1

1. A. H. Joy and M. L. Humason, *Pub. A.S.P.*, **61**, 133, 1949.
2. W. J. Luyten, *Ap. J.*, **109**, 532, 1949; *Pub. A.S.P.*, **61**, 179, 1949.
3. A. van Maanen, *Pub. A.S.P.*, **57**, 216, 1945.
4. K. C. Gordon and G. E. Kron, *Pub. A.S.P.*, **61**, 210, 1949.
5. A. van Maanen, *Ap. J.*, **91**, 503, 1940.
6. H. Shapley, *Harvard Repr.* No. 344.
7. A. D. Thackeray, *M.N.*, **110**, 45, 1950.
8. P. van de Kamp and S. L. Lippincott, *Pub. A.S.P.*, **63**, 141, 1951.

[5] *Ibid.*, p. 329.
[1] G. E. Kron, *A.J.*, **55**, 69, 1950.
[2] A. H. Joy and R. E. Wilson, *Ap. J.*, **109**, 231, 1949.
[3] A. D. Thackeray, *M.N.*, **110**, 45, 1950.
[4] A. H. Joy and M. L. Humason, *Pub. A.S.P.*, **61**, 133, 1949.

TABLE 2

OBSERVATIONS ON dM STARS

STAR	1900 α	1900 δ	m_v	SP.	INTERVAL	NO. NIGHTS	NO. EXP.	EXP. TIME (MIN.)	TOTAL EXP. TIME (HR.)
	Stars Showing H and K Emission Lines								
ADS 48B, F	0h 0m4	+45° 16′	9.4, 9.9	dM0, dM2	1923–51	33	287	½	10.8
Grb. 34A, B	0 12.7	+43 27	8.5, 10.9	dM2.5, dM4e	37–51	21	205	¾	37.4
Mlb 377A	0 26.2	+66 42	10.4	dM2.5	37–49	15	101	⅔	5.0
Ross 318	0 55.3	+71 9	9.9	dM3.5e	37–51	15	147	½	3.1
Wolf 47A	0 56.3	+61 49	9.5	dM2	38–44	5	5	30	2.5
L726-8A, B	1 34.0	−18 28	13.0, 13.5	dM5.5, dM5.5	48–51	17	73	13	15.8
ADS 1865	2 22.5	+ 3 59	8.6	dM1.5	38–51	22	270	½	2.5
Ross 556	2 38.4	+25 6	10.5	dM3	37–51	12	126	⅓	1.3
o^2 Eri C	4 10.7	− 7 49	11.1	dM4.5e	37–51	33	289	½	8.7
20C303	4 37.0	+18 47	9.8	dM2.5	37–48	10	47	2	4.1
Cin. 705	5 26.4	− 3 42	8.1	dM2	37–50	15	194	⅓	3.3
Ross 42	5 26.7	+ 9 45	11.8	dM4e	40–51	10	97	1½	4.0
Ross 614	6 24.3	− 2 44	11.3	dM4.5e	38–51	101	1089	1	49.8
YY Gem	7 28.2	+32 6	9.5	dM1e	38–51	23	325	½	3.0
Ross 882	7 39.4	+ 3 48	11.6	dM4.5e	40–51	9	74	2	4.9
BD+20°2465	10 14.2	+20 22	9.4	dM4e	38–51	81	809	1½	33.5
Wolf 359	10 51.6	+ 7 36	13.5	dM6e	37–50	50	84	15	44.7
Lal. 21185	10 57.9	+36 38	7.3	dM2	12–51	246	2972	¾	59.3
Lal. 21258A, B	11 0.5	+44 2	8.6, 14.8	dM2, dM5.5e	38–49	11	58	1½	3.6
Wolf 424A, B	12 28.4	+ 9 34	12.7	dM5.5e	38–51	63	192	6	42.8
AC+66°3955	12 45.1	+66 40	10.5	dM3	40–51	13	124	1½	5.7
Cin. 1633	12 45.6	− 0 13	8.7	dM0	40–41	6	23	4	1.5
ADS 8862	13 15.4	+48 18	8.8	dM2	45–51	16	185	1	3.1
AC+18°1204-96A, B	13 28.1	+17 16	11.0, 11.5	dM4e, dM4.5e	43–51	3	36	1	0.8
Lal. 25372	13 40.7	+15 26	8.6	dM2.5	38–51	42	501	¾	14.2
ADS 9090A, B	13 58.5	+46 49	9.9, 9.9	dM3, dM3,	38–50	15	121	⅓	2.4
Wolf 630A, B	16 50.1	− 8 8	9.9	dM3e	38–51	45	170	4	27.2
μ Herc B	17 42.5	+27 47	10.2	dM3.5	38–49	23	137	¾	6.0
BD+4°4048	19 12.1	+ 5 2	9.2	dM3	37–50	40	471	1½	11.5
Wolf 1084	20 40.3	+54 57	15.3	dM5e	37–51	11	12	30	10.4
Fu 54A	20 56.2	+39 41	10.2	dM3e	37–48	16	165	1	5.5
61 Cyg B	21 2.4	+38 15	6.3	dM0	12–51	130	1425	½	26.2
Ross 775	21 24.8	+17 12	10.4	dM4	38–51	29	387	½	8.8
Kr. 60B	22 24.4	+57 12	11.3	dM4.5e	31–51	71	713	⅓	16.4
L789-6	22 33.0	−15 52	12.3	dM5.5e	40–50	60	145	9	42.8
BD+43°4305	22 42.5	+43 49	10.2	dM4.5e	37–51	55	610	½	15.0
Ross 671	22 51.8	+16 2	9.0	dM2.5	37–51	36	355	1	13.2
BD+19°5116A, B	23 26.7	+19 23	10.3, 12.8	dM4e, dM5.5e	44–51	17	259	¾	3.5
Ross 248	23 37 0	+43 40	12.2	dM5.5e	37–51	196	949	3	128.3
	Stars Showing No H and K Emission Lines								
BD+5°1668	7 22.4	+ 5 32	10.0	dM4	37–51	125	1600	½	20.9
Barnard's star	17 52.9	+ 4 25	9.7	sdM4.5	16–51	451	6760	⅔	114.0
Wolf 1062	19 7.0	+ 2 44	11.3	dM4	38–50	31	206	2	8.8
Ross 165	19 41.7	+26 55	12.7	dM4.5	37–49	69	234	5	49.9
CC 1213	20 29.0	+65 6	11.5	dM3	38–51	54	542	1	22.4

Since the majority of near-by stars are M dwarfs, the Sproul Observatory has an accumulation of exposures of potential flare stars on its astrometric program. Recently, all images of dM stars known to exhibit H and K emission lines have been examined for variability. The material, representing 44 stars, consists of more than twenty-three thousand images, covering a total of 37 days of observation and a nightly average of ten exposures per star. These stars—plus a few nonemission-line M dwarfs—are listed in Table 2, which gives the interval over which the plates were taken, the number of nights, the number of exposures, the current exposure time, and the total exposure time. The apparent visual magnitudes and spectra are those given by Joy and Wilson.[2] The exposure times were appreciably longer before the summer of 1939, at which time the Eastman Super Panchro Press emulsion was introduced; another cut in exposure was made in 1945, when the I-C emulsion gradually came into use. It is difficult to make a generally valid quantitative statement, since exposure times depend on other factors besides plate speed. In the majority of cases, however, the change in emulsion in 1939 reduced the exposure times to less than half their former values, while the change to the I-C emulsion in 1945 resulted in another halving of the exposure time. Since the beginning of 1949 the 103-G emulsion has been generally employed.

The images were inspected by Miss Julia Damkoehler and the author. It must be remembered that these plates were taken for astrometric purposes, for which small, sharp, well-blackened images are desirable, and that the scale is large (1 mm = 18″.87), thereby increasing the effects of changes in seeing. Double stars with separations of less than 2″ generally appear as one blended image. It is difficult to establish the reality of any apparent variability of less than 0.2 mag. Obviously, short exposures are necessary to reveal a flare which may remain intense for only a few minutes. No certain variability was found, with the one striking exception of Krüger 60B, which exhibited a flare-up on July 26, 1939, and has been reported elsewhere.[5]

Although, with this one exception, the results are virtually negative, the present survey throws some light on the frequency of flares or, rather, on the elusive nature of these unpredictable and short outbursts. Inspection of plates for variability of late dwarf M stars will be continued at the Sproul Observatory.

SARAH LEE LIPPINCOTT

SPROUL OBSERVATORY
SWARTHMORE COLLEGE
SWARTHMORE, PENNSYLVANIA
November 19, 1951

[5] P. van de Kamp and S. L. Lippincott, *Pub. A.S.P.*, **63**, 141, 1951.

ERRATA

In *Ap. J.*, **113**, 475, 1951, Part I, equation (6), considerable uncertainty was expressed as to the correct form for the ratio of partition functions of the activated and normal states. It was not intended, however, that the uncertainty would extend so far as to use the reciprocal of the approximation finally adopted, as was erroneously done in equation (9), which should read

$$\frac{f^*}{f} = \frac{(1 - e^{-3\theta^*/4T})^{-2}}{(1 - e^{-3\theta_s/4T})^{-3}} \sim \frac{3}{4}\frac{\theta_s}{T}\left(\frac{\theta_s}{\theta^*}\right)^2,$$

and the first factor of equation (10) should be $(k\theta_s/h)$ rather than $(kT^2/\theta_s h)$. The numerical results in Table 1 change accordingly, but, as indicated in the paper, the exponential term in equation (9) is by far the governing factor. The average meteor surface temperature at maximum light becomes 4300° rather than 3100° for the case $\Lambda = 1$ of the paper. Recent work (R. N. Thomas and F. L. Whipple, *Ap. J.*, **114**, 448, 1951) indicates, however, that for the meteors $\Lambda_{av} \ll 1$, bringing the surface temperatures below this 4300° value. A discussion of this latter material in terms of the above methods will be presented shortly.

MELVIN A. COOK
HENRY EYRING
RICHARD N. THOMAS

In *Ap. J.*, **113**, 697, 1951, paragraph 1, line 5, *for* p.a. 52° *read* p.a. 308°. On page 699, paragraph 1, line 4, *for* p.a. 21° *read* p.a. 339°.

G. H. HERBIG

THE OBSERVATORY

FOUNDED 1877

* * *

A Magazine presenting current developments in Astronomy by means of Articles, Correspondence, Notes on discoveries and Reviews of important astronomical books. The papers read at the Meetings (Astronomical & Geophysical) of the Royal Astronomical Society and the discussions which follow are also fully reported.

* * *

Annual subscription for 6 issues, post free, £1 should be sent to

***The Editors,* ROYAL GREENWICH OBSERVATORY**

Horstmonceux Castle, Hailsham, Sussex, England

A Completely Revised Edition

THE ATMOSPHERES OF THE EARTH AND PLANETS

By GERARD P. KUIPER

Important new material has been added to make this edition the most modern and complete monograph on planetary atmospheres.

Additions include:

—Information recently obtained in V-2 flights about our upper air and the x-ray spectrum of the sun.

—Identification of the strong red and infrared emissions of the night sky.

—A new determination of the cosmic abundances of the chemical elements.

—A derivation of the ozone temperature in the upper stratosphere.

—A determination of the age of meteorites.

—A discussion of the presence of nitrous oxide in the lower atmosphere and its connection with the life cycle.

—A reconstruction of the conditions leading to the escape of the "proto-atmosphere."

—A new section on Jovian planets.

—A development of the atmospheric conditions on Mars.

Paperbound $5.50 *Clothbound $8.50*

THE UNIVERSITY OF CHICAGO PRESS

5750 ELLIS AVENUE **CHICAGO 37, ILLINOIS**

IMPORTANT BOOKS IN THE HISTORY OF ASTRONOMY

THE ARYABHATIYA OF ARYABHATA
An Ancient Indian Work on Mathematics and Astronomy

Translated with Notes by WALTER EUGENE CLARK

Aryabhata's work, which was composed in A.D. 499, is probably the earliest preserved Indian mathematical and astronomical text bearing the name of an individual author; the earliest Indian text to deal specifically with mathematics; and the earliest preserved astronomical text from the third or scientific period of Indian astronomy. This is the first complete translation from the Sanskrit of this historical document.

120 pages 7½ × 5½ *$2.50*

LATIN TREATISES ON COMETS BETWEEN 1238 and 1368 A.D.

By LYNN THORNDIKE

This volume publishes for the first time the Latin texts of important tracts on comets observed between 1238 and 1368 A.D. Among the treatises are works by Aegidius of Lessines, Gerardus de Silteo, Peter of Limoges, Geoffrey of Meaux, and John of Legnano. As a summary of the Aristotelian doctrine of comets, the commentaries of Thomas Aquinas and of Albertus Magnus on Aristotle's *Meteorology* are included in English translation.

286 pages 6 × 9 *Index* *$5.00*

THE SPHERE OF SACROBOSCO AND ITS COMMENTATORS

By LYNN THORNDIKE

A critical edition of the Latin text, together with an English translation, of the SPHERE of John of Sacrobosco—for centuries the best and best known manual of astronomy by a Western author. Also included is the hitherto unpublished commentary by Robert of England, with an English translation. In addition, the commentary of Cecco d'Ascoli and the commentary ascribed to Michael Scot are made available for the first time outside of rare books printed in abbreviated Latin.

506 pages 6 × 9 *Index* *$10.00*

THE UNIVERSITY OF CHICAGO PRESS